Project No. 16-10918

# Development and Application of a Data-Driven Methodology for Validation of Risk-Informed Safety Margin Characterization Models

## Reactor Concepts Research Development and Demonstration (RCRD&D)

**Nam Dinh**
North Carolina State University

**Collaborators**
George Washington University
The Ohio State University

Alison Hahn, Federal POC
Curtis Smith, Technical POC

NEUP Nuclear Energy University Programs
U.S. Department of Energy


## Milestone: M2NU-16-NC-NCSU-030401-151
### Final Technical Progress Report

Project Number: IRP-16-10918
DOE Contract No.: DE-NE0008530

# Development and Application of a Data-Driven Methodology for Validation of Risk-Informed Safety Margin Characterization Models

Project PI: Nam Dinh (ntdinh@ncsu.edu)
Technical Contact: Yong-Joon Choi
Federal Contact: Alison Hahn

**North Carolina State University**
Nam Dinh, Abhinav Gupta, Igor Bolotnov, John Baugh, and Maria Avramova
**Purdue University**
Hany Abdel-Khalik
**University of Michigan**
Xiaodong Sun
**The George Washington University**
Philippe Bardet
**Zachry Nuclear Engineering**
Jeffery Lane
**R.T. Sewell Associates**
Robert Sewell
**Centroid PIC, Inc.**
Ram Sampath
**Idaho National Laboratory**
Steven Prescott, Cristian Rabiti, Robert Youngblood
**Oak Ridge National Laboratory**
Weiju Ren

January 2021

**Abstract**

The document is the Final Technical Progress Report for the Nuclear Energy University Program's Integrated Research Project (IRP) on "Development and Application of a Data-Driven Methodology for Validation of Risk-Informed Safety Margin Characterization Models" that supports the LWR Sustainability Program's RISMC R&D Pathway. The project goal is to develop and demonstrate a data-driven methodology for validation of advanced computer models used in nuclear power plant safety analysis. Specifically, the advanced computer models are those in the toolkit developed to support risk-informed safety margin characterization (RISMC), an integrated deterministic/probabilistic safety analysis methodology developed in the Department of Energy's Light Water Reactor Sustainability (LWR-S) program.

The report reflects the progress made towards the project's stated goal by contributions by researchers and graduate students from universities, with support from researchers from national laboratories and industry companies. The project organization, effort coordination and technical implementation are summarized, followed by discussion of main findings, issues, and path forward. Selected chapters provide a more detailed description of tasks, approaches and respective findings and recommendations. Noteworthy are contributions that serve as guidelines for methodology development. It is also noted that this report is complemented by other milestone reports (as stand-alone deliverables) that provide detailed discussion of the technical developments. The project results have been documented in a number (12) dissertations and these, 50+ peer-reviewed publications in technical journals and conference proceedings.

**Acknowledgement**

The document is prepared as milestone report for the work performed under the Department of Energy's Nuclear Energy University Program's Integrated Research Project "Development and Application of a Data-Driven Methodology for Validation of Risk-Informed Safety Margin Characterization Models" in support of the DOE's LWR Sustainability program's RISMC R&D Pathway. The project received guidance from the RISMC Pathway Technical Lead, Dr. Curtis Smith, and the LWR Sustainability program RISMC Technical Point of Contact (TPOC) Dr. Yong-Joon Choi, both of Idaho National Laboratory (INL).

**Nomenclature**

| | |
|---|---|
| AMS | Advanced Modeling and Simulation |
| BN | Bayesian Network |
| BWR | Boiling Water Reactor |
| CA | Code Adequacy |
| CASL | Consortium for Advanced Simulation of Light Water Reactors |
| CAE | Claim, Argument, and Evidence |
| CFD | Computational Fluid Dynamics |
| CPT | Conditional Probability Table |
| CSAU | Code Scaling, Applicability, and Uncertainty |
| DA | Data Applicability |
| DD | Data-Driven |
| EM | Evaluation Model |
| EMDAP | Evaluation Model Development and Assessment Process |
| EMU | Experimental Measurement Uncertainty |
| EU | Expected Utility |
| EVSI | Expected Value of Sample Information |
| GSN | Goal Structuring Notation |
| GWU | The George Washington University |
| HMM | Heterogeneous Multiscale Integration |
| IET | Integrated Effect Test |
| INL | Idaho National Laboratory |
| ML | Machine Learning |
| M&S | Modeling & Simulation |
| NCSU | North Carolina State University |
| NPP | Nuclear Power Plant |
| ORNL | Oak Ridge National Laboratory |
| PCM | Physics-guided Covered Mapping |
| PCMM | Predictive Capability Maturity Model |
| PCMQ | Predictive Capability Maturity Quantification |
| PIRT | Phenomena Identification and Ranking Table |
| PP | Phenomenology Pyramid |
| PWR | Pressurized Water Reactor |
| PRA | Probabilistic Risk Analysis |
| QoI | Quantity of interest |
| ROM | Reduce Order Modeling |
| RAVEN | Risk Analysis Virtual Environment |
| RPP | Reactor Prototypicality Parameter |
| RISMC | Risk-Informed Safety Margin Characterization |
| SPH | Smoothed Particle Hydrodynamics |
| STH | System Thermal-Hydraulics |
| U-M | University of Michigan |
| UQ | Uncertainty Quantification |
| V&V | Verification and Validation |
| VUQ | V&V and UQ |

## Table of Contents

# 1. Project Overview

## 1.1. Goal, Vision, and Approach

The goal of the integrated research project is to develop and demonstrate a data-driven methodology for validation of advanced computer models for nuclear power plant safety analysis. Specifically, the advanced computer models are those in the toolkit developed to support the risk-informed safety margin characterization (RISMC), an integrated deterministic/probabilistic safety analysis methodology developed in the Department of Energy's Light Water Reactor Sustainability (LWR-S) program.

The project is carried out with vision that the new validation methodology for safety analysis codes will build upon the U.S. Nuclear Regulatory Commission's Code Scaling, Applicability and Uncertainty (CSAU) methodology, and its subsequent regulatory guide NRC 1.203 on "Transient and Accident Analysis Methods", also known as Evaluation Model Development and Assessment Process (EMDAP). The resulting methodology, called Risk-informed EMDAP or REMDAP, should meet requirements of the RISMC methodology. The project team brings to bear advanced methods and tools in verification, validation, sensitivity, and uncertainty analysis to facilitate the implementation of already demanding EMDAP in a risk-informed application.

The project's technical approach involves applying the developed validation methodology to guide the validation of computer models for flooding hazard analysis and for system thermal-hydraulics analysis. Respectively, the RISMC tools are (1) a Smoothed Particle Hydrodynamics code used in the LWR-S program for flooding simulation, and (2) a system-level reactor core thermal-hydraulics simulation code. In both cases, the RISMC models are applied to study a selected class of accident scenarios, for which sources of errors and uncertainties and predictive capability gaps are identified. Methods and tools of sensitivity, uncertainty and scaling analysis are applied to guide the development of a verification and validation plan, including the validation data plan. The latter identifies and characterizes existing and available data and databases and defines requirements for data to be obtained experimentally and computationally. Validation experiments (e.g., fluid dynamics, and fluid-structure interactions, turbulent mixing, and thermal stratification) and high-fidelity computer simulation ("numerical experiments") are formulated, designed, built, and operated to produce data for validation of the respective RISMC tools. Lessons learned by means of the two applications will serve as useful feedback for refining the proposed methodology and associated techniques.

One major challenge in validation is a lack of relevant data, including lack of confidence in the applicability of models and their supporting data in prototypic reactor conditions. In addition to this, the computational and methodological limitations of previous eras led to reliance on human judgment that can now be reduced. It is not that we no longer need data: rather, nowadays, it is possible to improve the use that we make of the data that we have (or can obtain).

In addition, in order to bridge the remaining gap in data, the project investigates and advances:

(a) a decision-theoretic framework for predictive capability maturity quantification;

(b) techniques for simulation-based scaling for evaluation of applicability of experiments and determination of the validation domain;

(c) reduced order modeling techniques to enable uncertainty quantification;

(d) data-driven multi-scale integration that enables effective use of "big data" generated by advanced experiments and validated computational simulations;

(e) validation data plan as a dynamic risk-informed instrument to guide design of experiments and simulation, and

(f) validation data management system that makes use of the Nuclear Energy Knowledgebase for Advanced Modelling and Simulation (NE-KAMS) infrastructure.

The proposed project will bring to bear advanced methods and tools in verification, validation, sensitivity, and uncertainty analysis to facilitate the implementation of already demanding EMDAP in a risk-informed application (see Figure 1.1). in REMDAP, the risk-informed dimension manifests itself through the requirements (Box 1.1 in Figure 1.1) and measured by PCMQ (Box 1.3 in Figure 1.1). The proposed approach will combine the NRC's CSAU methodology with the state-of-the-art uncertainty characterization techniques to provide a mathematically defendable basis for calculating biases and their uncertainties for the wide range of operating conditions that represent the intended range of model application. Our proposed approach will allow for a reliable scaling of the biases between the experimental and application conditions that precludes the need for model calibration. Quantitative metrics will be used to judge the relevance and value of available experimental information within the application scenario. Further, it will reduce reliance on the heuristics. The choice of models and model parameters will be based on the Phenomena Identification and Ranking Table (PIRT) process, increasingly aided by sensitivity/uncertainty analysis.

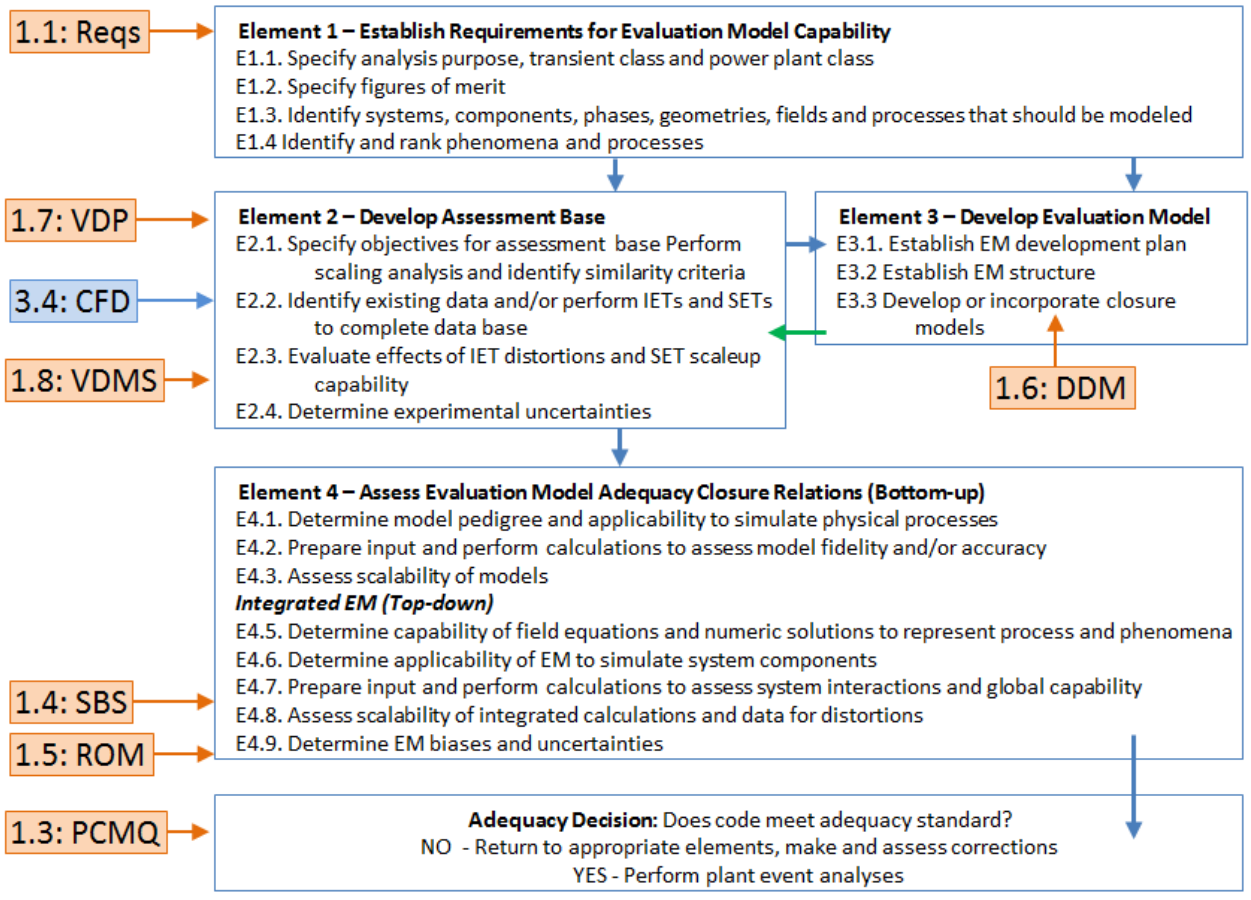


Figure 1.1. Risk-informed Evaluation Model Development and Assessment Process. Orange boxes denote developments in the project and indicate EMDAP elements where the advances are expected to impact.

Many limitations of a "validation" process arise because the experimental data correspond only partially to a scenario of interest. Consequently, a scenario-based approach for V&V-UQ proposed in this project is intended to overcome these limitations. Another challenge in validation is a lack of relevant data,

including lack of confidence in the applicability of models and their supporting data in prototypic reactor conditions. In addition to this, the computational and methodological limitations of previous eras led to reliance on human judgment that can now be reduced. It is not that we no longer need data: rather, nowadays, it is possible to improve the use that we make of the data that we have (or can obtain). In particular, a new physics-guided validation strategy based on first principles physics will rigorously map and bound the simulation errors in the domain of intended model use. To our knowledge, this represents a first-of-a-kind approach for the determination of the validation domain in the nuclear engineering community that presents a significant shift from the current approach for expert-determined scale distortion uncertainties. This is what we mean by "data-driven."

The project pursues a *simulation-aided uncertainty-guided data-driven* approach to enable effective implementation of the CSAU/EMDAP elements. The project investigates:

(a) Risk-informed approaches for collection and characterization of evidence,
(b) Decision-oriented framework for quantification of "validity" (or "maturity"), with a probabilistic criterion for adequate level of validation.
(c) Techniques for physics-based simulation-aided scaling, uncertainty, and sensitivity analysis (to compute and optimize the relevance and value of experiments),
(d) Methods for data-driven model development and assessment process that effectively utilizes data from physical and numerical experiments.

The project team applies the developed validation methodology to guide the validation of computer models for flooding risk-assessment and for system thermal-hydraulics analysis. Specifically, the RISMC tools selected in the proposed project are a Smoothed Particle Hydrodynamics (SPH-NEUTRINO) code for flooding simulation and the CTF code as surrogate for reactor system thermal-hydraulics simulation. In both cases, the RISMC models will be applied to study a selected class of accident scenarios, for which sources of errors and uncertainties and predictive capability gaps will be identified. Methods and tools of sensitivity, uncertainty and scaling analysis will be applied to guide the development of a verification and validation plan, including the validation data plan. The later identifies and characterizes existing and available data and databases and defines requirements for data to be obtained experimentally and computationally. Validation experiments (fluid dynamics, and fluid-structure interactions, turbulent mixing, and thermal stratification) and high-fidelity computer simulation ("numerical experiments") will be formulated, designed, built, and operated to produce data for validation of the respective RISMC tools. Through the two applications, lessons learnt will provide feedbacks to the methodology and associated techniques.

### 1.2. Project Organization and Execution

The project has three inter-related sub-domains and respective Tasks: (i) Task 1: Validation methodology development; (ii) Task 2: Flooding hazard simulation code application, and Task 3: System thermal-hydraulics simulation code application. The three sub-teams were organized, with overlapping participation, to ensure two-way information flow from methodology to applications, and between the two applications.

- The methodology group is led by NCSU, Purdue, ORNL and INL.
- The flooding application group is led by GWU, CPI, NCSU, RTS and INL.
- The system thermal-hydraulics (STH) application is led by UM, ZNE, Purdue and NCSU.

Table 1.1. The project's principal investigators.

| | Areas of Expertise | Special capability & contributions |
|---|---|---|
| Nam Dinh (NCSU) | Reactor safety, thermal-hydraulics | V&V, data-driven; project integration |
| Abhinav Gupta (NCSU) | Nuclear facilities, structures; hazards | PRA-based; Bayesian validation framework; |
| Hany Abdel-Khalik (PU) | Data assimilation; sensitivity/uncertainty | Reduced order modeling, coverage mapping |
| Xiaodong Sun (OSU) | Reactor system/core thermal-hydraulics | Advanced T-H experimentation; validation experi. |
| Philippe Bardet (GWU) | T-H experimentation; advanced diagnostics | Fluid-structure interaction; validation experiment |
| Igor Bolotnov (NCSU) | Multiphase flow direct numerical simulation | DNS (CFD) –informed STH; data analysis |
| John Baugh (NCSU) | Storm surge analysis; code assessment | ADCIRC; code interfacing; flooding scenarios |
| Maria Avramova (NCSU) | Reactor system/core thermal-hydraulics | COBRA-TF; RELAP; TRACE; CFD |
| Robert Youngblood (INL) | Risk, prevention & decision analysis; | Value of information; acceptance |
| Steve Prescott (INL) | Simulation-aided RISMC applications | RISMC validation requirements |
| Cristian Rabiti (INL) | Sensitivity/uncertainty analysis; RAVEN | S/UA support for design of experiments |
| Weiju Ren (ORNL) | Data management; relational database | NE-KAMS; VUQ-oriented data management |
| Jeff Lane (Zachry) | Reactor core/ plant thermal-hydraulics | GOTHIC, STH, SCA code assessment |
| Robert Sewell (RTSA) | Hazard analysis, External Event PRA | Industry requirements on code validation |
| Ram Sampath (CPL) | Flooding simulation; SPH modeling | NEUTRINO code improvement/support |
| Anh Bui (NCSU) | Turbulent and multi-phase CFD, SPH, V&V; | CFD-informed SPH; model calibration |

The coordination started from the kick-off meeting and reinforced and adjusted by the half-yearly and annual meetings. The exchanges were initiated and maintained via electronic communication, and teleconferences.

Capability and human resources development: The project team places a high significance on attracting young talented students and researchers for the project, and their training. The project recruited and involved two post-doctoral research scholars and thirteen graduate students.

Coordination and integration: The project coordination is conducted through project meetings, group meeting, and topical meetings. Three groups are organized along the Task areas, each has a coordinator. The project's principal investigator provides overall coordination that facilitates integration.

Milestones and deliverables:

The project is implemented through a series of milestones. The list of milestones (M2 and M3 reports) and delivery schedule were submitted and accepted by the NEUP program (Table 1.2).

Table 1.2. Major and minor milestones (left column includes milestone ID number, level, and schedule).

| | |
|---|---|
| N151 12/2019 | (M2) Final Report for (Project 16-10918) Development and Application of a Data-Driven Methodology for Validation of Risk-Informed Safety Margin Characterization Models |
| N152 12/2017 | (M2) Year 1 Status Report for (Project 16-10918) Development and Application of a Data-Driven Methodology for Validation of RISMC Models |
| N153 6/2018 | (M2) Formulation of a data-driven methodology for validation of RISMC models |
| N154 3/2019 | (M2) Methods and tools to support the data-driven methodology for validation of RISMC models |

| | |
|---|---|
| N155 6/2019 | (M2) Application of the data-driven methodology to validation of a system thermal-hydraulics-based simulation model |
| N156 9/2019 | (M2) Application of the data-driven methodology to validation of a computational fluid dynamics-based simulation model |
| N157 9/2017 | (M3) Assessment of predictive capability maturity |
| N158 12/2017 | (M3) Risk-informed approach to validation |
| N159 3/2018 | (M3) Reduced order model development and application |
| N1510 6/2018 | (M3) Approaches to implementation and evaluation of coupling of codes |
| N1511 12/2018 | (M3) System thermal-hydraulic model validation experiment |
| N1512 12/2018 | (M3) Computational fluid dynamics code validation experiment |
| N1513 3/2019 | (M3) Using high-fidelity CFD simulation to support calibration and validation of system thermal-hydraulics model |
| N1514 6/2019 | (M3) Using high-fidelity CFD simulation to support calibration and validation of coarse-grain CFD model |

Table 1.3. The project's milestones relationships. Each M2-level (major) milestone is supported by two M3-level (minor) milestones.

| | | | | | | | | |
|---|---|---|---|---|---|---|---|---|
| | N151: Final Report | | | | | | | |
| | ***Methodology Development*** | | | | ***Applications*** | | | |
| | | | | | STH/CTF | | Flooding/SPH | |
| M2 | N153 RFW | | N154 M&T | | N155 STH | | N156 CFD | |
| M3 | N157 PCMQ | N158 PRAV | N159 ROMT | N1510 CCVV | N1511 STHE | N1513 H2LS | N1512 CFDE | N1514 H2LC |
| | N152 Y1R | | | | | | | |

## 1.3. Project Technical Implementation

The project technical implementation is task-based, milestone-oriented, following the approach outlined in the original proposal. Project tasks and information flow are illustrated in Figure 1.2 and Figure 1.3. Relationship between the project tasks and milestones are presented in Table 1.4.

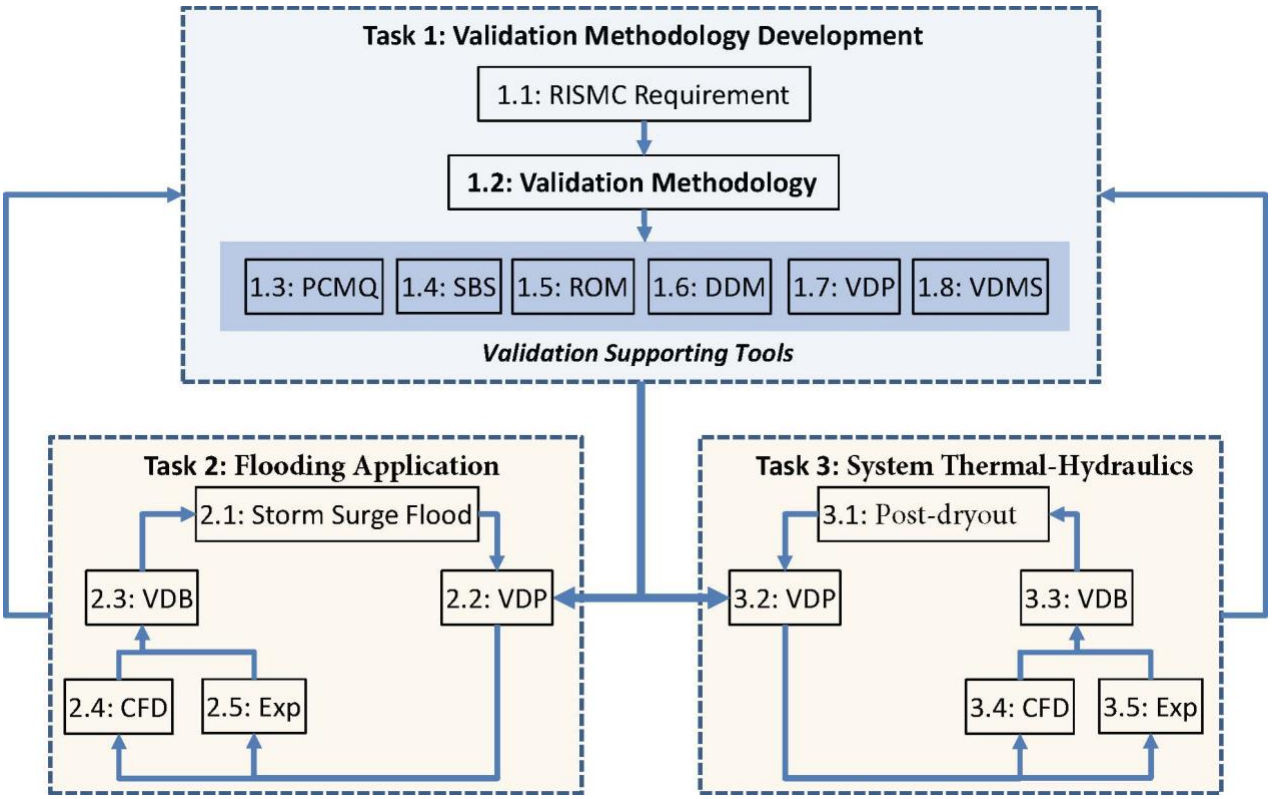


Figure 1.2. Project tasks and information flow.

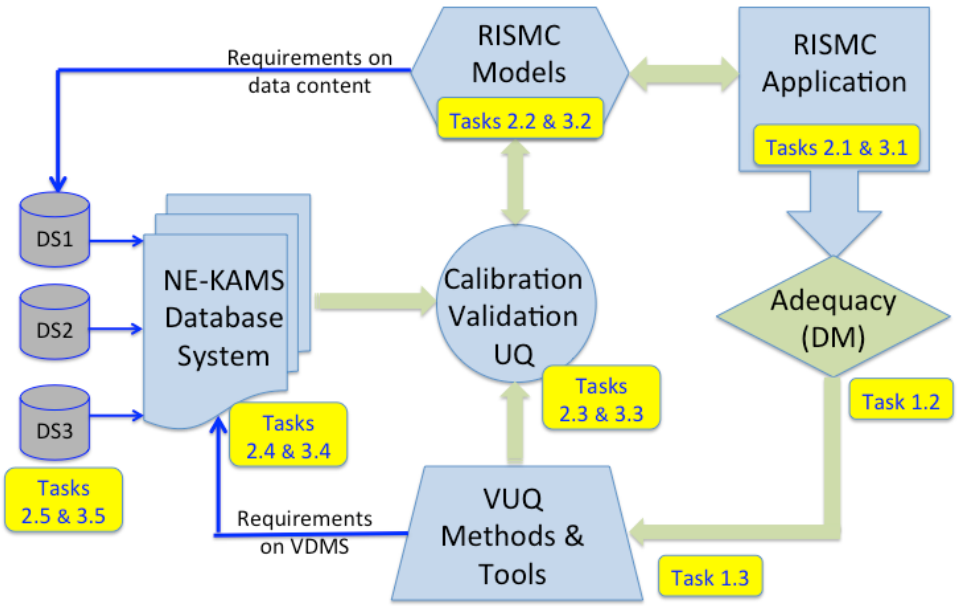


Figure 1.3. Information flow in application tracts.

Table 1.4. Relationship between the project tasks and milestones.

| Miles-tone N$^{O}$ | Task | | | | | | | | | | | | | | | | | |
|---|---|---|---|---|---|---|---|---|---|---|---|---|---|---|---|---|---|---|
| | 1.1 | 1.2 | 1.3 | 1.4 | 1.5 | 1.6 | 1.7 | 1.8 | 2.1 | 2.2 | 2.3 | 2.4 | 2.5 | 3.1 | 3.2 | 3.3 | 3.4 | 3.5 |
| 157 | | | x | | | | | | | | | | | | | | | |
| 158 | | x | | | | | | | | | | | | | | | | |
| 153 | x | x | # | * | * | * | x | x | * | * | | * | | * | * | | * | |
| 159 | | | | | x | | | | | | | | | | | | | |
| 1510 | | | | | | x | | | | | | | | * | | | | |
| 154 | | * | # | x | # | * | * | | | | | | | | | | | |
| 1511 | | | | | | | | | | | | | | | * | | | x |
| 1513 | | | | | | | | | | | | | | | * | | x | |
| 155 | | # | | | | | | * | | | | | | x | x | x | # | # |
| 1512 | | | | | | | | | | | * | | x | | | | | |
| 1514 | | | | | | | | | | | * | x | | | | | | |
| 156 | | # | | | | | | * | x | x | x | # | # | | | | | |
| 152 | | % | | % | | % | | % | % | | % | % | % | % | | % | % | % |
| 151 | Final Report (integration) | | | | | | | | | | | | | | | | | |

x – direct support; # – synthesized; * – input; % - progress report.

**Task Area 1 – Validation Methodology Development for RISMC Models:** Development of methodology, including framework and enabling methods for validation of RISMC models.

Task 1.1: Define RISMC requirements for model applications, RISMC models (codes), and their validation.
Task 1.2: Develop validation methodology of RISMC models.
Task 1.3: Predictive capability maturity quantification (PCMQ): evidence-based framework for quantifying maturity of predictive capability.
Task 1.4: Simulation-based scaling (SBS): an information-theoretic based method to quantify similarity and applicability of experiment to reactor prototypic process
Task 1.5: Reduced order modeling (ROM): to achieve computational efficiency much needed in RISMC applications.
Task 1.6: Data-driven multi-scale modeling (DDM): to make use of data for model improvement.
Task 1.7: Validation data plan (VDP): to identify data needs and planning experimental activities to meet data requirements.
Task 1.8. Validation data management system (VDMS) using NE-KAMS to support validation activities.

**Task Area 2 – Flooding Hazard Simulation Code Application:** Apply the methodology to flooding simulation model for a storm surge scenario.

Task 2.1: Perform RISMC analysis of storm surge flood scenarios to guide VDP
Task 2.2: Define data plan for SPH-NEUTRINO model validation (VDP).
Task 2.3: Develop flooding hazard analysis database (VDB).
Task 2.4: Generate numerical simulation data used for validation of NEUTRINO model (CFD).
Task 2.5: Design experiments used for validation of NEUTRINO model (Exp).

**Task Area 3 – System Thermal-hydraulics Application:** Apply the methodology to system-level core thermal-hydraulics model and CTF.

Task 3.1: Perform RISMC analysis to guide VDP for CTF in post-dryout regime
Task 3.2: Define CTF Validation data plan (VDP)
Task 3.3: Develop CTF validation data base (VDB)
Task 3.4: Generate numerical simulation data used for validation of CTF model (CFD)
Task 3.5: Design experiments used for validation of CTF model (Exp)

Note #1: Tasks 2.1 and 3.1 are focused on analysis that serves to guide development of the respective VDP (Validation Data Plan). As such, the analysis is intended to be limited in scope (as opposed to a full-scope RISMC treatment). Considering the available resources and timeline of the required input, the problem statement for Tasks 2.1 and 3.1 will allow for scenario assumptions and system simplification appropriate for methodology demonstration.

Note #2: The IRP focus is on methodology development for validation of advanced CFD-type code (SPH) and system thermal-hydraulics (STH). Initially, the choice for STH was RELAP-7, a next generation system thermal-hydraulics code under development in the LWR Sustainability program. As the project started, the team learned about the delay of RELAP-7 code release. At the kick-off meeting, the team evaluated options, and decided to focus the validation demonstration on core thermal hydraulics using CTF as surrogate for RELAP-7. The focus on the core thermal hydraulics is motivated by its high priority in safety analysis. CTF (aka COBRA-TF) is a sub-channel analysis code for core thermal-hydraulics based on multi-field two-fluid model, similar to the one in STH, but allowing for higher (sub-channel) resolution. We expect CTF-like capability be in advanced STH. In fact, CTF is currently used as the T-H component in CASL-VERA. The choice for CTF is also critical because the IRP team has access to the source codes and validation experiments for CTF, both are essential for the implementation and demonstration of the developed IRP methodology. The decision was communicated to the IRP TPOC and RISMC Technical Lead. The team put in place the backup option (with CTF) to cope with the delay of RELAP-7 release.

### 1.4. Project Technical Findings

The project technical findings are discussed on task basis and given in detail in the corresponding sections of this report. The main findings and issues are highlighted as follows:

(1) Risk-informed validation approach (RFW/PRAV): The project study proposed a formal validation approach that provides a basis to quantify credibility of risk assessments that are based on advanced simulation codes. The efficiency of the risk informed validation approach lies in the identification of critical structures, systems, and components (SSCs) that contribute to the system-level risk using Bayesian statistics. The validation methodology employs a data-driven approach to quantify the quality of data that is used to evaluate experimental fragilities for flooding failures. As the fragility assessment of a flooding scenario suffers from large epistemic uncertainties, the credibility of system-level validation is expressed using probabilistic distribution and maturity levels. To ensure that the system-level validation is complete and consistent, an additional validation index called consistency index is introduced. The risk informed validation approach is integrated with USNRC's Evaluation Model Development and Assessment Process (EMDAP) framework for a complete and wider applicability of the framework.

In the project's milestone report *M3NU-16-NC-NCSU-030401-158*, Bodda and Gupta (2018) explored a novel approach to quantitatively assess the validation of a system-level simulation based on the available information from component level validation. The proposed approach uses performance-based probabilistic risk assessment (PRA) as the basis for validation as well as for allocating resources towards improving the validation either by collecting additional data or by enhancing the accuracy of simulation tools. The approach builds upon characterizing the validation in terms of an overlapping coefficient which is described as the joint area under the experimentally obtained and simulation based probability density functions of basic parameters or events. The approach utilizes the power of Bayesian statistics by mapping fault trees

and event trees into a Bayesian network which allows consideration of non-Boolean relationships between events as well as allows consideration of correlated events in the network. Starting with the experimental and simulation based probability density functions of basic parameters or basic events, a Bayesian network is used to propagate the risk for the system. The experimental data is graded by RSU: Relevance ($\in_R$), Scaling ($\in_S$) and Uncertainty ($\in_U$). The experimental data is identified based on integral effect tests (IET) and relevant separate effect tests (SET). If experimental data is not available for any event, then the experimental fragility curve can be taken as the best estimate simulation fragility curve. The fragilities and the risk associated with each intermediate event and the top event is calculated separately for both the experimental and simulated data. This set of curves are then used for evaluating the overlapping coefficient of each event. The PRA based approach helps in identification of critical path thereby reducing the computational effort by focusing on only those events that lie on the critical path. Reliance on the events of critical path can also be used to determine the allocation of resources among different events for improving the validation at component or intermediate levels. When a validation between the experimental and simulation data is available for the basic parameters and not for the basic events directly in the network, a hidden layer is added below the basic events to relate the fundamental parameters to the basic events. The relationship between the hidden layer nodes and the basic event nodes can be defined by either a mechanistic model or a simulation-based generation of response surface. Availability of new validation data, either through new experimental information or enhanced simulation tools, can be incorporated in a relatively straightforward manner by employing Bayesian updating to calculate posterior fragilities and the corresponding overlapping coefficients.

For details, see Chapter 2 and cited therein references.

(2) Data-Driven Validation Methodology for RISMC M&S (RFW): Risk-Informed Safety Margin Characterization (RISMC) is a modern methodology for Nuclear Power Plant safety analysis that combines a dynamic probabilistic risk assessment (PRA) and "best estimate plus uncertainty" realization of the RISMC mechanistic models. Controlled by probabilistic tools with initial and boundary conditions, multiple simulations are performed with mechanistic tools to identify the safety margin and vulnerability of the reactor. Since the result of RISMC is used to inform and support the decision regarding design, operation, and safety of nuclear power plant, a mathematically defendable and robust approach is needed for the validation of the simulation tools, such that a confident and effective decision can be made regarding the high-consequence nuclear safety. Due to the lack of prototypical data and deficiencies of the simulation model, a framework is needed to guide the validation of RISMC Modeling & Simulation (M&S) tools in three major aspects: generating & gathering direct all related evidence, integrating evidence into a claim regarding the model credibility/uncertainty, and making confident and robust decision for the model credibility/uncertainty. Also, since RISMC requires a large number of simulations for every external event, it's sometimes inefficient to pursue high-order-accuracy M&S tools, where the facilities' margins are enormous compared to code uncertainty. As a result, the sufficiency of simulation accuracy depends on the characteristics of the scenario and validation that adapts such a concept is known as the risk-informed validation. The objective is to advise the safety management group on how to make a best and effective assessment for the model uncertainty, given the research goal and the scenario information. Although many validation frameworks have been developed, none of them explicitly adapts the risk-informed concept. Moreover, many elements are performed as black boxes due to the inherent limitations and challenges. When the system becomes large and complex, the uncertainties induced by these limitations could grow up and accumulate. Without proper investigations, such issues can be easily overlooked and the user may experience a loss of confidence on the validation decision. As a result, a risk-informed validation framework is needed for assessing the credibility/uncertainty of RISMC M&S tools. At the same time, new methodologies/technologies are needed to resolve the major issues and challenges of traditional validation methodologies.

In the project of "Development and Application of a Data-Driven Methodology for Validation of Risk-Informed Safety Margin Characterization Models", a validation framework, named Risk-informed

Evaluation Model Development and Assessment Process (REMDAP), is proposed for the validation of RISMC M&S tools. REMDAP is designed based on the framework of Evaluation Model Development and Assessment Process (EMDAP) and the methodology of Code Scaling Applicability, and Uncertainty (CSAU). By incorporating data-driven and risk-inform concept, REMDAP aims to present a significant shift from the current approach for expert-determined validation to the data-driven approach. In this study, a concept of sufficient accuracy is developed and adapted in the REMDAP framework to account for the unfrozen model forms, parameters and computational resources in the RISMC analysis. A tentative workflow is prepared based on the currently developing methodologies/technologies. Next, the progress of developing key methodologies in the REMDAP framework, including the data-driven closure development, data-driven uncertainty quantification, and Predictive Capability Maturity Quantification & Bayesian Network (PCMQBN) are demonstrated. Presently, this study demonstrates some initial developments of classifying methodologies based on assumptions and conditions, the objective is to identify the feature and create an initial proof-of-concept for applying Data Driven Modeling (DDM) in the model development and validation process. The application of REMDAP to sophisticated RISMC tools, including Cobra-TF and NEUTRINO-SPH, is still under development.

First, a data-driven closure development methodology is under initial development and the available data-driven methods are classified into two types. The parametric model is built upon the fixed model form that relies on human knowledge, while the nonparametric model solely depends the data. Illustrative examples are prepared for both types of model development methods and observations are analyzed. Second, a data-driven uncertainty quantification (UQ) methodology is developed and the present methods are classified into two types: global data-driven UQ and local data-driven UQ. The global approach targets at system code like Cobra-TF by assuming that the model has been well-verified and closures are the major source of uncertainties. The local approach uses Physics-Informed Machine Learning (PIML) to construct a surrogate between the simulation error and the input physical features. It's designed for the coarse-grid CFD like NEUTRINO-SPH, where error of each computing element is characterized with PIML. Illustrative examples are prepared for both types of data-driven UQ methods and observations are analyzed.

Another major challenge of RISMC M&S tools validation is the decision-making process under uncertainty. Traditional validation relies heavily on expert judgments and the process is obscure and heuristic. In this study, a decision-theoretic methodology PCMQBN is under development. The objective is to construct a transparent, consistent and improvable validation process with mathematical languages and effectively make decisions on model credibility with adequate confidence based on a set of uncertain beliefs and a set of utilities. Guidance is constructed for the uncertainty grade of the R/S/U (Relevance/Scaling/Uncertainty) grading system. Illustrative examples are prepared to demonstrate the guidance and major findings. In addition, a framework of Bayesian sensitivity study is proposed for PCMQBN and the objective is to improve the robustness of the PCMQBN's result.

For details, see Chapter 3 and cited therein references.

(3) Predictive Capability Maturity Quantification (with Bayesian Network) (PCMQ-BN): In this project study, a framework of PCMQBN is developed to formalize and quantify the validation decision-making process with mathematical languages. The objective is to support the decision-making process for simulation adequacy in a transparent, consistent, and improvable manner. PCMQBN first formalizes the mathematical representation of simulation adequacy as a triplet of scenario, predictive capability level, and belief. Next, argumentation theory is employed to formalize the decision-making process in validation as an argument for simulation adequacy that is based on evidence from the validation frameworks and activities. In this process, all related evidence is characterized such that its representation is consistent with the definition of simulation adequacy. Next, all evidence is quantified where the predictive capability is represented by maturity levels and the belief is quantified by probabilities. Next, Bayes' theorem is used to integrate the quantified evidence, and the Bayesian network is used to represent this integration by directed

acyclic graphs. To ensure the consistency of network connections and causal dependence on well-known physics, rules, and knowledge, a synthetic model is also suggested for evaluating the conditional probability among all nodes in the network by calculating the Reactor Prototypicality Parameter. A sensitivity analysis is performed to evaluate the impact of conditional probability and decision parameters. It is found that the conditional dependency between simulation adequacy and validation result has higher impacts on those between [R]elevancy/[S]caling/[U]ncertainty grade and data applicability. It is also found that relative weights of evidence from different databases have large impacts on the final data adequacy. Therefore, during a validation decision-making process, the correlations and dependencies among different databases and attributes need to be evaluated more carefully than accuracy assessments and scaling analysis for separate models and databases. Based on the sources and levels of uncertainty, three phases of development are defined for documenting and grading the quality of the assessment process and simulation adequacy results.

To demonstrate the capability of PCMQBN, a case study is performed to assess the adequacy of SPH methods in simulating the scenario of "floods damage the building structures, enter the room, and cause diesel generator (DG) malfunctioning". The validation framework CSAU and its regulatory guide EMDAP is used for collecting evidence and qualitative adequacy assessment. Since opposite conclusions are obtained from two numerical benchmarks, the PCMQBN framework is used to further refine the adequacy assessment with quantitative results. For separate benchmarks, it is found that the belief level on the adequacy claim for the SPH method is consistent with the qualitative results from CSAU/EMDAP. Meanwhile, it is found that the belief level for an adequate SPH simulation is 83% when evidence from both benchmarks are used. Comparing to the qualitative result, there is higher confidence that the SPH simulation is adequate for the designated purposes based on available evidence. Also, the uncertainty of simulation adequacy is less than that from the qualitative assessment since the contradictory results suggest a non-informative adequacy distribution. To further demonstrate how PCMQBN results can be used in risk-informed validation, a risk-informed safety analysis is performed to evaluate potential damages to SSCs of NPPs by water waves. SPH simulations are performed to determine the structural loads by a wave for 60 cycles. Based on a synthetic ensemble model, distributions of SPH predictions and corresponding consequences are made based on the simulation adequacy results. It turns out that the expected loss determined based on the PCMQBN results is 30% less than that loss from the qualitative assessment. As a result, the formalized PCMQBN framework is able to reduce the uncertainty in simulation adequacy assessment and the expected losses in the risk-informed analysis due to that uncertainty.

For details, see Chapter 4 and the project's milestone report *M3NU-16-NC-NCSU-030401-157*.

(4) Reduced Order Modeling (ROM) & Physics Coverage Mapping (PCM) (M&T): This project segment has focused on further development of reduced order modeling techniques and physics-guided coverage mapping methodology to support the validation of computerized physics models employed in support of engineering calculations. Two challenges are targeted by these developments. First, how to take advantage of high-fidelity software tools in a manner that is computationally feasible. High fidelity tools are sought because they are believed to enable better predictions of complex physics phenomena. Engineering analyses however require numerous executions of such tools to achieve engineering objectives such as design optimization, propagation of uncertainties, integration of measurements from separate effects of integral effects experiments, etc. The cost of running this analysis is prohibitively large, forcing analysts to revert back to lower-fidelity models. To address this challenge, reduced order modeling techniques with error preserving bounds are sought in this project. The project has started with recent advances in reduced order modeling techniques that rely on the use of randomization to seek optimum reduction conditions for a given model. The project has further developed a number of algorithms to enable reduction across multiple physics models and has integrated the use of neural networks with previously developed randomized reduction algorithms. The outcome is an advanced set of reduction algorithms suitable for reducing complexity of multi-physics models for both transient and steady state calculations,

with mathematically rigorous upper-bounds on the maximum errors resulting from the reduction. For the second challenge tackled by this project segment, the goal is to answer a recurring question in validation exercises, that is, why and how could analyst rely on experimental data, often collected in idealized conditions, to validate modeling results for other conditions, for which no experimental data exist, representing the envisaged domain of model application. To address this challenge, investments in a new methodology, called physics-guided coverage mapping has been made. The idea is to rely on high fidelity modeling tools to identify in a non-parametric fashion the relationship between experimental and application conditions. The non-parametric description implies that no assumptions are made about the functional form relating application responses to experimental responses. Instead, information theory principles are employed directly to find the best joint PDF relating the experimental responses and the application responses. Going beyond this initial rendition of physics-guided coverage mapping methodology, the project has invested into further developing this methodology to account for modeling errors and constraints that might be present, which if not respected, would lead to incorrect mapping results. Examples include constraints on the input model parameters that must be respected when the parameters are perturbed. Also, in many situations, model parameters are pre-calculated by other computer codes, and the model is validated along with these parameters. In principle, any perturbations to these parameters would result in additional modeling errors that are yet to be validated. Hence, algorithms have been developed to ensure no additional errors are introduced due to parameters perturbations. This is achieved via a constrained sensitivity analysis exercise to ensure zero sensitivities of the modeling errors to parameter perturbations.

In the study Zhou and Abdel-Khalik (2017) further develop a data-driven methodology called physics-guided coverage mapping (PCM) to support model validation with the primary objective of formulating mathematically defendable procedures for mapping biases from the experimental domain to the application domain where measurements are scarce. PCM-based bias mapping is demonstrated using an application of BWR full-size fine-mesh bundle test (BFBT) experiments axial void distributions. The transfer of biases is done directly using kernel density estimation techniques and a joint probability distribution constructed by a pseudo response obtained non-parametrically using alternating conditional expectation (ACE) algorithm, which maximizes the mutual information between the pseudo response and the application response. Central to these developments is the ability to measure the importance of individual experiments which can be done quantitatively using the proposed algorithm. Thus, this work has further developed the PCM methodology as a calibration-free methodology to estimate application responses using the available body of experimental data. PCM requires for its optimal performance high fidelity physics models for both the application and experimental conditions. It also requires performing multiple uncertainty analyses which are later harvested for correlations that directly relate the application to the experimental response. By doing so, one needs not to identify the individual sources of uncertainties which precludes the need to solve an ill-posed problem. The study was performed using TRACE code. Current effort is to apply the method to CTF and post-dryout experiments.

For details, see Chapter 5 ad peer-reviewed references listed therein.

(5) Multiscale Simulation by Code Coupling for Flooding Scenarios (CCVV): Events such as the flooding around the Fort Calhoun (2011), Vermont Yankee (2013), and St. Lucie (2014) nuclear power plants have highlighted the need for accurate simulations to determine the risk of flooding at these and other facilities around the country. However, plant response to flooding due to hurricane storm surge involves multiple spatiotemporal scales. While ocean circulation models can simulate large-scale storm surge events, assessment of the resilience of critical infrastructure to storm-induced flooding require much smaller scales that are more appropriate for fluid solvers, which can resolve finer scale processes. Therefore, bridging the gap between these simulation approaches is essential, and calls for the conception, development, and evaluation of a multi-scale methodology that can accommodate the substantial differences in scales.

We describe a modeling framework that incorporates the larger scale finite element (FE) model, ADCIRC, along with the smaller scale smoothed particle hydrodynamics (SPH) code, Neutrino, to provide finer level resolution for complex geometries. ADCIRC is an ocean circulation model that solves the shallow water equations over a mesh of nodes and triangular elements. The use of unstructured grids with varying element sizes means that a mesh can be gradually refined in areas that require greater levels of topographic detail. While these refinements can reach the meter scale, shallow water equations are not suitable for simulating the hydrodynamic processes that occur beneath that scale and that must account for the complex geometries of, for example, a nuclear power plant. Such simulations require smaller-scale models like the mesh-free fluid solver, Neutrino.

Our approach draws on a methodology called *subdomain modeling*, which allows local changes in a finite element model to be accommodated with less computational effort than would be required by re-running the entire simulation. Provided a subdomain is large enough to contain the altered hydrodynamics, changes can be made—such as refinements in spatial resolution and the addition of flood protection measures—and simulations performed on a subdomain without the need to calculate new boundary values. Objectives of the project include enhanced spatial resolution of subdomain meshes to get finite element simulations closer to facility-scale features and topography; data libraries and reuse to curtail the need for large, ocean-scale simulations, allowing modelers to instead start from the subdomain scale; ADCIRC-Neutrino coupling to facilitate subdomain-to-facility scale interactions; and verification and validation to ensure the correctness of computer implementations.

Results are based on datasets obtained from and through collaboration with the United States Army Corps of Engineers (USACE), and include (1) refinement and evaluation of subdomain modeling for its computational benefit and solution quality in actual, real-world applications that consider a range of USACE engineering design scenarios, (2) development of a post-processing approach that facilitates the use of spatially and temporally coarse datasets from USACE as boundary conditions for subdomain modeling, allowing us to adopt a library of states (LOS) perspective so that simulation results from a variety of historical and synthetic storms are available for reuse—this allows us to recover boundary conditions of a quality comparable to datasets with a much finer temporal resolution, (3) a prototype coupling approach using subdomain modeling to combine the larger scale finite element model, ADCIRC, with the smaller scale smoothed particle hydrodynamics code, Neutrino, to provide finer level resolution for complex geometries.

For details, see Chapter 6 and the project's milestone report *M3NU-16-NC-NCSU-030401-1510*.

(6) Validation acceptance criteria (RFW): In an early report, Youngblood (2017) provided an analysis of approaches of acceptance criteria for validation process, from "traditionalist" and 'revisionist" perspectives. Further, he highlighted scaling-induced uncertainty. If we lack data at full scale, and are not completely certain of the applicability of data obtained at reduced scale, then we have a residual epistemic uncertainty about our model, and we do not know how to deal with it except by making essential use of expert analysis and expert judgment. It may prove to be possible to address this issue at least partially in the likelihood model that we use in Bayesian analysis, but a convincing explication of this remains to be developed. Given relevant data obtained at multiple scales, there might be a way to "learn" (machine-learn) how to correct for scale differences. This would not qualify as classical "validation," but it may turn out to be useful: it would help in formulating a project-specific approach to scaling.

For details, see Appendix A in the project's milestone report *M2NU-16-NC-NCSU-030401-152*.

(7) Industry perspectives on risk-informed methodology: In an early study by the project's industry partner, Sewell (2018) analyzed external events PRA in the nuclear industry, bringing out four principal insights. Firstly, model validation approaches should address the entire uncertainty distribution, and thus

be keyed to development of (at least) the best estimate (eliminating model bias) and the aleatory variation (i.e., model error, or σ). The scope of models considered should also enable evaluation of the epistemic variation (i.e., differences existing among models that reflect data uncertainties and the competing hypotheses/theories of an informed technical community (ITC), plus code-to-code variations in results of models solving similar hypothesis/theory). Secondly, model validation should consider the broad scope of customer requirements. For PRA in the nuclear industry, customer requirements may pertain to safety analysis and regulatory requirements, as well as a licensee's own financial analyses toward effective operational management of their nuclear facility. Thirdly, owing to its past and existing role, and its demonstrated efficacy, the SSHAC approach logically serves as a de facto template for requirements and procedures for validating models and their use in the nuclear industry, particularly for PHA and PRA. Finally, as PHA and PRA are naturally compatible with decision science, validation approaches can be resolved, or tailored, to the needs of the specific decision.

(8) SPH/CFD model validation experiment (CFDE): The primary purpose of this task is to demonstrate an application of the data-driven validation methodology on a flooding simulation model. A large-scale oscillating tank experiment was designed, constructed, instrumented and conducted and then used to validate the SPH code Neutrino, as well as determine parameters that affect the simulation results. The 90% and 50% end-wall pressure bounds were compared, as was the pressure impulse. The simulation bounds fell mostly within the experimental bounds, with exceptions at the beginning of the cycle (~40% difference), at peak pressure (~75% difference), and at the end of the cycle (~40% difference). The simulation pressure impulse matched the experiments well and was within 10%. Additionally, seven parameters were identified and investigated to determine their significance. All seven parameters were identified as significant. However, the particle size, interaction-radius to particle-size ratio, and fluid settling seem to have a greater effect due to larger fluctuation in their results.

The next step is to quantify the significance of each parameter. Once this is done, those parameters that have the greatest effect on the simulation results can be optimized. The optimization goal would be to increase the accuracy of the simulation results while still accounting for the computational runtime of the simulation. This optimization will also depend on the scenario and a valid parameter range vs. result criteria needs to be established.

Further, insights gained from the experimental validation exercise led to suggestions on refinements of the initial framework. For details, see Chapter 7 in this report.

(9) Adequacy of SPH model for flooding analysis: In this study, a scoping-stage assessment is performed for SPH's adequacy in simulating the real-scale external flooding scenarios, especially in predicting the surface-wave impacts on SSCs at NPP sites. To ensure the completeness and consistency, validation frameworks, Code Scalability Applicability and Uncertainty (CSAU), and its regulatory guide, Evaluation Model Development and Assessment Process (EMDAP) are followed to guide validation activities and to make final code adequacy assessment. First, an external-flooding scenario is designed, and SPH simulations are performed with an SPH-based software named Neutrino. A Phenomenon Identification and Ranking Table (PIRT) is created, and the surface-wave impacts are identified as one of the high-rank phenomena. At the same time, a performance measurement standard is created for measuring the code adequacy in informing safety decisions consistently and transparently. At the scoping stage, these criteria are selected based on authors' knowledge and reviewed by researchers in related fields. Next, numerical benchmarks are designed for assessing the code adequacy of SPH methods and corresponding software implementations on Neutrino. Next, code accuracy is evaluated by comparing simulation results from Neutrino against experimental measurements in each benchmark. Meanwhile, a scaling analysis is performed to determine a group of dimensionless number for characterizing important physics and to assess the applicability of validation database collected in reduced-scale facility to the prototypic scenario. Finally, results from all activities are brought together to make an adequacy decision. It is found that, based on the current evidence, SPH methods and associated Neutrino software can predict the unbroken surface-wave

peak pressure onto stationary rigid with reasonable accuracy if the suggested sizes of particles are used. However, the available evidence is not sufficient to support the decisions of SPH's adequacy in predicting impact force on dynamic rigid structures.

The validation exercises of the SPH simulation highlighted several aspects of data for the data-driven methodology: general uncertainty values; data for scaling; and bands of applicable validation data. Through varying the SPH parameters it was shown that the particle size, interaction-radius to particle-size ratio, and fluid settling are important factors can have a large influence on the uncertainty of the results. The process used for this research can be used in developing validation cases against experiments for the flooding scenario areas of pressure, duration, max height/splash, and turbulence. The resulting uncertainty can then be used in correlation with scenario applicability in the PCMQBN data driven methodology for an overall model confidence rating.

For details, see Chapter 8 and Chapter 9 in this report.

(11) Industry perspectives on data-driven methodology: In an early phase of the project, a study by the project's industry partner (Zachry) concluded that if successful, the project could advance the safety analysis methods and offer better information to support the decision making process. Many of the proposed ideas seem promising, but additional progress and integration of the methods is necessary to determine the feasibility for industry application and regulatory acceptance. Over the course of the project, efforts were made to formalize and communicate developments (of methods and tools), including through peer-reviewed publications. A follow-up study by Zachry focused on "requirements for data-driven validation framework", outlining challenges (e.g., methodology inertia, overfitting, cost of changes). The study concluded that the integration of a data-driven methodology into RISMC models for nuclear safety analysis is a clear step forward for the industry. For the near future, we see the most promise in Physics-Separated and Physics Evaluated Machine Learning domains (for details, refer to Chang & Dinh, 2018, IJTS). We believe that the input space for these types of problems is too vast for the data-only type of approach that has gained traction in other applications. The strategy most likely to succeed will leverage the advantages of a physics-based approach with those of a data-driven approach.

(12) STH model validation experiment (STHE): The primary purpose of this study is to demonstrate an application of the data-driven validation methodology for a STH model. The task is to establish experimental facilities, conduct experiments, and provide data support for the data-driven validation methodology development. Compared to the traditional validation practices, data-driven validation relies on data from experiments (and advanced computational analyses) that are specifically designed for the model and use state-of-the-art methods to rigorously map and bound the simulation uncertainties in the domain of intended model use. Therefore, data-driven validation presents a significant shift from the current validation practices based on expert-determined scale distortions. CTF, a subchannel analysis code, was chosen as the subject of STH code validation. In addition, based on the literature and feedback from the STH code validation subgroup, dispersed flow film boiling (DFFB) regime, where droplets are dispersed in a continuous superheated vapor phase, was chosen as the phenomenon focus of the study.

Three phases for the experimental investigation were proposed. In the first phase (Phase I), an air-water experiment was to be carried out at room temperature to test necessary optical instrument for droplet measurements and to develop proper experimental procedures, which serve as guidelines for elevated-temperature and pressure experiments. The second and third phase (Phase II/III) experimental work would involve modification of the Phase I experimental facility and proper configuration of components, which is not included in this report. Data processing was completed using LaVision ParticleMaster package and in-house computer codes to obtain polydispersed droplets diameter and velocity statistics. Additionally, the particle diameter distribution was modeled using a lognormal distribution. The distribution uncertainty was used to represent the data uncertainty quantification. Also, the estimated parameters' confidence interval in

the distribution model fitting process was provided based on bootstrap resampling and central limit theorem. Finally, SMD calculation results based on two approaches, namely data-based and distribution-based, were provided. The processed data and quantified uncertainty from Phase I experiments would be valuable to the validation process in the data-driven model development.

The choice of CTF and post-dryout heat transfer in dispersed droplet film-boiling flow as the target for validation imposes demanding operating conditions for a UM test facility, while limiting the facility's flow diagnostic capability. Efforts are required to complete the facility construction and bring it to a reliable operation, to generate data for the STH/CTF validation task. While the test facility was constructed to generate data for the project, time (and resources) allocated within the IRP enabled completion of Phase I of the experimental plan, as summarized in Chapter 10 of this report. For details, see the project milestone report *M3NU-16-NC-NCSU-030401-155*.

(13) STH/MCFD Modeling and UQ using High-Resolution Experiments (STH): The project study introduced a modular Bayesian approach to quantify and reduce the uncertainties of Multiphase Computational Fluid Dynamics simulations. The proposed approach is supported by three machine learning methods: principal component analysis for dimensionality reduction, feedforward neural network for surrogate modeling, and Gaussian processes for model form uncertainty evaluation. The epistemic uncertainty is quantified through the modular Bayesian approach, then combined with the aleatoric uncertainty of the stochastic flow fluctuation for a comprehensive uncertainty evaluation of the MCFD predictions. Based on the obtained uncertainty, probability-boxes can be constructed for comprehensive risk analysis.

With the support of high-resolution experimental measurements acquired in a test section with a cross section of 10 mm × 30 mm, a comprehensive case study has been performed to evaluate the uncertainty of three quantities of interest: void fraction, liquid velocity, and gas velocity. The proposed approach is implemented based on the open-source deep learning library PyTorch and can be run on GPU for efficient and fast evaluation. The case study demonstrates that the proposed approach can effectively quantify and reduce the uncertainty of the MCFD predictions. With the consideration of the model parameter uncertainty only, the prediction uncertainty can be significantly reduced, and any unphysical predictions can be eliminated. The results can be further improved with the combination of the model parameter uncertainty and model form uncertainty. The proposed approach provides a general framework that utilizes different experimental measurements for a comprehensive UQ of high-resolution, low-fidelity numerical models, an example close to this work is the boiling and heat transfer problem.

Be that as it may, it should also be noted that discrepancies between the MCFD predictions and experimental measurements still exist after the UQ is performed. The main reason is the model form uncertainty trained with Gaussian process neglects the influence of the inlet conditions. To further improve the work, additional experiments need to be performed for a broader range of the inlet conditions. Based on larger measurement databases, a model form uncertainty that takes both the location and inlet conditions as input can be trained to better reflect the physics underlying the bubbly flows. Furthermore, the effect of data size on the UQ results could also be evaluated with the additional available data.

(14) High-fidelity Simulation Data Generation (H2LS/STH): To support data-driven modeling and validation of coarse-grid models, methods of Direct Numerical Simulation (DNS) for both single-phase and two-phase flow are employed to generate high-fidelity data. Large scale simulations running on massively parallel supercomputers, which constitute the major objective of this task, pose several problems for their successful execution and subsequent, or in-situ, post-processing and data analysis. Major challenges with the simulations performed herein with PHASTA were, understandably, of a logistical nature, which required efficient data management code, either integrated as subroutines within PHASTA using advanced MPI libraries or developed as separate programs capable of handling large volumes of data.

The technical objectives of the large-scale simulations include

- Implementing code functionalities in PHASTA to make DFFB simulations feasible. This includes suite of tools to assign fully turbulent inflow boundary conditions, droplet injection at the upstream spacer-grid location and scalable MPI I/O routines for high data throughput.
- Single-phase and two-phase simulations on large scale supercomputers for a range of operating DFFB conditions, including different flow Reynolds numbers and droplet collision Weber numbers.
- Data collection, post-processing and analysis from single and two-phase simulations.
    - Study of turbulent flow features including mean flow properties, Reynolds stresses and turbulent anisotropy to gain insight into the effect of spacer-grids and mixing vanes.
    - Analysis of the axial evolution of droplet volume, interfacial area and Sauter mean diameter, for different Weber numbers, and comparison with existing correlation in the STH code COBRA-TF [20] and empirical correlation from prior DFFB experiments, conducted at the rod bundle heat transfer facility
- Data archival to support future developments on data-driven, machine learning based turbulence and STH modeling.

The key conclusions from this project contribution are:

- The research herein highlights the capability of PHASTA, coupled with level-set method, to simulate the post-LOCA DFFB regime. Simulations with unprecedented resolution and fidelity were performed to illuminate droplet dynamics in this critical PWR regime.
- Advanced high-resolution data collection tools are implemented in PHASTA which enable detailed study of turbulence from DNS scale simulations, optimized for large scale supercomputers.
- The high spatial and temporal resolution of data collected from the single-phase and two-simulations is archived and would, potentially, serve as a data mine for the development of machine learning based turbulence and STH models.
- The results from single-phase simulations highlight the effect of spacer-grids and mixing vanes on convective enhancement. Further, invariant analysis of the data reveals that the mixing vanes modify the state of turbulence in the downstream region.
- The results from two-phase simulations emphasize the importance of considering droplet feedback to turbulence, in addition to the enhancement provided by spacer-grids and mixing vanes. The SMD results at the downstream locations match well with experimental data, establishing confidence in PHASTA and the incorporated level-set method in simulating the DFFB regime.
- All tools are in place for a more extensive parametric study of the DFFB regime, with a range of bulk Reynolds number and collision Weber numbers. Single droplet collision studies are recommended for characterizing uncertainties associated with collision events.
- The most limiting assumption of the current simulations, in contrast to the real DFFB conditions, is the lack of heat transfer modeling. Consideration of heat transfer mechanisms requires more extensive development efforts in PHASTA, including methods for phase change, conjugate heat transfer and modeling of radiative heat transfer.

For more details, see Chapter 11 of this report, and milestone report *M3NU-16-NC-NCSU-030401-1513.*

(15) CFD Modeling and Validation (SPH/CFD): The project study established that currently validation of SPH turbulence models has been conducted mostly for small-scale flows in simple geometries by comparison with mesh-based CFD results and small-scale experimental data. There is no study of the effects of particle resolution/size on the performance of the above-mentioned turbulence models. The study by Bui led to the following: (i) Either one-equation or two-equation equation turbulence model is recommended to be used in the SPH modeling of simple turbulent flows, such as open-channel flows or straight fluid spreading; (ii) More complex and computationally expensive algebraic Reynolds stress model

is suitable for more complex flow conditions and for fluid-structure interactions; (iii) Closure laws, such as wall functions and the mixing length, used in all previously mentioned turbulence models would need proper validation for different flow conditions and scales; (iv) Physics-constrained machine learning (ML) can be used to either to develop and validate closure model surrogates, or to construct a data-driven turbulence model to calculate turbulence viscosity directly. Both of these approaches require data from high-fidelity simulations and/or experiments.

(16) CFD Data-Driven Modeling: The project study introduced and implemented two data-driven approaches to model CFD error leveraging the potential of massive high-fidelity (HF) data. The first approach is type II approach, the advantage of it is code efficiency, machine learning (ML) process only needed to be done once based on a pre-calculated RANS results. The disadvantage of it is the error introduced because of the inaccuracy of the pre-calculated RANS result. The second approach is type I approach, which is use ML surrogate model to replace turbulence model in CFD iteration. Two case studies have been performed to demonstrate and evaluate these two approaches. According to the results of both case studies, the data-driven model largely improved RANS model. The improved RANS model allows more accurate and flexible prediction for turbulence flow, which is not only the aim of turbulence modeling but also fundamental for coarse mesh CFD in NPP. As nuclear safety problem becomes increasingly stringent and requires detailed analysis of thermal-hydraulics, computationally efficient CFD methods are needed to support the study of a broad range of accident scenarios. Current turbulence modeling requires different RANS models for different flow patterns, which largely hinder the use of CFD for complex scenarios with transient flow patterns.

(17) Data-Driven Modeling, Calibration, and Validation (H2LS/H2LC): The effort in this area aims to develop and assess a data-driven approach for turbulence modeling (DDTM) approach that could be leveraged in engineering analysis including simulation of thermal-hydraulic processes in nuclear power plants (NPP). Traditionally, the most common method in computational fluid dynamics (CFD) used in engineering practice is based on the solution of Reynolds-averaged Navier–Stokes (RANS) equations. The method has limitations in the calculation accuracy and complexity of choosing turbulence model and parameters for different flow configurations. High fidelity (HF) simulations, such as the Direct numerical simulation (DNS) and the Large eddy simulation (LES), could break the two limitations of RANS but their computational expenses are too large to be used in engineering practice. The DDTM approach aims to develop a RANS-based method which is as accurate as HF simulations and applicable to a broad range of flow patterns leveraging the power of machine learning. The potential advantages of DDTM are in three aspects: The first advantage is to let data automatically improves the model. Labor cost and human biases in devising the mathematical expressions are reduced; The second advantage is the potential to integrate the various types of turbulence models into one model, which could greatly simplify the CFD simulation process and system code coupling; The third advantage is the potential to largely reduce computational expense by applying the framework of DDTM into coarse mesh simulation, where the DDTM approach not only simulate the turbulence error but also the error caused by using coarse mesh.

The main contribution of this work is the proposal of a new DDTM approach. The new approach is named as “multi-model data-driven turbulence modeling (MDTM)”, compared to the “single-model data-driven turbulence modeling (SDTM)” approach proposed by other researchers. The term “model” here refers to the turbulence models in RANS. The SDTM approach is so far considered as the most suitable DDTM approach for our purpose. But it has two limitations that prevent it from being a practical approach: First, the single-model approach fails when the baseline model result is far from the true result; Second, the selection of baseline turbulence model form and parameters could make a difference in prediction accuracy. But one could not quantitatively determine which baseline model is the most suitable one for a certain flow configuration beforehand. Hence the MDTM approach is proposed to overcome these limitations by

increasing the degree of freedom to the machine learning surrogate model and let the machine learning surrogate model automatically select the most suitable baseline model to be used.

Numerical experiments have been performed to test the performance of DDTM. 5 case studies are performed to answer 5 critical questions about DDTM separately. The 1st question is whether the SDTM approach performs better than traditional turbulence model approach. 1D channel flow problem with DNS data is used to answer this question. The 2nd question is whether the MDTM approach performs better than the SDTM approach. This question is also answered by 1D channel flow problem with DNS data and 2D lid-driven cavity problem with LES data. The 3rd question is whether the MDTM approach could be applied to more complex flow configurations. The question is answered by 2D lid-driven cavity problem with LES data. The 4th question is whether the HF data could use LF data (such as RANS) instead. The question is answered by 2D lid-driven cavity problem with RANS data. The last question is whether the LF model could be coarse mesh RANS. The question is also answered by 2D lid-driven cavity problem.

For details, see the project's milestone report *M3NU-16-NC-NCSU-030401-1514*.

(18) Data-Driven Framework for error estimation and mesh-model optimization in STH (M&T): The project study, a data-driven framework (optimal mesh-model information system, or OMIS) was developed and demonstrated to improve applications of the coarse-mesh codes by predicting their simulation errors and suggesting the optimal mesh size and closure models. The OMIS framework was illustrated based on the mixed convection case study. By learning from massive data instead of human experience, the OMIS framework provides data-driven guidance to help a user improve the modeling and simulation. This modularized procedure is extendible to modeling and simulation using other coarse-mesh codes where mesh size is one of the key model parameters. Scalability of the OMIS framework in the GELI (Global Extrapolation via Local Interpolation) condition is achieved by exploring local physics instead of global physics with the usage of advanced deep learning techniques and statistical approaches. It is expected to improve the scale-distorted approaches that connect scaled data to the real full-scale applications and reduce the uncertainty of scaling. This work also contributes to the development of a data-driven framework for the validation and uncertainty quantification of CFD-like codes. The OMIS framework treats physical models, coarse mesh sizes, and numerical solvers as an integrated model, which can be considered as a surrogate for governing equations and closure correlations. The prediction of simulation error takes all the error sources into account and shows a promising accuracy in the case study. For details, see Bao et al (NED-2019); Bao et al (ANE-2020).

(19) Validation Data Management System (VDMS): In the project study Ren et al. established that in order to ensure successful further development in the project, an issue that must be addressed as soon as possible is the current lack of a clear understanding of the validation data structure for advanced thermal-hydraulics analysis in reactor safety applications. The project investigated capability of NE-KAMS: Nuclear Energy – Knowledge base for Advanced Modeling and Simulation. One of the major characteristics that made NE-KAMS stand out during a nationwide survey of existing database systems was its customizable management of data and data interrelationships based on the data structure of interest. The importance of customizable management of data and data interrelationships was illustrated, where each circle represents a model, which may comprise multiple sub-models; and each line indicates a relation between the two models. The sub-models and sub-interrelationships multiply inside each circle. Data from the models and sub-models reflect the complex structure. Apparently, to confidently interpret and correctly use the data, the data interrelationships must be accurately maintained and understood. The project recommends further development, and use of NE-KAMS. For more detail, see Chapter 12.

### 1.4.1. Summary

In summary, the research conducted in this project has made important steps to advance the technical state of knowledge in the area of model validation by addressing the fundamental limitation of existing validation exercises - that is how to provide scientific guarantees on the simulation predictability for the intended wide range of reactor conditions using limited set of experiments and simulation analysis datasets. The research findings to date supports an initial team vision that the proposed methodology will:

- enable the RISMC models to provide a prediction of plant safety characteristics with associated uncertainty, which are crucial in the RISMC decision making process.
- serve as an instrument to coordinate R&D program for validation of RISMC models, supporting the continued safe operation of existing nuclear plants.
- guide efforts to maintain and develop the supporting research infrastructures, such as experimental facilities and numerical tools.

The project research provides valuable input towards guiding the development of both the RISMC formulation and the RISMC toolkit. It is critical to realize that V&V should not be an afterthought. Instead, it is necessary to integrate the V&V efforts into the development of RISMC formulations and toolkit. Lack of appropriate and sufficient experimental data has been a historic concern and yet the perceived need for such data continues to grow because every piece of data is considered equally relevant. The project team believes that the information-guided decision-theoretic based approach proposed in this project can assist by ranking the relevance of data for a particular RISMC scenario and thereby guiding efficient management of resources for future experimental studies and in some cases eliminating the need completely.

## 1.5. Technical Products and Dissemination

### 1.5.1. Journal Publications


[AP.1] Linyu Lin and Nam Dinh, "Predictive Capability and Maturity Assessment with Bayesian Network", *ASME Journal of Verification, Validation, and Uncertainty Quantification*, 2020 (online September 2020)

[AP.2] Han Bao, Nam Dinh, Linyu Lin, Robert Youngblood, Jeffrey Lane, Hongbin Zhang, "Using Deep Learning to Explore Local Physical Similarity for Global-scale Bridging in Thermal-hydraulic Simulation", *Annals of Nuclear Energy* journal Volume 147, November 2020, 107684

[AP.3] L. Lin, S. Prescott, R. Sampath, N. Montanari, H. Bao, and N. Dinh, "Adequacy Evaluation of Smoothed Particle Hydrodynamics Methods for Simulating the External-Flooding Scenario", *Nuclear Engineering and Design* journal (NED-110720, online June 2020)

[AP.4] Saran Bodda, Abhinav Gupta and Nam Dinh, "Enhancement of Existing Risk-Informed Validation Framework", *Reliability Engineering and System Safety*, V.204, p.107140, 2020 https://doi.org/10.1016/j.ress.2020.107140.

[AP.5] Chih-Wei Chang, Jun Fang and Nam Dinh; "Reynolds-Averaged Turbulence Modeling Using Deep Learning with Local Flow Features – an Empirical Approach", *Nuclear Science and Engineering*, Vol.00, pp.1-15, 2020 (online January 2020).

[AP.6] Saran Bodda, Abhinav Gupta and Nam Dinh, "Risk-Informed Validation Framework for External Flooding Scenario", J. *Nuclear Engineering and Design*, 2020, Vol., pp.1-10 (online October 2019)

[AP.7] Botros Hanna, Nam Dinh, Robert Youngblood, and Igor Bolotnov, "Coarse-Grid Computational Fluid Dynamic Errors Prediction by Machine Learning", *Progress in Nuclear Energy*, Vol.118 (2020) 103140 (online September 2019)

[AP.8] Paridhi Athe and Nam Dinh, "A Framework for Assessment of Predictive Capability Maturity and Its Application in Nuclear Thermal Hydraulics", J. *Nuclear Engineering and Design*, 2019, Vol.354, 110201, pp.1-24.

[AP.9] Yang Liu, Xiaodong Sun, and Nam T. Dinh, "Validation and Uncertainty Quantification of multiphase-CFD solvers: A Data-Driven Bayesian Framework Supported by High-Resolution Experiments", J. *Nuclear Engineering and Design*, 2019, Vol.354, 110200, pp.1-19.

[AP.10] Han Bao, Nam T. Dinh, Jeffrey W. Lane, and Robert W. Youngblood, "A data-driven framework for error estimation and mesh-model optimization in system-level thermal-hydraulic simulation", *Nuclear Engineering and Design*, Volume 349, 1 August 2019, Pages 27-45

[AP.11] Yang Liu, Nam Dinh, Ralph Smith, and Xiaodong Sun, "Uncertainty Quantification of Two-Phase Flow and Boiling Heat Transfer Simulation Through a Data-Driven Bayesian Modular Approach", *International Journal of Heat and Mass Transfer*, Volume 138, August 2019, Pages 1096-1116

[AP.12] Chih-Wei Chang and Nam Dinh, "Classification of Machine Learning Frameworks for Data-Driven Thermal Fluid Models", *International Journal of Thermal Science*, 135, pp.559-579, 2019.

[AP.13] Yang Liu and Nam Dinh, "Validation and Uncertainty Quantification for Wall Boiling Closure Relations in Multiphase CFD Solver", *Nuclear Science and Engineering*. pp.1-19, 2018 (online Sep 2018)

[AP.14] Yang Liu, Nam Dinh, Yohei Sato and Bojan Niceno, "Data-driven modeling for boiling heat transfer: using deep neural networks and high-fidelity simulation results", *Applied Thermal Engineering*, 144, pp.305-320, 2018

[AP.15] "Interface Tracking Simulations of droplet interaction with spacer grids under DFFB conditions", N. Saini, I.A. Bolotnov, accepted for publication to *Nuclear Engineering and Design*, 2020.

[AP.16] "Interface tracking simulation of phase-change phenomena: an evaporation and condensation model", M. Li, I.A. Bolotnov, accepted for publication in *International Journal of Heat and Mass Transfer* (2020).

[AP.17] "Interface Resolved Simulations of Reactor Flows", J. Fang, J.J. Cambareri, M. Li, N. Saini, I.A. Bolotnov, *Nuclear Technology*, **206**:2, pp. 133-149 (2020).

[AP.18] "Development of a new contact angle control algorithm for level-set method", M. Li, K. Zeng, L. Wonnell, I.A. Bolotnov, 141(6), 061301, doi: 10.1115/1.4041987, *Journal of Fluid Engineering* (2019).

[AP.19] Jeongwon Seo, Hany S. Abdel-Khalik, and Zoltán Perkó, "Addressing Ambiguities in Constrained Sensitivity Analysis for Reactor Physics Problems," Nuclear Technology, March 2020.

[AP.20] Dongli Huang and Hany Abdel-Khalik, "Modeling Errors-Preserving Constrained Sensitivity Analysis," Nuclear Engineering and Design, June 2020.

[AP.21] Dongli Huang and Hany S. Abdel-Khalik, "Nuclear Data Uncertainty Propagation and Modeling Uncertainty Impact Evaluation in Neutronics Core Simulation," Progress in Nuclear Energy, under review.

[AP.22] Yeni Li, Acacia Brunett, Elise Jennings, and Hany S. Abdel-Khalik, "ROM-based Surrogate Modeling of EBR-II benchmark using ANL's SAM Code," to be submitted, currently under internal review at ANL.

[AP.23] Dongli Huang, Ugur Mertyurek, and Hany S. Abdel-Khalik, "Verification of the sensitivity and uncertainty-based criticality safety validation techniques: ORNL's SCALE case study," Nuclear Engineering and Design, pp.110571, 2020.

[AP.24] John Baugh and Alper Altuntas. Formal methods and finite element analysis of hurricane storm surge: A case study in software verification. Science of Computer Programming, 158:100–121, 2018

[AP.25] Xing Liu, Wensheng Jiang, Bo Yang, and John Baugh. Numerical study on factors influencing typhoon-induced storm surge distribution in Zhanjiang Harbor. Estuarine, Coastal and Shelf Science, 215:39–51, 2018

[AP.26] Xing Liu, Fatima Bukhari, John Baugh, Chris Massey, and Wensheng Jiang. Enabling reuse of large-scale ocean simulations for coastal modeling, in preparation, end of July submission

[AP.27] Fatima Bukhari, John Baugh, and Chris Massey. Subdomain modeling: case studies and retrospective analysis on USACE engineering projects, in two parts, in preparation, September submission

[AP.28] Fatima Bukhari, Niels Montanari, Ram Sampath, and John Baugh. Coupling shallow water and SPH codes: ADCIRC and Neutrino, in preparation, uncertain submission date

[AP.29] S. S. Bodda, A. Gupta, and R. T. Sewell, "Application of Risk Informed Validation Framework to a Real Life Like Flooding Scenario," *ASCE-ASME Journal of Risk and Uncertainty in Engineering Systems, Part A: Civil Engineering* (2020, Under Review).

[AP.30] P. Vaishanav, A. Gupta, and N. Dinh, "Illustrate the concept of scaling in uncertainties using laboratory experiments conducted at different scales in the context of flooding risk assessment," (In preparation).

[AP.31] S. Kwag, A. Gupta, and N. Dinh, "Probabilistic risk assessment based model validation method using Bayesian network," *Reliability Engineering & System Safety*, 169, 380 (2018); https://doi.org/10.1016/j.ress.2017.09.013.

[AP.32] M.A. Andre and P.M. Bardet, "Non-linear wave interaction in shallow water sloshing at harmonic resonance frequency". *Journal of Fluid Mechanics.* Under Review.

[AP.33] E. Florou, C. Fort, M.A. Andre, and P.M. Bardet, "Three dimensional transparent compliant interface reconstruction with structured illumination". *Experiments in Fluids*. In Preparation.

[AP.34] Yang Liu, Dewei Wang, Xiaodong Sun, Yang Liu, Nam Dinh, and Rui Hu, "Uncertainty quantification for Multiphase-CFD simulations of bubbly flows: a machine learning-based Bayesian approach supported by high-resolution experiments", *Reliability Engineering and System Safety*, 2021 (in press).

### 1.5.2. Conference papers

[RP.1] Saran Bodda, Abhinav Gupta and Nam Dinh, "Enhancement of Risk-Informed Validation Framework for External Hazard Scenario", ESREL-2020 & PSAM-15, Venice, Italy, May 2020

[RP.2] Han Bao, Jinyong Feng, Nam Dinh, Igor A. Bolotnov, and Hongbin Zhang, "Demonstration of a Data-Driven Physics-Based Approach for Computationally Efficient CFD Prediction of Two-Phase Bubbly Flow", International Conference on Advances in Thermal Hydraulics ATH-2020, Paris, France, March 2020.

[RP.3] Chih-Wei Chang, Jun Fang and Nam Dinh; "Reynolds-Averaged Turbulence Modeling Using Deep Learning with Local Flow Features", Proceedings of the 18th International Topical Meeting on Nuclear Reactor Thermal Hydraulics, Portland, OR, USA, August 2019, **(NURETH-18 Best Paper award)**

[RP.4] Yang Liu, Xiaodong Sun, Yang Liu, and Nam Dinh, "Uncertainty Quantification and Reduction for Constitutive Relations in Multiphase-CFD Solvers: A Data-Driven Bayesian Approach Supported by Advanced Measurement Techniques", Proceedings of the 18th International Topical Meeting on Nuclear Reactor Thermal Hydraulics, Portland, OR, USA, August 2019

[RP.5] Linyu Lin, S. Prescott, N. Montanari, R. Sampath, H. Bao, and N. Dinh, "Assessment of Smoothed Particle Hydrodynamics Methods for Simulating the External-Flooding Scenario", Proceedings of the 18th International Topical Meeting on Nuclear Reactor Thermal Hydraulics, Portland, OR, USA, August 2019

[RP.6] Han Bao, Robert Youngblood, Hongbin Zhang, Nam Dinh, Linyu Lin, and Jeffrey Lane, "A Data-Driven Approach to Scale Bridging in System Thermal-hydraulic Simulation", Proceedings

of the 18th International Topical Meeting on Nuclear Reactor Thermal Hydraulics, Portland, OR, USA, August 2019

[RP.7] Yangmo Zhu, Nam Dinh, and Rui Hu, "Development of Data-Driven Turbulence Model for 3D Thermal Stratification Simulation during Reactor Transients", Proceedings of the 18th International Topical Meeting on Nuclear Reactor Thermal Hydraulics, Portland, OR, USA, August 2019

[RP.8] Liu, Y., Shi, S., Qian, Y., Sun, X., and Dinh, N. Inverse Uncertainty Quantification of Turbulence Modeling in Multiphase-CFD Solver Using High-Resolution Data from Particle Image Velocimetry. In Proceedings of the Advances in Thermal Hydraulics (ATH-2018). Orlando, FL, USA, November, 2018.

[RP.9] Y. Liu, N. Dinh, Y. Sato, and B. Niceno, "Validation and Uncertainty Quantification of DNB Closures in MCFD Solver Using Inverse Bayesian Inference Method", Paper 198. Proceedings of ANS Conference on Best Estimate Plus Uncertainty (BEPU-2018), Lucca, Italy, May 2018

[RP.10] B. Hanna, N. Dinh, and I.A. Bolotnov, "Coarse-Grid Computational Fluid Dynamic Errors Prediction by Machine Learning", International Congress on Advanced Nuclear Power Plants, ICAPP 2018, Charlotte, NC, April 2018

[RP.11] Yang Liu and Nam Dinh, "Development of VUQ Framework for Wall Boiling Model in a MCFD solver", "- The 17th International Topical Meeting on Nuclear Reactor Thermal Hydraulics (NURETH-17), Xi'an, China, September 3 - 8, 2017.

[RP.12] Yangmo Zhu and Nam Dinh, "A Data-Driven Approach for Turbulence Modeling", "- The 17th International Topical Meeting on Nuclear Reactor Thermal Hydraulics (NURETH-17), Xi'an, China, September 3 - 8, 2017 ("***Best Student Paper Award***")

[RP.13] Linyu Lin, Nam Dinh, Niels Montanari, Ram Sampath, Nadir Akinci, Steven Prescott, 2017 "Assessment of Smoothed Particle Hydrodynamic in application of High-Wind risk analysis"- The 17th International Topical Meeting on Nuclear Reactor Thermal Hydraulics (NURETH-17), Xi'an, China, September 3 - 8, 2017.

[RP.14] Paridhi Athe, Nam Dinh, and Hany Abdel-Khalik, "Investigation of Similarity Metrics for Simulation based Scaling Analysis," International topical meeting on Advances in thermal hydraulics 2016 (ATH 16), New Orleans, LA, June 12-16, 2016

[RP.15] Xiaoqin Zhang, Yang Liu, Xiaodong Sun and Nam Dinh, "Design of Validation Experiments for Model Improvement of Dispersed Flow Film Boiling in COBRA-TF", ANS Winter Meeting, 2018, *ANS Transactions*

[RP.16] H. Bao, N. Dinh, J. Lane, and R. Youngblood, "Study of Data-Driven Mesh-Model Optimization in System Thermal-Hydraulic Simulation ", ANS Annual Meeting. Summer 2018. *ANS Transactions.*

[RP.17] Linyu Lin and Nam Dinh, "Predictive Capability Maturity Quantification with Bayesian Networks", ANS Annual Meeting. Summer 2018. *ANS Transactions*.

[RP.18] Chih-Wei Chang, Nam Dinh, and Sacit Cetiner, "Physics-Constrained Machine Learning for Two-Phase Flow Simulation Using Deep Learning-Based Closure Relation ", American Nuclear Society Winter Meeting, *ANS Transactions*, November 2017

[RP.19] Chih-Wei Chang aad Nam Dinh, "A Study of Physics-Informed Deep Learning for System Fluid Dynamics Closures", American Nuclear Society Winter Meeting, *ANS Transactions*, November 2016

[RP.20] Jia Zhou, Hany Abdel-Khalik, and Nam Dinh, "Model Calibration vs. Physics-guided Coverage Mapping: Case Study - Pressure Drop Calculations", *ANS Transactions*, June 2016

[RP.21] "Detailed Analysis of the Effects of Spacer-grid and Mixing Vanes on Turbulence in a PWR sub-channel under DFFB conditions based on DNS Data", N. Saini, I.A. Bolotnov, Advances in Thermal Hydraulics, Paris-Saclay, France, March 31st – April 3rd, 2020 – Postponed to October 20-23, 2020 (COVID-19).

[RP.22] "Interface Tracking Simulations of droplet interaction with spacer grids under DFFB conditions", N. Saini, I.A. Bolotnov, 18*th International Topical Meeting on Nuclear Reactor Thermal*

*Hydraulics (NURETH-18)*, Portland, OR, USA, Aug. 18-22, 2019. *** Invited for publication in a special issue of Nuclear Engineering and Design.

[RP.23] "Nucleate Boiling Simulation using Interface Tracking Method -- Bubble Departure diameter and Bubble Release Frequency", M. Li, I.A. Bolotnov, 18*th International Topical Meeting on Nuclear Reactor Thermal Hydraulics (NURETH-18)*, Portland, OR, USA, Aug. 18-22, 2019.

[RP.24] "High fidelity simulations for characterizing Sauter mean diameter of droplets in DFFB regime", N. Saini, S. Satpathy, I.A. Bolotnov, *2018 International Congress on Advances in Nuclear Power Plants (ICAPP 18)*, Charlotte, NC, USA, April 8-11, 2018.

[RP.25] "Multi-bubble Flow Boiling Simulation using Interface Tracking Method", M. Li, I.A. Bolotnov, *2018 International Congress on Advances in Nuclear Power Plants (ICAPP 18)*, Charlotte, NC, USA, April 8-11, 2018.

[RP.26] "Development of Evaporation and Condensation Model – Pool Boiling Simulation using ITM approach", M. Li, I.A. Bolotnov, *Transactions of 2018 ANS Annual Meeting*, Philadelphia, PA, June $17^{th}$ – $21^{st}$, 2018.

[RP.27] Dongli Huang and Hany Abdel-Khalik, 2019, "Investigative Study on Impact of Modeling Uncertainties in Uncertainty Quantification of Neutronics Core Simulation," Proc. M&C 2019, Portland, OR, August 2019.

[RP.28] Dongli Huang, Hany Abdel-Khalik, Ondrej Chvala[PD], and Ivan Maldonado, "Uncertainty Quantification for Nuclear Core Simulation," Proceedings of ICONE 26, London, UK, July 2018.

[RP.29] Dongli Huang, Hany S. Abdel-Khalik, Ondrej Chvala, and Guillermo I. Maldonado, "Efficient Evaluation of Core Simulator Few-Group Cross-Section Uncertainties via PCM", International Conference on Mathematics & Computational Methods Applied to Nuclear Science & Engineering (M&C2017), Jeju, Korea, April 16-20, 2017.

[RP.30] Siqi Zhang, Hany S. Abdel-khalik, Alberto Talamo, and Dimitri Rochman, "Physics-guided Neutronic Validation Methodology with Demonstration to KUCA cores," International Conference on Mathematics & Computational Methods Applied to Nuclear Science & Engineering (M&C2017), Jeju, Korea, April 16-20, 2017.

[RP.31] Jia Zhou and Hany S. Abdel-Khalik, "Avoiding Calibration via a Non-Parametric Physics-guided Coverage Mapping Algorithm," Transactions of the American Nuclear Society, Winter Meeting, October, 2017.

[RP.32] Zhang, X., Liu, Y., Sun, X., and Dinh, N., "Design of Validation Experiments for Model Improvement of Dispersed Flow Film Boiling in COBRA-TF," *Transactions of the American Nuclear Society*, Vol. **119**, ANS Winter Meeting, November 11-15, 2018, pp. 133-136, Orlando, FL.

[RP.33] Time Dependent Sensitivity Analysis of CTF, A. Tezbasaran, and M. Avramova, Best Estimate Plus Uncertainty International Conference (BEPU-2020), Oct 11-17, *In preparation*

[RP.34] Sensitivity Analysis of CTF For Coping Time Evaluation During Loss Of Coolant Accidents, A. Tezbasaran, and M. Avramova, Best Estimate Plus Uncertainty International Conference (BEPU-2020), Oct 11-17, *In preparation*

[RP.35] John Baugh and Tristan Dyer. State-based formal methods in scientific computation. In Abstract State Machines, Alloy, B, TLA, VDM, and Z: 6th International Conference, ABZ 2018, pages 392–396, Cham, 2018. Springer. Lecture Notes in Computer Science 10817

[RP.36] Alper Altuntas and John Baugh. Hybrid theorem proving as a lightweight method for verifying numerical software. In Proceedings of the Second International Workshop on Software Correctness for HPC Applications, Correctness'18, pages 1–8. IEEE, 2018

[RP.37] Tristan Dyer, Alper Altuntas, and John Baugh. Bounded verification of sparse matrix computations. In Proceedings of the Third International Workshop on Software Correctness for HPC Applications, Correctness'19, pages 36–43. IEEE/ACM, 2019

[RP.38] Tristan Dyer and John Baugh. Verifying and Visualizing Models of Scientific Software, in preparation for submission to ABZ 2021, International Conference on Rigorous State Based Methods

[RP.39] "Knowledgebase Structure Formulation and Requirements Development in a Data-Sparse Reality," Paper Number: VVS2017-4019, Program of the V&V 2017 ASME Verification and Validation Symposium, May 3–5, 2017, Las Vegas, Nevada, Weiju Ren and Lianshan Lin.
[RP.40] S. S. Bodda, A. Gupta, and N. Dinh, "Risk informed validation framework for external flooding scenario," In Transactions of the 25th International Conference on Structural Mechanics in Reactor Technology (2019).
[RP.41] S. S. Bodda, A. Gupta, and N. Dinh, "Enhancement of risk informed validation framework for external hazard scenario," Proceedings of the 15th International Conference on Probabilistic Safety Assessment and Management (2020).
[RP.42] S. S. Bodda, H. Sandhu, A. Gupta, and N. Dinh, "Risk Assessment Using Bayesian Approach: Risk Informed Validation Framework and Multi-Hazard Risk Assessment," NARSIS Workshop, Training on Probabilistic Safety Assessment for Nuclear Facilities (2019).
[RP.43] P. Vaishanav, A. Gupta, and N. Dinh, "Scaling of Uncertainty in Validation of Flooding Simulations: An Illustrative Case Study," In Transactions of the 25th International Conference on Structural Mechanics in Reactor Technology (2019).
[RP.44] C FORT, E FLOROU, M HABUKAWA, MA ANDRE, and PM BARDET. Towards experimental measurement of interfacial shear stress in a turbulent liquid-air layer, 33rd Symposium on Naval Hydrodynamics, Osaka, Japan, 31 May- 5 June. 6, 2020.
[RP.45] Philippe Bardet, Matthieu Andre. Validation of SPH Code NEUTRINO, SMIRT 25, Charlotte, NC, Aug. 5-9 2019.
[RP.46] Emerald Ryan, Philippe Bardet, Ramprasad Sampath, Niels Montanari, Steven Prescott, Matthieu Andre. Validation and Determination of Significant Simulation Parameters Using the SPH Code NEUTRINO, SMIRT 25, Charlotte, NC, Aug. 5-9 2019.
[RP.47] M Andre, PM Bardet, Ram Sampath, Niels Montanari, Linyu Lin, Steven Prescott, Emerald D. Ryan. Validation of Risk-Informed Safety Margin Characterization for Flooding of Nuclear Power Plants, NURETH 18, Portland, OR, Aug. 18-23 2019.

1.5.3. Presentations (invited lectures, keynotes)

1. S. S. Bodda, "Risk-informed validation," Workshop on Flooding Risk Assessment: Validation, Application, and Experimental Studies, 25th International Conference on Structural Mechanics in Reactor Technology (SMiRT) (2019).
2. A. Gupta, "Multihazard Bayesian Analysis: PSA," Invited Talk and Panel Member at NARSIS Workshop on Probabilistic Safety Assessment, European Commission, Warsaw, Poland, September 2 – 5 (2019).
3. A. Gupta, "Probabilistic Risk Assessment Based Model Validation Methods using a Bayesian Network," Invited Presentation at 2017 Pacific Rim Forum on Earthquake Resiliency of Nuclear Facilities, UC Berkeley, Berkeley, CA, January (2017).
4. "High resolution simulation of reactor flows", I.A. Bolotnov, Politecnico di Milano, Milan, Italy, December 5th, 2019.
5. "Two-phase flow simulations of turbulent nuclear reactor flows", I.A. Bolotnov, PSI, Zurich, Switzerland, October 31st, 2019.
6. "Interface Tracking Simulations of Two-phase Flows", I.A. Bolotnov, TU-Dresden, Dresden, Germany, October 28th, 2019.
7. "High resolution simulation of two-phase flows to support model development", I.A. Bolotnov, University of Leeds, Leeds, UK, October 10th, 2019.
8. "High resolution simulation of reactor flows", I.A. Bolotnov, Nuclear Energy Agency (NEA), Paris, France, September 20th, 2019.
9. "Well-resolved two-phase flow simulations of turbulent nuclear reactor flows", I.A. Bolotnov, CEA, Paris, France, September 19th, 2019.

10. “How DNS can help understand multiphase flow behavior?”, I.A. Bolotnov, Presentation at the Institute for Fluid Dynamics seminar, HZDR – Helmholtz-Zentrum Dresden-Rossendorf, Dresden, Germany, August 29th, 2019.
11. Hany S. Abdel-Khalik , Wuhan University, China, Short Course on “Data Mining in Engineering”, July 2018.
12. Hany S. Abdel-Khalik, Chalk River Laboratories, Canada, ZED-2 Summer School, “Uncertainty Methods in Reactor Physics,” May 2018
13. Hany S. Abdel-Khalik, Karlsruhe University, Germany, “Methods of uncertainty assessment and propagation,” The 2017 Frédéric Joliot/Otto Hahn Summer School, Karlsruhe, Germany, August 2017
14. R. Sampath, S. Prescott, E. Ryan, “Applying Flood Simulations” SMiRT 25, August 6 2019
15. E. Ryan, R. Sampath, S. Prescott, “Validation and Determination of Significant Simulation Parameters using the Smoothed Particle Hydrodynamic Code Neutrino” SMiRT 25, August 6 2019
16. Y. Liu, Design of Validation Experiments for Model Improvement of Dispersed Flow Film Boiling in COBRA-TF, Presentation, ANS Winter Meeting & Expo, November 15, 2018, Orlando, FL.
17. John Baugh, The role of Alloy in developing scientific software. Workshop on the Future of Alloy, MIT, Cambridge, MA, April 30–May 1, 2018
18. John Baugh, Formal methods in scientific computing. Johns Hopkins University Applied Physics Laboratory, invited lecture, December 2019
19. John Baugh, Lightweight formal methods in scientific computing. Logic for Systems, Brown University, invited lecture, February 2020
20. Philippe Bardet, “Molecular Tagging Velocimetry: Pushing the limits of velocimetry,” CEA-Saclay, Saclay, France, 2019/10/14.
21. Philippe Bardet, “Molecular Tagging Velocimetry: Pushing the limits of velocimetry,” KTH, Physics department, Stockholm, Sweden, 2019/10/04.
22. Philippe Bardet, “Molecular Tagging Velocimetry: Pushing the limits of velocimetry,” Technical Plenary Session, NURETH 18 conference, Portland, 2019/08/18-23.
23. Philippe Bardet, “Progress in Thermo-Fluids Lab,” COE CFD Center of Excellence, Chicago, IL, 2019/06/26.
24. Philippe Bardet, “Molecular Tagging Velocimetry - MTV,” Rencontre Technique and Scientifique, CEA Cadarache, France, 2018/06/04.
25. Philippe Bardet, “Advanced laser diagnostics development for Thermal Hydraulics,” *Paul Scherrer Institute,* Switzerland, 2018/10/16.

### 1.5.4. Dissertations/Theses

1. S. S. Bodda, “Risk Informed Validation Framework Using Bayesian Approach,” PhD Thesis, North Carolina State University (2019).
2. A. R. Dubey, “Seismic Fragility of Piping Systems: Consideration of Cyclic Behavior and Closed-Form Relationship,” PhD Thesis, North Carolina State University (2019).
3. Linyu Lin, “Development and Assessment of Smoothed Particle Hydrodynamics Method for Analysis of External Hazards”, PhD Dissertation in Nuclear Engineering, North Carolina State University, December 2018
4. Yangmo Zhu, “Development and Assessment of a Data-Driven Approach for Turbulence Modeling”, PhD Dissertation in Nuclear Engineering, North Carolina State University, December 2019
5. Mengnan Li, “High Resolution Boiling Simulation using Interface Tracking Method”, PhD Dissertation, NCSU, 2019
6. Nadish Saini, “High-fidelity Interface Capturing Simulations of the post-LOCA Dispersed Flow Film Boiling Regime in a Pressurized Water Reactor Sub-channel”, PhD Dissertation, NCSU, 2020

7. Shrey Satpathy, “Development of high-resolution computational fluid dynamics capabilities for LWR accident analysis”. MNE Report, NCSU, 2017
8. Xiaoqin Zhang, “Experimental Investigation and Data Uncertainty Analysis of Synthetic Dispersed Flow Film Boiling”, PhD Dissertation, University of Michigan, 2020
9. Dongli Huang, Efficient Uncertainty Characterization Framework In Neutronics Core Simulation With Application To Thermal-Spectrum Reactor Systems, PhD Dissertation, Purdue University, 2020
10. Emerald Ryan, “Determination, Development, and Validation of a Fluid Height Analysis Method and Particle Spacing Protocol for the Smoothed Particle Hydrodynamic Code Neutrino”, PhD Dissertation, Idaho State University, 2019

    [*] *Work supported by INL Research Fellowship, in collaboration with IRP researchers.*
11. Fatima Bukhari, “Performance Evaluation of Subdomain Modeling and Operational Enhancements for Large-Scale Storm Surge Simulations”, PhD Dissertation, NC State University, April 2020.
12. Andrew Dyer, “Lightweight Formal Methods in Scientific Computing”, PhD Dissertation, NC State University, June 2020.

### 1.5.5. Technologies or Techniques

- Developed a novel technique to quantitatively assess the system-level validation by connecting individual validation events through a probabilistic risk assessment (PRA) informed validation framework. The framework utilizes the power of Bayesian statistics to include uncertainty in both simulation and experimental models. In this technique, the system-level validation and the identification of critical events are evaluated based on fragility estimates. To improve the overall validation, it requires enhancement of simulation models of events along the critical path or collection of additional field data until the adequacy of the system-level validation is satisfied. This process helps in allocating the resources efficiently thereby reducing the effort to conduct high-fidelity simulations and large-scale experiments.
- Enhanced the proposed framework by developing a new set of validation metrics (overlapping coefficient and consistency index) and an additional attribute (Code adequacy) for making the framework more robust. The concept of overlapping coefficient (OC) is used to quantify the degree of validation within the context of uncertainty. OC is calculated by evaluating the percentage of overlapping area between simulation and experimental (data-driven) fragility curves. Consistency index (δ) ensures that the simulation and data-driven fragilities correspond to the same set of critical events. The interpretation of consistency index in the risk informed framework is illustrated for various cases of seismic and flooding scenarios. The concept of maturity levels are utilized to assess the decision regarding the adequacy of a simulation code for an intended application.
- Integrated the proposed risk informed validation framework with USNRC’s Evaluation Model Development and Assessment Process (EMDAP) framework. This allows transformation of EMDAP into a risk-informed EMDAP. The applicability of the proposed framework is evaluated by application to a real life like flooding scenario of a sunny day dam failure. Application to the realistic scenario illustrates that the credibility of flooding simulations can be assessed using formal quantification which is otherwise not possible in the existing EMDAP framework. The integrated framework formalizes the validation process by quantifying the expert knowledge and making it less heuristic.
- Developed a methodology which examines reduced scale experiments at multiple scales to infer the effect of scaling. Several advanced simulation tools used for studying real world flooding scenarios are validated through smaller scale laboratory experiments. An implicit extrapolation is performed on the reduced scale data generally beyond the domain of validation when these simulation tools are used for real-world applications. This leads to scale distortion and uncertainty in prediction. Such issues are often only resolved by professional experts. Hence, the current

methodology is an attempt to understand scaling phenomenon to enhance and support the scaling extrapolation and reduce the reliance on expert data analysis.

- Sterling, a web-based visualizer for Alloy, enables modeling of scientific software using lightweight formal methods by providing advanced visualization tools that address shortcomings of the existing Alloy visualizations. These tools focus particularly on the ability to express the types of dynamic and spatial relationships that are embedded throughout models of scientific software.
- As a part of her PhD dissertation work, Fatima Bukhari demonstrates the appreciable computational savings provided by Subdomain Modeling for storm surge simulation, while maintaining solution integrity. Additionally, a one-way coupling methodology has been developed that allows for coupling between the large-scale finite element model, ADCIRC, and the small-scale smoothed particle hydrodynamics code, Neutrino. This work facilitates simulation of storms and their effects at 'facility level' scales, in turn enabling the quantitative assessment of the resilience of critical (nuclear) infrastructure to storm-induced flooding.
- (PU) The project has matured the physics-guided coverage mapping methodology to effectively and rigorously map biases between two sets of modeling conditions, representing experimental and application domain or high and low fidelity models. The developed technology provides a solution to a key challenge in existing regulatory/licensing framework, that is how to transition from heavy reliance on experiments to a science-based risk-informed validation strategy capable of leveraging advances in predictive science, information theory, and data analytics to develop transformational approaches for the evaluation of biases and uncertainties when limited experimental data exist. Addressing this challenge is critically needed to support the expected adoption of advanced reactor technologies, which require scientifically-defendable analysis capabilities for model validation of first-of-a-kind reactor technologies. The proposed helped develop the basic algorithms required to realize this vision.
- (GWU) The project developed a new experimental diagnostics to measure the interface of rough water waves in 3D + time.
- (UM) The project developed ParticleMaster Integrated Optical Imaging System Data Acquirement Procedures.

### 1.5.6. Inventions, Patent Applications, and/or Licenses

- Hany Abdel-Khalik and Ugur Mertyurek, "A Novel Capability to Support Nuclear Model Validation and Mapping of Biases and Uncertainties," August 2019, Invention Disclosure. Given interest in this technology, the co-PI has initiated collaborative discussions with various researchers in the DOE complex. Based on a recently executed inter-institution agreement between Purdue and ORNL, the co-PI is working with both institutions to file for a provisional patent regarding this technology and is currently working on a licensing agreement to help commercialize this technology. A startup company by the co-PI has been formed in 2018, and will be leveraged to apply for future funding opportunities in support of technology further development and adaption to nuclear industry needs.

### 1.5.7. Other products, notable achievements

- The work on risk informed validation framework got Saran Bodda recognized as one of the three winners of the Shibata Early Career Award at SMiRT 25 Conference, 2019.
- Saran Bodda and Ankit Dubey were awarded Zia Graduate Fellowship for their research contributions at NC State University.
- Yangmo Zhu is recipient of Student Paper Award at NURETH-17 (2017)
- Chih-Wei Chang receives Best Paper Award at NURETH-18 (2019)

1.5.8. Opportunities for training and professional development

- Conference attendance supported through the project by graduate students and faculty have contributed to the professional development.
- Students Saran Bodda and Pragya Vaishnav worked closely with industry collaborators on the project.
- Students Saran Bodda and Ankit Dubey spent a summer as interns at Idaho National Lab and getting familiar with MOOSE and related modules.
- Saran Bodda also developed codes for PRA that have been incorporated into MASTODON which is part of MOOSE.
- Ankit Dubey worked closely with INL researchers for simulating a scenario of internal flooding risk assessment at a nuclear plant.
- Internships for participating students:
    - Innovative Systems Software: Basic RELAP/SCDAPSIM Training June-July 2017
    - Idaho National Lab: RAVEN Training and RAVEN-CTF Coupling June-July 2018
- The development of Sterling led to an invited lecture opportunity for PhD student Tristan Dyer, who has secured a postdoctoral research position at Brown University to continue its development for use as the primary visualization tool for Forge, a language built for teaching formal methods and model checking.
- The demonstration of the applicability of Subdomain Modeling as a tool that affords appreciable computational savings while maintaining solution quality led to an internship with US Army Corps of Engineers - Engineering Research and Development Center (USACE-ERDC) for former PhD Student Fatima Bukhari. Upon completion of her degree, this internship was converted to a full-time employment opportunity as a Research Civil Engineer.
- At GWU, the project has supported a postdoctoral fellow, one doctoral student part time, one MS student, and served as capstone design for 5 undergraduate students at GWU. The postdoctoral fellow designed the experimental facility, which required significant structural analysis, an area in which he was not trained (he is an experimentalist in fluid dynamics). He managed to leverage the excellent and challenging work and is now doing structural testing for SpaceX Dragon capsule that brought back US astronauts to space in 2020!
- At Purdue University, the material developed has been the basis for two internships, one in the summer of 2019 for then-PhD candidate, Ms. Dongli Huang, who has graduated in May 2020, and another in the fall of 2019 for PhD candidate, Ms. Yeni Li, who is expected to graduate in December 2020. The material developed has contributed to a new course on data mining in Engineering, which was taught in TU-DELFT, Netherlands, 2018.
- At University of Michigan, the project created opportunity for facility design and construction training; experiment quality control training; LaVision ParticleMaster system package training.

# 2. Risk Informed Validation Framework Using Bayesian Approach

## 2.1. Summary

Safety of nuclear plants against external flooding has gained significant attention following the accident at Fukushima Daiichi nuclear power station. In United States, Oyster Creek nuclear plant was safely shutdown when high storm surge during hurricane Sandy caused a potential flooding threat. Subsequently, the nuclear energy industry experienced a significant activity in Probabilistic Risk Assessment (PRA) for external flooding. Past few decades have seen a rapid growth in the availability of computational power and that induces continually reducing cost of simulation. This rapidly changing scenario together with availability of high precision and large-scale experimental data has enabled development of high fidelity simulation tools capable of simulating multi-physics multi-scale phenomena. Increasingly, methods of computational fluid dynamics including advanced simulation codes are being considered to evaluate the sequence of events during different scenarios of flooding at a plant. One of the key limitations in validation is the lack of relevant experimental data at system-level. This limitation leads to a decrease in the confidence of system-level risk predictions. Therefore, a robust validation framework is needed to formalize the confidence in predictive capability of advanced simulation results.

In this project, we propose a formal validation approach that provides a basis to quantify credibility of risk assessments that are based on advanced simulation codes. The efficiency of the risk informed validation approach lies in the identification of critical structures, systems, and components (SSCs) that contribute to the system-level risk using Bayesian statistics. The validation methodology employs a data-driven approach to quantify the quality of data that is used to evaluate experimental fragilities for flooding failures. As the fragility assessment of a flooding scenario suffers from large epistemic uncertainties, the credibility of system-level validation is expressed using probabilistic distribution and maturity levels. To ensure that the system-level validation is complete and consistent, an additional validation index called consistency index is introduced. The risk informed validation approach is integrated with USNRC's Evaluation Model Development and Assessment Process (EMDAP) framework for a complete and wider applicability of the framework.

## 2.2. Introduction

Given the events at Fukushima-Daiichi nuclear power plant, there is an increased emphasis on using high fidelity simulation tools to evaluate the vulnerability of nuclear facilities subjected to external hazards. Availability of sophisticated computer models capable of simulating multi-physics multi-scale phenomena has increased the need for verification and validation of such high fidelity simulations. In this report, we aim to develop and demonstrate a comprehensive risk informed decision-oriented methodology for validation of advanced computer models used in nuclear power plant safety analysis. Specifically, the advanced computer models are those in the toolkit developed to support risk-informed safety margin characterization (RISMC), an integrated deterministic/probabilistic safety analysis methodology developed in the Department of Energy's Light Water Reactor Sustainability (LWR-S) program. The project investigated a decision oriented framework for quantification of validity with a probabilistic criterion for adequate level of validation.

The two primary challenges encountered in this project are: (1) lack of relevant plant-level data needed for validation of high-fidelity simulations, and (2) non-availability of a rational, consistent, and quantitative approach for validation. While first item above is essential in any validation effort, it is usually restricted by high cost of collecting such data and in some cases inability to conduct large-scale experiments. The confidence in high-fidelity simulations decreases due to excessive reliance on expert opinion for establishing the acceptability of high simulation models. The uncertainties due to inherent randomness and lack of knowledge about real physical complex systems as well as natural hazards pose significant challenges to the model validation assessment. Fidelity of a system-level computer simulation

model is difficult to assess even though a model for each component of the system can be individually validated with available component-level data. The system-level validation process involves a validation at component level, determine a relationship between component-level and system-level performance, and finally establish an inference of the degree of validation at system-level. The validation goal is difficult to achieve particularly in a quantitative sense because of the uncertainties in the relationship between different levels as well as in the parameters used for characterizing the performance at both the component and system levels. Consequently, six key aspects in this process are:

1. Validation metric: Characterization of appropriate validation indices for quantitative comparison of simulation and test data
2. Inference on the degree of validation at system-level
3. Ranking of Components and Subsystems: Any component or subsystem on the critical path would be considered most significant and assigned a higher priority
4. Confidence Bands: The component-level validation metric can be combined with the failure probabilities for a specific risk-scenario to develop confidence bands
5. Acceptability/Hypothesis Testing: Probabilistic criteria can be used to evaluate the acceptability of the validation for a particular component or simulation of an event in the given scenario
6. Identification of Validation Gaps: The prioritization described above would then help identifying appropriate validation gaps and allocating resources for data collection to reduce these gaps.

This research explored the development of a novel performance-based risk-informed validation approach that is rational, efficient, and quantitative in nature. A framework based on Bayesian statistics is proposed in validation of RISMC Models (Task 1 - Methodology Development) to implement and explore the proposed validation data plan (IRP-RC-1, 2016). The intent of the proposed approach is to provide a quantitative assessment of validation for a system-level simulation model based on component-level validation information. It uses performance-based criteria to judge the efficacy of a particular validation and a risk-informed framework to determine whether additional validation of a certain component or subsystem is needed or not. The specific steps of Bayesian framework are: The applicability and effectiveness of the proposed approach is explored in the context of a synthetic example of an accident sequence in nuclear plant subjected to storm surge, for which sources of errors and uncertainties and predictive capability gaps are identified. The proposed validation framework developed in this research is described in detail in Bodda (2020).

### 2.3. Scope of Work

The project goal is to develop and demonstrate a comprehensive risk-informed decision-oriented methodology for the validation of RISMC models (1.3.1 Project Scope, IRP-RC-1, 2016). In this project, we pursued a simulation-aided uncertainty-guided data-driven approach to enable effective implementation of the EMDAP elements and we investigated:

- Risk-informed approaches for collection and characterization of evidence.
- Decision-oriented framework for quantification of “validity” (or “maturity”), with a probabilistic criterion for adequate level of validation.
- Illustration and quantification of uncertainty in scaling phenomenon.
- Methods for data-driven model development and assessment process that effectively utilizes data from physical and numerical experiments.

To accomplish the work, our team has performed following subtasks corresponding to the major Task 1: Validation of RISMC Models (Methodology Development) and Task 2: Validation of Flood Simulation Capability for Plant Safety Analysis.

- Task 1.1: RISMC model applications and validation requirements
- Task 1.2: RISMC model validation methodology
- Task 1.3. Predictive capability maturity quantification
- Task 1.4. Simulation-based scaling

- Task 1.6. Data-driven multi-scale modeling
- Task 1.7. Validation data plan
- Task 2.1. Perform RISMC analysis of storm surge flood scenarios
- Task 2.2: Define flooding validation data plan

The specific information (technical approach and assumptions) required to carry out the validation of advanced simulation codes using the proposed validation framework is listed below (Bodda et al. 2020b):

- It is assumed that the event and fault trees needed as the first step in implementation of the proposed approach are available which is generally true for a major engineering facility or project. If not, then one would need to start by creating the logic tree and accident sequences. Subsequent mapping of this information into a Bayesian network does not require any additional input.
- A logic tree based risk assessment approach requires fragility curves for basic events. These are in general the simulation-based fragilities for a specific implementation. Therefore, it is assumed that these are available.
- The biggest challenge in implementing the proposed approach lies in developing the data-driven fragility curves that are used for validation. The data could come from experiments, experience, or high fidelity simulations. This aspect also involves establishing the grade levels for Relevance, Scaling, and Data Uncertainty (R/S/U) for the data used (Dinh, 2012).
- In the initial implementation of risk informed validation methodology, it is possible that the development of data-driven fragility for a certain event might not be available. This is similar to initial implementation of PRA in 1970s when there was not much information available on fragilities of components. The initial implementation of PRA relied significantly on expert opinion. Similar expert-based knowledge can be used for the initial implementation of the data-driven fragilities for such events. The initial implementation of the framework can then be used to determine the specific events that contribute more to the overall validation and therefore ideal candidates for collecting more data. As more information becomes available either through high fidelity simulations or experiments, the complete validation process can be updated.
- If the data-driven fragility cannot be generated for a certain event, then one can assume the data-driven fragilities to be same as the simulation-based fragilities in the initial implementation. These can then be updated as additional information become available.
- It is assumed that Fussell-Vesely importance measures can be used to identify the critical path for the entire system.
- In the context of overlapping coefficient as the validation metric, alternative validation metrics such as KL Divergence, Mutual Information, and Bayes Factor can be potential candidates.
- In order to quantify the adequacy of the various simulation codes used for generating the simulation fragility curves, it would be required to assess a maturity level for each simulation code.
- Finally, stakeholders would need to agree on an acceptance criterion for evaluating the degree of validation at the system-level.

## 2.4. Key Findings

### *Technical Findings*

- Developed a novel technique to quantitatively assess the system-level validation by connecting individual validation events through a probabilistic risk assessment (PRA) informed validation framework (Bodda et al. 2020a). The framework utilizes the power of Bayesian statistics to include uncertainty in both simulation and experimental models. In this technique, the system-level validation and the identification of critical events are evaluated based on fragility estimates. To improve the overall validation, it requires enhancement of simulation models of events along the critical path or collection of additional field data until the adequacy of the system-level validation is satisfied. This process helps in allocating the resources efficiently thereby reducing the effort to conduct high-fidelity simulations and large-scale experiments. ***Addresses Tasks 1.1, 1.2, 1.7, 2.1, 2.2.***

- Developed a data-driven approach to incorporate the quality of experimental data quantitatively in experimental fragility or data-driven fragility (Bodda et al. 2020a). The quality of experimental data is graded by three attributes: Relevance, Scaling, and Data Uncertainty (R/S/U). Relevance reflects the degree of applicability of experimental data from existing studies to the current application. Scaling uncertainty incorporates both geometric and physics scaling uncertainties. Data uncertainty reflects the uncertainty in the measured data. In the absence of appropriate experimental data, one could use experience data (given in terms of failure rates) or even high fidelity simulations to develop the data-driven fragilities especially if high fidelity simulations have been validated against experiments. The uncertainties due to each of these three attributes are quantified by assigning grades on a 4-point scale (from 1 to 4 with 1 being poor and 4 being excellent) based on the quality of data. ***Partially addresses Task 1.6***
- Proposed a new set of validation metrics (overlapping coefficient and consistency index) and an additional attribute (Code adequacy) for making the risk informed validation framework more robust (Bodda et al. 2020b). The concept of overlapping coefficient (OC) is used to quantify the degree of validation within the context of uncertainty. OC is calculated by evaluating the percentage of overlapping area between simulation and experimental (data-driven) fragility curves (Figure 2.1). Consistency index (δ) ensures that the simulation and data-driven fragilities correspond to the same set of critical events. The interpretation of consistency index in the risk informed framework is illustrated for various cases of seismic and flooding scenarios. The concept of maturity levels are utilized to assess the decision regarding the adequacy of a simulation code for an intended application. ***Addresses Tasks 1.1, 1.2, 1.3***

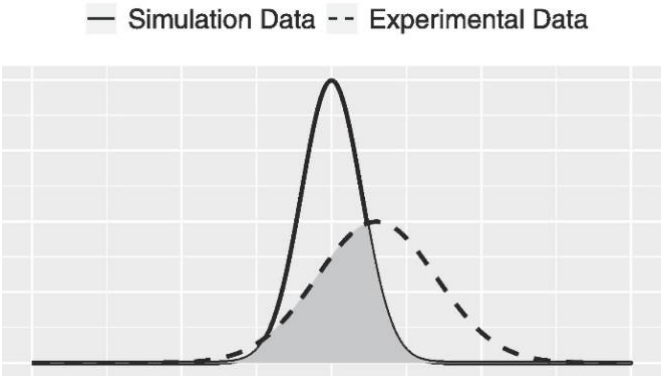


Figure 2.1. Overlapping Coefficient (Kwag et al. 2018)

- Integrated the proposed risk informed validation framework with USNRC's Evaluation Model Development and Assessment Process (EMDAP) framework as shown in Figure 2.2 (Bodda et al. 2020c). This allows transformation of EMDAP into a risk-informed EMDAP. The applicability of the proposed framework is evaluated by application to a real life like flooding scenario of a sunny day dam failure. Application to the realistic scenario illustrates that the credibility of flooding simulations can be assessed using formal quantification which is otherwise not possible in the existing EMDAP framework. The integrated framework formalizes the validation process by quantifying the expert knowledge and making it less heuristic. ***Addresses Tasks 1.1, 1.2, 1.3, 1.7, 2.1, 2.2.***

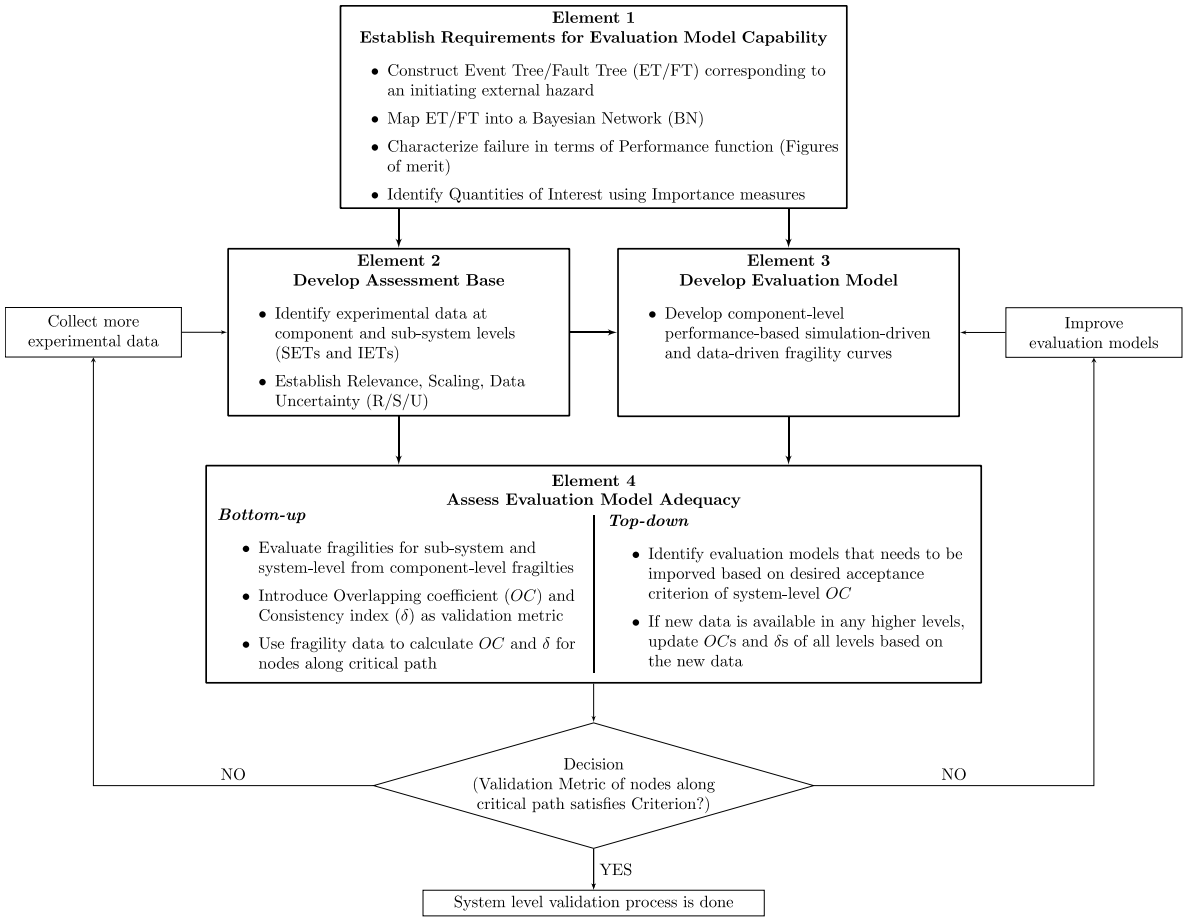


Figure 2.2. Integrated Risk informed EMDAP framework (Bodda et al. 2020c)

- Developed a methodology which examines reduced scale experiments at multiple scales to infer the effect of scaling (Vaishanav et al. 2019). Several advanced simulation tools used for studying real world flooding scenarios are validated through smaller scale laboratory experiments. An implicit extrapolation is performed on the reduced scale data generally beyond the domain of validation when these simulation tools are used for real-world applications. This leads to scale distortion and uncertainty in prediction. Such issues are often only resolved by professional experts. Hence, the proposed methodology is an attempt to understand scaling phenomenon to enhance and support the scaling extrapolation and reduce the reliance on expert data analysis. ***Addresses Tasks 1.4, 1.6***

***Highlights of technical innovations***

- Risk informed methodology for system-level validation within the context of uncertainty.
- Quantitative validation to assess credibility of system-level estimates.
- Bayesian approach for system-level validation.
- Grade quality of experimental data for quantitative representation of uncertainty.
- Incorporate the quality of experimental data quantitatively by adopting a data-driven approach.
- Identification of events critical for improving system-level validation.
- Concept of overlapping coefficient as validation index.
- Propose consistency index to ensure system-level validation is complete.
- Adequacy of a simulation code for an application is characterized by maturity level.

- Integration of risk informed validation approach with USNRC's Evaluation Model Development and Assessment Process (EMDAP) framework.
- Examination of reduced scale experiments at multiple scales to infer the effect of scaling.

## 2.5. Path Forward

Some of the key challenges and the recommendations for future work are discussed below. In practice, computational cost of the proposed approach can be a challenge. This is particularly true for generating multiple simulation-based fragility curves due to a large number of simulations that may be needed to account for uncertainties within a Monte Carlo approach. This challenge can be addressed to a certain degree by employing statistical inference for fragility estimates while minimizing the number of computationally intensive simulations. Another challenge relates to generation of data-driven fragility curves especially for all the basic events in the Bayesian network. The impact of this aspect is reduced in the proposed approach by recommending the development of assessment base for only the critical events first. Then, the non-critical events can be considered in the subsequent steps. In the absence of experimental data, one can use either experience data or high fidelity simulations to generate the data-driven fragilities. In the absence of any of these potential options, one could use expert judgment to come up with an initial estimate of data-driven fragilities and if that is also not desired for any specific event under certain extreme circumstances then it would be appropriate to use simulation-based fragility curve as a substitute for data-driven fragility for that specific event (indicating a perfect validation for this event). This can be updated in future as additional information becomes available. Another way could be to consider two different options for this event, that of perfect validation as well as no validation, and evaluate the impact on the overall system level validation. However, this aspect is not considered in this study and is a good candidate for future studies. This concept can also be extended to study the cliff-edge effect that is often observed in real life fragility estimates for certain events. An event with cliff-edge fragility could be considered using the two potential options of perfect validation as well as no validation. It is recommended to consider this aspect in future studies. The case studies considered in this manuscript do not include common cause failures (CCF). However, CCF events can be incorporated into the validation framework using Bayesian approaches (Mi et al., 2012; Li et al., 2019; Nguyen et al., 2020), and it does not require special attention. In this methodology, the non-critical paths in the Bayesian network are ignored for the system-level validation. Therefore, this assumption may cause some impact on the system-level code adequacy. For future work, the effect of assumption can be treated as a model uncertainty or incompleteness uncertainty and should be analyzed as part of uncertainty analysis in PRA (Drouin et al., 2017). The computational cost of Bayesian analysis is a limitation of using Bayesian approach in itself but availability of increasing computational resources have helped overcome this limitation in recent years.

## 2.6. Conclusions

The key conclusions of this study are summarized as follows:

- The risk informed methodology is mapped into four elements of the EMDAP framework to enable consistency and completeness in the validation process.
- The proposed integrated risk informed EMDAP framework enables us to quantify the validation for a realistic flooding scenario.
- It is also illustrated that the proposed framework allows implementation of Bayesian inference to identify the critical events for which collecting additional data would reduce the uncertainty and improve the validation of overall risk estimates.
- The integrated framework formalizes the validation process by quantifying the expert knowledge and making it less heuristic.
- The non-physical events in the PRA model are identified and treated as either completely safe or fail in the validation process.

- The data-driven fragilities are generated only for critical events. For non-critical events, the data-driven fragilities are considered to be same as simulation-based fragilities.
- The critical path in a Bayesian network is identified by using extended definition of
- Fussell-Vesely (FV) Importance measure for Bayesian networks.
- Introduced the concept of consistency index (δ) in the validation metric which ensures that the simulation and data-driven fragilities correspond to the same set of critical events.
- Overlapping coefficient is used as the standardized validation metric.
- The quality of experimental data used in the validation study is quantified and incorporated in the data-driven fragility curves.
- Multiple fragility curves are evaluated using different confidence levels instead of just the mean fragility curves.
- The robustness of the modified framework is illustrated by enabling clarity, consistency, and completeness for a synthetic and realistic examples of flooding scenario.

The performed project reinforced its potential for broader impacts as follows:

- The proposed framework will provide a better understanding of uncertainty in safety margins, and subsequently, help identify vulnerability and risk of nuclear systems. From the perspective of the nuclear industry, this understanding is central to a more efficient design, operation, and emergency management, of current and future NPPs.
- Presently, most of the regulators around the world as well as organizations developing codes and standards (ANS, ASME, USNRC, IAEA, etc.) are in the process of developing regulatory guidelines for probabilistic flooding risk assessment particularly for advanced reactors. Therefore, the scenario-based RISMC applications proposed in this project can be used as an assessment tool to evaluate the value of new frameworks.
- Historically, the nuclear industry has not been effective in communicating the risks to public and media. Effective communication of risk requires an extremely simple characterization and powerful simulation/visualization of scenarios, which can then be used as a confidence builder through public's understanding of the extensive defense-in-depth measures followed by the industry experts. RISMC toolkit can be quite powerful in simplifying and in enabling the visualization of defense-in-depth measures for appropriate communication to the public and the media.

## 2.7. References


H. Nguyen and E. Gouno, "Bayesian inference for Common cause failure rate based on causal inference with missing data," *Reliability Engineering & System Safety*, 197, 106789 (2020).

IRP-RC-1, "Development and Application of a Data-Driven Methodology for Validation of Risk-Informed Safety Margin Characterization Model," A Proposal for an Integrated Research Project In Response to Funding Opportunity Announcement (FOA) No. DEFOA-0001281 IRP-RC-1 (2016).

J. Mi, Y. Li, H.-Z. Huang, Y. Liu, and X. Zhang, "Reliability analysis of multi-state systems with common cause failure based on Bayesian Networks," 2012 International Conference on Quality, Reliability, Risk, Maintenance, and Safety Engineering, 1117-1121, IEEE (2012).

M. Drouin, A. Gilbertson, G. Parry, J. Lehner, G. Martinez-Guridi, J. LaChance, and T. Wheeler, "Guidance on the Treatment of Uncertainties Associated with PRAs in Risk-Informed Decision making, Final Report (NUREG-1855, Revision 1)," US Nuclear Regulatory Commission Office of Nuclear Regulatory Research (2017).

N. Dinh, "CIPS Validation Data Plan," INL/EXT-12-25347, Idaho National Laboratory (2012); https://doi.org/10.2172/1044197.

P. Vaishanav, A. Gupta, and N. Dinh, “Scaling of Uncertainty in Validation of Flooding Simulations: An Illustrative Case Study,” In Transactions of the 25th International Conference on Structural Mechanics in Reactor Technology (2019).

S. Kwag, A. Gupta, and N. Dinh, “Probabilistic risk assessment based model validation method using Bayesian network,” *Reliability Engineering & System Safety*, 169, 380 (2018).

S. S. Bodda, “Risk Informed Validation Framework Using Bayesian Approach,” PhD Thesis, North Carolina State University (2019).

S. S. Bodda, A. Gupta, and N. Dinh, “Risk informed validation framework for external flooding scenario,” *Nuclear Engineering and Design*, 356, 110377 (2020a).

S. S. Bodda, A. Gupta, and N. Dinh, “Enhancement of risk informed validation framework for external hazard scenario,” *Reliability Engineering & System Safety*, 204, 107140 (2020b).

S. S. Bodda, A. Gupta, and R. T. Sewell, “Application of Risk Informed Validation Framework to a Real Life Like Flooding Scenario,” *ASCE-ASME Journal of Risk and Uncertainty in Engineering Systems, Part A: Civil Engineering* (2020c, Under Review).

Z. Li, T. Xu, J. Gu, H. Wang, and J. Zhao, “Reliability modeling of redundant systems considering CCF based on DBN,” *Arabian Journal for Science and Engineering*, 44, 3, 2567 (2019).

# 3. Data-Driven Methodology for Validation of RISMC Models

## 3.1. Summary

Risk-Informed Safety Margin Characterization (RISMC) is a modern methodology for Nuclear Power Plant safety analysis that combines a dynamic probabilistic risk assessment (PRA) and "best estimate plus uncertainty" realization of the RISMC mechanistic models. Controlled by probabilistic tools with initial and boundary conditions, multiple simulations are performed with mechanistic tools to identify the safety margin and vulnerability of the reactor. Since the result of RISMC is used to inform and support the decision regarding design, operation, and safety of nuclear power plant, a mathematically defendable and robust approach is needed for the validation of the simulation tools, such that a confident and effective decision can be made regarding the high-consequence nuclear safety. Due to the lack of prototypical data and deficiencies of the simulation model, a framework is needed to guide the validation of RISMC Modeling & Simulation (M&S) tools in three major aspects: generating & gathering direct all related evidence, integrating evidence into a claim regarding the model credibility/uncertainty, and making confident and robust decision for the model credibility/uncertainty. Also, since RISMC requires a large number of simulations for every external event, it's sometimes inefficient to pursue high-order-accuracy M&S tools, where the facilities' margins are enormous compared to code uncertainty. As a result, the sufficiency of simulation accuracy depends on the characteristics of the scenario and validation that adapts such a concept is known as the risk-informed validation. The objective is to advise the safety management group on how to make a best and effective assessment for the model uncertainty, given the research goal and the scenario information. Although many validation frameworks have been developed, none of them explicitly adapts the risk-informed concept. Moreover, many elements are performed as black boxes due to the inherent limitations and challenges. When the system becomes large and complex, the uncertainties induced by these limitations could grow up and accumulate. Without proper investigations, such issues can be easily overlooked and the user may experience a loss of confidence on the validation decision. As a result, a risk-informed validation framework is needed for assessing the credibility/uncertainty of RISMC M&S tools. At the same time, new methodologies/technologies are needed to resolve the major issues and challenges of traditional validation methodologies.

In the project of "Development and Application of a Data-Driven Methodology for Validation of Risk-Informed Safety Margin Characterization Models", a validation framework, named Risk-informed Evaluation Model Development and Assessment Process (REMDAP), is proposed for the validation of RISMC M&S tools. REMDAP is designed based on the framework of Evaluation Model Development and Assessment Process (EMDAP) and the methodology of Code Scaling Applicability, and Uncertainty (CSAU). By incorporating data-driven and risk-inform concept, REMDAP aims to present a significant shift from the current approach for expert-determined validation to the data-driven approach. In this study, a concept of sufficient accuracy is developed and adapted in the REMDAP framework to account for the unfrozen model forms, parameters and computational resources in the RISMC analysis. A tentative workflow is prepared based on the currently developing methodologies/technologies. Next, the progress of developing key methodologies in the REMDAP framework, including the data-driven closure development, data-driven uncertainty quantification, and Predictive Capability Maturity Quantification & Bayesian Network (PCMQBN) are demonstrated. Presently, this study demonstrates some initial developments of classifying methodologies based on assumptions and conditions, the objective is to identify the feature and create an initial proof-of-concept for applying Data Driven Modeling (DDM) in the model development and validation process. The application of REMDAP to sophisticated RISMC tools, including Cobra-TF and NEUTRINO-SPH, is still under development.

First, a data-driven closure development methodology is under initial development and the available data-driven methods are classified into two types. The parametric model is built upon the fixed model form that relies on human knowledge, while the nonparametric model solely depends the data. Illustrative

examples are prepared for both types of model development methods and observations are analyzed. Second, a data-driven uncertainty quantification (UQ) methodology is developed and the present methods are classified into two types: global data-driven UQ and local data-driven UQ. The global approach targets at system code like Cobra-TF by assuming that the model has been well-verified and closures are the major source of uncertainties. The local approach uses Physics-Informed Machine Learning (PIML) to construct a surrogate between the simulation error and the input physical features. It's designed for the coarse-grid CFD like NEUTRINO-SPH, where error of each computing element is characterized with PIML. Illustrative examples are prepared for both types of data-driven UQ methods and observations are analyzed.

Another major challenge of RISMC M&S tools validation is the decision-making process under uncertainty. Traditional validation relies heavily on expert judgments and the process is obscure and heuristic. In this study, a decision-theoretic methodology PCMQBN is under development. The objective is to construct a transparent, consistent and improvable validation process with mathematical languages and effectively make decisions on model credibility with adequate confidence based on a set of uncertain beliefs and a set of utilities. Guidance is constructed for the uncertainty grade of the R/S/U (Relevance/Scaling/Uncertainty) grading system. Illustrative examples are prepared to demonstrate the guidance and major findings. In addition, a framework of Bayesian sensitivity study is proposed for PCMQBN and the objective is to improve the robustness of the PCMQBN's result.

## 3.2. Introduction

This chapter aims to demonstrate the motivation of developing a new validation framework for the RISMC M&S tools from the perspective of practical challenges/gaps.

### 3.2.1. Risk-Informed Reactor Safety Analysis

Risk-Informed Safety Margins Characterization (RISMC) Pathway is conducting research and development for advanced methods and tools to support Nuclear Power Plant (NPP) safety assessments and management [1]. Presently, RISMC is applied to address the NPP safety margin during external hazards, including flooding, high winds and so on. Because the RISMC approach explicitly couples probabilistic approaches (the "scenario") with phenomenological representations (the "physics") through a modeling-and-simulation-based approach, it is ideally suited to serve as a framework to address the interactions of external hazards on NPPs and their potential impacts on the NPP safety. Figure 3.3 shows a simple representation of load and capability in both traditional safety analysis (left) and RISMC (right). Originally, the load and capability on the Structures Systems Components (SSCs) are calculated deterministically by the system code with less uncertainty information. In RISMC analysis, uncertainty of the load and capability are considered, and the safety margin is characterized by the region where the load exceeds the capacity.

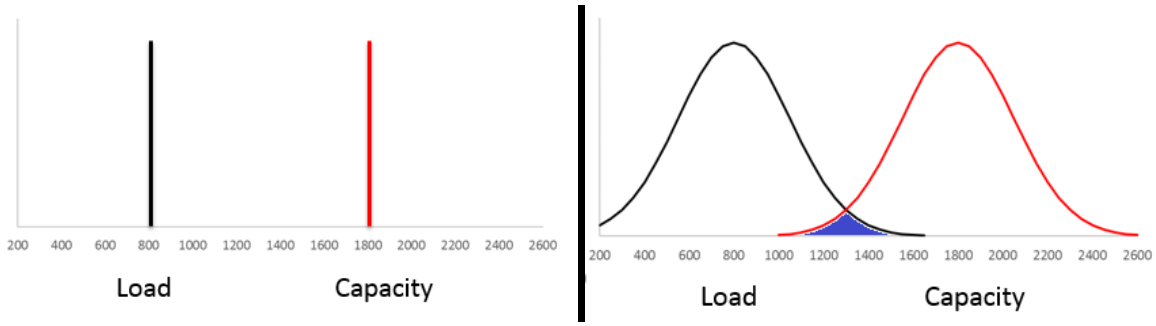


Figure 3.3: Simple representation of load and capability in traditional safety analysis (left) and RISMC (right) analysis. The shaded region in the right plot is where the load exceeds the capacity, exhibiting potential failure risk.

Usually, the capacity distribution does not vary too much from one scenario to another since they are determined by the physical designs and material properties or regulatory safety limits. But distributions of the load will depend on scenarios and RISMC simulation tools are needed to determine the time and scenario-dependent outcomes for a family of accident scenarios. Figure 3.4 shows an example for a family of load and capacity distributions under different accident scenarios. The plot is extracted from the RISMC document by C. Smith et al, 2015 (Smith C. , Rabiti, Martineau, & Szilard, Risk-Informed Safety Margins Characterization (RISMC) Path Technical Program Plan, 2015).

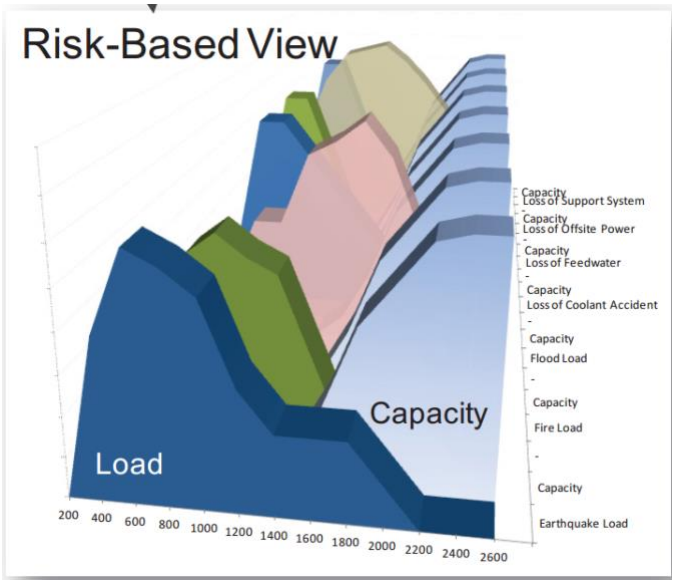


Figure 3.4: Family of load and capacity distributions for different accident scenarios. This plot is extracted from figure 2-4 of RISMC document (Smith C. , Rabiti, Martineau, & Szilard, Risk-Informed Safety Margins Characterization (RISMC) Path Technical Program Plan, 2015).

In recent works (Smith C. , Rabiti, Martineau, & Szilard, Risk-Informed Safety Margins Characterization (RISMC) Path Technical Program Plan, 2015) [3] [4], RISMC has been applied to analyze the risk induced by flooding hazards, and Figure 3.5 shows the corresponding flowchart for tsunami events. RAVEN (Risk Analysis in a Virtual Control Environment) is the statistical package that samples, executes, and evaluates the simulation with uncertain parameters. NEUTRINO, one of the Smoothed Particle Hydrodynamics (SPH) software packages, is applied as the Computational Fluid Dynamics (CFD) tool for simulating the flooding generation, propagation, and interaction with NPP sites. RELAP-7 is the system code designed for the reactor thermal-hydraulics simulation. For the CFD simulation, three-dimensional terrains and building models are constructed by SPH particles for the entire NPP site. Next, multiple full-size and real-time fluid simulations with various initial conditions characterized by RAVEN are performed with NEUTRINO. Event sequences and plant responses, including the dynamic water height, force acting on a certain SSC, and so on, can be extracted for tsunami events. Reference document (Smith C. , Rabiti, Martineau, & Szilard, Risk-Informed Safety Margins Characterization (RISMC) Path Technical Program Plan, 2015) has demonstrated detailed procedures and findings.

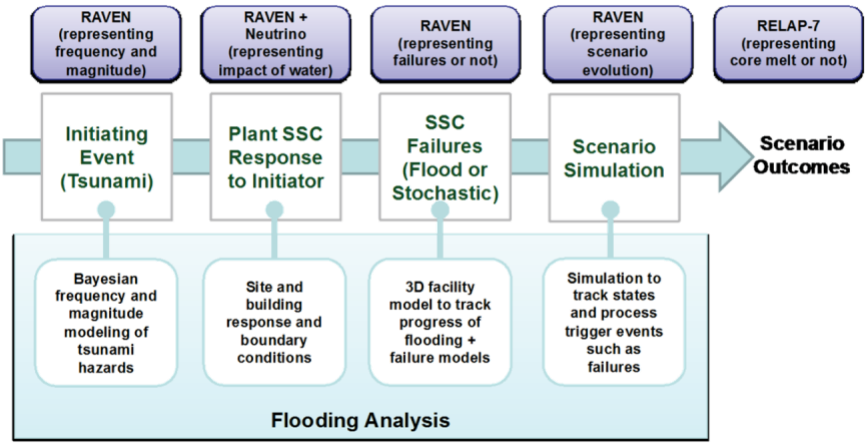


Figure 3.5: Flowchart of applying RISMC in external flooding analysis by C. Smith, et al. (Smith C. , Rabiti, Martineau, & Szilard, Risk-Informed Safety Margins Characterization (RISMC) Path Technical Program Plan, 2015).

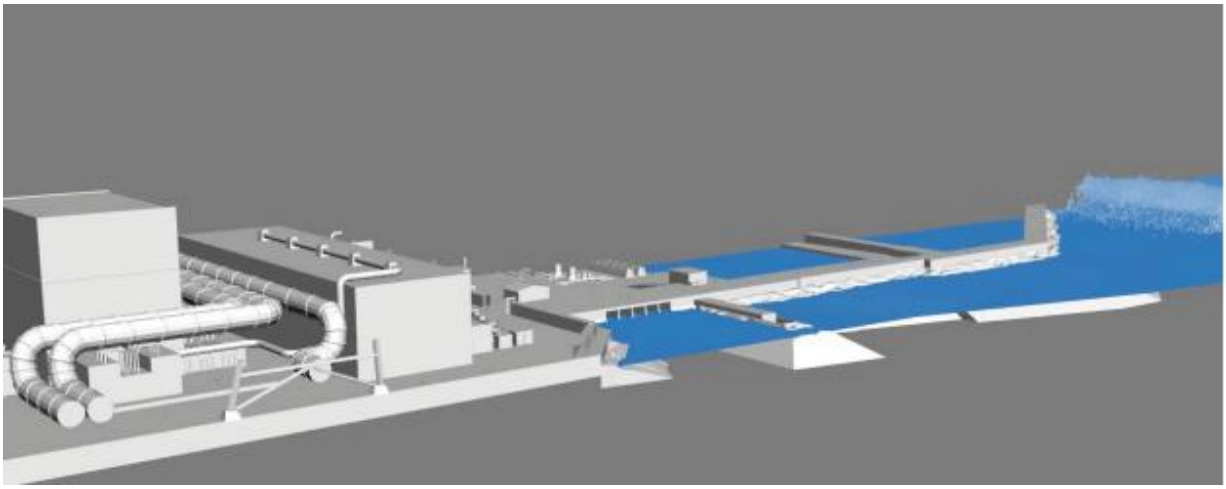

Figure 3.6: NEUTRINO simulation for the tsunami event [5].

Figure 3.6 shows a snapshot of tsunami simulation using NEUTRINO with a ¼ slice of the nuclear facility. The impact of the tsunami, whose wave height ranges from 14 to 38 meter, are determined based on the SPH simulation. Based on the information from NEUTRINO, the system code can predict the thermal-hydraulic status inside the reactor core. The scenario-based and risk-informed safety margin can be obtained for the reactor and facilities using the statistical analysis. Reference document [6] shows the safety margins risk for a Pressurized Water Reactor during the tsunami event. Though NEUTRINO has shown great capability in performing the large-scale fluid simulation, the simulation's credibility or uncertainty remains to be a problem. Some initial assessments have been performed for SPH and NEUTRINO (Smith C. , Rabiti, Martineau, & Szilard, Risk-Informed Safety Margins Characterization (RISMC) Path Technical Program Plan, 2015), however, due to the complexity of physics and phenomenon, a comprehensive validation is still needed to accurately characterize the uncertainty of simulations. What's more, although SPH can be treated as a DNS software, whose accuracy can be improved by refining particles, it is not realistic to perform RISMC analysis with DNS configurations. In addition, for facilities that have much more margins than the code uncertainty, it is not effective to keep pursuing high accuracy.

Therefore, the accuracy of characterized M&S credibility/uncertainty needs to be sufficient but also practical.

### 3.2.2. Model Validation Framework

This section aims to review the previous standards and methodologies for the M&S credibility assessment in the nuclear discipline, including their features, limitations and applications.

**CSAU/EMDAP**

Code Scaling, Applicability, and Uncertainty (CSAU) evaluation methodology is introduced in 1989 [7] to accommodate the revised rule on the acceptance of Emergency Core Cooling System (ECCS) entitled "Emergency Core Cooling System; Revision to Acceptance Criteria". The objective is to provide a practical engineering approach that can quantify the code reliabilities and uncertainties. It's mainly composed by three elements [8]: (1) requirements and code capability; (2) assessment and ranging of parameters; (3) sensitivity and uncertainty analysis; The first element aims to identify the code applicability and potential code limitations for the particular scenarios. This is usually achieved with a phenomenon identification and ranking process, (e.g., Phenomenon Identification and Ranking Table (PIRT) [9]), such that the assessment process can be sufficient and efficient. The product of the first element is a hierarchy of relevant tests for the code validation, including the separate effect tests (SETs), mixing effect tests (METs), and integral effects tests (IETs). The second element aims to assess the capability of the code by comparing simulation results against experimental data. The scaling methodology is needed in this element to guide the development of simulation codes and assess the code scale-up capability. The third element aims to assess the uncertainty due to the code limitations, scaling distortions, data quality, and so on. Usually, the second and third element are performed at the same time and the ultimate product is a simple and direct statement of the code uncertainty or credibility in the primary safety criteria (e.g. the Peak Cladding Temperature (PCT)). For obvious and inevitable limitations in knowledge, a conservative margin is added to compensate for the effect of epistemic uncertainty.

Evaluation Model Development and Assessment Process (EMDAP) is a regulatory guide developed by U.S. NRC [10] for code development and assessment. The objective is to describe an acceptable process of developing and assessing the evaluation models that are used to analyze transient and accident behavior within the design basis of a nuclear power plant. The principle of EMDAP is developed based on the CSAU methodology, while EMDAP has formal and explicit descriptions for most of the assessment process, including the PIRT, evaluation model, assessment base, scaling analysis, and so on. After the validation, the system code will be "frozen" and applied to accident scenario for reactor transient and risk analysis. Though CSAU and EMDAP have a logical and comprehensive structure, the decision process for the adequacy is not explicitly specified, and the judgment is made based on experts' opinion. Therefore, for an individual researcher, it's difficult to conduct EMDAP independently and transparently, and the epistemic uncertainty are easily overlooked. For a group of researchers, problems of expert elicitation become serious and challenging. In addition, though CSAU/EMDAP emphasizes the importance of VUQ, they have a vague classification between the verification and validation. CSAU has been successfully applied to the RELAP-5 simulation code for the Small Break Loss-of-Coolant Accidents of AP600 [11], while EMDAP has not been widely applied.

**Predictive Capability Maturity Model**

Predictive Capability Maturity Model (PCMM) [12] is developed by Sandia National Laboratory and it aims to assess the credibility of M&S tools based on the decision consequence. Comparing to CSAU/EMDAP, PCMM explicitly treats the model credibility/uncertainty assessment as a decision-making process with explicit structures. First, a specific application and the corresponding model is selected. Also,

based on the nature and consequence of the application, requirements and targets can be designated. Next, for the chosen scenario, six attributes are designed and assessed separately: representation and geometric fidelity; physics and material model fidelity, code variation, solution verification, model validation, and uncertainty quantification and sensitivity analysis. At the same time, a qualitative assessment for each attribute is performed based on a PCMM matrix, and it characterizes each attribute with maturity levels. Finally, the model's achieved level is compared against the target level and the decision of validation adequacy can be made. Since the final decision can either be made based on a stringent requirement or a trade-off between the fulfillment and limitation, PCMM can effectively guide the development and validation of M&S tools. In addition, PCMM presents a formal definition for credibility assessment using the maturity level and it also explicitly distinguishes the difference between verification and validation. Though the maturity descriptor of PCMM includes statements of IETs and SETs, the scaling analysis and the hierarchical structure are not explicitly discussed. As a result, the capability of PCMM is limited in validating complex systems with multiple scales, physics, and phenomenon. In 2013, PCMM has been specifically discussed in the report by U.S. NRC [13], which emphasizes the use of maturity for the model credibility assessment. CASL also adopts PCMM for assessing Multiphysics computational tools [14].

In general, previous validation frameworks either do not have a formalized decision model or do not have the capability of scaling. Also, none of them is built on the risk-informed concept. As a result, a new risk-informed framework is needed to better validate the RISMC M&S tools. What's more, the proposed framework should be built based on the best-existing knowledge and show the capability of evolution with new data, information, and knowledge.

### 3.2.3.Data-Driven Modeling and Application

This section aims to review the development of Data-Driven Modeling (DDM), and in fact, the concept of data-driven modeling is not new to the nuclear discipline. For a complicated physical process that has not been fully understood, the classical data-driven approach aims to gain insights and mechanistic understanding of the physics through the data analysis and mining process. Figure 3.7 shows a classical cycle of the modeling process. The cycle usually starts from a specific application, where requirements and specifications are designated for each scenario. At the same time, the prediction made based on the knowledge base is compared against the observation from the application. If the inconsistency is not acceptable, the database will be renewed with more data collection. Next, the data will be "formatted" to information that is valuable and meaningful to the human being for understanding a subject [15] and form an information base. Next, knowledge is extracted from the information based on people's understandings, beliefs, and assumptions, such that a theory/model can be designed for the application purpose. Next, the model prediction from the compact theory/model is again compared to the observation and the consistency is against evaluated. This cycle is repeated until the consistency is acceptable and it usually takes decades to develop a satisfactory model. Moreover, the modeling evolution of this cycle is driven by human's knowledge and capability. Sometimes, data analysis and mining are employed in addition to human efforts for information collection and knowledge abstraction.

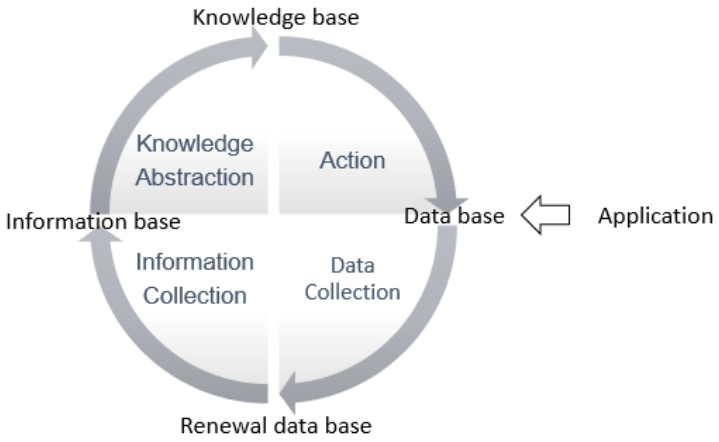


Figure 3.7: Classical cycle of modeling process

In the last few decades, with the rapid growth of computational powers and data availability from high-resolution experiments and high-fidelity simulation, the role of data analysis and data mining becomes more important. Techniques, including calibration and statistical inference, are widely applied for estimating the parameters of deterministic models. Domingos [16] has classified data-driven methods into five tribes based on their learning algorithm and targeting problem (Table 3.).

Table 3.1: Five tribes of data-driven techniques [16].

| **Tribe** | **Targeting Problem** | **Origins** | **Master Algorithm** |
|---|---|---|---|
| Symbolistic | Knowledge Composition | Logic, philosophy | Inverse deduction |
| Evolutionaries | Structure Discovery | Evolutionary biology | Genetic programming |
| Analogizers | Similarity | Psychology | Kernel machines |
| Connectionists | Credit Assignment | Neuroscience | Backpropagation |
| Bayesians | Uncertainty | Statistics | Probabilistic inference |

At the same time, as the statistical inference algorithms become more sophisticated and feasible, it is possible to assimilate and extract information from the large amount of data, like those generated by DNS simulations. In recent years, with the advancement of machine learning, DDM shows potential in extracting and learning knowledge without being explicitly programmed. In a word, the development of statistical inference and machine learning show potential of carrying one or more modeling steps and the reliance on human knowledge is getting less. Depending on the level of involvement for the DDM and human knowledge, a DDM hierarchy structure for the modeling process can be developed based on the data-information-knowledge-wisdom hierarchy by Ackoff [17] and Rowley [18].

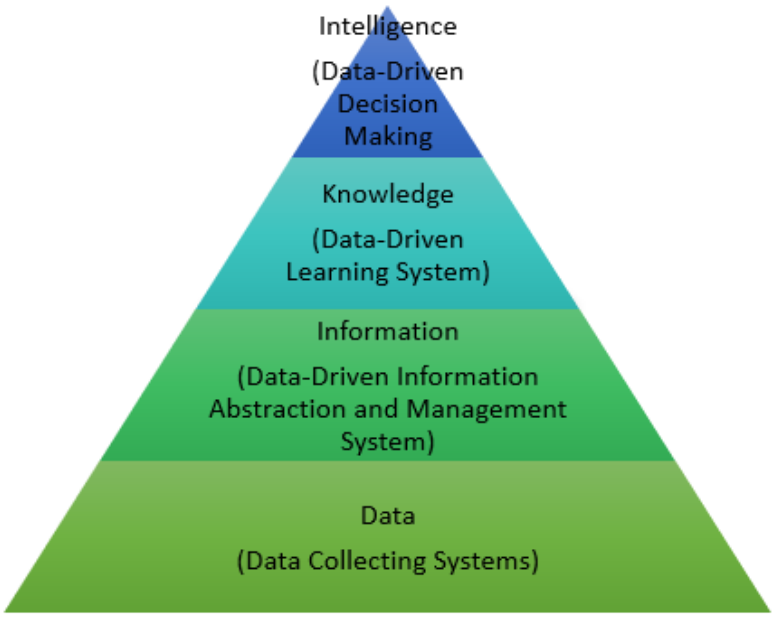


Figure 3.8: DDM hierarchy system modified according to Ackoff [17] and Rowley [18].

In the present nuclear discipline, DDM is mainly used for extracting information from data, including the uncertainty, similarity, and so on. Attempts have been made in the thermal fluid area, especially in the turbulence modeling and the Nuclear System Thermal Hydraulics (NSTH). For turbulence modeling, efforts have been made to accelerate the calculation speed [19] and to improve the accuracy [20] [21]. For the NSTH development, initial works have been performed for classifying the DDM application [22]. Besides, some efforts have been made to recognize and recover the underlying physics from a large amount of data, including constructing the governing equation [23] and closure relations [24] [25]. Although DDM shows excellent potential in information abstraction and knowledge abstraction, the problem of data collection limits its application. In one hand, the quality of nuclear data is not properly guaranteed, where information of experimental setups and uncertainty are poorly recorded. In another hand, the amount of nuclear data is far less than the requirements for "big data" and data gaps are commonly seen in nuclear studies. Therefore, to properly apply DDM in the nuclear discipline, a data collection system with proper requirements on data quality, data amount, and data coverage is needed in addition to the system of data analysis and mining.

One major challenge in validation of nuclear discipline is the data gap. Previously, validation relies on human judgment to bridge the gap and improve confidence. However, such expert-determined process is highly heuristic and takes decades to develop and validate a model. Nowadays, with the rapid growth of computer powers and experimental instruments, a large amount of data is generated by both the high-fidelity simulations and advanced experiments. Also, data analysis and mining are getting more sophisticated and tools like Bayesian inference and machine learning have proven to be successful in many areas. It has become possible to improve the use that we make of data we have (or can obtain) and present a significant shift from the previous expert-determined model development/validation to a new data-driven path. As a result, this study aims to investigate the DDM and its application to model development and validation in the nuclear discipline, especially the Nuclear System Thermal Hydraulics and coarse-grid Computational Fluid Dynamics (CFD).

### 3.2.4.Remarks

This chapter first describes the RISMC technology and its application in the reactor safety analysis, where both accuracy and sufficiency are required. It's claimed that a comprehensive validation is needed to characterize the uncertainty of RISMC M&Ss. The objective is to ensure the reliability of RISMC results, meanwhile, to maintain the M&S efficiency to the best extent. Next, this chapter describes the state of art for the present model validation framework in nuclear discipline, including CSAU/EMDAP and PCMM. By comparing the requirement of risk-informed technology against the capability of existing validation methodologies, it's found that the practical gaps/challenges are too large to apply conventional validations. Next, the recent development and applications of DDM for the M&S in the nuclear discipline. To properly assess the uncertainty/credibility of the RISMC M&S tool, a new validation framework is needed based on the current best knowledge, including the decision theory, scaling analysis and DDM. In addition, risk-informed technology should be incorporated into the proposed validation framework.

## 3.3. Technical Developments

This chapter aims to demonstrate the development of Risk-Informed Evaluation Model Development and Assessment Process framework, including the central concept, present progress of key technologies/methodologies, and recommendations from the expert group.

### 3.3.1. Concept of Sufficient Accuracy

To validate selected RISMC simulation tools, a validation framework is needed for uncertainty quantification and scaling. In the EMDAP framework, the M&S is "frozen" for the specific scenario after the validation. However, model forms and parameters of RISMC tools are subject to change since efficiency is another important consideration in addition to accuracy. Moreover, since RISMC analysis aims to evaluate the reactor's safety margin during external hazards, the uncertainty is significant and the result is subjective. Under such conditions, the way that traditional frameworks validate the M&S by characterizing one single error number is not very meaningful. Indeed, reducing the number of error implies better accuracy, but the work becomes more complicated and less scrutable. Even though the simulation error appears to be acceptable or far less than the criteria for a specific large-scale scenario, the credibility of the M&S remains suspicious. As a result, this study proposes the concept of sufficient accuracy that aims to adapts the accuracy requirements according to scenarios and tools' limitations. In this study, the "accuracy" of a simulation result is represented by the maturity level that is characterized by errors and the "sufficient" is characterized by the utility on the M&S maturity. The utility on the model maturity is assessed based on the expect rewards by multiplying the reward function by subjective beliefs. The rewards function depends on the consequence and human preference on each level, while the subjective belief is assessed with validation metrics and expert elicitations. Note that the concept of sufficient accuracy has many commons with the risk-informed or risk-oriented concept. Therefore, validation adopting such concept can be claimed as a risk-informed validation. Further, to ensure the reliability and avoid confusion, it's required that the sufficient accuracy and its analysis are transparent, complete, consistent and improvable.

Table 3.2: Example of reward levels and their meaning. The reward function ranges from 0 to 1.

| Expected Rewards | Characteristics |
|---|---|
| 0.9 | The uncertainty of M&S is well characterized and successfully maintained at a very low level for the application purpose. |
| 0.5 | The uncertainty of M&S is partially characterized and successfully maintained at a reasonable level for the application purpose. |
| 0.1 | The uncertainty of M&S is poorly characterized and likely to amplify for the application purpose. |

Sufficient accuracy has two sub-attributes: acceptance domain and bounded error. The acceptance domain is assessed by on the scenario and requirement, while the bounded error is characterized based on the discrepancy between the model prediction and the true value. Table  shows their definition and features.

Table 3.3: Definition and notation for sufficient accuracy, acceptance domain and bounded error.

| **Terminology** | **Definition** | **Notation** |
|---|---|---|
| Sufficient Accuracy | A risk-informed concept for M&S validations by adapting the accuracy requirements according to scenarios and tools' limitation | The sufficient accuracy is the theoretical basis for the risk-informed validation framework. It is designated for situations where the effect of uncertainties are dominant. The "sufficient" is measured by the utility on the model accuracy. It requires the validation to be transparent, complete, consistent and improvable. |
| Acceptance Domain | An accuracy requirement for simulating the generation, propagation, and interaction of accident scenarios | The acceptance domain is inherited from the concept of sufficient accuracy and arisen from the application requirements. Other than the practical consideration, no explicit restriction is placed on the acceptance domain. |
| Bounded Error | An error analysis for the M&S based on the discrepancy between the model prediction and the true value | The bounded error is inherited from the concept of sufficient accuracy and estimated by comparing the model prediction against the true value or high-fidelity data. The bounded error has to be consistent, therefore, the analyzing process should be transparent, complete and robust. |

Comparing to the accuracy concept in traditional validations, the sufficient accuracy has three major differences. First, it aims to establish that the belief is high enough to regard the M&S as a tool of certain maturity rather than seeking the precise error. Though such concept appears to be trivial when conservative treatment is available, it avoids the excess conservatism while maintains convincing. This conservatism suggests that sufficient accuracy has to be transparent, while the convincement suggests that the analysis (of both logical and evidential) towards the sufficient accuracy should be complete. Second, it clearly separates the aspects of well-posed error/discrepancy calculation and the aspects of human confidence that are subject to large variations. The former aspect can be classified as a "causal relation" that is deterministic and obtained by direct comparisons. The latter one is "intangible" that is probabilistic depending on the scenario and human articulates. As a result, this requires a properly document for human articulates. Also, a robust and consistent process is needed for making confident decision regarding the M&S accuracy. Third, the concept of sufficient accuracy focuses on the area where large uncertainties exist. Instead of qualitatively defining the model credibility, the sufficient accuracy aims to bound the uncertainty. Therefore, as uncertainties being reduced, the process guided by sufficient accuracy should be improved. In conclusion, this study proposes a risk-informed validation framework that is transparent, complete, consistent, and improvable. To ensure the logical completeness and consistency, the framework is suggested to be built upon the existing studies.

### 3.3.2. RISMC Model Validation Methodology

Risk-Informed Evaluation Model Development and Assessment Process (REMDAP) is a validation framework first proposed by Dr. N. Dinh, et al. [26] in the project of "Development and Application of a Data-Driven Methodology for Validation of Risk-Informed Safety Margin Characterization Models." The objective is to "provide a mathematically defendable basis for calculating biases and their uncertainties for a wide range of operating conditions that represent the intended range of model application" by combining the CSAU/EMDAP methodology with advanced DDM methods, including Reduce Order Modeling (ROM) [27], Simulation-Based Scaling (SBS) [28], Validation Data Planning (VDP) [29], and Validation Data

Management System (VDMS) [30]. Figure 3.9 shows the advanced methods and tools to facilitate the implementation of already demanding EMDAP in a risk-informed application. Orange boxes represent methodologies that will be developed in this project and their task number.

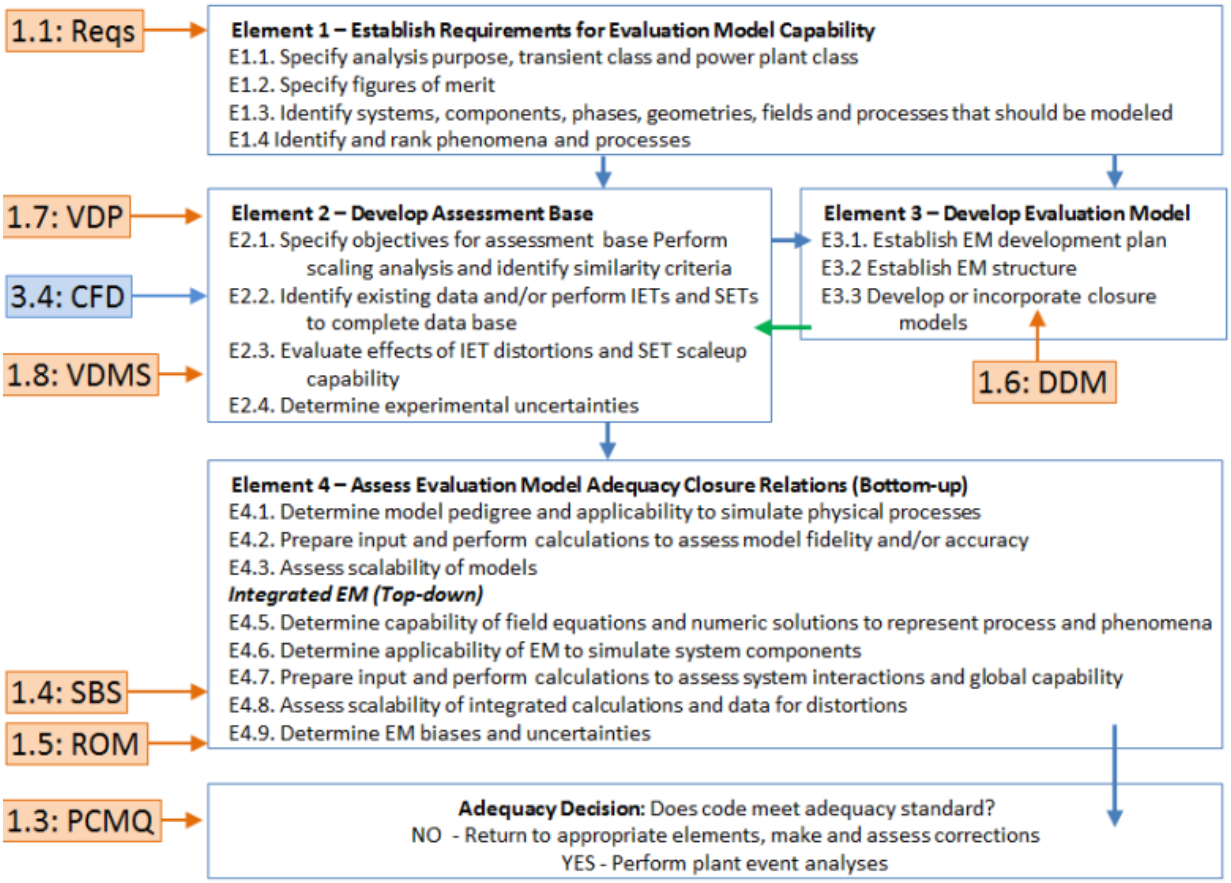


Figure 3.9: Risk-informed Evaluation Model Development and Assessment Process. Orange boxes denote developments in the project and indicate EMDAP elements where the advances are expected to impact [26].

The present section discusses and demonstrates the progress of Task 1.3, Task 1.6, and Task 1.7. Details of Task 1.3 and Task 1.7 have been initially addressed in a previous milestone report [31], this study will further develop the PCMQBN framework by constructing guidance for the R/S/U (Relevance/Scaling/Uncertainty) grading system. Also, this study will discuss the present development on the robustness of PCMQBN. Task 1.6 DDM is the most critical and challenging problem since it presents a significant shift from the current approach of expert-driven to data-driven analysis and this project aims to prove its feasibility. Presently, the DDM is applied to two elements: closure development and uncertainty quantification. The data-driven closure development aims to construct or calibrate closure models with data-driven techniques, while the data-driven UQ seek s to evaluate the uncertainty of simulation. Furthermore, the data-driven UQ has two approaches: the global approach aims to evaluate the uncertainty of NSTH codes like Cobra-TF, where closures and correlations are assumed to be the major uncertainty source; the local approach aims to evaluate the uncertainty of Coarse-Grid CFD code like NEUTRINO, where each element is the source of uncertainties. Presently, this study demonstrates some initial developments of classifying methodologies based on assumptions and conditions, the objective is to identify the feature and create an initial proof-of-concept for applying Data Driven Modeling (DDM) in the model development and validation process.

Figure 3.10 shows a tentative structure of the REMDAP framework according to the present methodology development. Elements #1 - #4 are inherited from the EMDAP framework, while new components, including data-driven closure development, data-driven validation and PCMQBN are developed and included. Element 1 and 2 are the same as EMDAP process, and a similar procedure should be followed. For element 3, the data-driven closure development is incorporated. Techniques, including machine learning and statistical inference, are used for the model construction. At the same time, the data-driven concept is also employed in the model assessment process by quantifying the simulation uncertainty, and two approaches are developed for the system code and coarse-grid CFD separately. If models are consistent and uncertainties are bounded by an acceptable range. The uncertainty information will be fed into the PCMQBN framework for the model maturity analysis. The code adequacy, represented by the probabilistic maturity level, will guide the M&S credibility decision. If the achieved credibility has reached the target level, a robustness test will be performed to ensure the robustness of the validation process. Next, the similar validation process will be performed multiple times with different combination of model forms, model parameters, and computational resources. Finally, a function of the M&S credibility against model forms, model parameters, and computational costs will be constructed, based on which model suggestions will be made for the full-scale safety analysis. For cases that fail to satisfy the criteria or has a major issue like model inconsistency or unbounded error, information will be fed to the validation data plan and guide the update of validation database and evaluation models.

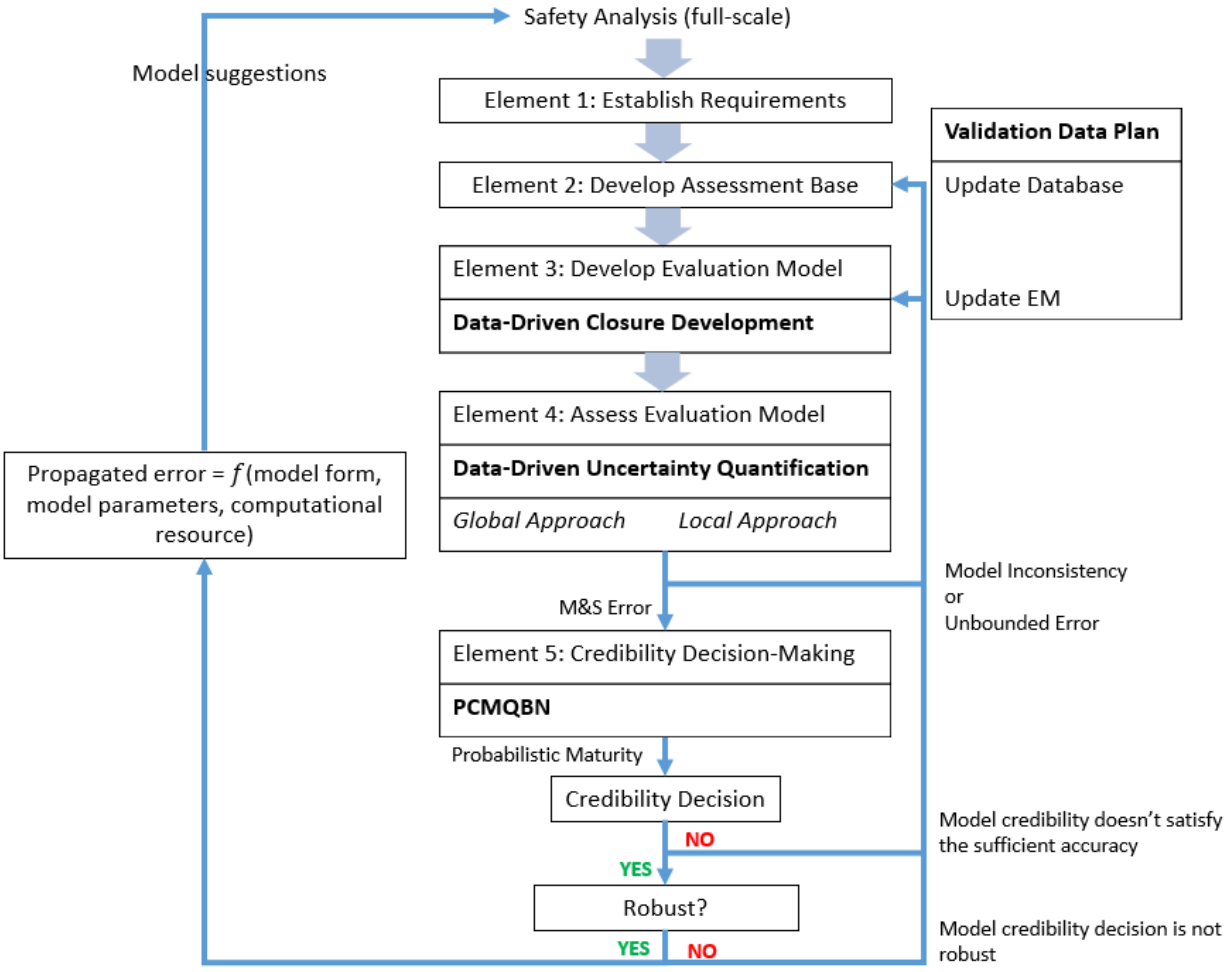


Figure 3.10: Schematic flowchart of REMDAP framework (tentative). The innovative methodologies/techniques are bolded.

Comparing to the EMDAP process, the information flow and element 1 & 2 are maintained. Element 3 and 4 have been greatly simplified and only essential components that have data-driven concept are included since the project aims to demonstrate the feasibility of the data-driven and risk-informed concept in the validation. Scaling analysis is not explicitly discussed, but it's performed as part of the data-driven UQ. The adequacy decision of EMDAP has been rebuilt into a new decision-making element. Moreover, in addition to the model credibility decision, REMDAP also requires a sensitivity study for the decision-making such that the final decision can be robust.

### 3.3.3. Progress of the Key Technology/Methodology

This section aims to demonstrate the progress of crucial methodologies in the present REMDAP framework. For each methodology, assumptions, objective, technical approach and illustrative examples are provided.

**Data-Driven Closure Development**

With the rapid growth of computer powers, data-driven techniques, especially statistical inference and machine learning, have been continuously gaining success in the computer vision and healthcare. Machine learning, especially the deep learning technique, has shown to be more capable than human contestants in the area of image processing, pattern recognition, and so on. Inspired by such successes, researchers have been trying to apply machine learning in closure model developments. The expectation is that machine learning can help researcher identify the essential physical features from the data, and thus shorten the model development cycle. Recently, general guidance for machine-learning-based data-driven closure development has been developed by Chang et al [22] for the NSTH. Figure 3.11 shows his schematic workflow for the NSTH closure development using supervised machine learning. $\boldsymbol{X}$ represents the input flow features, $\boldsymbol{Y}$ represents the targets associated with the input flow features, $k$ represents the $k_{th}$ measurement for a single flow feature point. Both inputs and targets will be fed into the machine-learning engine. After sufficient training, a NSTH closure will be developed.

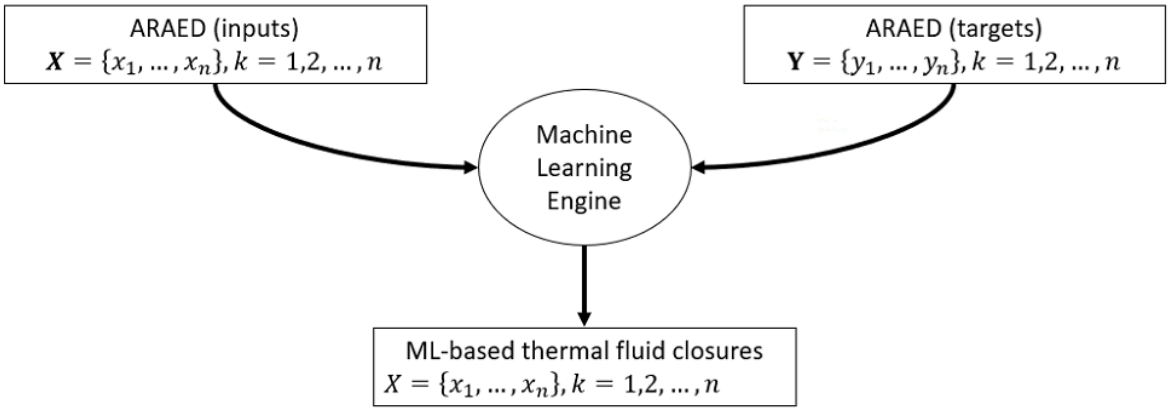


Figure 3.11: Schematic workflow of data driven NSTH closure development using machine learning by Chang et al. [22]

Detailed information for each type can be found in the reference document [22]. Until now, machine-learning-based data-driven closure development has been used in constructing single-phase turbulence models [20] [21] and simple two-fluid models [24] [25]. Ling et al. [32] evaluates the predictive capability of different machine learning algorithms for predicting the averaged Navier-Stoke uncertainty in a high Reynolds region.

The present study mainly investigates the application of statistical inference and machine learning algorithm in data-driven closure development process. To adapt the concept of sufficient accuracy and investigate the feature of various types of development process, this study classifies the present closure development methods into two types. Table  shows a summary of two types of methods, including their assumptions and master algorithms. Compared to the parametric model, the nonparametric model makes fewer assumptions and requires no priori information [33]. Therefore, the nonparametric model is more robust and simpler, however, it requires a large amount of data to draw a confident conclusion. In many application, the parametric and nonparametric form are mixed [34] but mathematically transferring them from one to another remains challenging.

Table 3.4: Summary of closure development techniques

| **Closure Development** | **Assumption** | **Master Algorithm** |
|---|---|---|
| Parametric | 1. Fixed model form,<br>2. The errors are normally distributed,<br>3. Random variables are independent and identically distributed. | Maximum Likelihood Estimation.<br>Bayesian Inference. |
| Nonparametric | Two unspecified continuous distributions are identical | Neural Network.<br>Gaussian Process. |

An illustrative example is prepared to demonstrate the feature and difference between two types of methods. This example assumes that the closure is a correlation for the Nusselt number with respect to Reynold and Prandtl number. It's also assumed that the data from Petukhov correlation [35] is high-fidelity and they will be used as the training data. By employing a deterministic correlation as the training data source, the effect of data amount and data bias on the closure quality can be illustrated. For the parametric method, a fixed form of Dittus-Boelter correlation is employed, while for nonparametric method, the neural network is used. Since neural network randomly generates the initial weight and bias, which will be updated by the optimizer, multiple (100 times) training is performed with a sequence of random number and a mean value of all training results is used. This example uses Mean Squared Error (MSE) to measure the quality of model prediction. Figure 3.12 shows the plot of MSE for closures constructed by both methods. As more data is used for training and calibration, the MSE value reaches the asymptotic range for all types of methods. It's also found that a similar error is obtained from the Bayesian Inference and Least Squared Error since the closure's quality is limited by the fixed model form. In addition, the MSE from the neural network can be reduced to a very small value ($10^{-3}$). What's more, both closures are sensitive to the amount of data. However, when the data amount is small, the neural network tends to have larger error than the parametric error. In the appendix document (Appendix B) by Zachry Inc., it's also suggested that machine learning algorithm like neural network has the problem of overfitting.

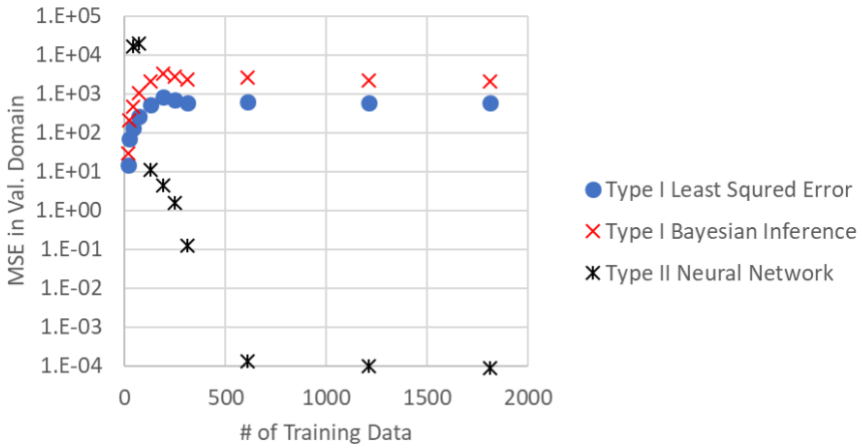


Figure 3.12: Mean Squared Error (MSE) of closures constructed by parametric and nonparametric methods.

**Data-Driven Uncertainty Quantification**

This session demonstrates the study of data-driven Uncertainty Quantification (UQ), and the objective is to accurately quantify and propagate the simulation error. This study classifies the data-driven UQ methods into two types: the global data-driven UQ and the local data-driven UQ. Table  shows the summary of two types of methods that are underdeveloped.

Table 3.5: Summary of data driven UQ

| **Data-Driven UQ** | **Assumption** | **Targeting Problem** | **Master Technique** |
|---|---|---|---|
| Global Approach | Closure models are the major source of uncertainty | Model Form and Parameter Error | Forward/Inverse UQ |
| Local Approach | | Discretization Error, Model Form, and Parameter Error. | Physics-Informed Machine Learning |

Although Data-Driven UQ aims to propagate/predict the simulation uncertainty, it's more straightforward and feasible to compare the corrected simulation result against the real result rather than comparing the predicted uncertainty against real uncertainty. In addition, most of the present validation metric is designed for estimating the credibility/uncertainty of simulation result rather than the credibility/uncertainty of uncertainty. Therefore, the quantified uncertainty will be substituted back to the simulation and the corrected result will be compared against the real value to test the applicability of proposed methods.

*Global Data-Driven Uncertainty Quantification*

By assuming closure models are the major source of uncertainty, the global data-driven UQ aims to quantity the uncertainty induced by the closure model. The simulation is assumed to be well-verified before this process. Therefore, the capability of global approach is limited to the model error quantification, including the model form and model parameters. In this study, the global approach is designed for the system code of Cobra-TF. Figure 3.19 shows workflows for the inverse UQ component of the global approach. Note that the global approach calibrates the model based on the quantity of interest, therefore,

the field data from the CFD or system code simulation needs additional processing. In addition, the result of uncertainty quantification depends on the selection of validation metrics. In addition, since inverse UQ usually requires a sampling process, to save computational resources in complex problems, methodology of Reduced Order Modeling (ROM) is used to construct a surrogate model for the solver. As another major methodology developed by the data-driven project, detailed discussions will be prepared in a separate report. After the inverse UQ, uncertainties of model parameters and forms will be propagated by perturbing their values according to the known distribution.

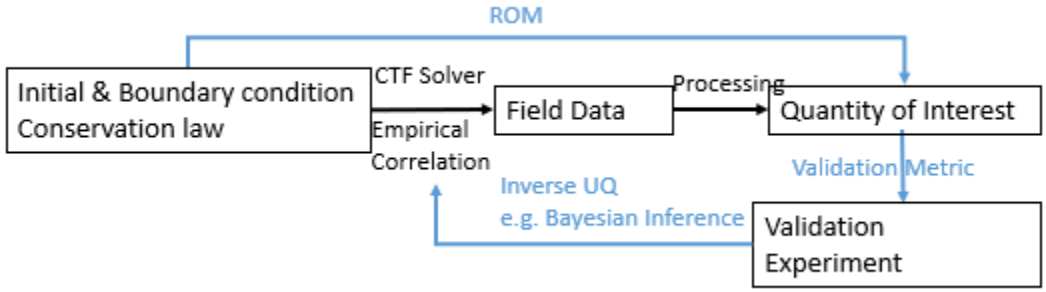


Figure 3.13: Schematic workflow for the global approach of data driven UQ.

To demonstrate the application of global approach, an illustrative example is prepared and the objective is to quantify the parameter uncertainty of Dittus-Boelter correlation. Also, the uncertainty of a machine-learning-based model is analyzed. This example assumes that the data from Petukhov correlation is high-fidelity and Bayesian inference is used for quantifying the parameter uncertainties based on data from validation domain. Next, the quantified uncertainty will be propagated to the application domain. Figure 3.14 shows the coverage mapping of model inputs variables, including the Reynolds (Re) and Prandtl (Pr) number. The red region represents the validation domain, while the region with blue diagonal stripes represents the application domain. In addition, the application domain fully covers the validation domain.

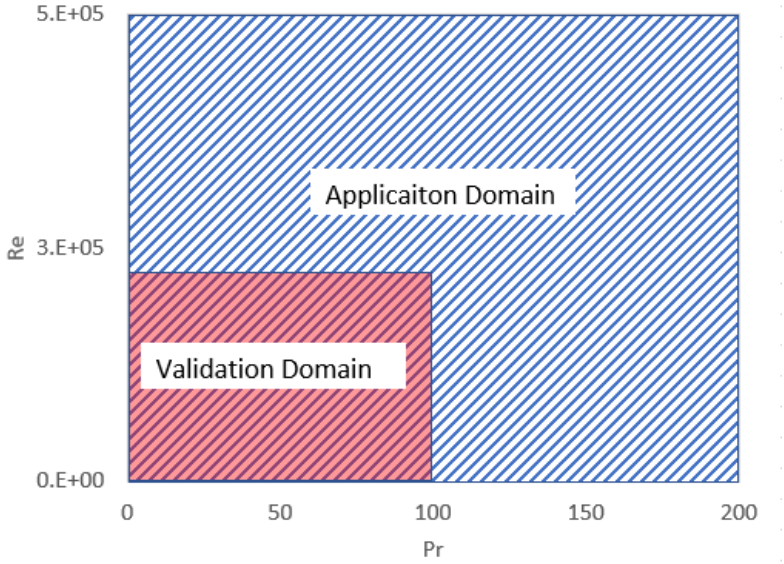


Figure 3.14: Coverage mapping of input variables.

Figure 3.15 shows the plot of MSE for the Dittus-Boelter correlation and the machine-learning-based closure in the application domain. It's found that the error reaches the asymptotic range in the application and increasing the number of training data will not change the error. However, comparing to the error in the validation domain (Figure 3.12), uncertainties of both parametric and nonparametric methods are

amplified in the application domain. And the amplification turns to be much higher for the machine-learning-based closure (nonparametric method) than the Bayesian inference or least square error (parametric method). As a result, the problem of data gap remains challenging even with sophisticated data-driven closure development and pursuing high accuracy is very likely to induce large scaling distortion.


Figure 3.15: MSE of Dittus-Boelter correlation and machine-learning-based closure in the application domain.

Moreover, this study performs the same example with the metric of confidence interval and the closure quality is measured by the percentage of real values being bounded by the 95% confidence range of closure predictions. Figure 3.16 shows the plot of bounded percentage for closure constructed by both types of data-driven methods. Comparing to the MSE, a similar trend of converge is found. However, the confidence ranges from Bayesian Inference bounded more real data points than the one from Neural Network. The reason is that the uncertainty from Bayesian inference is much larger than the one form Neural Network (refer to Figure 3.12). Such finding again indicates that pursing higher accuracy is likely to result in large distortion when there is a data gap.


Figure 3.16: Percentage of real values being bounded by the 95% confidence range of model prediction in the application domain.

The effect of data bias is also investigated by introducing constant error to the high-fidelity data. In this study, the error is introduced in two ways: total fractional error by adding a constant fractional error to the high-fidelity output (Nu); parameter fractional error by adding a constant fractional error to the high-fidelity input (Re, Pr). Figure 3.17 shows how data bias influences the model quality and it's found that as more bias is introduced, the model quality keeps deteriorating. Although the data bias has a significant effect on the closure quality, there is rarely an effective way of analyzing or avoiding the bias. However, it's important that the information of high-fidelity data, especially the uncertainty information, needs to be properly characterized and recorded. Otherwise, a poorly documented low-quality data can induce terrible and irreversible effect on the quality of closures and simulations.

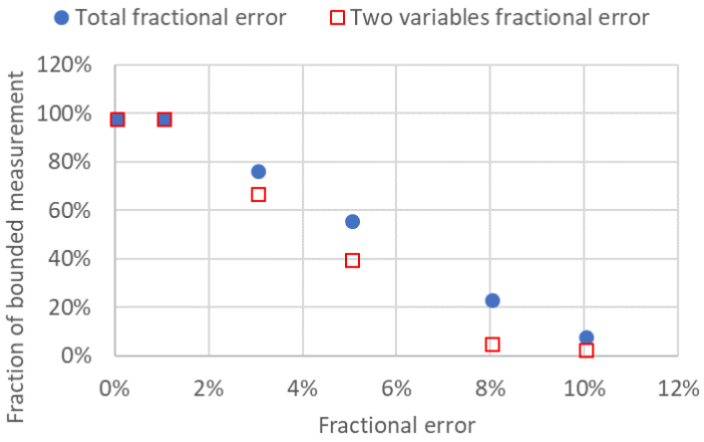


Figure 3.17: Effect of data bias on the percentage of real values being bounded by the 95% confidence range of model prediction in the application domain.

Another successful application of global approach for complex problems is the Total Data Modeling Integration (TDMI). In addition to the data-driven UQ, TDMI also has the component of surrogate construction, sensitivity study and closure evaluation. Figure 3.18 shows its complete workflow for the multiphase CFD application. It is first proposed by Bui et al [36] and the objective is to calibrate models of multiscale and multi-physics phenomena in thermal hydraulics. The master methodology of TDMI is inverse UQ, where uncertainties of model are inferred according to experimental measurements. Compared to the traditional method, TDMI is based on a strategy of model-data integration, where all models are simultaneously analyzed and calibrated using multiple sets of data from various scales. In addition to the model parameters, recent developments also aim to characterize and calibrate the model form error [37] [38]. Figure 3.18 shows Liu's schematic workflow of TDMI for validating a MCFD code.

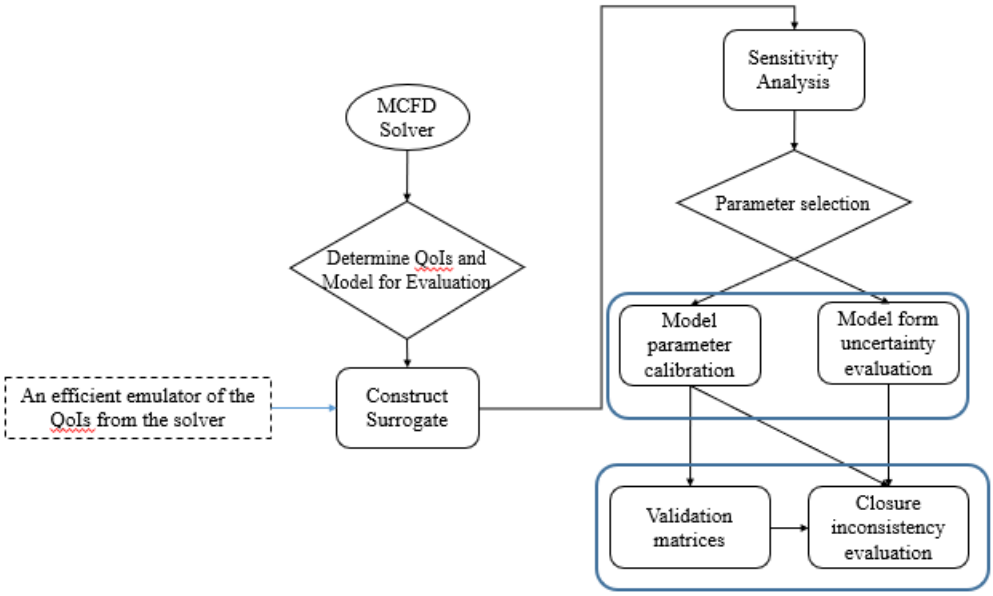


Figure 3.18: Schematic workflow of TDMI framework for validating the Multiphase CFD (MCFD) by Liu [34].

*Local Data-Driven Uncertainty Quantification*

For the local approach, since no explicit assumptions are made for the uncertainty source, it shows more capabilities than the global approach. Figure 3.19 shows the schematic workflow for the local approach of data-driven UQ. Different from the global data-driven UQ, the local approach targets at the field data directly and objective is to estimate the simulation uncertainty of field data. Therefore, the data from each calculation element will be extracted and analyzed.

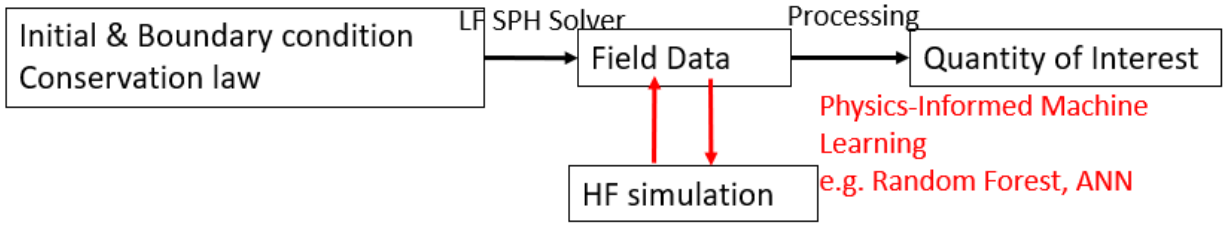


Figure 3.19: Schematic workflow for the local approach of data-driven UQ

In this study, the method of Physics-Informed Machine Learning (PIML) is used for the local approach and it is mainly designed for the coarse-grid SPH simulation. PIML has first been proposed for characterizing the simulation error of each computing element that is induced by turbulence models [20] [21]. The objective is to construct a surrogate model between the simulation error and the physical features.

$$\varepsilon_{d,V_i}(\vec{\boldsymbol{v}}_i) = \vec{\boldsymbol{v}}_i(HF) - \vec{\boldsymbol{v}}_i(LF) \qquad \text{Eq. 3.1}$$

In the previous work, it is assumed that the targeting simulation has reached the grid convergence range. However, since it is challenging to ensure grid convergence for large-scale simulations, especially when there are additional closures, the grid assumption is not employed in this study. Since the local approach targets at coarse-grid SPH simulations, one challenge is that the high-fidelity data is obtained from mesh-

based simulation. A mapping method is needed to transfer the field data (pressure, velocity, energy) from Eulerian method to Lagrangian method. In this study, a simple averaging method is used by assuming that each particle has a stable size the properties in the particle volumes are approximately the same.

To demonstrate the application of the local approach, an illustrative example is prepared, and the objective is to demonstrate how PIML predicting the uncertainty of SPH in simulating the velocity field. A lid-driven simulation is constructed with LAMMPS-SPH and OpenFOAM, where OpenFOAM is used as the source of high-fidelity data. Multiple simulations with different configuration are constructed and Table shows the ID and setups for each simulation. Currently, only the dynamic viscosity is changed, therefore, the Reynolds number is used to characterize each case. To test the applicability of PIML, it will be trained with selected cases, named as training sets, and applied to other cases, named as application sets.

Table 3.6: Summary of simulation ID and configurations. Dynamic viscosity is currently the only variables being changed.

| **ID** | $\delta r$ | $\nu$ | $Re$ |
|---|---|---|---|
| **dp1** | 0.02 | $10^{-3}$ | 1000 |
| **dp8** | 0.02 | $5 \times 10^{-4}$ | 2000 |
| **dp4** | 0.02 | $2 \times 10^{-4}$ | 5000 |
| **dp6** | 0.02 | $10^{-4}$ | 10000 |

First, the high-fidelity mesh-based simulation data need to be mapped to the SPH simulation. A simple averaging method is used and Figure 3.20 shows the velocity comparison for the original SPH, mapped SPH and the reference simulation by STARCCM. After the mapping, the target variables are calculated by Eq. 3.1.

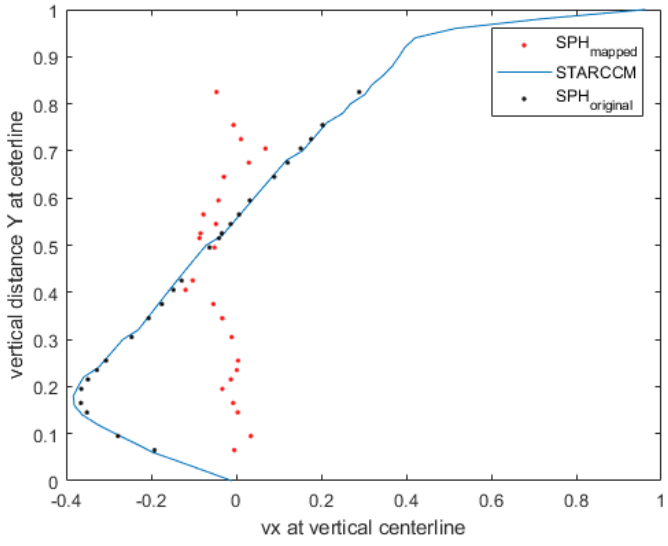


Figure 3.20: Comparison of $V_x$ at the vertical centerline.

Next, based on the SPH equation for velocity calculation and the theoretical analysis for the truncation and discretization error, five physical features are selected as the input variables (Eq. 3.2) of PIML. For a two-dimensional simulation, each physical feature is propagated to two direction and there will be ten features in total.

$$\left(\vec{F}_p\right)_i ; \left(\vec{F}_v\right)_i ; \vec{v}(\boldsymbol{r}_i) \sum_j w_h(\boldsymbol{r}_i - \boldsymbol{r}_j) V_j ; \nabla \vec{v}(\boldsymbol{r}_i) \sum_b w_h(\boldsymbol{r}_i - \boldsymbol{r}_j) \cdot (\boldsymbol{r}_i - \boldsymbol{r}_j) V_j ; \boldsymbol{r}_{i_{wall}} \quad \text{Eq. 3.2}$$

Next, both input features and target variables are fed into the machine-learning engine and the simulation error of velocity is predicted for each particle. To characterize the accuracy of PIML for SPH application, the SPH's velocity field is corrected based on the predicted error by substituting the error into Eq. 3.1. The corrected velocity is then compared against the high-fidelity data and L2 relative error norm is used as the comparing metric. As a result, if the corrected L2 error is less than the original simulation, it can be claimed that PIML can predict the simulation error of velocity. Table  shows a summary of all cases, including their training datasets, application datasets, error of corrected velocity field based on the PIML result, and error of original SPH velocity field. For both case studies, it can be found that except for the PIML trained by the first training set, which has the most distant Reynolds number from the application dataset, all other PIMLs successfully predict the error of field data. It is also found that as more datasets are used for training, the error of corrected fields becomes smaller. For case study #2, as the Re of training set becomes closer to the application set, the error of corrected field gets smaller.

In addition to the random forest machine-learning engine, this study also tests the neural network engine. It turns out that random forest is faster and more robust than the neural network, however, the error reduction with respect to the data amount is more obvious for the neural network.

Table 3.7: Summary of PIML results with Random Forest as the machine-learning engine.

| Case Study | Training Set Re | Application Set Re | Error of Corrected Fields | Error of Original Fields |
|---|---|---|---|---|
| #1 | 10000 | 5000 | $4.54 \times 10^{-4}$ | $4.31 \times 10^{-4}$ |
| | 1000+10000 | | $3.23 \times 10^{-4}$ | |
| | 2000+10000 | | $3.44 \times 10^{-4}$ | |
| | 1000+2000+10000 | | $3.23 \times 10^{-4}$ | |
| #2 | 1000 | 10000 | $6.10 \times 10^{-4}$ | $5.37 \times 10^{-4}$ |
| | 2000 | | $4.88 \times 10^{-4}$ | |
| | 5000 | | $3.99 \times 10^{-4}$ | |
| | 1000+2000 | | $4.44 \times 10^{-4}$ | |
| | 1000+5000 | | $4.18 \times 10^{-4}$ | |
| | 2000+5000 | | $3.74 \times 10^{-4}$ | |
| | 1000+2000+5000 | | $4.00 \times 10^{-4}$ | |

**Predictive Capability Maturity Quantification & Bayesian Network**

Predictive Capability Maturity Quantification Bayesian Network (PCMQBN) is a decision framework that can quantitatively measure the model credibility with maturity level and subjective belief. Next, with a synthetic reward function, the decision regarding the selection of models and parameters can be made by maximizing the expected rewards. The conceptual development has been included in a separate report [31]. This study aims to demonstrate the new development on the R/S/U grade and Bayesian sensitivity study.

***R/S/U Grade***

In PCMQ framework, data attribute of data applicability is determined based on the qualitative Relevance/Scaling/Uncertainty grade, where the uncertainty (U) measures the data uncertainty due to instrumentation errors and limited resolution of measurement instruments. However, there is no explicit guidance for evaluating and assigning the grading number to each attribute. As suggested by the previous study on the effect of data bias (Figure 3.17), a proper document of data is crucial to the development and

quality of closures. Therefore, recent developments have focused on designing a guidance for the uncertainty (U) grade, while the other two attributes remain to be investigated. Table  shows the present guidance of specifying uncertainty grade.

Table 3.8: Guidance for specifying the uncertainty grade in the R/S/U grade system.

| **Data Type** | **Uncertainty Grade** | **Description** |
|---|---|---|
| Type I | <U>=1 | Largely biased data |
| Type II | <U>=2 | No uncertainty information |
| Type III | <U>=3 | Either the model prediction or the high-fidelity data has uncertainty information |
| Type IV | <U>=4 | Both the model prediction and the high-fidelity data have uncertainty information |

To better use the data uncertainty information, various validation metrics are needed. Table  summarizes most of the popular validation metrics in the engineering discipline.

Table 3.9: Summary of validation metrics and their applicability to each type of data.

| **Validation Metric** | **Type II** | **Type III** | **Type IV** | **Range** |
|---|---|---|---|---|
| *Deterministic Metric* | | | | |
| Root Mean Square Error | ✔ | | | $[0,\infty)$ |
| Euclidean Distance | ✔ | | | $[0,\infty)$ |
| Normalized Euclidean Metric | | ✔ | | $[0,\infty)$ |
| Mahalanobis Distance | | ✔ | ✔ | $[0,\infty)$ |
| *Probability-based Metrics* | | | | |
| Confidence Interval | | ✔ | | |
| Kullback-Leibler Divergence | | | ✔ | $[0,\infty)$ |
| Symmetrized Divergence | | | ✔ | $[0,\infty)$ |
| Jensen-Shannon Divergence | | | ✔ | $[0,\ln 2]$ |
| Hellinger Metric | | | ✔ | [0,1] |
| *Hypothesis Testing* | | | | |
| Kolmogorov-Smirnov Test | | ✔ | ✔ | [0,1] |
| Total Variation Distance | | | ✔ | [0,1] |

To demonstrate the applicability of this grading system, the illustrative example of section 2.3.2 is prepared with a simple PCMQBN structure (shown in Figure 3.21). The goal is to estimate the model credibility in the application domain in Figure 3.14 based on the result in the validation domain. The maturity level of validation result is estimated according to the MSE from machine-learning based closure

(Figure 3.15) in the validation domain, while the maturity level of code adequacy is measured according to the MSE in the application domain.

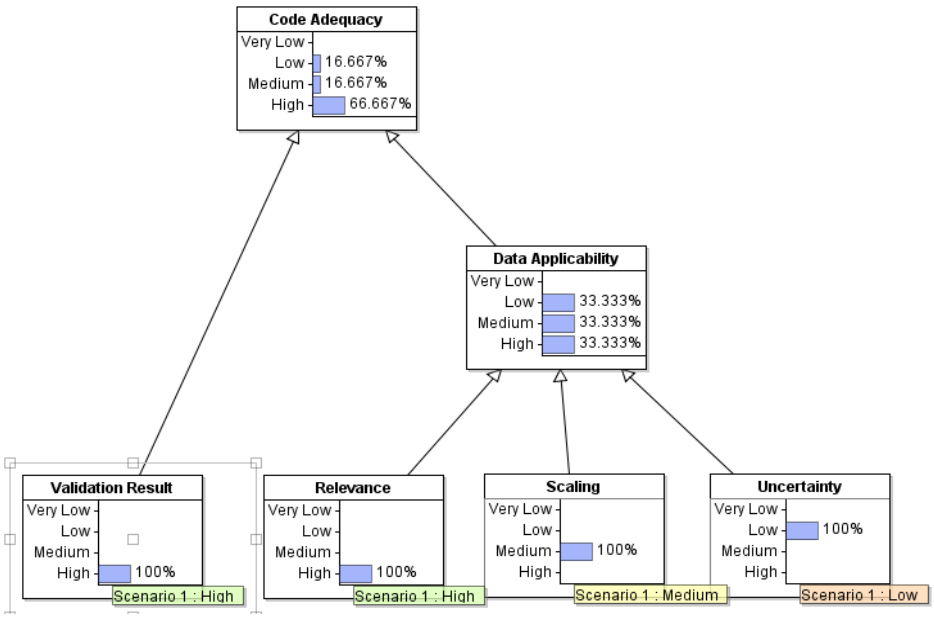


Figure 3.21: Illustrative example with a simple PCMQBN structure.

Table  shows the range of outputs from validation metrics that corresponds to each maturity level of the validation result attribute. A fabricated reward for each maturity level of code adequacy is also included. The expected reward is obtained by multiplying the belief by the reward of each level, based on which decision of the model credibility can be made.

Table 3.10: Summary of maturity levels with their corresponding MSE ranges and maturity rewards.

| Maturity Level | Validation Metrics Output | Reward of Maturity Level for Code Adequacy |
|---|---|---|
| VL | $[10^3, \infty)$ | $-\$100$ |
| L | $[10^2, 10^3)$ | $-\$50$ |
| M | $[1,100)$ | $\$50$ |
| H | $[0,1)$ | $\$100$ |

Table  shows the summary of the estimated probabilistic maturity, expected rewards and real rewards for the code adequacy. In addition, to better use the data uncertainty information, various validation metrics are employed. As more uncertainty information becomes available, both the probabilistic maturity level and expected rewards are getting closer to the real value.

Table 3.11: Summary of the estimated probabilistic maturity, expected rewards and real rewards for the code adequacy.

| **Uncertainty Grade** | **Validation Metric** | **Probabilistic Maturity** | | | **Rewards** | |
|---|---|---|---|---|---|---|
| | | **PCMQ Estimate** | | **Real** | **Expected** | **Real** |
| 2/Type II | Mean Squared Error | VL | 0% | 100% | $66.75 | -$100 |
| | | L | 16.67% | 0% | | |
| | | M | 16.67% | 0% | | |
| | | H | 66.66% | 0% | | |
| 3/ Type III | Normalized Euclidean Distance | VL | 0% | 0% | $83.34 | -$50 |
| | | L | 0% | 100% | | |
| | | M | 33.33% | 0% | | |
| | | H | 66.67% | 0% | | |
| 4/Type IV | Symmetric Divergence | VL | 0% | 0% | $57.8 | $73.39 |
| | | L | 0% | 0% | | |
| | | M | 53.22% | 53.22% | | |
| | | H | 46.78% | 46.78% | | |

***Bayesian Sensitivity Analysis for PCMQBN***

To ensure the robustness of the credibility assessment from the validation framework, a sensitivity study is needed to ensure the uncertainty has been maximumly reduced based on the present knowledge and data. As a quantified credibility assessment and decision-making framework, PCMQBN supports sensitivity study in a more feasible manner, where mathematical analysis can be performed by perturbing the parameters of each component. PCMQBN has three major components: prior belief on maturity level, update rule and utility/reward of each maturity level. Figure 3.22 shows the scheme of validation decision process and the Bayesian sensitivity analysis for the entire loop. The objective is to reach a consistent result or an interval of results. The present study focuses on the sensitivity study of the prior belief estimation, especially the prior belief on the maturity of validation result. Presently, the sensitivity study is still under investigation.

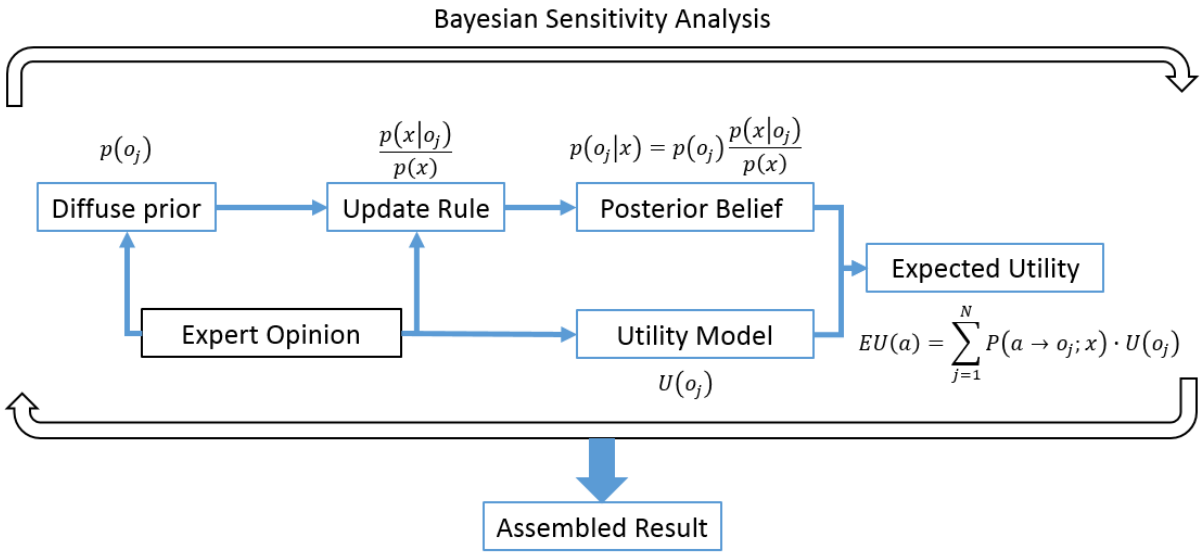


Figure 3.22: Scheme of validation decision and the performance of Bayesian Sensitivity Study

### 3.3.4. Remarks

This chapter first describes concept of sufficient accuracy. Next, a tentative REMDAP framework is constructed based on the concept sufficient accuracy and DDM. The progress of key technologies/methodologies is introduced, including the data-driven closure development, data-driven uncertainty quantification and PCMQBN. In addition, illustrative examples are prepared for each methodology. Recommendations for the data-driven validation have been provided by researchers in Zachry Inc. and the document is attached in Appendix B.

## 3.4. Summary and Outlook

In this study, a novel data-driven concept is incorporated into the model validation process to help shorten the closure development and validation process. The concept of sufficient accuracy is developed based on the risk-informed concept to guide the validation of RISMC simulation tool, which has a significant portion of uncertainties and intangibles. Based on the data-driven concept and sufficient accuracy, a validation framework named Risk-Informed Evaluation Model Development and Assessment Process (REMDAP) is proposed and under development. A tentative workflow is prepared based on the currently developing methodologies/technologies. Next, the progress of developing key methodologies in the REMDAP framework, including the data-driven closure development, data-driven uncertainty quantification, and Predictive Capability Maturity Quantification & Bayesian Network (PCMQBN) are demonstrated. Presently, this study demonstrates some initial developments of classifying methodologies based on assumptions and conditions, the objective is to identify the feature and create an initial proof-of-concept for applying Data Driven Modeling (DDM) in the model development and validation process.

For the data-driven closure development, the present study classifies it into two types. The parametric method assumes a fixed model form that relies on human knowledge, while the nonparametric method uses nonparametric forms that solely depend on the data. From the condition of illustrative examples, it's observed that as more data is used for training and calibration, the error will reach an asymptotic range for all types of methods. Also, it is observed that a similar error is obtained from the Bayesian Inference and Least Squared Error since the closure's quality is limited by the fixed model form. Moreover, the error from the nonparametric form can be reduced to a very small value ($10^{-3}$). In addition, both types are sensitive to the amount of data, however, when the data amount is small, the nonparametric model tends to have larger error than the parametric error.

For the data-driven uncertainty quantification (UQ) methodology, the present study classifies them into two types: global data-driven UQ and local data-driven UQ. Schematic workflows are constructed for both approaches. The global approach targets at system code like Cobra-TF by assuming that the model has been well-verified, and closures are the major source of uncertainties. The illustrative examples show that the error reaches the asymptotic range in the application domain and increasing the number of training data will not change the error. When the UQ is performed for both parametric and nonparametric closure development methods, errors are amplified when the closure of both types is used in the application domain. And the amplification turns to be much higher for the machine-learning-based closure (nonparametric method) than the Bayesian inference or least square error (parametric method). As a result, the problem of data gap remains challenging even with sophisticated data-driven closure development and pursuing high accuracy is very likely to induce large scaling distortion. A same procedure is performed with a difference validation metric of confidence interval, where the closure quality is measured by the percentage of real values being bounded by the 95% confidence range of closure predictions. In addition to the similar finding of error amplification, the confidence ranges from Bayesian Inference bounds more real data points than the one from Neural Network, because the uncertainty of Bayesian inference is much larger than the one of Neural Network. This suggests that though the parametric model with fixed model form limits the model quality in the validation domain, however, when there is a data gap, it also helps to restrain the error amplification in the application domain due to the failure of capturing the correct pattern with the nonparametric model. The effect of data bias is also investigated by introducing constant error to the high-fidelity data. From the illustrative examples, it's observed that as more bias is introduced, the model quality keeps deteriorating. Although the data bias has a significant effect on the closure quality, there is rarely an effective way of analyzing or avoiding the bias. However, it's important that the information of high-fidelity data, especially the uncertainty information, needs to be properly characterized and recorded. Otherwise, a poorly documented low-quality data can induce significant and irreversible effect on the quality of closures and simulations.

As for the local data-driven approach, Physics-Informed Machine Learning (PIML) is employed to construct a surrogate between the simulation error and the input physical features. It is designed for the coarse-grid computational fluid dynamics like NEUTRINO-SPH, where the error of each computing element is characterized with PIML. Since there is no validation metric available to characterize the accuracy of error prediction, this study substitutes the estimated error from PIML back to the original simulation and measures the capability of PIML by comparing the corrected data against the high-fidelity data. In the conditions of the illustrative example, it is observable that the error of corrected field data by PIML is lower than the original SPH simulation, except for the one trained by data with the furthest fluid characteristics to application dataset. It is also found that as more datasets are used for training, the error of corrected fields becomes smaller. In addition, as the fluid characteristics of training set becomes closer to the application set, the error of corrected field gets smaller. In addition to the random forest machine-learning engine, the same process is performed with the neural network engine. The result suggests that random forest is faster and more robust than the neural network, however, the error reduction with respect to the data amount is more obvious for the neural network.

Finally, further developments are made for the decision-theoretic methodology of PCMQBN. Guidance is constructed for qualitatively evaluating the uncertainty grade in the R/S/U (Relevance/Scaling/Uncertainty) grading system. It's found from the illustrative example that as more uncertainty information becomes available; both the probabilistic maturity level and expected rewards are getting closer to the real value. Furthermore, a framework of Bayesian sensitivity study is proposed for PCMQBN and the objective is to improve the robustness of the PCMQBN's result, which is presently under investigation.

### 3.5. References


[1] C. Rabiti, A. Alfonsi, J. Cogliati, D. Mandelli, R. Kinoshita and C. Smith, "A novel method of controlling thermal hydraulics codes using RAVEN," LWRS Newsletter, 2014.

[2] C. Smith, C. Rabiti, R. Martineau and R. Szilard, "Risk-Informed Safety Margins Characterization (RISMC) Path Technical Program Plan," Idation National Laboratory, Idaho Falls, 2015.

[3] C. Smith, S. Prescott, J. Coleman, E. Ryan, B. Bhandari, D. Sludern, C. Pope and R. Sampath, "Progress on the Industry Application External Hazard Analyses Early Demonstration," Idaho National Laboratory, Idaho Falls, 2015.

[4] S. Prescott, D. Mandelli, R. Sampath, C. Smith and L. Lin, "3D Simulation of External Flooding Events for the RISMC Pathway," Idaho National Laboratory , Idaho Falls, 2015.

[5] S. Prescott, R. Sampath, C. Smith and T. Yang, "3D Modeling Engine Representaiton Summary Report," Idaho National Laboratory, Idaho Falls, 2014.

[6] C. Smith, D. Mandelli, S. Prescott, A. Alfonsi, C. Rabiti, J. Cogliati and R. Kinoshita, "Analysis of pressurized water reactor station blackout caused by external flooding using the RISMC toolkit," Idaho National Laboratory, Idaho Falls, 2014.

[7] N. Zuber, G. E. Wilson, M. Ishii, M. Wulff, B. Boyack and A. Dukler, "An integrated structure and scaling methodology for severe accident technical issue resolution: Development of methodology," *Nuclear Engineering and Design,* vol. 186, pp. 1-21, 1998.

[8] B. Boyack, I. Catton, R. Duffey, P. Griffth, K. Katsma, G. Lellouche, S. Levy, U. Rohatgi, G. Wilson, W. Wulff and N. Zuber, "Quantifying reactor safety margins part 1: An overview of the code scaling, applicability and uncertainty evaluation methodology," *Nuclear Engineering and Design,* vol. 119, no. 1, pp. 1-15, 1990.

[9] T. Olivier and S. Nowlen, "A phenomena Identificaiton and Ranking Table (PIRT) exercise for nuclear power plant fire modeling applications," U.S. NRC, Washington DC, 2008`.

[10] U.S. NRC, "Transient and accident analysis methods," U.S. Nuclear Regulatory Commission, Washington D.C., 2005.

[11] C. Fletcher, P. Bayless, C. Davis, M. Ortiz, S. Sloan, R. Shaw, R. Shultz, C. Slater, G. Johnsen, J. Adams, L. Ghan and D. Bessette, "Adequacy Evaluation of RELAP5/MOD3, Version 3.2.1.2. for simulating AP600 Small Break Loss-of-Coolant Accidents," Idaho National Engeneering and Environment Laboratory, Idaho Falls, 1997.

[12] W. Oberkampf, M. Pilch and T. Trucano, "Predictive Capability Maturity Model for computational modeling and simulation (SAND2007-5948)," Sandia National Laboratories, Albuquerque, 2007.

[13] J. Kaizer, "Fundamental Theory of Scientific Computer Simulation Review," U.S. NRC, Washington DC, 2013.

[14] V. A. Mousseau and N. Dinh, "CASL Verification and Validation Plan," Consortium for Advanced Simulation of Light Water Reactors, CASL-U-2016-1116-000, 2016.

[15] E. Turban, R. Rainer and R. Potter, Introduction to information technology, New York: Wiley, 2005.

[16] P. Domingos, The master algorithm, Basic Books, 2015.

[17] R. Ackoff, "From data to wisdom," *Journal of Applied System Analysis,* vol. 16, pp. 3-9, 1989.

[18] J. Rowley, "The widwom hierarchy: representations of the DIKW hierarchy," *Journal of Information Science,* vol. 33, no. 2, pp. 163-180, 2007.

[19] L. Ladicky, S. Jeong, B. Solenthaler, M. Pollefeys and M. Gross, "Data-driven fluid simulations using regression forests," in *The 8th ACM SIGGRAPH Conference and Exhibition on Computer Graphics and Interactive Techniques in Asia,* Kobe, 2015.

[20] E. Parish and K. Duraisamy, "A paradign for data-driven predictive modeling using field inversion and machine learning," *Journal of Computatinal Physics,* vol. 305, pp. 758-774, 2016.

[21] J. Wang, J. Wu and H. Xiao, "Physics-informed machine learning approach for reconstructing Reynolds stress modeling discrepancies based on DNS data," *Physical Review Fluids,* vol. 2, 2017.

[22] C. Chang and N. Dinh, "Classification of machine learning frameworks for data-driven thermal fluid models," *International Journal of thermal sciences (revision under review).*

[23] S. Brunton, J. Proctor and J. Kutz, "Discovering governing equations from data by sparse identification of nonlinear dynamical systems," *Proceedings of the National Academy of Sciences,* vol. 113, pp. 3932-3937, 2016.

[24] M. Ma, J. Lu and G. Tryggvason, "Using statistical learning to close two-fluid multiphase flow equations for a simple bubbly system," *Physics of Fluids,* vol. 27, 2015.

[25] M. Ma, J. Lu and G. Tryggvason, "Using statistical learning to close two-fluid multiphase flow Using statistical learning to close two-fluid multiphase flow," *International Journal of Multiphase Flow,* vol. 85, pp. 336-347, 2016.

[26] N. Dinh, A. Gupta, J. B. I. Bolotnov, M. Avramova, H. Abdel-Khalik, X. Sun, P. Bardet, R. Sewell, R. Sampath, J. Lane, A. Bui, S. Prescott, C. Rabiti, R. Youngblood and W. Ren, "Development and Application of a Data-Driven Methodology for Validation of Risk-Informed Safety Margin Characterization Models," North Carolina State University, Raleigh, 2015.

[27] A. Alfonsi, C. Rabiti, D. Mandelli, J. Cogliati, C. Wang, P. Talbot, D. Maljovec and C. Smith, "RAVEN theory manual and user guide," Idaho National Laboratory, Idaho Falls, 2017.

[28] P. Athe, N. Dinh and H. Abdel-Khalik, "Investigation of similarity metrics for simulation based scaling analysis," in *Advances in Thermal Hydraulics,* New Orleans, 2016.

[29] T. Dinh, "Validation data to support advanced code development," in *The 15th International Topical Meeting on Nuclear Reactor Thermal Hydraulics,* Pisa, 2013.

[30] W. Ren, "Nuclear enerugy knowledge based for advanced modeling and simulation - functionalities and operation (Beta) - NE-KAMS Version Beta," Oak Ridge National Laboratory, Oak Ridge, 2012.

[31] L. Lin, P. Athe and N. Dinh, "Predictive capability maturity assessment with Bayesian network," North Carolina State University , Raleigh, 2017.

[32] J. Ling and J. Templeton, "Evaluation of machine learning algorithms for prediction of regions of high Reynolds averaged navier Stokes uncertainty," *Physics of Fluids,* vol. 27, 2015.

[33] A. Stuart, J. Ord and S. Arnold, Kendall's Advanced Theory of Statistics: Volume 2A—Classical Inference and the Linear Model (sixth edition), Wiley, 1999.

[34] Y. Liu, "Development of a data-driven analysis framework for boiling problems with multiphase-CFD solver," North Carolina State University, Raleigh, 2018.

[35] B. Petukhov, "Heat transfer and friction in turbulent pipe flow with variable physical properties," Academy of Science of the USSR, Moscow, 1970.

[36] A. Bui, N. Dinh and B. Williams, "Validation and calibration of nuclear thermal hydraulics multiscale multiphysics models - subcooled flow boiling study," Idaho National Laboratory, Idaho Falls, 2013.

[37] Y. Liu and N. Dinh, "Development of a Data-driven Analysis Framework for Pool Boiling and Subcooled Flow Boiling Problems," U.S. Department of Energy, Washington DC, 2017.

[38] X. Wu, T. Kozlowski, H. Meidani and K. Shirvan, "Inverse Uncertainty Quantification using the Modular Bayesian Approach based on Gaussian Process, Part 1: Theory," *Nuclear Engineering and Design*, vol. 335C, pp. 339-355, 2018.

# 4. Predictive Capability Maturity Quantification using Bayesian Network

## 4.1. Introduction

Nowadays, an increasing amount of research has been conducted for developing and applying advanced modeling and simulation (M&S) tools in nuclear discipline. In risk-informed safety analysis [1] [2], M&S tools are used to investigate the effects of uncertain scenarios, simulate accident progressions, characterize the reactor safety margin, improve the operational procedures, locate design vulnerabilities, etc. Compared to classical risk analysis, the risk-informed analysis aims to address both aleatory and epistemic uncertainty within a well-defined issue space, rather than trying to work with arbitrarily defined point values of load and capacity. Meanwhile, in complex systems like Nuclear Power Plants (NPPs), since the interactions among systems, components, and external events can be highly nonlinear, risk-informed safety analysis uses advanced simulations to fully represent the generations, progressions, and interactions of accident scenarios with the NPPs. However, the classical risk-informed approach does not consider the impacts of simulation adequacy [3] [4], which includes model parameter uncertainty, model form uncertainty, numerical approximations, scaling errors, etc. As a result, a validation framework is needed to not only determine whether the M&S code is adequate for representing the issue spaces but also to be directly used in the risk-informed safety analysis.

Code Scaling, Applicability, and Uncertainty (CSAU) evaluation methodology was introduced in 1989 [5] to demonstrate a method that "can be used to quantify uncertainties as required by the best-estimate option described in the U.S. Nuclear Regulatory Commission (NRC) 1988 revision to the ECCS Rule (10 CFR 50.46) [6]". A Regulatory Guide (RG 1.203), Evaluation Model Development and Assessment Process (EMDAP), is developed at 2005 to "describe a process that the U.S. NRC considers acceptable for use in developing and assessing evaluation models that may be used to analyze transient and accident behavior that is within the design basis of a nuclear power plant [7]." In the CSAU/EMDAP framework, the complexity of physics and phenomena is emphasized, and scaling analysis is suggested to resolve the lack of data issues. The objective is to ensure both the sufficiency and necessity of validation data, modeling, and simulation, such that the simulation can adequately describe the scenarios investigated. Although the evidence involved is objective, the assessment process requires subjective information, including phenomena ranking and identification, decisions regarding data applicability, selection of validation metrics, etc. In CSAU/EMDAP, such subjective evidence is treated implicitly, and it causes the validation process to lack transparency. Meanwhile, due to a lack of formalized treatment, it becomes hard for analysts and decision makers to ensure the consistency of elicitation and processing of subjective information. Therefore, a decision model is needed for integrating all sources of evidence and determining final simulation adequacy. Meanwhile, the decision model needs to be practical, transparent, and consistent, such that the simulation adequacy results can be used with sufficient confidence.

The Predictive Capability Maturity Model (PCMM) (Oberkampf, Pilch, & Trucano, Predictive Capability Maturity Model for computational modeling and simulation (SAND2007-5948), 2007) was developed by W.L. Oberkampf et al. in 2007. As a decision model for Verification, Validation, and Uncertainty Quantification (VVUQ), PCMM explicitly treats the model credibility/uncertainty assessment as a decision-making process. For designated scenarios, six attributes are designed and assessed qualitatively based on a PCMM matrix, which is designed according to the context and consequence of applications. Since the final decisions are informed by requirements and consequences, PCMM can effectively guide the development and validation of M&S tools. However, since the PCMM matrix is constructed using descriptive statements, the representations of performance standards can be obscure and suggest inconsistent criteria. Meanwhile, although validation and uncertainty quantification are discussed as major attributes, other critical components, including scaling analysis, data applicability, data quality, etc., are not explicitly discussed. As a result, when there are data gaps induced by differences between the

prototypical and experimental systems, such implicitness could suggest results in inconsistent maturity levels.

Other frameworks include “Guide for Verification and Validation in Computational Solid Mechanics (VV10)” [9] and “Standard for Verification and Validation in Computational Fluid Dynamics and Heat Transfer (VV20)” [10] by ASME for quantifying the degree of accuracy to consider the errors and uncertainties in both the solution and the data. Since the adequacy results are used to support nuclear risk analysis, while VV10 and VV20 are designed as a general guidance for the V&V of computational model, CSAU/EMDAP and PCMM are more appropriate and relevant to the context of this study.

In this paper, a new decision model named Predictive Capability Maturity Quantification using Bayesian network (PCMQBN) is presented. Developed based on argumentation theory and Bayes’ theorem, PCMQBN aims to formalize the decision-making for assessing simulation adequacy assessment such that the process is transparent, consistent, and improvable with new evidence. This paper is organized as follows (Figure 4.1): section 2 limits the scope of this study by introducing assumptions, conditions, and limitations of proposed framework. Section 3 formalizes the interpretation of simulation adequacy based on the nature of validation. Section 4 introduces PCMQBN, where the first two subsections describe technical basis that characterizes and integrates evidence based on the argumentation theory and Bayes’ theorem; the last two subsections evaluate the behavior of this framework. Section 5 illustrates the application of PCMQBN in evaluating the adequacy of a Smoothed Particle Hydrodynamic simulation for predicting the hydrodynamic forces onto static structures during an external flooding scenario.

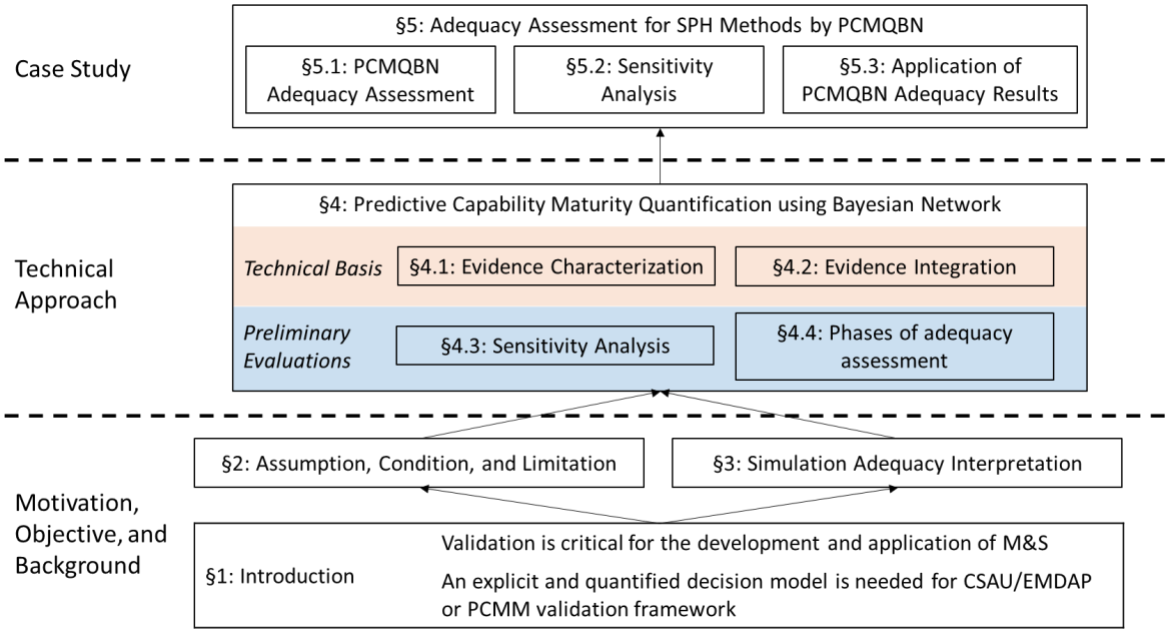


Figure 4.23: The schematic structure for this chapter.

## 4.2. Assumption, Condition, and Limitation

To properly identify the scope of this study, important conditions and assumptions are listed in Table 4.1. Category A aims to define the scope and application of this study; category B lists the assumptions in PCMQBN for formalizing the decision-making process in validations; category C suggests the conditions and assumptions used in case studies.

Table 4.1: Important conditions and assumptions with respect to aspects of investigation.

| ID | Conditions/Assumptions |
|---|---|
| **A** | **Investigation Scope** |
| A1 | Current work only focuses on validation activities to support the risk-informed safety analysis |
| A2 | There are data gaps between the validation databases and target applications |
| A3 | The SPH-based computer code is assumed to be verified |
| **B** | **Validation Formalization** |
| B1 | Formalism can reduce the uncertainty |
| B2 | Decision makings in validation is a structured argument process supported by a body of evidence; |
| B3 | Risks due to model uncertainty are characterized by expected losses |
| **C** | **Case Study** |
| C1 | If simulation is not adequate, it can predict the QoIs with maximum 100% errors |
| C2 | If simulation is adequate, it can predict the QoIs with maximum 20% errors |
| C3 | If simulation adequacy is uncertain, QoIs are assembled according to predictions and beliefs at each adequacy level |
| C4 | Preference over different simulation-adequacy levels can be characterized by the magnitude of expected loss |

Assumption A1 limits the application to risk-informed safety analysis, and the objective is to determine the error distribution of the quantity of interest predicted by M&S. More specifically, this study focuses on situations with data gaps. As a result, to better characterize adequacy of M&Ss and to avoid unreliable expert judgments, this study aims to reduce the uncertainty in estimating the simulation adequacy and corresponding risks induced by such uncertainty. Assumption A3 mainly assumes that the code verification has been performed. The confidence on such assumption is built on the theory manual of NEUTRINO [11], together with code and solution verifications from various literature (Lin L. , Assessment of the smoothed particle hydrodynamics method for nuclear thermal-hydraulic applications, 2016) [13] [14].

Assumption B1 suggests the formal methods to improve the reliability and robustness of the validation decision-making process. Formal methods have continuously proven its success in financial, computer system, etc. in reducing major losses due to unverified errors [15]. It is argued that the formal methods do not obviate the need for testing, experiments, and other assertion techniques, it is mainly designed to help identify errors in reasoning which could be overlooked or left unverified. Assumption B2 aims to formalize the validation process as an argument process and to further represent the validation argument with Bayes' theorem. However, it has been suggested that the prior probability and likelihood cannot be known precisely [16] [17]. In this study, a sensitivity analysis is suggested by performing standard Bayesian analysis with a class of prior and likelihood functions. Next, all important parameters, which have high impacts on the results, are carefully examined. If no significant discrepancy is witnessed, the result is claimed to be robust. Assumption B3 aims to suggest expected losses for representing the risks of adopting code predictions to risk-informed safety analysis. Since M&Ss are mainly used to support safety decisions and alternatives in designated applications, the corresponding "adequacy" should be defined based on the consequence of adopting the predicted QoIs. This study makes a table of synthetic monetary loss for each possible consequence, and the expected losses are calculated based on the simulation adequacy result.

Assumptions 1, 2 and 3 in category C are made to define the error distributions of QoIs in the case study based on the simulation adequacy results. It is criticized that the current assembly of simulation adequacy and model predictions is arbitrary. Therefore, the claim that the proposed framework can reduce uncertainty in simulation adequacy results is questionable [18]. However, at the initial developmental phase, it is acceptable to have a crude ensemble method for demonstration purposes. It is stressed that the parameters in the proposed framework are not fixed. As more evidence is gathered, the parameters need to

be calibrated and refined. Moreover, since formal methods are designed to avoid or reduce unverified errors, it is argued that the validity of this claim should not be greatly deteriorated by assumptions for simplification purposes. Assumption 4 suggests a rational agent who prefers to have fewer expected monetary losses. It is criticized in [19] that the expected value cannot fully represent the agents' choices, where subjective and psychological impacts are neglected. It is argued that this study is at the scoping stage, and the objective is to formalize the decision-making process. In the future developmental stage, different decision analysis models can be tested and optimized for validation purposes.

### 4.3. Simulation adequacy Interpretation

To formalize the decision-making process in simulation-adequacy assessment, a consistent and transparent interpretation is needed for "simulation adequacy" as a theorical basis of the proposed framework. This section first reviews definitions from relevant works and identifies requirements for interpreting simulation adequacy. Next, the simulation adequacy is interpreted as a triplet set by answering three key questions. Meanwhile, examples are given for illustrating each of the three elements.

In validation, simulation adequacy is usually defined as the degree to which a simulation can adequately represent the system quantities of interest from the perspective of the intended uses [20]. In works by P. Athe et al. [21] and J.S. Kaizer et al. [22], the simulation adequacy is represented by a binary term "credibility – the determination that an object (in this particular instance, a model) can be trusted for its intended purpose." Furthermore, the concept of assurance case is adopted in the definition of credibility, and a "validation case" is developed for arguing the trustworthiness of a model to the decision maker for certain applications. This definition emphasizes the effects of expert belief and connections between simulation adequacy and the consequences of application. However, as an argument process, the assessment process heavily relies on expert opinions in claiming, reasoning, justifying, and reaching final goals. It could also become expensive to reach agreements when a group of experts with different backgrounds and knowledge is presented. Although the decision-making has been formalized in [22], it is suggested here that the process should be further quantified for better transparency and for reducing uncertainties due to inconsistent assessment results. In works by S. Mahadevan et al. [23], simulation adequacy is quantified by Probability Density Function (PDF) of model predictions or their uncertainty. The Bayes' theorem is used for either testing the hypothesis about model uncertainty or estimating the probability that model predictions represent the target phenomena. The uncertainty distribution definition emphasizes mathematical representations of uncertainty such that the reliability or probability of success of the model can be measured in a direct, objective, and quantitative manner. Although such interpretations are consistent and rigorous in mathematics, its applicability is greatly limited by assumptions in the assessment process. For example, the uncertainty distribution and likelihood function are assumed to have explicit forms and parameters [24], such that they can be determined by probabilistic inference. Moreover, these distributions are assumed to be fixed in different scenarios and applications. However, for situations with a lack of prototypical data, the uncertainty can be seriously distorted when it is propagated across different scales. Meanwhile, when there are multiple scales and phenomena involved in application scenarios, the inference of uncertainty distributions relies heavily on the quality of multi-physics and multi-scale models. If the multi-physics and multi-scale interactions are poorly captured, results from uncertainty inference can be misleading (Liu & Dinh, Validation and uncertainty quantification for wall boiling closure relations in multiphase-CFD solver, 2018). Meanwhile, these models are usually developed based on reduced-scale and separate-effect databases. Therefore, when the data are not fully applicable to the target applications due to scaling distortions, uncertainty due to model forms can hardly be characterized, and results from uncertainty inference can be further distorted. Besides, the quality of data also affects the results from uncertainty inference, however, the uncertainty inference can hardly capture its impacts without an informative prior [26]. As a result, although the simulation adequacy assessment needs to be quantified, the framework is suggested to have more flexible forms and adaptable structures than PDF-based distributions in uncertainty inference. At last, in the CSAU/EMDAP framework, simulation adequacy is defined by both accuracy

information of model predictions and the applicability of the validation database [27]. Such a definition is more comprehensive and flexible since it not only considers the effect of scale gaps in assessing data applicability but also the uncertainty distributions of model predictions. In the present study, the interpretation of simulation adequacy will be made based on that from CSAU/EMDAP. Moreover, the impacts of scenarios and applications are also considered.

As a result, this study describes simulation adequacy as the degree to which M&S tools can adequately represent the system quantities of interest in the target applications. The objective is not only to determine if an M&S is good or bad but also to describe the uncertainty in the real application, especially when it is understood from non-prototypical data. In this study, simulation adequacy is suggested to be composed of three components: scenario, uncertainty/predictive capability levels, and beliefs. Note the purpose of this interpretation is not to resolve fundamental issues of uncertainty classifications through a sophisticated interpretation. Instead, this study focuses on practical resolutions for deciding simulation adequacy in complex engineering problems with a transparent and consistent framework. In the context of nuclear engineering, the term "transparent" requires a formalized interpretation and representation for simulation adequacy; the term "consistent" requires the formalization to have a mathematical basis, and allow for assumptions that cannot be violated in real applications; the term "practical" requires that the formalized simulation adequacy assessment should be easily applied to risk analysis. Eq. 4.1 shows a representation of simulation adequacy as a triplet set: scenarios, beliefs, and levels of uncertainty or predictive capability for M&S.

$$\text{Simulation adequacy} = \{\text{scenario}, \text{belief}, \text{predictive capability}\} \qquad \text{Eq. 4.1}$$

The structure of interpretation in this study is similar to the triplet by Kaplan and Garrick [28] for probabilistic risk analysis. The definition for simulation adequacy aims to answer three questions:

1. *What scenario does the M&S apply to?*

In the nuclear accident and transient analysis, results of M&S are used to support system designs and risk management within a range of issue spaces. Meanwhile, since risk-informed safety analysis aims to address the scenario uncertainty, a scenario set $S = [S_1, \dots, S_i, \dots]$ is defined, and each element corresponds to one sampled scenario $S_i$ according to designated distributions. Therefore, the selections of computational methods and simulations naturally depend on the investigated scenario. Moreover, in scenarios with minor impacts, the reactor systems can be robust enough to withstand much higher loads than those being exerted. In this circumstance, safety decisions do not heavily rely on M&S results, requirements on model predictive capability and confidence do not need to be high. Similarly, when scenarios loads are likely to exceed system capacities and the uncertainty of M&S results could alter the safety decisions, the requirements on the predictive capability and confidence will be strict.

2. *What is the predictive capability of M&S?*

The "Predictive Capability" refers to the capability of M&Ss in predicting QoIs during accident and transient scenarios. As a major product of classical validation methods, the capability is quantified by errors between simulation results and observations. Such techniques, as validation metrics, statistical analysis, etc. are usually used. Meanwhile, Oberkampf et al. [20] represent the model's predictive capability by maturity levels, which are further explained by sub-attributes and descriptive terms. In this case, argumentation theory and corresponding techniques, including Goal Structure Notation (GSN), Claim, Argument, and Evidence notation (CAE), etc. are used.

3. *What is the belief in the M&S predictive capability?*

Due to imperfect knowledge and insufficient data, predictive capability cannot be precisely estimated, and belief is used to describe a state of knowledge regarding estimations. Although belief is represented by probability, it does not refer to the frequency or statistics in the sense that it does not represent a property of the 'real' world. Rather, belief describes our state of knowledge and discusses its effects on decisions. Table 4.2 shows an example of belief scales in probabilities together with their characteristics. This scale provides the definition of unreasonable model maturity levels as involving the independent combination of an end-of-spectrum condition with a condition that is expected to be outside the main body of the spectrum but cannot be positively excluded. The spectrum in this study refers to the spectrum of physics, scales, data applicability, and prediction errors. For example, when a solid-mechanistic code is applied to simulate fluid dynamics, its prediction errors for certain QoIs can occasionally be small at certain locations. However, the belief that this simulation generally has low prediction errors and high maturity should be low since the physics in solid mechanics are outside the spectrum of fluid dynamics; when experimental data for validating a simulation in kilometer-scale and multi-physics scenarios is collected from a centimeter facility that focuses on one of the involving phenomena, the belief that the experimental data are applicable to the target scenarios should be low since the scale are different and phenomena are separate. However, such reduced scale and separate-effect data cannot be positively excluded from the main body of the spectrum in target applications since the involving physics and phenomena are in the spectrum of target scenarios.

Table 4.2: Assignment of screening probability with characteristics and examples.

| **Belief scales in Probabilities** | **Characteristics** | **Examples** | |
|---|---|---|---|
| | | **Validation Result** | **Data Applicability** |
| 1 | Corresponding levels are well-known and obtainable on the major spectrum | Applying CFD-based M&S with very fine grids (DNS scales) | High-quality validation databases are collected from prototypical systems for the directly relevant phenomena |
| 0.1 | Corresponding levels are known but obtainable only at the edge of spectrum | Applying CFD-based M&S with coarser grids (Asymptotic range or outside) | Validation databases are collected from reduced-scale systems for the highly relevant phenomena |
| 0.01 | Corresponding levels cannot be excluded, but it is outside the spectrum of reason | Applying CFD-like or correlation-based M&S | Validation databases are collected from low-quality and reduced-scale systems with the poorly relevant phenomena |
| 0.001 | Corresponding levels are unreasonable and violates well-known reality. Its occurrence can be argued against positively | Applying solid mechanistic M&S | Validation databases are collected from low-quality and reduced-scale systems with irrelevant phenomena |

As a result, the objective is to find the belief $P_i(level_j)$, represented by probabilities, such that Eq. 4.2 can be satisfied for any investigated scenarios $S_i$ within the designated scenario set or issue space $S = [S_1, \dots, S_i, \dots]$; $P_s$ is the screening probability for beliefs in simulation's validation result, data applicability, and simulation adequacy for a given set of scenarios. It is to ensure consistent belief assignments across the entire issue space in the risk-informed safety analysis. Similar definitions can also be found in the Risk-Oriented Accident Analysis Methodology by T.G. Theofanous [2], which focuses on the scenarios spectrum and aims to distinguish unreasonable and small-probability events.

$$P_i(level_j) < P_s \text{ for all } S_i \qquad \text{Eq. 4.2}$$

Table 4.2 shows an example of screening probability assigned by expert knowledge. Examples are also provided assuming that an M&S simulation is applied to predict the generation and progression of surface waves in the flooding scenarios. Validation Result (VR) is assessed by comparing simulation predictions against validation databases, while Data Applicability (DA) is assessed by the scale of facilities, relevancy of phenomena, and quality of data.

The probability values $P_i(level_j)$ are computed from the probabilistic framework that represents a map of parameters in the causal relationships $\{d_i\}$, prior knowledge $\{\tilde{p}_i\}$, and decision parameters $\{k_i\}$:

$$P_i(level_j) = F(d_1, d_2, \dots, \tilde{p}_1, \tilde{p}_2, \dots, k_1, k_2, \dots) \quad \text{Eq. 4.3}$$

The prior knowledge $\{\tilde{p}_i\}$ and corresponding uncertainties are distributions and can be quantified according to the probability scale in Table 4.2. Causal relationships and decision parameters should not violate well-known physics and laws, and a synthetic model can be developed to support the value assignment. Meanwhile, they are assumed to be well-posed problems in the sense that they are not subject to major discontinuities and the uncertainty can be reduced to the parameter level without major modeling uncertainty. It is argued that the three questions above are sufficient for guiding validation activities and adequacy assessment. However, since simulation results are usually applied in risk analysis and safety decisions, the preferences and consequences of accepting certain simulation adequacy results need to be evaluated, especially when results contain uncertainties. Although such topics are beyond the scope, for completeness, this study briefly discusses a fourth attribute of simulation adequacy as an additional concern. Meanwhile, a synthetic model, together with a review of other sophisticated options, is included regarding the application of simulation adequacy results.

Since the simulation adequacy results are mostly applied to support safety-related decisions or alternatives, the adequacy should be judged not only based on model predictions and validation databases, but it should also consider the target decisions. For example, in scenarios with severe consequences, requirements on belief and M&S's predictive capability levels should be more stringent than for those with less severe consequences. In the risk-informed analysis, the predictive capability level and belief should be higher for regions where loads distributions and capacity distributions overlap. If the adequacy result satisfies the requirements, a cost-benefit analysis is performed based on the consequence of simulation's uncertainty and risk. If the adequacy of results does not satisfy the requirements or it is net beneficial for improving the predictive capability level and belief, additional iteration will be conducted to either continue developing new models, collecting new data, or updating the validation techniques. By adding risk and performance measurement results, the validation process becomes risk-informed in the sense that the acceptance criteria of simulation adequacy are informed by risks of target applications, which are caused by both model and scenario uncertainty.

### 4.4. Predictive Capability Maturity Quantification using Bayesian Network

To avoid expert biases and unreliable judgement within an implicit decision scheme, this study proposes a quantitative decision-making framework, named Predictive Capability Maturity Quantification using Bayesian Network (PCMQBN) to formalize the assessment of simulation adequacy. Considering the similarity between assurance case to simulation validation, the simulation adequacy assessment can be described as a "confidence argument" supported by evidence that justifies the claim that simulation provides reliable prediction in the domain of application. The evidence is collected from the validation framework and characterized mathematically such that it is consistent with the interpretation of simulation adequacy. Moreover, such an argument process can be further quantified by probabilities and maturity levels, and further represented graphically by Bayesian networks. In this framework, all evidence is

integrated by probabilistic inferences and can be further represented graphically by a Bayesian network. At the same time, to integrate evidence from various sources, a synthetic decision model is suggested for determining the relative weights and conditional probabilities in Bayesian networks. Figure 4.24 shows the scheme for assessing and applying simulation adequacy by PCMQBN. Evidence of validation result and data applicability are firstly collected from validation activities guided by validation frameworks like CSAU/EMDAP. Sub-section 4.4.1 discusses in detail how evidence is collected and characterized consistently based on the maturity level assignment (4.1.1) and belief assignment (4.1.2). Next, the characterized evidence, together with decision parameters regarding the conditional dependencies among different evidence and attributes, are integrated for simulation adequacy results. Sub-section 4.4.2 discusses details of how evidence is integrated based on the argumentation theory and further quantified by probabilistic inference. To evaluate the sensitivity of decision parameters, sub-section 4.4.3 suggests a sensitivity analysis for the simulation adequacy result with the same set of evidence. At last, the simulation adequacy result is applied to safety analysis by assembling the predictions by Modeling and Simulation (M&S) and beliefs. At the same time, the parameter assignment and integration structures are subject to refinement. Sub-section 4.4.4 discusses different phases of simulation adequacy assessment based on qualities of each step.

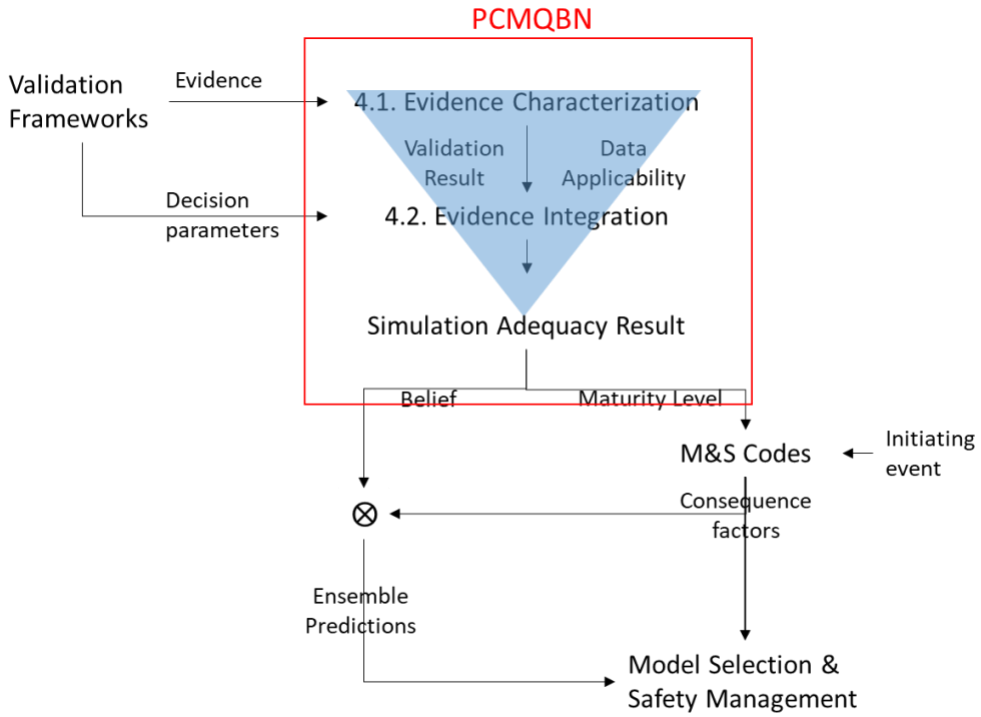


Figure 4.24: Scheme for the assessment and application of simulation adequacy by PCMQBN.

### 4.4.1.Evidence Characterization

During a validation process like CSAU/EMDAP, different activities and materials, including validation databases, scaling analysis of experimental databases, simulation assessment results, phenomenon identification and ranking process, etc., are used to support the adequacy assessment of a simulation. To make better use of these materials, this study characterizes all related evidence based on the argumentation theory and the triplet definition for simulation adequacy. The characterization is required to be transparent, practical, and consistent. The term “transparency” requires a clear representation of evidence by mathematical forms such that the meaning and substance of evidence are maintained and visible. The term “practice” requires all related evidence to be effective for practical purposes and easily obtainable. In the context of nuclear safety analysis, the evidence should be characterized such that it can be directly used to

support safety-related decisions. The term "consistency" requires the characterizations to be theoretically defendable, mathematically sound, and consistent with common knowledge and well-known rules.

There are various ways of characterizing evidence. Sun [29] categorizes evidence as direct evidence, backing evidence or counter evidence, based on its association with confidence. In the context of assurance case that focuses on safety [30], the evidence is defined as "the information that serves as the grounds and starting point of (safety) arguments, based on which the degree of truth of the claims in arguments can be established, challenged and contextualized". Furthermore, in Toulmin's argument model [31], the evidence is classified into six groups: claim, data, warrant, backing, qualifier, and rebuttal. Since validation shares many common features with the assurance case, Table 4.3 shows examples in simulation adequacy assessment for each element based on the Toulmin's argument model. In this study, information including simulation predictive capability, validation data, scaling results, data relevance, data uncertainty, assumptions, and conditions, are considered as evidence for assessing simulation adequacy. In addition, although indirect evidence, including process quality assurance, use history, M&S management, etc. [32], will affect the adequacy assessment for M&S, this study mainly investigates direct evidence for validation.

Table 4.3: Elements of Toulmin's Argument model with simulation adequacy example.

| | | |
|---|---|---|
| **Claims** | The statement we wish to justify | e.g., Simulation predictive capability for an intended reactor application |
| **Data** | The fact we appeal to, the grounds or information on which our claim is based | e.g., Validation data and results collected from experiments, observations, and knowledge |
| **Warrant** | A statement authorizing the step from data to claim is true; an inference rule | e.g., Results from the scaling analysis that infer system behaviors in prototypical conditions based on validation data in reduced-scale conditions |
| **Backing** | A reason for trusting the warrant | e.g., Argument that authorizes the relevance of investigated phenomena and processes for the target applications |
| **Qualifier** | A term or phrase reflecting the degree to which the data support the claims, e.g. generally, probably | e.g., Argument that evaluates the uncertainty of data and experiment |
| **Rebuttal** | Specific circumstances in which the argument will fail to support the claims as exceptions | e.g., Assumptions and conditions about validation data, model, and adequacy assessment |

Since simulation adequacy is to estimate the degree that model predictions represent the real values, the errors, referred to as validation result, between model predictions and the validation data should be used to support the adequacy assessment. In some validation methods, simulation adequacy is interpreted as uncertainty distributions of model predictions [23]. However, it is argued that in nuclear applications, the difficulties, and costs in collecting data under prototypical conditions are so high that only data from small-scale facilities and separate (or mixed) effect tests are practically obtainable. Therefore, the uncertainty distribution estimated by validation data on different scales can be significantly distorted. To avoid the problem of scaling distortion, it becomes necessary to evaluate the applicability of validation data to the target applications, referred to as data applicability, in addition to the validation result. As a result, the top claim of simulation adequacy is supported by sub-claims of validation result and data applicability. The validation result is to determine the errors between simulation results and the validation data, while the data applicability is to determine the applicability of validation data from reduced scales and experimental conditions in the context of applications. Next, the corresponding evidence is collected and evaluated.

The following sections discuss how evidence for validation results and data applicability are characterized. Specifically, the predictive capability is described by maturity levels, while the belief is represented by probability.

**Maturity Level Assignment**

There have been a lot of research performed to quantitatively measure the level of predictive capability for an M&S tool. Harmon and Youngblood [33]suggested a five-point maturity ranking scale based on the concept of credibility, objectivity, and sufficiency of accuracy for the intended use. Long and Nitta [34] suggested a 10-point scale by the concepts of completeness, credibility, and sufficiency of accuracy for the intended use. Pilch et al. [35] suggested a four-point scale dominated by the level of formality, the degree of risk in the decision based on the M&S effort, the importance of the decision to which the M&S effort contributes, and sufficiency of accuracy for the intended use. It is discussed by Pilch et al. that the maturity level of each element should be made based on the risk tolerance of the decision maker. NASA suggested a four-point scale based on the level of believability, formality, and credibility [36]. It was suggested by NASA that the credibility assessment should be separated from the requirements for a given application of M&S. In this study, the maturity level by W.L. Oberkampf (Oberkampf, Pilch, & Trucano, Predictive Capability Maturity Model for computational modeling and simulation (SAND2007-5948), 2007) is used to represent and rank the predictive capability of M&Ss. It is believed that the maturity assessment and adequacy assessment should be dealt with independently as much as possible to reduce misunderstandings or misuse of an M&S maturity assessment. As a result, the maturity level in this study is defined by the intrinsic and fundamental attributes in the M&S validation and decision-making process. The objective is to objectively track all intellectual artifacts obtained during all related validation activities.

*Validation Result*

In this study, the "validation result" is defined as the comparisons between the model predictions and validation data. Based on the comparisons, maturity levels can be further defined by descriptive terms in Predictive Capability Maturity Model (Oberkampf, Pilch, & Trucano, Predictive Capability Maturity Model for computational modeling and simulation (SAND2007-5948), 2007), value bounds from probabilistic or distance metrics, confidence interval, or hypothesis testing. The results from different validation metrics are in different ranges, and the corresponding interpretations can be distinct. Maupin *et al.* [37] has reviewed and tested a class of validation metrics with a synthetic example, it is found that the selection of metrics is problem dependent. For example, when both the experimental measurement uncertainty and model uncertainty is available, probabilistic metrics are more preferred than distance metrics. Otherwise, for results from deterministic models, the distance metrics are more appropriate. The descriptive terms are composed of two elements: model accuracy and performance standards. Performance standards are criteria for measuring "acceptability" of simulation accuracy, and they are defined according to applications and scenarios. These number are not fixed such that the upper and lower bounds can be floating in a single application, especially when multiple phenomena and databases are available. At the same time, it is suggested that the designation of value bounds should be consistent with the meaning of metrics outputs. For example, if hypothesis testing is used, higher values suggest a higher confidence level, and the corresponding level should be higher; if distance metrics are used, higher values usually suggest larger error, and the corresponding levels should be smaller.

When validation data is collected directly from the prototypical system, the validation result can directly support the argument of simulation adequacy. However, when the data is collected from reduced-scale facilities or separate effect tests, additional evidence is needed for assessing the simulation adequacy in target applications. Different from the maturity level definitions in PCMM, attributes of data applicability and scaling analysis are not included in the validation result. Rather, a separate evidence characterization,

data applicability, is prepared to account for the effect of data relevance, scaling analysis, and data uncertainty. Meanwhile, the involvements of expert knowledge and judgment in selecting metrics and designing acceptance criteria are not included, and they will be discussed separately in the belief assessment.

*Data Applicability*

In addition to the levels from validation results, evidence of data applicability is also needed when the data is collected from reduced-scale facilities, Separate Effect Tests (SETs) or Integral Effect Tests (IETs), etc. The "data applicability" is defined by the similarity between validation facilities and reactor prototypical conditions. In this study, the maturity level of data applicability is characterized by a R/S/U grading system. The R/S/U is firstly developed by N. Dinh's works in 2013 [38] and has been used in [39] to evaluate the quality of validation data. The R/S/U system categorizes evidence of data applicability into three sub-attributes: [R]elevance, [S]caling, and [U]ncertainty, and each of them is designed according to their intrinsic properties. In this study, focuses have been put on extreme cases with binary grades for relevance and scaling attributes. In practical applications, intermediate grades can be introduced with higher resolutions. The relevance grade [R] is determined according to relationships of phenomenon and physics between application and reduced-scale validation databases. For example, the flow data collected from a curved tube is irrelevant to those in a straight tube since the phenomena are different; and the channel flows with $Re$ around $100$ is irrelevant from those around $5000$ since the dominating physics is different. The relevance grade is mostly determined by expert opinions. PIRT [40] and the corresponding quantitative version QPIRT [41] are strategies for identifying and ranking the relevance between validation databases and applications. The (physics) scaling grade [S] measures the degree of similarity between phenomena in the prototypical systems and reduced-scale experiments on the basis of physics scaling. At the same time, the scaling grade aims to determine if the validation databases are sufficient to justify extending the experimental model assessment results to applications. A formalized scaling analysis can be found in [5], and a recent review on scaling methodology can be found in [42]. In classical scaling analysis [27], dimensionless parameters are used for measuring the similarity between prototypical systems and reduced-scale facilities. If the dimensionless space of the validation databases covers the space of application, scaling analysis is claimed to be sufficient. Meanwhile, the database is claimed to be capable of representing behaviors and phenomena in the designated scenarios. For example, it is assumed that the lid-driven cavity flow can be sufficiently characterized by the Reynolds number ($Re$). It is also assumed that behaviors in the prototypical system can be represented by reduced-scale lid-driven cavity flow, while geometries, driven velocity, and fluid properties are different. As a result, the scaling grade for the validation databases can be decided by comparing the range of $Re$ for the reduced-scale database against the range under prototypical conditions. If the $Re$ range of validation databases covers that in prototypical systems, the scaling is graded as 1. Otherwise, scaling is graded as 0. In addition, scaling grade equals to 1 only if and only if the relevance [R] is not 0. Moreover, considering the effects of measurement errors, the uncertainty grade [U] is suggested for measuring the data uncertainty due to instrumentation errors and limited resolution.

For example, the data applicability assessment is performed when the target application is a channel flow, and the quantities of interest are the averaged flow velocity $v_0$. It is assumed that the flow can be fully characterized by Reynolds number ($Re$), and the target Re equals to $5 \times 10^3$. Meanwhile, it is required that the uncertainty, quantified by L1 relative error norm $\varepsilon_{QoI}$, in measuring $v_0$ is less than 50% of the characterized velocity $v_0$. It is further assumed that four databases are available from four different experiments. The experiment #1 is performed in a curved pipe with $Re \in [10^2, 10^4]$ and measurement error $\varepsilon_{QoI} = \pm 0.1 v_0$. The experiments #2, #3, and #4 are performed in straight pipes. Experiment #2 has $Re \in [10, 10^3]$ and $\varepsilon_{QoI} = \pm 0.1 v_0$; Both experiment #3 and #4 have $Re \in [10^2, 10^4]$, while experiment #4 has higher measurement errors $\varepsilon_{QoI} = \pm 2 v_0$. For experiment #1, since the phenomena in the curved pipe (case #1) is different from those in the straight pipe, the collected data is not relevant to the target application

even though the Reynolds number and data uncertainty satisfies the target conditions. Databases of case #3 and #4 are sufficient since the physical characterization ($Re$) of validation database covers the same characterization in the target application. However, case #2 does not cover the target application. Therefore, the scaling attribute of case #3 and #4 is rated as 1, while case #2 is rated as 0. The uncertainty of case #4 in measuring quantities of interest $\varepsilon_{QoI}$ is higher than the acceptance criteria, and the corresponding attribute is rated as 0. Uncertainty of case 2 and 3 satisfies the criteria and rated to be at least 1. As a result, case #3 is found to be applicable.

*Beliefs Assessment*

In addition to the maturity, belief in levels of validation results and data applicability needs to be assessed based on the prior knowledge. Considering the subjective and intangible nature of beliefs, a table of belief scales is prepared for the temporary quantification of intangibles, and the results are rendered in qualitative terms by applying this scale in reverse. Table 4.2 provides an example with an arbitrary assignment of probabilistic values; more sophisticated evaluations might be made by different sources and groups. The objective is to reach an agreement on a single or a class of scales, and the defense in depth is assured with better scrutability and communicability [2]. Also, beliefs can be estimated by metrics, including confidence interval, probability boxes, etc. [16] [37]However, their results cannot violate Eq. 4.2 such that an adequate margin can be ensured. Meanwhile, the belief can also be assessed based on expert opinions and represented by splinter probabilities. The value assignment in this study is arbitrary, and it is also suggested that the values are problem dependent. For scenarios with severe consequences and small margins, the belief assessment and the belief scales can be more stringent.

It is suggested that the attributes of data applicability and validation result are not independent. For example, it has been pointed out by [37] that the selection of validation metrics depends on the uncertainty grades. It is also suggested by [27] that the gradings for scaling and relevance are also correlated. Meanwhile, the assessment for data applicability and selection of validation metrics relies on expert opinions. Considering the objective nature of maturity level and R/S/U grades by their definitions, an evidence integration process is needed for integrating intercorrelations and dependencies among attributes, subjective and objective information to the final simulation adequacy. Although GSN provides structural representations of validation arguments, no quantitative result can be obtained. To better support risk analysis and guide model selections, additional techniques are needed to quantify evidence and to transform validation arguments into computable networks.

### 4.4.2. Evidence Integration

To integrate evidence in a transparent and consistent manner, many studies have employed Goal Structuring Notation (GSN) to integrate evidence to final simulation adequacy with the diagrammatic notation [43]. Based on the evidence characterization, the claim of overall simulation adequacy is supported by sub-claims of validation result and data applicability, which is further argued based on the R/S/U grade. **Error! Reference source not found.** depicts the network of simulation adequacy assessment by GSN [44] and defines principal components in GSN. The top objective (Goal #1) is to assess the adequacy of M&S for a designated scenario, and it is argued based on sub-claims of validation results and data applicability. Furthermore, the data applicability is argued based on three sub-claims: relevance, scaling, and uncertainty (R/S/U). The goals at bottom levels are solved by corresponding evidence and corresponding characterizations.

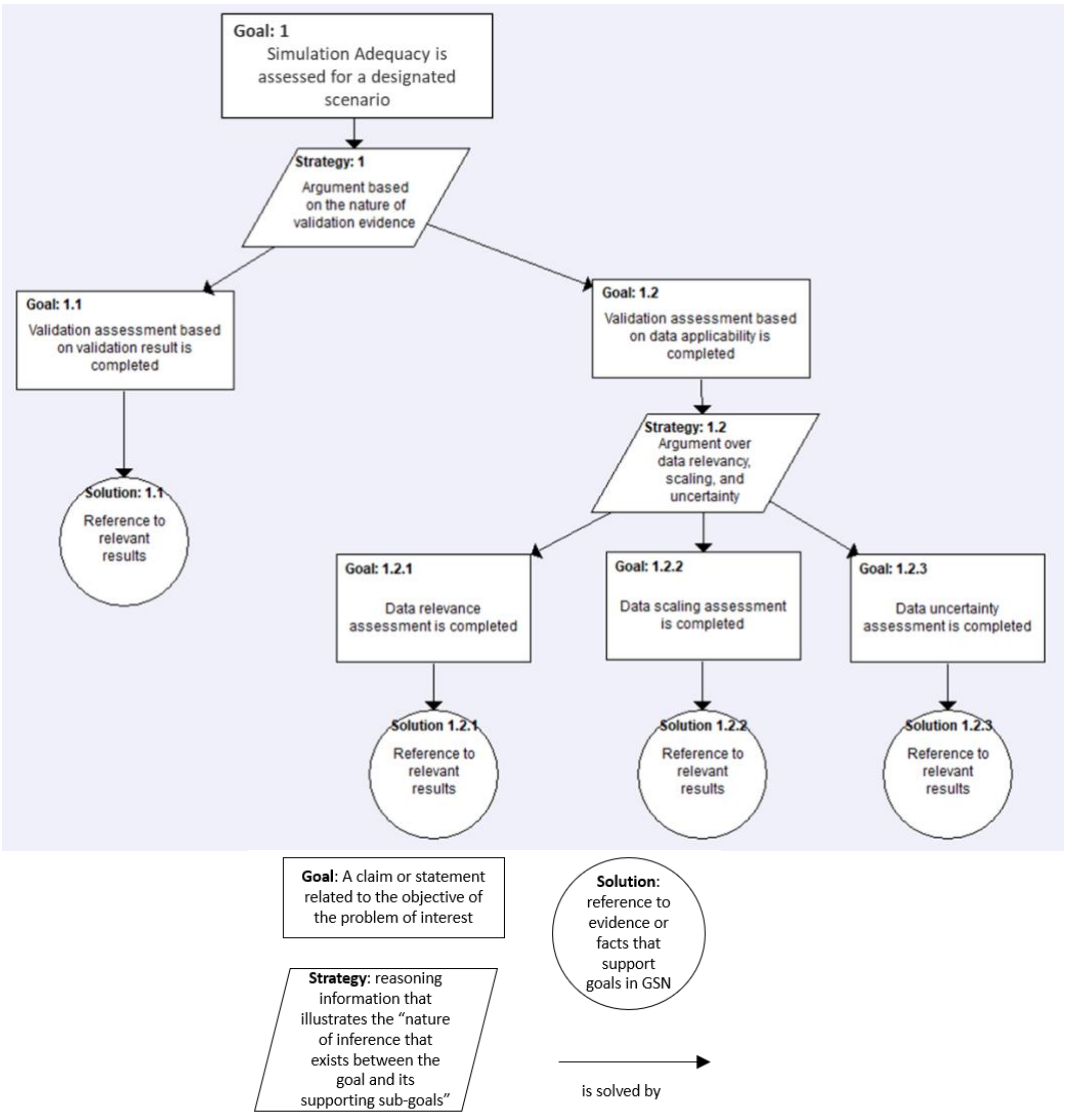


Figure 4.25: Decision model for simulation adequacy assessment in a designated scenario. Principal components and their descriptions in global structure notation (GSN).

To quantify the validation argument with mathematical languages, this work uses probabilities and connects them with logic for quantitative reasoning. Comparing to the classical logics with rigid and binary characters, probabilistic approaches soften the constraints of Boolean logic and allow truth values to be measured on a belief scale [45]. According to Eq. 4.3, the belief is represented as a function of causal relationships $\{d_i\}$, prior knowledge $\{\tilde{p}_i\}$, and decision parameters $\{k_i\}$. The prior knowledge, represented by probability, has been estimated as belief and collected from the validation framework, together with the evidence of validation result and data applicability. Causal relationship includes direct and indirect dependency among all attributes. Since the dependence can be uncertain, the dependence becomes conditional to all possible states of attributes or intermediate variables. Such a process enables reasoning "by assumption" and decompose the reasoning task into a set of independent subtasks. It also allows us to use local chunks of information taken from diverse domains and fit them together to form a global interference in stages, using simple, local vector operations. Since the quantification of conditional dependency relies on conceptual relationships and expert opinions, decision models are needed for assessing conditional probabilities. A validation knowledge base is constructed by quantifying components $\{d_i\}$, $\{\tilde{p}_i\}$, and $\{k_i\}$. In addition to different evidence characterizations, PCMQBN also aims to integrate

evidence from different databases, and a synthetic model is needed for assessing the conditional probabilities according to their levels in relevancy, scaling, data uncertainty, data applicability, and validation results.

For better visualizations, this study uses the Bayesian network to represent the statistical relationships between different evidence and attributes. A Bayesian Network (BN) is a directed acyclic graph (DAG) that is created by using the nodes represented by circles, arrows, and the conditional probability table. Each node defines either a discrete or a continuous random variable. An intermediate node serves as a parent as well as a child node. The nodes which have arrows directed to other nodes are parent nodes and nodes that have arrows coming from other nodes are called child nodes A node that does not have any arrow coming from another node is called as the root node, and it does not have any parent node. Arrows represent direct relationships between interconnected parent and child nodes. The conditional probability table assigned to each node describes the quantitative relationships between interconnected nodes. A BN analysis is performed based on the conditional probability as in Eq. 4.4 and the conditional independence assumption, i.e. $P(x, y|z) = P(x|z)P(y|z)$ if and only if $x \perp y|z$. The joint probability distributions can be described by conditional probability as:

$$P(X_1, X_2, \dots, X_n) = \prod_{i=1}^{n} P(X_i|X_1, \dots, X_{i-1}) \qquad \text{Eq. 4.4}$$

The conditional independence assumption simplifies Eq. 4.4 further as:

$$P(X_1, X_2, \dots, X_n) = \prod P(X_i|\text{Parent } (X_i)) \qquad \text{Eq. 4.5}$$

Parent $(X_i)$ is parent nodes for $X_i$; $P(X_i|\text{Parent } (X_i))$ is the conditional probability table of $X_i$; $n$ is the number of nodes in the network. A Bayesian network can also be used as an inference tool to evaluate beliefs of events when evidence becomes available. For evidence $e$, the joint probability of all the nodes can be inferred as:

$$\begin{aligned} P(X_1, X_2, \dots, X_n|e) &= \frac{P(X_1, X_2, \dots, X_n, e)}{P(e)} \\ &= \frac{P(X_1, X_2, \dots, X_n, e)}{\sum_{X_1,\dots,X_n} P(X_1, X_2, \dots, X_n, e)} \end{aligned} \qquad \text{Eq. 4.6}$$

In this study, node $X_i$ includes Simulation Adequacy (SA), Validation Result (VR), Data Applicability (DA), Relevancy [R], Scaling [S], and Uncertainty [U], and each node is further characterized by maturity levels. Based on Eq. 4.4 and Eq. 4.5, the joint probability distributions are calculated as a product of probability distributions of each of the variable's conditional on other variables. The conditional probability table is determined based on expert knowledge in casual relationships and dependencies among different nodes. Table 4.4 shows an example of assigning conditional probabilities when the data applicability is assessed based on evidence from R/S/U grades. First of all, it is 0% confident that corresponding data is applicable if the phenomena and involving physics are 100% not relevant; Meanwhile, the data is applicable with 100% confidence only if the data is relevant, scaling is sufficient, and data uncertainty is acceptable with 100% confidence [27]. Second, the confidence level of having applicable data drops to 60% if the data uncertainty becomes unacceptable; the level drops to 20% if the scaling becomes insufficient; the level further drops to 5% if both scaling and uncertainty are not acceptable. These number are required to be less than 100% based on findings by D' Auria [46] such that insufficient scaling and low-quality data are expected to have negative impacts on simulation adequacy assessment. However, the values are arbitrarily assigned to quantify the relative impacts due to different root causes, and it is assumed in this study that the negative impact due to insufficient scaling is higher than that due to low-quality data. Similar techniques

also apply to the conditional probabilities for simulation adequacy assessment. The simulation is 100% adequate if the data is applicable and the validation result satisfies the acceptance criteria. Moreover, it becomes 30% or less confident that the simulation is adequate if either validation result or data applicability does not satisfy the criteria.

Table 4.4. Example of conditional probabilities based on expert knowledge on causal relationships and dependencies among different evidence characterizations.

| **Conditional Probability** | **Value** |
|---|---|
| P(Yes-Applicable data \| No-relevant data) | 0 |
| P(Yes-Applicable data \| Yes-relevant & Yes-scaling & Yes-uncertainty) | 1 |
| P(Yes-Applicable data \| Yes-relevant & Yes-scaling & No-uncertainty) | 0.6 |
| P(Yes-Applicable data \| Yes-relevant & No-scaling & Yes-uncertainty) | 0.2 |
| P(Yes-Applicable data \| Yes-relevant & No-scaling & No-uncertainty) | 0.05 |
| P(Yes-Adequate simulation \| Yes-Applicable data & Yes-Validation result) | 1 |
| P(Yes-Adequate simulation \| Yes-Applicable data & No-Validation result) | 0.3 |
| P(Yes-Adequate simulation \| No-Applicable data & Yes-Validation result) | 0.25 |

**Error! Reference source not found.** shows examples of the Bayesian network with the conditional probabilistic prepared with GeNie [47]. Although the data is relevant and has good quality, the confidence for applicable validation data is 20% since the dimensionless space of validation data does not cover the space of the target application. Meanwhile, since the confidence of getting an adequate simulation given an acceptable validation and not applicable data is 0.25. the confidence for an adequate simulation is 40% even the simulation predictions have good accuracy in predicting the validation data.

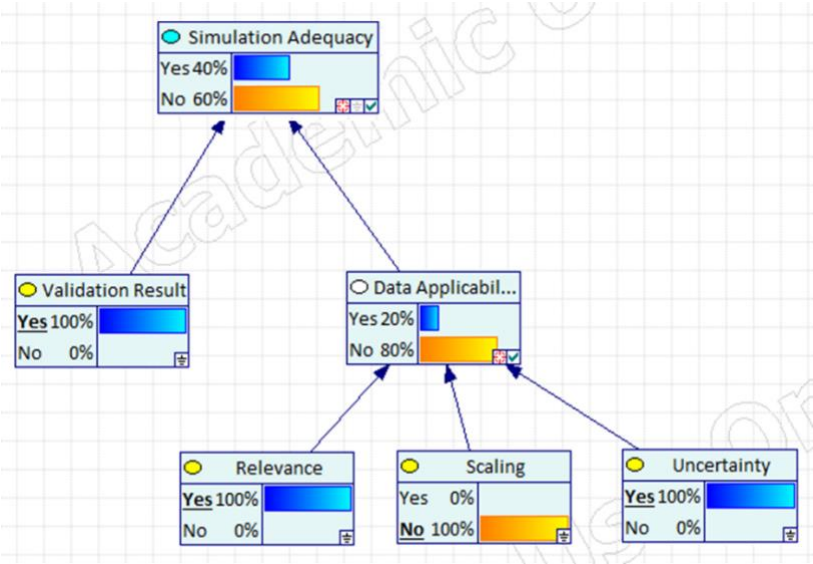


Figure 4.26: Example of Bayesian network for simulation adequacy assessments with designed conditional probability table by expert knowledge.

In practice, since multiple databases are usually used in the validation process, the overall simulation adequacy should account for impacts from multiple nodes that represent the simulation adequacy result from each database. In this study, a synthetic integration model is designed to determine the conditional probability based on the Reactor Prototypicality Parameter (RPP) and Experimental Measurement Uncertainty (EMU).

The concept of validation cubic was first suggested in [38], and the objective is to measure how close the given test conditions are to the reactor conditions in scenario of interest to the application. The term "cubic" refers to three-dimensional and normalized space, which is filled by a body of validation evidence from validation experiments. At the same time, each "dimension" is normalized to the range of 0 to 1 such that each face has a square shape. Three dimensions include Reactor Prototypicality Parameter (RPP), system decomposition, and physics models. RPP, Reactor Prototypicality Parameter, is defined as the significance of certain evidence in supporting claims in reactor conditions. In this study, a numerical value equal to 1 stands for highly significant evidence, in the sense that the data from validation experiments are relevant, sufficient, and high-quality. 0 means insignificant evidence where the data can be irrelevant, insufficient or low-quality. System decomposition represents the separation of target scenarios into sub-phenomena and sub-physics. As a result, the validation experiments can be classified into separate or mixed effect tests, where separate phenomena and physics are investigated in different facilities. Physics models refer to the micro-scale closures, equation sets, and macro-scale effective-field model for simulating the prototypical system. Figure 4.27 shows an example of a validation cubic. A body of evidence ($E_1, \dots, E_i, \dots$) is collected from experiments with different system decomposition, i.e. Separate Effect Test (SET), Mixed Effect Test (MET), Small-Scale Integral Effect Test (SS-IET), and Large-Scale Integral Effect Test (LS-SET). Meanwhile, each evidence $E_i$ is to develop the model and to support the validation over a range of models from sub-grid-scale models (closures) to macroscale Effective-Field Model (EFM). In this study, the RPP value is proposed to integrate the dimension of system decomposition and physics model, and it represents the relative importance of each evidence from the perspective of the physics model and system decomposition. Also, it is found that the status of evidence collection and simulation adequacy support is correlated with the filling of the Cubic's upper layer (RPP->1) across physics and system decomposition dimensions.

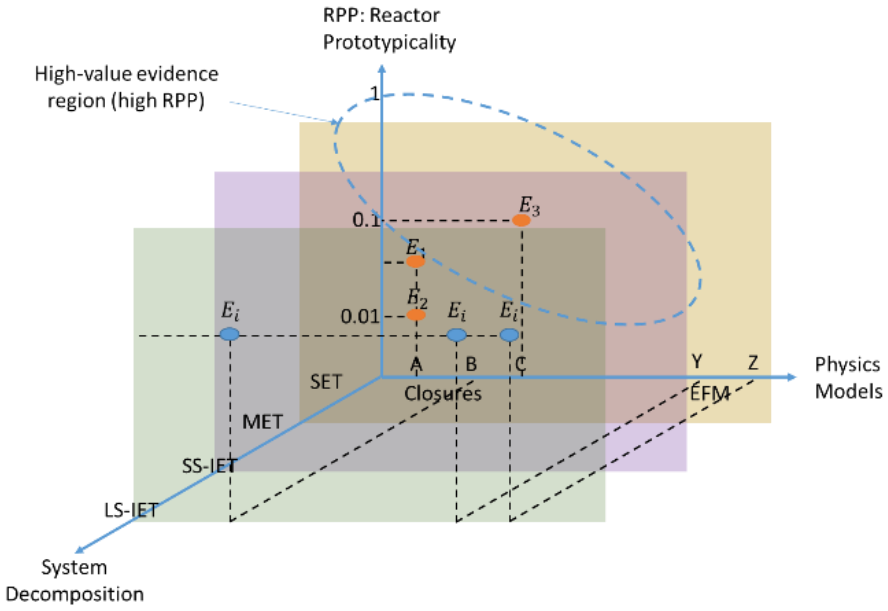


Figure 4.27: Validation Cubic for a body of evidence for validating sub-grid-scale models (closures) to macroscale effective-field model EFM. Evidence included ($E_1, \dots, E_i, \dots$) is notational and they are collected from different experiments or databases with different levels of system decompositions. The relative importance of evidence is represented by RPP values. The status of validation evidence and

simulation adequacy support is correlated with filling of the Cubic's upper layer (RPP->1) across physics and system decomposition dimensions.

This study suggests a synthetic model for determining the RPP values based on the ratio of scaling parameters (Sc) in the experiments $\left[Sc_{Mod_K}\right]_{EXP}$ and in the applications $\left[Sc_{Mod_K}\right]_{APP}$:

$$RPP = \left[Sc_{Mod_K}\right]_{EXP} / \left[Sc_{Mod_K}\right]_{APP} \quad \text{Eq. 4.7}$$

The $Mod_K$ represents the physical process $K$ calculated from test/experimental conditions, which is also a high-ranked physics in the application conditions. $\left[Sc_{Mod_K}\right]_{EXP}$ represents the scaling parameters of $Mod_K$ in experimental conditions, while $\left[Sc_{Mod_K}\right]_{APP}$ is the scaling parameters in the application's conditions. In fluid mechanics, $Sc_{Mod_K}$ can be quantified by dimensionless parameters, like Reynolds number and Mach number, which describe the relative magnitude of fluid and physical system characteristics, such as density, viscosity, speed of sound, flow speed, etc. To determine the conditional probability, a weight factor $\psi_{E_i}$ for each evidence $E_i$ is first calculated by Eq. 4.8 based on the EMU and RPP. in the validation cubic model [38].

$$\psi_{E_k} \sim m \cdot EMU_J + n \cdot RPP_{K,J} \quad \text{Eq. 4.8}$$

EMU is Experimental Measurement Uncertainty that measures the uncertainty of a certain experiment, and it is determined based on the level of uncertainty characterizations of experimental measurements. A similar characterization for uncertainty levels can be found in [37]. $m$ and $n$ are grades that represent the significance of experiment $J$ and the physics $K$. The experimental significance is affected by the quality and relevance of a given experiment, while the physical significance is ranked according to the PIRT process, where highly ranked phenomena and their corresponding physics should have high a significance factor $n$. Table 4.5 provides an example of parameter selections and their definitions in the validation cubic decision model.

Table 4.5. Summary of parameters in the validation cubic decision model.

| Experimental Measurement Uncertainty (EMU) for a given experiment $J$ | |
|---|---|
| [0, 1] | EMU = 0.001 ⇔ Level 0: Experimental uncertainties are unknown or largely biased |
| | EMU = 0.01 ⇔ Leve 1: Experimental uncertainties are qualitatively analyzed only |
| | EMU = 0.1 ⇔ Level 2: Experimental uncertainties are well characterized for most important measurements, but some remains poorly known |
| | EMU = 1 ⇔ Level 3: Experimental uncertainties are well characterized for all tests |
| Significance factor for a given experiment $J$: $m$ | |
| [0, 1] | Value ranging from 0 to 1. 0 represents insignificant experiments due to low relevance or low quality. 1 means highly significant experiments that are directly relevant to the applications, and the experimental quality is great. |
| Significance factor for a given physics $K$: $n$ | |
| [0, 1] | Value ranging from 0 to 1. 0 represents low-ranked phenomena and physics, while 1 means high-ranked ones based on PIRT results |
| Governing scaling parameters for model $\left[Sc_{Mod_K}\right]_{EXP}$ and application $\left[Sc_{Mod_K}\right]_{APP}$ | |
| [0, ∞) | Dimensionless quantities that measure the system invariance according to the model |

Figure 4.28 illustrates both 2D and 3D views of the validation cubic. To demonstrate the effects of significance factors, ranges of weight factors against the EMU values are made with three arbitrarily assigned values for $m$ and $n$. The minimum bound is obtained with RPP equals 0, while the maximum bound is obtained with RPP equals 1. It is emphasized that the current formulation is to illustrate the qualitative correlations between important decision parameters, i.e., the weight of evidence, and validation evidence, including scaling parameters, experimental VUQ qualities, etc.

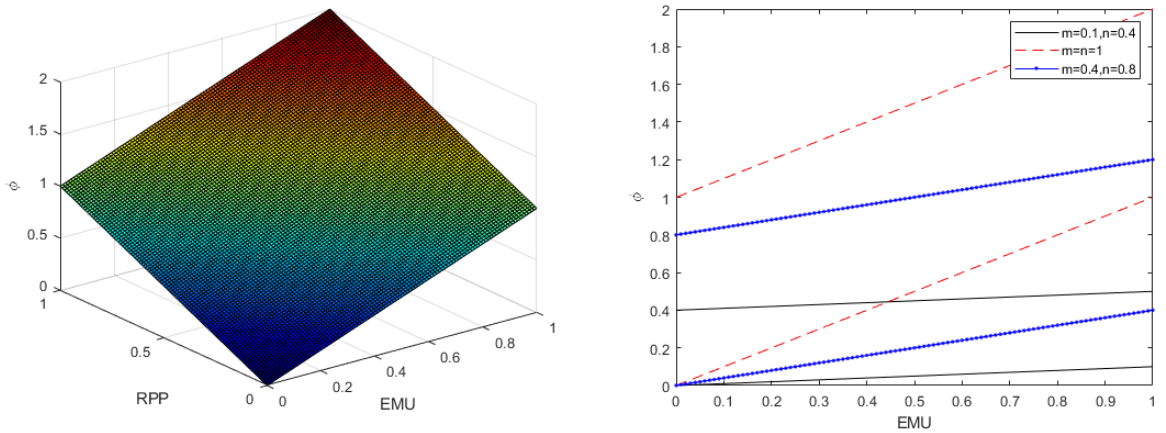


Figure 4.28: Illustration of validation cubic: left: 3D surface plot for weight factor $\psi_{E_i}$ given $m = n = 1$; right: ranges (minimum and maximum) of weight factors $\psi_{E_i}$ with three arbitrary values of $m$ and $n$. The uncertainty is introduced by samples of RPP values.

After determining the weight factor $\psi_{E_i}$ for each evidence $E_i$, they are normalized to $\tilde{\psi}_{E_i}$ according to Eq. 4.9 and used as the conditional probabilities between overall simulation adequacy $CA$ and individual simulation adequacy from separate databases.

$$P\left(SA\middle|SA_{E_i}\right) = \psi_{E_i} / \sum_{i=1}^{n} \psi_{E_i} \qquad \text{Eq. 4.9}$$

Considering the previous discussion on validation result and data applicability, the general standards for simulation adequacy can be identified as:

**Adequate** – For the high-rank phenomena, the accuracy in predicting the quantity of interest is acceptable. The simulation can also be confidently used in similar applications with relevant, scaling, and high-quality validation databases (high R/S/U grades or answer yes). The accuracy in predicting corresponding quantities of interest should also be acceptable.

**Inadequate** – For the high-rank phenomena, the accuracy in predicting the quantity of interest is unacceptable. The simulation cannot be confidently used in similar applications with irrelevant, insufficient, or low-quality validation databases (low R/S/U grades or answer no).
The inadequacy can be caused by reasons including unacceptable validation result, irrelevant, low-quality data insufficient validation data. In classical validations, the simulation is inadequate if one of these conditions is satisfied. In the PCMQBN framework, the simulation becomes "partial" inadequate, and the degree is defined based on beliefs in probability.

### 4.4.3. Sensitivity Analysis

Sensitivity analysis is the study of how the uncertainty in the output of a system can be divided and allocated to different sources of uncertainty in its inputs [48]. In Bayesian-network applications, sensitivity

analysis investigates the effect of small changes in numerical parameters (prior probability, conditional probability) on the output parameters (posterior probabilities). Since the design and parameter selection of PCMQBN requires expert inputs, it is necessary to evaluate that induced uncertainty in the PCMQBN framework. A list of uncertain parameters is designed, including beliefs on the levels of evidence, conditional probability, and evidence integration structures. Next, a sensitivity analysis is performed to assess the impact of each parameter on any target nodes. In this study, an algorithm by Kjaerulff and van der Gaag [49] is used for calculating a complete set of derivatives of the posterior probability distributions over the target nodes over each of the uncertain parameters. Figure 4.29 shows an example of a tornado plot for the Bayesian network in **Error! Reference source not found.**. Twelve variables are sampled, including the belief in the evidence of validation result is acceptable (VR=Yes), validation data is relevant (DA_R=Yes), validation data is sufficient for scaling (DA_S=Yes), the probability of having an adequate simulation given that the data is applicable and validation result is acceptable (SA=Yes|DA=Yes, VR=No). All parameters are sampled from 0 to 1, and the width of each bar represents the range of belief values on the target attribute (Simulation adequacy = Yes). It can be found that evidence of validation result has the most significant impact on simulation adequacy. This is reasonable since the comparison between model predictions and experimental data directly represents the simulation's degree of accuracy. The conditional dependencies of simulation adequacy on data applicability and validation result have more impacts on the target belief than other dependencies.

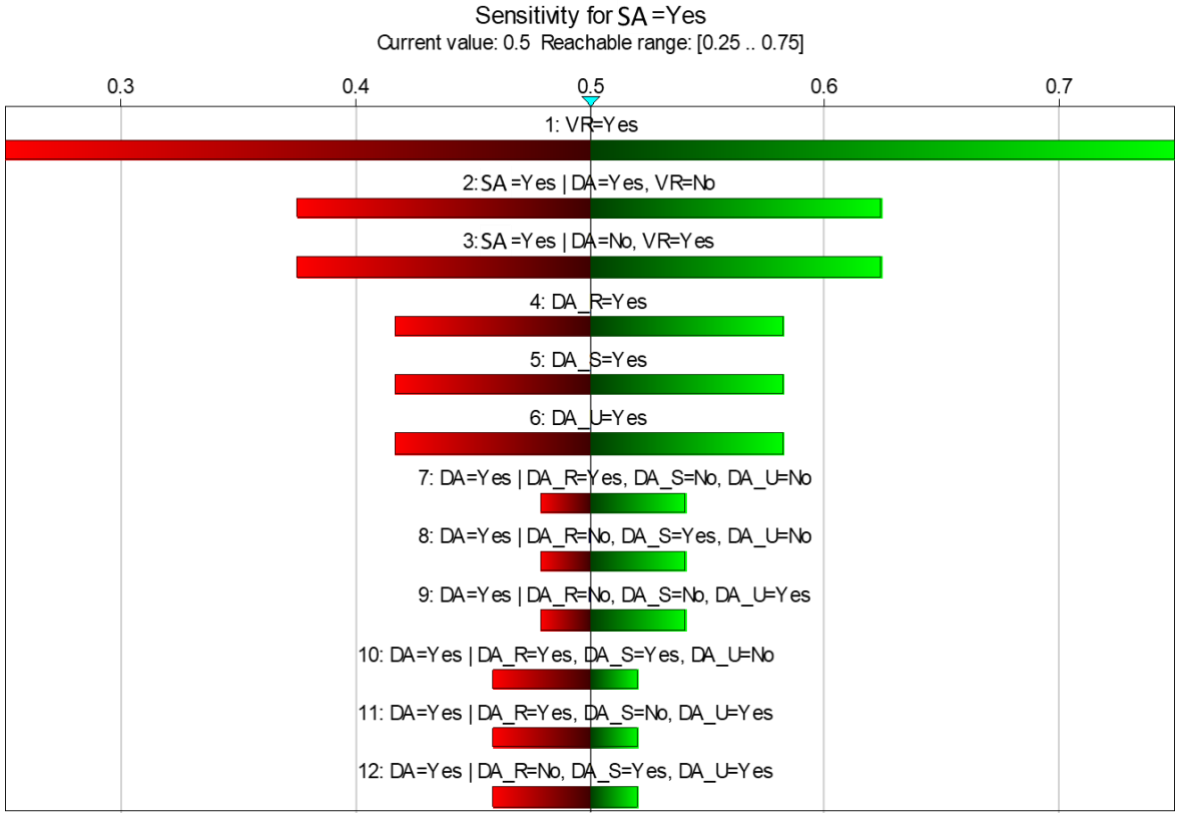


Figure 4.29: Example of tornado sensitivity plot. All listed evidence and conditional probabilities are sampled by 40% of their current values, the colored bar shows the maximally reachable ranges for the final simulation adequacy results. These ranges are arranged based on their widths, while the number indicates their ranks of importance to the simulation adequacy.

Sensitivity analysis is a unique feature enabled by formalizing and quantifying the decision-making process. It improves the robustness of the assessment results for simulation adequacy in the presence of uncertainty. It also helps the understanding of correlations between different attributes in the validation

decision-making process such that the structure can be continuously refined. Moreover, by identifying the most sensitive attribute, simulation adequacy can be improved by collecting evidence of specific phenomena, improving the model performance for local predictions, and refining the conditional-dependency parameters. In addition, the sensitivity analysis offers a simple strategy against the imprecision issue in classical Bayesian analysis, where the uncertainty is required to be measured by a single (additive) probability, and values can be measured by a precise utility function [16]. However, such an assumption is very hard to achieve in validation since the data is too few to make precise estimates on the probability and the distribution. By performing a sensitivity study on various sources of uncertainty, the standard analysis is applied to all possible combinations of the decision including parameters, evidence, integration structure, etc. Next, a class of simulation adequacy is determined, and if the class of decisions is approximately the same, it can be claimed that a robust result is obtained. Otherwise, the range can be taken as an expression of confidence from the analysis. As a "convenient" approach against the imprecision issue, this method is also known "Robust Bayes" or "Bayesian sensitivity study" [50] [51].

#### 4.4.4. Phase of Simulation Adequacy Assessment

To manage the progress of validation activities, PCMQBN adequacy assessment, sensitivity analysis, and applications, this study defines three phases of development for grading the quality and confidence in the simulation adequacy results based on the sources and levels of uncertainties. **Error! Reference source not found.** defines the phases of development based on the sources and levels of uncertainties in simulation adequacy assessment by PCMQBN. At each stage, evidence needs to be collected and characterized accordingly. Meanwhile, the uncertainty in each evidence, parameter, integration structure, and the final simulation adequacy need to be evaluated. Complete documentation and review of this process mark the completion of each phase. Phase 1 is designed for initial adequacy assessment. Although the uncertainty in final adequacy is large, the objective is to agree on the evidence selection, conditional dependencies, acceptance criteria, and qualitative impacts on the target applications. Meanwhile, it serves as the foundation for phase 2. Most validation activities and decision-making efforts will be conducted in Phase 2, and the objective is to have an adequate simulation that can support designated decisions with confidence. The quality assurance for the simulation is also required to prevent defects and issues in software products. Phase 3 involves licensing and regulatory activities, and the objective is to provide confirmatory results and define a defense-in-depth in evaluation.

Table 4.6. Definition of phases of development.

| Phase # | | Sources of Uncertainty | Levels of Uncertainty |
|---|---|---|---|
| 1 | Scoping | Largely uncertain conditional dependency with unknown bounds.<br>Insufficient evidence or imprecise beliefs on evidence with uncertain bounds.<br>Unverified or low-quality evidence. | Uncertainty in the final simulation adequacy is so large that preliminary sensitivity analysis shows that the uncertainty will alter the decisions in designated scenarios and applications. |
| 2 | Refinement | Uncertain conditional dependency with known bounds.<br>Sufficient evidence with imprecise beliefs but known bounds. | Uncertainty in the final simulation adequacy has known ranges or distributions with confidence levels. The uncertainty can alter the decisions only at the edge of scenario spectrum |
| 3 | Maturation | Conditional dependency with precisely known distributions.<br>Sufficient evidence with beliefs on evidence and precisely known distributions. | Uncertainty in the final simulation adequacy is precisely characterized, and they are not likely to alter the decisions. |

To illustrate the process and help the understanding, a case study is prepared for assessing the simulation adequacy for Smoothed Particle Hydrodynamics (SPH) methods in external-flooding scenarios. A validation process has been performed and discussed in [52]. The current case study is at the scoping stage, and the decision parameters are subject to sensitivity analysis.

### 4.5. Adequacy Assessment for SPH Methods by PCMQBN

To demonstrate the capability of PCMQBN in assessing the adequacy of simulation results, this study assesses the adequacy of SPH simulations in predicting the impact forces during an external-flooding scenario. Evidence is collected from the CSAU/EMDAP framework, which is performed and explained in detail by a separate work [53]. Sub-section 5.1 describes the assessment process for simulation adequacy. Sub-section 5.2 evaluates the sensitivity of simulation-adequacy results by sampling decision parameters and evidence characterizations. Sub-section 5.3 describes the application of simulation adequacy from PCMQBN results.

There are different types of flooding scenarios evaluated by the nuclear industry, and each may have multiple criteria for adequacy acceptance. For this external-flooding example, the analysis purpose is to assess if the simulation adequacy of SPH to model impact forces when simulating the scenario of "floods damage the building structures, enter the room, and cause diesel generator (DG) malfunctioning" is acceptable. The validation framework CSAU and its regulatory guide EMDAP is used for qualitative adequacy assessment. Figure 4.30 shows the scheme of the CSAU-guide validation process, and results from all activities lead to a qualitative decision of simulation adequacy for SPH methods in designated applications. The SPH methods and the simulation code, Neutrino, are explained in [53].

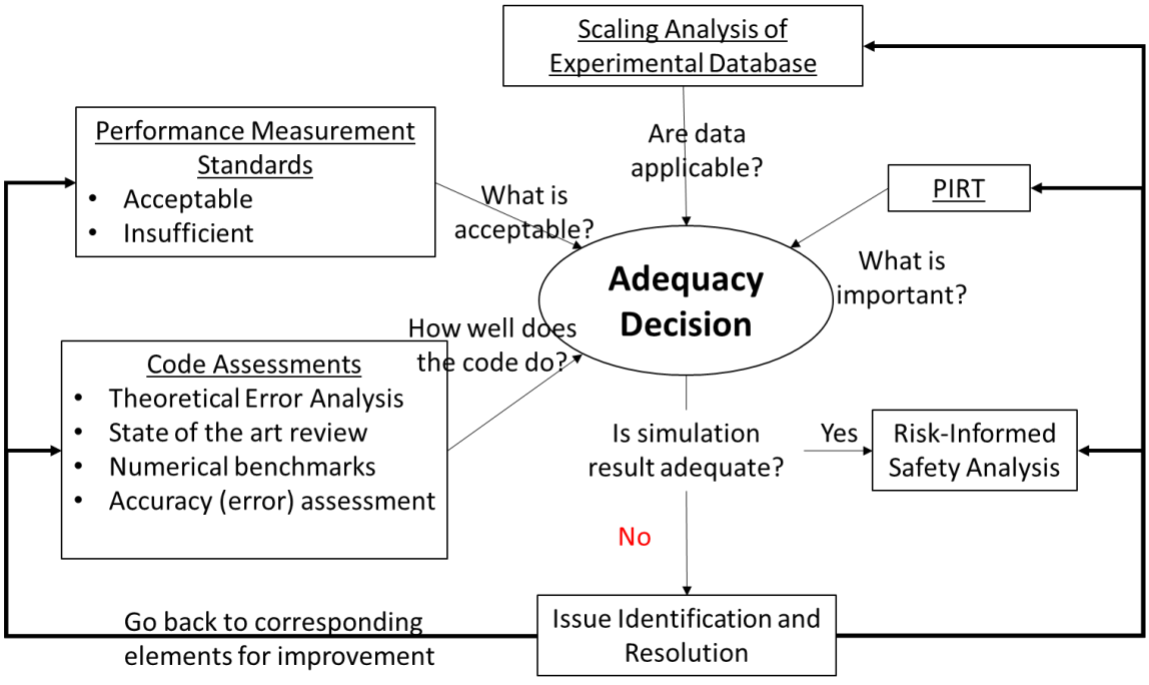


Figure 4.30: Demonstration of adequacy assessment based on CSAU/EMDAP.

The corresponding QoIs include the response time and the structural loads on Systems, Structures, and Components (SSCs) by floods. The response time is the time for the external floods to reach the DG building and to potentially fail the DGs, while the structural loads are the pressure forces acting on the

nuclear SSCs by the floods. This study focuses on the adequacy assessment of SPH methods in predicting the structural loads. An SPH-based software, Neutrino [11], is used to simulate an external-flooding scenario.

A PIRT process is performed to rank the importance of separate phenomena for evaluating the simulation adequacy in the designated scenarios. To estimate the structural loads with sufficient accuracy, the adequacy of SPH methods in simulating the hydrodynamic forces on stationary structures is highly important. As a result, a validation database is constructed with a list of numerical benchmarks, and evidence of simulation accuracy (validation result) is collected by comparing simulation predictions against measurements from each benchmark. At the same time, a scaling analysis is performed to evaluate the applicability of all databases. Table  shows a list of benchmarks together with qualitative results for each assessment. In both benchmarks, the peak pressure forces are selected as the quantity of interest, and SPH simulations are performed with different simulation parameters for complete uncertainty quantification. Next, simulation results are compared against the experimental measurements, and an L1 metric (L1 relative error norm) described in Eq.  4.10 is used to evaluate the accuracy of SPH's performance. The accuracy is acceptable if $L_1$ is less than 20%.

$$L_1 = |\frac{QoI_{preds} - QoI_{meas}}{QoI_{meas}}| \qquad \text{Eq. 4.10}$$

where $QoI_{preds}$ represents the predicted quantity of interest by Neutrino, while $QoI_{meas}$ represents the measurements from experiments. More details about the accident scenario, PIRT process, performance measurement standards, accuracy and scaling analysis can be found in [52].

Table 4.7. Validation results for SPH methods in simulating hydrodynamic forces on stationary structures in the external-flooding scenario.

| **Benchmark** | **Simulation Adequacy** | **Accuracy (L1 error)** | **Data Applicability** | | |
|---|---|---|---|---|---|
| | | | **Relevancy** | **Scaling** | **Data Quality** |
| Dam Break | Adequate | Acceptable ($L_1$=3.6%) | Yes | Yes | High |
| Moving Solids in Fluid | Inadequate | Falling: Acceptable ($L_1$=5.52%) | Yes | No | High |
| | | Floating: Acceptable ($L_1$=4.41%) | | | |

It is found from the dam break benchmark that the SPH method can adequately predict the hydrodynamic forces on the stational object with acceptable accuracy and applicable databases. At the same time, an opposite conclusion is obtained from the moving solids in fluid benchmark since the experimental scale is too small to cover the application scenarios. Therefore, based on the collected databases, it is hard to decide whether SPH methods can predict the hydrodynamic force on solid objects with acceptable accuracy since claims from two benchmarks seem to be contradictory. To reduce uncertainty, PCMQBN is applied to assess the simulation adequacy with the validation cubic model.

### 4.5.1.PCMQBN Adequacy Assessment

Since evidence from two experimental databases is used, the weight factor needs to be calculated, and Table 4.8 shows the assignment of decision parameters based on validation activities from CSAU/EMDAP. Parameter $m$ represents the significance of dam-break and moving-solid-in-fluid experiments. It ranges from 0 to 3, and it is mainly determined by the quality of experiment and collected data. Since the dam break data is collected by extracting graphical points from literatures, its experimental significance is rated as low (=1). The moving solid data is collected directly from experimental facilities, and repeated runs are

performed to quantify the experimental uncertainties from sensors, equipment, operating conditions, etc. Therefore, the moving-solid experiment is rated as high (=3). Parameter $n$ represents the significance of physics in two experiments, and it is rated according to the PIRT process. Since both experiments are investigating the phenomenon of hydrodynamic forces on stationary structures, they are rated as high, and the corresponding value is 3. $\left[Sc_{Mod_K}\right]_{EXP}$ and $\left[Sc_{Mod_K}\right]_{APP}$ are scaling parameters in experimental and prototypical conditions respectively. A scaling analysis has been performed and discussed in [52]. A dimensionless number $x^*$ is suggested for the dam break benchmark according to Eq. 8.50. $L$ is the distance between the gate and the solid object, $h$ is the initial depth of surface wave.

$$x^* = h/L \qquad \text{Eq. 4.11}$$

Table 4.8: A list of decision parameters in validation cubic model. The value is assigned based on author's knowledge.

| **Decision Parameters** | **Dam Break** | **Moving Solid in Fluid** |
|---|---|---|
| $m$ | 1 (Low) | 3 (High) |
| $n$ | 3 (High) | 3 (High) |
| $\left[Sc_{Mod\_K}\right]_{EXP}$ | 0.1~0.26 ($x^*$ EXP) | 0.017 ($x^*$ EXP) |
| $\left[Sc_{Mod\_K}\right]_{APP}$ | 0.1 ($x^*$ APP) | 0.1 ($x^*$ APP) |
| $RPP$ | 1 | 0.17 |
| $EMU$ | 0.1 (Level 1) | 0.01 (Level 2) |
| $\psi_{E_i}$ | 0.43 | 0.16 |
| $\overline{\psi_{E_i}}$ | 0.73 | 0.27 |

For the moving-solid benchmark, the scaling analysis shows that the accuracy in predicting the buoyance force depends on the particle intensity around the solid object. Therefore, for the moving object calculation, the cube density ratio ($\rho^*$ defined in Eq. 4.12) and the ratio between cube volume and average particle volume ($V^*$ defined in Eq. 4.13), are selected as the dimensionless parameters. $\bar{V}_{dp}$ is the average particle volume defined by Eq. 4.14 [54], and $d$ is the initial particle diameter.

$$\rho^* = \rho_{cube}/\rho_{fluid} \qquad \text{Eq. 4.12}$$

$$V^* = V_{cube}/\bar{V}_{dp} \qquad \text{Eq. 4.13}$$

$$\bar{V}_{dp} = d^3 \qquad \text{Eq. 4.14}$$

Based on the scaling parameters, the RPP can be determined according to Eq. 4.7. The dam break has RPP equal to 1 since the range of dimensionless parameters in validation databases covers those in the application scenario. The EMU is rated according to the characterization of experimental uncertainties (Table 4.5). Since the dam break data does not have any uncertainty information, the uncertainty level is rated as level 1 (EMU=0.1). The uncertainty of moving solid measurements is quantified by repeated runs and rated as level 2 (EMU=0.01). At last, all parameters are substituted into Eq. 4.8, and the weight factor

$\psi_{E_i}$ for each benchmark can be determined. They are further normalized to $\overline{\psi_{E_i}}$ such that they can be further used in PCMQBN for calculating the conditional probabilities.

Figure 4.31 shows the Bayesian network for simulation adequacy assessment based on evidence and decision parameters for two numerical benchmarks. It is found that the belief level on the claim that the SPH method is adequate in predicting the hydrodynamic force is 100% when the simulation adequacy is estimated solely by evidence from the dam break benchmark. This finding is consistent with the qualitative result given the simulation accuracy and data applicability for the dam break benchmark. Meanwhile, the belief level on the same claim becomes 36% when the simulation adequacy is estimated by evidence from the moving-solid experiment. This result is similar to the qualitative results where the simulation is not adequate in simulating pressures in the moving-solid benchmarks. Furthermore, it is found that the belief level for an adequate SPH simulation is 83% when evidence from both benchmarks is used. Compared to the qualitative results, there is higher confidence that the SPH simulation is adequate for the designated purposes based on available evidence. Also, the uncertainty of simulation adequacy is less than that from the qualitative assessment since the contradictory results suggest a non-informative adequacy distribution.

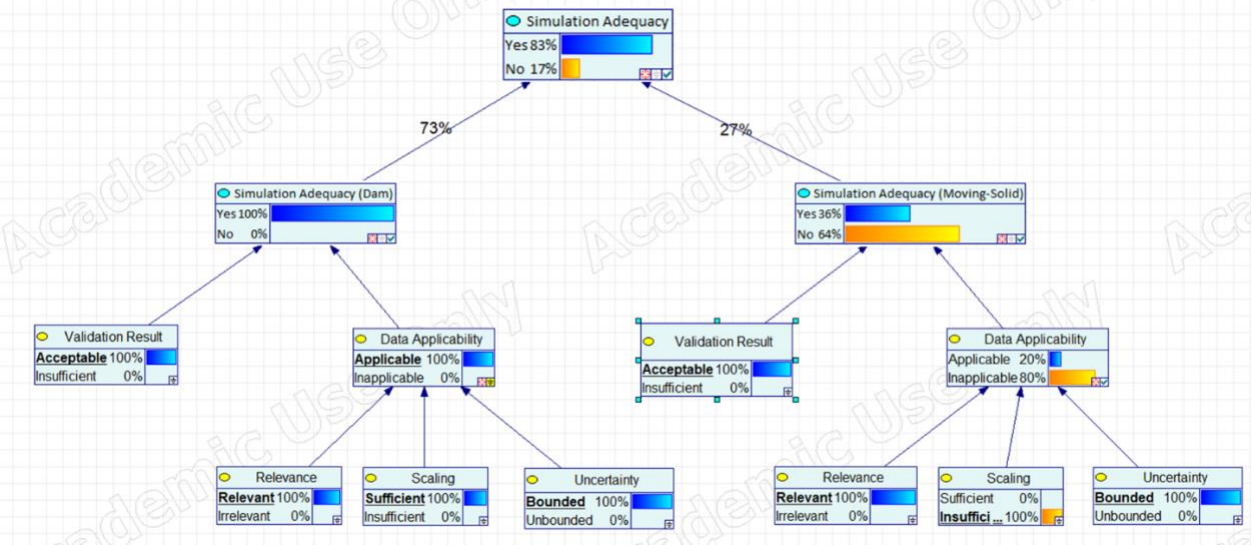


Figure 4.31: Simulation adequacy estimated by the evidence from two benchmarks and weight factors estimated by the listed decision parameters.

### 4.5.2. Sensitivity Analysis

Considering the uncertainty of assigning decision parameters, a sensitivity study is performed by sampling all conditional probabilities by 10% of their current values. Figure 4.32 shows the sensitivity tornado, and it turns out that the relative importance of two validation databases, i.e. P(SA=Adequate|SA_DAM = Adequate, SA_Moving = Inadequate), has the highest impact on the final simulation adequacy. When the conditional probability is sampled from 0.438 to 1 (currently at 0.73 based on the RPP model), the probability of having an adequate simulation range from 0.64 to 1.

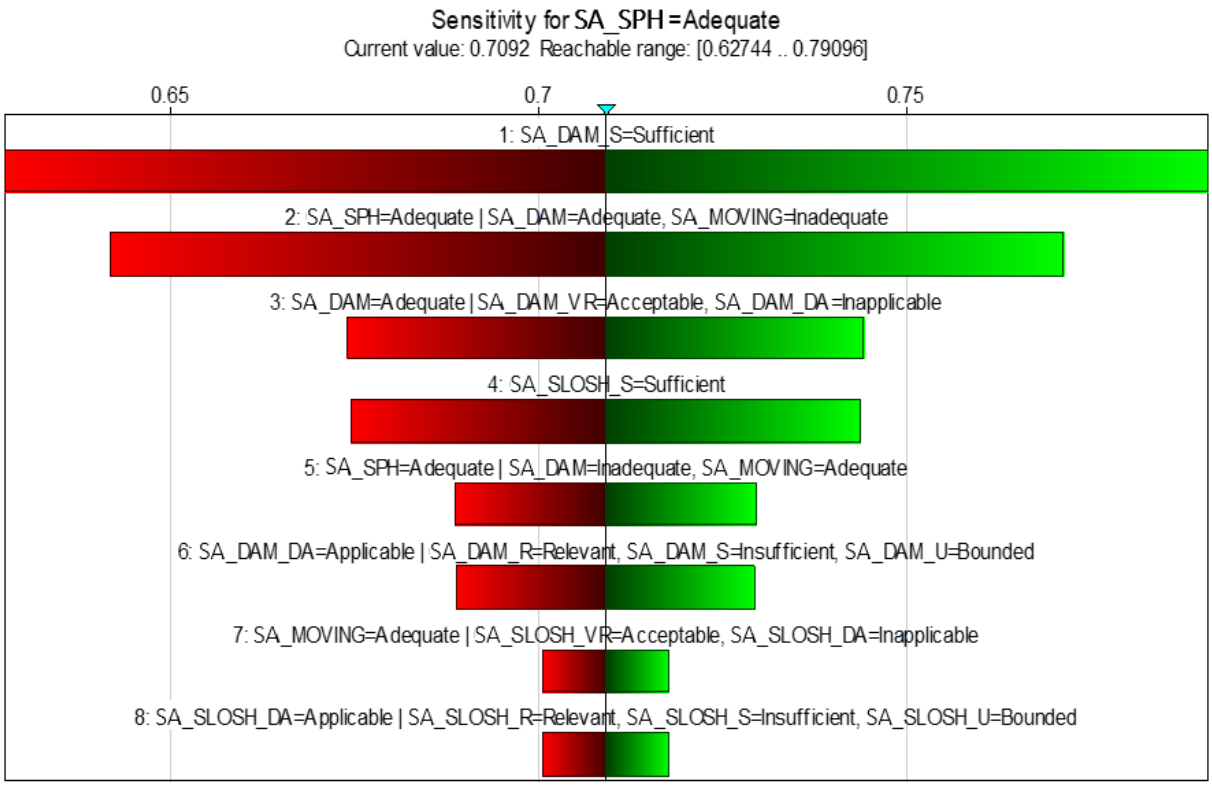


Figure 4.32: Sensitivity plot for the simulation adequacy assessment with uncertain scaling grade and uncertain conditional probabilities. All conditional probabilities are sampled by 40% of their current values, the maximally reachable belief in an adequate simulation range from 0.63 to 0.8.

At the scoping stage, the evidence of scaling grade can be unverified. Thus, another sensitivity analysis is performed by excluding the evidence on scaling grade and setting the belief in sufficient/insufficient scaling as 50%/50%. The belief in an adequate simulation has reduced to 71%. Figure 4.32 shows the sensitivity tornado of simulation adequacy result with uncertain scaling grade and conditional probability. It is found that the scaling analysis for the dam break benchmark has the highest impact on the simulation adequacy result. When the parameter is sampled from 0.3 to 0.7 (currently at 0.5), the simulation adequacy ranges from 0.63 to 0.8. Meanwhile, the relative importance of two validation databases, i.e. P(SA=Adequate|SA_DAM = Adequate, SA_Moving = Inadequate), still has a high impact. Therefore, it is recommended that the sufficiency analysis (scaling grade) for validation databases needs to be verified and ensured with high confidence levels. At the same time, the relative weights of two evidence from the RPP model need to be carefully examined. However, in both cases, where scaling grade and conditional probabilities are uncertain, the beliefs on an adequate simulation are higher than 50%, and it suggests a more informative distribution than the qualitative decision analysis.

### 4.5.3. Application of PCMQBN Adequacy Results

To further demonstrate how PCMQBN results can be used in risk-informed validation (Figure 4.24), a risk-informed safety analysis is performed to evaluate potential damages to SSCs of NPPs by water waves. SPH simulations are performed to determine the structural loads by a wave for 60 cycles. The cycle is defined based on the frequency of hydrodynamic pressures by the surface-wave. Figure 4.33 shows the predicted time transient of hydrodynamic pressure $Pr(t)$ and impulse, and 1 cycle lasts for 9.09sec. The impulse is calculated by:

$$Im(t) = \int_{T_0}^{T_0+t} Pr(t)\, dt \qquad \text{Eq. 4.15}$$

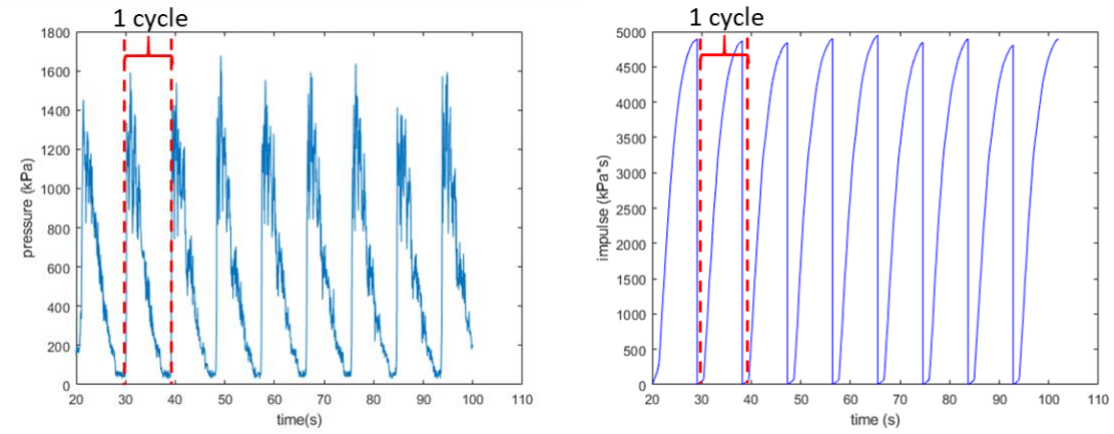


Figure 4.33: Predicted time transient of hydrodynamic pressures (left) and impulse (right) onto the structure by water surface waves.

To evaluate damages from structural loads in each wave cycle, the pressure-impulse (P-I) diagram is calculated for each cycle. The pressure-impulse diagram is determined by finding the maximum pressure and maximum impulse in each cycle. In structural engineering, the P-I diagram is used to describe a structure's response to blast load. Depending on the P-I values in each cycle, damages to the structure by surface waves can be characterized by 4 damage levels as in Figure 4.34. This study uses the P-I diagrams for Reinforced Concrete (RC) structures, and the curve of damage levels is made based on experimental data from [55].

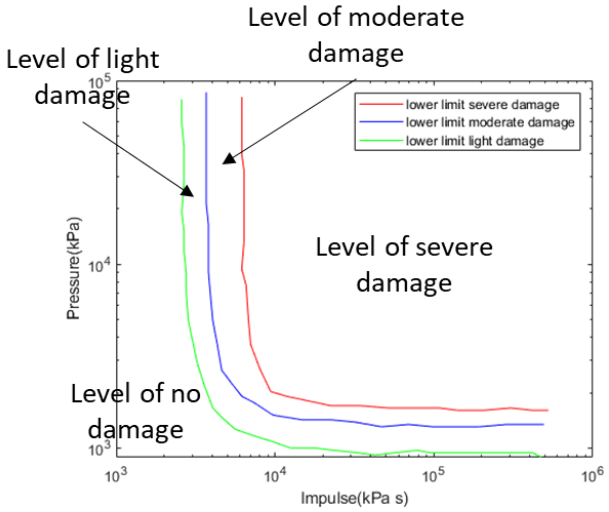


Figure 4.34: Logarithm plot of damage levels. Four levels of damage are defined based on the P-I values.

Based on the adequacy definition, the accuracy is acceptable when the L1 error in predicting hydrodynamic pressure is less than 20%. It is further assumed that when the simulation is not adequate, either due to unacceptable error or inapplicable data, the prediction will have maximally 100% L1 errors. As a result, error bands are added to the SPH predictions by:

$$y = Y_{prd} + \varepsilon_r Y_{prd} \qquad \text{Eq. 4.16}$$

$Y_{prd}$ is the SPH prediction for the hydrodynamic pressure and impulse, $\varepsilon_r$ is the maximum L1 error by the requirements: $\varepsilon_r$ equals to 20% when the simulation is adequate, and the accuracy is acceptable; $\varepsilon_r$ equals

to 100% when the simulation is not adequate. When the simulation adequacy is uncertain, the prediction is linearly assembled based on the confidence:

$$y_{en} = P(adq) \cdot y_{adq} + (1 - P(adq)) \cdot y_{inadq} \quad \text{Eq. 4.17}$$

$y_{en}$ is the ensembled predictions; $P(adq)$ is the confidence in the claim that the simulation is adequate; $y_{adq}$ is the SPH predictions with error bands when the simulation is adequate ($\varepsilon_r = 20\%$); $y_{inadq}$ is the predictions with error bands when simulation is not adequate ($\varepsilon_r = 100\%$). Figure 3.35 shows the distribution of P-I values onto the damage-level plots for all 60 cycles in four conditions: (1) the simulation is 100% adequate; (2) the simulation is 100% inadequate; (3) the simulation is 50% adequate and 50% inadequate; (4) the simulation is 83% adequate and 17% inadequate.

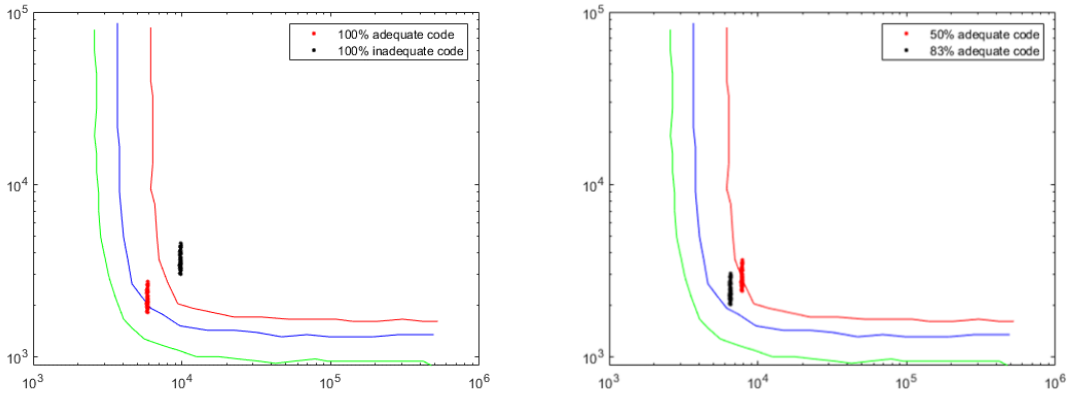


Figure 3.35: Distribution of P-I values onto the damage levels for all 60 cycles when the simulation is 100% adequate or 100% inadequate (left) and when the simulation is 50% adequate or 83% adequate (right).

The number of cycles in each different damage levels can be found with different simulation adequacy results. Table 4.9 shows the number of cycles in each damage level for four distributions of P-I values based on the simulation adequacy results. If no validation decision is made, on one hand, when the simulation is presumably 100% inadequate, all damages are predicted to be severe; on the other hand, when the simulation is presumably 100% adequate, there are no severe damages, and 21 out of 60 cycles result in light damages. If validation activities are performed, and when a qualitative validation decision is made with 50/50 adequacy results, 26 out of 60 cycles (43.3%) turn to be severe. However, when a quantitative validation decision is made 83/17 adequacy results based on the PCMQBN framework, all cycles turn to be moderate.

Table 4.9. Number of cycles in each damage levels for four different simulation adequacy results.

| **Damage Level (DL)** | **Loss (C)** | **Probability of Occurrence $P_{DL}$ among 60 cycles** | | | |
|---|---|---|---|---|---|
| | | **100% Adequate** | **100% Inadequacy** | **Ensembled 50/50** | **Ensembled 83/17** |
| *No* | 0 | 0/60 | 0/60 | 0/60 | 0/60 |
| *Light* | $10 | 21/60 | 0/60 | 0/60 | 0/60 |
| *Moderate* | $50 | 39/60 | 0/60 | 34/60 | 60/60 |
| *Severe* | $100 | 0/60 | 60/60 | 26/60 | 0/60 |

To further demonstrate how these predictions affect the safety analysis, an expected loss $\langle C \rangle$ is calculated based on a table of synthetic monetary loss and the probability of each damage levels.

$$\langle C \rangle = \int P_{DL} \cdot CdC = \sum_{i=1}^{4} P_{DL(i)} \cdot C_{DL(i)} \quad \text{Eq. 4.18}$$

$C_{DL(i)}$ is the consequence in monetary losses for the damage level $i$, and a synthetic value is assigned in Table 4.9; $P_{DL(i)}$ is the chances that the predicted cycles will fall into the damage level $i$, and it is determined in Table 4.9. $i$ ranges from 1 to 4 and it represents four damage levels from no damage to severe damage. Table 4.10 shows the value of expected loss $\langle C \rangle$ based on Eq. 4.18 and corresponding values in Table 4.9.

Table 4.10. Expected losses for four simulation adequacy results.

| **Decision Analysis** | **Expected Loss $\langle C \rangle$** |
|---|---|
| Qualitative and Implicit framework (Ensembled 50/50) | \$71.67 |
| PCMQBN decision framework (Ensembled 83/17) | \$50 |
| Optimistic decision maker (100% Adequate) | \$36 |
| Conservative decision maker (100% Inadequate) | \$100 |

It is found that if the decision maker is willing to accept potential risks by the simulation errors and completely trust the simulation with 100% simulation adequacy, the expected loss is the smallest, which suggests an optimistic attitude to the simulation prediction errors. However, if the decision maker is not willing to accept any risks by simulation errors, the expected loss is greatest, which suggests a conservative attribute to the simulation and its prediction errors. Meanwhile, it is found that with simulation adequacy result assessed by PCMQBN (83/17), the expected loss is reduced by 30% compared to the qualitative and implicit decision framework (50/50) in classical validations. Assuming our goal is to make the expected loss less than \$60. The currently available evidence is sufficient to achieve this target. However, with the qualitative decision framework, we need additional validation efforts to further improve our confidence in simulation adequacy. Therefore, it is found that compared to the qualitative decision analysis, the PCMQBN framework is able to reduce costs by effectively conducting and planning validation activities.

## 4.6. Conclusion

In this study, a framework of PCMQBN is developed to formalize and quantify the validation decision-making process with mathematical languages. The objective is to support the decision-making process for simulation adequacy in a transparent, consistent, and improvable manner. PCMQBN first formalizes the mathematical representation of simulation adequacy as a triplet of scenario, predictive capability level, and belief. Next, argumentation theory is employed to formalize the decision-making process in validation as an argument for simulation adequacy that is based on evidence from the validation frameworks and activities. In this process, all related evidence is characterized such that its representation is consistent with the definition of simulation adequacy. Next, all evidence is quantified where the predictive capability is represented by maturity levels and the belief is quantified by probabilities. Next, Bayes' theorem is used to integrate the quantified evidence, and the Bayesian network is used to represent this integration by directed acyclic graphs. To ensure the consistency of network connections and causal dependence on well-known physics, rules, and knowledge, a synthetic model is also suggested for evaluating the conditional probability

among all nodes in the network by calculating the Reactor Prototypicality Parameter. A sensitivity analysis is performed to evaluate the impact of conditional probability and decision parameters. It is found that the conditional dependency between simulation adequacy and validation result has higher impacts on those between [R]elevancy/[S]caling/[U]ncertainty grade and data applicability. It is also found that relative weights of evidence from different databases have large impacts on the final data adequacy. Therefore, during a validation decision-making process, the correlations and dependencies among different databases and attributes need to be evaluated more carefully than accuracy assessments and scaling analysis for separate models and databases. Based on the sources and levels of uncertainty, three phases of development are defined for documenting and grading the quality of the assessment process and simulation adequacy results.

To demonstrate the capability of PCMQBN, a case study is performed to assess the adequacy of SPH methods in simulating the scenario of "floods damage the building structures, enter the room, and cause diesel generator (DG) malfunctioning". The validation framework CSAU and its regulatory guide EMDAP is used for collecting evidence and qualitative adequacy assessment. Details about SPH simulations and evidence collection are discussed in [52]. Since opposite conclusions are obtained from two numerical benchmarks, the PCMQBN framework is used to further refine the adequacy assessment with quantitative results. For separate benchmarks, it is found that the belief level on the adequacy claim for the SPH method is consistent with the qualitative results from CSAU/EMDAP. Meanwhile, it is found that the belief level for an adequate SPH simulation is 83% when evidence from both benchmarks are used. Comparing to the qualitative result, there is higher confidence that the SPH simulation is adequate for the designated purposes based on available evidence. Also, the uncertainty of simulation adequacy is less than that from the qualitative assessment since the contradictory results suggest a non-informative adequacy distribution. To further demonstrate how PCMQBN results can be used in risk-informed validation, a risk-informed safety analysis is performed to evaluate potential damages to SSCs of NPPs by water waves. SPH simulations are performed to determine the structural loads by a wave for 60 cycles. Based on a synthetic ensemble model, distributions of SPH predictions and corresponding consequences are made based on the simulation adequacy results. It turns out that the expected loss determined based on the PCMQBN results is 30% less than that loss from the qualitative assessment. As a result, the formalized PCMQBN framework is able to reduce the uncertainty in simulation adequacy assessment and the expected losses in the risk-informed analysis due to that uncertainty.

### 4.7. References


[1] S. Hess, N. Dinh, J. Gaertner and R. Szilard, "Risk-informed safety margin characterization," in *Proceedings of the 17th International Conference on Nuclear Engineering*, Brussels, 2008.

[2] T. Theofanous, "On the proper formulation of safety goals and assessment of safety margins for rare and high-consequence hazards," *Reliability Engineering and System Safety*, vol. 54, pp. 243-257, 1996.

[3] C. Smith, C. Rabiti, R.Martineau and R. Szilard, "Risk-informed safety margins characterization (RISMC) pathway technical program plan," Idaho National Laboratory, Idaho Falls, 2015.

[4] C. Smith, D. Schwieder, C. Phelan, A. Bui and P. Bayless, "Risk informed safety margin characterization (RISMC) advanced test reactor demonstration case study," Idaho National Laboratory, Idaho Falls, 2012.

[5] N. Zuber, G. E. Wilson, M. Ishii, M. Wulff, B. Boyack and A. Dukler, "An integrated structure and scaling methodology for severe accident technical issue resolution: Development of methodology," *Nuclear Engineering and Design*, vol. 186, pp. 1-21, 1998.

[6] U.S. NRC, "50.46 Acceptance criteria for emergency core cooling systems for light-water nuclear power reactors," U.S. NRC, 29 August 2017. [Online]. Available: https://www.nrc.gov/reading-rm/doc-collections/cfr/part050/part050-0046.html. [Accessed 18 February 2020].

[7] U.S. NRC, "Transient and accident analysis methods," U.S. Nuclear Regulatory Commission, Washington D.C., 2005.

[8] W. Oberkampf, M. Pilch and T. Trucano, "Predictive Capability Maturity Model for computational modeling and simulation (SAND2007-5948)," Sandia National Laboratories, Albuquerque, 2007.

[9] ASME, Guide for Verification and Validation in Computational Solid Mechanics, ASME, 2006.

[10] ASME, Standard for Verification and Validation in Computational Fluid Dynamics and Heat Transfer, ASME, 2009.

[11] R. Sampath, "Neutrino document (release 1.0)," March 2018. [Online]. Available: https://media.readthedocs.org/pdf/neutrinodocs/master/neutrinodocs.pdf. [Accessed 10 October 2018].

[12] L. Lin, "Assessment of the smoothed particle hydrodynamics method for nuclear thermal-hydraulic applications," North Carolina State University, Raleigh, 2016.

[13] D. Violeau, Fluid mechanics and the SPH method: theory and applications, Oxford: Oxford University Press, 2012.

[14] Q. Zhang, L. Hernquist and Y. Li, "Numerical Convergence in Smoothed Particle Hydrodynamics," *The Astrophysical Journal*, vol. 800, no. 1, 2015.

[15] E. Clarke and J. Wing, "Formal Methods: State of the Art and Future Directions," *ACM Computing Surveys*, vol. 28, no. 4, 1996.

[16] P. Walley, Statistical Reasoning with Imprecise Probabilities, Chapman and Hall/CRC, 1990.

[17] R. Youngblood, "Recommendations on validation of models to be developed in "Development and Application of a Data-Driven Methodology for Validation of Risk-Informed Safety Margin Characterization Models"," North Carolina State University, Raleigh, 2017.

[18] R. Youngblood, *Personal Communication in PCMQBN and risk-informed validation*, Feburary 2020.

[19] D. Kahneman, Thinking, fast and slow, New York: Farrar, Straus and Giroux, 2011.

[20] W. Oberkampf and C. Roy, Verification and Validation in Scientific Computing, Cambridge University Press, 2010.

[21] P. Athe, "A framework for predictive capability maturity assessment of simulation codes," North Carolina State University , Raleigh, 2018.

[22] J. Kaizer, R. Anzalone, E. Brown, M. Panicker, S. Haider, J. Gilmer, T. Drzewiecki and A. Attard, "Credibility assessment framework for critical boiling transition models," U.S. NRC, Washington DC, 2018.

[23] R. Zhang and S. Mahadevan, "Bayesian methodology for reliability model acceptance," *Reliability Engineering & System Safety*, vol. 80, no. 1, pp. 95-103, 2003.

[24] R. Smith, Uncertainty quantification: theory, implementation, and applications, Philadelphia: Society for Industrial and Applied Mathematics, 2013.

[25] Y. Liu and N. Dinh, "Validation and uncertainty quantification for wall boiling closure relations in multiphase-CFD solver," *Nuclear Science and Engineering,* vol. 193, no. 9, pp. 1-19, 2018.

[26] X. Wu, K. Shirvan and T. Kozlowski, "Demonstration of the relationship between sensitivity and identifiability for inverse uncertainty quantification," *Journal of Computational Physics,* vol. 396, pp. 12-30, 2019.

[27] C. Fletcher, P. Bayless, C. Davis, M. Ortiz, S. Sloan, R. Shaw, R. Shultz, C. Slater, G. Johnsen, J. Adams, L. Ghan and D. Bessette, "Adequacy Evaluation of RELAP5/MOD3, Version 3.2.1.2. for simulating AP600 Small Break Loss-of-Coolant Accidents," Idaho National Engeneering and Environment Laboratory, Idaho Falls, 1997.

[28] S. Kaplan and B. Garrick, "On the quantitative definition of risk," *Risk Analysis,* vol. 1, no. 1, pp. 11-27, 1981.

[29] L. Sun, "Establishing confidence in safety assessment evidence," Department of Computer Science, University of York, 2012.

[30] U.K. MoD, "Interim Standard 00-55: The procurement of safety critical software in defence equipment," UK Ministry of Defence, 1991.

[31] S. E. Toulmin, The Use of Argument, U. K.: Cambridge University Press, 2003.

[32] NASA, "Standard for models and simulation (NASA-HDBK-7009)," National Aeronautics and Space Administration, Washington D.C., 2008.

[33] S. Harmon and S. Youngblood, "A proposed model for simulation validation process maturity," *The Journal of Defense Modeling and Simulation,* vol. 2, no. 4, pp. 179-190, 2005.

[34] R. Logan and C. Nitta, "Validation, uncertainty, and quantitative reliability at confidence (QRC)," in *41st AIAA Aerospace Sciences Meeting and Exhibit*, Reno, 2003.

[35] M. Pilch, T. Trucano, D. Peercy, A. Hodges and G. Froehlich, "Concepts for stockpile computing (SAND2004-2479)," Sandia National Laboratories, 2004.

[36] NASA, "Interim NASA technical standard for models and simulations (NASA-STD-(I)-7009)," National Aeronautics and Space Administration, 2006.

[37] K. Maupin, L. Swiler and N. W. Porter, "Validation metric for deterministic and probabilistic data," *Journal of Verification, Validation and Uncertainty Quantification,* vol. 3, no. 3, 2019.

[38] N. Dinh, "Validation data to support advanced code development," in *The 15th International Topical Meeting on Nuclear Reactor Thermal Hydraulics (NURETH-15)*, Pisa, 2013.

[39] S. Bodda, A. Gupta and N. Dinh, "Risk informed validation framework for external flooding scenario," *Nuclear Engineering and Design,* vol. 356, 2020.

[40] T. Olivier and S. Nowlen, "A phenomena identification and ranking table (PIRT) exercise for nuclear power plant fire modeling applications (NUREG/CR-6978)," U.S. NRC, Washington DC, 2008.

[41] J. Yurko and J. Buongiorno, "Quantitative phenomena identification and ranking table (QPIRT) for reactor safety analysis," *Transactions of the American Nuclear Society,* pp. 1843-1853, 2001.

[42] OECD Nuclear Energy Agency, "Scaling in system thermal-hydraulics applications to nuclear reactor safety and design: a state-of-the-art report," OECD NEA, 2016.

[43] P. Athe and N. Dinh, "A Framework to Support Assessment of Predictive Capability Maturity of Multiphysics Simulation Codes," Consortium for Advanced Simulation of LWRs (CASL) , Oak Ridge, 2017.

[44] J. Spriggs, GSN - the Goal Structuring Notation, London: Springer-Verlag London, 2012.

[45] J. Pearl, Probabilistic reasoning in intelligent systems: networks of plausible inference, San Francisco: Morgan Kaufmann Publishers, Inc., 1988.

[46] F. D'Auria and G. Galassi, "Scaling in nuclear reactor system thermal-hydraulics," *Nuclear Engineering and Design,* vol. 240, pp. 3267-3293, 2010.

[47] BayesFusion, LLC, "GeNie Moderler User Manual," BayesFusion, LLC, 2019.

[48] A. Saltelli, M. Ratto, T. Andres, F. Campolongo, J. Cariboni, D. Gatelli, M. Saisana and S. Tarantola, Global Sensitivity Analysis: The Primer, John Wiley & Sons, 2008.

[49] U. Kjaerulff and L. C. v. d. Gaag, "Making sensitivity analysis computationally efficient," in *Proceedings of the Sixteenth Annual Conference on Uncertainty in Artificial Intelligence* , 2000.

[50] J. Berger, "The robust Bayesian viewpoint (with discussion)," *Robustness of Bayesian Analyses*, pp. 63-144, 1984.

[51] J. Berger, Statistical Decision Theory and Bayesian Analysis, New York: Springer-Verlag, 1985.

[52] L. Lin, S. Prescott, N. Montanari, R. Sampath, H. Bao and N. Dinh, "Adequacy evaluation of smoothed particle hydrodynamics methods for simulating the external-flooding scenario," *Nuclear Engineering Design,* vol. 365, 2020.

[53] L. Lin, "Development and Assessment of Smoothed Particle Hydrodynamics Method for Analysis of External Hazards," North Carolina State University, Raleigh, 2019.

[54] D. Violeau, Fluid Mechanics and the SPH Method: Theory and Applications, Oxford: OXFORD UNIVERSITY PRESS, 2012.

[55] M. Abedini, A. Mutalib, S. Raman, R. Alipour and E. Akhlaghi, "Pressure-Impulse (P-I) diagrams for Reinforced Concrete (RC) structures: a review," *Archives of Computational Methods in Engineering,* vol. 26, pp. 733-767, 2019.

# 5. Reduced Order Modeling Techniques and Physics-guided Coverage Mapping Methodology

## 5.1. Summary

This project investigation has focused on further development of reduced order modeling (ROM) techniques and physics-guided coverage mapping (PCM) methodology to support the validation of computerized physics models employed in support of engineering calculations. Two challenges are targeted by these developments. First, how to take advantage of high-fidelity software tools in a manner that is computationally feasible. High fidelity tools are sought because they are believed to enable better predictions of complex physics phenomena. Engineering analyses however require numerous executions of such tools to achieve engineering objectives such as design optimization, propagation of uncertainties, integration of measurements from separate effects of integral effects experiments, etc. The cost of running this analysis is prohibitively large, forcing analysts to revert back to lower-fidelity models. To address this challenge, reduced order modeling techniques with error preserving bounds are sought in this project. The project has started with recent advances in reduced order modeling techniques that rely on the use of randomization to seek optimum reduction conditions for a given model. The project has further developed a number of algorithms to enable reduction across multiple physics models and has integrated the use of neural networks with previously developed randomized reduction algorithms. The outcome is an advanced set of reduction algorithms suitable for reducing complexity of multi-physics models for both transient and steady state calculations, with mathematically rigorous upper-bounds on the maximum errors resulting from the reduction. For the second challenge tackled by this project segment, the goal is to answer a recurring question in validation exercises, that is, why and how could analyst rely on experimental data, often collected in idealized conditions, to validate modeling results for other conditions, for which no experimental data exist, representing the envisaged domain of model application. To address this challenge, investments in a new methodology, called physics-guided coverage mapping has been made. The idea is to rely on high fidelity modeling tools to identify in a non-parametric fashion the relationship between experimental and application conditions. The non-parametric description implies that no assumptions are made about the functional form relating application responses to experimental responses. Instead, information theory principles are employed directly to find the best joint PDF relating the experimental responses and the application responses. Going beyond this initial rendition of physics-guided coverage mapping methodology, the project has invested into further developing this methodology to account for modeling errors and constraints that might be present, which if not respected, would lead to incorrect mapping results. Examples include constraints on the input model parameters that must be respected when the parameters are perturbed. Also, in many situations, model parameters are pre-calculated by other computer codes, and the model is validated along with these parameters. In principle, any perturbations to these parameters would result in additional modeling errors that are yet to be validated. Hence, algorithms have been developed to ensure no additional errors are introduced due to parameters perturbations. This is achieved via a constrained sensitivity analysis exercise to ensure zero sensitivities of the modeling errors to parameter perturbations.

## 5.2. Introduction

First, we discuss work related to reduced order modeling. Despite the explosive growth in computer power enabling scientists to model systems at unprecedented levels of accuracy, the resulting high-fidelity models are too expensive for routine engineering analyses at the production level, which often require many repeated model executions for applications such as design optimization, uncertainty quantification, inference, etc. These engineering activities are needed to demonstrate the safety basis of advanced nuclear reactor designs with sufficient characterization of system performance as per modern regulatory frameworks. To address this challenge, a need exists for a formal approach that establishes a rigorous basis for reducing the complexity of high-fidelity models in order to enable fast turn-around times for routine

executions with acceptable and known accuracy. Reduced order modeling (ROM) refers to a wide class of methods designed to achieve this goal. ROM approaches may be classified into three categories, physics-based, pattern-based, and regression-based. The first category, physics-based, refers to approaches that rely on reducing the modeling complexity by incorporating assumptions and approximations to simplify the representation of the physics operator used to describe the system behavior. Examples of this include the use of RANS (Reynolds-averaged Navier-Stokes) models or LES (Large Eddy simulation) instead of direct numerical simulation (DNS) methods. The specific example employed in our recent work is the physics-based simulation of the protected and unprotected Shut Down Heat Removal Tests (SHRT-17 and SHRT-45R) for the Experimental Breeder Reactor II (EBR-II), modeled using the System Analysis Module (SAM), developed at Argonne National Laboratory for advanced non-LWR safety analysis. The physics-based reduction approach, while based on intuitive physical principles, cannot credibly estimate the uncertainties resulting from the various introduced assumptions and approximations, which is referred to as modeling uncertainties over the model validation domain. The validation domain refers to the range of conditions over which the modeling accuracy is assumed to be acceptable. Practitioners often resort to code-to-code comparisons and/or complicated scaling studies to justify the use of the model over the range of conditions envisaged for code use. In principle, one can estimate modeling uncertainties if one could execute both the high fidelity and reduced order model. This is however not practical, especially when considering the wide range of conditions expected during normal or abnormal operation. If the cost were acceptable, one would not need the reduced order model. The idea however is to use few executions of the high-fidelity model to estimate the modeling uncertainties, and then based on scaling arguments augmented by expert-judgment-based recipes, the uncertainties are mapped to other conditions for which no high fidelity model predictions exist. If high fidelity models are not available, one would resort to experiments to estimate modeling uncertainties, but this is outside the scope of the paper, as the focus is on how to reduce the complexity of simulation-based models. Thus, physics-based reduction is challenged by the lack of a rigorous approach to quantify the modeling uncertainties resulting from the reduction. Different from physics-based reduction, the basic idea for pattern-based methods is to construct a low-rank approximation to the model variables whose physics correlations are not explicitly available. Pattern-based methods rely on finding recurring patterns in the variability of the various model interfaces described by the input variables, representing measured or design independent variables i.e., model input parameters such as thermal conductivity, heat transfer coefficients, flow conditions, etc.; the state variables, e.g., the temperature distribution; and the output variables, representing performance metrics, e.g., peak fuel and clad temperatures. The state variables represent the solution of the physics equations, with the output variables being functions thereof. Specifically, pattern-based methods employ unsupervised methods such as principal component analysis (PCA), singular value decomposition (SVD), and proper orthogonal decomposition-type techniques to identify dominant behavior over the range of variations for the various model variables. The dominant behavior is described using few degrees of freedom, referred to as active degrees of freedom (DOFs), designed to capture a large percentage of the variability. Unlike physics-based reduction, these methods require no physics insights or intimate knowledge of the models being reduced but only nonintrusive access to allow multiple executions to generate training data, i.e., snapshots. The reduction errors have been conventionally estimated using a trial-and-error approach, where the number of active DOFs is changed until the error resulting from the reduction meets user tolerance. This however does not guarantee the reduction errors will be bounded over the range of conditions envisaged for model application, i.e., the model validation domain. In the recent past, randomized linear algebra techniques have resurfaced, offering a theoretical basis for estimating upper-bounded on the reduced models using pattern-based methods. One typical approach for achieving this is the randomized range finding algorithm, whose theoretical development allows one to estimate a realistic, i.e., non-conservative, upper-bound on the reduction error that is met with very high probability. Regarding the third category, regression-based, the basic idea is to try to regress one set of variables, referred to as responses, to other set of variables, called regressors. To regress, by definition, is to explain the cause of responses. In doing so, the relationship between the regressors and responses, referred to as response surface or a surrogate model, is often based on trial and error until an acceptable surface is identified which minimizes the regression errors. Some of

the notable choices for the surrogate model include linear/polynomial functions, artificial neural network-based functions, Gaussian process models, etc. The selection of a certain surrogate model is often guided by the nature of the physics model or phenomena being analyzed, and hence is generally a subjective process. Thus, it is not surprising that multiple surrogates could be developed with essentially similar accuracy. In our work, both linear regression and artificial neural network (ANN) based reduction are employed to construct surrogate models in terms of the active DOFs generated using pattern-based reduction. The construction of regression-based surrogate models represents the ultimate goal of any complexity reduction exercise, as it provides an inexpensive tool for repeated model executions for applications like sensitivity analysis, uncertainty quantification, and probability risk assessment. The key challenge however is that it is not clear how to estimate the reliability of the surrogate model for all conditions in the validation domain. This challenge is not addressed in the current work.

Second, we discuss work related to physics-guided coverage mapping. This project has laid the foundations for the development of a new methodology for the integrated use of uncertainties -- including parameters and modeling uncertainties and experimentally determined biases/uncertainties -- to support a recurring theme in a number of DOE's programs, that is how to improve modeling predictability via an optimized use of minimal targeted experiments and high-fidelity modeling and simulation tools. This vision recognizes the huge investments made by DOE in modeling and simulation over the past two decades, the climbing cost and challenges of first-of-a-kind measurements. This theme -- of increased reliance on modeling and simulation to guide the experimental activities and identify data needs -- represents an umbrella vision for a wide range of nuclear reactor and non-reactor applications, such as material testing, and advanced reactors/fuel concepts, etc. Realizing this vision will have far reaching implications for a wide range of nuclear systems, achieved via effective inference of the dominant sources of uncertainties, thus leading to better designs, more informed regulatory process, and ultimately to better economy for the associated systems. This project has developed and implemented a recently emerging methodology denoted by physics-guided coverage mapping (PCM) that employs data analytics, information theory, and high-fidelity simulation to develop novel computational capabilities that would be instrumental in meeting this vision. These capabilities include novel mathematical kernels capable of transferring biases/uncertainties between two generic user-specified domains, referred to hereinafter as the experimental domain and application domain. The experimental domain is considered small as it represents conditions which are difficult to obtain, realize, or measure, e.g., conducting a real experiment to analyze rare events or new evaluations of nuclear data, execution of computationally expensive high-fidelity model at few conditions when one is interested in replacing a high-fidelity model by a low-order model for routine calculations. The application domain is much bigger as it represents all conditions at which predictions are sought, e.g., design of experiments for fundamental research to support new reactor concepts and/or advanced fuel design, predicting reactor hot full power operating conditions for at normal and off-normal conditions, etc. The PCM methodology exploits uncertainties in a non-traditional manner which is primarily concerned with inferring the best possible correlations between the application's quantities of interest and the experimental responses. These relationships can be identified mathematically without making any adhoc assumptions by minimizing entropy-based measures, referred to as the mutual information. The implication is that even if the propagated uncertainties are high, one can find relationships -- via mathematical search through the uncertainty analysis results -- between the experimental responses and the application's quantities of interest which allow for an effective mapping of experimental biases. To ensure mathematical rigor of the PCM mapping kernels, both parameter and modeling uncertainties are simultaneously characterized in both the application and experimental domains based on high fidelity simulation, which represents the key contribution of this project, beyond what was done previously. This methodology departs markedly from the existing predictive modeling and validation methods which essentially decouple predictive simulation from uncertainty analysis -- sometimes performing the former and completely forgoing the need for the latter -- and basing model validation on expert-based customized recipes for bias mapping between the experimental and the application conditions. In doing so, the code-based uncertainty analysis -- in which known sources of uncertainties are propagated through the simulation -- may be

completely skipped and deemed unnecessary because the associated uncertainties are too high to be realistic for operation; instead, they are estimated via direct comparisons between experimental measurements and code predictions, referred to as "biases". To make up for the analyst's lack of knowledge on the exact mapping of these biases between the experimental and the application conditions, several system-specific recipes have been developed by practitioners.

### 5.3. Scope of Work

Regarding Reduced Order Modeling, as detailed in one of the listed papers (to be published; see sub-section 5.5), our goal is two-fold; first, to explore the reducibility of the SAM code using pattern-based techniques which are used to identify a small number of active DOFs for time-varying responses, e.g., fuel temperature, and model input parameters. In tandem with that, the reduction errors are rigorously quantified; second, regression-based reduction is used to regress the responses' active DOFs to input parameters active DOFs. Different regression surfaces are employed to explore best scenarios for SAM reducibility. In doing so, we recognize that it is difficult to assess the errors resulting from SAM's own physics-based reduction and regression-based reduction, which remain as open research topics for future work. The scope of work is directly related to the IRP objectives, as it provides an enabling tool for fast-execution of accuracy-preserving tools to enable scientific validation of computer models. Specifically, the goal here is to explore the reducibility of the SAM code using pattern-based and surrogate-based reduction techniques. The overarching goal here is to determine whether additional reducibility can be incorporated into the SAM physics model, based on the range of its intended application, thereby providing an efficient solver capable of performing computationally intensive analyses such as uncertainty quantification, inference, etc., especially when the number of model parameters is significantly increased. A representative model with 25 input model parameters expected to directly influence key performance metrics (fuel, clad, and coolant temperatures) is employed. The training snapshot are generated based on 1000 model executions, each randomizing the input parameters within their prior uncertainties. Each execution records the model responses and the associated state. The time-dependent fuel temperature is selected as the state variable, while the peak temperature over the transient time is selected as the model response. The goal is to create a reliable ROM model relating input parameter variations to both the state and response variations over the range of uncertainties for the model parameters. The transient time is selected to be 900 seconds, which corresponds to benign termination of the transient. The details can be found in the attached paper.

For PCM, the focus has been on the design of the noted mapping kernel and its associated enabling algorithms -- representing the key contribution of this project -- as it provides a mathematical construct in the form of a joint probability distribution function (PDF) which encodes all possible variations for the application's quantities of interest and the experimental responses. One key distinction of this work is the ability to include both parameter and modeling errors when performing the PCM analysis. Specifically, a neutronic model was used for demonstrating how modeling errors could interact with parameter uncertainties, leading to incorrect results, if modeling errors are ignored. Representative lattice physics models and core-wide models are employed wherein nuclear parameters, e.g., cross-sections, uncertainties are propagated using two different models, one representing a high fidelity and the other a low fidelity models, to assess the impact of modeling errors on the propagated uncertainties. A constrained sensitivity analysis algorithm is developed to identify all parameter perturbations that impact the modeling errors and are thus removed when performing the PCM or uncertainty analysis. Two attached papers describe the details of the new algorithms. These algorithms are expected to have many follow-up applications in support of data-driven validation of software tools. For example, they can be used to quantify the modeling errors based on few numbers of high-to-low fidelity models comparisons and employ PCM to estimate the modeling errors using the low-fidelity models at conditions for which the high-fidelity model predictions are considered computationally expensive. These algorithms can also be employed to estimate both modeling and parameters uncertainties, in a manner than ensures modeling errors are not stretching the low-fidelity models outside their validation domain.

## 5.4. Conclusions and Path Forward

This work has explored the reducibility of the SAM model using both pattern-based and regression-based methods. The two reduction methods are applied for two representative transient benchmark models, the EBR-II SHRT-17 and SHRT-45R tests. The pattern-based methods are capable of reducing the effective dimensionality of the model variables in a manner that establishes realistic upper-bounds on the reduction errors that are met with high probability. The reduced dimensions are referred to as the active degrees of freedom (DOF). The implication is that model responses of interest, despite their nominal high dimensionality, can be well-approximated by a much smaller number of DOFs. Next, regression-based methods are employed to functionalize model responses of interest in terms of the active DOFs as the regressor variables instead of the original number of model variables, which is typically much higher than the number of active DOFs. Although regression-based methods suffer from their lack of a rigorous approach for bounding their prediction errors, their performance is typically improved when the number of regressor variables is significantly reduced. These encouraging results are expected to lay the foundation for future work focused on devising new methods for incorporating the active DOFs directly into the numerical solver of the SAM code to allow for a faster execution by constraining the search for the solution along the active subspaces. Further, when straightforward application of ANN is not adequate, hybrid methods relying on physics-based reduced order modeling techniques will be employed to guide the construction of the ANN-based surrogate models. Overall, these results are expected to drive future work of more sophisticated application-targeting reduced order modeling techniques with superior computational efficiency and accuracy-preserving capability to help realize the value of high-fidelity modeling and simulation tools, in which a great deal of investments have been made by DOE over the past two decades.

With regard to PCM, the contributed methodology paves the way for a philosophy shift in the value of traditional uncertainty analysis in support of predictive model validation, shifting from a conventional measure of confidence in the calculated results to a mathematically-rigorous -- rooted in information theory -- approach by which experimental evidence, i.e., rare or expensive measurements, could be integrated with high fidelity simulation to directly produce inference on the quantities of interest, i.e., quantities that are costly to measure, cannot be directly measured, or computationally expensive to calculate on a routine basis. The work has upgraded previous PCM developments to take into account the impact of modeling errors on the inference analysis, typically ignored in previous work. The work has highlighted the key dependencies between modeling errors and parameter uncertainties for representative neutronic models and how modeling errors could have a significant impact on propagated parameter uncertainties. An algorithm to ensure non-contamination of parameter uncertainties by modeling errors has been presented and applied to a representative steady state and transient reactor models. Results indicate that one must carefully remove the modeling errors before propagating uncertainties. Future work will focus on the implication of these results for inference studies and bias calculations in support of model validation for first-of-a-kind reactor systems. Going beyond neutronics, it is important to note that modeling errors from other physics, e.g., thermal hydraulics, could feedback into neutronic modeling errors, expected to occur in a multi-physics simulation of core-wide performance. In this case, one must take into account the impact of other physics on neutronic errors. Algorithms, similar in function, to the ones proposed here could be envisioned, where one employs both a high and low fidelity multi-physics solver to estimate the modeling discrepancies for the responses of interest and ensure their insensitivity to the parameter perturbations.

## 5.5. Peer-Reviewed Documented Work

The following 5 peer-reviewed articles document the key aspects of the work performed under this contract.

1. Jeongwon Seo, Hany S. Abdel-Khalik, and Zoltán Perkó, "Addressing Ambiguities in Constrained Sensitivity Analysis for Reactor Physics Problems," Nuclear Technology, March 2020. This paper discusses a key enabling algorithm for PCM to ensure all parameter perturbations respect established constraints, prior to application of PCM
2. Dongli Huang and Hany Abdel-Khalik, "Modeling Errors-Preserving Constrained Sensitivity Analysis," Nuclear Engineering and Design, June 2020. This paper discusses how modeling errors could be integrated under the PCM framework with neutronics as example.

3. Dongli Huang and Hany S. Abdel-Khalik, "Nuclear Data Uncertainty Propagation and Modeling Uncertainty Impact Evaluation in Neutronics Core Simulation," Progress in Nuclear Energy, under review. This paper discusses our initial work on assessing the impact of modeling errors on uncertainty analysis studies used in support of model validation. This paper is still under review.

4. Yeni Li, Acacia Brunett, Elise Jennings, and Hany S. Abdel-Khalik, "ROM-based Surrogate Modeling of EBR-II benchmark using ANL's SAM Code," to be submitted, currently under internal review at ANL. This paper discusses ROM developments hybridizing both pattern-based and regression-based methods for reduction.

5. Dongli Huang, Ugur Mertyurek, and Hany S. Abdel-Khalik, "Verification of the sensitivity and uncertainty-based criticality safety validation techniques: ORNL's SCALE case study," Nuclear Engineering and Design, pp.110571, 2020. This paper is byproduct of our research on forward-based methods for sensitivity analysis.

# 6. Approaches to Implementation and Evaluation of Coupling of Codes

While having the potential to threaten nuclear infrastructure, external flooding hazards are often qualitatively assessed as risk-insignificant and excluded from detailed quantitative evaluation (Ma et al., 2017). However, lessons learned from Fort Calhoun (2011), the accident at Arkansas Nuclear One (2013), and the flooding of Vermont Yankee (2013) and St. Lucie (2014) have underscored the need for quantitative simulations to evaluate the risk of flooding to nuclear power plants.

## 6.1. Summary

Coastal flood hazard studies rely on many hundreds of design storm events, both historical and synthetic, to inform more comprehensive risk-based analyses, giving rise to the need for fast, deterministic simulations. As a part of the broader Integrated Research Project (IRP), we develop a methodology that supports probabilistic, risk-based design and decision-making by making deterministic, large-scale simulations more practical and efficient.

Events such as the flooding around the Fort Calhoun (2011), Vermont Yankee (2013), and St. Lucie (2014) nuclear power plants have highlighted the need for accurate simulations to determine the risk of flooding at these and other facilities around the country. However, plant response to flooding due to hurricane storm surge involves multiple spatiotemporal scales. While ocean circulation models can simulate large-scale storm surge events, assessment of the resilience of critical infrastructure to storm-induced flooding require much smaller scales that are more appropriate for fluid solvers, which can resolve finer scale processes. Therefore, bridging the gap between these simulation approaches is essential, and calls for the conception, development, and evaluation of a multi-scale methodology that can accommodate the substantial differences in scales.

We describe a modeling framework that incorporates the larger scale finite element (FE) model, ADCIRC, along with the smaller scale smoothed particle hydrodynamics (SPH) code, Neutrino, to provide finer level resolution for complex geometries. ADCIRC is an ocean circulation model that solves the shallow water equations over a mesh of nodes and triangular elements. The use of unstructured grids with varying element sizes means that a mesh can be gradually refined in areas that require greater levels of topographic detail. While these refinements can reach the meter scale, shallow water equations are not suitable for simulating the hydrodynamic processes that occur beneath that scale and that must account for the complex geometries of, for example, a nuclear power plant. Such simulations require smaller-scale models like the mesh-free fluid solver, Neutrino.

Our approach draws on a methodology called *subdomain modeling*, which allows local changes in a finite element model to be accommodated with less computational effort than would be required by re-running the entire simulation. Provided a subdomain is large enough to contain the altered hydrodynamics, changes can be made—such as refinements in spatial resolution and the addition of flood protection measures—and simulations performed on a subdomain without the need to calculate new boundary values. Objectives of the project include enhanced spatial resolution of subdomain meshes to get finite element simulations closer to facility-scale features and topography; data libraries and reuse to curtail the need for large, ocean-scale simulations, allowing modelers to instead start from the subdomain scale; ADCIRC-Neutrino coupling to facilitate subdomain-to-facility scale interactions; and verification and validation to ensure the correctness of computer implementations.

Results are based on datasets obtained from and through collaboration with the United States Army Corps of Engineers (USACE), and include (1) refinement and evaluation of subdomain modeling for its computational benefit and solution quality in actual, real-world applications that consider a range of USACE engineering design scenarios, (2) development of a post-processing approach that facilitates the

use of spatially and temporally coarse datasets from USACE as boundary conditions for subdomain modeling, allowing us to adopt a library of states (LOS) perspective so that simulation results from a variety of historical and synthetic storms are available for reuse—this allows us to recover boundary conditions of a quality comparable to datasets with a much finer temporal resolution, (3) a prototype coupling approach using subdomain modeling to combine the larger scale finite element model, ADCIRC, with the smaller scale smoothed particle hydrodynamics code, Neutrino, to provide finer level resolution for complex geometries.

In this report, we elaborate on these objectives, technical approaches, and results, describing their relationship with other components of the project, summarizing key findings, and presenting highlights of the technical innovations and implications of our work, as well as paths forward.

## 6.2. Technical Background

Flooding risk from hurricane storm surge is a multi-scale issue. Hurricanes develop and evolve over a period of weeks at spatial scales of hundreds of miles as they progress across the deep ocean and move onto the continental shelf and coastal floodplains. While numerical ocean circulation models can simulate storms and their flooding effects, they operate on spatiotemporal scales that are too coarse for evaluating the resilience of coastal infrastructure. Conversely, fluid solvers can resolve complex hydrodynamic processes beneath the meter scale but are incapable of simulating the large-scale processes that lead up to these more localized events.

Therefore, bridging the gap between these simulation approaches is essential, and calls for the conception, development, and evaluation of a multi-scale methodology that can accommodate the substantial differences in scales. In this study, we address practical needs identified through interactions with the Department of Energy (DOE), the United States Army Corps of Engineers (USACE), and other stakeholders by (1) refining and evaluating a subdomain modeling approach for its computational benefit and solution quality in actual, real-world applications that consider a range of USACE engineering design scenarios, (2) developing tools that facilitate the use of spatially and temporally coarse datasets from USACE as boundary conditions for subdomain modeling, and (3) prototyping a coupling approach using subdomain modeling to combine the larger scale finite element (FE) model, ADCIRC, with the smaller scale smoothed particle hydrodynamics (SPH) code, Neutrino, to provide finer level resolution for complex geometries, which we introduce below.

ADCIRC (Luettich et al., 1992; Luettich and Westerink, 2004; Westerink et al., 2008) is an ocean circulation model that uses finite element methods to solve the shallow water equations over a mesh of nodes and triangular elements. The use of unstructured grids with varying element sizes means that a mesh can be gradually refined in areas that require greater levels of topographic detail. While these refinements can reach the meter scale, shallow water equations are not suitable for simulating the hydrodynamic processes that occur beneath that scale and that must account for the complex geometries of, for example, a nuclear power plant. Such simulations require smaller-scale models like the mesh-free fluid solver, Neutrino.

Neutrino is a smoothed-particle hydrodynamics (SPH) model developed by the Neutrino Dynamics Initiative (Sampath et al., 2016; Sampath, 2018). It solves continuous fluid flow equations through the use of discrete moving particles (Liu and Liu, 2010) and simulates single-phase, isothermal, incompressible, Newtonian fluid flows with viscosity assumed to be constant with respect to space, and surface tension forces neglected. Discontinuities of physical quantities occurring at boundaries, such as densities and non-physical pressure forces, are generally challenging for SPH codes. Neutrino uses frozen particles to accommodate multiple bodies and circumvent underestimation of physical quantities at the boundaries.

## 6.3. Previous Work

Bridging the gap in modeling scales and coupling codes as diverse as ADCIRC and Neutrino present a technical challenge. There is some precedent, however, for nesting and coupling strategies that facilitate model integration across smaller differences in scales. A substantial body of work in both ocean and atmospheric modeling addresses both one-way and two-way nesting strategies (Spall and Robinson, 1989; Debreu and Blayo, 2008). As-Salek and Yasuda (1995) develop and employ a one-way nesting technique using flow velocities and water surface elevations as boundary conditions to drive finer, local meshes in their investigation of the effects of storm surge in the Bay of Bengal. Their results demonstrate that solutions from the nested model agree better with observed data than those from the coarser large-scale model alone.

Hubbert et al. (1990) compare large-grid non-nested models with nested models using water surface elevations as boundary conditions and demonstrate that the nested model outperforms the large-scale non-nested model. Fox and Maskell (1995) compare one-way and two-way nesting models and show that two-way nesting is advantageous when there are concerns about noise being generated at the interface of the nested domain and the larger domain. Similarly, Sheng et al. (2005) describe a two-way nesting method that obtains accurate results compared to large-scale outer models with one-way nesting. Debreu and Blayo (2008) review several two-way nesting techniques and conclude that the choice of technique involves trade-offs between conservation properties, accuracy, robustness, and coding challenges.

With respect to coupling between ADCIRC models, Baugh et al. (2015) present an approach for simulating storm surge and tides called *subdomain modeling* that allows local changes in a subdomain to be accommodated with less computational effort than would be required by re-running the full domain. Provided a subdomain is large enough to contain the altered hydrodynamics, changes can be made—such as refinements in spatial resolution and the addition of flood protection measures—and simulations performed on a subdomain without the need to calculate new boundary values. Using subdomain modeling, a library of states (LOS) perspective can therefore be adopted so that simulation results from a variety of historical and synthetic storms are available for reuse.

## 6.4. Relevant Methods

Analysis of plant response to external flooding requires a methodology and workflow that can accommodate the broad range of spatiotemporal scales involved. We begin by defining three modeling scales and two points of interaction between them. These scales are: (1) **ocean scale** (kilometers) in ADCIRC, (2) **subdomain scale** (tens of meters) in ADCIRC, and (3) **facility scale** (meter-level and below) in Neutrino, which have the following points of interaction:

- **Ocean-to-subdomain scale** – the interface between full domain and subdomain ADCIRC models, which differ in scale and resolution, using the subdomain modeling extension of ADCIRC.

- **Subdomain-to-facility scale** – the interface between a subdomain ADCIRC model to a Neutrino model, using a one-way handoff of data from ADCIRC to Neutrino.

Below we describe the modeling scales they entail and the coupling approaches at both of these points of interaction. We also introduce general verification and validation issues that are further explored in subsequent sections.

**Ocean scale:** well-validated ADCIRC simulations, test cases, and meshes composed of elements graduated in size with the largest elements over the deep ocean, smaller ones to resolve finer scale processes, and still smaller ones next to the coastline.

**Subdomain scale:** areas around a nuclear power plant facility selected from large-scale meshes using strategically placed boundaries to define a region of interest, and within which a variety of flood protection measures can be modeled and evaluated using ADCIRC.

**Facility scale:** local simulations using Neutrino, who's initial and boundary conditions are informed by and generated from subdomain scale simulations in ADCIRC.

In the workflow we advance, full domain simulations are performed that generate boundary conditions and initial conditions for subdomains in the form of time histories of water surface elevations, depth averaged velocities, and wet/dry states of nodes. Subdomain simulations are then performed at increased spatiotemporal resolutions without the need for additional full domain simulations.

With respect to coupling, because of the complexity involved in combining a mesh-based FE ocean circulation model and a mesh-free SPH model, our initial prototypes rely on a one-way handoff of output data from ADCIRC subdomains to the Neutrino domain. This requires: (1) geographical overlapping of the Neutrino domain with the ADCIRC subdomain, and (2) the ADCIRC subdomain to model local hydrodynamic behavior with sufficient fidelity so that boundary conditions around the peripheries of the Neutrino domain are meaningful. That is, subdomain simulations should behave as if a facility is present by matching topography and by including roughness coefficients to account for local hydrodynamic behavior.

This in turn requires that spatiotemporal gaps be bridged between the respective models and—since ADCIRC grids are typically resolved locally at larger scales than those of Neutrino—enhanced spatial resolution in ADCIRC subdomain simulations to account for protective structures, the facility itself, and any other finer topographic features. Temporal refinement is also required in combination with the spatial refinements in order to satisfy the Courant-Friedrichs-Lewy (CFL) condition.

### 6.5. Technical Objectives

As a part of the broader Integrated Research Project (IRP), we develop a methodology that supports probabilistic, risk-based design and decision-making by making deterministic, large-scale simulations more practical and efficient.

Technical objectives, approach, and relationship within the overall project are presented below. Additional details can be found in the doctoral dissertations of Bukhari (2020) on enhanced spatial resolution of subdomain meshes, data libraries and reuse, and ADCIRC-Neutrino coupling, and Dyer (2020) on verification and validation.

Coastal flood hazard studies rely on many hundreds of design storm events, both historical and synthetic, in their efforts to quantify larger risk-based goals, giving rise to the need for fast, deterministic simulations. In this project, we develop a modeling framework that includes a) enhanced spatial resolution of subdomain meshes – to get finite element simulations closer to facility-scale features and topography, b) data libraries and reuse – to curtail the need for large, ocean-scale simulations, allowing modelers to instead start from the subdomain scale, c) ADCIRC-Neutrino coupling – to facilitate subdomain-to-facility scale interactions, and d) verification and validation – to ensure the correctness of computer implementations. We describe these objectives below.

**Enhanced spatial resolution of subdomain meshes.** While subdomain modeling preserves the accuracy of solutions obtained from full domain simulations, its ability to accommodate *ex post facto* refinements of a subdomain have not been attempted or evaluated, particularly within the context of actual coastal projects that could benefit from such enhanced resolution. Our work here is with actual projects

obtained from and in coordination with the US Army Corps of Engineers (USACE) and their Engineering Research and Development Center (ERDC) in Vicksburg, MS. For each case study and project alternative defined, we determine whether and to what extent hydrodynamic effects remain local in subdomains, subsequent to mesh refinements and modifications; how sensitive subdomain solutions are to boundary locality, and placement; and how spatial mesh refinements for real world scenarios affect boundary conditions for subdomains when combined with variations in project configurations.

**Data libraries and reuse.** Existing datasets of historical and synthetic storm results—such as those developed and maintained at USACE, NOAA, and other agencies and oceanographic institutes—are widely available, providing a rich set of storm surge data that could in principle be used in combination with subdomain modeling in the design of coastal protective structures. Because the necessary output is commonly stored at intervals of as much as 5 to 15 minutes, however, we consider the role of higher order interpolation and smoothing of those results based on the following intuition: when results are infrequently recorded, since they represent points along a relatively smooth solution to the shallow water equations, it may be possible to recover any peaks that were inadvertently clipped—as the result of coarse-resolution temporal output—using cubic splines, Fourier analysis, and other numerical techniques. We develop an effective approach in the form of a post-processing step that can be applied to existing ADCIRC files before subdomain modeling is attempted on those existing datasets.

**ADCIRC-Neutrino coupling.** Interactions between ADCIRC and Neutrino can be realized through a one-way data handoff, proceeding from the kind of observable data produced by a shallow-water model like ADCIRC, and then made available to an SPH code like Neutrino through its available types of boundary conditions. Beyond the mechanics of the exchange, we consider modeling and scale differences in both space and time that require, for instance, working with parameters, terminology, and assumptions that vary between diverse modeling approaches and their respective communities, e.g., local and latitude-longitude coordinates and their transformations, devising an approach for finding and extracting small, appropriately-placed time windows from larger-scale output, and other differences between localized hydrodynamic and large-scale ocean circulation models. Our scope includes a) the details of the computer formats and requirements for data exchange, b) consideration of the modeling assumptions made between two diverse scientific areas with distinct paradigms, c) development of a series of coupling test cases, from simpler to more complex and with more realism, and their comparative evaluation, and d) observations and recommendations for continued development.

**Verification and validation.** Given the nature of the coupling approach being developed and its likely applications, it is particularly important that the software does what it is intended to do. Two key aspects of this determination, in the vernacular of the software engineering community, are verification and validation, where verification asks, "Is the product right?" and validation asks, "Is it the right product?" Verification, then, is concerned with whether an implementation satisfies its specification, i.e., is bug-free. Beyond traditional testing and code reviews, we develop static program verification techniques, which are based on providing a formal, or mathematical, specification of functional behavior and showing that an implementation satisfies the specification. This process involves concepts from mathematical theorem proving, and thus relies on modeling or manipulating computer programs instead of executing them, hence the term *static*. Doing so allows one to make strong correctness claims since coverage is more complete than can be obtained via testing alone.

### 6.6. Technical Approach

In this and the following sections, we lay out our technical approach for each of the above objectives, describe the relationship between our study and other components of the project, summarize key findings, present highlights of technical innovations and the implications of our work, and finish with a discussion on paths forward and conclusions.

**Enhanced spatial resolution of subdomain meshes.** To narrow the gap between large-scale storm surge simulations and more local facility-scale simulations, we address subdomain scale models and mesh refinements that are intended to capture a finer level of land surface detail than has previously been attempted. Three extensive case studies on the US Gulf and Atlantic coastlines—each with differing characteristics—have been developed and evaluated with respect to both computational benefits of the approach and its accuracy, at the following three sites:

(1) *Dyke Marsh Wildlife Preserve*, located between Mount Vernon and Alexandria, VA, along the west bank of the Potomac River, with project alternatives on the order of several miles long, which seek to restore a natural promontory structure and the surrounding area to its pre-1940s and '50s conditions, prevent further loss of the marsh, and potentially expand and protect the wetland and its delicate ecosystem.

(2) *Ike Dike*, located at Galveston Bay, TX, with project alternatives on the order of tens of miles long, which would enhance and extend the Galveston Seawall and provide further protection for an area at significant risk from storm-induced flooding, such as the damage resulting from Hurricane Ike. As part of a larger "coastal spine," the concept includes a gated coastal barrier that would limit inflow of hurricane storm surge into the bay and thus provide additional protection for Galveston Bay, the Bolivar Peninsula, Houston, and other surrounding communities.

(3) *New York-New Jersey Harbor and Tributaries* (HATS), an area affected by Hurricane Sandy and identified by USACE as one of nine high-risk, focus areas on the North Atlantic Coast that is most susceptible to storm-induced flooding. For this project, several flood control structures have been proposed to reduce costs and risks associated with storm events, and to support overall resilience and sustainability of coastal communities. Alternatives include the Throg's Neck barrier, a 1-mile flood control barrier, and a 13-mile flood control system referred to as the Jamaica Bay barrier. Each case study incorporates a full, base mesh along with several refined with-project alternatives.

**Data libraries and reuse.** To take advantage of existing datasets of historical and synthetic storm results, techniques have been developed to reuse existing datasets as boundary conditions for subdomain modeling. The original datasets may have the necessary output but are recorded at temporal resolutions of 15 to 30 minutes, which is too coarse for meaningful subdomain boundary conditions. We consider the role of higher order interpolation and smoothing of those results based on the following intuition: when results are infrequently recorded, since they represent points along a relatively smooth solution to the shallow water equations, it may be possible to recover any peaks that were inadvertently clipped—as the result of coarse-resolution temporal output—using cubic splines, Fourier analysis, and/or other numerical techniques.

Collectively, we consider four different interpolation approaches. The simplest of the approaches is one that leaves wet-dry states unforced, but that is otherwise equivalent to subdomain modeling, an approach we call SSM, or simplified subdomain modeling. Such an approach relies on linear interpolation of the time histories of water surface elevations and velocities. As a variation on the SSM approach, we also include results from SML+, a technique we define that uses linear interpolation, but that also adds points of maximum water surface elevation into those time series. Of the higher order approaches, the simplest cubic spline method, SMC, does not make use of the recorded maximum water surface elevation, whereas SMC+ *does* by inserting it into the time series. We compare the accuracy of subdomain solutions that make use of each of the SSM, SML+, SMC, and SMC+ approaches.

For our case studies, we utilize two example problems forced by tides that are taken from the official ADCIRC website, and two problems forced by winds that use the NC FEMA Mesh Version 9.98 as a large-scale domain. These include: 1) Idealized inlet with tidal forcing (adcirc.org, 2019a), 2) Shinnecock Inlet,

NY, with tidal forcing (adcirc.org, 2019b), 3) Cape Fear, NC, forced by Hurricane Fran (1996), and 4) Cape Hatteras, NC, forced by Hurricane Isabel (2003). In each case, subdomains of three different sizes are defined: small (S), medium (M), and large (L). Results of the simulations are evaluated by comparing the water surface elevations of a subdomain at each node to that of the full domain at every output time step. We present the cumulative distribution function (CDF) of the averaged error (AE) and maximum error (ME) of the water surface elevations for storm surge and tidal cases.

**ADCIRC-Neutrino coupling.** We have developed, as a proof of concept, a methodology that facilitates communication between the large-scale FE model, ADCIRC, and the small-scale SPH model, Neutrino. Both models simulate propagation of a flooding front, either over a broad area of interest (ADCIRC) or at the facility scale (Neutrino). While both models operate on distinctly different spatiotemporal scales, they can interact meaningfully by having ADCIRC provide boundary conditions for Neutrino runs. To do so requires bridging the gap between them in spatiotemporal scales, a disparity we have addressed by improving the local spatial resolution of large-scale ADCIRC meshes within a subdomain.

With respect to coupling, two case studies have been developed and used to evaluate the approach:

(1) *Pseudo One-Dimensional Test Case,* a highly idealized problem previously reported in the literature and used to evaluate the fidelity of the movement of the wetting and drying fronts produced by large-scale ocean circulation models.

(2) *Alligator River National Wildlife Refuge,* a more realistic study area located on North Carolina coast, with surrounding topography that is relatively smooth and vulnerable to flooding.

Though local in the context of this study, the results at the Alligator River site were produced by large-scale storm surge simulations on validated finite element meshes, in this case NC FEMA Mesh Version 9.98, produced through the North Carolina floodplain mapping program by the ADCIRC development group. This particular mesh, for instance, models a domain that encompasses the western North Atlantic Ocean, the Caribbean Sea, and the Gulf of Mexico. It consists of 620,089 nodes and 1,224,714 elements and has a steady open ocean boundary condition along its eastern edge.

With respect to data exchange between models, we have developed and implemented Python scripts that make use of ADCIRC solution outputs to produce inputs for Neutrino. A one-way handoff between the two models allows for the ADCIRC (subdomain) simulation to be run to completion before beginning the Neutrino simulation. Considering the difference between the formats of ADCIRC outputs and Neutrino inputs, ADCIRC solutions are mechanically translated into a format that is compatible with Neutrino inputs (see Appendix A).

**Verification and validation.** Coupling between a full domain and subdomain in ADCIRC is shown to be mathematically equivalent to ADCIRC itself through a combination of informal proofs (Baugh et al., 2015) and a static verification technique using state-based formal methods (Baugh and Altuntas, 2018; Baugh and Dyer, 2018). To explore implementation choices and ensure soundness, we made use of Alloy (Jackson, 2012), a declarative modeling language with tool support and an automatic form of analysis performed within a bounded scope using a SAT solver. Using Alloy, we have modeled finite element domains and simulations on them so we can experiment with and reason about the type of boundary conditions that might be imposed on subdomain runs. The approach allows us to draw useful conclusions about implementation choices and guarantees about the subdomain modeling extensions, that it is equivalence preserving.

## 6.7. Relationship within the Overall Project

ADCIRC models can produce highly accurate simulations, but they are computationally expensive, making them impractical for iterative design scenarios that seek to evaluate a range of hypothetical engineering design and failure scenarios of levees and other protective structures. As a result, and to support other components of the IRP project, it is particularly important to have accurate and efficient *deterministic* simulation approaches that can inform and feed into *probabilistic* risk assessments.

At the broadest level, deterministic simulations of this type are essential components in probabilistic frameworks like JPM-OS (Joint Probability Method with Optimal Sampling) that consider the full range and overall impacts of potential flooding scenarios by including variations in storm parameters such as track, size, forward speed, and intensity (USACE, 2007). At a more local level, these deterministic simulations are necessary if meaningful simulations of flooding are to be carried out at a nuclear power plant facility.

Neutrino is an impressive tool, and one that is especially capable of this type of facility-scale assessment, and yet it must be informed by a larger context. Our work aims to provide boundary conditions for Neutrino from large-scale ADCIRC models to make Neutrino's facility-level simulations more meaningful. As a result, we have been working closely with Centroid Lab, and we are continuing to do so, in order to provide perspective and appropriate data for loading into Neutrino so that simulations can be carried out by their lab.

## 6.8. Technical Findings

We present a summary of our technical findings, highlights of our technical innovations, and implications of the work with respect to our objectives of enhanced spatial resolution of subdomain meshes, data libraries and reuse, ADCIRC-Neutrino coupling, and verification and validation.

### 6.8.1. Enhanced Spatial Resolution of Subdomain Meshes

Results of our three USACE case studies at Dyke Marsh Wildlife Preserve, Ike Dike, and New York-New Jersey Harbor and Tributaries show that subdomain modeling provides computational savings of as much as 83 percent, depending on the site and the size of the subdomain used. To compare subdomain (SD) solutions with equivalent full domain (FD) solutions in cost and accuracy, *without-project* full domain meshes (spatially unrefined and refined versions) are used to obtain boundary conditions using a simulation time step of 50 seconds. This interval is selected to satisfy the recommendation that, for subdomain models, boundary conditions should be recorded at intervals of around or less than one minute in time. This output is used to enforce the boundaries of subdomains generated from refined *with-project* full domains. ADCIRC solutions are then generated for these subdomains and compared against corresponding full domain solutions (see Figure 6.1).

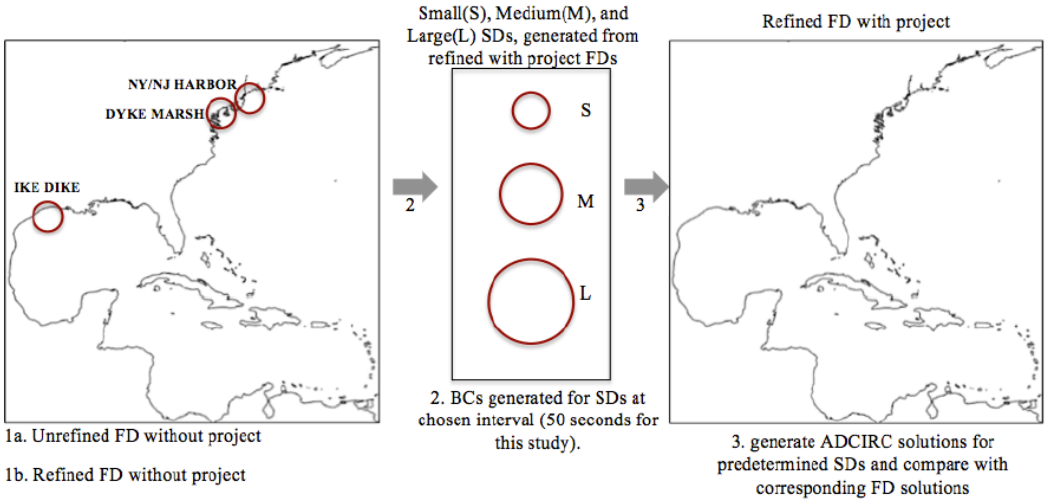


Figure 6.1: (1a) use unrefined without-project full domain or (1b) refined with-project full domain to (2) generate subdomain boundary conditions at a user defined interval of less than one minute (in our case 50 seconds), (3) the subdomain simulation is performed and compared against corresponding full domain solutions.

These comparisons indicate that, for studies without multiple, spatially distributed flood control structures, subdomain modeling can produce solutions within model tolerance levels of 15 to 30 cm. For studies incorporating more than a single flood control measure, subdomains must be generated that are large enough to encompass all structures, along with several layers of elements between the structures and the subdomain boundaries. These larger subdomains result in a decrease in computational savings unless flood control structures are spatially close enough together to be accommodated in smaller subdomains and still result in solutions within model tolerance levels.

In general, our results support the use of the smallest possible size of subdomain for case studies such as the Dyke Marsh, which are geographically isolated and incorporate relatively small project alternatives, e.g., on the order of several miles. Where possible, smaller subdomains produce results that are more accurate and with greater reductions in computational effort, a savings of at least 50 percent when compared with the standard ADCIRC workflow. There is only an incremental benefit in solution quality when starting from the refined *without-project* full domain to generate subdomain boundary conditions, as opposed to starting from the unrefined *without-project* full domain. This benefit, though small, is likely a result of the refined *without-project* full domain a) having enough resolution so there is less changed when a project is inserted, and b) incorporating the higher resolution bathymetry data used in subsequent subdomain runs. For larger project alternatives, e.g., those on the order of tens of miles, such as those incorporated in the Ike Dike case study, our results show that the most effective subdomain is one that encompasses the project with a distance between the subdomain boundary and project site of at least one-and-a-half times the span of the project itself. The largest sized subdomain used in the Ike Dike case study produces solutions that are accurate within model tolerance levels and have a computational savings of about 36 percent, compared with the standard ADCIRC workflow.

On problems like the NY-NJ HATS case study, which incorporate multiple, spatially distributed flood control structures, solution quality is well outside of model tolerance levels. Since the largest subdomain considered in this case study is smaller than the smallest subdomain in the Ike Dike case study, choosing a larger subdomain size could prove beneficial, though at the cost of a further reduction in the computational benefit, which we estimate to be about 36 to 39 percent. Even on these more challenging problems,

however, subdomain modeling could be used as a screening tool for eliminating project alternatives from further consideration, and their full domain simulations, since they provide sufficient accuracy to determine whether or not project alternatives are able to meet performance objectives. In addition, subdomain modeling could be used in such cases as a means of analyzing the interaction of various flood control measures with each other.

Our results show that subdomain modeling can be a beneficial tool that substantially reduces computational cost, and that *ex post facto* refinements to subdomains can be made to bring modeling results closer to the facility scale needed by tools like Neutrino. Its use, however, requires engineering judgment, and projects with multiple, spatially diverse protection measures over a large area see less computational benefit, though these are more typical of regional flood control strategies, in contrast with more local ones developed around nuclear power plant facilities.

*Guidelines for Computational Benefits and Subdomain Sizing*

Informed by these case studies above, we have developed a simple model for predicting the computational benefit achievable by subdomain modeling, based on the number of project alternatives considered, the number of nodes in a subdomain mesh, and the number of nodes in a full domain mesh. Development of such a relationship for automatically determining subdomain size and placement, however, is a more challenging issue. An *a priori* approach for subdomain sizing based on case study characteristics, e.g., bathymetry, project size, and storm features, would require a more concentrated effort that looks at a larger range of case studies to develop empirical guidelines, potentially using machine learning techniques.

Until such a study is conducted, however, it is nevertheless practical to generate subdomains of a variety of sizes, simultaneously, without any additional computational cost. As demonstrated by the current study, selection of multiple subdomains would only result in an incremental increase in data produced by an already low-cost workflow. This approach results in the user having a range of subdomain sizes, such that the user can force the selected domains with data from the first storm event, and then converge on the most appropriate subdomain size before forcing other subdomains with data from the remainder of the storm events.

6.8.2. Data Libraries and Reuse

Our approach to storm surge simulation introduces three modeling scales with one-way interactions between them: ocean, subdomain, and facility scales. At the subdomain scale, boundaries are defined far enough away from a nuclear power plant facility to be hydrodynamically independent of any design or failure scenarios, but close enough to reduce computational effort by eliminating substantial parts of the ocean domain from each subdomain simulation. Doing so enables the creation of validated datasets, libraries consisting of spatially varying time series of water surface elevations, depth-averaged velocities, and wet/dry status along subdomain boundaries.

The approaches we consider are based on a cubic spline interpolation of water surface elevations and velocities. As an example of possible approaches, Figure 6.2 shows an actual, high resolution time history of elevations, $\eta(t)$, for a two-hour period (in red), with standard ADCIRC output produced on the half-hour (black dots). The corresponding node is located near shore, and superimposed on the hydrograph is a shallower, higher frequency component with a period of about 30 minutes.

We note that a straightforward use of the available output with linear interpolation would mean that, between sample points A and B, the most substantial portion of the elevation forcing would be “clipped”, resulting in an under-prediction of its surge effects, when used as a subdomain boundary condition. If the maximum water surface elevation $\eta(t^*)$ is available (the open dot), however, it can be inserted into the time

series. Three possible cubic spline interpolation functions S are shown. Of the three, the best fit is obtained when η(t*) is inserted, so long as a condition S′(t∗) = 0 is also added (in black). By way of contrast, if the derivative at t* is not forced to be zero (in blue dots), the actual maximum is exceeded by spline S, and if the maximum η(t*) is not inserted at all (in green dashes), the elevation forcing is still under-predicted, but is nevertheless a modest improvement over linear interpolation. We also note that using the recommended post-processing approach, we are able to recover boundary conditions that would be available from data with a temporal resolution of 5 minutes as opposed to 30 minutes.

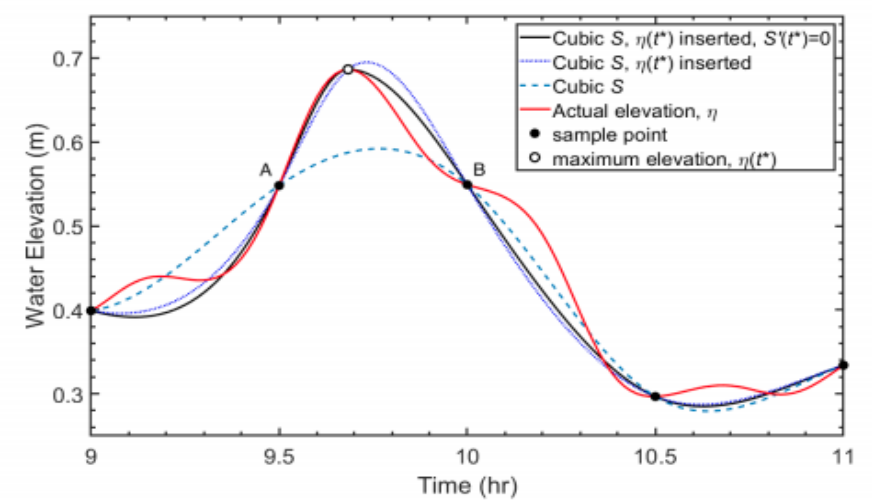


Figure 6.2: Water surface elevation forcing on a boundary node using different interpolation techniques. The cubic spline hydrographs are interpolated from water surface elevations that are sampled every half hour, with and without maximum elevation.

In comparing the best cubic and linear approaches, SMC+ and SML+, we find that in all cases cubic interpolation substantially outperforms linear interpolation. However, the absolute performance of the SMC+ approach still depends on the nature of the problem being simulated, whether simple or more complex, and whether boundary or meteorological forcing is used. In the idealized inlet case, the CDF curves for water surface elevation are nearly the same for the cubic approaches, and likewise for the linear ones, whether or not the maximum surface elevations are inserted; this is because the M2 tidal constituent is the only boundary forcing and the bathymetry is simple, with no wetting and drying involved, and this results in simpler hydrographs that are easier to recover without making use of the maximum water surface elevations.

For more complex situations, the performance of the SMC+ approach is affected by other factors, such as oscillations due to edge waves and ADCIRC's wetting and drying algorithm. The Cape Hatteras case is an example in which the process of edge waves form over a four-hour period at 30-minute intervals. The long gravity waves imposed by the atmospheric pressure system propagate to the coastal area and are trapped by the bathymetry, at which point they degenerate into a series of smaller scale longshore edge waves. This process starts early on and lasts until the hurricane makes landfall. By extending subdomain boundaries further out into the ocean, the effects of the edge waves can be contained, resulting in better performance of the SMC+ approach. Although the expansion of the subdomain area requires more computational resources, the use of oblong or other specially shaped subdomains can effectively reduce the demand on computing resources. By positioning more boundary nodes further from the coastline, better results can be obtained within the same computation time.

### 6.8.3. ADCIRC-Neutrino coupling

With respect to prototype development and coupled simulations, our approach starts simply, beginning with relatively smooth terrains, with the expectation that future work will draw on the lessons learned here to develop more complex case studies, potentially adding topographic variety, protective structures, and additional realism to capture hydrodynamic behavior around nuclear power plant facilities.

**Pseudo One-Dimensional Test Case.** This case study follows Luettich and Westerink (1995) and subsequently Dietrich et al. (2004) and is chosen as a simple test case with linear bathymetry before moving on to more complex test cases with complicated bathymetric profiles. In their study, Dietrich et al. (2004) develop and present a nearly frictionless version of the true 1D test case simulated in their 1D implementation of ADCIRC. Without access to a stable 1D implementation of ADCIRC, we follow Dietrich et al. (2004) by developing a pseudo-one-dimensional test case that can be simulated in the standard 2D implementation of ADCIRC.

Following Dietrich et al. (2004), the problem has the following parameters: a linear slope, a width of 10 m, an undisturbed length of 24 km, a bathymetric depth at the open ocean boundary of 5 m, a grid spacing of 10 m, a time step of 0.5 s, and a tidal forcing amplitude of 0.25. The bottom friction parameter *cftau* and the continuity equation parameter *G* are set to 0.001, and the wetting and drying parameters *Hmin* and *Umin* are set to 0.01. Flow is imposed only in the x-direction, and an 80-m subdomain is selected toward the shallow end of the full domain. Elevation and velocity time series at relevant stations/gauges that are output every 10 s for a duration of 10 min. These outputs are passed through Python scripts that translate data into a format suitable for Neutrino to use as inputs. A second mesh is developed with all parameters left constant except for an increase in mesh resolution from 10 m to 5 m.

**Alligator River National Wildlife Refuge.** The study area features a smooth terrain located in eastern North Carolina along the Atlantic Coast (Figure 6.3a). We select an area of 103 m x 116 m to refine to a grid spacing of 10 m. This area of interest is located near the Alligator River National Wildlife Refuge in a low-lying part of the domain that is vulnerable to flooding (Figure 6.3b) and forced by meteorological input data from Hurricane Isabel (2003). We define 48 boundary nodes at about 10 m apart around an area where the Neutrino domain is to be located. The area starts dry and floods in a 2-day simulation, from which we extract 90 s of output data for Neutrino at 5 s intervals. These data values are passed through the Python script and converted to a format suitable for use as input for Neutrino.


Figure 6.3: (a) Location of Alligator River National Wildlife Refuge and (b) a finite element mesh refined and laid over an area of interest located near the Alligator River National Wildlife Refuge

Together, these case studies provide a basis for a methodology of one-way coupling between ADCIRC and Neutrino that can inform additional, more complex, case studies in the future.

**Results and Observations.** Presented here are results from our efforts to implement and validate a coupling methodology for ADCIRC with Neutrino. In what follows, we provide both quantitative and qualitative comparisons between results from ADCIRC simulations and results from corresponding Neutrino solutions.

We begin with the Alligator River case study, and show side-by-side qualitative comparisons between ADCIRC solutions and Neutrino solutions. Figures 4 through 6 represent the status of the flooding front at particular snapshots in time in ADCIRC (left) and Neutrino (right).

At a point 20 s into the simulation (Figure 6.4), ADCIRC has inundated more of the domain, in comparison with Neutrino, where a faint flooding front can be seen aligned along its boundaries below and to the right. In ADCIRC, the flooding front is moving diagonally from the southeast to the northwest; in Neutrino, the shape of the front is clearly affected by the shape of its boundary, presumably indicating a problem with the way in which boundary conditions are being imposed in the smoothed particle hydrodynamics code.

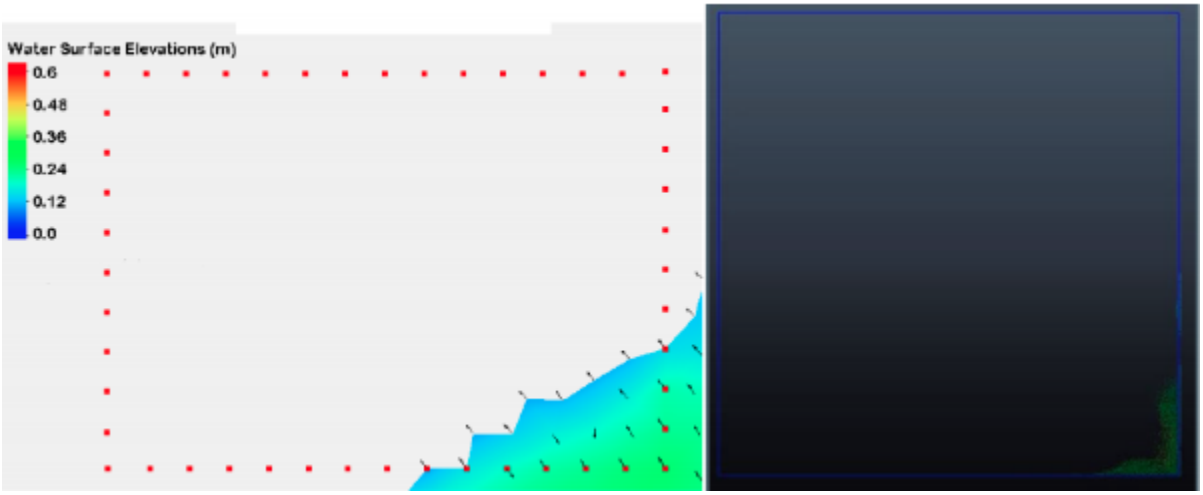


Figure 6.36: ADCIRC output (left) and Neutrino output (right) 20 seconds into the simulation. The ADCIRC image includes velocity direction (black arrows) and boundary input (red dots) used by the Neutrino domain.

At about 30 s into the simulation (Figure 6.5), the ADCIRC domain is about halfway inundated and continues to maintain a nearly linear wetting front, whereas about a third of the Neutrino domain is inundated; its wetting front continues to reflect the shape of its domain. At about 65 s into the simulation (Figure 6.6), the ADCIRC is nearly fully inundated, and the Neutrino front continues to lag a bit.

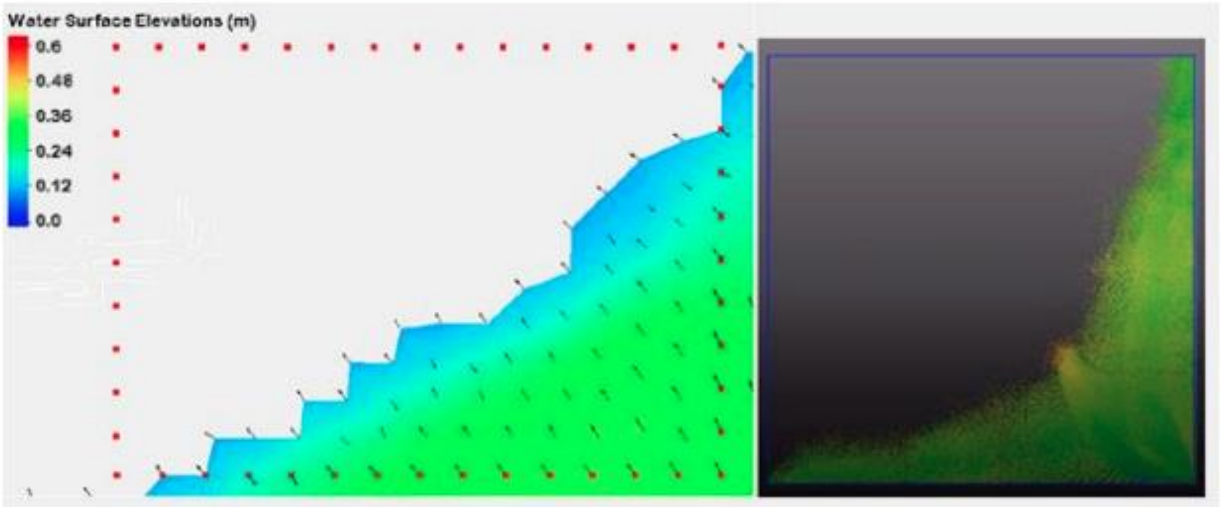


Figure 6.37: ADCIRC output (left) and Neutrino output (right) 30 seconds into the simulation.

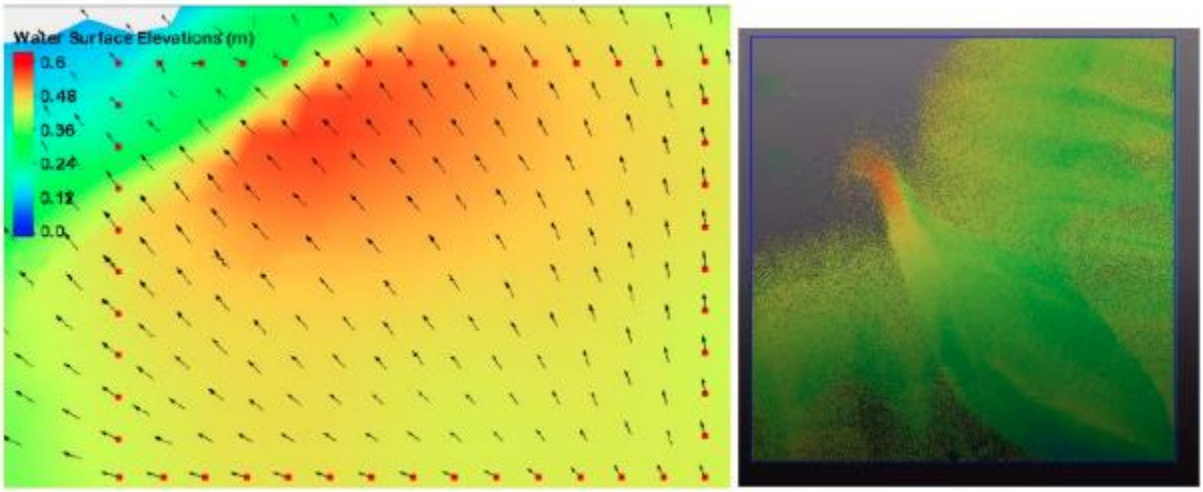


Figure 6.38: ADCIRC output (left) and Neutrino output (right) 65 seconds into the simulation.

In each of the snapshots, Neutrino shows a flooding front entering the domain from the southern and eastern boundaries in a way that seems to reflect the shape of the domain. Further into the simulation, it also seems to create an unusual artifact, an oblong build-up of water on a diagonal from the southeast corner of the domain to the northwest corner of the domain, which does not appear in ADCIRC output. In order to better understand the reason behind these discrepancies, we take a step back to the simpler pseudo-one-dimensional case study.

In the pseudo-one-dimensional case study, similar to Dietrich et al. (2004), the ADCIRC tides-only simulation on this domain results in minimums in water surface elevation (of about -0.3 m) when the wetting and drying front is 18.7 km into the domain. These results agree with Dietrich et al., which report the same minimum elevations and movement into the domain, though with marginally different timing, probably as a result of the respective differences in the models used. Similarly, maximum elevations (of about +0.3 m) occur when the wetting and drying front is 21.2 km into the domain. These results are again in agreement with Dietrich et al., with marginal differences in timing.

The discrepancies in the times to reach minimum and maximum elevations between our results and those of Dietrich et al. may be due to (1) the fact that we are capturing two-dimensional physics in our use of the production version of ADCIRC, as opposed to the simplified 1D model used by Dietrich et al., and (2) the selection of the lateral eddy viscosity parameter. The lateral eddy viscosity parameter plays a crucial role in 2D ADCIRC by allowing either slower or more rapid inundation, depending upon the selected value, and its relationship with similar parameters in Neutrino requires further study to see if better agreement may be had by doing so, either on the ADCIRC or the Neutrino side.

Continuing with the pseudo-one-dimensional case study, when comparing ADCIRC solutions with Neutrino at a particular time step (Figure 6.7), water surface elevations in Neutrino are about 28 percent lower earlier in the domain, and the gap between ADCIRC solutions and Neutrino increases progressively from about 54 percent lower at 20.55 km into the domain, to 98 percent at 20.56 km, and finally to 100 percent at 20.57 km.

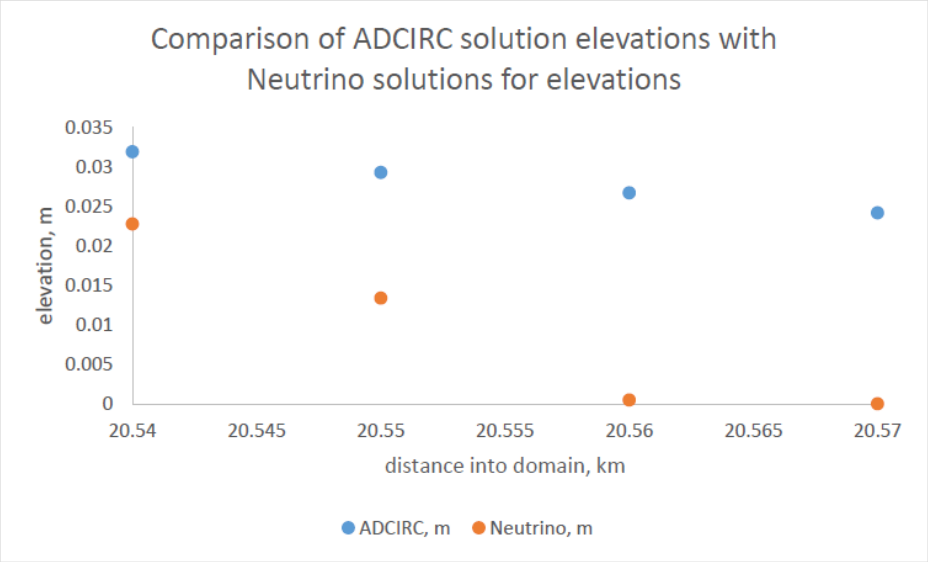


Figure 6.7: Comparison of ADCIRC and Neutrino water surface elevations at various points in pseudo-one-dimensional case study.

Discrepancies between ADCIRC and Neutrino in the pseudo-one-dimensional case study indicate the need to better understand the quantitative relationships between the modeling parameters used in Neutrino and ADCIRC (e.g., lateral eddy viscosity, bottom friction, and tidal amplitude). In addition, the notion of state captured in shallow-water models like ADCIRC is not easily transferred as boundary conditions to a smoothed particle hydrodynamics code, which is being asked to handle arbitrary flow behavior along its boundaries. Like most SPH solvers, Neutrino only handles the creation of fluid particles on one side of a boundary and does not have the ability to handle arbitrary backflows, time dependent changes in the magnitude and direction of velocities along its boundaries, and so on. Further work may be needed to advance the state of the art in handling arbitrary boundary conditions in SPH codes.

## 6.9. Highlights of Technical Innovations

Beyond the broader innovations already described, we note the following concrete contributions made during this project.

**A priori predication of computational benefits of subdomain modeling.** We develop an empirical relationship for percent reduction in computational cost achievable by subdomain modeling based on comparisons of computational costs associated with the standard ADCIRC workflow and those associated with the subdomain modeling workflow. The relationship is a function of the number of alternatives being considered ($N$), the number of full domain nodes ($nf$), and the number of subdomain nodes ($ns$). With this, the percent reduction achievable by subdomain modeling can be obtained.

**Internal weirs in subdomains.** ADCIRC supports several types of internal and external boundary conditions types. Prior to this research effort, subdomain modeling lacked the capability to accommodate island boundary conditions and internal weir boundary conditions. These boundary condition types are regularly used (in the case of the island boundary condition type) to denote islands, and (in the case of internal weirs) to represent project alternatives considered by United States Army Corps of Engineers (USACE). Prior to this research effort, when generating subdomains, island boundary conditions or internal weir boundary conditions would result in an error rather than a successful simulation. This research effort involved enhancing and refining subdomain modeling scripts to incorporate island and internal weir boundary condition types.

**Smoothing and interpolation for subdomain modeling.** Prior to this research effort, subdomain modeling could not accommodate reuse of existing full simulation datasets, which are only available at 15- or 30-min intervals, where subdomain simulations traditionally require boundary conditions at an interval of about one minute or less. This research effort resulted in the improvement of subdomain modeling scripts to include the recommended cubic spline interpolation with maximum surface elevation to generate, from existing archived full simulation solutions, subdomain boundary conditions using this interpolation technique.

**Scripts for converting ADCIRC output to Neutrino input.** ADCIRC deals with large-scale finite element simulations where domains are in geographic coordinates and simulation run times are on the order of several days. On the other hand, Neutrino deals with mesh-free simulations at facility-level scales where domains are in cartesian coordinates and simulation run times are on the order of several minutes. Considering the difference between the formats of ADCIRC outputs and Neutrino inputs, we have developed a Python script as a method of communication between two different models with two different paradigms. This script serves to take ADCIRC outputs and convert them to a format suitable for use as input for Neutrino.

**Validation of correctness models.** To support the verification of scientific software, we developed a web-based visualizer for state-based formal methods called Sterling. As an interface for lightweight tools like Alloy, it provides advanced visualization capabilities that address the shortcomings of existing approaches and includes the ability to visualize the types of dynamic and spatial relationships that are needed for modeling scientific software.

### 6.10. Implications of the Work

The demonstrated ability of subdomain modeling to reduce computational cost led initially to an internship opportunity and ultimately to a staff research position for PhD student Fatima Bukhari with the US Army Corps of Engineers at its Engineering Research and Development Center (USACE-ERDC). Her position with USACE-ERDC is based on this work, which she is now presenting to others at the center via team talks and other collaborations within the center.

In addition, beyond this personal recognition, USACE is now undertaking an initiative to incorporate our subdomain modeling approach in its regular workflow so that computational resources can be reduced

while maintaining solution quality. In USACE's current workflow, project alternatives are defined by large-scale ADCIRC grids that differ locally in a geographic region of interest. These project domains are forced by thousands of selected storms, and individual ADCIRC simulations are performed on each of them. This results in thousands of full domain ADCIRC simulations *per project alternative*, after which the results are analyzed and archived on a server. The running and archiving of these simulations results in a significant burden on computational resources, which are expected to be reduced by incorporating subdomain modeling and its approach to reuse in the workflow.

With respect to software verification, our Sterling tool has been adopted as the primary visualization interface for Forge, a language built for teaching formal methods and model checking. Forge and Sterling were used as the primary teaching tools in the Spring 2020 Logic for Systems undergraduate course in the Computer Science department at Brown University.

### 6.11. Path Forward

We describe future directions with respect to our objectives of enhanced spatial resolution of subdomain meshes, data libraries and reuse, ADCIRC-Neutrino coupling, and verification and validation.

**Enhanced spatial resolution of subdomain meshes.** In all test cases, a sampling interval of 50 seconds is used for recording boundary conditions for subdomain simulations. Conducting similar experiments with a broader range of sampling intervals, both smaller and larger than 50 seconds, would aid in providing a clearer relationship between computational savings and quality of subdomain solutions. A repetition of these experiments with additional variety of subdomains could also prove fruitful. In addition, future studies might benefit from a wider variety of real-world test cases, from which a wider range of subdomain sizes could be generated and subjected to a broader range of sampling intervals for recording subdomain boundary conditions. This would provide the tools necessary to develop an empirical relationship for subdomain sizing based on case study characteristics. Finally, further exploration is warranted for case studies with multiple flood control structures that are close together and case studies with multiple flood control structures that are spatially separate.

In addition, in depth evaluation of subdomain modeling indicates that it produces solutions within model tolerance levels and has resulted in the development of an empirical formula for the computational benefit achievable by subdomain modeling. However, further investigation is necessary to develop guidelines for subdomain sizing based upon case study characteristics.

**Data libraries and reuse.** The results of our smoothing approach for reusing large-scale datasets are representative in the sense that subdomain boundaries are sized and placed without consideration given to the hydrodynamic particulars of nodes appearing on subdomain boundaries. Additional improvements in accuracy, however, could be obtained by treating the creation of subdomains as a modeling exercise, looking for boundary placements that avoid regions with more complex hydrodynamics and higher frequency components. Because such assessments can be made *a priori*, future work could focus on an additional post-processing step that optimizes subdomain boundary placement.

**ADCIRC-Neutrino coupling.** A prototype approach for handing off data between ADCIRC and Neutrino has been developed but needs further work. Preliminary models and a comparison of results suggests a follow up study that would look more carefully at the physical parameters and types of boundary conditions employed by SPH solvers to better match anticipated coastal flooding scenarios. In addition, because our experiments began by focusing on relatively smooth terrains and simplified domains, future work might successively add complexity by including more topographic variety; protective structures, such as levees or dune systems; variations in storm parameters such as track, size, forward speed, intensity; and finally, additional realism to mimic hydrodynamic behavior around nuclear power plant facilities.

**Verification and Validation.** As we have noted, subdomain modeling has been shown to be mathematically equivalent to ADCIRC through a combination of informal proofs and static verification techniques using state-based formal methods, but much additional work remains on the topic of software quality in scientific arenas. Despite broad and recognized impacts, meeting quality and reproducibility standards is a growing concern, as is productivity. Not merely anecdotes, numerous empirical studies of software thwarting attempts at repetition or reproduction of scientific results have been cataloged, along with their concomitant effects, including a widespread inability to reproduce results and subsequent retractions of papers in scientific journals.

## 6.12. Conclusions

Assessing the vulnerability of nuclear infrastructure to hurricane storm surge requires both high-fidelity simulations and a methodology that accommodates the spatiotemporal scales over which hurricanes operate. Our approach introduces three modeling scales with one-way interactions between them: ocean, subdomain, and facility scales. For ocean and subdomain scales, we make use of the parallel, unstructured-grid finite-element hydrodynamic code, ADCIRC, and for the facility scale, the mesh-free SPH model, Neutrino.

We address both modeling and data exchange concerns, as well as the gap in resolution between typically the coarsest Neutrino and finest ADCIRC models. The need for spatial—and therefore temporal—refinement of large-scale ADCIRC simulations is made practical through the use of subdomain modeling. These questions are explored within the context of three real-world case studies provided by the USACE Engineering Research and Development Center (ERDC) in Vicksburg, MS. The sites are located along the Atlantic and Gulf coastlines of the United States, and each has differing characteristics, with project alternatives varying in size from on the order of several miles long to tens of miles long, and with both single and multiple, simultaneous project alternatives considered. Our study shows that subdomain modeling can in fact accommodate enhanced *ex post facto* refinements, and thereby reduce computational effort substantially, making more practical the use of large-scale storm surge models in an iterative design scenario.

In cases where the need for subdomain modeling is unanticipated at the time simulations are originally performed, a post-processing step in the workflow has been developed so that existing, archived results can be reused. We show that the coarse output ordinarily produced by ADCIRC still allows for subsequent localized simulations of high quality when the datasets are post-processed using the techniques we describe. Of those considered and evaluated, cubic spline interpolation works best at recovering water surface elevations and velocity time histories, and modest additional improvements can be had when maximum water surface elevations are available, as they typically are in ADCIRC output. Such an approach results in the recovery of boundary conditions with a quality comparable to those obtained from temporally more refined datasets. The approach enables a workflow that accommodates the construction, maintenance, and reuse of large-scale simulation libraries.

Our coupling approach is based on a one-way handoff of data from ADCIRC to Neutrino, and tested within the context of a pseudo one-dimensional problem and a more realistic case study at the Alligator River National Wildlife Refuge. These studies start from validated, large-scale ADCIRC simulations, which produce results that are then converted to a suitable format for Neutrino using a Python script for data exchange. Preliminary datasets from both case studies have been developed and provided to the Centroid Lab, which has successfully loaded them into Neutrino and performed the corresponding simulations. Comparisons between the ADCIRC and Neutrino solutions indicate a need for further scrutiny and study of the quantitative relationships between ADCIRC and Neutrino modeling parameters. Further

sensitivity studies are suggested for exploring these relationships and the nature of the boundary conditions supported by SPH solvers like Neutrino.

### 6.13. References


**As-Salek, J. A., and Yasuda, T. (1995).** Comparative study of the storm surge models proposed for Bangladesh: Last developments and research needs. Journal of Wind Engineering and Industrial Aerodynamics, 54–55(C), 595–610.

**Baugh, J., Altuntas, A., Dyer, T., and Simon, J. (2015).** An exact reanalysis technique for storm surge and tides in a geographic region of interest. Coastal Engineering, 97, 60-77.

**Baugh, J. and Altuntas, A. (2018).** Formal methods and finite element analysis of hurricane storm surge: A case study in software verification. Sci. Comput. Program. 15: 100–121.

**Baugh, J. and Dyer, T. (2018).** State-based formal methods in scientific computation. In Abstract State Machines, Alloy, B, TLA, VDM, and Z: 6th International Conference, ABZ 2018, pages 392–396, Cham, 2018. Springer Lecture Notes in Computer Science 10817.

**Bukhari, F. (2020).** Performance evaluation of subdomain modeling and operational enhancements for large-scale storm surge simulations. (Doctoral dissertation, North Carolina State University, Raleigh, NC). Retrieved from https://www.lib.ncsu.edu/resolver/1840.20/37415

**Debreu, L., and Blayo, E. (2008).** Two-way embedding algorithms: A review. Ocean Dynamics, 58(5–6), 415–428.

**Dyer, T. (2020).** Lightweight formal methods in scientific computing. (Doctoral dissertation, North Carolina State University, Raleigh, NC). Retrieved from https://www.lib.ncsu.edu/resolver/1840.20/38064

**Hubbert, G. D., Leslie, L. M., and Manton, M. J. (1990).** A storm surge model for the Australian region. Quarterly Journal of the Royal Meteorological Society, 116(494), 1005–1020.

**Dietrich, J.C., Kolar, R.L., and Luettich, R.A. (2004).** Assessment of ADCIRC's wetting and drying algorithm. Developments in Water Science. 55(2):1767-1778.

**Fox, A. D., and Maskell, J. S. (1995).** Two-way interactive nesting of primitive equation ocean models with topography. Journal of Physical Oceanography, 25, 2977–2996.

**Jackson, D. (2012).** Software Abstractions: Logic, Language, and Analysis, revised edition, MIT Press.

**Liu, M.B. and Liu, G.R. (2010).** Smoothed particle hydrodynamics (SPH): an overview and recent developments. Archives of Computational Methods in Engineering 17(1): 25–76.

**Luettich, R. A., Westerink, J. J., and Scheffner, N. W. (1992).** ADCIRC: An Advanced Three-Dimensional Circulation Model for Shelves, Coasts, and Estuaries. Report 1. Theory and Methodology of ADCIRC-2DDI and ADCIRC-3DL. Retrieved from http://agris.fao.org/agris-search/search.do?recordID=AV20120114600

**Luettich, R.A. and Westerink, J.J. (1995).** "An Assessment of Flooding and Drying Techniques for Use in the ADCIRC Hydrodynamic Model: Implementation and Performance in One-Dimensional Flows", Report for the Department of the Army, Contract Number DACW39-94-M-5869 (1995).

**Luettich, R.A., and Westerink, J.J. (2004).** Formulation and Numerical Implementation of the 2D/3D ADCIRC Finite Element Model Version 44.XX.

**Ma, Z., Smith, C., and Prescott, S. (2017).** 'A Simulation-Based Dynamic Approach for External Flooding Analysis in Nuclear Power Plants'. Proceedings of the 20th Pacific Basin Nuclear Conference. PBNC 2016. Springer, Singapore.

**Sampath, R., Montanari, N., Akinci, N., Prescott, S., and Smith, C. (2016).** Large-scale solitary wave simulation with implicit incompressible SPH. Journal of Ocean Engineering and Marine Energy. 2(3): 313–329.

**Sampath, R. (2018).** Neutrino Documentation. Neutrino Dynamics Initiative. Retrieved from: https://media.readthedocs.org/pdf/neutrinodocs/master/neutrinodocs.pdf

**Sheng, J., Tang, L., and Wang, L. (2005).** Simulating the upper ocean circulation on the Belize shelf: An application of a triply nested-grid ocean circulation model. Journal of Ocean University of China, 4(4), 315–328.

**Spall, M., and Robinson, A.R. (1989).** A new open ocean, hybrid coordinate primitive equation model. Mathematics and Computers in Simulation. 31. 241-269. 10.1016/0378- 4754(89)90162-6.

**USACE (2007).** Elevations for Design of Hurricane Protection Levees and Structures: Lake Pontchartrain, Louisiana and Vicinity Hurricane Protection Project, West Bank and Vicinity, Hurricane Protection Project. Report, Prepared by New Orleans District, U.S. Army Corps of Engineers, October.

**Westerink, J. J., Luettich, R. A., Feyen, J. C., Atkinson, J. H., Dawson, C., Roberts, H. J., et al. (2008).** A Basin- to Channel-Scale Unstructured Grid Hurricane Storm Surge Model Applied to Southern Louisiana. Monthly Weather Review, 136(3), 833–864.

# 7. Flooding Model Validation Experiment

## 7.1. Introduction

The safe production of power from nuclear facilities has always been a concern. In 1975 the NRC was established to protect public health and safety relating to nuclear energy. One of the risk areas addressed by the NRC is that of flooding. Several guides and evaluation methods have been published over time by NRC to assist commercial nuclear facilities in verifying and improving flood safety. In 2008 the Regulatory Guide 1.200 (https://www.nrc.gov/docs/ML0904/ML090410014.pdf) describes methods to meet technical adequacy for PRA models, including internal and external flooding. Just before the Fukushima Tsunami event of 2011 NRC published "Design-Basis Flood Estimation for Site Characterization at Nuclear Power Plants in the United States of America." (https://www.nrc.gov/docs/ML1132/ML11321A195.pdf). This NRC document outlines the different types of flooding hazards and the process to evaluate the risk of each. After determining the frequency of various events, the effects of those flooding events need to be evaluated. The growth in computer power has enabled the development of advanced predictive modeling, referred to as high fidelity modeling. The capabilities of high-fidelity modeling ultimately enable engineers develop better understanding of the behavior of complex systems, based on multi-scale multi-physics simulation. This understanding will translate into evaluating current designs and optimizing protective measures. Realizing these benefits however continues to be handicapped by the conventional nature of the validation process and how to account for uncertainties.

## 7.2. Requirements

There are seven main categories for flooding at nuclear facilities identified by the NRC:

- Local Intense Precipitation (LIP)
- Stream & River Rise Flooding
- Dam Failure
- Storm Surge
- Wave (Rouge, Tsunami, Seiche)
- Pipe Rupture
- Ice-Induced Flooding

Each nuclear facility has different items that it is susceptible to and must have assessed each risk. First the facility evaluates the likely hood of events in the categories. If the risk is significant, then further analysis is performed by developing probable flooding scenarios. Conservative estimates are often used in these stages to make sure that uncertainty and other unknowns do not jeopardize the safety of the plant. Because of this conservatism, some scenarios may have misleading importance and require mitigation efforts. To avoid unnecessary and costly plant modifications, a detailed flooding analysis can be performed using several tools available to the utilities. The development of advanced predictive modeling, referred to as high fidelity modeling, with high levels of accuracy as compared to legacy codes. The premise of high-fidelity modeling is that it will ultimately enable engineers develop better understanding of the behavior of complex systems, based on multi-scale multi-physics simulation. However, this requires these tools to be relevant and validated for the key aspects of the scenarios being evaluated and a methodology for determining the confidence level when using multiple tools and crossing different domains. Facilities can

now evaluate fields such as impact forces, water or wave height, debris flow, and splashing using these advanced tools such as the SPH approach used in Neutrino and outlined in this report.

With these new capabilities available, a good framework for validation and evaluating the uncertainty between tools needs to be available as well. Which tools can be used in the different scenarios, what confidence level do they provide, and how does the confidence from individual codes or methods combine to give and overall confidence level?

Historically evaluating flooding risk and protection methods involved data gathering and then expert judgment. While we will never and should never, fully eliminate the need of human expertise, by following a proper methodology and using these maturing technologies, comes the opportunity to minimize errors and conflicts in expert judgement. Other modeling and simulation strategies have shown a "Human In The Loop" approach is the most effective. In summary, the validation methodology outlined in this report allows for the following key capabilities:

- Site specific adjustments
- Varied detail level
- Scaling of validation data and uncertainties
- Simulation features uncertainty
- Multi-Stage uncertainty propagation

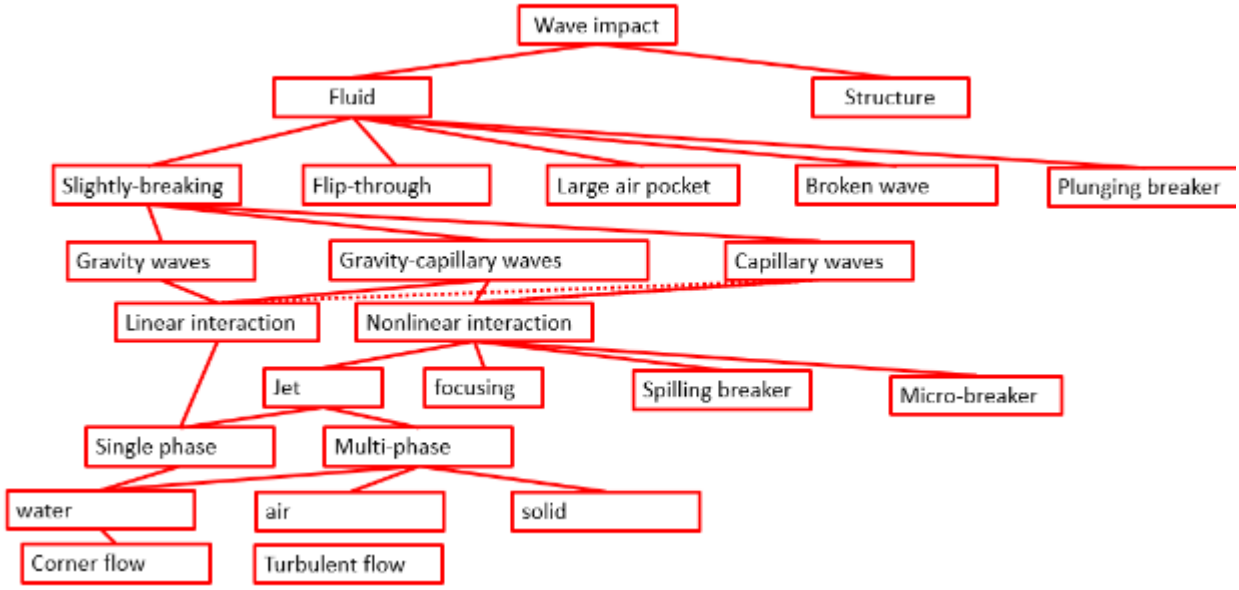


Figure 7.1 Proposed Validation Pyramid for Flooding Scenarios.

### 7.3. SPH Simulation Code

While performing validation studies of Neutrino code and the underlying SPH fluid models, we obtained insights on key limitations faced by the Neutrino code version currently in use. In this section, we describe the main enhancements and developments made during the project implementation to the Neutrino code and SPH fluid model, in relation to the modeling of external-flooding scenarios. A large part of the investigation and enhancements done were collaborative work with, on fluid-solid interaction capability, the COSMER laboratory at the University of Toulon and, on coupling with shallow-water model, the Department of Civil, Construction, and Environmental Engineering at North Carolina State University, the

Department of Mathematics at Boise State University, and the Idaho National Laboratory. We emphasize that most of the simulations run during the project did not benefit from these enhancements.

### 7.3.1. Wall boundary handling and fluid-solid interaction

Accurate fluid-solid interaction is crucial to account for debris impact and push further the flooding risk assessment. Neutrino code incorporates a rigid-body solver and two-way couples it with the SPH fluid solvers. However, we noticed difficulties to simulate floating and sinking bodies in water, especially when the density ratio is close to 1, thereby advocating the need to enhance the wall boundary handling and fluid-solid coupling.

There are two wall conditions imposed in the SPH fluid model: a slip condition and a pressure condition. Correct choices of conditions and proper impositions are important to obtain reliable pressure forces and friction forces. Initially, we were imposing a partial-slip condition and, for the pressure field, a homogeneous Neumann condition. However, both are problematic. Firstly, the partial-slip condition requires tuning a numerical parameter to decide on how much friction is applied to the fluid, and it is not clear what would be a suitable default value for this parameter. Secondly, the homogeneous Neumann condition on the pressure field neglects the acceleration of the solid body and effects due to all non-pressure forces (from gravity and viscosity, in particular). To overcome these limitations, we added a no-slip condition, that does not require any numerical parameter and could serve as a default setting, and we replaced the pressure wall condition by a non-homogeneous Neumann condition, accounting for the solid-body acceleration and the non-pressure force effects.

The way the Neumann boundary conditions are imposed was also problematic. We were using a mirroring technique, which is computationally very efficient and consists in, in the SPH particle-particle interactions, “mirroring” fields from the fluid particle to the boundary particle. Investigating the impacts on particle pressures and pressure forces on a hydrostatic test case, we noticed that this technique yields significantly over-estimated fluid pressures near the boundary, and especially at the corner of the fluid-solid interface. We decided to implement and use instead an extrapolation technique based on Shepard’s method; we observed that the hydrostatic solution is correctly reproduced, while still retaining the computational efficiency [Gartner, Montanari, Richier, Hugel, Sampath, 2019].

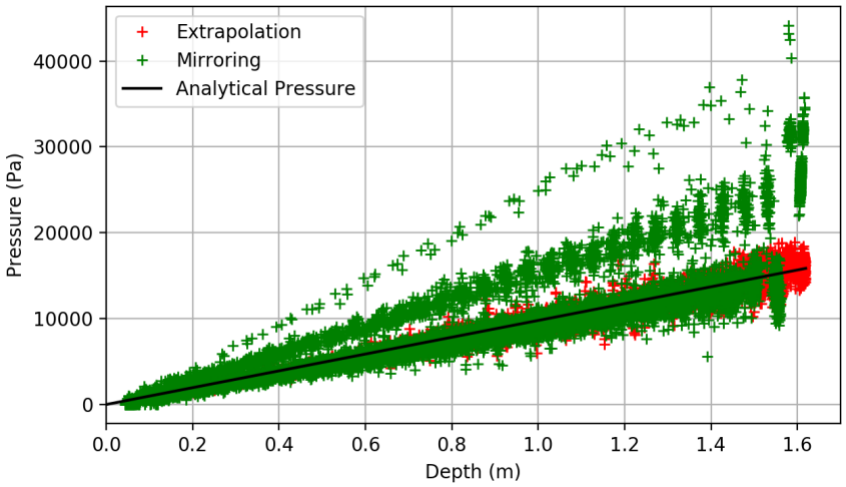


Figure 7.2. Evolution of particle pressures over depth for the analytical hydrostatic solution, Neutrino with pressure mirroring and homogeneous Neumann boundary condition, and Neutrino with pressure extrapolation and non-homogeneous Neumann boundary condition.

We tested it further on dynamic test cases, such as a falling sphere in water, to which we derived an approximate solution based on added mass and velocity damping [Gartner, Montanari, Richier, Hugel, Sampath, 2019]; the results are encouraging but show that attention on numerical-parameter setting (choice of smoothing kernel, interaction radius, etc.) is required, at least at coarse resolution, to reproduce the expected dynamic behavior. We realized a few other, more minor enhancements, such as: more choices of smoothing kernels (quartic B-spline, quantic B-spline, quantic Wendland); and a better time-step synchronization between the SPH fluid solver and the rigid-body solver.

Efforts were also made on handling negative relative pressures (with respect to atmospheric pressure), which may occur at the back-side of a solid body past the flow. It is challenging to design a SPH fluid model that can deal with negative pressures for, mainly, three reasons: inter-particle pressure forces may become attractive instead of repulsive, causing occurrences of the so-called tensile instability; the imposition of the dynamical condition on pressure at free-surface, relative pressure = 0, becomes challenging; and the matrix of the pressure Poisson equation loses interesting properties, such as the diagonal dominance, some of which are requirements for the convergence of the linear-system solver implemented in Neutrino. Although we were able to find a partial solution and to obtain encouraging results, we have not been able yet to device a suitable method, that solves all three sub-problems simultaneously and in a robust and stable manner, to handle the negative pressures.

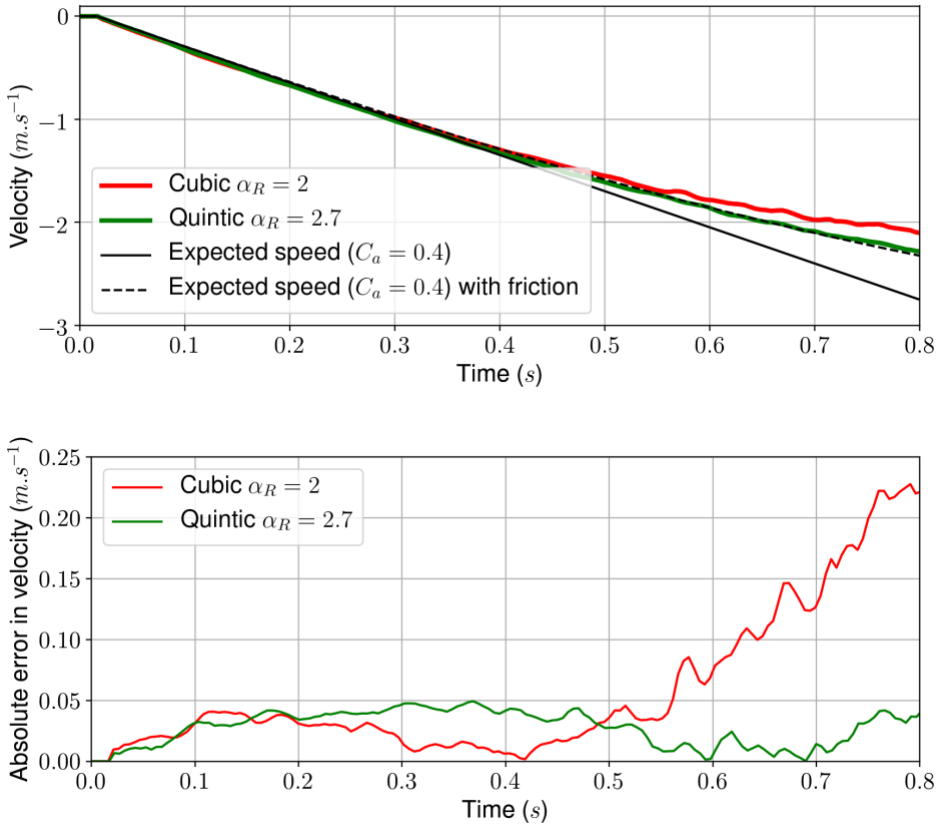


Figure 7.3. Speed and absolute error over time for the falling sphere in Neutrino against an approximate solution based on added mass and velocity damping. We tested two numerical settings, which differ in the choice of smoothing kernel (cubic B-spline or quantic B-spline) and the ratio between interaction radius and particle size.

### 7.4. Topography and coupling with shallow-water models

Preliminary work has been done on a one-way coupling from shallow-water models to 3D Navier-Stokes SPH models in Neutrino, resulting on a proof-of-concept of the methodology [Montanari, Sampath, Calhoun, Prescott, Smith, 2018]. However, no rigorous validation study had been undertaken and not all necessary modeling tools to deploy it in the industry have been implemented yet.

We implemented a new node, called Rigid Topography in Neutrino code [Montanari, Sampath, Calhoun, Prescott, Smith, 2018], that is specifically intended to model the solid surface of the ground or sea floor. It can produce a high-quality triangle-mesh of the solid surface from topography data by performing a 2D Delaunay triangulation. The triangle mesh is then sampled with boundary particles used in the SPH framework to model wall boundaries and impose the pressure wall condition and slip condition. We also added a mesh visualization based on the relative elevation.

Topography data comprises elevations of the ground surface or sea floor at many locations. Similarly, simulation output data from shallow-water code consists of the water height and horizontal velocity fields sampled at different locations. Generally, these locations of topography data and shallow-water data are specified in latitude-longitude-height (LLH) coordinates defined for a given geodetic system, which approximates the Earth's surface as a certain sphere or ellipsoid. We added the support of two widely used geodetic systems: the world geodetic system (WGS) 84, defined with respect to the average of stations all over the world and used by the global positioning system; and the North American datum (NAD) 83, designed to be particularly accurate for points on the North American Plate. Conversely, the much smaller scale of the simulation domains in Neutrino is more simply handled using 3D Cartesian geographic coordinates. One convenient choice is, for instance, the local north-east-up (NEU) coordinate system, which is defined on a local plane tangent to the Earth's surface. Therefore, to make use of topography data and shallow-water data in Neutrino, we enabled converting the locations from an LLH coordinate system to a local NEU coordinate system. This conversion is a multi-step process; indeed, it also requires: an intermediate conversion to the Earth-centered, Earth-fixed (ECEF) geocentric coordinates, which correspond to a Cartesian system that is geocentric instead of being local; and a reference location to define the local NEU coordinate system.

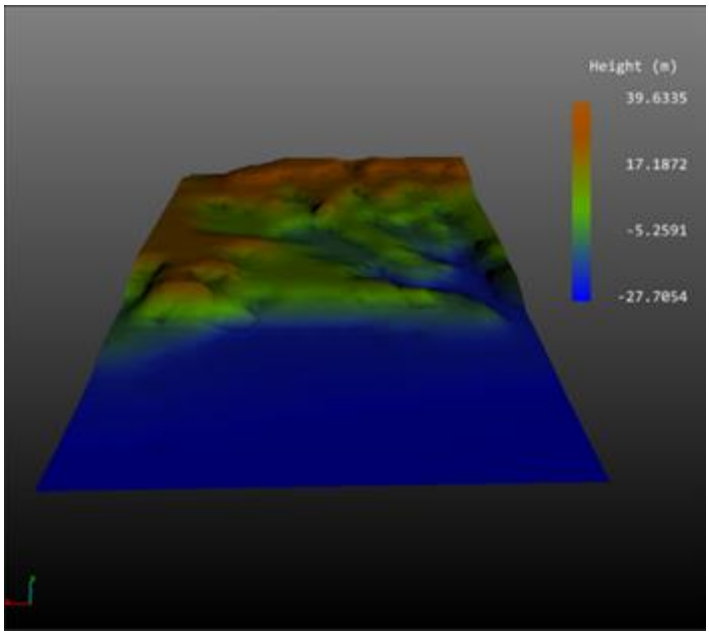


Figure 7.4. Visualization in Neutrino of a topography mesh generated from topography data after geographic coordinate conversion and Delaunay triangulation. The color represents the relative elevation of the ground surface and sea floor with respect to the average elevation of the topography.

We improved the method to couple from shallow-water code to 3D SPH fluid model. There were significant deviations between the flow rates prescribed by the shallow-water code and the ones modeled through the SPH particle representation in Neutrino, eventually causing large errors in the total mass and total volume simulated in Neutrino. The issue comes from the fact that the fluid height at the coupling boundary is unavoidably approximated as the closest multiple of particle size. To enforce the right flow rate, at each time step we apply an adjustment process in two steps: first, the flow-rate deviation is computed; then, the rate of particle emission is adjusted to account for the flow-rate deviation. If, at the coupling boundary, the number of fluid particles along the vertical direction is higher than the prescribed fluid height, then the rate of particle emission is decreased accordingly; conversely, if the number of fluid particles along the vertical direction is lower, then the rate of particle emission is increased by a right amount. We tested this coupling-method improvement on a tidal simulation run first using ADCIRC over a large domain then refined in Neutrino on a small subdomain and a 10-min time slice. The results show a superior behavior after adjustment, without any pseudo-oscillation-like evolution of the accumulated fluid volume error anymore. Note that it appears a drift, regardless the adjustment is used or not; the cause has not been clearly identified, but it could simply be an artefact coming from the approximations done when calculating the reference accumulated fluid volumes.


Figure 7.5. Fluid height, flow speed and flow rate over time in the tidal simulation for ADCIRC (input of the coupling) and Neutrino (output of the coupling) with and without adjustment. The flow rate, which combines fluid height and flow speed, is correctly recovered by adjusting the rate of particle emission (governed by the flow speed).

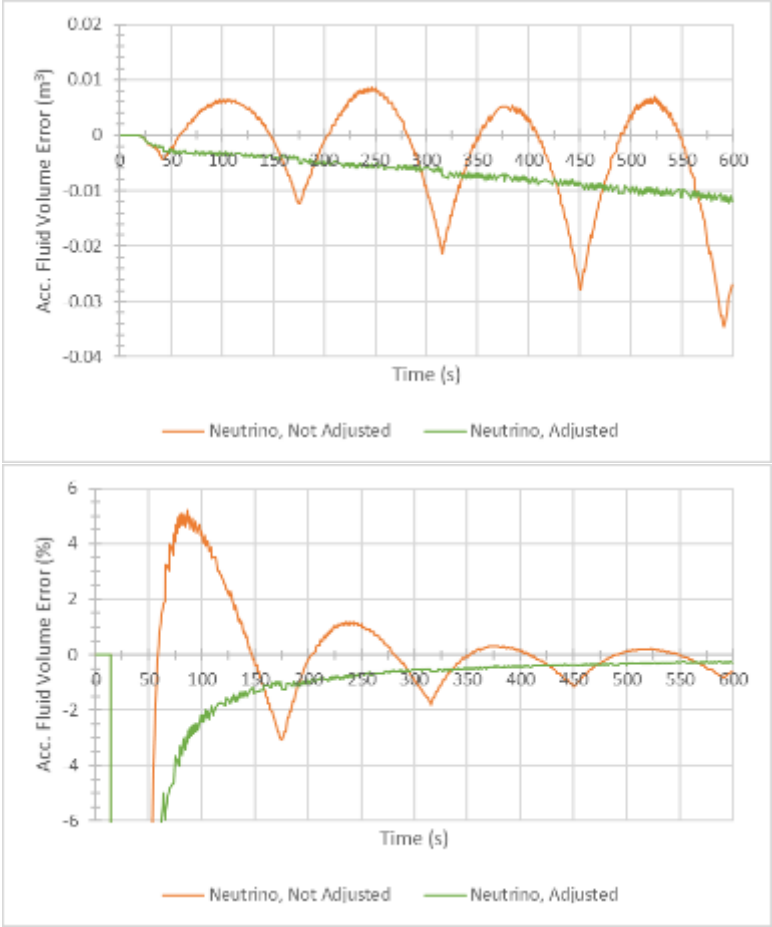


Figure 7.6. Absolute and relative accumulated fluid volume errors over time in the tidal simulation for Neutrino with and without adjustment. The errors are calculated with respect to the prescribed flow-rate time series; the reference accumulated fluid volume is estimated by integrating over time the prescribed flow rates and approximating using a Riemann sum with middle point rule.

## 7.5. Turbulence modeling

We incorporated a large-eddy simulation (LES) turbulence model to the SPH fluid models. It is a simple turbulent modeling based on a spatial filtering of the Navier-Stokes equations; it makes use of the mixing-length and turbulent viscosity concepts and is parametrized by the Smagorinsky constant.

Such SPH-LES fluid models have been used to simulate with satisfactory results in coastal and ocean engineering. However, recent research demonstrated that several extra terms appear in the SPH equations when adopting the Lagrangian viewpoint (as conventionally done with SPH) and properly applying a spatial filtering to the Navier-Stokes equations [Montanari, Sampath, Calhoun, Prescott, Smith, 2018] [Di Mascio, Antuono, Colagrossi, Marrone, 2017]. It appears that some of these extra terms significantly affect the simulation accuracy, which strongly advocates towards the need to rework our SPH-LES model to account for it.

## 7.6. Definition of validation experiment

### 7.6.1. Basic Geometry

The experimental facility is based on a **rectangular tank** mounted on linear bearing to allow forcing in the **horizontal direction by oscillating the entire tank.** It is expected that this configuration will allow for many oscillations, thus enabling the acquisition of repeat iterations to obtain statistics of phenomena of interest. This approach should prove more efficient in instrumenting and acquiring validation data than the traditional approach of running individual dam break runs (for example).

The rectangular shape was chosen because this geometry is simpler and easier to build. The tank will also be wide enough to allow for significant 3D flows, as encountered in real situations.

The choice of the forcing type (entire tank) instead of a more traditional wave paddle on one end was motivated by the following factors:

- Better excitation (more control) than wave paddle type.
- Can impart more energy to the fluid.
- Could be used for studying seismic effects (on spent fuel pool or liquid metal/salt pool reactor) in the future, presenting a better investment of DOE resources.

### 7.6.2. Principle of operation

Unlike a dam break experiment, waves can be generated continuously by oscillating the whole tank as described above. The continuous operation will allow recording many datasets in a single run in order to obtain good statistical convergence of the data. This is possible only if the flow has returned to a similar initial state between each event.

The design plans for a relatively long tank so that the 3D effects introduced by the obstacle are dissipated and the flow returns to 2D for the next event. Preliminary simulations will also play a key role in checking this aspect of the design.

## 7.7. Preliminary Design with NEUTRINO

### 7.7.1. Modeling tools

We aimed to use neutrino in assisting in the design of the facility (determining its optimal dimensions, type of motions, etc). Preliminary work focused on getting the software running and getting familiar with its functions. An example of dam break impacting a rigid body was computed following a tutorial:

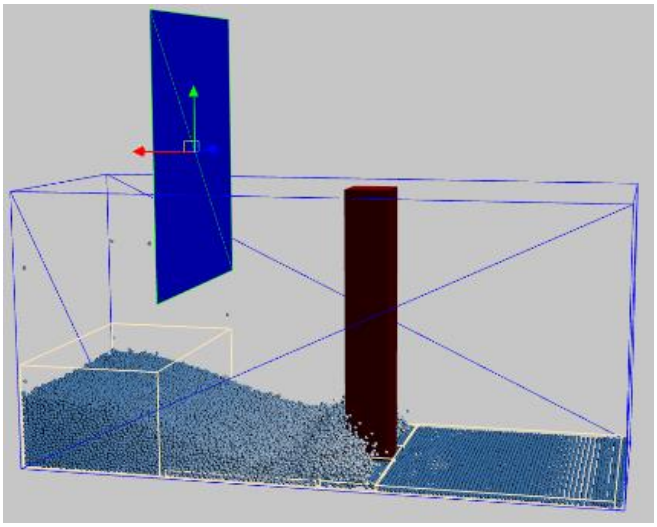

Figure 7.7. dam break impacting a rigid body configuration.

A rectangular tank was then modelled, and an external forcing was implemented. The waveform of the forcing is prescribed in Python programming language which allows a wide range of expression, including mathematical equation and conditional statements which can be varies as function of time during the simulation. For instance the expression:

*prop = vec3f(0,0,0.2*(math.cos(1.15*Scene.ElapsedTime)-1))*

oscillates the tank horizontally following a cosine function with an amplitude of 0.2 m and period of $2\pi/1.15=5.464$ s.

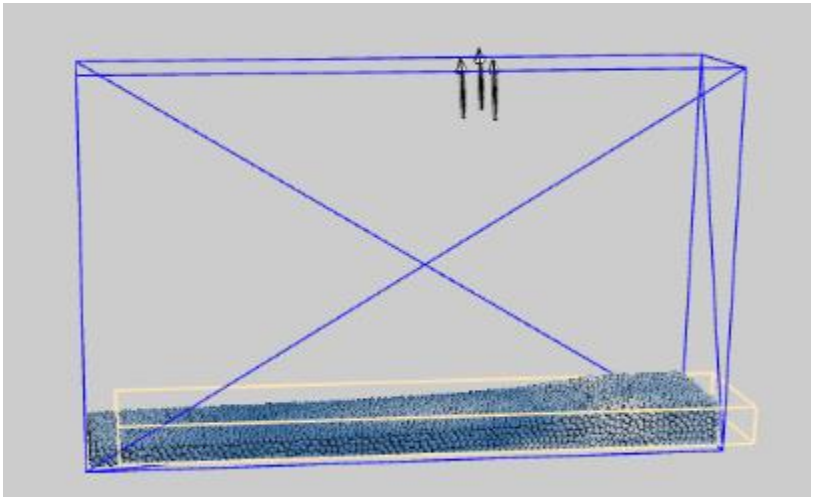

Figure 7.8. Tank oscillation schematic.

These first tests allowed checking that the wave phase velocity is in agreement with the theory for gravity waves in shallow water, given by the following dispersion equation: $\omega^2 = gk\,Tanh(kh)$.

The analytical solution for this type of flow is given below for the free surface profile (Ibrahim 2005):

$$\eta = \Omega^2 \frac{X_0}{g} \sin\Omega t \left\{ x - \sum_{n=0}^{\infty} \frac{(-1)^n 4L}{\pi^2(2n+1)^2} \frac{\Omega^2}{(\omega_n^2 - \Omega^2)} \sin\left((2n+1)\frac{\pi x}{L}\right) \right\}$$

and the dynamic pressure field (ignoring hydrostatic pressure):

$$p = \rho X_0 \Omega^2 \sin\Omega t \left\{ x + \sum_{n=0}^{\infty} \left[ \frac{(-1)^n \sin\left((2n+1)\frac{\pi x}{L}\right) \cosh\left((2n+1)\frac{\pi(z+h)}{L}\right)}{\pi^2(2n+1)^2 \cosh\left((2n+1)\frac{\pi h}{L}\right)} \times \frac{4L\Omega^2}{(\omega_n^2 - \Omega^2)} \right] \right\}$$

This theory is only for linear (i.e. low amplitude) waves. Such solutions were not used further because the present study focuses on large amplitude event, and because of the limited spatial resolution of SPH (limited by particle size). A better way to validated Neutrino results is with experiments of more advanced non-linear numerical simulations.

7.7.2. Comparison to experimental data

The resulting flow is visualized in Neutrino. Useful data such as velocity and pressure then have to be exported and processed with a different software such as Matlab. For an oscillating tank, an example of velocity field is shown below:

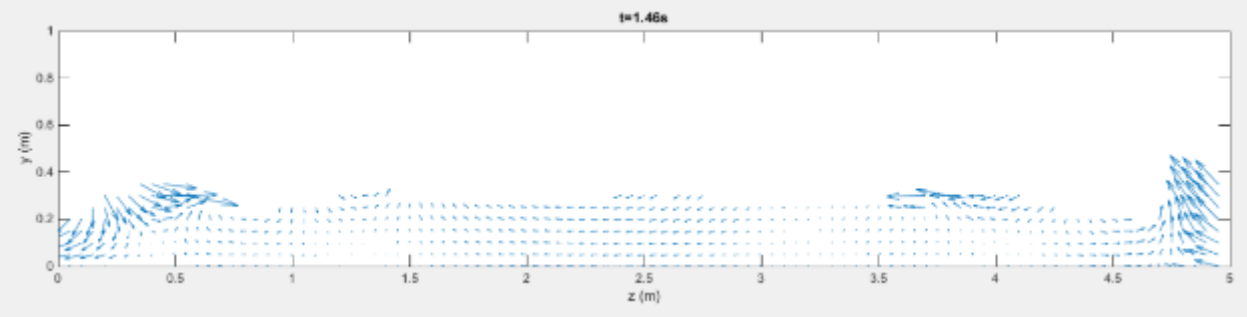


Figure 7.9. Oscillating tank velocity field

The experiment by Faltinsen et al. ("Multidimensional modal analysis of nonlinear sloshing in a rectangular tank with finite water depth." Journal of Fluid Mechanics 407 (2000): 201-234) was used as a benchmark for investigating large amplitude 2D free surface flows.

The below figure shows a very good agreement over the first 10 seconds of forcing. After that, the Neutrino solution departs from the experimental results in term of amplitude, which is likely due to viscous dissipation. The latter is sometimes increased in simulations (artificial viscosity) to help with stability. Identifying and improving this aspect is an example of how experiment can help improve simulation accuracy.

Nevertheless, these results are deemed satisfactory to use Neutrino for developing a preliminary design of the experimental facility.

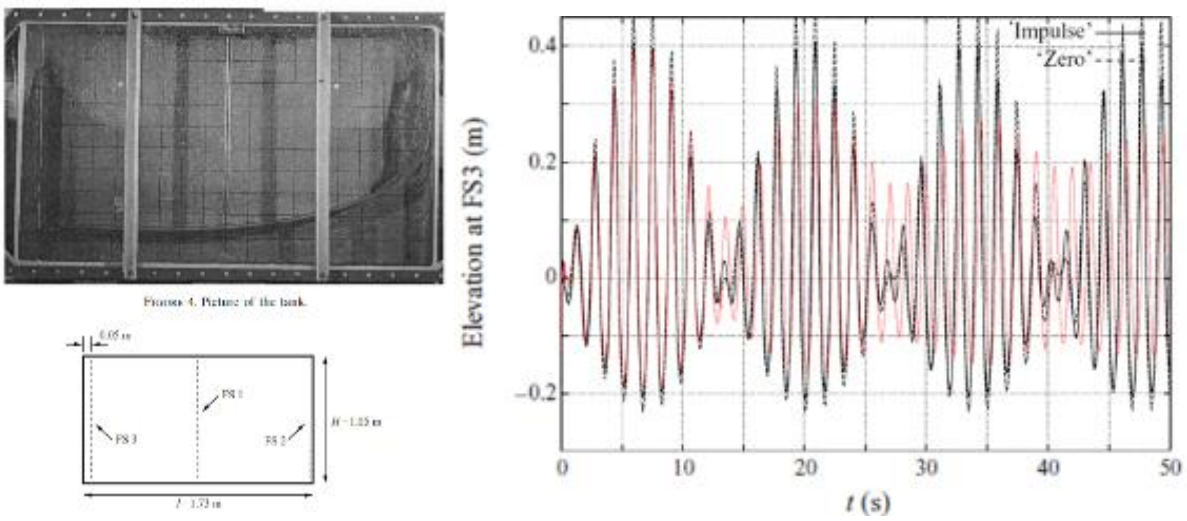


Figure 7.10. Left: Faltinsen's experimental test section and geometry. Right: Experimental data (black) vs. Neutrino data (red) for the free surface elevation at FS3 location.

## 7.8. Design of the Experiment

### 7.8.1. Neutrino simulation results

A wide range of tank size, water level, object (if any), forcing amplitude and frequency were modeled in Neutrino. The following table shows some of the forcing studied in term of period ($T$), and forcing amplitude ($X$). Of particular interest for the design is to estimate the resulting force required to move the tank.

| | $T$ (s) | Ramp (s) | $X$ (m) | $V$ (m/s) | $a$ (m/s$^2$) | Force (N) |
|---|---|---|---|---|---|---|
| Design1 | 4 | 1 | 0.06 | 0.094 | 0.30 | 1,777 |
| Design2 | 8 | 1 | 0.06 | 0.094 | 0.30 | 1,777 |
| Design3 | 2 | 1 | 0.06 | 0.094 | 0.30 | 1,777 |
| Design4 | 1 | 1 | 0.06 | 0.094 | 0.30 | 1,777 |
| Design5 | 1 | 1 | 0.1 | 0.157 | 0.49 | 2,961 |
| Design6 | 6 | 1 | 0.1 | 0.157 | 0.49 | 2,961 |
| Design6_1 | 5 | 1 | 0.1 | 0.157 | 0.49 | 2,961 |
| Design6_2 | 5 | 1 | 0.1 | 0.157 | 0.49 | 2,961 |
| Design6_3 | 4.5 | 1 | 0.1 | 0.157 | 0.49 | 2,961 |
| Design6_4 | 4.5 | 1 | 0.1 | 0.157 | 0.49 | 2,961 |
| Design6_5 | 4.8 | 1 | 0.1 | 0.157 | 0.49 | 2,961 |
| Design6_6 | 4.8 | 1 | 0.1 | 0.157 | 0.49 | 2,961 |
| Design6_7 | 4.7 | 0.5 | 0.1 | 0.314 | 1.97 | 20,844 |
| Design6_7b | 4.7 | 0.5 | 0.1 | 0.314 | 1.97 | 18,844 |
| Design6_7c | 4.7 | 0.5 | 0.1 | 0.314 | 1.97 | 20,844 |
| Design6_8 | 4.7 | 0.3 | 0.1 | 0.524 | 5.48 | 44,899 |
| Design7_1 | 4.7 | 0.3 | 0.1 | 0.524 | 5.48 | 32,899 |
| Design9_3 | 4 | 0.6 | 0.2 | 0.524 | 2.74 | 16,449 |
| Design9_4b | 5 | 0.6 | 0.2 | 0.524 | 2.74 | 22,449 |

Below are shown a few examples of tests, with an object representing a structure to study at various locations. The initial tests are coarse and preliminary to keep the processing time short and allow many cases to be studied in a reasonable amount of time. As the results are analyzed, the model is refined and becomes more complex.

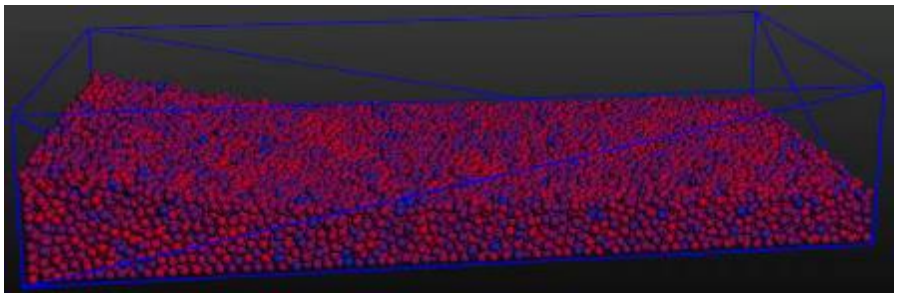

Design 6_1

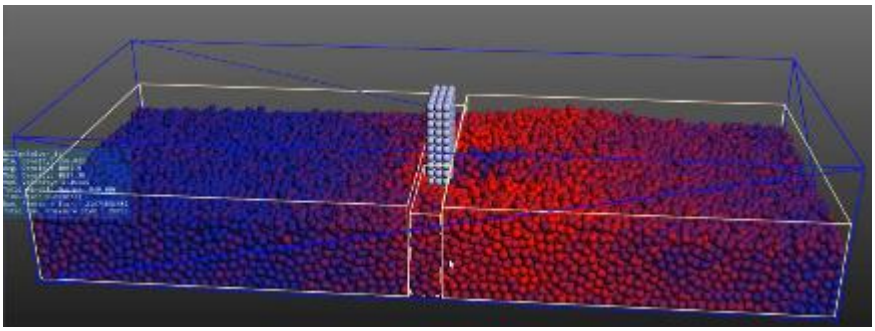

Design 6_7

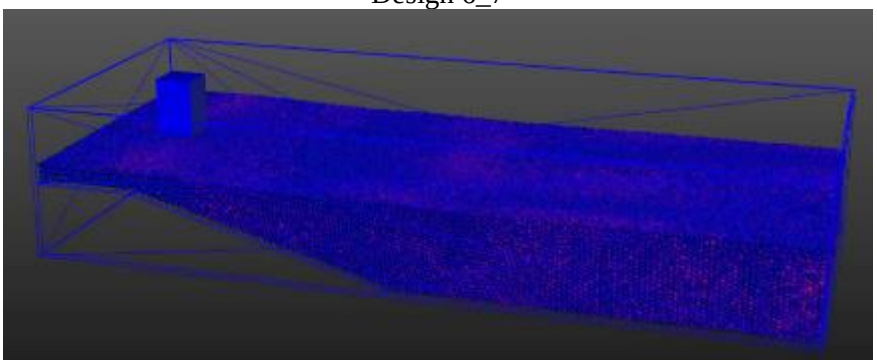

Design 9_4

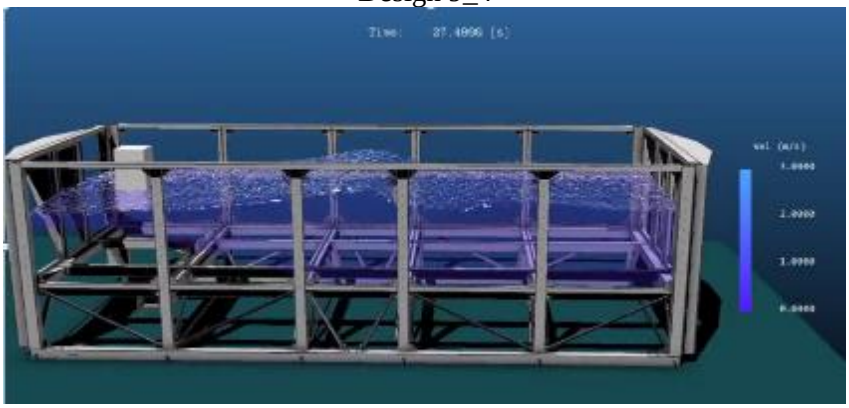

Figure 7.11. Design 9_4b (with tank CAD model shown and surface rendering).

For this last case, the impact for on the object (the grey cuboid on the left) was reported for 15 cycles, and is plotted below:

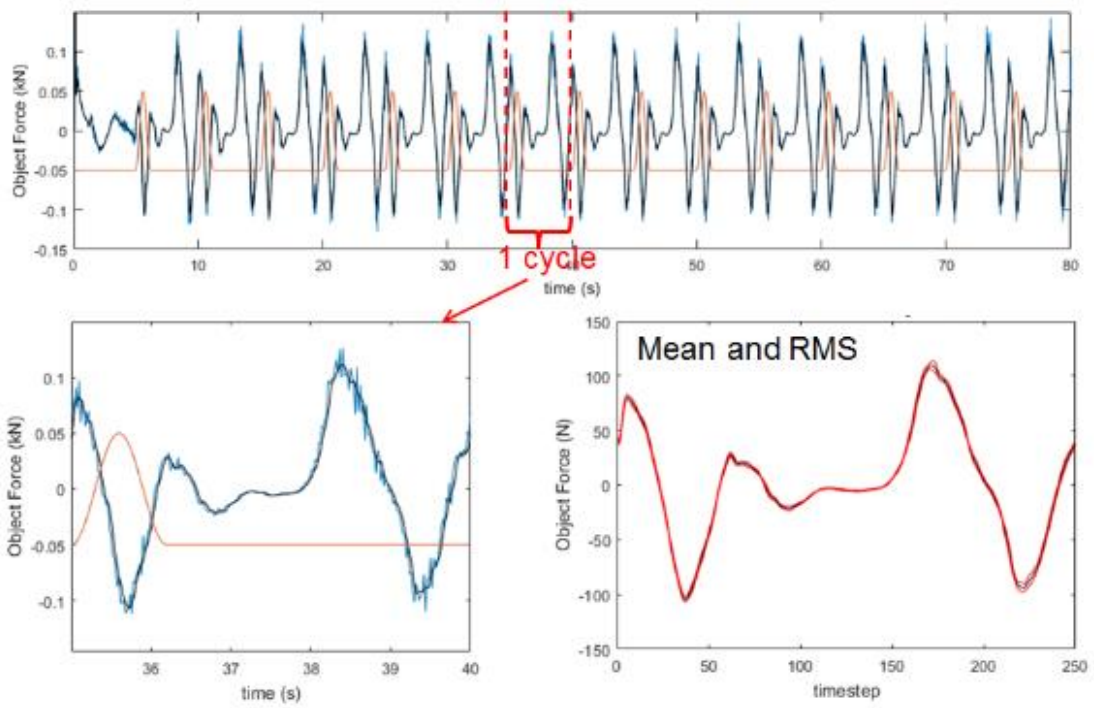


Figure 7.12. Top: Force of the structure (raw/blue smoothed/black) and forcing motion (orange). Left: Zoom-in one cycle. Right: Phase averaged mean and RMS.

The reported force on the object is very repeatable from cycle to cycle, which is a necessary condition to gather good statistical data from both experiment and simulation. When validating the simulation with the experiment, it will be invaluable to have access to not one, but hundreds of events to assess the uncertainties due to random error. For the above results, the deviation from the calculated mean force is shown as a histogram plot:

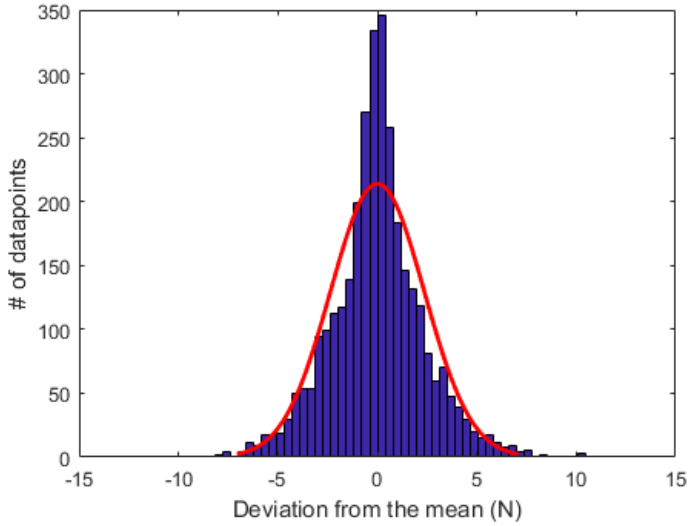


Figure 7.13. PDF of the deviation to the mean. Red curve is Gaussian (normal) distribution.

When the experiment is running, similar data will be collected. The correlation between PDFs will inform on the agreement between experiment and simulation and will determine to which degree the numerical model is validated.

The various simulations pointed to a successful tank geometry of 20 feet long by 8 feet wide by 4 feet high. This design is shown in the previous figure of design_9_4b. This choice of size was driven by the following factors:

- Maximize the size to match as well as possible the scale of real-world events.
- Size limited by the area of the available strong floor in Tompkins Hall at GWU.
- Cost of the actuator limited the maximum force that can be imparted to the tank.

It is planned to have the nominal water depth at 2 feet, which represents a volume of about 10 $m^3$.

Various types of forcing were also studied: pure sine wave, rectangular function, sine wave with off-times, etc. The behavior of the flow was studied, as well as the required acceleration and speed. For instance, a perfectly rectangular function would require unrealistic infinite acceleration.

Using Fourier analysis, the frequency components of each type of forcing were analyzed to make sure the actuator could deliver such forcing. See below an example for the following forcing amplitude function:

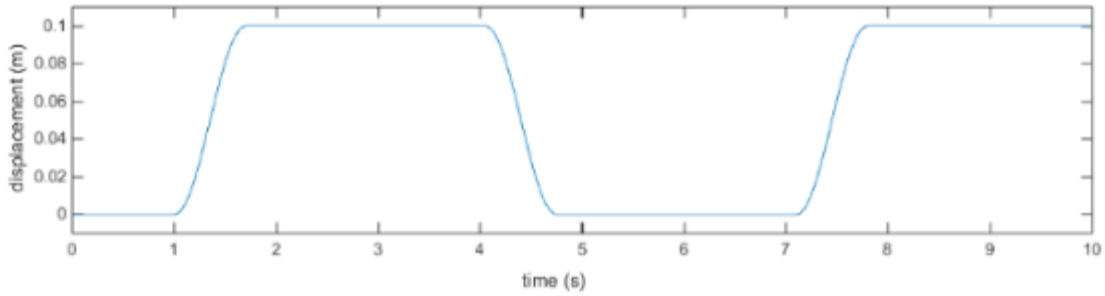


Figure 7.14. example of forcing amplitude function.

Here is the spectral analysis showing the corresponding acceleration for each frequency component.

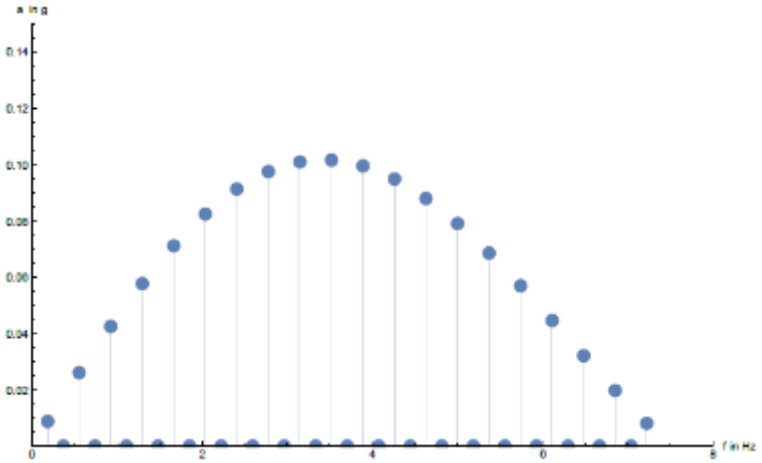

Figure 7.15. Acceleration for each frequency component.

In this case, the max frequency is below 8 Hz and the corresponding acceleration is quite low (<0.01 $m/s^2$).

7.8.2.Components Selection

The experiment is composed of several main components:

- Hydraulic actuator and supporting hardware (i.e., pump, controller)
- Tank
- Reaction frame supporting the tank and the actuator.

A few companies selling hydraulic test actuators offer turn-key systems for 1D forcing including hydraulic system and reaction frame. The tank would have to be added on top of these systems. The following table summarizes two such systems that we considered:

| **Manufacturer** | **Size** | **Forcing capacity** | **Price** |
|---|---|---|---|
| MTS | 5' x 5' | 16", 11 kips, 4,000 lbs payload | $450k |
| ETS solution | 4' x 4' | 3.5", 4.4 kips, 660 lbs payload | $140k |

In fact, we had proposed to buy a turn-key system from ETS solution for the proposal. However, once the funds were awarded and we started sizing the system, the sale representative from ETS solution realized that they had made a mistake in the initial quote of $100k and they could not honor it. This forced back to the drawing board. By leveraging several legacy pieces of equipment left in a new laboratory space that we were given to us (controller MTS hydraulic actuator, load cell, worth more than $70k at current list price), we realized that we could do a much more capable system for a fraction of the price than any turn-key system.

These systems do not match the final size (20' x 8') or forcing capacity (10,000 lbs.) of the system we designed. The pricing is also prohibitive considering the tank is not included.

It was therefore chosen to build a custom system. Furthermore, the new laboratory has a strong floor and, the tank and the actuator can be directly mounted on the floor, which remove the need for a reaction table. The tank would then simply sit of linear rails mounted to the floor.

***Hydraulics***

The hydraulic system is the most expensive and arguably the most important component of the experiment. We worked with MTS Corporation since we already have a MTS controller and load cell. We selected 22 kips (22,000 lbs.), 10" amplitude actuator with a 30 GPM 3000 psi hydraulic pump. We also added an accumulator to take advantage of the forcing off-time for increasing actuator velocity during on-time.

Figure 7.16. MTS 22 kips actuator

The actuator was delivered in January 2018.

***Rails***

Rails and linear bearing carriages have been selected based on the required loads and speed and ordered from Schneeberger. They arrived in February 2018. Structural I-beams will be used to connect these rails to the strong floor.

Figure 7.17. Linear bearing carriage on rails.

***Tank***

The tank will be built of carbon steel and acrylic. The steel will form a frame to support the structural load on the water and forcing, and the acrylic will allow optical access to all sides of the experiment. The previous figure of design9_4b showed the steel frame with the acrylic side and bottom wall panels. The tank sits 0.6 m above the linear bearings. While this complicates the structural design, it enables the deployment of optical systems (lasers, cameras, etc) below the tank. Thus, the facility was designed to be modular and allow the deployment of a broad class of diagnostics.

The steel frame and acrylic panels were designed and dimensioned using a combination of analytical and FEM analysis with the software ProE, as described in the next section.

7.8.3. Structural Design

The frame is subjected to the following loads:

- Gravity
- Water weight on the bottom walls
- Water hydrostatic load on the side walls
- Horizontal acceleration of 5 $m/s^2$ (max from the design table)
- Water load (estimated with Neutrino) on the end wall

Using an iterative approach, the tank frame design was refined to minimize deflection, while making sure the maximum stress (Van Misses) remains well below the elastic limit of carbon steel (250 MPa). Below are a few examples of iterations. Maximum stress is typically located where the carriages are attached, while maximum deflection can be found in the center of the tank floor, and top of side and end walls:

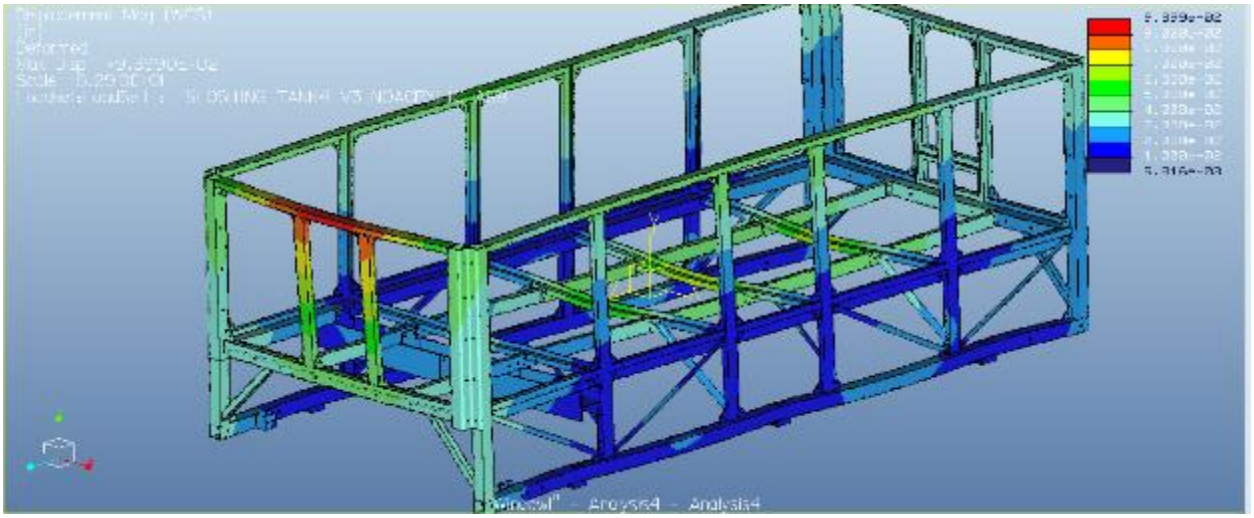

Figure 7.18. Version 4. Displacement map (amplitude of displacement is magnified for visualization purpose). Max displacement is on the order of 2.5 mm

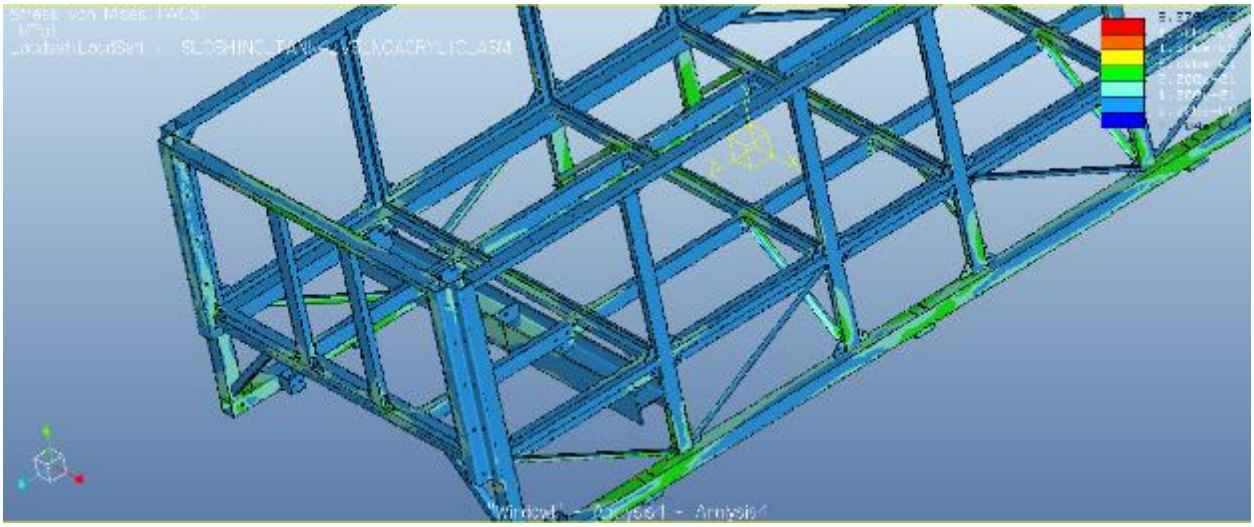

Figure 7.19. Version 4. Stress map. Max stress is below 50 MPa (limit is 250 MPa)

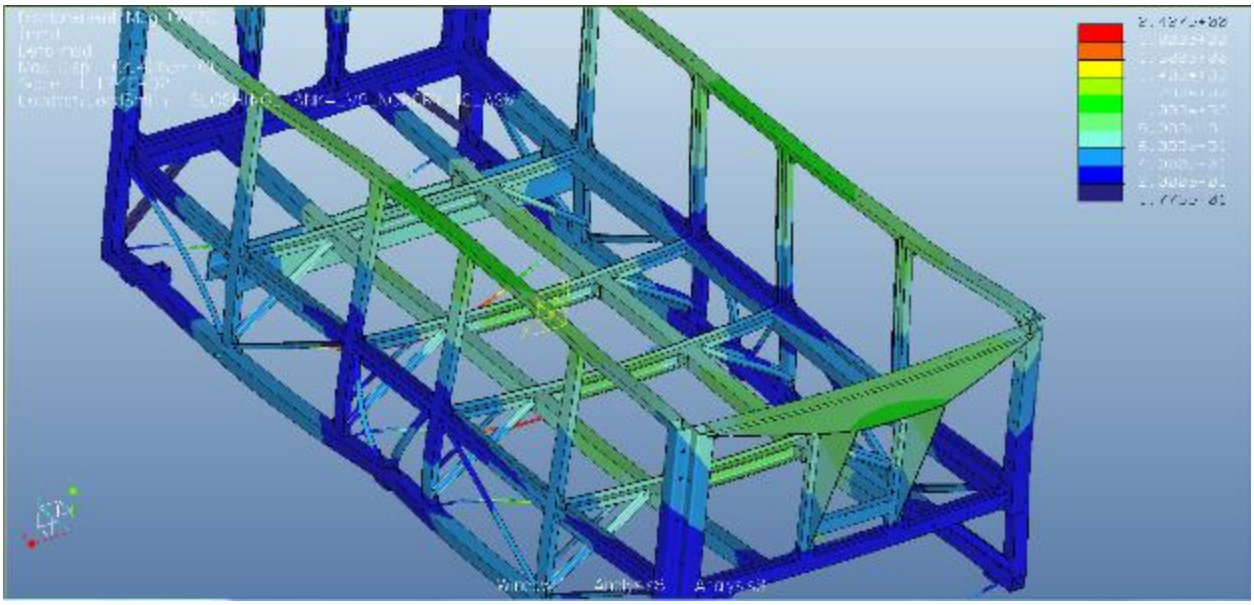

Figure 7.20. Version 8. Displacement map. Max displacement on the order of 1.2 mm. Structural elements have been added to stiffen the end wall assembly without adding too much weight.

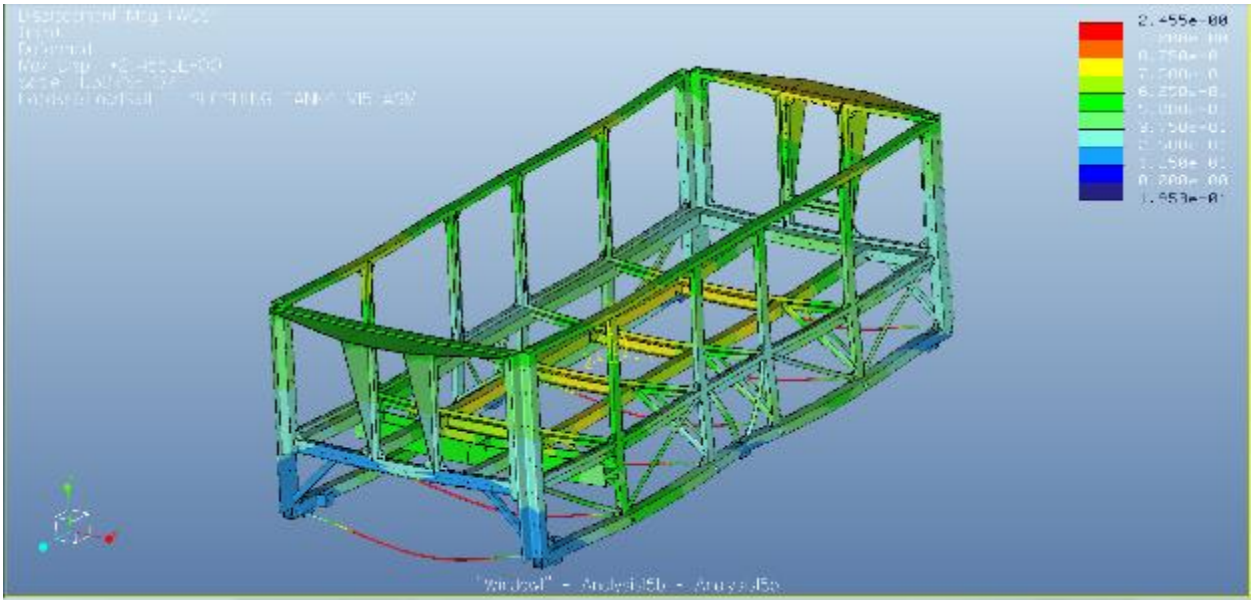

Figure 7.21. Version 15b (final). Displacement map. Max displacement is on the order of 0.85 mm (neglecting the rods at the bottom that are made to release load on the linear bearings.

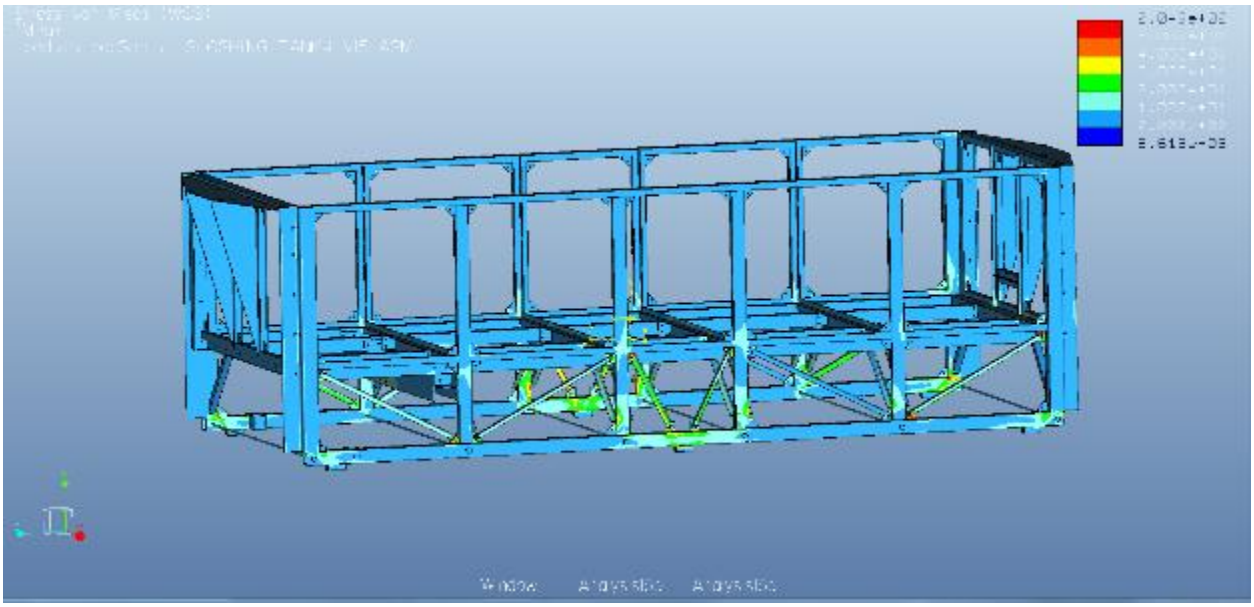

Figure 7.22. Version 15b (final). Stress map. Max stress on the order of 50 MPa. Localized higher stress is a result of mesh size and singularities at sharp edges.

The acrylic walls will be 1” thick on the side panels, and 1.5” thick at the bottom. Metal threaded inserts on the acrylic (on a 6” x 6” pattern) will allow mounting on structures and other objects in the tank.

### 7.8.4. Integration and sample tests

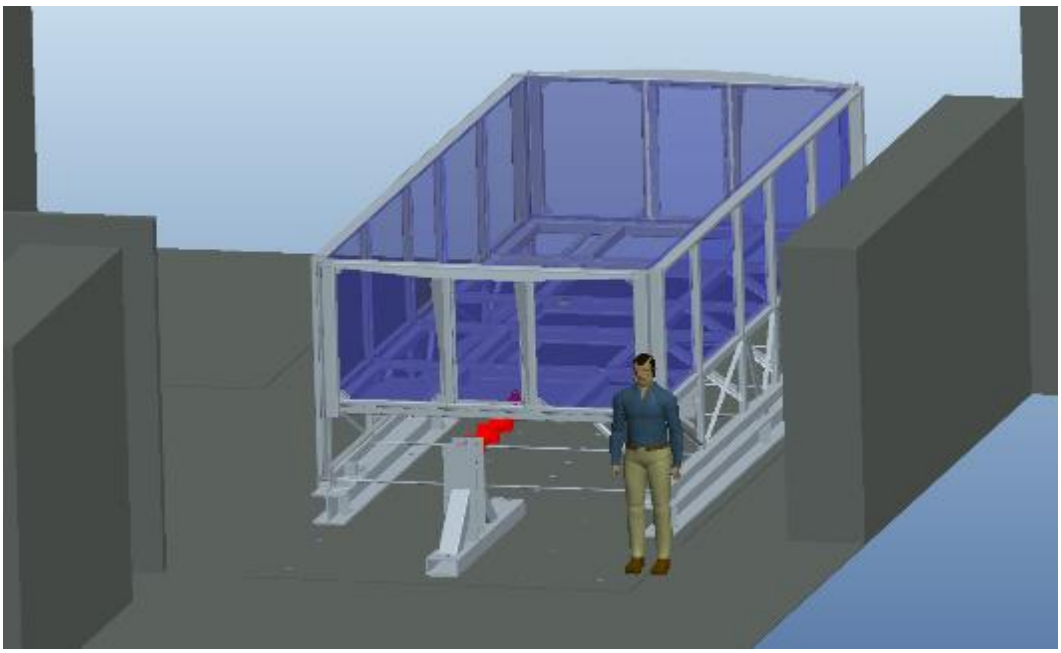

Figure 7.23. Tank installed on rails connected to the strong floor with I-beams. Actuator (red) is also connected to the strong floor and to the tank. The overall tank is 8’ high. Manikin shown for scale

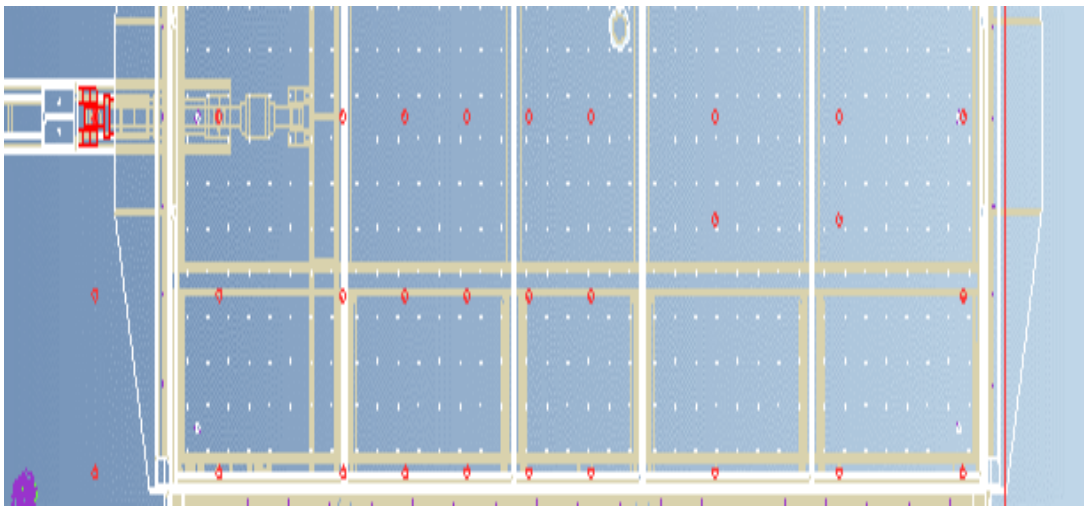

Figure 7.24. Top view of the experiment. Red lines show the strong floor area.

Drawings were generated for acrylic and metal frame components and sent for fabrication in January 2018. The list of drawings was 93 pages long for the frame and 18 pages long for the acrylic panels. We approached several companies and ended selecting a supplier we have worked successfully with in the past and which was the most competitive.

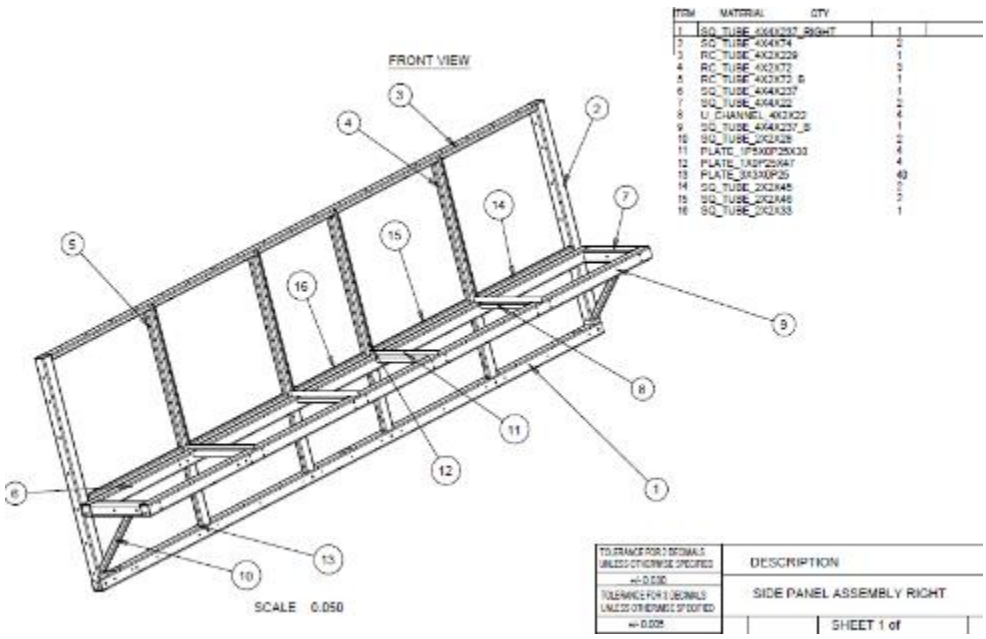


Figure 7.25. Tank side panel welding instructions.

## 7.9. Assembly of the facility

### 7.9.1. Tank Frame

The tank frame is composed of 13 main components, weighting up to 1,700 lbs. and up to 20 ft long. A team of riggers were hired to bring these parts into the basement of the Engineering building and assemble the facility in April 2018.


Figure 7.26. Test facility assemble.


Figure 7.27. Test facility assemble.

The tank frame was carefully aligned to be level (with 1.2 mm) and positioned on the linear rails supported by I-beams mounted to the strong floor.

Precise alignment of all 6 carriages ensured that the tank could move with minimum friction. In fact, a single person could move the whole tank (4,000 lbs.) by hand.

7.9.2.Hydraulics

The hydraulic actuator was then fitted to the experiment. MTS performed on-site calibration and commissioned the hydraulic system. Some troubleshooting took place to avoid cavitation in the oil line, limit oil compressibility oscillations, and maximize the flow rate. Shakedown tests of the hydraulic system and tank frame were performed to verify the performances were as expected. This was completed in late May 2018, with the final problem (cavitation in the hydraulic return line) resolved by October 2018. Cavitation was limiting only the largest forcing and would start acquiring data for smaller forcing.

Figure 7.28. Actuator connected to the tank and strong floor support.

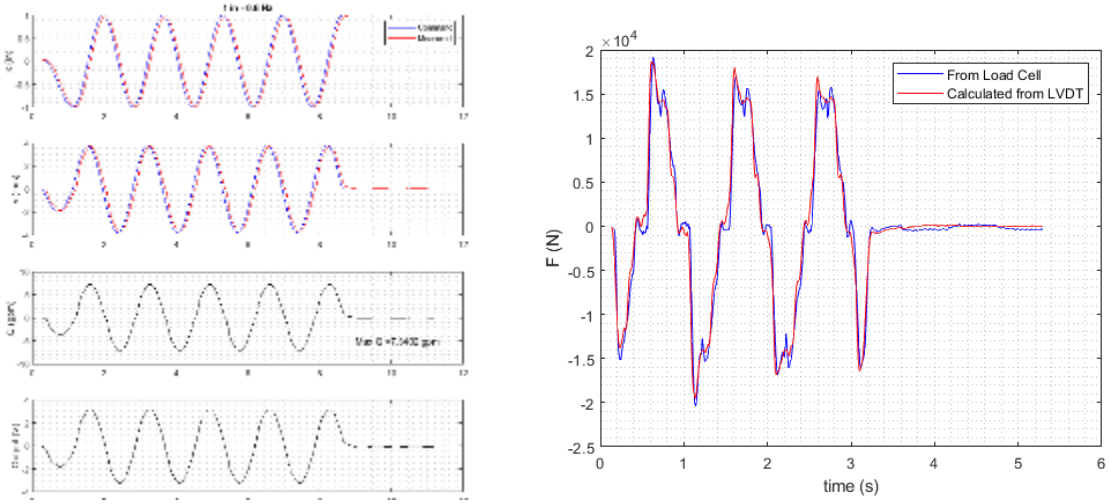


Figure 7.29. Examples of shakedown test results

### 7.9.3. Acrylic Panels

Once the tank framed moved correctly and the actuator performed well, the acrylic panels were installed. A special adhesive (Sikaflex 295UV, typically used for marine application) was used to bond the acrylic to the steel. Such adhesive also ensures water tightness and form a seal thick enough (1.2 cm) to allow some small relative motion between tank and panel (to accommodate for differential thermal expansion for example).

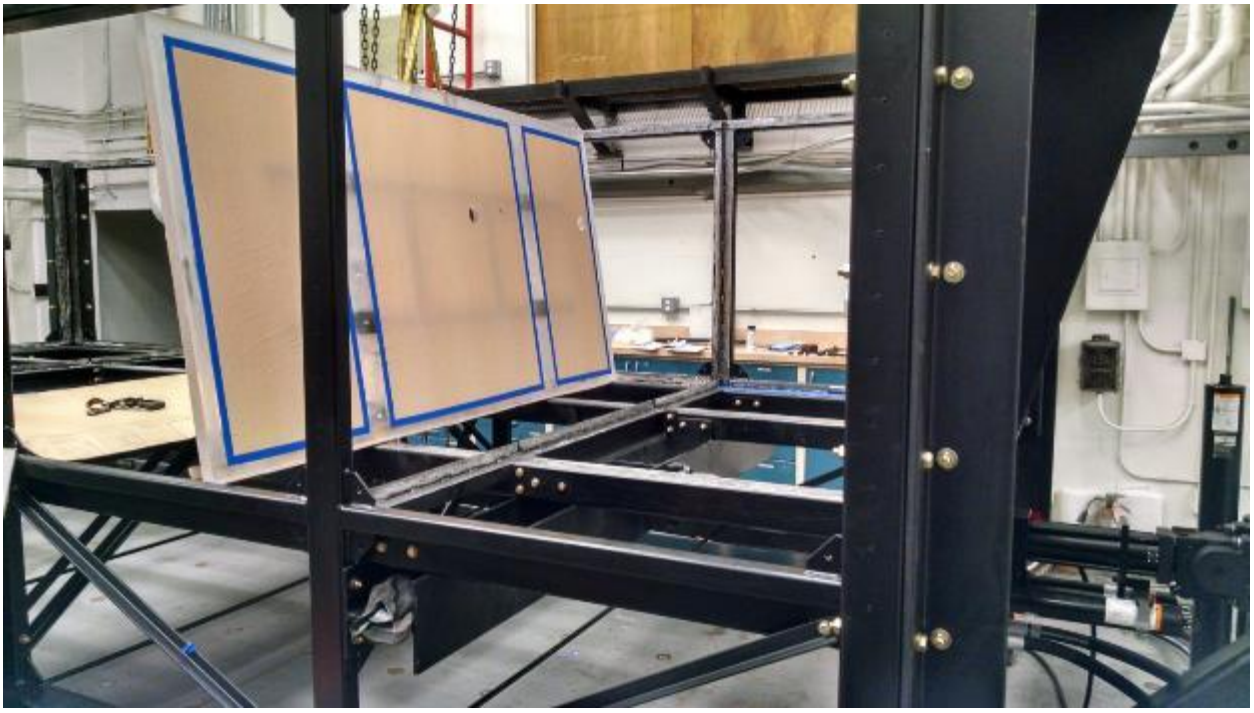

Figure 7.30. Bottom acrylic panel being prepared for installation. Drainage holes are visible.

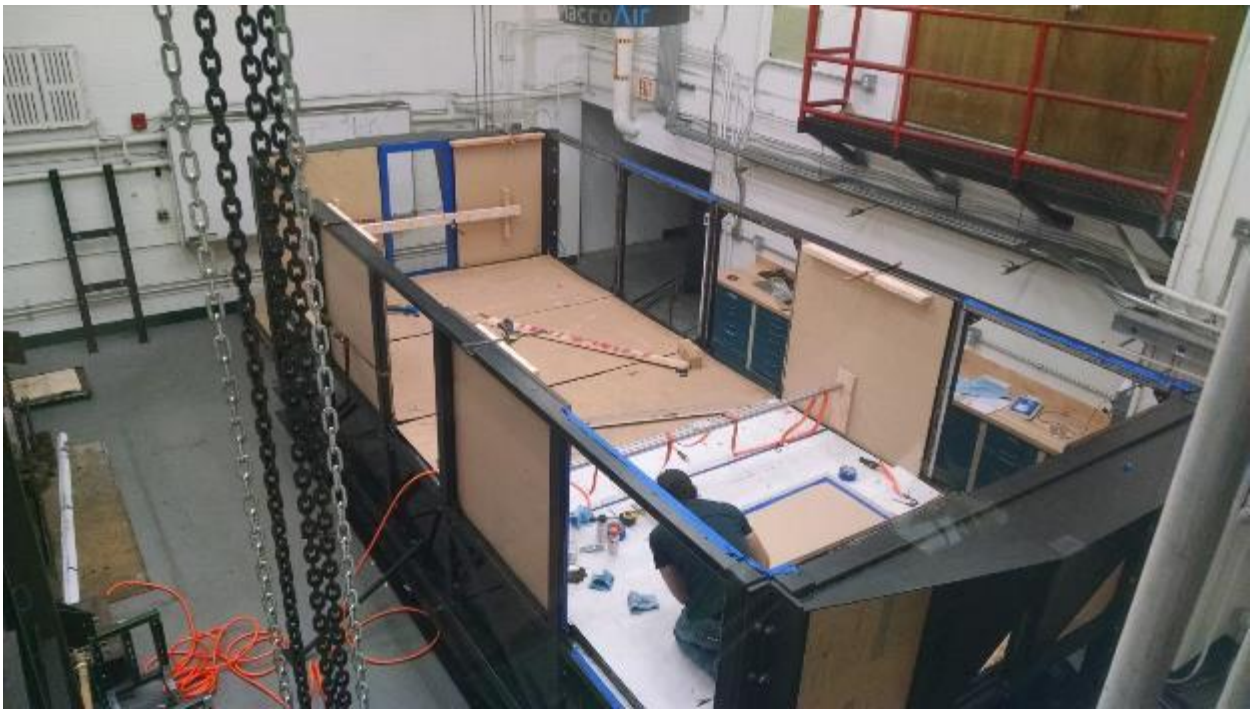

Figure 7.31. Installation of the side wall panels.

The acrylic installation took place during June 2018. The adhesive then required one month of curing time before water could be added in the tank mid-August 2018. A very small leak was identified and patched. The tank has been leak-free since.

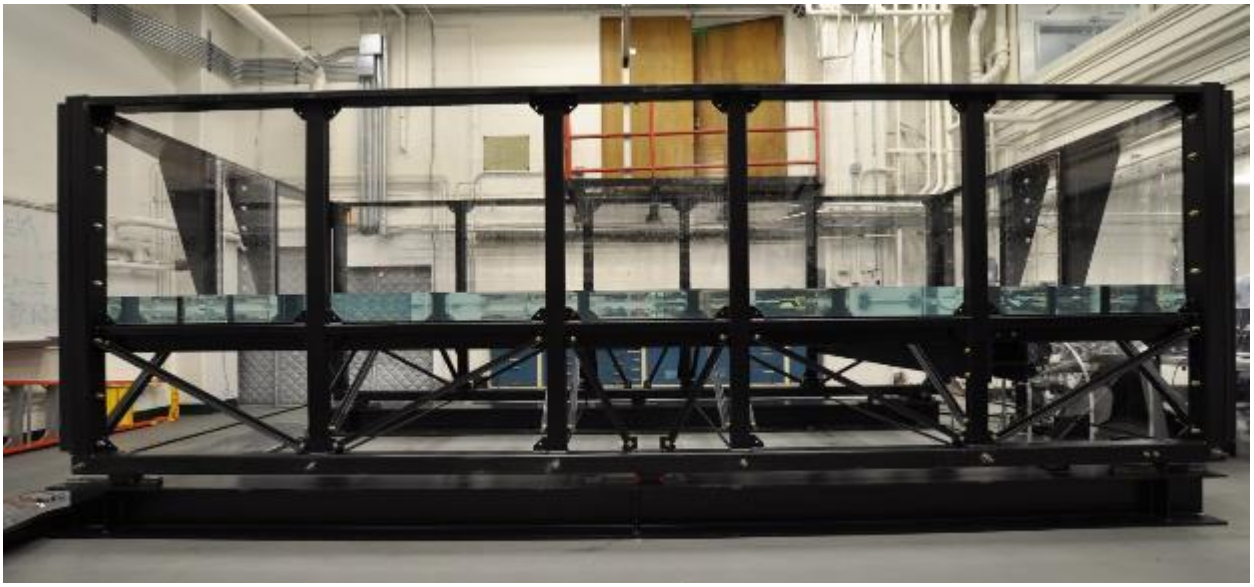

Figure 7.32. Operational tank with 6” of water (design allows for up to 24” depth)

## 7.10. Instrumentation

### 7.10.1. Tank Motion

The computer generates a waveform that is executed by the actuator which is rigidly connected to the tank. The displacement control is a closed loop based on LVDT feedback (and force stabilization to damp oscillations due to oil compressibility). The LVDT voltage signal is sampled at 2,048 Hz with a 16-bit LabView DAQ. The accuracy in the tank motion is assessed by comparing a perfect input function (pure sine wave) to the actual measurement obtained through the LVDT sensor. Any difference between the two can be attributed to the control system or to the LVDT. The calibration report of the LVDT indicates accuracy better than 0.52 mm (0.41 % of full range). The 16 bit -10V/+10V DAQ results in a 0.3 mV digitalization, which translates into a resolution of 0.004 mm, which is negligible.

The position accuracy is evaluated using 183 cycles of a 4” (101.6 mm) 0.11 Hz sine wave. The difference between requested and measured displacements over the entire sequence is as follow:

- **0.814 mm peak deviation** (0.8 % of amplitude)
- **0.384 mm RMS deviation** (0.38% of amplitude)

These results are also consistent with the LVDT accuracy.

The accuracy on the forcing frequency is evaluated by comparing the time of position zero-crossing versus pure sine wave for the same sequence.

The difference between requested and measured timing over the entire sequence is as follow:

- **ms peak deviation** (0.01 % of period)
- **0.72 ms RMS deviation** (0.008% of period)

These values are consistent with the sampling frequency.

### 7.10.2. Surface Elevation

***Initial profile (water at rest)***

The water in the tank is allowed to come to a rest before each run. The level of disturbances is characterized using the RMS of the surface slope. The latter is measured by reflecting a laser beam on the surface of the water near the center of the tank. A camera records the reflected beam imaged on a screen. The camera resolution is 0.4 mm/pixel, and a subpixel ($1/50^{th}$) accuracy fit yields a precision of $2\times10^{-4}$ degrees on the surface slope.

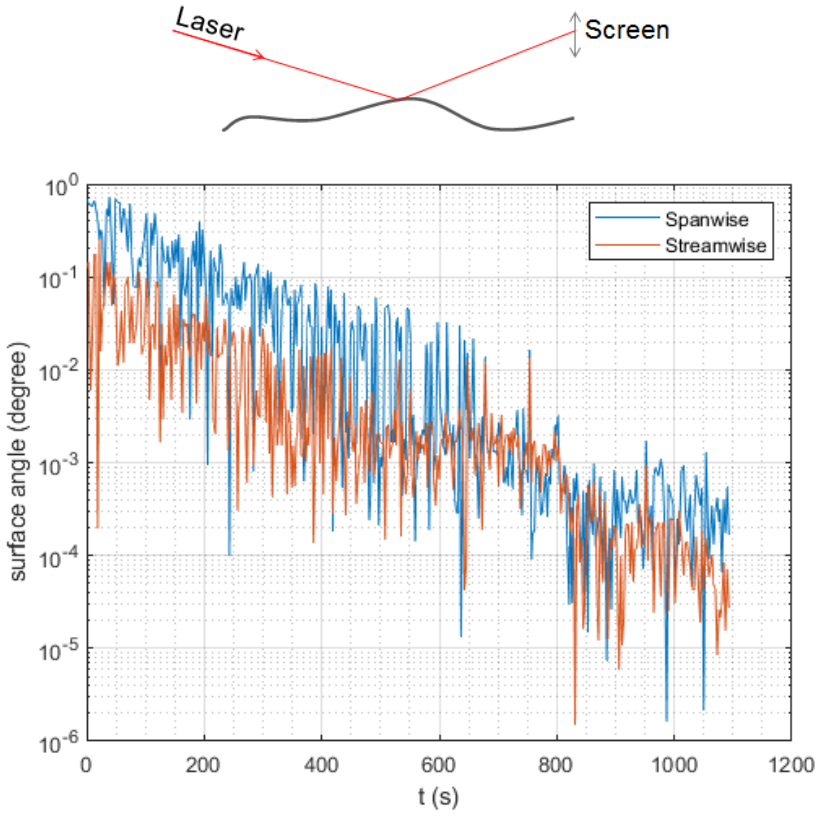


Figure 7.33. Surface slope as function of time: Natural decay of surface disturbances.

The slope of the disturbances decays exponentially, by a factor of 10 every ~200 seconds. The total time to reach a particular level of disturbance depends on the initial level of disturbance (1 degree in the above example due to FOV limitations). After 1000 s, the equivalent amplitude of the surface waves is below 10 μm.

***2D Profiles***

This is recorded with a single camera pointing at the long side of the tank, fitted with a wide angle lens that allows the entire tank length to fit in the frame. As a result of the large FOV, the spatial resolution is limited to ~5 mm/pixel. The surface profile is extracted with an image processing code that locates the location of the surface based on the intensity gradient. No subpixel analysis is performed, thanks to temporal over-sampling, temporal averaging allows improving the accuracy by a factor of $\sqrt{N}$, with $N$ the number of samples over which the averaging is conducted in a boxcar manner. The final accuracy is estimated at 2 mm. This is sufficient for a coarse characterization of the evolution of the surface profile at a full tank length scale.

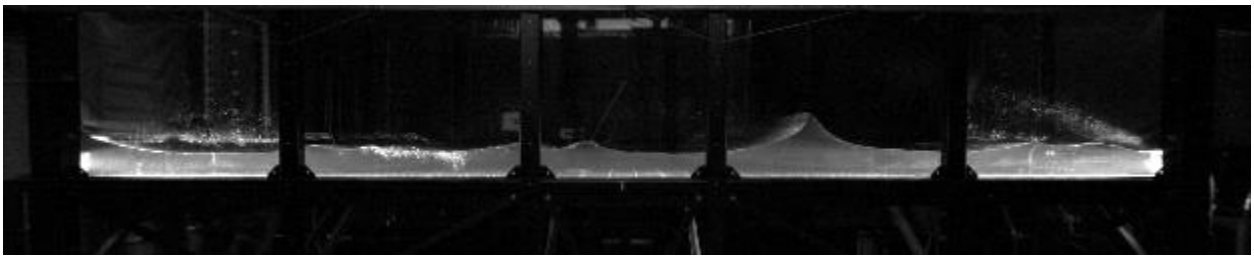

Figure 7.34. Raw image used for surface profile identification at large scale

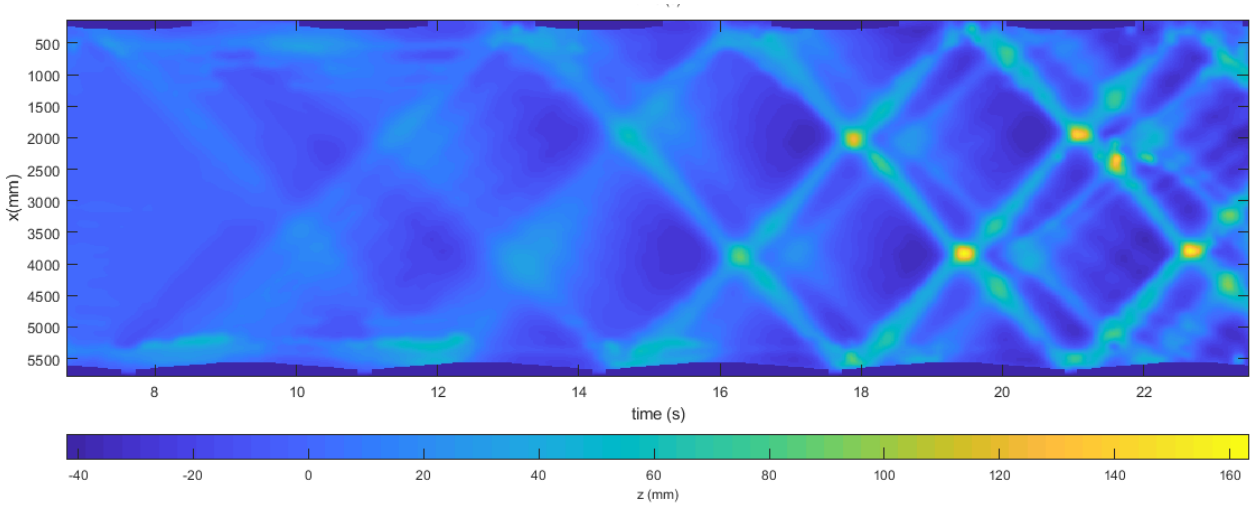


Figure 7.35. Example of 2D surface elevation map as function of time

### 7.10.3. Pressure

The pressure at the end wall of the tank is measured at several elevations using the following pressure transducers:

Omega PXM309-0.14G10V (140 mBar gauge range) and Omega PXM309-0.35G10V (350 mBar gauge range). The linearity/hysteresis/repeatability (called accuracy in Omega datasheet) is 0.25% of full scale (35 Pa and 70 Pa, respectively).

In the experiments, the reading will depend on the ambient atmospheric pressure. By setting the pressure to zero in absence of water at the beginning of a run, we can take advantage of the very good linearity/hysteresis/repeatability for our measurements.

The 16 bit -10V/+10V DAQ results in a 0.3 mV digitalization, which translates into a resolution of 0.43 Pa and 1.07 Pa, for the respective transducers, which is negligible compared to the sensor accuracy.

When recording a static signal, the noise level is on the order of 5 Pa RMS and 10 Pa RMS for the respective transducers, which is below the static accuracy stated.

As mentioned earlier, we focus our study on the gauge pressure (relative to ambient). The precision of the measurement with respect to ambient pressure is much better and is estimated at 35 Pa for the 140 mBar sensor and 70 Pa for the 350 mBar sensor. Pressure is sampled by the DAQ at 2,048 Hz, which is twice the cut-off frequency (time response) of the sensor.

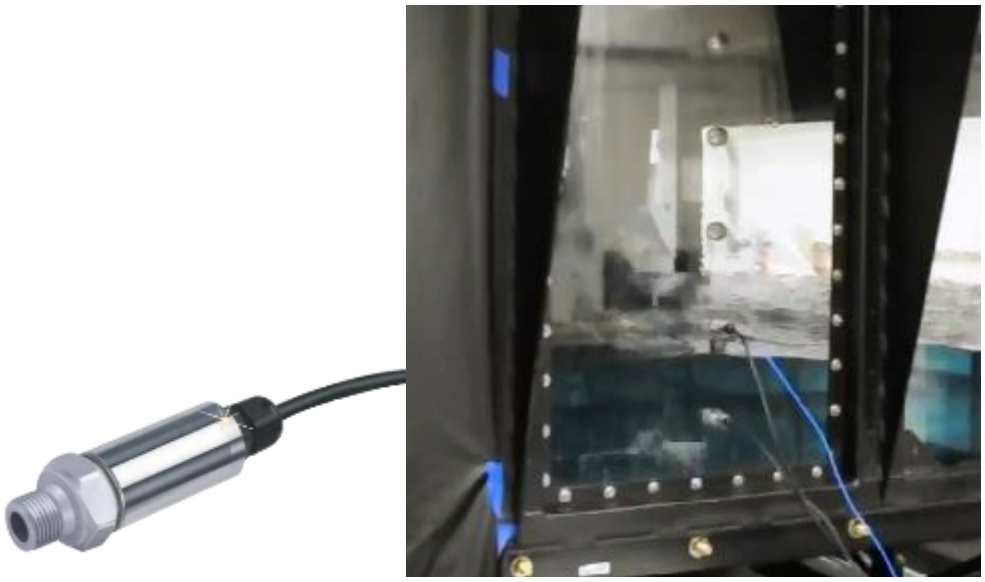

Figure 7.36. Left: Pressure transducer. Right: Mounting locations on the tank endwall.

## 7.11. Results

### 7.11.1. Tank modes

A repeatable flow can be obtained by exciting waves with a frequency that matches the natural frequency of water wave in the tank. The phase velocity of a water wave in shallow water defined as follow:

$$c = \sqrt{\frac{g\lambda}{2\pi}\tanh\left(\frac{2\pi h}{\lambda}\right)}$$

with $\lambda$ the wavelength and $h$ the water depth.

For a successful amplification, the wavelength is constrained by the tank length: The crest of a wave must be at one end of the tank, while the trough of a wave must be at the other end (because on one side the tank moves towards the flow, while it moves away at the end side). Therefore, the following relation between wavelength and tank length must be satisfied:

$$L = \lambda n + \frac{\lambda}{2} = \lambda\left(n + \frac{1}{2}\right)$$

With $n$ a positive integer that specifies the mode. At any time, there are $2n + 1$ waves traveling in the tank. To be able to amplify a wave (until breaking for instance), the tank must move towards the wave every time a crest impacts the end wall. Therefore, the forcing frequency must match the time it takes for a wave to travel back and forth along the tank, multiplied by the number of waves:

$$f = \frac{c}{2L}(2n + 1)$$

Combining these equations, the tank frequency becomes

$$f = \sqrt{\frac{(2n+1)g}{4\pi L}\tanh\left(\frac{(2n+1)\pi h}{L}\right)}$$

The following figure shows *f* as function of *h* for the first 6 modes:

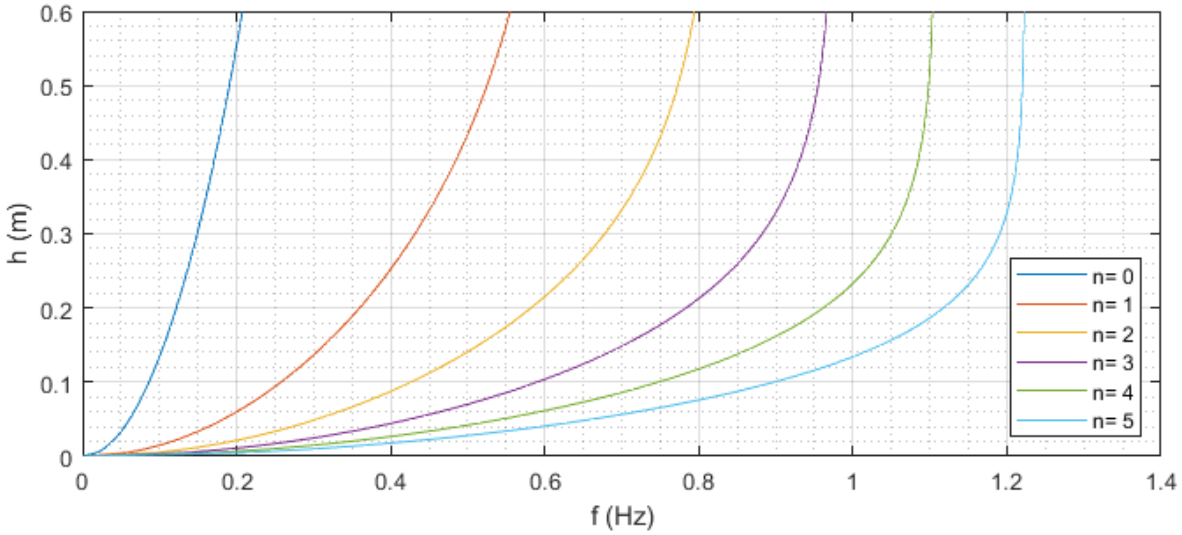


Figure 7.37. Frequency function of height.

Due to the tank motion, the effective tank length is slightly smaller than the physical length. Because the tank moves towards the waves as the crests approaches, the effective length is:

$$L_{eff} = L - 2A$$

with *A* is the forcing amplitude.

Example of mode 1 (n=0):

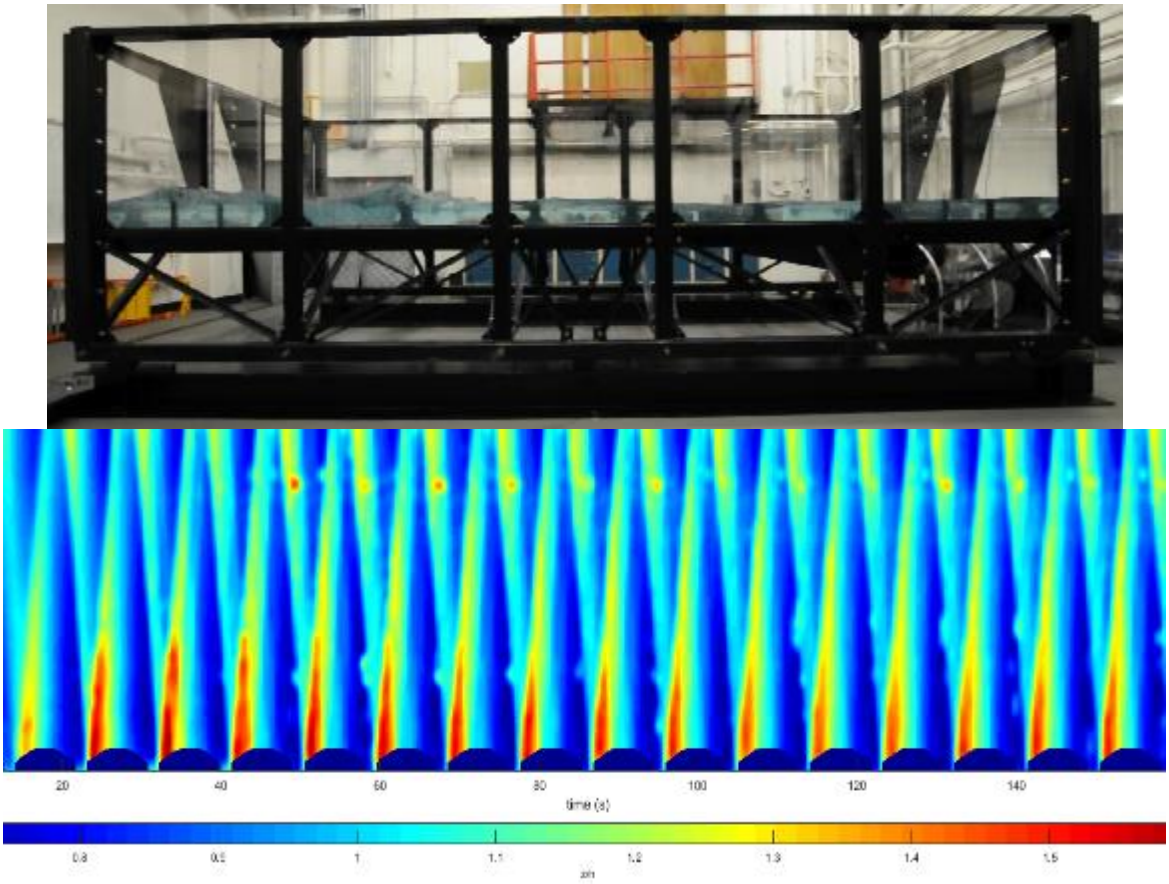


Figure 7.38. Measured 2D profile evolution (mode 1).

Example of mode 2 (n=1):

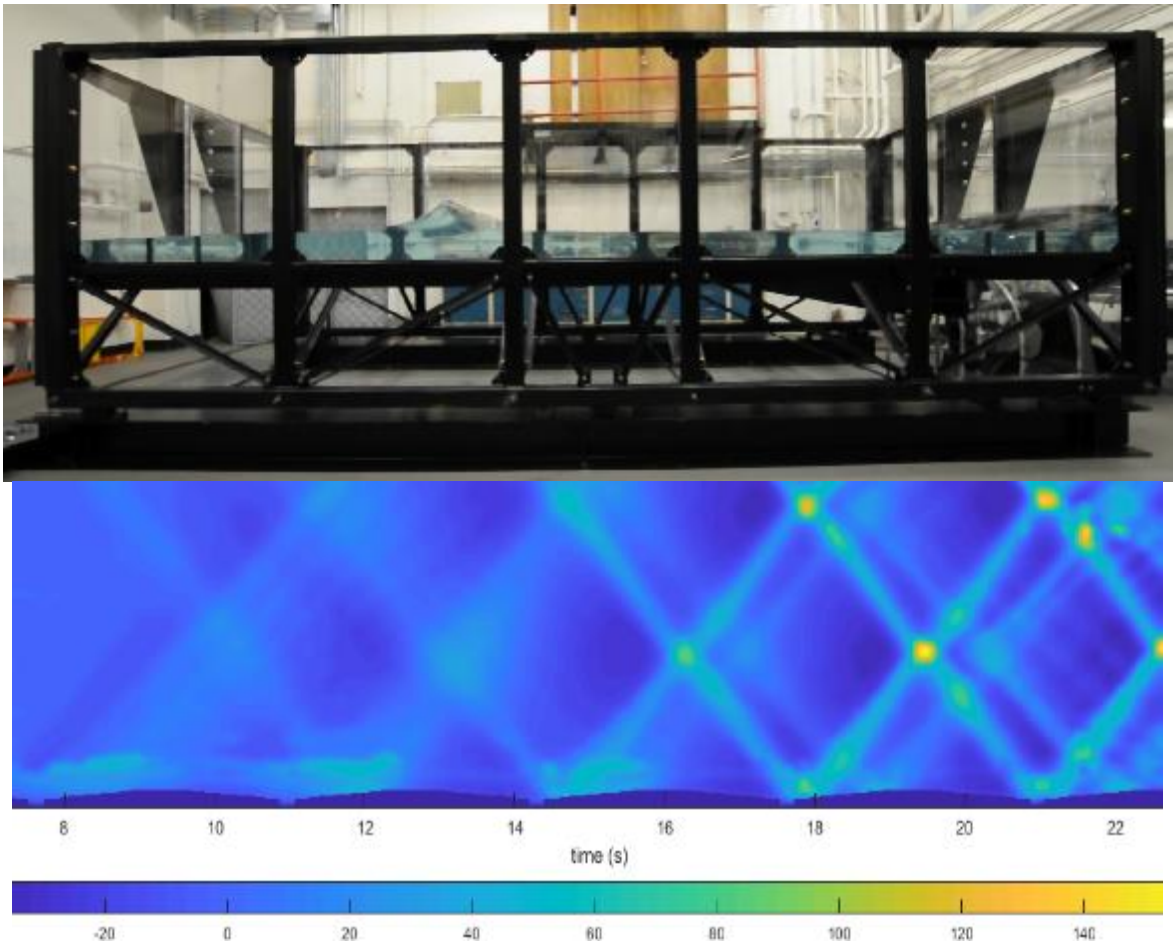


Figure 7.39. Measured 2D profile evolution (mode 2).

### 7.11.2. Panel Deflection

The effect of tank panel deformation on the pressure measurements was investigated using an accelerometer. The main concern was that water impact would induce vibration of the panel that holds the transducer, and that the resulting acceleration would lead to spurious reading of the pressure. Another important reason for monitoring the panel deformation for the purpose of validation is because the pressure resulting from the impact on a compliant structure is significantly lower than that on a rigid structure.

During a typical wave impact, the panel oscillates at ~120 Hz, with acceleration up to 0.5 g. This translates into a deflection of ~9 μm. As shown below the pressure spectrum does not correlate with the acceleration spectrum, which means that oscillations of the panel do not induce spurious pressure measurements.

However, the deflection of the panel will still affect the physical pressure during the impact; therefore, the deflection must still be monitored.

Future tests could look into making the panel stiffer (with metal braces for instance) and studying the effect on the pressure data.

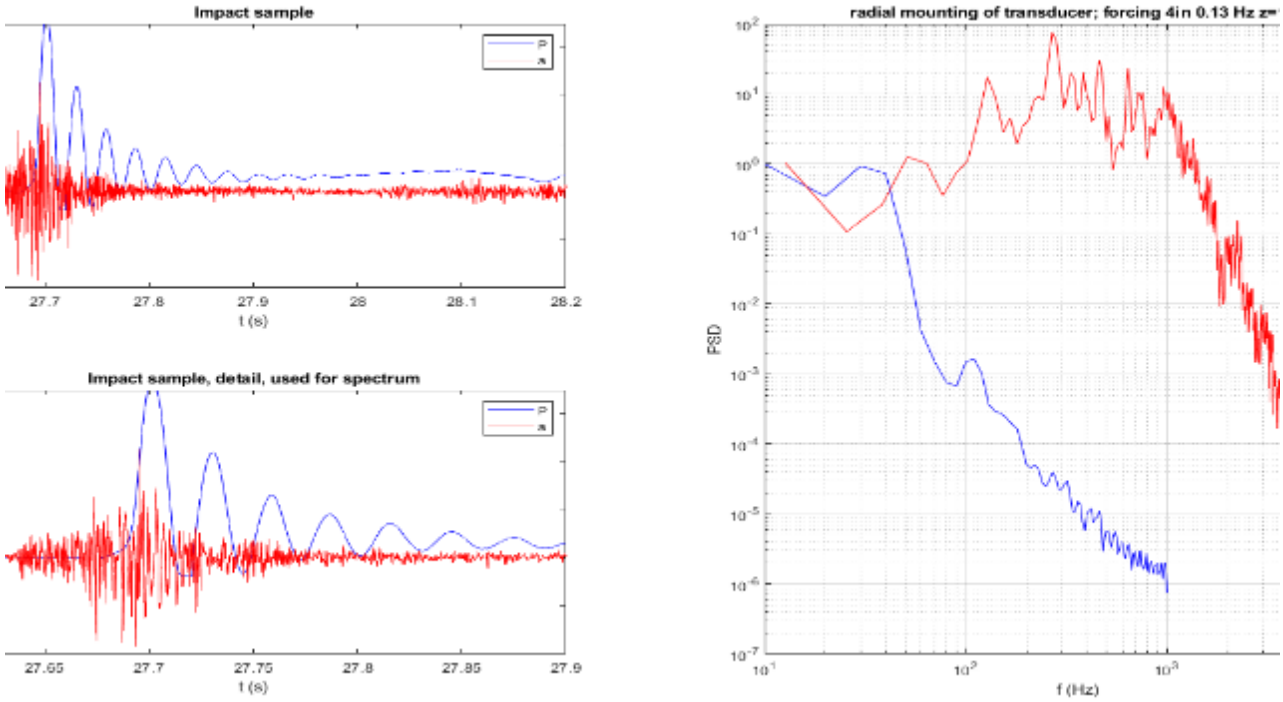


Figure 7.40. Temporal pressure and acceleration profiles (left) and frequency spectrum (right).

### 7.11.3. Repeatability

Repeatability and sensitivity of the pressure measurement was evaluated for the following conditions:

- Forcing: 4.000” (101.6 mm), 0.1100 Hz (mode 1)
- Water depth: 6” (152 mm)

The flow that develops consists into a breaking wave that goes back and forth along the tank, with a period that matches that of the forcing (mode 1). Pressure is collected using the 350 mBar sensor located at z=4” (101.6 mm) above the tank bottom (2” below mean water level). The flow is initially 2D, but slowly becomes 3D as the breaking event generates 3D structures. Four tests are conducted:

| Run | h (mm) | f (Hz) | A (mm) | Comments |
|---|---|---|---|---|
| 1 | 152.4 | 0.11 | 101.6 | Reference run |
| 2 | 152.4 | 0.11 | 101.6 | Identical to Run 1 |
| 3 | 152.4 | 0.11 | 102.108 | Change of the forcing amplitude by 1% |
| 4 | 153.4 | 0.11 | 101.6 | Change of the water depth by 1 mm |

The change of the water depth by 1.0 mm was done by adding a precisely measured volume of water to the tank. The frequency was not modified as the uncertainty analysis showed that this parameter is very accurately controlled (better than 0.01 %).

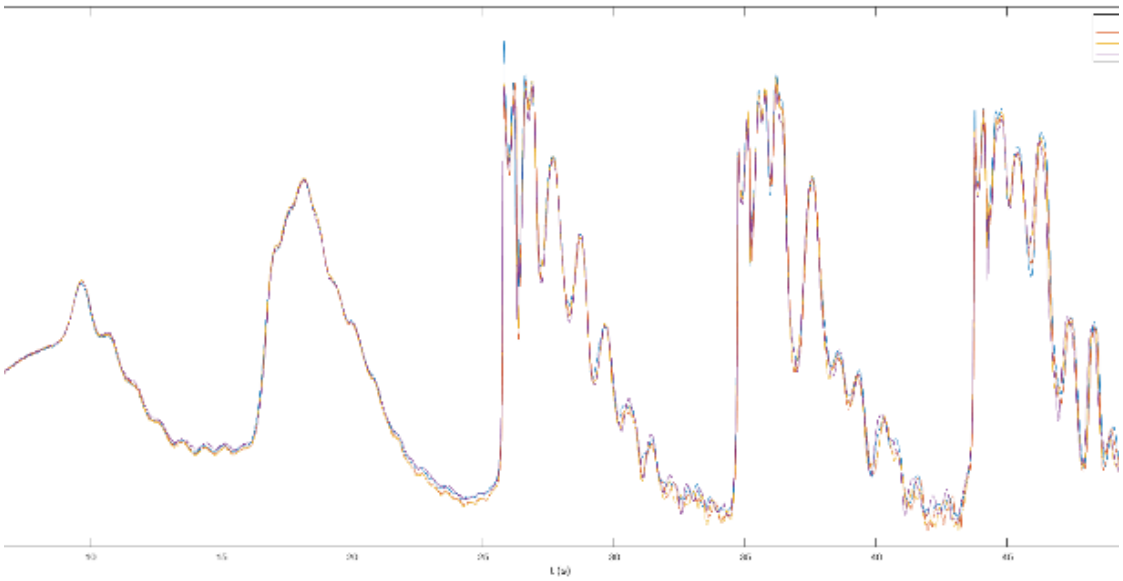

Figure 7.41. Time evolution of pressure.

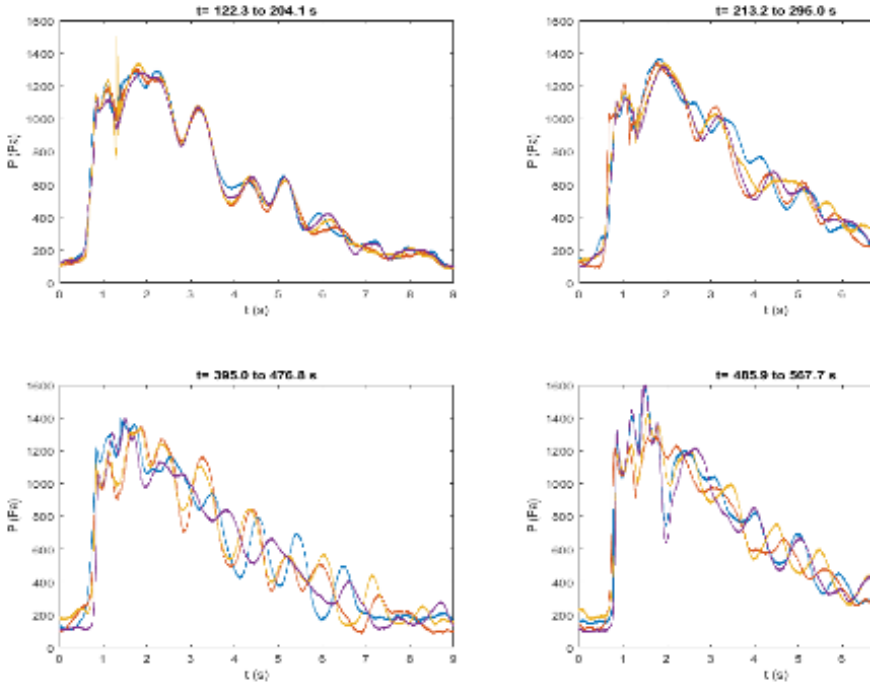


Figure 7.42. Ten cycles moving average for the first 10 minutes.

For the first 10 cycles, the difference is on the order of the precision (70 Pa), except for the peak pressure. Even for identical condition (runs 1 and 2), the pressure timeline starts diverging after about 20 cycles, because of turbulence and other chaotic processes. The main findings are as follow:

- The comparison between experiment and simulation must be limited to the first 10-20 cycles or look at the overall envelop of the pressure during the impact.
- Over the first 10-20 cycles, modifying an initial condition by an amount similar to the respective uncertainty does not affect the repeatability. Therefore, the initial condition are well-enough characterized for the purpose of validation and repeatability (for this particular set of tests).

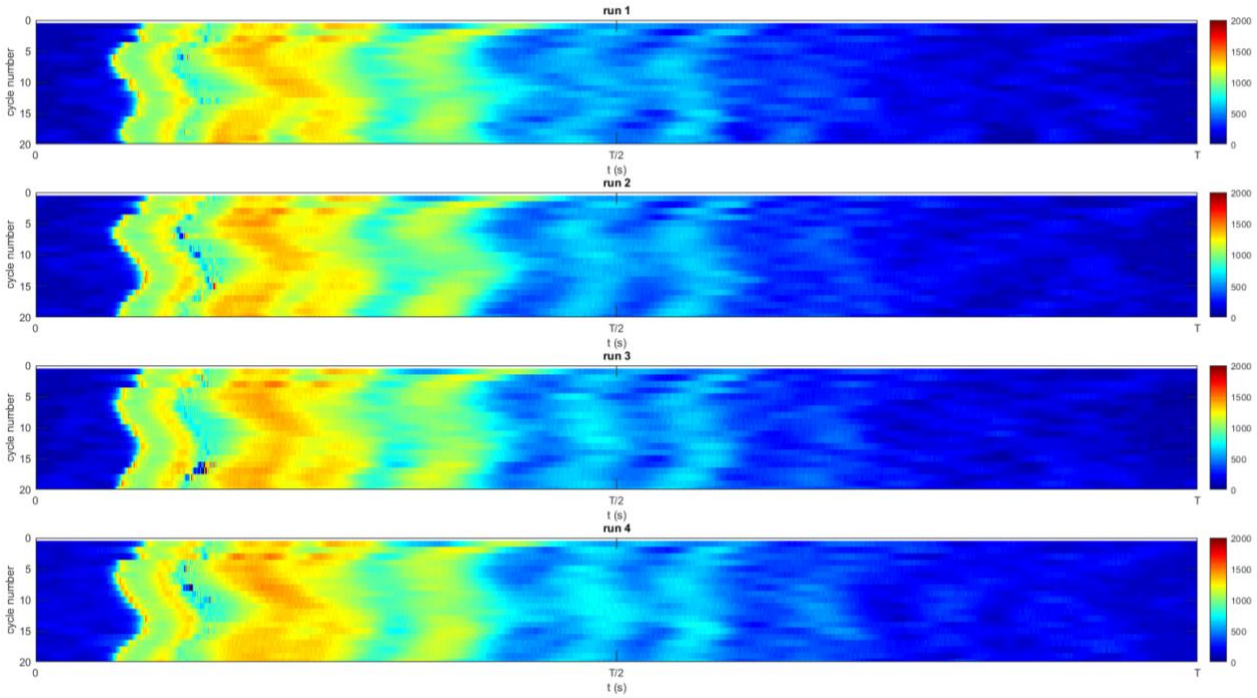


Figure 7.43. Time evolution of the pressure profile for the first 20 cycles of each runs.

### 7.11.4. Wave Impact Statistics

The four runs presented in the previous section were aggregated, which resulted in 459 single wave impact events from which good statistics can be extracted.

The first metrics to be studied are: the average pressure profile during an impact, the standard deviation (RMS), and the minimum and maximum pressure, as plotted below:

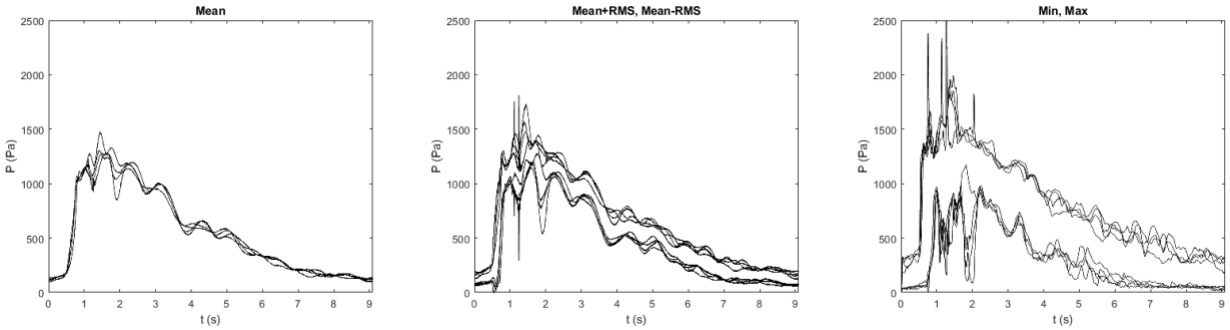


Figure 7.43. Average pressure profile during an impact.

The variation in the measured profile is mostly due to several factors: random turbulent unsteady bubbly flow and 3D waves. The percentile bound are also plotted below. These may be more appropriate for studying the spread of data with a non-normal distribution.

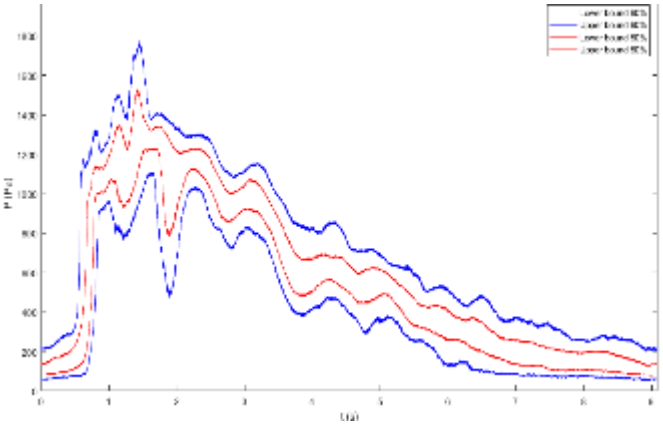

Figure 7.44. Percentile bound of pressure profiles.

The variation in the measured profile is mostly due to several factors: random turbulent, unsteady bubbly flow, and 3D waves. These curves show that the pressure evolution is bounded between quantified intervals. Compared the percentile graph with the min max graph, one can see that there are a few events that largely deviate from the mean values, mostly near the peak pressure. These correspond to event for which the wave impact happens exactly at the time of wave breaking. This highlight the need to preforms hundreds of cycle to be able to characterize the frequency of occurrence of such rare events.

The cycle plotted above is discretized in 9 segments of 1 second each, and the distribution of the pressure around the mean is plotted as a histogram:

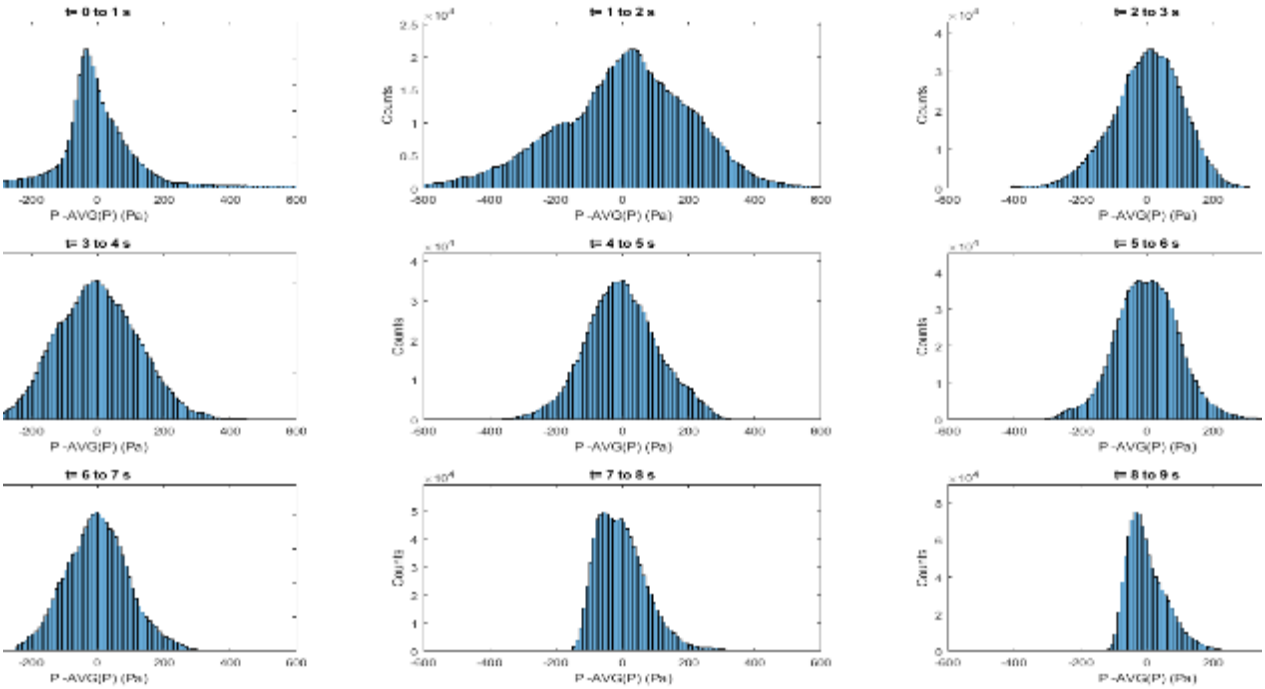


Figure 7.45. Pressure histograms.

This highlights the larger (non-Gaussian) distribution of pressure during the impact phase (t=1 to 2 s).

The distribution of the first and last segment is skewed. This is because the pressure sensor is momentarily above the water surface at these times, which causes a bias toward $P$ = 0 Pa.

### 7.11.5. Pressure-Impulse

When studying the failure of a structure, the main parameter is the maximum stress (or pressure) that can be withstood. However, for short transient, the peak pressure can exceed the static limit for a brief moment without causing failure. This is due to the dynamic response of the structure (inertia) which acts as a low-pass filter. For such event, the occurrence of failure is better predicted by the impulse, which is defined as:

$$P(\mathbf{x}) = \int_{\text{before}}^{\text{after}} p(\mathbf{x}, t)\mathrm{d}t$$

The threshold for failure for a given structure can then be given by a pressure-impulse (P-I) diagram:

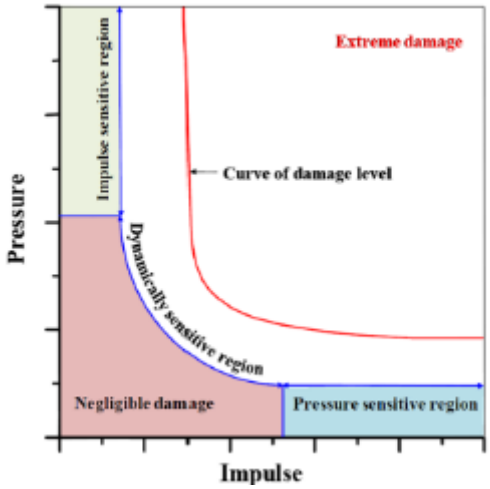


Figure 7.46. Pressure-impulse (P-I) diagram.

From the experimental data, the maximum pressure and impulse are calculated from each cycle, see a sample below:

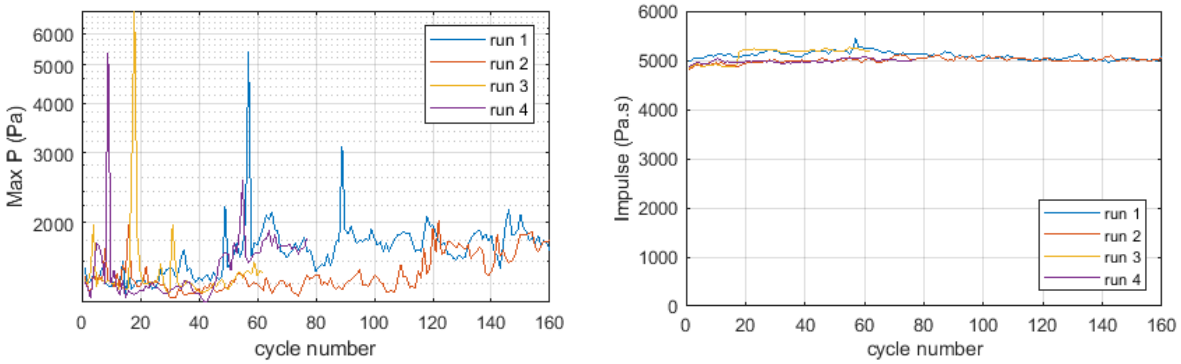


Figure 7.47. Maximum pressure and impulse.

It should be noted that while the max pressure shows large fluctuation (as discussed earlier), the impulse is remarkably consistent, as noted by Peregrine 2003. These data-points can then be plotted in a P-I diagram. The failure limit shown in red is arbitrary and for illustrative purposes only. The few outliers on the max pressure are related to breaking modes of waves on the wall. The physical processes describing this will be highlighted in the next section.

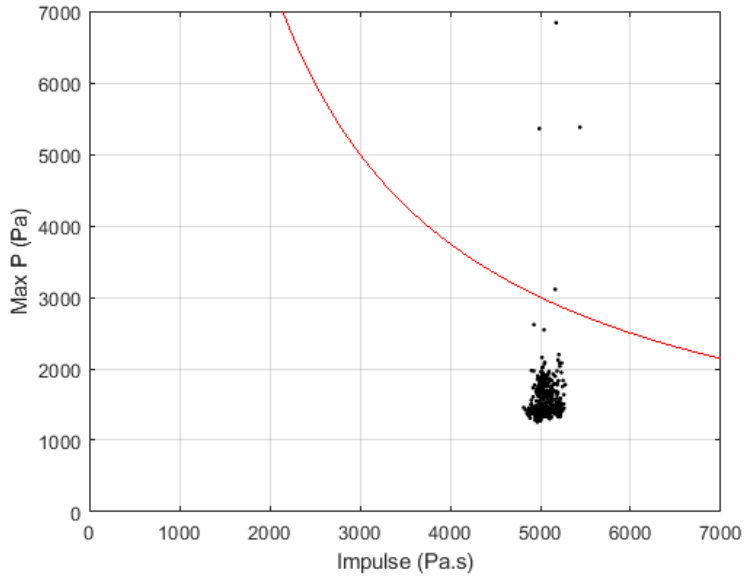


Figure 7.48. Maximum pressure versus impulse.

### 7.11.6. Pressure Peak and Bubble-Induced Pressure Oscillations

The few occurrence of very large peak pressure was investigated. The following figure shows the pressure time history for two consecutive waves during run 1:

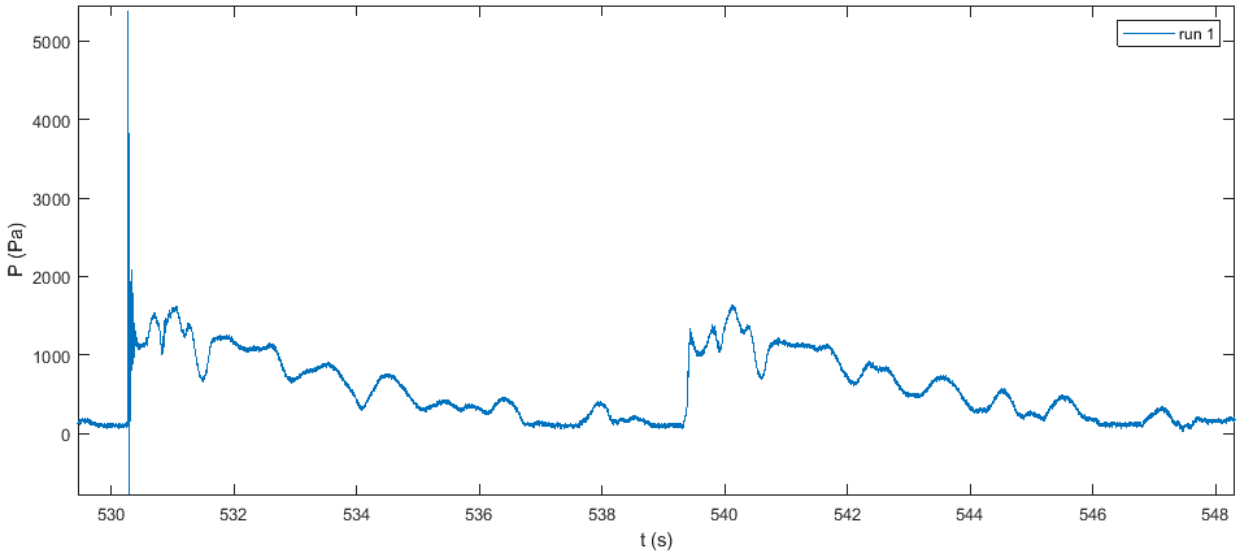


Figure 7.49. Pressure history.

The overall profiles are similar, except for the initial peak Here is a magnified view of that first peak:

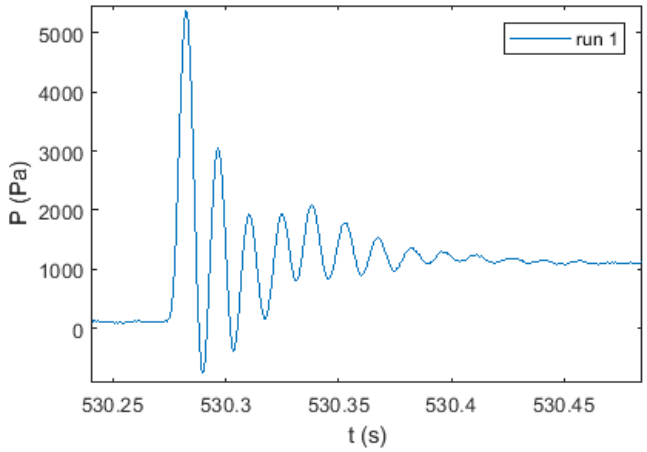


Figure 7.50. Zoomed-in pressure history.

This shows large pressure oscillations at a frequency of 70 Hz. Further tests showed that the large pressure peak occurs when the wave break exactly on the wall. This was studied by Chan and Melville (1988):

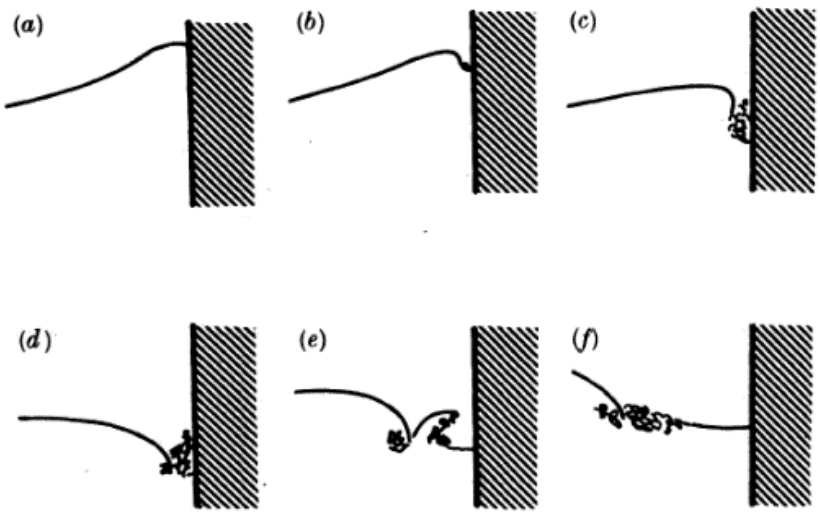


Figure 7.51. Schematic of breaking waves incident on a surface wall.

However, pressure oscillation and large peak pressure are not correlated; one can occur without the other.

The oscillations are caused by the presence of bubbles in the flow. This was studied using high speed imaging. The following image shows the flow in the direct vicinity of a pressure transducer during wave impact.

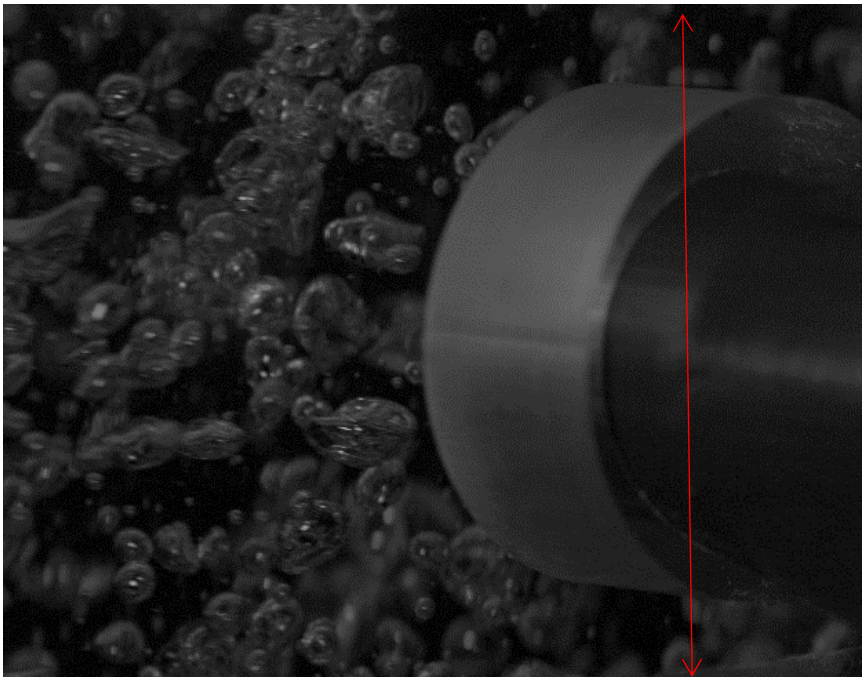

Figure 7.52. High speed movie snapshot. Pressure transducer is on the right. For scale, the arrow is 1.25”.

The effect of bubbles on the pressure oscillations is shown in the following two sets of figures. In the first set, oscillations are limited in amplitude. The high speed image shows a few small bubbles. In the second set of figures, larger pressure oscillations are recorded, and many larger bubbles are visible near the pressure port. This supports the hypothesis that the oscillations are caused by bubbles.

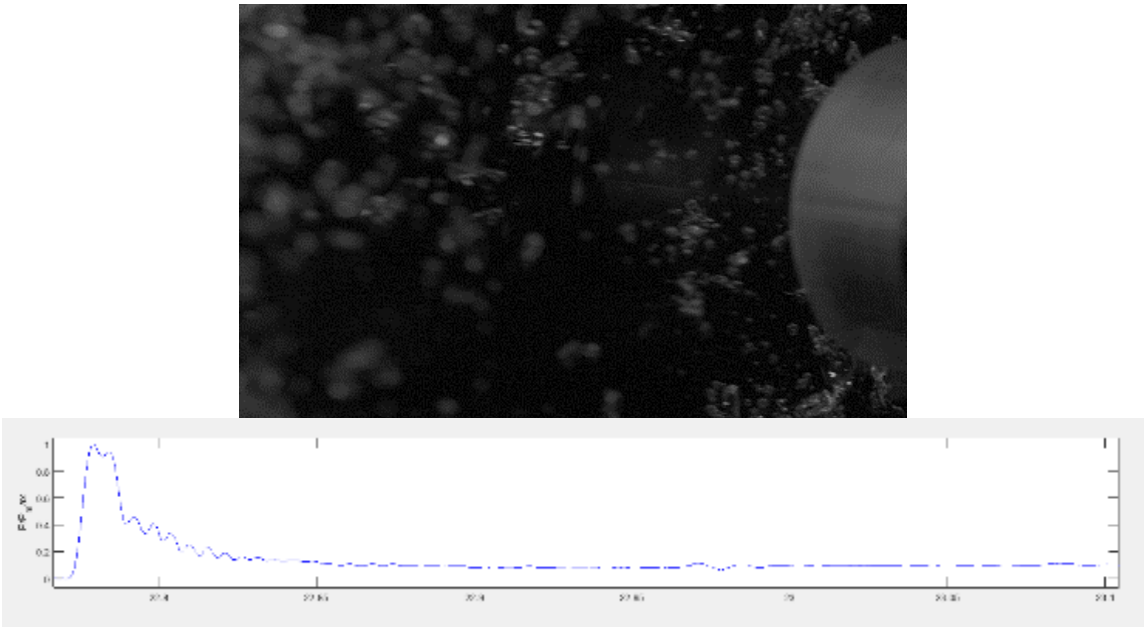

Figure 7.53. Top: Raw image. Bottom: Corresponding pressure plot

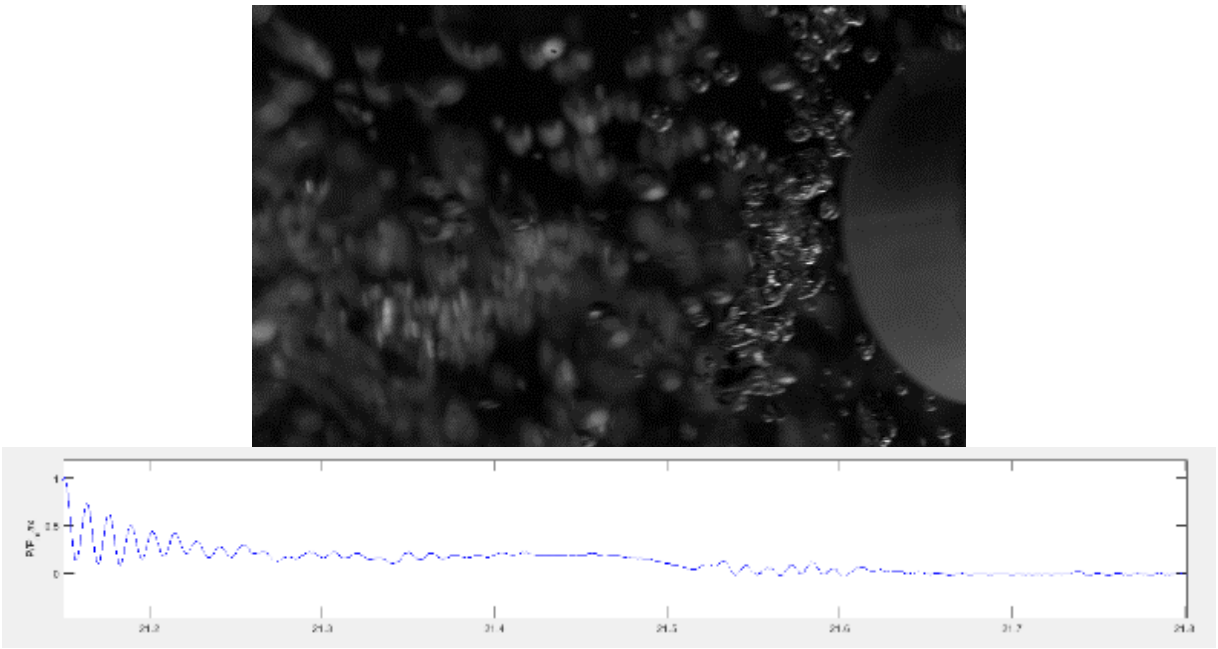

Figure 7.54. Same as above for a different impact event

In nearly all the wave impact data acquired so far, the waves become too steep in the tank and spilling breakers develops as the wave travels between the walls. However, in a few cases, the wave reaches the wall without breaking first and breaks on the wall directly. In the first phase of the impact, a large air cavity is trapped and its compression by the breaking wave results in the much higher peak pressure observed occasionally in our runs. In fact the peak pressure during those events is about 3 times larger than during impacts when the wave "spills" on the way to the tank edge.

### 7.11.7. Comparison with simulation

The statistical results are used for comparison with the Neutrino simulations.

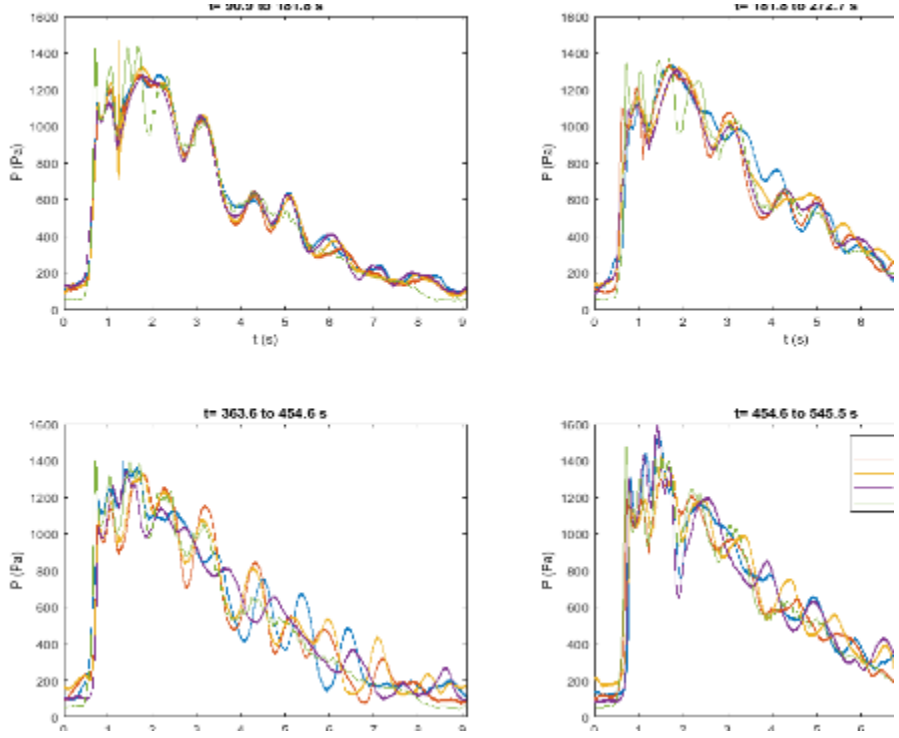


Figure 7.55. Neutrino results overlaid with the experimental data.

The SPH simulation captures remarkably well the general envelope of the pressure time-history. The match is very good for the first 90s (top left panel). The percentile plot and impulse are also presented below:

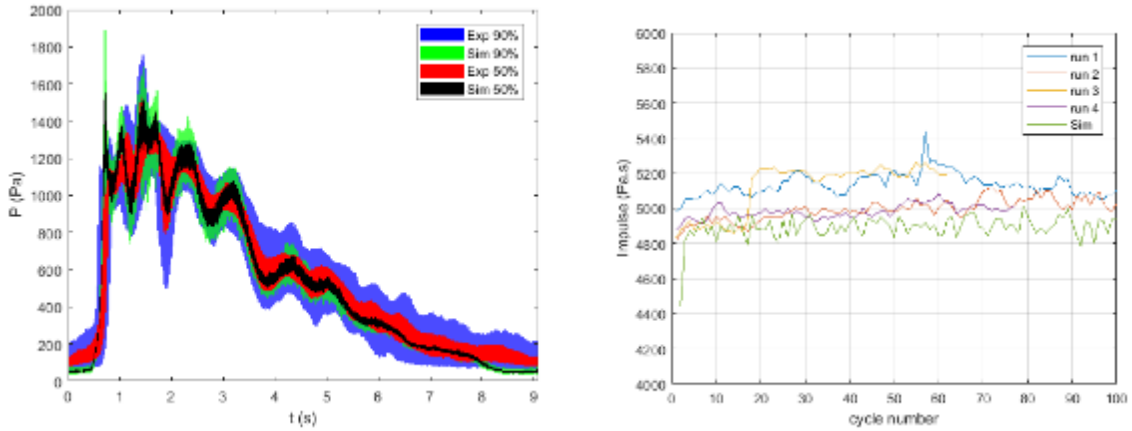


Figure 7.56. Simulation results: pressure and impulse.

The left plot shows that the simulation results are more consistent from cycle to cycle than in the experiment. For instance, the 50% band is narrower in the simulation than in the experiment. This difference is explained in part by the 3D effect (spanwise waves, turbulence, bubbly flow, etc.) not being fully captured by Neutrino. On the other hand, Neutrino captures well the impulse, with an error of about 4%.

Such comparisons between experiment and simulation are extremely useful to identify the limitations of a code for real scenarios. In the context of RISMC, we need to define a way to quantify the performances of the code. For multivariable and multidimensional quantities, advanced metrics are being explored.

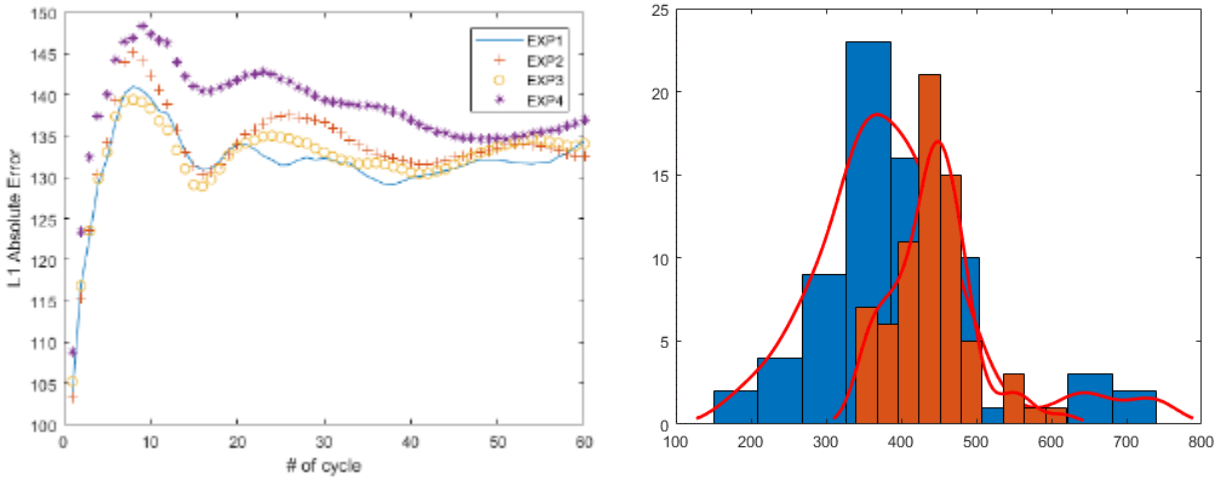


Figure 7.57. Left: Convergence of the L1 error. Right: Comparison of the pressure distributions at one instant in time (blue is simulation, orange is experiment).

Comparison of the pressure distribution allows computing metrics based on the histogram overlap (K-L Divergence and Hellinger metrics).

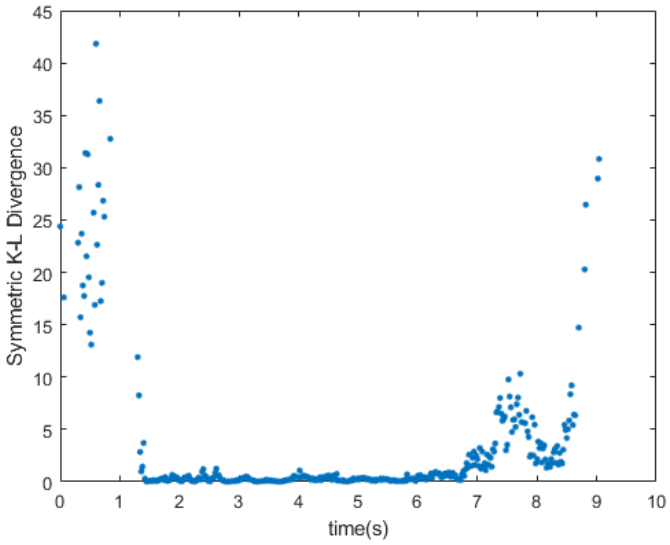


Figure 7.58. K-L divergence.

This example shows large discrepancy at the beginning and end of the cycle. When looking at the time history of the pressure (see figure below), these correspond to the absence of impact, i.e. only hydrostatic pressure, which is a region of the pressure time history that is not relevant for validating neutrino in flooding scenarios:

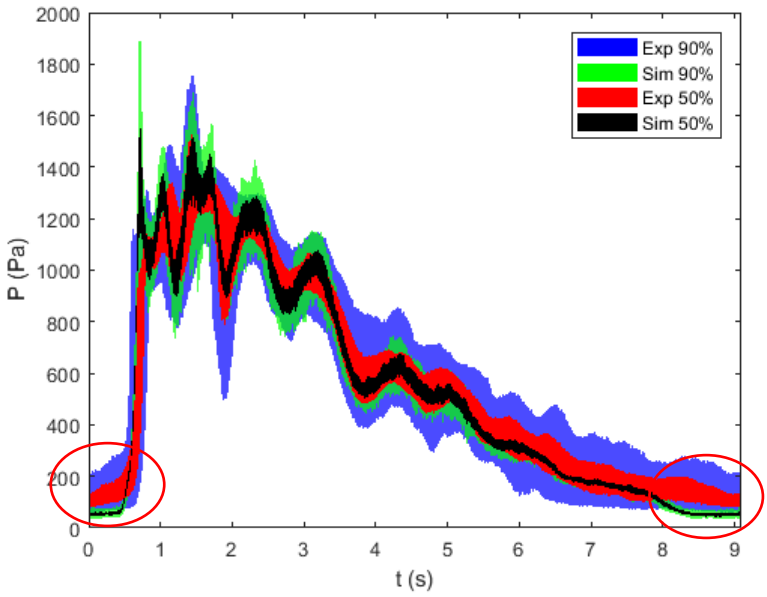


Figure 7.59. Region of large discrepancy highlighted in red circles.

The reason for the large discrepancy there is because the relative error is large (~100%). However, the absolute error is about 50 Pa, which is on the order of the sensor accuracy, and correspond to a hydrostatic head of 0.5 cm, which is smaller than the particle size in the simulation. Therefore, this emphasizes the importance of choosing the correct metric(s), and correctly interpreting its results.

### 7.11.8. Scaling Analysis

We seek a way to estimate the behavior of the flow at large scale from the data we collect in the experiment, in other words, looking for a physics-based argument to extrapolate between validation and application domain. Doing so involves identifying scaling parameters for the impact pressure. In single phase regimes (when there is not air entrapment during the impact), the dynamic pressure normalizes the pressure, $P$:

$$P^* = \frac{P}{\frac{1}{2}\rho V^2}$$

The characteristic velocity is that of the shallow water wave: $V = c = \sqrt{gh}$. The equation becomes:

$$P^* = \frac{P}{\frac{1}{2}\rho g h}$$

The denominator is half the hydrostatic pressure at the bottom of the tank (or the hydrostatic pressure at half depth), which means that for shallow water wave, we can use either dynamic pressure or hydrostatic pressure for normalizing.

This result shows that the impact pressure for shallow wave should scale directly with the water depth.

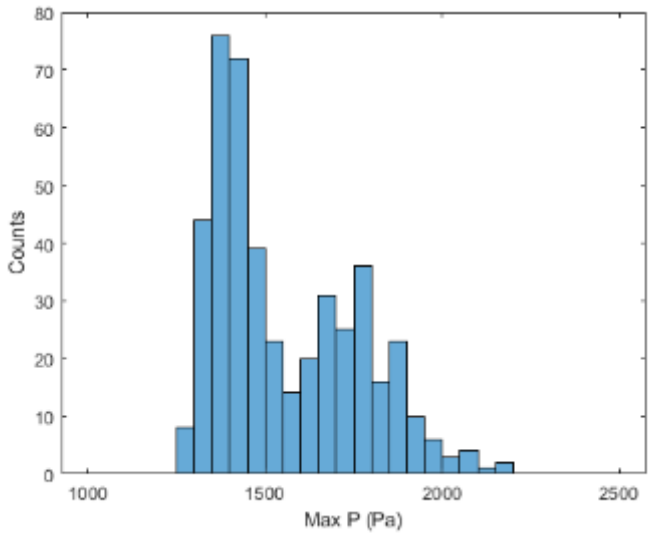


Figure 7.60. Max impact pressure distribution at $z$=0.101 m for $h$=0.152 m. $z$ is the sensor elevation and $h$ the mean surface elevation.

The mean of max impact is around 1600 Pa. We now double the depth. We would expect the impact pressure to double as well. We conducted tests are twice the depth (0.304 m) and the histogram is shown below (the histogram is coarser as we have taken fewer runs):

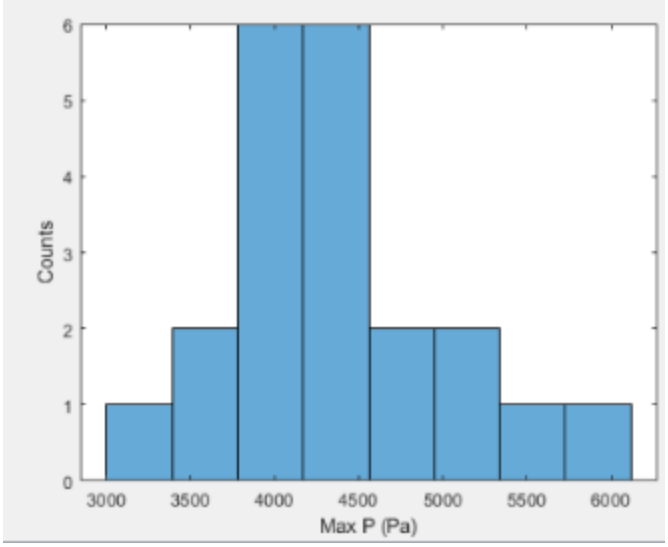


Figure 7.61. Max impact pressure at $z$=0.101 m for $h$=0.304 m.

The mean is close to 4200 Pa, which is more than double. The main discrepancy appears to be due to the sensor location. The physical location is the same is both cases, but what appears to matter is the sensor depth relative to the surface elevation. If the latter is different, an offset results due to the difference in hydrostatic pressure. When correcting the data above for the hydrostatic pressure, one obtains:

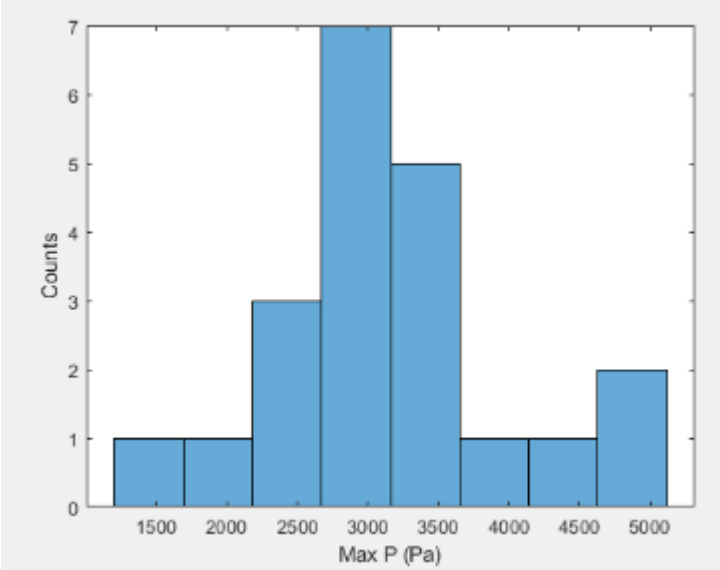


Figure 7.62. Max impact pressure at $z$=0.270 m for $h$=0.304 m.

The mean max pressure is ~3200 Pa, or twice that of the 0.152 m depth case when the sensor is at the same depth (5 cm below the mean surface elevation) which agrees with the scaling presented above. More data will be acquired for $h$=0.304 m and other depth to confirm scaling.

## 7.12. SPH Neutrino benchmark

### 7.12.1. Experimental setup

A large-scale oscillating tank was designed and constructed at the George Washington University. The tank measures 5.951 m long × 1.2 m high × 2.468 m wide. The tank is constructed of a steel frame and acrylic walls and bottom. The tank is oscillated through a sine-forcing function using a hydraulic actuator capable of amplitudes up to 0.25 m and velocities up to 0.5 m/s. Additionally, a pressure transducer is located at the end-wall of the tank, 0.1016 m above the tank bottom, to measure the pressure from wave impacts.

The experiment for the end-wall pressure measurement consisted of a water depth of 0.1524 m. The forcing function had a 0.1016 m amplitude, with a 0.11 Hz frequency. The experiment ran for 60 cycles and was repeated four times, with minor variations to account for some uncertainties. Two of the runs were identical; one run varied the depth by adding a precisely measured volume of water to the tank, and the last run varied the forcing function amplitude. Table  shows the variations on the four experimental model runs.

Table 7.11: Experimental model run variations.

| Run | Water Depth (m) | Frequency (Hz) | Amplitude (m) | Variation |
|---|---|---|---|---|
| 1 | 0.1524 | 0.11 | 0.1016 | Reference run |
| 2 | 0.1524 | 0.11 | 0.1016 | Identical to Run 1 |
| 3 | 0.1524 | 0.11 | 0.102108 | Change of forcing amplitude by 1% |
| 4 | 0.1534 | 0.11 | 0.1016 | Change of water depth by 1 mm |

### 7.12.2. Smoothed Particle Hydrodynamics

The fluid-simulation code Neutrino was investigated and used to numerically reproduce the experiment. An incompressible SPH solver was selected, considering its high computational efficiency (Sampath et al. 2016). It solves the incompressible Navier-Stokes equations for isothermal, single-phase flows in a Lagrangian, velocity-pressure formulation. The water-air mixing and surface-tension effects, with air entrainment and formation of bubbles and foam, as occur from wave breaking, are not modelled. To avoid excessive complexity, only the water phase is considered, and the air-water interface is approximated as a free surface. The SPH method is well suited to simulate violent flows with a highly evolving free surface. Thus, it is expected to perform well for water waves and oscillating motions.

In accordance with the physical properties of water, the fluid is assumed to be Newtonian, with viscosity constant in both space and time. The water is discretized into a set of fluid particles, with fixed mass and volume that move along with the flow. Because SPH is a mesh-free numerical method, there is no explicit inter-particle connectivity. Instead, the spatial-differential operators are approximated by modeling inter-particle interactions. Using a Gaussian-like function, smoothing kernel, with compact support, the respective contributions of each interacting particle-pair are weighted based on the inter-particle distances. In this work, the smoothing kernel used is the cubic B-spline.

### 7.12.3. Simulation Setup

The Neutrino model was constructed to match the experimental setup as closely as possible. The oscillating tank experiment can be characterized as a two-dimensional (2-D) experiment, resulting in the simulation tank having the same length and height dimensions, but a smaller width of 0.2 m. By reducing the width of the simulation tank, the computational runtime of the simulation is also reduced without compromising accuracy. A simulation with a particle size of 0.01 m (181,387 fluid particles total) takes about 16.7 hours for 30 cycles using an Intel Xeon central processing unit E5-2683 v3 @ 2.00 GHz with 28 core and 56 logical processors.

The simulation tank was filled with particles to the correct fluid depth. The number of fluid particles was carefully controlled to ensure that the numerical volume of the fluid simulation corresponds to the correct physical fluid depth. A measurement field is used to measure the pressure on the end-wall. This measurement field compares to the pressure transducers used in the experimental setup. Figure 9.2. shows the large-scale oscillating tank on the left and a cross-sectional view of the simulation setup on the right.

Figure 7.63. Large-scale oscillating tank at the George Washington University (left) and Neutrino simulation setup (right).

Once the simulation setup was complete, the simulation tank and end-wall measurement field needed to be oscillated at the same forcing function as the experiment. To create these oscillations, a python script for each object was created and added to the position of the object as a dynamic expression. The python scripts adjust the position of the items based on Equation 7.9.2.

$$z(t) = A \sin(2\pi f t) \quad \text{(Eq.7.1)}$$

where z is the new position, t is the time, A is the amplitude, and f is the frequency. The amplitude and frequency values are set in the python script to match the experimental values, and the time is extracted from the simulation. The equation allows for the movement of each object to be continuous and evaluated for every time step of the simulation. Without using the equation and, instead, using a dataset of positions, the movement of the objects may not shift smoothly with the time step, causing jumps with overlapping particles, which results in erratic or explosion-like behavior from the simulation tank impact.

### 7.12.4. Validation Simulation Conditions

Several parameters were varied to match the simulation to experimental results. Those parameters included particle size and measurement-field size and location. The first parameter that was varied was particle size. Three different particle-size values were used to determine the effect of spatial resolution on the pressure results. The three values used were 0.03, 0.02, and 0.01 m. Each cycle of the simulation results was then sorted and analysed to determine the 90% and 50% bounds (the point at which 90% [or 50%] of the data are within that band). Figure  shows the 90% pressure bounds for the different particle sizes on the left and the 50% pressure bounds on the right.

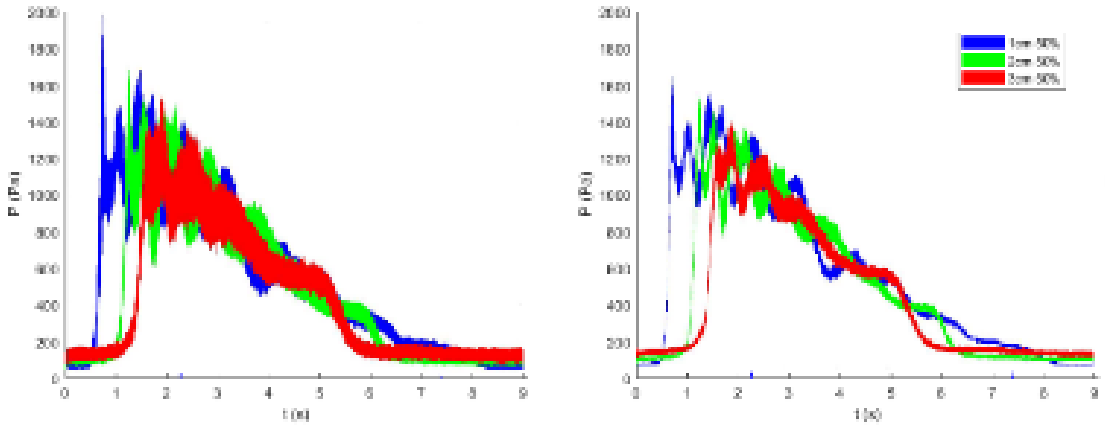

Figure 7.64. Particle size pressure bounds comparison.

As shown in the plots in Figure , the pressure bounds shift to the right as the particle size becomes larger. The left-most pressure bound using 0.01 m particles matched the experimental results with enough accuracy that smaller particles were not tested. Therefore, a particle size of 0.01 m was selected for both accuracy and acceptable run times.

Next, the measurement field size and location were adjusted. A particle size of 0.03 m was used for these comparisons to reduce the computational runtime. For changes to the measurement field size, the y-axis height of the measurement field stayed constant at a value equal to the particle size (0.03 m) because the field must be at least the size of the particles. The x-axis width value also stayed constant at 0.15 m because the experiment is considered 2-D. The z-axis length of the experiment was adjusted to see the effect on the results. Two z-axis length values were used: 0.15 m and 0.1 m.

For the location changes, only the x-axis position was varied to determine if a slight shift in location had an effect though the experiment is considered 2-D, particles are still 3-D in nature, and a shift may cause more or less particle interaction on the measurement field. The y-axis position was not adjusted because its location is based on the location of the pressure transducer in the experiment. The z-axis location

also was not varied because it must stay on the end-wall of the tank. Figure 7.65 shows the measurement field length comparison on the left and the measurement field x-axis location comparison between centered and shifted 0.015 m on the right. These plots show the last 10 cycles of the 60 cycle simulation averaged together.

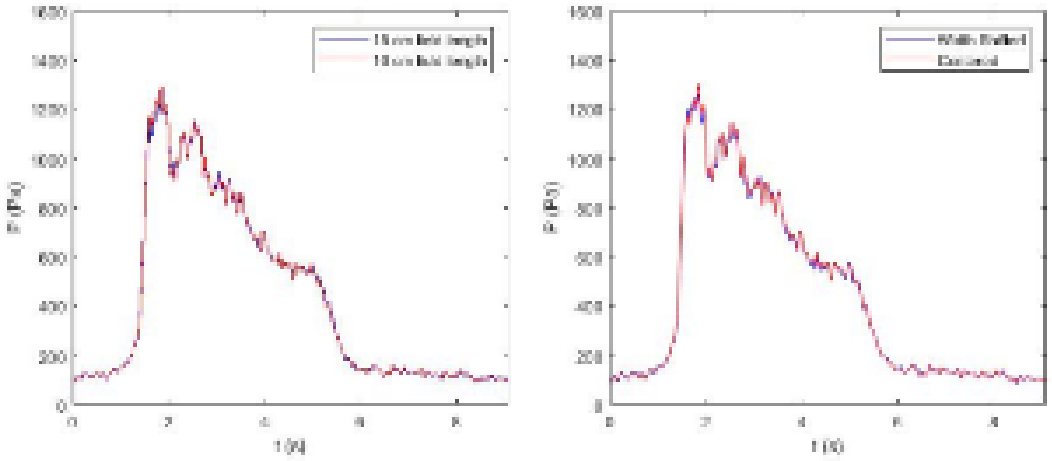

Figure 7.65. Measurement field size and location pressure comparison.

Based on the plots above, there is nearly no difference between the varied sizes and locations of the measurement field. Therefore, the measurement field was left centered in the simulation tank, and the size of the measurement field for the results below was 0.05 m long by 0.05 m wide by 0.01 m high. These dimensions were scaled down from the 0.03 m particle size results to a 0.01 m particle size.

The values selected for each of these parameters were based on a brief parametric study of the parameter. More parameters could be adjusted, which might affect the simulation results. The following section will discuss these other parameters as well as the methodology for determining their significance.

### 7.12.5. Significant parameter determination

**Investigated Parameters**

More than 30 parameters or settings are associated with a Neutrino simulation as well as parameters associated with the experiment. However, not all of these parameters have an effect on the accuracy of the simulation. Table 7.12 shows a list of the parameters and an initial discussion on whether the parameter was investigated to determine its significance. Highlights show parameters that were investigated.

Table 7.12: Parameter discussion table.

| **Parameters** | **Importance Discussion** |
|---|---|
| Time step pressure iteration coefficient | Important, but not investigated because it is expected to be soon deprecated after replacing the pressure solver |
| Non-static reference frame | Not important because it only affects simulations with fast-moving dynamic solid objects |
| Stop criterion | Important, but not investigated because the default value is known to be optimal |
| Stop threshold | Important because it affects the level of incompressibility enforcement. |

| | |
|---|---|
| Minimum number of iterations | Important, but not investigated because the default value is known to be optimal |
| Maximum number of iterations | Not important because it is only used to prevent occurrence of infinite loops due to non-convergence of the pressure solver |
| Relaxation factor | Not important because default value leads to optimum convergence (Sampath et al. 2016) |
| Old pressure weight | Important, but not investigated because the default value is known to be optimal |
| Particle shifting | Not important because particles should not be enforced to a particular configuration |
| Buoyance model | Not important because it only affects simulation of non-isothermal flows |
| Density computation | Important, but not investigated because the default value is known to be optimal |
| Enable negative pressures | Not important because it only affects the fluid-solver interaction with dynamic solid objects |
| Enable tensile instability control | Not important because it only affects the fluid-solver interaction with dynamic solid objects |
| SPH Laplacian for viscosity | Not important because it is known to yield very similar simulations |
| Wall boundary pressure method | Important, but not investigated because the default value is known to be optimal |
| Wall boundary extrapolation | Important, but not investigated because the default value is known to be optimal |
| Wall hydrostatic pressure correction | Important, but not investigated because the default value is known to be optimal |
| Wall viscous correction | Important, but not investigated because the default value is known to be optimal |
| Free-surface density correction | Important, but not investigated because the default value is known to be optimal |
| Free-surface pressure correction | Important, but not investigated because the default value is known to be optimal |
| Near-free-surface identification coefficient | Important, but not investigated because it only affects simulations with free-surface correction, which is not used |
| Open boundary extrapolation | Not important because there is currently only a single choice and would only affect simulations with open boundaries |
| CFL number | Important, but not investigated because the default value is known to be close to optimal |
| Time step diffusion coefficient | Not important because it only affects simulations with highly viscous flow |
| Clamp to multiple of Solid-Solver time step | Not important because it only affects fluid-solver interaction with dynamic solid objects |
| Adaptive time step | Important, but not investigated because the default value is known to be optimal |
| SPH kernel | Important, but not investigated since the same methodology can used to other smoothing kernels. |
| Particle size | Important because it changes the resolution of the simulation. |
| Interaction-Radius to Particle-Size Ratio | Important because it changes the number of particles influencing the particle of interest. |
| Fluid settling uncertainty | Important because it effects the fluid depth. |

| | |
|---|---|
| Fluid depth uncertainty | Not important because the correct number of particles for a given fluid depth can be calculated. |
| Fluid properties | Not important because they will match the fluid properties of the experiment. |
| Measurement field size | Important, but not being investigated due to initial research results. |
| Dimension uncertainty | Important, but not investigated due to very small uncertainty range. |
| Forcing function amplitude uncertainty | Important because it effects the forcing function of the simulation. |
| Forcing function frequency uncertainty | Important because it effects the forcing function of the simulation. |
| Pressure transducer location uncertainty | Important because it effects the measurement field location in the simulation. |

Based on Table 7.12, 7 of the 37 parameters were investigated to determine their significance. These seven parameters were analyzed using the method described below.

### 7.12.6. Methodology Using Risk Analysis Virtual Environment (RAVEN)

RAVEN is an Idaho National Laboratory developed analysis software. It can run external codes and performing analysis on the results. RAVEN has a wide range of capabilities, a few of which include reduced order models, advanced sampling methods, data post-processing, and model parameter optimization (Rabiti et al. 2017). The Neutrino and RAVEN coupling was used so that RAVEN would sample parameter values, modify the Neutrino's input file, and run Neutrino continuously without any user need after running the RAVEN input file (Ryan and Pope 2019).

The methodology for determining the significance of parameters consisted of, first, randomly sampling across the range of possible values of a single parameter. The values were sampled from a uniform distribution across the range of values using a Monte Carlo sampler. The value range for each parameter was selected based on previous simulation investigation or the uncertainties associated with the physical experiment. The results were then analysed to determine whether the parameter caused a change in the results. If the different parameters values did not cause a change in results, then the parameter was considered insignificant. Table  shows the range of values for each parameter, as well as the default value that was used when other parameters were being sampled. These ranges are all considered uniform although many have other distributions.

Table 7.13: Investigated parameter value ranges and default value.

| **Parameters** | **Value Range** | **Default Value** |
|---|---|---|
| Stop threshold | 0.0001 to 0.01 | 0.001 |
| Particle size | 0.007 m to 0.02 m | 0.01 m |
| Interaction-radius to particle-size ratio | 2.0 to 2.4 | 2.0 |
| Fluid settling uncertainty | $-0.4\delta_r$ to $0.4\delta_r$* | 0 |
| Forcing function amplitude uncertainty | 0.1012 m to 0.102 m | 0.1016 m |
| Forcing function frequency uncertainty | 0.1099868 Hz to 0.110011 Hz | 0.11 Hz |
| Pressure transducer location uncertainty | 0.1006 m to 0.1026 m | 0.1016 m |

* where $\delta_r$ is the particle size

## 7.13. Results

### 7.13.1. Validation

The 90% and 50% pressure bounds for the experiment and simulation were compared. Additionally, the pressure of each cycle was integrated over time to compare the pressure impulse. Figure  shows the pressure bound comparison with the 90% bound plot on the left and the 50% bound plot on the right. Figure  shows the absolute percentage error plots between the simulation and experiment upper and lower bounds for the 90% bounds on the left and the 50% bounds on the right.

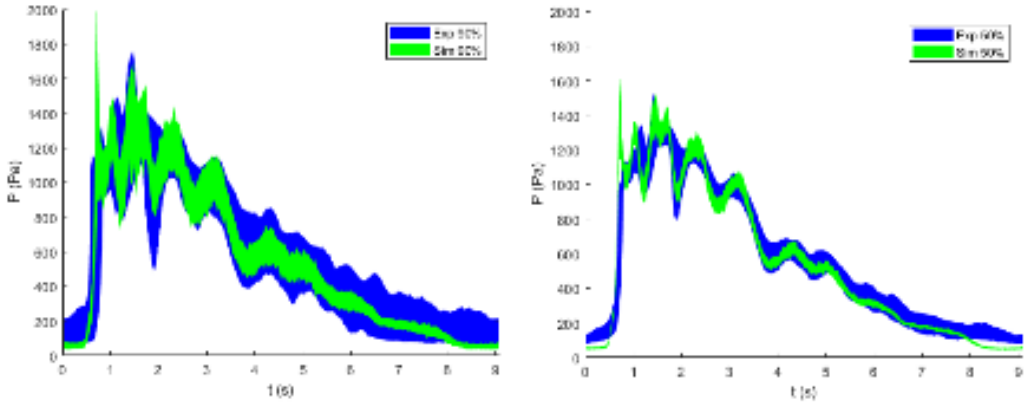

Figure 7.66. Pressure bounds comparison plots.

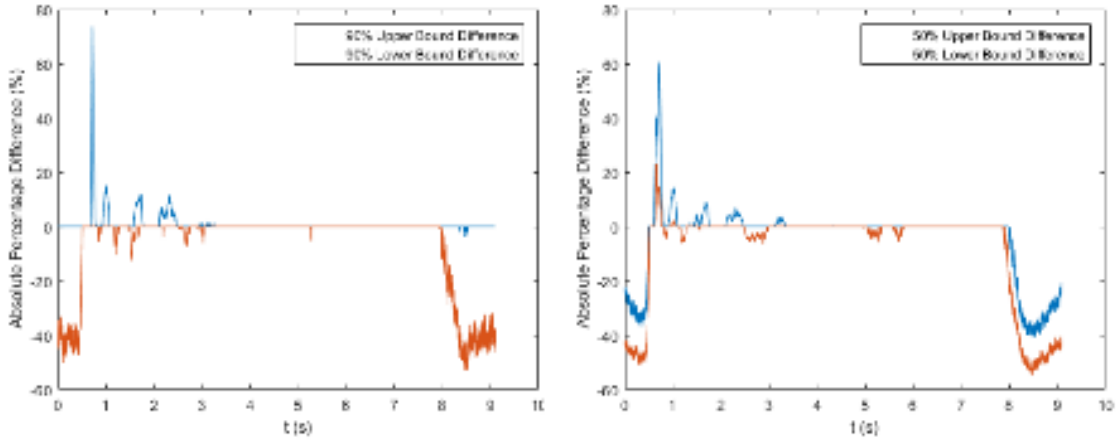

Figure 7.67. Pressure bounds simulation error plots.

The above plots show that both the 90% and 50% simulation pressure bounds mostly fall within the experimental bound. A few exceptions do occur in the low-pressure areas at the very beginning of the cycle (~40% difference) and the very end of the cycle (~40% difference); however, these low-pressure differences are typically insignificant for applications. The peak pressure tends to have a short but high initial peak variation (~75% difference) compared to the experiment. Overall, the simulation results match well with the experimental results for most of the time. However, refinement of parameters could possibly increase the accuracy of the simulation.

The simulation impulse pressure was compared to the pressure impulse for each experimental run. The absolute percentage difference between the simulation and each experimental run was also computed. Figure 8 shows the impulse pressure comparison plot on the left and the absolute percentage difference plot on the right.

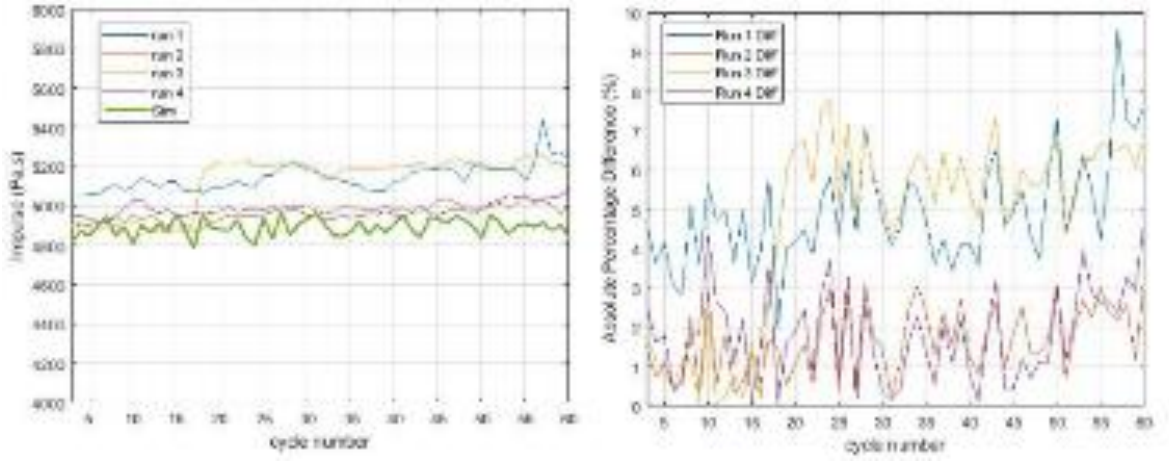


Figure 7.68. Impulse pressure comparison plots.

The absolute percentage difference plot shows that the pressure impulse of the simulation is within 10% of all four experimental runs. However, for two of the runs, the simulation is within 5% of the experiment. This shows that the simulation pressure impulse matches the experimental very well.

### 7.13.2. Significant Parameters

The parameters and their range of values identified above were sampled five times using RAVEN. The pressure results for all five runs were compared to determine whether the parameter is significant. To reduce the computational runtime, 30 rather than 60 cycles were simulated. Table  shows the five sampled values for each parameter and Figure .69 shows the average pressure plot comparison for the different parameters.

Table 7.14. Sampled values for each parameter.

| **Parameter** | **Sample 1** | **Sample 2** | **Sample 3** | **Sample 4** | **Sample 5** |
|---|---|---|---|---|---|
| Stop threshold | 0.005188 | 0.009604 | 0.000482 | 0.008365 | 0.004260 |
| Particle size | 0.009004 | 0.009710 | 0.018166 | 0.011869 | 0.017700 |
| Interaction-radius to particle-size ratio | 2.083384 | 2.149816 | 2.013502 | 2.042695 | 2.089326 |
| Fluid settling uncertainty | 0.027887 | 0.920035 | -0.922877 | 0.669684 | -0.691674 |
| Forcing function amplitude uncertainty | 0.101436 | 0.101541 | 0.101956 | 0.101291 | 0.101270 |
| Forcing function frequency uncertainty | 0.110007 | 0.110008 | 0.110011 | 0.109989 | 0.109992 |
| Pressure transducer location uncertainty | 0.102298 | 0.102340 | 0.101516 | 0.102578 | 0.101047 |

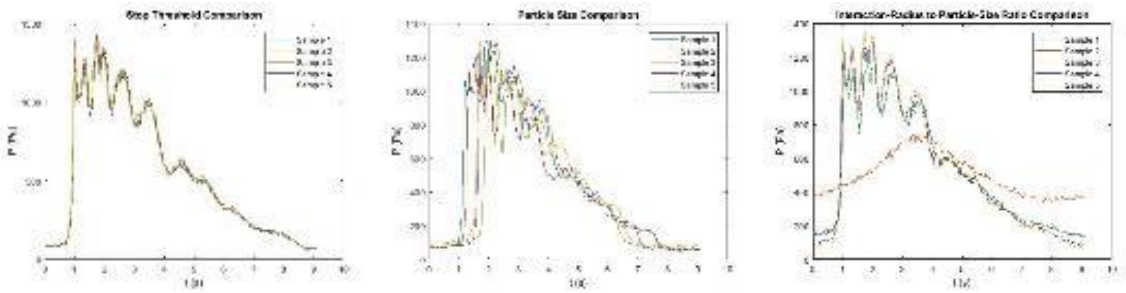

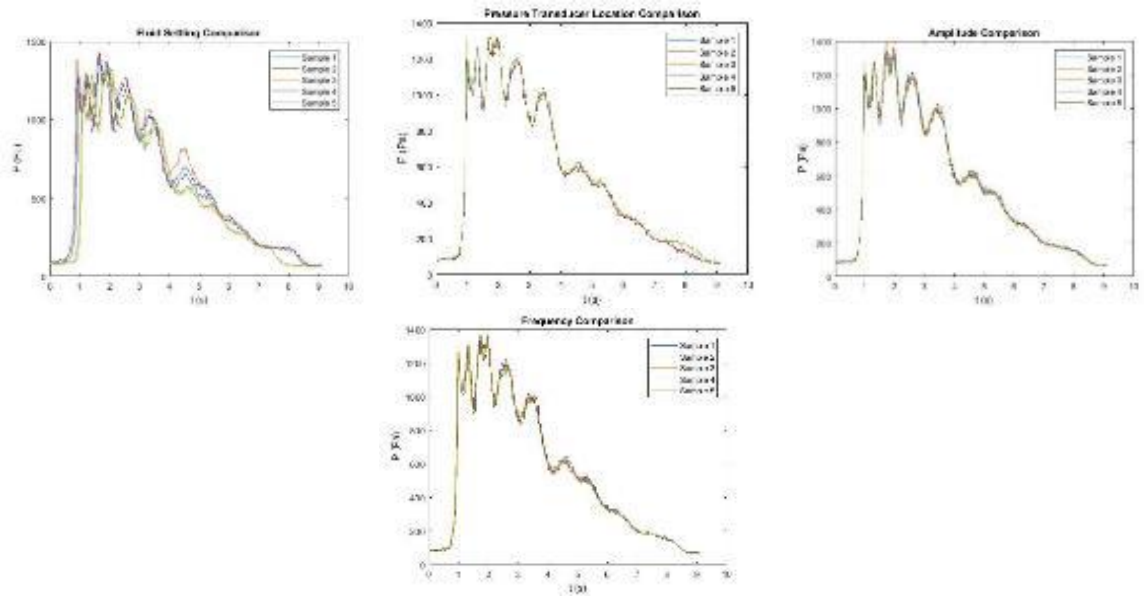


Figure 39.69. Average pressure comparison plots for each investigated parameter.

Based on the plots above, all seven parameters influence the simulation results. However, some of these parameters seem to be more important based on the amount of fluctuation that occurred between the results. For example, the particle size, interaction-radius to particle-size ratio, and fluid settling plots showed greater fluctuation than the stop threshold, amplitude, frequency, and pressure transducer location plots. This indicates that more research is needed to quantify the significance of each parameter.

## 7.14. Conclusions

A large-scale oscillating tank experiment was conducted and then used to validate the SPH code Neutrino, as well as determine parameters that affect the simulation results. The 90% and 50% end-wall pressure bounds were compared, as was the pressure impulse. The simulation bounds fell mostly within the experimental bounds, with exceptions at the beginning of the cycle (~40% difference), at peak pressure (~75% difference), and at the end of the cycle (~40% difference). The simulation pressure impulse matched the experiments well and was within 10%. Additionally, seven parameters were identified and investigated to determine their significance. All seven parameters were identified as significant. However, the particle size, interaction-radius to particle-size ratio, and fluid settling seem to have a greater effect due to larger fluctuation in their results.

The next step is to quantify the significance of each parameter. Once this is done, those parameters that have the greatest effect on the simulation results can be optimized. The optimization goal would be to increase the accuracy of the simulation results while still accounting for the computational runtime of the simulation. This optimization will also depend on the scenario and a valid parameter range vs result criteria needs to be established.

## 7.15. Lessons Learned and Revision of Methodology

### 7.15.1. Issues and Challenges

First, one challenge of SPH validation is to define validation goals and requirements for all involved phenomena, processes, and components from the perspective of risk analysis. In this chapter, for clarification, the validation goals of each numerical benchmark are defined by accuracy and calculated by

validation or error metrics. Furthermore, they are assumed to be the same for all involved phenomena. However, for RISMC applications, the requirement on model accuracy is subject to change given uncertain scenarios. For scenarios where facilities have enormous safety margins, the tolerance for simulation uncertainties can be much larger than scenarios that have the fragile equipment. In addition, for scenarios that have risks with severe consequences, the requirement on model credibility will be more stringent than scenarios that have slight effects. Second, for complex scenarios with multiple phenomena, processes, and components, the requirements on model accuracy in simulating each separate effect should be inferred rigorously according to the requirements for integral behaviors. In CSAU and EMDAP framework, none of such connection has been explicitly discussed. Besides, the subjective components of model credibility in nuclear safety-related applications cannot be ignored when external hazards are analyzed, and the uncertainties are significant. To be specific, the subjective component is mainly introduced by two aspects: scaling analysis and physical pattern recognition. The first aspect mainly depends on the similarity (sufficiency, relevancy, and distortion) of the validation database to prototypic conditions. The second aspect depends on the understanding of all involving physics and their interactions. Both aspects require subjective assessments and their criteria for success depend on the subjective confidence level. With the same validation goal, scenarios with complex physics require higher confidence in the scaling analysis and physical pattern recognition than those with simple phenomena, such that the model can be used for full-scale applications. However, neither CSAU or EMDAP has formalized or explicitly discussed such situations.

Second, there is no framework or procedure in the previous validation that formalizes the decision-making process for validation adequacy. Although **Error! Reference source not found.** shows a schematic structure with all inputs, detailed information, like relative importance, dependency, acceptance criterion, etc., are not explicitly discussed. At the same time, due to a lack of data from integral facilities under prototypic conditions, adequacy of simulation models must be decided according to their performances in predicting data from separate phenomena and reduce-scale facilities. Considering the complexity of scenarios and the multitude of evidence, human assessments can be heuristic and obscure. As a result, to remain convincing, the adequacy decision-making process needs to be formalized and represented transparently. At the same time, the formalization needs to be consistent and robust, such that the decision-making process can be defendable and satisfactory across a wide range of plausible situations. Besides, for scenarios that evidence has not been exhaustively collected, the formalized decision-making process should be theoretically improvable when new knowledge and data become available.

Third, SPH methods are found to be insufficient in predicting various high-rank phenomena. Although an “excellent” performance is desirable for every phenomenon, it can hardly be achieved for SPH methods based on the previous assessments. When an insufficient performance is found for high-rank phenomena, SPH methods can still be considered adequate despite the deficiency if (1) the phenomenon can subsequently be demonstrated to not have the dominant influence on the course of the application or (2) an appropriate method can be demonstrated for quantifying the calculational uncertainty resulting from the deficiency, and the uncertainty is acceptable. The database in this study is not sufficient for verifying the PIRT, efforts are devoted to the uncertainty quantification of SPH methods. Regular UQ methods require separations of total uncertainty with respect to sources and properties and assumes that each source is scale invariant. However, all sources of uncertainties, including discretization errors, simulation errors, model form errors, and input errors, are tightly coupled, and characterizing each of them by independent error distributions is difficult. Besides, it is found that the simulation error of SPH methods depends on the characteristics of scales. Moreover, the uncertainties of situations, where the regular UQ methods apply, are much smaller than those of external-hazards scenarios. Therefore, new UQ methodologies are needed for estimating total simulation uncertainties under large uncertainties. At the same time, the new methodologies are expected to propagate (interpolate and extrapolate) the uncertainties from reduce-scales to full-scale conditions.

### 7.15.2. RISMC Model Validation Framework

Since the objective of this study is to assess the credibility of NEUTRINO and to improve the EMDAP framework. New methodologies discussed in this chapter are incorporated into the EMDAP framework for (1) Identifying credibility requirements in validation process; (2) formalizing the decision-making process in the validation process (3) quantifying the uncertainty of SPH simulations in a transparent, consistent, and robust manner. Figure  shows a schematic flowchart for the improved EMDAP framework. The solid blocks (Elements #1 - #4) are inherited from the EMDAP framework, meanwhile, new components in bold fonts, including sufficient accuracy, data-driven validation, and PCMQBN are developed and included. The dashed blocks are defined with respect to their scopes and requirements.

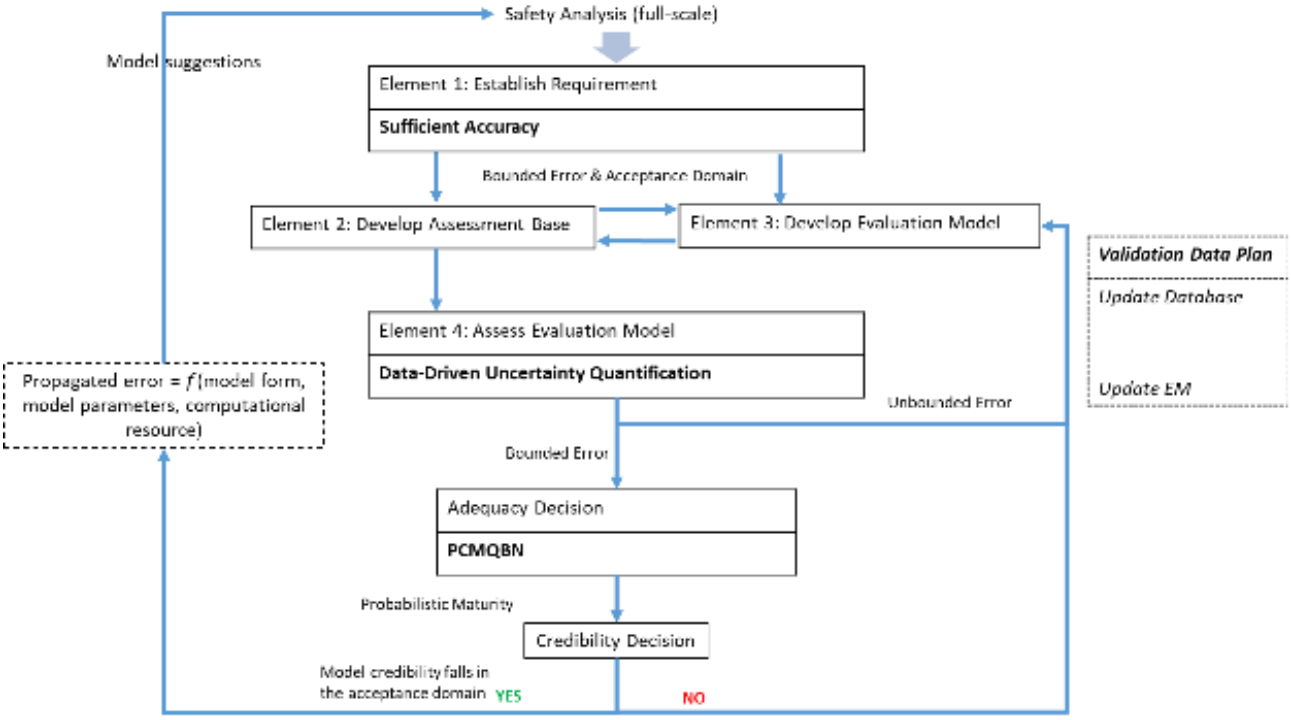


Figure 7.70. A schematic flowchart of the improved EMDAP framework. The solid blocks are mainly inherited from the well-established EMDAP framework, and three of them have been improved with new methodologies (in bold font). The definitions and case studies of bold methodologies have been demonstrated in this study. The scopes and requirements of dash blocks have been defined for the dashed blocks.

### 7.15.3. Revised Blocks

The concept of sufficient accuracy is applied to Element 1. The validation goal, represented by maturity level and corresponding subjective beliefs, is determined according to the safety goal, where a critical belief and a range of acceptance domain for model credibility are identified. The transparency and consistency of this process is ensured by formalized procedures and mathematical derivations. At the same time, by admitting the subjective nature of validation and introducing qualitative validation goal, the robustness of this process is ensured by achieving a designated level of "credibility" across the validations and assumptions that are consistent with known facts. The PCMQBN is applied to the element for adequacy decision. The validation decision-making process is first defined as an argument process. Next, aiming at three components (evidence, structure, and acceptance criterion) of the validation arguments, PCMQBN

further represents the argument process with Bayesian Decision theory: the evidence is characterized according to the concept of sufficient accuracy; the argument structure is constructed according to the validation cubic model; and the acceptance criterion is made according to the sufficient-accuracy-guided validation goal. Again, the transparency and consistency are ensured with formalized procedures and mathematical representations. The robustness is ensured by a formalized Bayesian sensitivity analysis, also known as Robust Bayes. The Data-Driven Uncertainty Quantification is applied to Element 4. The uncertainty of SPH simulations are quantified with techniques of PEML, where a surrogate model is constructed between the local physical features and simulation uncertainties. Presently, Random Forest is used as the major algorithm for constructing the surrogate model. Meanwhile, the capabilities of constructed PEML are tested for both the interpolated and extrapolated scenarios. The transparency is ensured by the opensource simulation engines and the open-access validation data management system. Meanwhile, the consistency is ensured by treating the surrogate model as a fast data extraction from high-fidelity database. The robustness is mainly ensured by the reliability and robustness of modern machine learning algorithms.

Validation Data Plan (VDP) is “a dynamic planning instrument to guide, and potentially optimize activities on data production and acquisition, data analysis and management, and data usage so that they enable effective support for development, assessment and application of simulation tools intended for challenge problem”. In the flowchart of Figure 7.70, VDP refers to a decision model that (1) integrates information from all related validation activities, and (2) prioritizes data activities, based on cost-benefit analysis of possible activities. In this study, the cost-benefit analysis is performed based on the value of information theory, and a decision tree is used for calculating the expected value of sample information (EVSI). The EVSI refers to the expected increase in utility or monetary value that a decision-maker could obtain from gaining access to a sample of additional observations before making decision. A synthetic example is prepared for demonstrating the procedure of calculating EVSI according to the adequacy maturity from PCMQBN and a “postulated” new model. For the vent overflow model that has been discussed in previous milestone (M2NU-16-NC-NCSU-030401-153), it is assumed that a postulated model is designed such that the maturity level of validation result is improved as in Figure .


Figure 7.71. Demonstration of maturity and code adequacy improvement by a "postulated" model.

It is further assumed that the chance of getting such an improvement is 40%, and there is 60% chance that a model as bad as the SET-Calibrate model is obtained. A decision tree, shown in Figure , can be built for determining the expected increase in monetary value by having an improved model rather than having the TDMI-calibrated model. In this scenario, the expected value is found to be negative, and it indicates that the efforts devoted to the development of such new model are more than those being already obtained. Therefore, the VDP for such a model is not preferred.

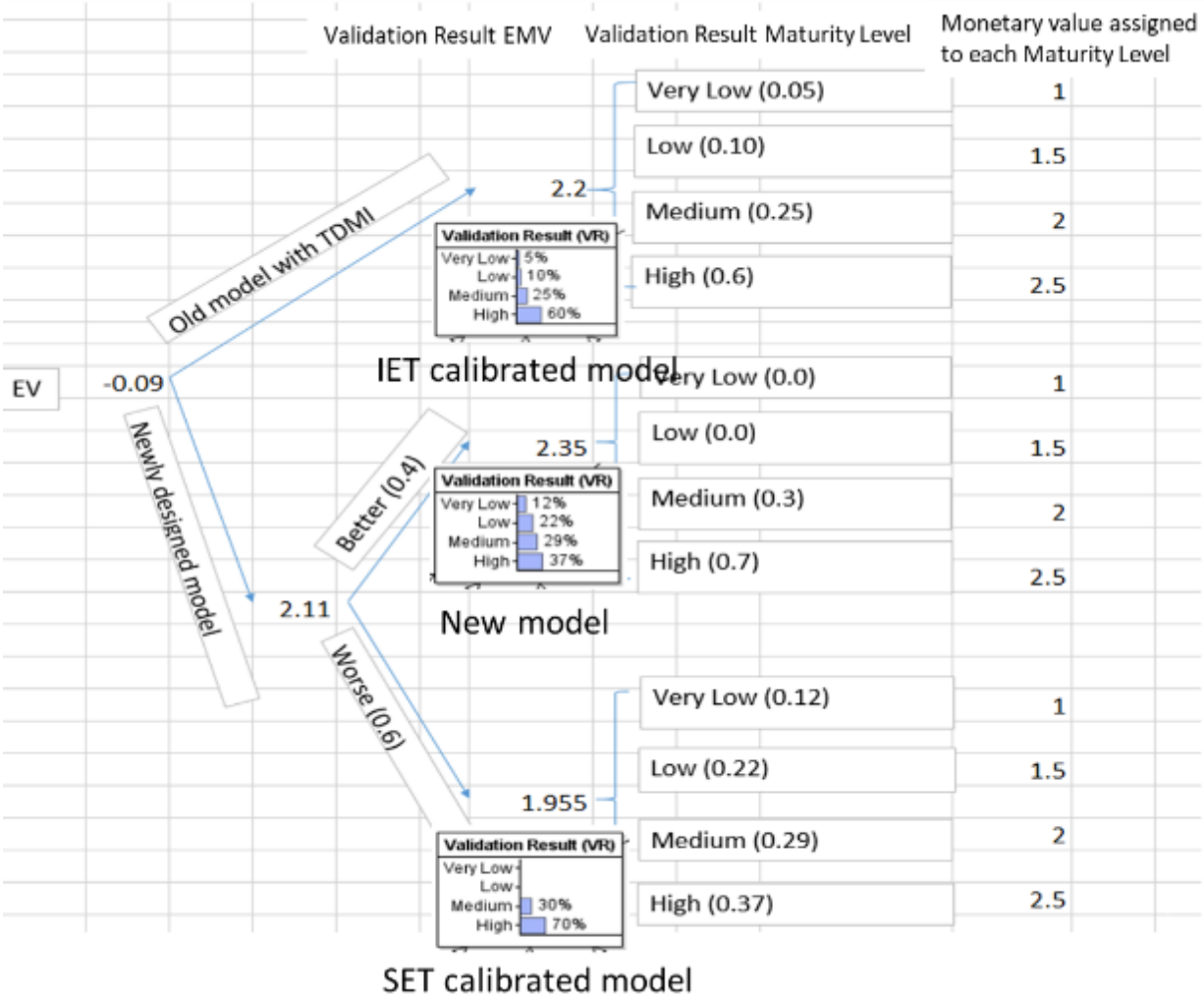


Figure 7.72. Decision tree for calculating the expected increase in the monetary values by having a postulated new model rather than having the IET-calibrated model.

Another block being developed is the error propagation, where the simulation uncertainty will be propagated from validation to application scenarios. Data-driven methods are used to construct a correlation between local physical features and simulation uncertainties. Detailed works can be found in the previous milestone (M2NU-16-NC-NCSU-030401-153). Since the biggest challenge of such propagation comes from the scaling analysis, such error propagation is also named as uncertainty scaling. The objective is to (1) characterize the applicability of reduce-scale validation to full-scale application. (2) construct a mathematical relationship between the simulation error and the characterized applicability. In previous section, a qualitative relationship has been constructed between the PEML corrected simulation error and the dimensionless number. An initial study has been performed for constructing a mathematical relationship between the simulation uncertainty and the similarity index. Presently, for the case study of lid-driven cavity, similarity indexes refer to the Reynolds ratio and symmetric Kullback-Leibler Divergence, and their goal is to identify the similarity of training and testing scenarios. The Reynold ratio is estimated by the ratio of $Re_\tau$, while the symmetric Kullback-Leibler Divergence is estimated by probability distributions of local physical features. In this study, the Reynold ratio $r^*$is defined in Eq. 7.19, while the symmetric Kullback-Leibler Divergence $D_{KL}$ is defined in Eq. 7.21.

$$r^* = Re_{target}/\overline{Re}_{training} \qquad \text{Eq. 7.19}$$

$$\overline{Re}_{training} = \sum_{i}^{n} Re_i \,/n \qquad \text{Eq. 7.20}$$

$$D_{KL}(P,Q) = \sum_{i} P(i) \log\left(\frac{P(i)}{Q(i)}\right) + Q(i) \log\left(\frac{Q(i)}{P(i)}\right) \qquad \text{Eq. 7.21}$$

$$P(i) = \frac{1}{N h_1 h_2 \dots h_d} \sum_{i=1}^{N} \prod_{j=1}^{d} k\left(\frac{x_j - y_{ij}}{h_j}\right) \qquad \text{Eq. 7.22}$$

where $Re_{target}$ is the Reynolds number of the target scenario; $\overline{Re}_{training}$ is the average Reynolds number of the training scenarios calculated by Eq. 7.20; $P(i)$ and $Q(i)$ are the probability density distribution of physical features $y$ approximated by multivariate kernel distributions; $k(\cdot)$ is the one-dimensional kernel smoothing function; $x$ is the d-dimensional random vector for the physical features. $N$ is the number of samples drawn from each group of physical features. 7.73 shows the plot of L2 relative error norm for the corrected velocity field against the Reynolds ratio $r^*$ and symmetric K-L Divergence $D_{KL}$ when the target scenario has $Re_{target} = 10000$. However, no strong mathematical correlation has been found between the suggested representation of similarity and the PEML performance.

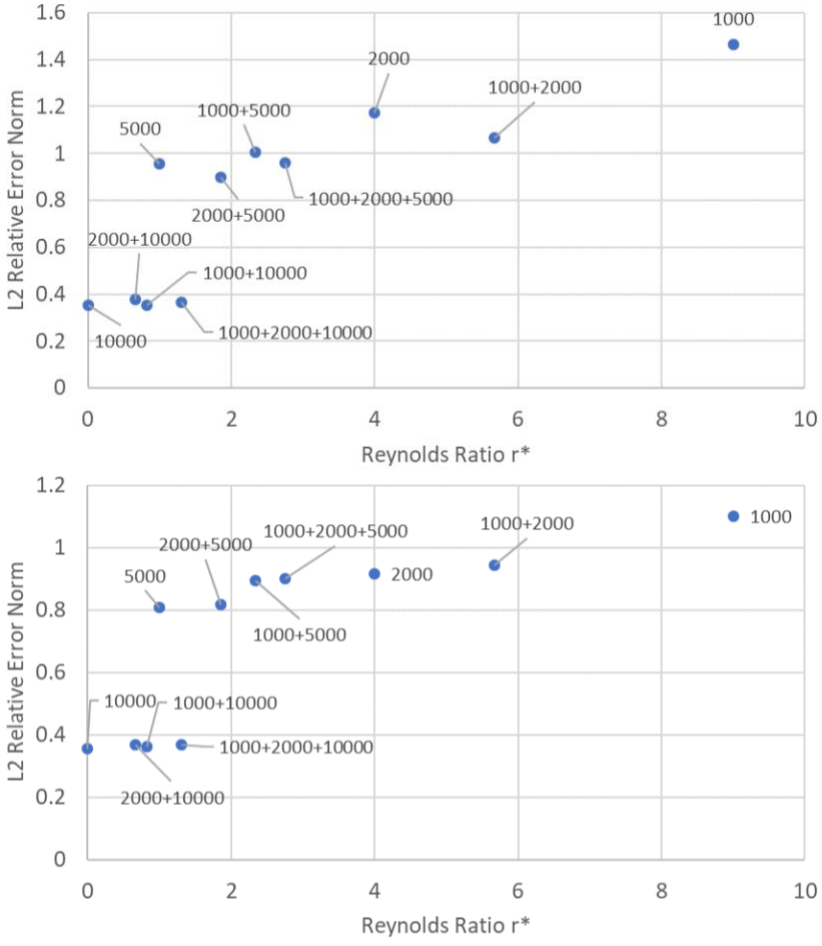


(a) L2 relative error norm versus Reynold ratio $r^*$ for x (upper) and y (lower) directions' velocity field

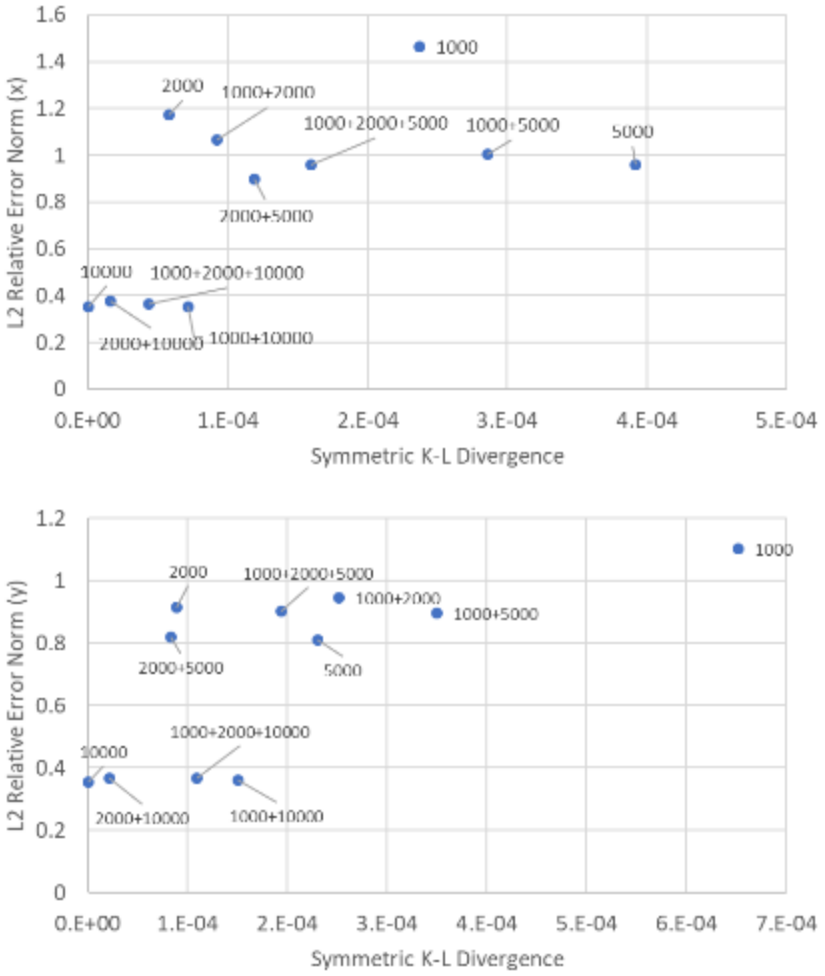


(b) L2 relative error norm versus symmetric K-L Divergence of all physical features for x (upper) and y (lower) directions' velocity field.

Figure 7.73. Plot of NMSE for the corrected low-fidelity simulation against the Reynolds ratio $r^*$ and K-L Divergence when the target scenario has $Re_{target} = 10000$.

## 7.16. References


Gingold RA, Monaghan JJ (1977) Smoothed particle hydrodynamics: theory and application to non-spherical stars. Mon Not R Astron Soc 181:375–389

Ihmsen M, Orthmann J, Solenthaler B, Kolb A, Teschner M. (2014) SPH fluids in computer graphics.

Zhang, A-man, et al. "Smoothed particle hydrodynamics and its applications in fluid-structure interactions." Journal of Hydrodynamics, Ser. B 29.2 (2017): 187-216.

Shadloo, M. S., G. Oger, and D. Le Touzé. "Smoothed particle hydrodynamics method for fluid flows, towards industrial applications: Motivations, current state, and challenges." *Computers & Fluids* 136 (2016): 11-34.

Violeau, Damien, and Benedict D. Rogers. "Smoothed particle hydrodynamics (SPH) for free-surface flows: past, present and future." *Journal of Hydraulic Research* 54.1 (2016): 1-26.

Liu, Mou-Bin, and Shang-ming Li. "On the modeling of viscous incompressible flows with smoothed particle hydrodynamics." *Journal of Hydrodynamics* 28.5 (2016): 731-745.

Monaghan, J. J. "Smoothed particle hydrodynamics and its diverse applications." *Annual Review of Fluid Mechanics* 44 (2012): 323-346.
Gotoh, Hitoshi, and Abbas Khayyer. "Current achievements and future perspectives for projection-based particle methods with applications in ocean engineering." *Journal of Ocean Engineering and Marine Energy* 2.3 (2016): 251-278.
Sampath, Ramprasad, et al. "Large-scale solitary wave simulation with implicit incompressible SPH." *Journal of Ocean Engineering and Marine Energy* 2.3 (2016): 313-329.
Ibrahim, Raouf A. *Liquid sloshing dynamics: theory and applications*. Cambridge University Press, 2005.
Peregrine, D. H. "Water-wave impact on walls." Annual review of fluid mechanics 35, no. 1 (2003): 23-43.
Di Mascio, A., Antuono, M., Colagrossi, A., & Marrone, S. (2017). Smoothed particle hydrodynamics method from a large eddy simulation perspective. *Physics of Fluids, 29*(3).

Gartner, N., Montanari, N., Richier, M., Hugel, V., & Sampath, R. (2019). Towards real-time simulation of physically realistic pressure applied to submerged bodies using explicit and semi-implicit SPH algorithms. *OCEANS.* Marseille, France.

Montanari, N., Sampath, R., Calhoun, D., Prescott, S., & Smith, C. (2018). Coupling large-scale and detailed site flooding simulations. *Probablistic Safety Assessment and Management.* Los Angeles, CA, USA.

# 8. Adequacy Evaluation of Smoothed Particle Hydrodynamics Methods for Simulating the External-Flooding Scenario

## 8.1. Summary

In modern nuclear risk analysis for external-flooding scenarios, Computational Fluid Dynamics (CFD) tools are used to simulate the generation, propagation, and interactions of Nuclear Power Plants (NPPs) with the nuclear Systems, Structures, and Components (SSCs). Smoothed Particle Hydrodynamics (SPH), as a Lagrangian and mesh-free method, is one of the particle-based CFD methods. Since SPH methods can effectively handling large-scale fluid simulations with complex interfacial structures, SPH-based software has been used to simulate the impacts of external flood onto nuclear facilities, and the simulation results have been used to support nuclear safety analysis. However, previous risk analysis assumes that SPH methods and the corresponding simulation packages are applicable to the external-hazards risk analysis, and their simulation uncertainties do not affect the confidence of safety decision. Considering the high consequences to nuclear safety induced by simulation errors, a systematic and complete validation process is needed to evaluate the adequacy of SPH simulations in informing related safety decisions.

In this study, a scoping-stage assessment is performed for SPH's adequacy in simulating the real-scale external flooding scenarios, especially in predicting the surface-wave impacts on SSCs at NPP sites. To ensure the completeness and consistency, validation frameworks, Code Scalability Applicability and Uncertainty (CSAU), and its regulatory guide, Evaluation Model Development and Assessment Process (EMDAP) are followed to guide validation activities and to make final code adequacy assessment. First, an external-flooding scenario is designed, and SPH simulations are performed with an SPH-based software named Neutrino. A Phenomenon Identification and Ranking Table (PIRT) is created, and the surface-wave impacts are identified as one of the high-rank phenomena. At the same time, a performance measurement standard is created for measuring the code adequacy in informing safety decisions consistently and transparently. At the scoping stage, these criteria are selected based on authors' knowledge and reviewed by researchers in related fields. Next, numerical benchmarks are designed for assessing the code adequacy of SPH methods and corresponding software implementations on Neutrino. Next, code accuracy is evaluated by comparing simulation results from Neutrino against experimental measurements in each benchmark. Meanwhile, a scaling analysis is performed to determine a group of dimensionless number for characterizing important physics and to assess the applicability of validation database collected in reduced-scale facility to the prototypic scenario. Finally, results from all activities are brought together to make an adequacy decision. It is found that, based on the current evidence, SPH methods and associated Neutrino software can predict the unbroken surface-wave peak pressure onto stationary rigid with reasonable accuracy if the suggested sizes of particles are used. However, the available evidence is not sufficient to support the decisions of SPH's adequacy in predicting impacts force on dynamic rigid.

## 8.2. Introduction

Since the Fukushima accident and other site flooding events in the United States, the risk of NPP due to external flooding has drawn attention from both regulatory and research departments. Responding to the concerns of NPP safety due to external flooding, U.S. Nuclear Regulatory Commission (NRC) has developed recommendations for further regulatory actions in the seismic and flooding designs, and emergency preparations. In addition, U.S. NRC also requests a flooding reevaluation at NPP sites from power reactor licensees and holders of construction permits. One task of the Risk-Informed Safety Margin Characterization (RISMC) methodology is to develop methods for systematically analyzing the risk and accurately determining the safety margins. In RISMC, advanced simulations are used for capturing the propagation and impact of hazards on NPPs. Meanwhile, validation frameworks, including Code Scalability, Applicability, and Uncertainty (CSAU) and Evaluation Model Development and Assessment

Process (EMDAP), are needed for assessing the adequacy of selected simulation methods and tools in simulating high-ranked phenomena.

Researches on the RISMC methodology were formulated as a pathway in the U.S. Department of Energy's Light Water Reactor Sustainability program in 2008 (Hess, Dinh, Gaertner, & Szilard, Risk-informed safety margin characterization, 2008), and its application scope has covered a wide range of issues in nuclear safety analysis and risk management [2] [3] [4]. RISMC has also been conducting research and development for advanced methods and tools to support NPP safety assessments and management. Within an identified issue space, RISMC analyzes the system's Quantities of Interest (QoIs) and the corresponding safety margins probabilistically, where a broader range and type of uncertainties are considered. Considering the complexity of external flooding, advanced simulation tools are needed for a comprehensive analysis of scenario progressions. Because the RISMC approach explicitly couples probabilistic approaches (the "scenarios") with phenomenological representations (the "physics") through a modeling-and-simulation-based approach, it is ideally suited to serve as a framework to address the interactions of external hazards on NPPs and their potential impacts on the NPP safety.

In previous works [4], RISMC has been applied to analyze the risk induced by flooding hazards, and an SPH-based CFD tool named Neutrino is used for simulating the generation, propagation, and interaction of floods with NPP sites. Next, based on the information from Neutrino, the system code can predict the thermal-hydraulic status inside the reactor core. Next, the scenario-based and risk-informed safety margin can be obtained for the reactor and facilities using the statistical analysis. Though Neutrino has shown great capability in performing large-scale fluid simulations [5], due to the complexity of involving physics and phenomena, the simulation's adequacy remains unknown. Although SPH, with sufficiently refined particles, can be used to perform Direct Numerical Simulation (DNS), the computational cost is too high to be practical in the RISMC analysis. As a result, a comprehensive validation is still needed to accurately characterize the adequacy of SPH simulations. Meanwhile, it is also necessary to consider the simulation efficiency as another important code adequacy criterion.

The Code Scaling, Applicability, and Uncertainty (CSAU) evaluation methodology was introduced in 1989 [6] to accommodate the revised rule on the acceptance of the Emergency Core Cooling System (ECCS). The objective is to demonstrate a method that "can be used to quantify uncertainties as required by the best-estimate option described in the NRC's 1988 revision to the ECCS Rule (10 CFR 50.46) [6]". Evaluation Model Development and Assessment Process (EMDAP) is a regulatory guide developed by U.S. NRC based on CSAU methodology [7]. The objective is to describe an acceptable process of developing and assessing the evaluation models that are used to analyze transient and accident behavior within the design basis of a nuclear power plant. The CSAU/EMDAP framework is mainly composed by five activities:

- Identify the importance and adequacy of mathematical model, code and data for all related systems, components, processes, and phenomena;
- Establish standards against which code models and adequacy can be measured;
- Construct code-assessment case studies and database;
- Perform code assessment by comparing the code results against the standards;
- Perform scaling analysis for database in terms of their relevance and sufficiency for the intended application.

After the implementation of all activities, an adequacy decision will be made, and suggestions on model forms and parameters are provided. Next, the simulation code will be "frozen" and applied to the accident scenario for reactor transient and risk analysis. CSAU/EMDAP framework has been successfully applied to assess the adequacy of RELAP-5 simulation code for the Small Break Loss-of-Coolant Accidents of AP600 [8]. In this study, CSAU/EMDAP framework will be followed for the systematic and consistent assessment of SPH methods and the corresponding software Neutrino.

### 8.3. Smoothed Particle Hydrodynamics

In 1977, SPH was first invented to deal with astrophysical problems in three-dimensional open space [9], and it is found that the collective movement of particles can be used to represents the fluid flow. Since then, SPH has advanced tremendously in hydraulics with a large amount of work being performed both theoretically and computationally. Though mesh-based methods are still the dominant tools for multi-phase simulations, SPH has built its fidelity in simulating fluid problems with complex and irregular interfaces [10]. Recently, SPH has grown popular and become an essential part of the numerical arsenal of several industrial and laboratory institutions, and its capability has been assessed for high-wind [11], micro-boiling [12], etc. For RISMC analysis of flooding hazards, as a Lagrangian method, SPH can predict the particle motion through space and time with no requirement for any underlying mesh. This brings some key advantages with SPH in the field of long surface-wave production and development [13] [14], sloshing [5], floating objects [15] [16], surface-wave impacts and interacting force estimate [17] [18], which is perfectly suitable for the RISMC simulation in flooding scenarios. In general, the success of SPH in these fields relies on its capabilities in simulating scenarios with nonlinear and multi-scale phenomena. In addition, as suggested by D. Violeau and B.D. Rogers, [19]: "SPH has been able to generate results in close agreement with reference solutions/data in validation tests, without highly sophisticated algorithms required in mesh-based schemes." Since SPH is likely to provide more promising futures in complex free-surface and very large-scale flow simulation than mesh-based methods, it is selected as the major simulation tool for RISMC analysis in flooding.

In SPH, the elements are represented as particles, while the physical properties are distributed and smoothed across a spatial distance (smoothing length) by certain rules (e.g., kernel function). Therefore, the physical quantities of any particle can be obtained by summing the relevant properties of all the particles lying within the range of kernel. In SPH, the summing of property or function $f$ is governed by:

$$f(\vec{r}) \cong \int f(\vec{r}')W(\vec{r}-\vec{r}',h)d\vec{r}' \quad \text{Eq. 8.23}$$

where $h$ is the smoothing length; $W(\vec{r}-\vec{r}',h)$ is the kernel function. The kernel function assigns weights to discretized properties $f(\vec{r}')$ at different locations $\vec{r}'$ and takes an interval in its supporting length $h$. The objective is to approximate the real function values at location $\vec{r}$. It is argued that when the kernel function becomes a Dirac delta function, the left-hand side and right-hand side of Eq. 8.23 will be equal. The smoothing function $W$ has a finite range of $\kappa h$, where $\kappa$ is a constant that defines the support domain of the smoothing function. In general, the properties of the weight function can be summarized as:

$$\int W(\vec{r}-\vec{r}',h)d\vec{r}' = 1 \quad \text{Eq. 8.24}$$

$$\lim_{h\to 0} W(\vec{r}-\vec{r}',h) = \delta(\vec{r}-\vec{r}') \quad \text{Eq. 8.25}$$

$$W(\vec{r}-\vec{r}',h) = 0 \; when \; |\vec{r}-\vec{r}'| > \kappa h \quad \text{Eq. 8.26}$$

Regarding the properties of kernel functions, Eq. 8.24 represents the normalization property, Eq. 8.25 represents the Dirac delta function property, and Eq. 8.26 represents the compact condition. If the equation is further approximated with particles, which means to represent the problem domain with a set of particles and estimate the field variables based on these particles, Eq. 8.23 becomes Eq. 8.27:

$$f(\vec{r}) \cong \sum_b f(\vec{r}_b)W(\vec{r}-\vec{r}_b,h)\,\Delta V_b \quad \text{Eq. 8.27}$$

where b represents any discrete region within the affecting region. If each discrete region has mass, which can be represented as $\rho dV$, the equation will then be written as:

$$f(\vec{r_a}) \cong \sum_b \frac{m_b}{\rho_b} f(\vec{r}_b) W(\vec{r}_a - \vec{r}_b, h) \quad \text{Eq. 8.28}$$

$m_b$ and $\rho_b$ represents the mass and density of each particle. Eq. 8.28 is usually referred as "summation interpolation", which is the basis of all SPH formalisms. Since mass and density are introduced during the particle approximation, it makes SPH very suitable for hydrodynamic problems where mass need to be conserved, like multiphase flow. Similar technique can also be applied for approximating the divergence $\nabla \cdot f(\vec{r})$ and gradient $\nabla f(\vec{r})$.

$$\nabla f(\vec{r}) \cong \rho \sum_b m_b [\left(\frac{f(\vec{r}_b)}{\rho_b^2}\right) + (\frac{f(\vec{r})}{\rho^2})] \cdot \nabla W(\vec{r} - \vec{r}_b, h) \quad \text{Eq. 8.29}$$

$$\nabla \cdot f(\vec{r}) \cong -\frac{1}{\rho} \sum_b m_b (f - f_b) \cdot \nabla W(\vec{r} - \vec{r}_b, h) \quad \text{Eq. 8.30}$$

In this work, the cubic B-spline kernel function, as shown in equation Eq. 8.31, is applied, with $q = r/h$.

$$W(r) = \frac{1}{\pi h^3} \begin{cases} 1 - \frac{3}{2}q^2 + \frac{3}{4}q^3, & 0 \le q \le 1 \\ \frac{1}{4}(2-q)^3, & 1 < q \le 2 \\ 0, & 2 < q \end{cases} \quad \text{Eq. 8.31}$$

### 8.4. IISPH Discretization of the Navier-Stokes Equations

In this study, a single-phase, isothermal, incompressible and Newtonian fluid flow is considered, and an Implicit Incompressible Smoothed Particle Hydrodynamic (IISPH) algorithm is used to solve the governing fluid equations. Meanwhile, the viscosity is assumed to be constant in space, and the surface tension forces are ignored. The Navier-Stokes equations can be written as

$$\frac{d\vec{v}}{dt} = -\frac{1}{\rho}\nabla p + \upsilon \nabla^2 \vec{v} + \vec{g} \quad \text{Eq. 8.32}$$

$$\frac{d\rho}{dt} = -\rho \nabla \cdot \vec{v} \quad \text{Eq. 8.33}$$

where $\vec{v}$, $p$, $\upsilon$, $\vec{g}$ represent velocity, pressure, kinetic viscosity, and gravitational acceleration respectively. $d/dt = \partial/\partial t + \vec{v} \cdot \nabla$ is the Lagrangian derivative. At the preliminary step, the density of all SPH particles are calculated based on Eq. 8.34.

$$\rho_a(t) = \sum_b m_b W_{ab}(t) \quad \text{Eq. 8.34}$$

where $t$ represents the time, $a$ represents the target particle, $b$ represent the surrounding particles, $W_{ab}$ is the kernel function values calculated based on the distance between each pair of particles $a$ and $b$. Eq. 8.34 is also a SPH discretization of the continuity equation (Eq. 8.33) with exact time integrations. The pressure-velocity coupling is solved by splitting the momentum equation Eq. 8.32 into two steps:

(1) The intermediate velocity $\vec{v}_a^*$ is calculated by solving momentum equation without pressure term. The Monaghan artificial viscosity formulation [20] is used for particle discretization, while the explicit Euler scheme is used for time integrations.

$$\vec{v}_a^* = \vec{v}_a(t) + \Delta t(-\sum_b m_b \Pi_{ab} \nabla W_{ab}(t) + \vec{g}) \quad \text{Eq. 8.35}$$

$$\Pi_{ab} = -\upsilon \frac{\min(\left(\vec{v}_a(t) - \vec{v}_b(t)\right) \cdot \left(\vec{x}_a(t) - \vec{x}_b(t)\right), 0)}{|\vec{x}_a(t) - \vec{x}_a(t)|^2 + 0.01h^2} \quad \text{Eq. 8.36}$$

where $\upsilon$ is the viscous factor that equals to $^{2\alpha h}/_{\rho_a(t) + \rho_b(t)}$, $\alpha$ is the artificial viscosity coefficient. Next, the intermediate densities are computed with Eq. 8.33 and the implicit Euler scheme:

$$\rho_a^* = \rho_a(t) + \Delta t \sum_b m_b(\vec{v}_a^* - \vec{v}_b^*) \nabla W_{ab}(t) \quad \text{Eq. 8.37}$$

(2) The momentum equation is calculated with only the pressure term, while it is combined with the mass equation to ensure the incompressibility condition $^{d\rho}/_{dt} = 0$. The Poisson equation is used to solve the pressures $p_a$:

$$\nabla^2 p_a(t) = \frac{\rho_0 - \rho_a^*}{\Delta t^2} \quad \text{Eq. 8.38}$$

More details of solving the Poisson equation can be found in [5] [21]. At last, the new velocity and position are computed with Euler-Cromer scheme for the time integration:

$$\vec{v}_a(t + \Delta t) = \vec{v}_a^* + \Delta t \sum_b m_b (\frac{p_a(t)}{\rho_a(t)^2} + \frac{p_b(t)}{\rho_b(t)^2}) \nabla W_{ab}(t) \quad \text{Eq. 8.39}$$

$$\vec{x}_a(t + \Delta t) = \vec{x}_a(t) + \Delta t \vec{v}_a(t + \Delta t) \quad \text{Eq. 8.40}$$

The time step $\Delta t$ is updated based on the Courant-Friedrichs-Lewy (CFL) condition $\Delta t_{CFL}$ and an empirical correlation for $\Delta t_{max}$, which is designed to avoid unreasonable numbers of iterations in the pressure solver:

$$\Delta t = \min(\Delta t_{CFL}, \Delta t_{max}) \quad \text{Eq. 8.41}$$

$$\Delta t_{CFL} = \min\left(\frac{\lambda_{CFL} h}{|\vec{v}_{max}|}, \sqrt{\frac{\lambda_{CFL} h}{|\vec{g}|}}\right)$$

$$\Delta t_{max} = \frac{\lambda_{max} h}{|\vec{g}|}$$

where $\lambda_{CFL}$ is the CFL coefficient, $\lambda_{max}$ is a coefficient for $\Delta t_{max}$, and $\vec{v}_{max}$ is the maximum velocity for all particles. The calculation of particle properties depends on properties of neighboring particles, and a

neighborhood searching algorithm is constructed in Neutrino with a combination of compact hashing and Z-curve index sorting. More details can be found in [5].

At the boundaries, the kernel support domain of fluid particles can be insufficiently sampled, and it leads to an underestimation of densities. As a result, the neighboring boundary particles are also taken into account when densities and forces are calculated for fluid particles. The surface of rigid objects is sampled by a single layer of boundary particles, and they are implemented based on the directly analytical shapes or the mesh of rigid objects [22]. The spacing of the boundary particle is, wherever possible, enforced equal to the rest particle distances of fluid particles. To avoid density peaks because of the boundary-particle oversampling, a relative contribution factor $\Psi_s$ for boundary particles $s$ is calculated as:

$$\Psi_s = \frac{\rho_0}{\sum_k W_{sk}(t)} \quad \text{Eq. 8.42}$$

where $k$ represents boundary particle neighbors. The boundary particles contribute to the densities of fluid particles $a$ as:

$$\rho_a(t) = \sum_b m_b W_{ab}(t) + \sum_s \Psi_s W_{as}(t) \quad \text{Eq. 8.43}$$

Two wall boundary conditions are imposed, constraining the velocity and pressure fields: a partial-slip condition and a homogeneous Neumann boundary condition, ${\partial p}/{\partial \vec{n}} = 0$, with $\vec{n}$ as the unit vector normal to the boundary. As a result, the pressure force $\vec{F}^p_{a\leftarrow s}$ and friction force $\vec{F}^v_{a\leftarrow s}$ applied from a boundary particle $s$ to a fluid particle $a$ are expressed as:

$$\vec{F}^p_{a\leftarrow s} = -m_a \Psi_s \frac{p_i(t)}{\rho_i(t)} \nabla W_{as}(t) \quad \text{Eq. 8.44}$$

$$\vec{F}^v_{a\leftarrow s} == -m_a \Psi_s \Pi_{ab} \nabla W_{as}(t) \quad \text{Eq. 8.45}$$

where $\Pi_{ab}$ is calculated by Eq. 8.36 with a reformulated viscous factor $v = {\sigma h}/{2\rho_a(t)}$. $\sigma$ is the fluid-solid coefficient, which is tuned for each solid surface to impose a partial-slip condition and account for different levels of rugosity, similarly as the Manning coefficient. Moreover, incorporating the fluid-rigid boundary handling requires modifications for solving the intermediate velocity $\vec{v}^*_a$ and density $\rho^*_a$:

$$\vec{v}^*_a = \vec{v}_a(t) + \Delta t(-\sum_b m_b \Pi_{ab} \nabla W_{ab}(t) - \sum_s \Psi_s \Pi_{ab} \nabla W_{as}(t) + \vec{g}) \quad \text{Eq. 8.46}$$

$$\rho^*_a = \rho_a(t) + \Delta t \sum_b m_b (\vec{v}^*_a - \vec{v}^*_b) \nabla W_{ab}(t) + \sum_s \Psi_s (\vec{v}^*_a - \vec{v}_s) \nabla W_{as}(t) \quad \text{Eq. 8.47}$$

In addition, the fluid-rigid pressure is also considered to update the velocity at $t + \Delta t$:

$$\vec{v}_a(t+\Delta t) = \vec{v}^*_a + \Delta t \sum_b m_b \left( \frac{p_a(t)}{\rho_a(t)^2} + \frac{p_b(t)}{\rho_b(t)^2} \right) \nabla W_{ab}(t) + \sum_s \Psi_s \frac{p_a(t)}{\rho_a(t)^2} \nabla W_{as}(t) \quad \text{Eq. 8.48}$$

With the fluid-rigid boundary handling scheme, the SPH software, Neutrino, is able to predict the hydrodynamic forces onto solid objects from the surface waves by calculating the pressure Eq. 8.44 and friction Eq. 8.45 forces. Moreover, by incorporating a solid-mechanistic solver, Neutrino is able to simulate the motion of dynamic objects and solid deformation. More details can be found in [22].

The free-surface conditions are implicitly imposed without the need of boundary particles. The kinematic condition and dynamic condition on the tangential stress are automatically satisfied with, respectively, the Lagrangian approach and an appropriate choice of SPH operators [23], while the dynamic condition on the pressure is indirectly imposed by:

(1) Defining the pressure as the relative pressure with respect to the atmospheric pressure, so that when the fluid pressure equals to the atmospheric pressure, a zero relative pressure is exerted.
(2) Clamping all negative pressures to zero due to the incomplete fluid neighborhood at the free-surface during the execution of the pressure-solving algorithm.

It can be seen from equation Eq. 8.27 – Eq. 8.48 that the information from neighboring particles is crucial to the final results. Theoretical error analysis has been performed for the mathematical formulation of SPH methods in [24]. The goal is to identify sources of error for SPH simulations. Meanwhile, the numerical error analysis is an important input towards the adequacy assessment of the SPH methods in predicting application quantities of interest. It is found that the particle size is the major source of uncertainty for SPH methods. Since the properties are assumed to be homogeneous for every single particle and smoothed across its neighboring particles, low particle number density will result in significant errors. Therefore, the particle size is a major source of uncertainty. It is also found that the continuous Lagrangian operator has a second order of accuracy for approximating an arbitrary scale (or vector) field and gradients of any order. However, most errors come from the discretization process, and the particle distribution deviates from a perfectly regular configuration after simulation starts. As a result, the math to derive the error in the general case turns to be more complicated than for mesh-based methods. In [24], a theoretical error analysis is performed given that the particles are uniformly distributed, and the second order of accuracy can be achieved with SPH approximations. However, it is found from a simple laminar scenario, where particle distributions are relatively uniform, that SPH methods with weakly compressible SPH formulation have the first order of accuracy. In general, to confidently apply SPH's simulation results to external-flooding simulations and nuclear safety analysis, the adequacy of SPH needs to be analyzed systematically for the intended uses.

### 8.5. SPH Adequacy Assessment with CSAU/EMDAP Framework

To systematically assess the adequacy of SPH methods for the external flooding, the CSAU/EMDAP framework is applied, with four key activities. Figure 8.40 shows the scheme of such process, and results from all activities lead to the decision for the adequacy of SPH methods in designated applications.

Both the verification by theoretical error analysis and the literature reviews for SPH have been performed in [24], and the corresponding software package Neutrino has been verified in [25]. The rest components, including target applications, performance measurement standards for code adequacy, code assessments, and scaling analysis will be further discussed. Finally, a code adequacy decision will be made together with a summary of findings and lessons learned. In addition, Figure 8.40 also suggests that the code adequacy assessment is an iterative process, and efforts are continuously required in achieving sufficient levels of details, improving models, collecting new data, etc. **Error! Reference source not found.** defines phases of code adequacy assessment based on the sources of uncertainties and their consequences in supporting safety-related decisions in applications. This study is currently at the scoping stage, and the objective is to qualitatively evaluate the adequacy of SPH methods and the corresponding package Neutrino in simulating important phenomena in external flooding. Comparing to the maturation stage, the scoping stage potentially has large uncertainties and biases. Regular code assessments usually

start with phase #1, and it mainly aims to focus the issues and maximizing effectiveness in addressing them, including appropriate research efforts, databases, requirements, decision analysis, and assessment process. The completion of phase #2 would take place outside and after sufficient resolutions have been achieved. At the same time, the adequacy results are reinforced by target applications. That is, phase #2 can be regarded as confirmatory, but can only be judged on a case-by-case basis.

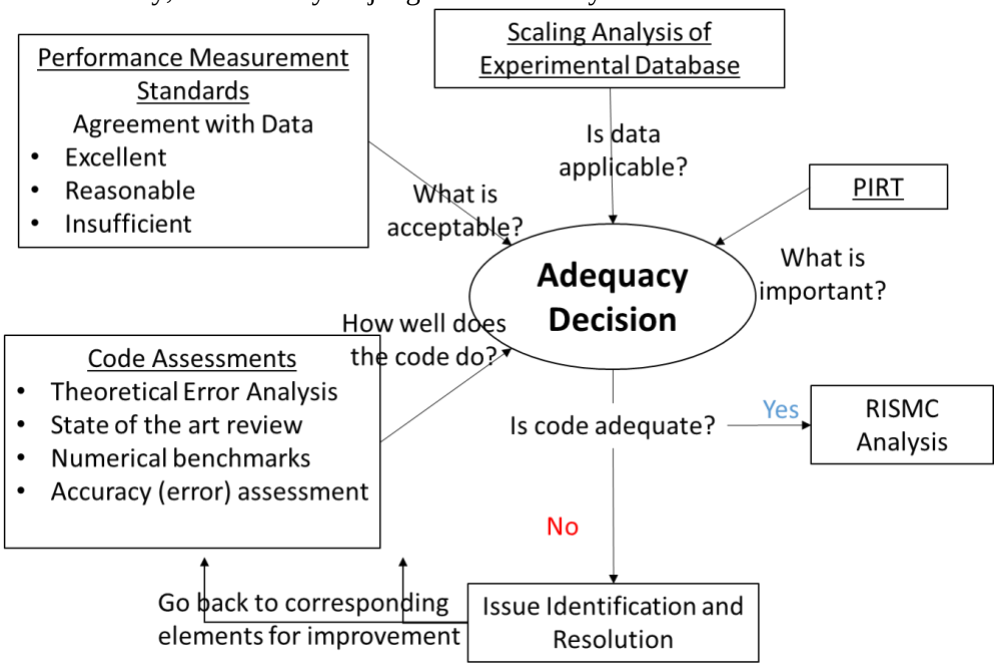


Figure 8.40. Demonstration of adequacy decision process.

Table 8.1. Definition of phases of assessment

| Phase # | | Sources of Uncertainties | Consequence |
|---|---|---|---|
| 1 | Scoping | Important phenomena are identified and ranked with potentially large uncertainties and biases;<br>The assignment of acceptance criteria could be uncertain and biased;<br>Adequacy decisions are qualitative;<br>Validation data and evidence are potentially insufficient; | Uncertainty in the final code adequacy is large, and it could potentially alter the decisions in applications |
| 2 | Maturation | Important phenomena are identified and verified<br>The assignment of acceptance criteria is verified;<br>Verified adequacy decisions with acceptable uncertainties;<br>Validation data and evidence are sufficient; | Uncertainty in the final code adequacy is negligible compared to the defense-in-depth |

### 8.5.1. Scenario Description

There are several different types of flooding scenarios evaluated by the nuclear industry, and each may have multiple criteria for adequacy acceptance. For this external-flooding example, the analysis purpose is to assess if the code adequacy of SPH to model impact forces when simulating the scenario of “floods damage the building structures, enter the room, and cause diesel generator (DG) malfunctioning” is acceptable. Detailed event progressions are listed as follows:

- If there is external flooding after a dam breaching, water overflows the NPP site, and the AC power fails immediately.
- If the water reaches the DG building, and the peak forces acting on the building exceed a limit, water starts to penetrate the room.

The corresponding QoIs include the response time and the structural loads on Systems, Structures, and Components (SSCs) by floods. In this study, the response time is the time for the external floods to reach the DG building and to potentially fail the DGs. The response time is crucial for the nuclear safety analysis, including estimating the decay heat, initiating emergency procedures, and determining responses of SSCs, etc. The structural loads on stationary SSCs are important for determining the structural integrity and operational status of SSCs during external-flooding scenarios. For example, if the load exceeds the regulatory limits, certain SSCs need to be shut down; if the force exceeds the operational limits, certain SSCs malfunction or fail. Additionally, the structural loads on moving objects are important for the flooding-induced debris analysis, including the debris transport and its impacts on SSCs. Figure 8.41 shows a postulated scenario of external flooding induced by dam failures. Flooding simulations have been performed with Neutrino, and some key configurations for this simulation are listed in Table .

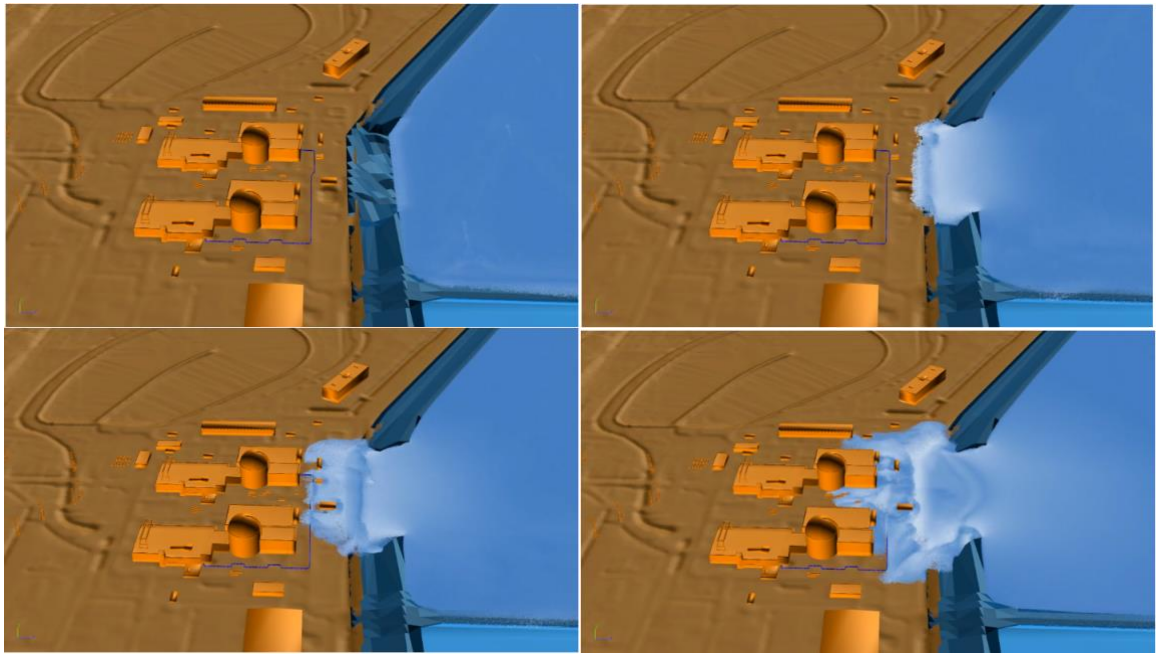

Figure 8.41. Demonstration for a postulated external flooding scenario induced by dam failures. A full-scale simulation is prepared with Neutrino software package.

Table 8.2. Scenario configurations, Neutrino setups, and predicted QoIs

| **Scenario Configurations** | |
|---|---|
| Water level at the dam breaching | 5m |
| Breaching width | 10m |
| Distance to buildings | 20m |
| **Neutrino Setups** | |
| Particle size | 2cm |
| CFL number | 0.6 |
| **Predicted QoIs** | |
| Response time | 20min |

| | |
|---|---|
| Peak force | 400N |

At the scoping stage, this study does not design new facilities, and validation data is collected from existing literature. To ensure the data applicability to the application scenarios, a scaling analysis is needed to ensure the relevance and sufficiency for all collected data. **Error! Reference source not found.** shows the PIRT high-rank phenomena for the FoMs of response time and structural loads, where the shaded areas represent the FoMs. Since SPH has been applied to simulate the violent flow for a long time [19], its model and code are adequate for generating the surface wave with a wave generator [26] [27], surface-wave propagation, and force estimation on static objects [28]. Comprehensive reviews for SPH methods and codes in simulating these phenomena can be found in the reference documents [29]. Therefore, most rankings for these phenomena are "**H**igh" except for the math model and code adequacy of structural loads. SPH methods have shown good agreements in predicting the hydrodynamic forces. Although, the results can be unstable and additional smoothing techniques are usually needed, they are ranked as "**M**edium" since these issues are considered moderate. For the phenomenon of vortex shedding, the math model and code in SPH is very limited, and they are all ranked as "**L**ow". To achieve a comparable accuracy to mesh-based simulations, SPH either needs to refine its particle to DNS scales or to be incorporated by closures. However, since the number of neighboring elements (particles) for an SPH element (particle) is typically 3-4 times more than that for a mesh cell in mesh-based simulations, SPH methods are more computationally expensive than mesh-based methods in DNS scales. Besides, since the nature of particle-based methods deviates from the mesh-based methods, most well-known closure models in established CFD studies may not be perfectly suitable for SPH. Therefore, better SPH closures are still needed for such phenomenon from the aspects of math and model adequacy. Finally, the data of full-scale solitary surface wave can be obtained analytically, while the data from aerospace engineering for large-scale vortex shedding phenomenon are quite adequate. Therefore, the ranking of data adequacy for solitary surface wave and vortex shedding is "**H**igh". But for the rest of phenomena, there is a lack of large-scale data.

Table 8.3: PIRT process and lists of numerical benchmarks designed for each phenomenon in external flooding scenarios.

| ID | Phenomenon Description | Imp | Adequacy | | |
|---|---|---|---|---|---|
| | | | Math Model | Code | Data |
| A | Response Time | | | | |
| | Solitary Surface Wave | H | H | H | H |
| | Surface-Wave Propagation | H | H | H | L |
| | Vortex Shedding | H | L | L | H |
| B | Structural Loads | | | | |
| | Hydrodynamic Force on Stationary Structures | H | M | M | L |
| | Hydrodynamic Force on Moving Structures | H | M | M | L |

Considering the limitation of databases from literature, this study only assesses the adequacy of Neutrino in predicting hydrodynamic forces on stationary structures.

### 8.5.2. Performance Measurement Standards

To decide if the code is adequate for the specific application, standards need to be established, against which code models and adequacy can be measured. In this study, the standards are described as – the code is considered adequate for each separate phenomenon or process if:

- The code state of the art is known, documented, and acceptable.
- The code is generally acceptable for simulating each separate phenomenon of the application.
- The code predicts the high-fidelity data from separate effect tests with acceptable accuracy.
- The code is acceptable for the scale of the specific target applications.

The code is considered adequate for integral scenarios if:

- The field equations represent the key processes and phenomena.
- The code is generally acceptable for simulating the application scenarios with various phenomena and processes.
- The code predicts the behavior of important phenomena as observed in appropriate integral effects tests with acceptable accuracy.
- The code represents the interactions of between phenomena, process, and system components.

To provide a quantitative measure for the term "acceptability," criteria are needed for assessing the code accuracy and quality of the validation database. In this study, the code accuracy is measured by simulation errors in predicting selected QoIs, while the quality of the validation database is measured according to the attributes of scaling analysis. **Error! Reference source not found.** shows the accuracy standards measured by error ($L_1$ relative error norm) in predicting selected QoI. At the scoping stage, the acceptance criteria for code accuracy are made by authors' knowledge, and they have been reviewed by researchers in relevant fields. In the refinement stage, the acceptance criteria will be adjusted based on the code adequacy and risk analysis results. The $L_1$ relative error norm is defined by

$$L_1 = |\frac{QoI_{preds} - QoI_{meas}}{QoI_{meas}}| \qquad \text{Eq. 8.49}$$

where $QoI_{preds}$ and $QoI_{meas}$ represent the predicted QoI by simulations and measured QoI by experiments. Considering the limitations of this study, current error analysis is at preliminary stages with simple uncertainty quantification metrics. Advanced metrics and the corresponding quantification methods [30] [31] will be evaluated.

Table 8.4. Simulation code accuracy standards measured by error in predicting selected QoIs

| **Accuracy Statement** | **$L_1$ Relative Error Norm in Predicting Selected QoIs** |
|---|---|
| Excellent Accuracy | $\leq 10\%$ |
| Reasonable Accuracy | $\leq 20\%$ |
| Insufficient Accuracy | $> 20\%$ |

A systematic scaling analysis [6] is composed by "top-down" and "bottom-up" analysis. The scaling analysis is tightly coupled with the model assessment process. Starting from the Phenomenon Ranking and Identification Table (PIRT), the physical characteristics are identified, and the interconnections among system components, phenomena, and processes can be understood. Meanwhile, by identifying important phenomena, necessary data can be collected with required physical characteristics. In this study, the dimensionless groups are used to represent the physical characteristics that governs the system responses. Next, the relative importance of the dimensionless groups is investigated through various code assessment process until a relationship is developed between the selected phenomena and the dimensionless groups. Next, simulations will be validated by comparing results against databases until the code adequacy is acceptable. Once validation is finished, it can be claimed that all data involved in this process have been "compressed" into the simulation codes. As a result, the scaling process is to find the "encodings" for the database, and the model assessment processes can be treated as an adequacy and applicability test for the condensed form of data. The adequacy is decided based on collected data and

validation results, while the applicability is verified according to the sufficiency of databases. In this study, the dimensionless number of experiments are compared to the applications, and the sufficiency is verified if the test data envelops the application behavior. In another word, the dimensionless number in applications should be covered by the min-max range of dimensionless groups in the database. However, since the PIRT process relies on expert knowledge of systems, phenomena, and processes, the selected physical characteristics can be only peculiar to the experiments and is not expected in the applications. Such an issue is usually known as scaling distortion [6]. To avoid distortions, a relevance analysis is needed for the database to ensure that all selected phenomena are also typical under prototypic conditions. At the same time, the distortion needs to be evaluated by making model predictions at different spatial and time scales. Next, uncertainty analysis is performed with respect to each scale. If the uncertainty of model predictions can be bounded, the scale distortion is claimed as acceptable. **Error! Reference source not found.** shows general descriptions of three attributes in scaling analysis and corresponding acceptance criteria. In this study, when the code adequacy is evaluated, the acceptance criteria of scaling analysis (**Error! Reference source not found.**) and code accuracy (**Error! Reference source not found.**) will be considered at the same time. Although, scaling and code accuracy are correlated since model is treated as a compact form of data, this study assumed them to be independent. Such an assumption is valid under the condition that the current SPH model and the software package Neutrino are developed without scaling analysis. However, in the later stage, as SPH models become sophisticated during the iterative development and assessment process, sophisticated techniques are needed to further improve model accuracy, data sufficiency, relevance, and distortion.

Table 8.5. Attributes and criteria of systematic scaling analysis.

| **Attribute** | **Criterion** |
|---|---|
| Sufficiency | The physical characteristics of database bound those for applications. |
| Relevance | The physical characteristics of database are relevant to those for applications |
| Distortion | The uncertainty of model predictions can be bounded when it is propagated through scales |

Considering the previous discussion on code accuracy and scaling analysis, the general standards for code adequacy can be identified as:

**Excellent** – For the high-rank phenomena, the accuracy in predicting the quantity of interest is excellent. The code can also be confidently used in similar applications, and the accuracy in predicting corresponding quantities of interest should also be excellent.

**Reasonable** – For the high-rank phenomena, the accuracy in predicting the quantity of interest is reasonable. The code can also be confidently used in similar applications, and the accuracy in predicting corresponding quantities of interest should also be excellent.

**Insufficient** – For the high-rank phenomena, the accuracy in predicting the quantity of interest is insufficient. The errors of most predictions lie outside the uncertainty bounds, and major modifications are needed before the code can be used in similar applications with sufficient confidence.

In this study, the minimum standard for acceptable code in terms of code adequacy is “reasonable”. Meanwhile, due to a lack of data from integral effect tests, this study focuses on the code adequacy assessment of SPH methods for separate phenomena.

8.5.3. Develop Assessment Base and Evaluation Model

To ensure the data applicability to the application scenarios, a scaling analysis is needed to ensure the relevance and sufficiency for all collected data. Table  shows the list of related numerical benchmarks for all high-rank phenomena collected from various sources, while the QoIs for each benchmark are also listed. In this study, not all benchmarks have been demonstrated, but at least one benchmark will be discussed for each phenomenon.

Table 8.6. Numerical benchmarks for all high-rank phenomena. Benchmarks in blue and italic fonts are investigated but not discussed in this study.

| ID | High-Rank Phenomena | Numerical Benchmarks | QoI |
|---|---|---|---|
| A | Response Time | | |
| | Solitary Surface Wave | *Wave Piston Machine* [26] [32] | Surface-Wave Height |
| | Surface-Wave Propagation | Dam Break [33] [34] | Time of Peak Force |
| | Vortex Shedding | *Flow around Cylinder* [28] | Velocity Field |
| B | Structural Loads | | |
| | Hydrodynamic Force on Stationary Structures | Dam Break [33] [34] | Force Magnitude |
| | Hydrodynamic Force on Moving Structures | Moving Solids in Static Fluid [35]; *Flow-Induced Motion of Floating Bodies with Wave Maker;* [36] | Moving Trajectory |

8.5.4. Code Assessment and Scaling Analysis

In flooding scenarios, since the force exerted by the flow to the structures is an important quantity to measure, dam break is selected to test the capability of SPH methods in predicting force magnitude and flow propagation. The first simulation is designed based on the setups from S.J. Cummins, et al. [33] The simulation is one-to-one scale to real experiments and set up as in Figure 8.42 according to Cummins work [33]. The scene consists a rectangular tank with 0.61m width, 1.6m length, and 0.75m height; a vertical column with a 0.12m squared base; and a planar gate for suddenly releasing water. The rigid column is located 0.9m from one of the tank boundaries, and the gate is located at a distance of 0.5m from the rigid column. A water column with 0.3 height is initially contained behind the gate. In Neutrino, a gate is first put in position and held for 1 sec until all fluid particles are settled down. Then the gate is completely opened, and fluid collapses driven by gravity. Figure 8.43 shows the evolution of fluid over the surface. The maximum Reynolds number for this case is around $1.68 \times 10^5$ with characteristic length equal to the width of the dam. The particle size ranges from 5mm to 50 mm, and there are around 64k fluid particles when particle size is 10mm. The time stepping parameters $\lambda_{CFL}$ and $\lambda_{max}$ are set to 0.4 and 0.5 respectively.

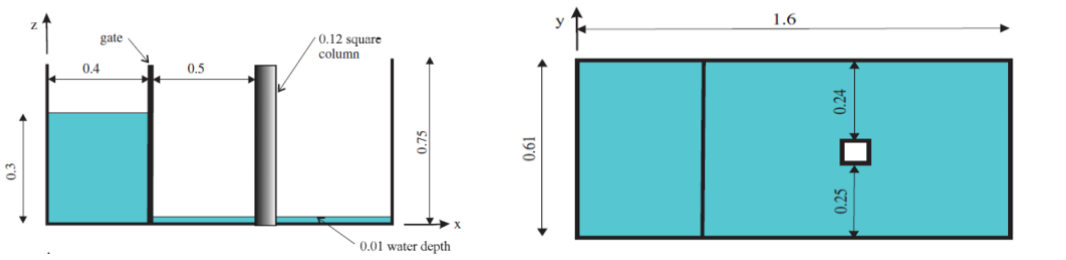

Figure 8.42. Schematic diagram of the dam geometry from Cummins et al. 2012 [33].

Figure 8.43 shows the evolution of water collapsing and hitting the rigid column. The gate is removed at the beginning of the simulation, and a surface wave is induced by gravitational effects. The first (primary) surface-wave impact happens at around 0.3s, then, the wave reaches the other end at 0.6s. The surface wave is reflected back and hitting the column again at 1.5s. The impact forces for the primary and reflected surface waves are measured and compared against the experimental measurements.

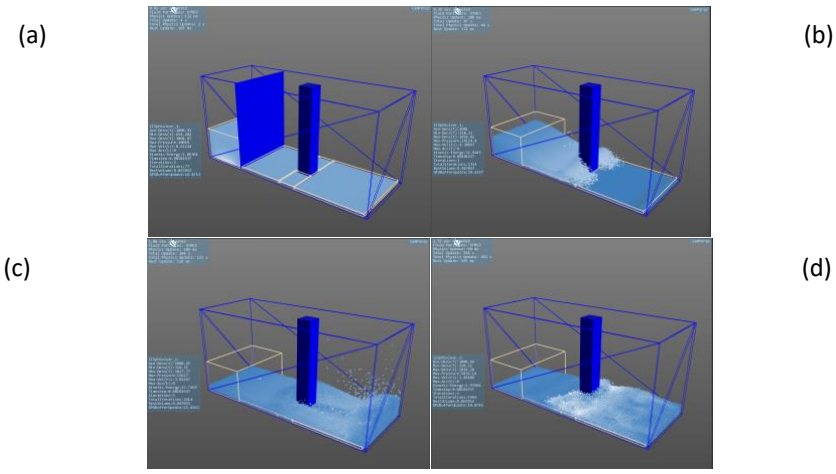


Figure 8.43. Evolution of the water collapse and interaction with the column simulated by Neutrino. (a) start of simulation; (b) primary surface wave hitting dam structure; (c) surface wave reflected; (d) Reflected surface wave hitting dam structure;

The transient comparison of simulation results again experimental data can be found in previous work [28]. The time step is affecting little on the results, as long as the CFL number is lower or equal to 0.5. Figure 8.44 shows the convergence plot of particle size in predicting different QoIs, including the maximum force of primary and reflected surface wave exerting on the structure, the time of those maximum forces. The percentage represents the relative error of simulation results against experimental data. When particle size reaches 0.01m, further refinement does not continue to improve the accuracy. Comparing to the force magnitude, contacting time of surface-wave propagation is affected more by the particle size.

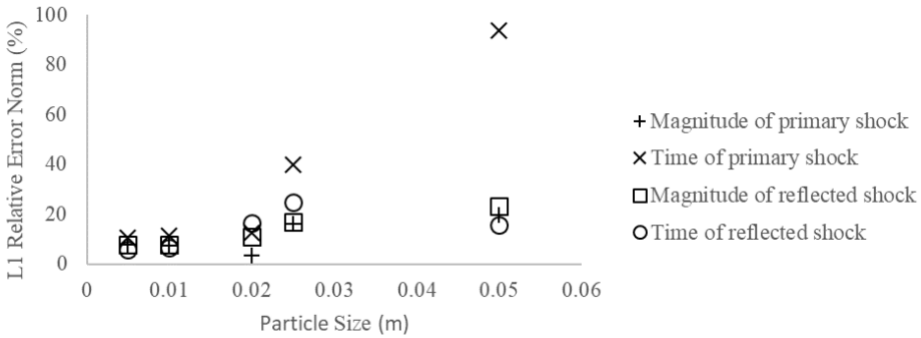


Figure 8.44. Particle size convergence plot for force magnitude and contacting time of primary and reflected surface wave.

Figure 8.45 shows the plot of relative error against the computational time. When the particles are refined, better results are obtained with more computational time needed. Note that when particle size is 0.02m, the simulation results are better (70% improvement in magnitude of primary surface-wave impact; 60% in the time of primary surface-wave impact; 34% improvement in magnitude of reflected surface-wave impact; 33% improvement in time of reflected surface-wave impact) but consuming less time (5%)

than the one with 0.025m particle size. Because the CFL condition is applied for every time step, the simulation with coarse particle size is not as stable as the one with finer size. Therefore, using a finer particle size requires smaller time step and longer time to simulate.

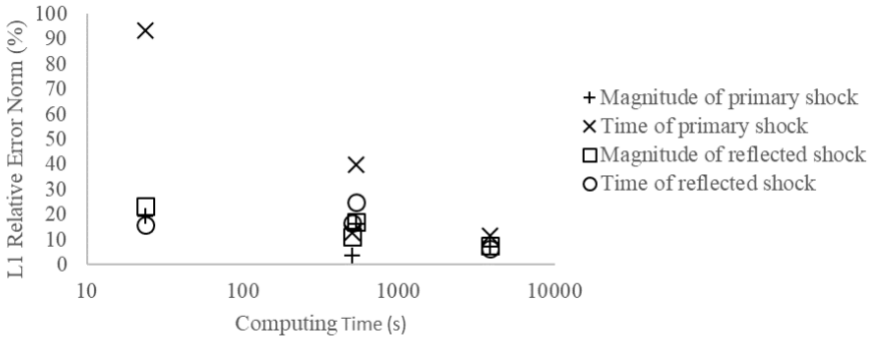


Figure 8.45. Plot of relative error against computing time for force magnitude and contacting time of primary and reflected surface wave.

Table shows the list of simulation parameters that have the error of simulated QoIs fall into the bounded region. The yellow shaded row represents the parameter combination with lowest computational time, which is suggested as the optimal simulation parameters for numerical benchmarks.

Table 8.7: Simulation parameters with 20% bounded absolute relative error for the case of dam break.

| **Particle Size (m)** | **Simulation Time/Physical Time** | **$L_1$ Relative Error Norm (%)** | |
|---|---|---|---|
| | | **Max. Force Magnitude** | **Time of Peak force** |
| 0.05 | 11.96 | 19.58% | 93.55% |
| 0.025 | 265.8 | 16.16% | 40% |
| 0.02 | 252.4 | 3.58% | 12.73% |
| 0.01 | 1929 | 7.66% | 10.53% |
| 0.005 | 57364.5 | 7.26% | 11.43% |

In addition, a second simulation is performed according to experiments by F. Aureli [34], where forces with respect to various water height are measured, and the optimum particle size identified by the previous study (0.02m) is used for all simulations. The Aureli's data can also be used to verify the scaling analysis. In this study, it is found that the QoIs, the peak pressure force magnitude, are proportional to the design wave heights without exhibiting impulsive breaking wave pressures of high intensities [37]. The design wave height refers to the highest wave height expected under the given wave condition. In dam-break benchmarks, the design wave height equals to the initial water depth $h$, which is the highest wave height during the transient.

To investigate the sufficiency and distortion of database for dam break, the initial depth $h$ is non-dimensionalized as $x^*$ by Eq. 8.50, where $L$ is the distance between the gate and the stationary object. Figure shows the comparison of the measured against SPH predicted peak force with different dimensionless ratios $x^*$ (Eq. 8.50). At the same times, linear functions are fitted to both datasets, based on which an error plot is made with respect to the dimensionless ratio $x^*$.

$$x^* = h/L \qquad \text{Eq. 8.50}$$

Figure  shows the plot of error for predicting peak force with respect to the dimensionless ratio $x^*$ given the same particle size as 0.02m. When the $x^*$ is larger than 0.2, the error can be properly bounded and reasonably accepted.

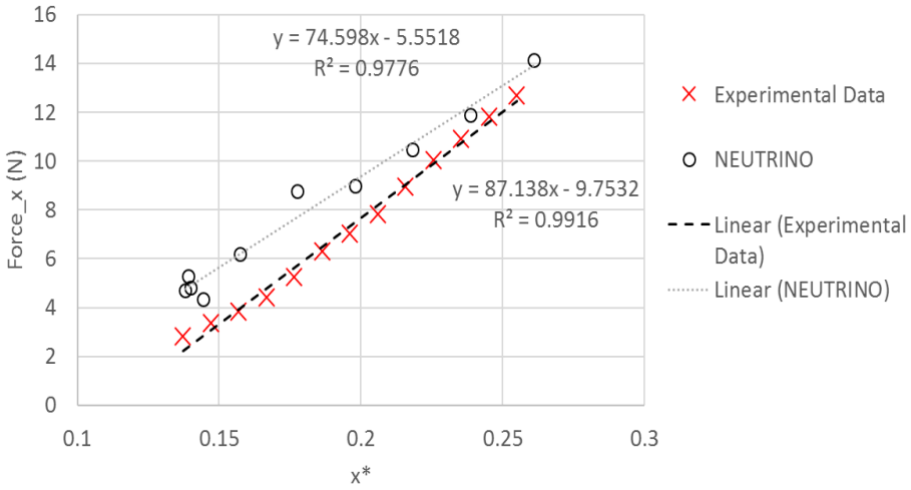


Figure 8.7. Comparison of the measured against SPH predicted peak force with different dimensionless ratio $x^*$.

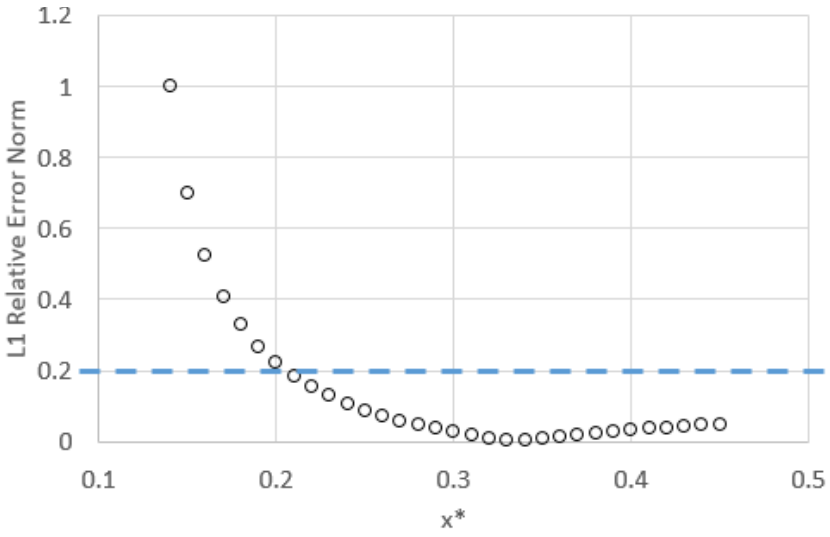


.

Figure 8.8. Plot of $L_1$ relative error norm for predicting the peak force versus the dimensionless ratio $x^*$ with particle size as 0.02m.

Considering the effect of particle size and dimensionless ratio, the error in predicting the peak force by SPH can be propagated to the application scenario. Assuming that the dimensionless ratio is the major physical characteristic that measures the similarity, suggestions of simulation parameters can be made according to previous studies on particle size and dimensionless ratio. Table  shows the suggested simulation parameters for the application scenario based on the SET analysis. Since this study does not have data that has the same dimensionless ratio but different facility sizes, the particle size is suggested to be the same as or smaller than 2cm, such that the $L_1$ relative error norm for the predicted peak force is less than 20%.

Table 8.7. Simulation parameters that are scaled from numerical benchmarks to a postulated scenario with the same dimensionless group.

| | **Numerical Benchmarks** | **Scenario Simulation** |
|---|---|---|
| Water height | 0.1 ~ 0.13m | 5m |
| Distance to the static structure | 0.51m | 20m |
| Dimensionless ratio $x^*$ | 0.2 ~ 0.26 | 0.25 |
| Suggested particle size | 0.02m | 0.02m |
| Predicted peak force error ($L_1$ relative norm) | 5%~20% | 3.6% |
| Predicted time of peak force error ($L_1$ relative norm) | 4%~18% | 12.73% |

Since this study does not focus on experimental developments, the adequacy of Neutrino is assessed only for the phenomenon of hydrodynamic forces on stationary structures. Dam break is selected to test the capability of SPH methods in predicting force magnitude and flow propagation. An assessment has been performed for Neutrino based on the Cummins [33]'s data. It is found that the accuracy of Neutrino prediction for the magnitude of peak force is reasonable when the particle size is 2cm; the accuracy is excellent when the particle size is less than or equal to 1cm. Although particle refinements provide better accuracy, the computational expenses grow drastically. Considering the minimum acceptance criteria, particle size is suggested to be 2cm for better efficiency.

In order to evaluate the accuracy of moving solids in flow, simulations with falling and floating block in the fluid are set based on the experiments by T.R. Wu, et al [35]. A rectangular tank with 140mm width and 140mm height is used for both simulations, and it is filled by water with density equal to 997 $kg/m^3$. For the case of falling cube, a cubic block with density equals to 2120 $kg/m^3$ is used. The cube is initially held half submerged in the water with depth equal to 131mm. Next, the block is released, and it falls to the bottom of the tank. For the floating block, a rectangular wooden block with density equal to 800.52 $kg/m^3$ is initially held at the bottom of the tank. The tank is filled by water with depth equal to 52mm. When simulation starts, the wooden block is released and floated to the water surface. The block will oscillate sometimes and finally become stable. For the falling case, the time it takes for the cube to reach the bottom is measured; For the floating case, the time it takes for the block to reach maximum height is measured. Both quantities are then compared against experimental measurements. Figure 8.46 shows the dimensions of the water tank and cube for both the falling and floating experiments. Different particle sizes are sampled for both cases, which range from 0.5mm to 6mm. The time stepping parameters $\lambda_{CFL}$ and $\lambda_{max}$ are set to 0.4 and 0.5 respectively.

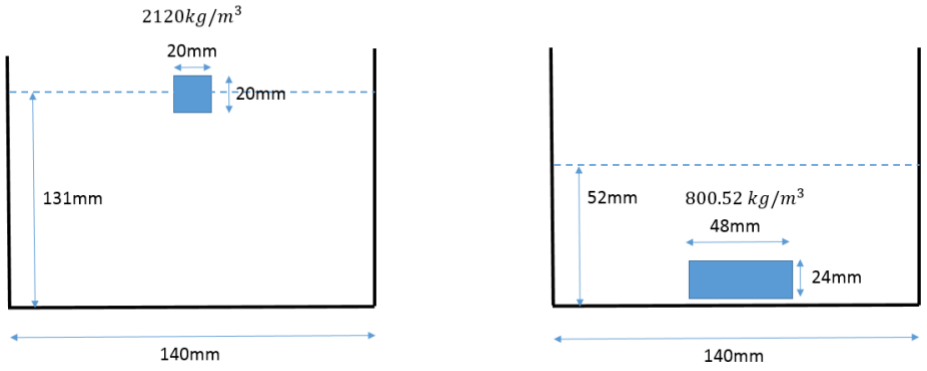

Figure 8.46. Dimensions of the water tank and cube for both the falling and floating experiments

Figure 8.47 shows the plot of the cube vertical displacement against the time from both Neutrino simulation and experiment. Note that both the displacement and time have been non-dimensionalized, where t* and z* are defined in Eq. 8.51 and Eq. 8.52. Three different particle sizes are tried with the simulation and a good agreement is found when the particles are 2.5mm. In this case, the falling time of the cube, defined as the non-dimensional time spent for the heavy cube to reach the bottom of the tank from its initial position, is selected as the quantity of interest.

$$z^* = z/H \qquad \text{Eq. 8.51}$$

$$t^* = t \Big/ \sqrt{\frac{2H}{g}} \qquad \text{Eq. 8.52}$$

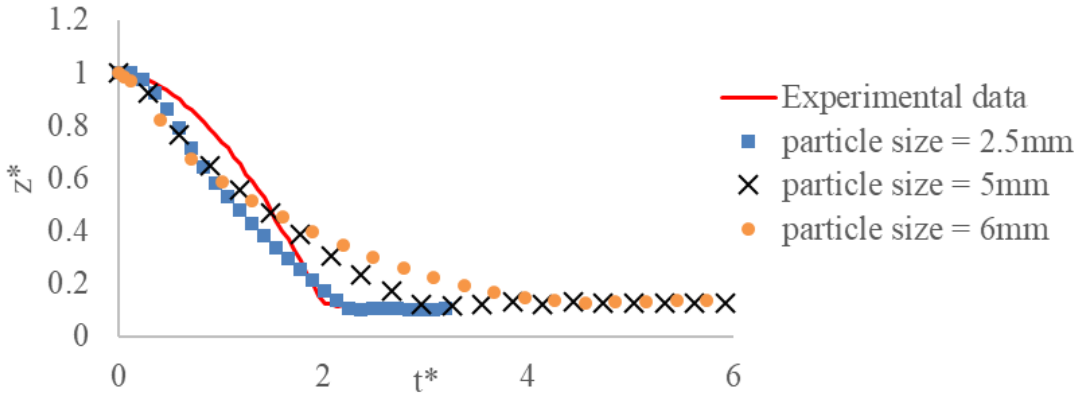


Figure 8.47. Comparison of vertical displacement of falling block simulated by LAMMPS and Neutrino

Table  shows the L1 relative error norm by comparing the simulated cube falling non-dimensional time against the measured data. Error is decreasing as the particle being refined, and the heavy cube will fall slower as the particles get larger. If the particle size is larger than 6mm, the heavy cube will float on top of the fluid. Because the mass of cube is constant and the insufficient number of particles will cause high simulation error, especially in pressure calculation, large particle size will result in unphysically high buoyance forces.

Table 8.9: List of particle sizes in Neutrino simulations for falling cube, and the L1 relative error norm of each simulation in predicting the cube falling time.

| **Particle Size** | **L1 Relative Error Norm (%)** |
|---|---|
| 6mm | >100% |
| 5mm | 52.73% |
| 2.5mm | 5.52% |

Figure 8.48 shows the time transient of block's non-dimensional vertical displacements from Neutrino with three different particle sizes. However, the oscillations are dampened faster than experiments, since the numerical diffusion of SPH simulation tends to be larger than expected. Because a large deviation is found between the simulated results and experimental measurement, and the current computing power doesn't allow Neutrino to have more refined particle size, LAMMPS 2D [38] simulation is executed with 0.5mm particles.

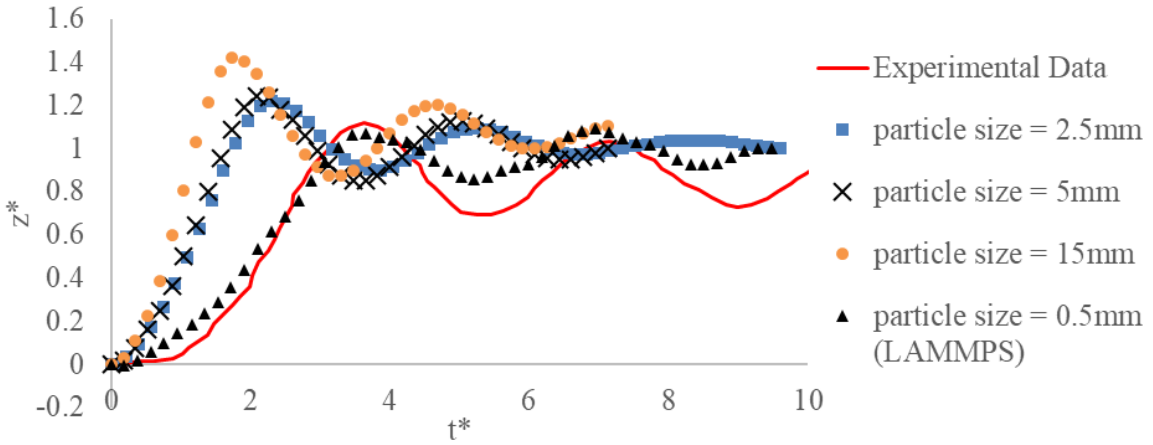


Figure 8.48. Comparison of vertical displacement of floating block simulated by LAMMPS and Neutrino

Table  shows the L1 relative error norm by comparing the simulation result against the measured data for selected QoI. Error is decreasing as the particle being refined, and a very good agreement is found with very refined particles in LAMMPS simulation.

Table 8.10: List of particle sizes in Neutrino simulations for floating cube, and the L1 relative error norm of each simulation in predicting the cube floating time and oscillation period.

| **Particle Size** | **L1 Relative Error Norm (%)** |
|---|---|
| 6mm | 54.64% |
| 5mm | 45.57% |
| 2.5mm | 39.67% |
| 0.5mm (LAMMPS) | 4.41% |

Both simulations suggest that particle size is crucial to the accuracy of SPH in predicting the falling and floating time, which is affected by the force balance between gravity and the buoyance force. The accurate prediction of buoyance force depends on the particle intensity around the cube. Therefore, for the moving object calculation, the cube density ratio ($\rho^*$ defined in Eq. 8.53) and the ratio between cube volume and average particle volume ($V^*$ defined in Eq. 8.54), are selected as the dominant physics. $\bar{V}_{dp}$ is the average particle volume defined by Eq. 8.55 [39], and $d$ is the initial particle diameter:

$$\rho^* = \rho_{cube}/\rho_{fluid} \quad \text{Eq. 8.53}$$

$$V^* = V_{cube}/\bar{V}_{dp} \quad \text{Eq. 8.54}$$

$$\bar{V}_{dp} = d^3 \quad \text{Eq. 8.55}$$

Suggestion on particle size will be made with these parameters being kept constant. Table  shows the suggestion on particle size selection for corresponding scenarios. For the case of falling cube, the simulation with 2.5mm particles is selected for scaling, while the simulation with 0.5mm particles is selected for the floating cube. However, since there is only one dataset for this phenomenon, the dimensionless group cannot be verified, and the dimensionless parameters for application scenarios are assumed to be the same as the numerical benchmarks.

Table 8.11. Simulation parameters that are scaled from numerical benchmarks to a postulated scenario with the same dimensionless group.

| | **Numerical Benchmarks** | **Application Scenario** |
|---|---|---|
| **Falling object** | | |
| Cube volume | 8000mm$^3$ | 8m$^3$ |
| Density | 2120kg/m$^3$ | 2120kg/ m$^3$ |
| Density ratio $\rho^*$ | 2.1 | 2.1 |
| Volume ratio $V^*$ | 512 | 512 |
| Suggested particle size | 2.5mm | 0.25m |
| Predicted error $L_1$relative norm) | 5.52% | ~5.52% |
| **Floating object** | | |
| Cube volume | 56448mm$^3$ | 451.584m$^3$ |
| Density | 800.52kg/m$^3$ | 800.52kg/ m$^3$ |
| Density ratio $\rho^*$ | 0.8 | 0.8 |
| Volume ratio $V$ | 451584 | 451584 |
| Suggested particle size | 0.5mm + Equation of State | 0.1m |
| Predicted error ($L_1$ relative norm) | 4.41% | ~4.41% |

In above sections, simulations of dam break and moving solids have been run, and the results are compared against experimental measurements. For both cases, SPH has shown good performances in predicting the selected QoIs, including the force magnitude, water propagation speed to dry surface, falling and floating time, and the errors are properly bounded. By requiring the predicted QoIs in scenario simulations to have less than 20% absolute relative error, simple scaling has been performed for both cases.

For the external-flooding scenario, the FoMs are the response time and structural loads on SSCs. Next, according to the PIRT process, all high-rank phenomena are identified, and numerical benchmarks are set correspondingly. Next, the accuracy of SPH methods in simulating each scenario is assessed by comparing the SPH predicted QoIs against the measured data. Table  shows the assessment results of all numerical benchmarks for both scenarios, and their code adequacy is rated by the performance measurement standards.

Table 8.12. Comparison of measured and SPH predicted QoIs for high-rank phenomena of external-flooding scenarios.

| **Numerical Benchmarks** | **QoI** | **Accuracy** |
|---|---|---|
| Dam break | Force magnitude;<br>Water propagation speed | Excellent |
| Falling cube | Falling time | Excellent |
| Floating cube | Floating time;<br>Oscillation period | Excellent |

8.5.5. Scaling Analysis

To determine the relevance and sufficiency of database for the intended applications, a scaling analysis is needed. A systematic scaling analysis is composed by “top-down” and “bottom-up” analysis. As discussed previously, the scaling analysis is tightly coupled with the model assessment process. Starting from the PIRT, the identifications of physical characteristics require complicate procedures such that the interconnections among system components, phenomena, and processes are well understood. In this study, the dimensionless groups are used to represent the physical characteristics that govern the system responses. Next, the relative importance of the dimensionless groups is investigated through various code assessment

process until a relationship is developed between the selected phenomena and the dimensionless groups. A combination of various relationships is usually known as a "workable form". Next, the workable form will be validated by comparing against data until a final form is determined. Until this point, it can be claimed that all data involved in this process have been "compressed" into an equation-based workable form. As a result, the scaling process is to find the "encodings" for the database, and all the model assessment process is to test the applicability of this form. At the same time, scaling also aims to verify that the database is sufficient.

When estimating the structural loads exerted by water waves, there are three parts of forces being considered: the static pressure, the dynamic pressure, and impulsive forces. When the structure is placed such that the incident waves are unbroken, the standing wave will exist seaward of the wall, and only the static and dynamic forces will exist. In such situations, the forces can be approximated based on the linear wave theory. Tadjbaksh et al. first drived the third order approximation in terms of pressure due to standing waves [40], Based on their approximation, Goda [41] extended it to the fourth order approximation. Meanwhile, a series of laboratory tests are conducted to calibrate parameters in the model and it is found that the pressure forces are proportional to the design wave heights $h$ [37], and the correlations between the peak pressure forces and water wave depth can be simplified into Eq. 8.56 [42].

$$P = w_0 h(\alpha_1 + \alpha_2 \cos^2 \beta) \qquad \text{Eq. 8.56}$$

where $\alpha_1$ and $\alpha_2$ are empirical parameters, $\beta$ is the angle of wave approach, $w_0$ is a constant as the specific weight of the water (9.807kN/m$^3$). Such a relationship has been verified in various scales, including experiments with monochromatic waves [43] and field measurements [44]. In the dam-break benchmark, the peak pressure force is assumed to be linearly correlated with the initial water depth $h$, which is non-dimensionalized by the distance $L$ between the gate and the stationary object. It is reasonable to build the relationship in small-scale dam break benchmarks and extend it to large-scale water waves.

Next, the dimensionless number of experiments are compared to the applications, and the sufficiency can be verified if the test data envelops the application behavior. In another word, the dimensionless number of a sufficient validation database should cover those numbers in the application scenarios. Otherwise, the selected phenomena can be only peculiar to the experiments and is not expected in the applications. Such issue is usually known as the scaling distortion. As a result, a relevance analysis is needed for the database to ensure that all selected phenomena are also typical under prototypic conditions. Finally, the model predictions are made for the applications, and an uncertainty analysis is performed with respect to each evaluated phenomenon. **Error! Reference source not found.** shows general descriptions for the attributes and criteria of scaling analysis.

Table  shows the summary of numerical benchmarks and their physical characteristics for external-flooding scenarios. Compared to the list of benchmarks in Table , some cases are not discussed due to a lack of validation data. It is known that the phenomena of turbulence and vortex shedding are governed by the Reynolds number that are differently defined. For the rest phenomena, the dimensionless groups are characterized based on author's best knowledge, and verification is still needed. For phenomena of hydrodynamic force on stationary structures, the QoI (peak force) is found to be linearly related to the initial height of water column according to Figure . In this study, the initial column height is non-dimensionalized by Eq. 8.50 Since the values of dimensionless group in the postulated full-scale scenario are covered by the range of experimental database, simulation errors are expected to be less than 10% with particle size equals to 0.02m. A similar analogy also applies to the phenomenon of surface-wave propagation, where the time of peak force is the QoI. Differently, the simulation errors are expected to be less than 20% with particle size of 0.02m. However, more data from facilities with different configurations are still needed to verify the scalability of dimensionless group. For the phenomenon of hydrodynamic force on moving structures, the density ratio $\rho^*$ (Eq. 8.53) and volume ratio $V^*$ (Eq. 8.54) are used, and they are assumed to be same in

application and experiment scenarios. However, such a theory is not verified, and more data from different facilities and configurations are needed. Furthermore, this study assumes that the values of dimensionless group in the postulated full-scale scenario are the same as those from experimental database.

Table 8.13: summary of numerical benchmarks and their physical characteristics for external-flooding scenarios

| **Phenomenon Description** | **Numerical Benchmarks** | **Dimensionless Group** | | |
|---|---|---|---|---|
| | | **Symbolic Representation** | **Validation Database** | **Application** |
| Response Time | | | | |
| Surface-Wave Propagation | Dam Break | $x^*$ (Eq. 8.50) | 0.2~0.26 | 0.25 |
| Structural Loads | | | | |
| Hydrodynamic Force on Stationary Structures | Dam Break; | $x^*$ (Eq. 8.50) | 0.2~0.26 | 0.25 |
| Hydrodynamic Force on Moving Structures | Falling Objects | $\rho^*$ (Eq. 8.53) $V^*$ (Eq. 8.54) | $\rho^* = 0.8$ $V^* = 512$ | $\rho^* = 0.8$ $V^* = 512$ |
| | Floating Objects | | $\rho^* = 2.1$ $V^* = 4.5E5$ | $\rho^* = 2.1$ $V^* = 4.5E5$ |

Based on the criteria in **Error! Reference source not found.** and the dimensionless group, outputs of scaling analysis can be determined. Table  shows qualitative judgements for the sufficiency, relevance, and distortion obtained from the scaling analysis.

8.5.6. Adequacy Decision

To decide the adequacy of SPH methods in simulating the designated external-flooding scenarios, results from reviews, theories, assessments, PIRT, and scaling analysis are combined by the scheme in Figure 8.40. Since the database is mainly collected from literature, this study focuses on the accuracy assessment of separate phenomena, while the integral code adequacy has not been properly measured. Although a scaling analysis has been performed, the dimensionless groups and their relationships to QoIs are not verified. Table  summarizes the results from various components. Meanwhile, suggestions for particle-size selections are included according to the results of accuracy assessments and scaling analysis.

Table 8.14. Validation results for SPH methods in simulating the external-flooding scenario

| **Phenomenon Description** | **Code Adequacy** | **Accuracy (L1 error)** | **Scaling Analysis** | | | **Suggested Particle Size** |
|---|---|---|---|---|---|---|
| | | | **Relevance** | **Sufficiency** | **Distortion** | |
| Response Time | | | | | | |
| Surface-Wave Propagation | Reasonable | Reasonable (12.7%) | Yes | Yes | Bounded | 0.02m |
| Structural Loads | | | | | | |
| Hydrodynamic Force on Stationary Structures | Excellent | Excellent (3.6%) | Yes | Yes | Bounded | 0.02m |
| Hydrodynamic Force on Moving Structures | Falling – Insufficient | Excellent (5.52%) | Yes | No | N/A | Falling – 0.25m |
| | Floating – Insufficient | Excellent (4.41%) | | | | Floating – 0.1m |

For the scenario of "floods damage the building structures, enter the room, and cause diesel generator malfunctioning", SPH methods can predict the hydrodynamic force on both stationary and moving structures with acceptable accuracy. For the phenomena with stationary structures, the present analysis suggests that the particle size of Neutrino simulation should be less than or equal to 0.02m. At the same time, according to the scaling analysis by dimensionless group $x^*$, the database is sufficient for predicting a similar phenomenon in full-scale scenarios. However, the present decision is limited to predicting peak pressure force under unbroken surface waves. The validity of such conditions in the target application needs evidence from larger scales. At the same time, it has been suggested by the independent reviewers that other important phenomena, like turbulence, can be critical in predicting the target QoIs in addition to the static and dynamic pressures [45]. For the phenomena with moving structures, the suggested particle size for a postulated scenario is 0.25m for falling cubes and 0.1m for floating cube. Since there is only one dataset for this phenomenon, distortion analysis is not applicable (N/A).

## 8.6. Conclusion

The present study demonstrates a validation of SPH methods and the corresponding software Neutrino in simulating a designated external-flooding scenario. To ensure the consistency and completeness, validation frameworks CSAU, and its regulatory guide EMDAP is followed. An external-flooding scenario is defined, and a PIRT process is performed, which identifies the surface-wave impacts on rigid structures as one of the high-rank phenomena. At the scoping stage, acceptance criteria of 20% is set based on authors' knowledge and reviewed by researchers in relevant fields. Two numerical benchmarks are designed, and the simulation results are compared against the experimental measurements. It is found that for all benchmarks, SPH methods can predict the hydrodynamic force acting on both stationary and moving structures with excellent accuracy, where the $L_1$ relative error norm is less than 10%. At the same time, for the phenomenon of surface-wave propagation, SPH simulation accuracy appears reasonable ($L_1$<20%). For each case, suggestions on particle-size selections are also made according to the results of the convergence study. Next, a scaling analysis is performed for identifying the sufficiency, relevancy, and distortion of validation database from the perspective of the full-scale applications. In addition, dimensionless groups are suggested for evaluating the full-scale behaviors based on the existing database. It is found that SPH can be used to predict unbroken surface-wave peak-pressure impacts on stationary structures with adequate performance, while evidence is not sufficient to justify its adequacy in predicting forces onto moving objects. Meanwhile, independent reviews suggest that the validity of major assumptions in target applications need to be evaluated with large-scale experiments, and the relevancy of other phenomena like turbulence need to be identified with more benchmarks. Consequently, additional validation-grade experiments and high-fidelity simulations must be collected for new data. Meanwhile, it is recommended that an adequacy decision model is needed to assess code adequacy and to reduce uncertainties due to the lack of data and heuristic biases.

## 8.7. References


[1] S. Hess, N. Dinh, J. Gaertner and R. Szilard, "Risk-informed safety margin characterization," in *Proceedings of the 17th International Conference on Nuclear Engineering*, Brussels, 2008.

[2] C. Rabiti, A. Alfonsi, J. Cogliati, D. Mandelli, R. Kinoshita and C. Smith, "A novel method of controlling thermal hydraulics codes using RAVEN," LWRS Newsletter, 2014.

[3] H. Bao, H. Zhao, H. Zhang, L. Zou, P. Sharpe and N. Dinh, "Safe reactor depressurization windows for BWR Mark I Station Blackout accident management strategy," *Annals of Nuclear Energy,* vol. 114, pp. 518-529, 2018.

[4] C. Smith, C. Rabiti, R. Martineau and R. Szilard, “Risk-Informed Safety Margins Characterization (RISMC) Path Technical Program Plan,” Idaho National Laboratory, Idaho Falls, 2015.

[5] R. Sampath, N. Montanari, N. Akinci, S. Prescott and C. Smith, “Large-scale solitary wave simulation with implicit incompressible SPH,” *Journal o f Ocean Engineering and Marine Energy*, vol. 2, no. 3, 2016.

[6] N. Zuber, G. E. Wilson, M. Ishii, M. Wulff, B. Boyack and A. Dukler, “An integrated structure and scaling methodology for severe accident technical issue resolution: Development of methodology,” *Nuclear Engineering and Design*, vol. 186, pp. 1-21, 1998.

[7] U.S. NRC, “Transient and accident analysis methods,” U.S. Nuclear Regulatory Commission, Washington D.C., 2005.

[8] C. Fletcher, P. Bayless, C. Davis, M. Ortiz, S. Sloan, R. Shaw, R. Shultz, C. Slater, G. Johnsen, J. Adams, L. Ghan and D. Bessette, “Adequacy Evaluation of RELAP5/MOD3, Version 3.2.1.2. for simulating AP600 Small Break Loss-of-Coolant Accidents,” Idaho National Engeneering and Environment Laboratory, Idaho Falls, 1997.

[9] L. B. Lucy, “A numerical approach to the testing of the fission hypothesis,” *Astronomical Journal*, vol. 82, no. 12, pp. 375-389, 1977.

[10] D. Violeau and R. Issa, “Numerical modelling of complex turbulent free-surface flows with the SPH method: an overview,” *International Journal for Numerical Methods in Fluids*, vol. 53, no. 2, pp. 277-304, 2007.

[11] L. Lin, N. Dinh, N. Montanari, R. Sampath, N. Akinci and S. Prescott, “Assessment of Smoothed Particle Hydrodynamics in Application of High-Wind Risk Analysis,” in *17th International Topical Meeting on Nuclear Reactor Thermal Hydraulics*, Xi'an, 2017.

[12] L. Lin, N. Dinh, R. Sampath and N. Akinci, “A computational study of think film dynamics on micro-structured surfaces,” in *Proceedings of the ASME 2016 Summer Heat Transfer Conference*, Washington DC, 2016.

[13] T. Capone, A. Panizzo and J. Monaghan, “SPH modelling of water waves generated by submarine landslides,” *Journal of Hydraulic Research*, vol. 48, pp. 80-84, 2010.

[14] R. Vacondio, B. Rogers, P. Stansby and P. Mignosa, “Shallow water SPH for flooding with dynamic particle coalescing and splitting,” *Advances in Water Resources*, vol. 58, pp. 10-23, 2013.

[15] S. Marrone, B. Bouscasse, A. Colagrossi and M. Antuono, “Study of ship wave breaking patterns using 3D parallel SPH simulations,” *Computers and Fluids*, vol. 69, pp. 54-66, 2012.

[16] A. Zhang, X. Cao, F. Ming and Z. Zhang, “Investigation on a damaged ship model sinking into water based on three dimensional SPH method,” *Applied Ocean Research*, vol. 42, pp. 24-31, 2013.

[17] S. Lind, P. Stansby, B. Roger and P. Lloyd, “Numerical predictions of water-air wave slam using incompressible-compressible smoothed particle hydrodynamics,” *Applied Ocean Research*, vol. 49, pp. 57-71, 2015.

[18] X. Ni, W. Feng and D. Wu, "Numerical simulations of wave interactions with vertical wave barriers using the SPH method," *International Journal for Numerical Methods in Fluids,* vol. 76, no. 4, pp. 223-245, 2014.

[19] D. Violeau and B. D. Rogers, "Smoothed particle hydrodynamics (SPH) for freesurface flows: past, present and future," *Journal of Hydraulic Research,* vol. 54, pp. 1-26, 2016.

[20] J. Monaghan and R. Gingold, "shock simulation by the particle method SPH," *Journal of Computational Physics,* vol. 52, no. 2, pp. 374-389, 1983.

[21] "M. Ihmsen; J. Cornelis; B. Solenthaler; C. Horvath; M. Teschner," *IEEE Transactions on Visualization and Computer Graphics,* vol. 20, no. 3, pp. 426-435, 2014.

[22] N. Akinci, J. Cornelis, G. Akinci and M. Teschner, "Coupling elastic solids with smoothed particle hydrodynamics fluids," *Journal of Computer Animation and Virtual Worlds,* vol. 24, no. 3-4, pp. 195-203, 2013.

[23] A. Colagrossi, M. Antuono and D. Touze, "Theoretical considerations on the free-surface role in the smoothed-particle-hydrodynamics model," *Physical Review,* vol. 79, no. 056701, 2009.

[24] L. Lin, "Development and Assessment of Smoothed Particle Hydrodynamics Method for Analysis of External Hazards," North Carolina State University, Raleigh, 2019.

[25] N. Akinci, "Interface handling in smoothed particle hydrodynamics," University of Freiburg, Freiburg im Breisgau, 2014.

[26] D. Goring, "Tsunamis-the propagation of long waves onto a shelf," California Institute of Technology, Pasadena, 1978.

[27] B. Ren, M. He, P. Dong and H. Wen, "Nonlinear simulations of wave-induced motions of a freely floating body using WCSPH method," *Applied,* vol. 50, pp. 1-12, 2015.

[28] L. Lin, "Assessment of the smoothed particle hydrodynamics method for nuclear thermal-hydraulic applications," North Carolina State Uninversity, Raleigh, 2016.

[29] C. Smith, S. Prescott, J. Coleman, E. Ryan, B. Bhandari, D. Sludern, C. Pope and R. Sampath, "Progress on the industry application external hazard analyese early demonstration (INL/EXT-15-36749)," Idaho National Laboratory, Idaho Falls, 2015.

[30] Y. Liu, N. Dinh, R. Smith and X. Sun, "Uncertainty quantification of two-phase flow and boiling heat transfer simulations through a data-driven modular Bayesian approach," *International Journal of Heat and Mass Transfer,* vol. 138, pp. 1096-1116, 2019.

[31] H. Bao, N. Dinh, J. Lane and R. Youngblood, "A data-driven framework for error estimation and mesh-model optimization in system-level thermal-hydraulic simulation," *Nuclear Engineering and Design,* vol. 349, pp. 27-45, 2019.

[32] G. Katell and B. Eric, "Accuracy of solitary wave generation by a piston wave maker," *Journal of Hydraulic Research,* vol. 40, no. 3, pp. 321-331, 2002.

[33] S. J. Cummins, T. B. Silverster and P. W. Cleary, "Three-dimensional wave impact on a rigid structure using smoothed particle hydrodynamics," *International Journal for Numerical Methods in Fluids,* vol. 68, pp. 1471-1496, 2012.

[34] F. Aureli, S. Dazzi, A. Maranzoni, P. Mignosa and R. Vacondio, "Experimental and numerical evaluation of the force due to the impact of a dam-break wave on a structure," *Advances in Water Resources*, vol. 76, pp. 29-42, 2015.

[35] T. Wu, C. Chu, C. Huang, S. Chien and M. Chen, "A two-way coupled simulation of moving solids in free-surface flows," *Computers & Fluids*, vol. 100, pp. 347-355, 2014.

[36] I. Hadzic, J. Hennig, M. Peric and Y. Xing-Kaeding, "Computation of flow-induced motion of floating bodies," *Applied Mathematical Modelling*, vol. 29, pp. 1196-1210, 2005.

[37] Y. Goda, Random Seas and Design of Maritime Structures, Advanced Series on Ocean Engineering, New Jersey: World Scientific, 2000.

[38] "LAMMPS-SPH," Sandia National Laboratory, [Online]. Available: http://lammps.sandia.gov.

[39] D. Violeau, Fluid Mechanics and the SPH Method: Theory and Applications, Oxford: OXFORD UNIVERSITY PRESS, 2012.

[40] I. Tadjbakhsh and J. Keller, "Standing surface waves of finite amplitude," *Journal of Fluid Mechanics*, vol. 8, no. 3, 1960.

[41] Y. Goda, "The Fourth Order Approximation to the Pressure of Standing Waves," *Coastal Engineering in Japan*, vol. 10, no. 1, pp. 1-11, 1967.

[42] Y. Goda, "New wave pressure formulae for composite breakwaters," in *14th International Conference on Coastal Engineering*, Copenhagen, Denmark, 1974.

[43] H. Takagi, T. Shibayama and M. Esteban, "An expansion of the reliability design method for caisson-type breakwaters towards deep water using the fourth order approximation of standing waves," in *Asian and Pacific Coasts*, Nanjing, China, 2007.

[44] E. Marchi, E. Raiteri, G. Scarsi and S. Sturo, "Storm wave pressures on the breakwater of Genoa Harbor measurement station," in *the 16th Congress of the Interational Association for Hydraulic Research*, 1975.

[45] Nuclear Engineering and Design, "Reviewer feedbacks from the journal submission," 2020.

[46] B. Bouscasse, A. Colagrossi, S. Marrone and M. Antuono, "Nonlinear Water Wave Interaction with Floating Bodies in SPH," *Journal of Fluids and Structures*, vol. 42, pp. 112-129, 2013.

# 9. Validation of SPH for Nuclear Power Plant Scenarios using Neutrino

## 9.1. Summary

The validation of Smoothed Particle Hydrodynamics (SPH) has many different facets such as impact forces, wave formation, turbulent flows, etc. Additionally, in the nuclear power industry, there are many different types of flooding concerns with different factors affecting the protection features. The purpose of this area of work was to determine applicable or correlated test cases, develop experimental validation methods and then perform some validation cases against experimental results on a large scale in order to provide data for scalability.

The critical validation factors of SPH for flooding scenarios are Impulse pressure, Duration, Wave Height, velocity, and Turbulence. Different validation factors are applicable for varying flood scenarios and protection strategies. This work provides a method for determining those factors so that the correct uncertainty factors can be used in the overall data driven methodology for uncertainty.

Historically several validation cases for SPH have been done to both small scale experiments and numerical comparison of results vs CFD. The impact validation case of wave impact forces was chosen for initial validation. George Washington University constructed the wave tank and performed necessary experiments and Neutrino's SPH code was used for the fluid simulation [3].

Both experimental and simulation parameter variations can affect the validation results. To minimize uncertainty and optimize simulation costs in simulation results, modelers need guidance on parameter values. Along with experimental parameters, Neutrino has over 30 different parameters that can be adjusted, using expert judgement this was reduced to 7 parameters, to perform importance measures on including:

- Stop Threshold
- Particle Size
- Interaction-Radius to Particle-Size Ratio
- Fluid Settling uncertainty
- Forcing function amplitude uncertainty
- Forcing function frequency uncertainty
- Pressure transducer location uncertainty

The most significant parameters were particle size, fluid settling, and interaction-radius to particle size ratio.

Using the optimal parameter values for computation time and accuracy, the impulse pressure of the experiment and simulation results were compared (Figure 9.1). The simulation results averaged around 3-4% difference from the experiment results, with a max of less than 10% for the four different experimental runs. The experiment results varied 2-3% with a max of 8% variation. This data combined with other validation results, including scaling factors can then be used in the overall data driven methodology.

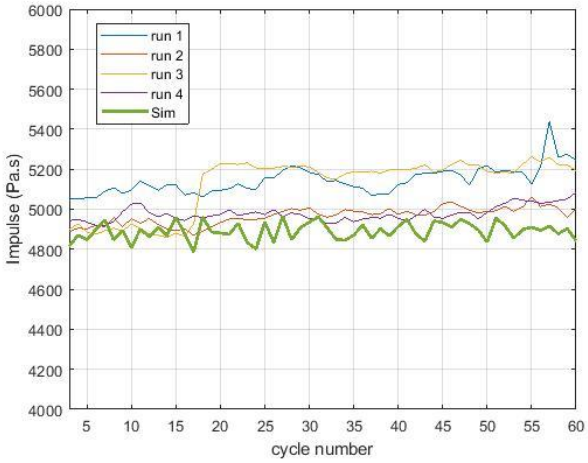


Figure 9.1. Experimental and simulation impulse.

## 9.2. Introduction

Mitigation efforts are often designed or retrofitted into structure to reduce the damage to critical areas—i.e., removable barriers or dikes. Since floods will always be a concern, improvements or new tools to optimize the cost of mitigation efforts are always valuable. Simulating flooding events is conducted through many different methods and at varying levels of detail. These tools help determine general flooding inundation height, down to the specific components or infrastructure that might be damaged. Modelling can help guide mitigation efforts to prevent damage from occurring. However, for these simulations to be useful, they must match reality, which requires code validation. Because there are many different flooding scenarios, from barrier overtopping to debris impact, there are also many different features that need validation, and one code could be very effective for simulating overtopping but not work at all for debris. The following PIRT style table lays out scenario types and the key factors for validation which can then be used for proper uncertainty analysis of that scenario type.

| | Pressure /Impulse | Duration | Max Height / Splash | Velocity | Turbulence |
|---|---|---|---|---|---|
| Door Failure | High | - | - | - | - |
| Barrier Over-Top | - | High | Med | Med | - |
| Barrier Failure | High | *Low | - | - | *Med |
| Penetration | - | High | - | High | - |
| Exhaust Vent | - | - | High | - | - |
| Ducting | High | - | - | - | - |
| Debris Impact | - | - | Low | High | Med |

"*" Type Dependent

To develop the methodology and generate initial data, different experiment cases were established using the large-scale oscillating designed and constructed at George Washington University. The tank measures 5.951 m long × 1.2 m high × 2.468 m wide and is constructed of a steel frame and acrylic walls and bottom. The adaptive design allows for attaching structures inside the tank and both pressure transducers and high imagery cameras measure forces and fluid movement. The tank is oscillated through a sine-forcing function using a hydraulic actuator. The first validation case chosen was wave impact force as this is a common case and would provide additional data for scaling analysis.

By recreating the physical tank and experiments using SPH we can then determine a few critical aspects of the simulation. First, what features of the experiments is the SPH code able to recreate with sufficient accuracy and speed. Second, what SPH parameters are critical for good simulation results? To do this a

virtual tank was set up using Neutrino, matching the physical model of the tank. A forcing function using the same oscillation formula as the physical tank was used to move the virtual tank model, in order to most closely match the actual movement.

The results of the experiment vs simulation and parameter importance can then be used to help determine the confidence for a specific type of flooding scenario and contribute to the data driven validation.

### 9.3. Scope of Work

The main objective of this work consisted of simulation validation with two test areas. First, the comparison of SPH simulation results to experiment results for the wave oscillation tank. Second, the importance of specific SPH parameters affecting the accuracy of the simulation. The next objective was the application of this validation data in how to correctly apply uncertainty results.

Experiment data was generated by using wall pressure transducers set at a depth of 0.1524m. The experiment ran for 60 cycles and was repeated four times with minor variations as shown in Table . Of the 60 cycles, the last 10 were averaged for the result, to establish a steady state for the results.

Table 9.1. Experimental model run variations.

| Run | Water Depth (m) | Frequency (Hz) | Amplitude (m) | Variation |
|---|---|---|---|---|
| 1 | 0.1524 | 0.11 | 0.1016 | Reference run |
| 2 | 0.1524 | 0.11 | 0.1016 | Identical to Run 1 |
| 3 | 0.1524 | 0.11 | 0.102108 | Change of forcing amplitude by 1% |
| 4 | 0.1534 | 0.11 | 0.1016 | Change of water depth by 1 mm |

The Neutrino model was constructed to match the experimental setup as closely as possible. The oscillating tank experiment can be characterized as a two-dimensional (2-D) experiment, resulting in the simulation tank having the same length and height dimensions, but a smaller width of 0.2 m. By reducing the width of the simulation tank, the computational runtime of the simulation is also reduced without compromising accuracy. A simulation with a particle size of 0.01 m (181,387 fluid particles total) takes about 16.7 hours for 30 cycles using an Intel Xeon central processing unit E5-2683 v3 @ 2.00 GHz with 28 core and 56 logical processors.

The simulation tank was filled with particles to the correct fluid depth. The number of fluid particles was carefully controlled to ensure that the numerical volume of the fluid simulation corresponds to the correct physical fluid depth. A measurement field is used to measure the pressure on the end-wall. This measurement field compares to the pressure transducers used in the experimental setup. Figure 9.2. shows the large-scale oscillating tank on the left and a cross-sectional view of the simulation setup on the right.

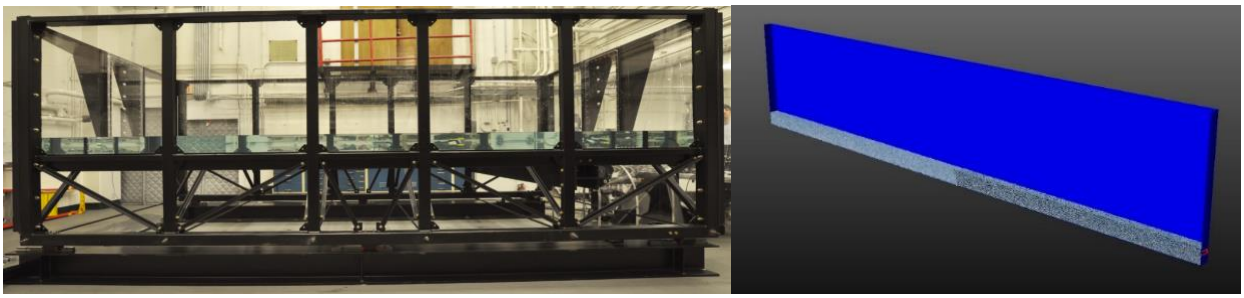

Figure 9.2. Large-scale oscillating tank at the George Washington University (left) and Neutrino simulation setup (right).

Once the simulation setup was complete, the simulation tank and end-wall measurement field needed to be oscillated at the same forcing function as the experiment. To create these oscillations, a python script for each object was created and added to the position of the object as a dynamic expression. The python scripts adjust the position of the items based on Equation 9.9.2.

$$z(t) = A \sin(2\pi f t) \tag{9.2}$$

where z is the new position, t is the time, A is the amplitude, and f is the frequency. The amplitude and frequency values are set in the python script to match the experimental values, and the time is extracted from the simulation. The equation allows for the movement of each object to be continuous and evaluated for every time step of the simulation. Without using the equation and, instead, using a dataset of positions, the movement of the objects may not shift smoothly with the time step, causing jumps with overlapping particles, which results in erratic or explosion-like behavior from the simulation tank impact.

The RAVEN software developed at INL [1] along with a coupling module [2] was used for performing advanced sampling, parameter optimization, and run the Neutrino simulation and then post-process results. The methodology for determining the significance of parameters consisted of, first, randomly sampling across the range of possible values of a single parameter. The values were sampled from a uniform distribution across the range of values using a Monte Carlo sampler. The value range for each parameter was selected based on previous simulation investigation or the uncertainties associated with the physical experiment. The results were then analysed to determine whether the parameter caused a change in the results. If the different parameters values did not cause a change in results, then the parameter was considered insignificant. Table  shows the range of values for each parameter, as well as the default value that was used when other parameters were being sampled. These ranges are all considered uniform although many have other distributions.

Table 9.2. Investigated parameter value ranges and default value.

| **Parameters** | **Value Range** | **Default Value** |
|---|---|---|
| Stop threshold | 0.0001 to 0.01 | 0.001 |
| Particle size | 0.007 m to 0.02 m | 0.01 m |
| Interaction-radius to particle-size ratio | 2.0 to 2.4 | 2.0 |
| Fluid settling uncertainty | $-0.4\delta_r$ to $0.4\delta_r$* | 0 |
| Forcing function amplitude uncertainty | 0.1012 m to 0.102 m | 0.1016 m |
| Forcing function frequency uncertainty | 0.1099868 Hz to 0.110011 Hz | 0.11 Hz |
| Pressure transducer location uncertainty | 0.1006 m to 0.1026 m | 0.1016 m |

* where $\delta_r$ is the particle size

## 9.4. Key Findings

The 90% and 50% pressure bounds for the experiment and simulation were compared. Additionally, the pressure of each cycle was integrated over time to compare the pressure impulse. Figure  shows the pressure bound comparison with the 90% bound plot on the left and the 50% bound plot on the right. Figure  shows the absolute percentage error plots between the simulation and experiment upper and lower bounds for the 90% bounds on the left and the 50% bounds on the right.

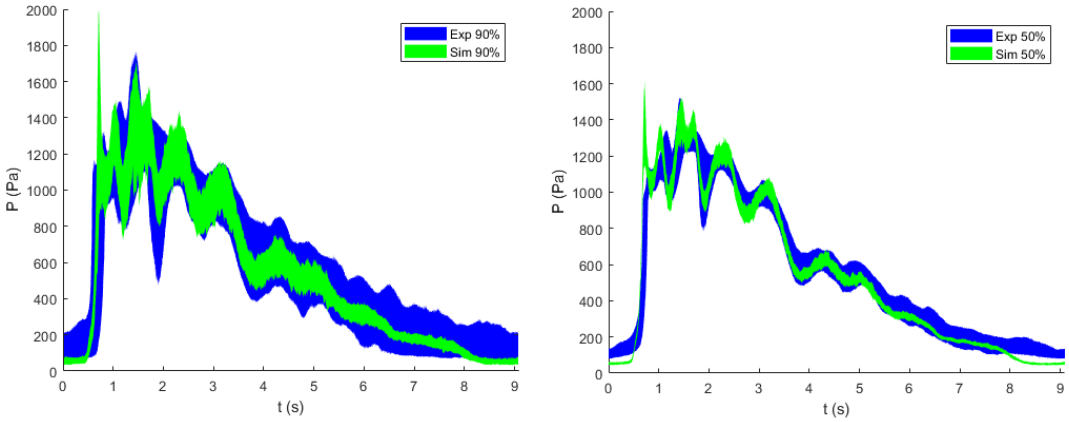


Figure 9.3. Pressure bounds comparison plots.

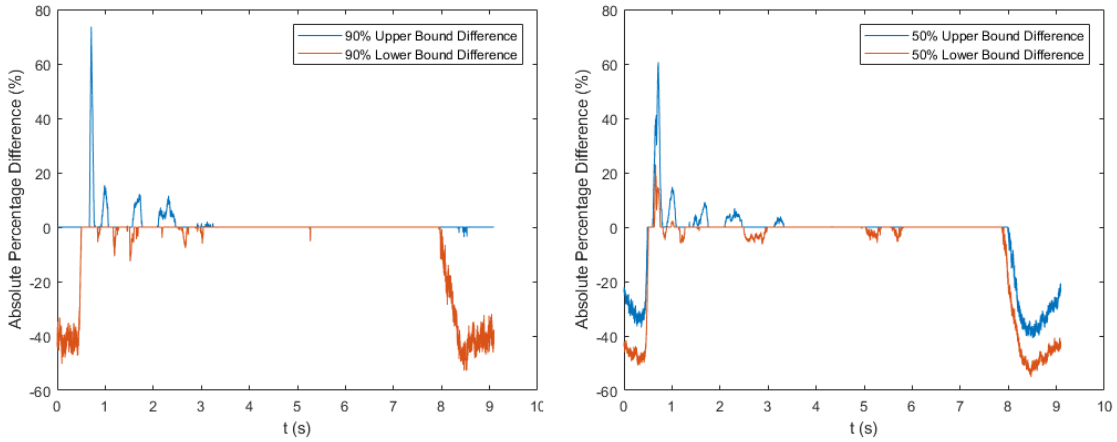


Figure 9.4. Pressure bounds simulation error plots.

The above plots show that both the 90% and 50% simulation pressure bounds mostly fall within the experimental bound. A few exceptions do occur in the low-pressure areas at the very beginning of the cycle (~40% difference) and the very end of the cycle (~40% difference); however, these low-pressure differences are typically insignificant for applications. The peak pressure tends to have a short but high initial peak variation (~75% difference) compared to the experiment. Overall, the simulation results match well with the experimental results for most of the time. However, refinement of parameters could possibly increase the accuracy of the simulation.

The simulation impulse pressure was compared to the pressure impulse for each experimental run. The absolute percentage difference between the simulation and each experimental run was also computed. Figure  shows the impulse pressure comparison plot on the left and the absolute percentage difference plot on the right.

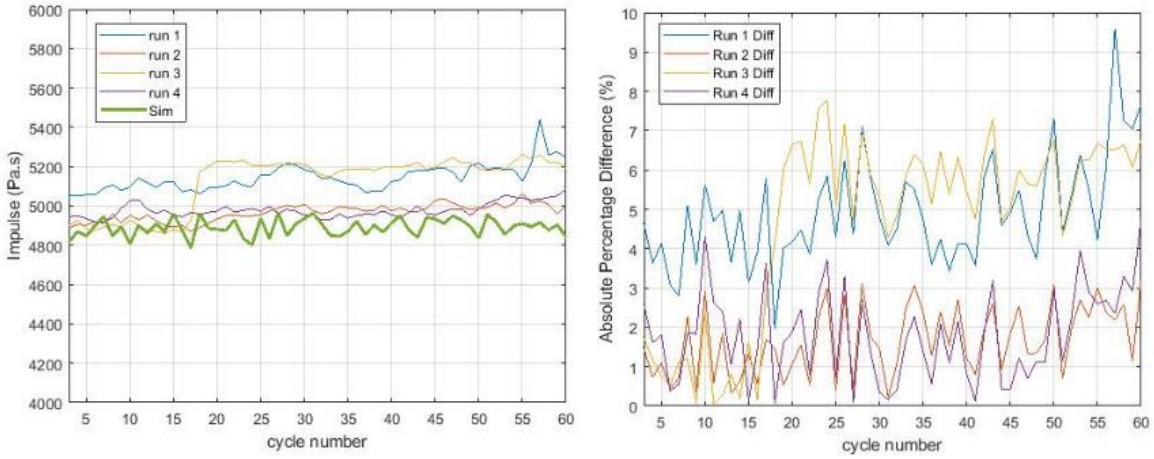


Figure 9.5. Impulse pressure comparison plots.

The absolute percentage difference plot shows that the pressure impulse of the simulation is within 10% of all four experimental runs. However, for two of the runs, the simulation is within 5% of the experiment. This shows that the simulation pressure impulse matches the experimental very well.

The parameters and their range of values identified above were sampled five times using RAVEN. The pressure results for all five runs were compared to determine whether the parameter is significant. To reduce the computational runtime, 30 rather than 60 cycles were simulated. Table  shows the five sampled values for each parameter and Figure  shows the average pressure plot comparison for the different parameters.

Table 9.3. Sampled values for each parameter.

| **Parameter** | **Sample 1** | **Sample 2** | **Sample 3** | **Sample 4** | **Sample 5** |
|---|---|---|---|---|---|
| Stop threshold | 0.005188 | 0.009604 | 0.000482 | 0.008365 | 0.004260 |
| Particle size | 0.009004 | 0.009710 | 0.018166 | 0.011869 | 0.017700 |
| Interaction-radius to particle-size ratio | 2.083384 | 2.149816 | 2.013502 | 2.042695 | 2.089326 |
| Fluid settling uncertainty | 0.027887 | 0.920035 | -0.922877 | 0.669684 | -0.691674 |
| Forcing function amplitude uncertainty | 0.101436 | 0.101541 | 0.101956 | 0.101291 | 0.101270 |
| Forcing function frequency uncertainty | 0.110007 | 0.110008 | 0.110011 | 0.109989 | 0.109992 |
| Pressure transducer location uncertainty | 0.102298 | 0.102340 | 0.101516 | 0.102578 | 0.101047 |

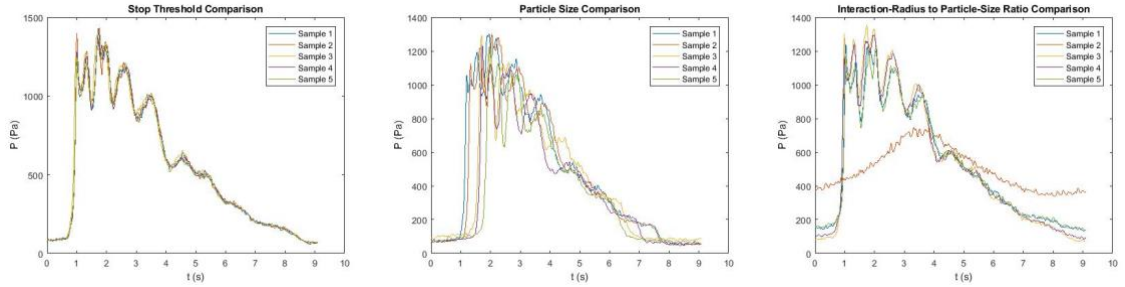

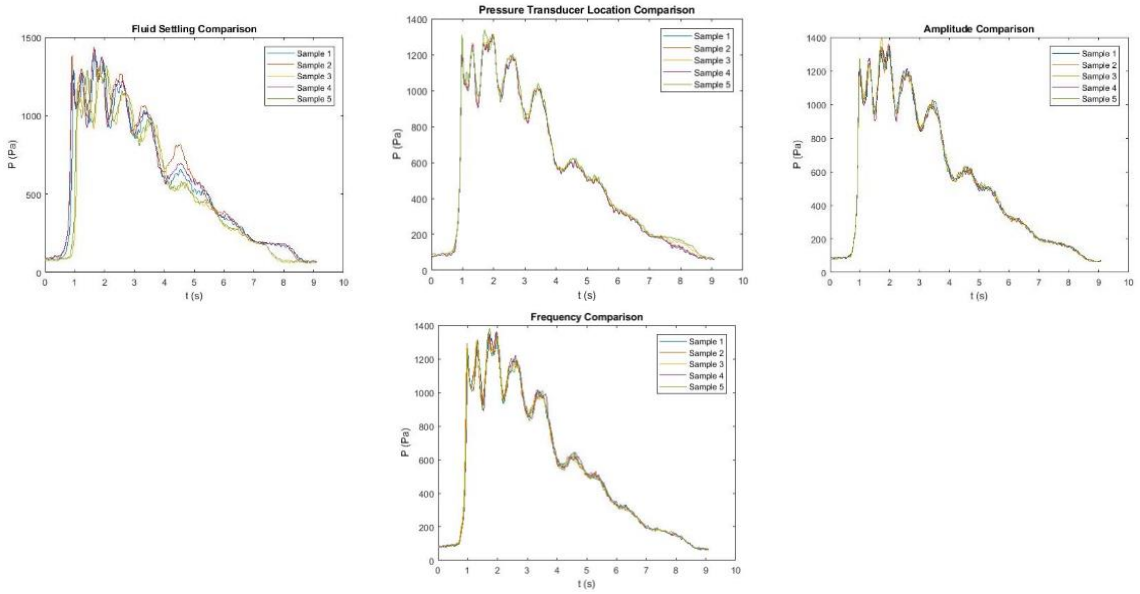


Figure 9.6. Average pressure comparison plots for each investigated parameter.

Based on the plots above, all seven parameters influence the simulation results. However, some of these parameters seem to be more important based on the amount of fluctuation that occurred between the results. For example, the particle size, interaction-radius to particle-size ratio, and fluid settling plots showed greater fluctuation than the stop threshold, amplitude, frequency, and pressure transducer location plots. This indicates that more research is needed to quantify the significance of each parameter.

These results can then be used for uncertainty in the categories of the PIRT diagram for use by specific scenarios feed into the PCMQBN framework. For example, the experiment results show above provide the pressure validation this can be used for door failures. Validation data from the experiment could be used as a whole, but any data that does not fall into the range of causing a door failure is irrelevant (Figure 9.7). In this case the validation attribute of concern is the difference band of the simulation peek pressure or the band above a threshold in impulse pressure vs the experiment. If the simulation is significantly different for low pressures but accurate for higher pressures, the simulation outcome uncertainty would be very low. However, if the simulation were accurate for low pressures, but more inaccurate for higher pressures, using the overall uncertainty would indicate the outcome results better than what they are.

| | Pressure /Impulse | Duration | Max Height / Splash | Velocity | Turbulence |
|---|---|---|---|---|---|
| Door Failure | High | - | - | - | - |
| Barrier Over-Top | - | High | Med | Low | - |
| Barrier Failure | High | *Low | - | - | *Med |
| Penetration | - | High | - | High | - |
| Exhaust Vent | - | - | High | - | - |
| Ducting | High | - | - | - | - |
| Debris Impact | - | - | Low | High | Med |

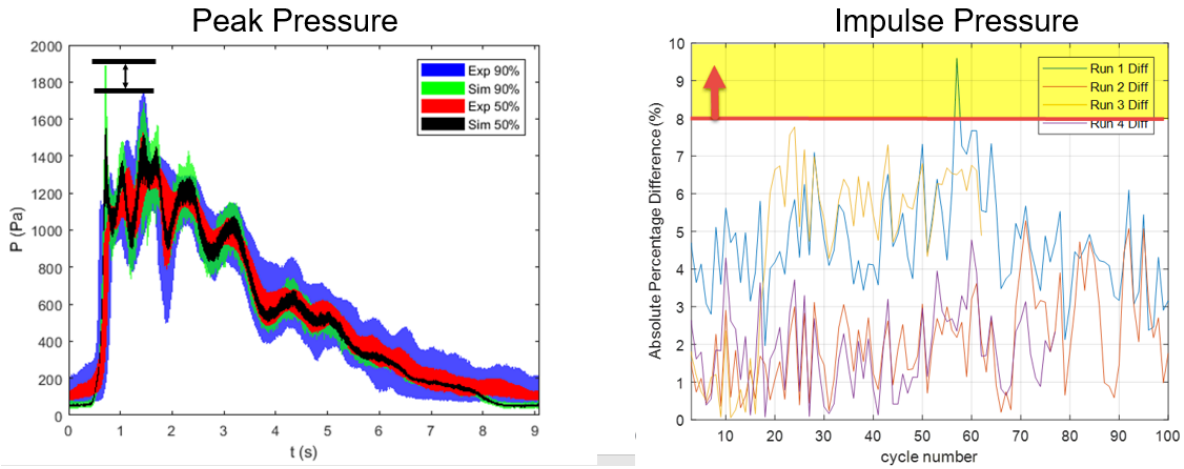


Figure 9.7. Key validation areas for door failures.

## 9.5. Conclusions

The validation results of the SPH simulation provided several aspects of data for the data-driven methodology: general uncertainty values; data for scaling; and bands of applicable validation data. Through varying the SPH parameters it was shown that the particle size, interaction-radius to particle-size ratio, and fluid settling are important factors can have a large influence on the uncertainty of the results.

The process used for this research can be used in developing validation cases against experiments for the flooding scenario areas of pressure, duration, max height/splash, and turbulence. The resulting uncertainty can then be used in correlation with scenario applicability in the PCMQBN data driven methodology for an overall model confidence rating.

## 9.6. References


[1] Rabiti, C., Alfonsi, A., Cogliati, J. Mandelli, D., Kinoshita, R., Sen, S., Wang, C., Talbot, P. W., Maljovec, D. P., and Chen, J. (2017). "RAVEN User Manual," Idaho National Laboratory, Idaho Falls, ID, INL/EXT-15-34123.

[2] Ryan, E. D., and Pope, C. L. (2019). "Coupling of the Smoothed Particle Hydrodynamic Code Neutrino and the Risk Analysis Virtual Environment for Particle Spacing Optimization," *Submitted for publication.*

[3] Sampath, R., Montanari, N., Akinci, N., Prescott, S., and Smith, C. (2016). "Large-Scale Solitary Wave Simulation with Implicit Incompressible SPH," *Journal of Ocean Engineering and Marine Energy*, Volume 2, Issue 3.

# 10.System Thermal-Hydraulics Model Validation Experiment

## 10.1. Summary

This work is part of an integrated research project (IRP) titled "Development and Application of a Data-Driven Methodology for Validation of Risk-Informed Safety Margin Characterization Models" supported by the U.S. Department of Energy Office of Nuclear Energy's Nuclear Energy University Program (NEUP) to develop a data-driven validation methodology for risk-informed safety margin characterization (RISMC) models. The primary purpose of this study is to demonstrate an application of the data-driven validation methodology. The work presented in this report is to establish experimental facilities, conduct experiments, and provide data support for the data-driven validation methodology development.

Compared to the traditional validation practices, data-driven validation relies on data from experiments (and advanced computational analyses) that are specifically designed for the model and use state-of-the-art methods to rigorously map and bound the simulation uncertainties in the domain of intended model use. Therefore, data-driven validation presents a significant shift from the current validation practices based on expert-determined scale distortions.

The work introduced in this report is to design and establish an experimental facility (or facilities), conduct experiments, and provide data support for the validation of a system thermal-hydraulics (STH) code based on the proposed data-driven validation methodology. RELAP-7 was proposed as the STH code of interest in the original proposal. However, since RELAP-7 is not available for validation, COBRA-TF (CTF), a subchannel analysis code, was chosen as the subject of STH code validation. In addition, based on the literature and feedback from the STH code validation subgroup, dispersed flow film boiling (DFFB) regime, where droplets are dispersed in a continuous superheated vapor phase, was chosen as the phenomenon focus of our study.

Three phases for the experimental investigation were proposed. In the first phase (Phase I), an air-water experiment was to be carried out at room temperature to test necessary optical instrument for droplet measurements and to develop proper experimental procedures, which serve as guidelines for elevated-temperature and pressure experiments. The second and third phase (Phase II/III) experimental work would involve modification of the Phase I experimental facility and proper configuration of components, which is not included in this report. Data processing was completed using LaVision ParticleMaster package and in-house computer codes to obtain polydispersed droplets diameter and velocity statistics. Additionally, the particle diameter distribution was modeled using a lognormal distribution. The distribution uncertainty was used to represent the data uncertainty quantification. Also, the estimated parameters' confidence interval in the distribution model fitting process was provided based on bootstrap resampling and central limit theorem. Finally, SMD calculation results based on two approaches, namely data-based and distribution-based, were provided. The processed data and quantified uncertainty from Phase I experiments would be valuable to the validation process in the data-driven model development.

## 10.2. Introduction

An integrated research project (IRP) titled "Development and Application of a Data-Driven Methodology for Validation of Risk-Informed Safety Margin Characterization Models" was initiated in October 2016 under the support of the U.S. Department of Energy Office of Nuclear Energy's Nuclear Energy University Program (NEUP). The project aims to develop and demonstrate a data-driven methodology for validation of advanced computer models for nuclear power plant safety analysis. Specifically, the advanced computer models are those in the toolkit developed to support the risk-informed safety margin characterization (RISMC), an integrated deterministic/probabilistic safety analysis

methodology developed in the Department of Energy's Light Water Reactor Sustainability (LWR-S) program.

One major challenge in model validation is lack of relevant data, including lack of confidence in the applicability of models and their supporting data in prototypic reactor conditions. It is possible to improve how we acquire and use the data for model validation. In particular, a new physics-guided validation strategy based on first principles physics will rigorously map and bound the simulation uncertainties in the domain of intended model use. To our knowledge, this represents a first-of-a-kind approach for the determination of the validation domain in the nuclear engineering community that presents a significant shift from the current approach for expert-determined scale distortion uncertainties. The project team plans to apply the developed validation methodology within this project to guide the validation of computer models for flooding hazard analysis and for system thermal-hydraulics (STH) analysis. In the original proposal, the RELAP-7 reactor system simulation code that has been under development at the Idaho National Laboratory was chosen as the STH code for validation. However, the code did not appear to be at the maturity level for a meaningful validation when this IRP was initiated. Therefore, COBRA-TF (CTF) was then chosen as the STH code of interest in this project.

Nucleate boiling is a highly efficient and desirable cooling mechanism in high power density systems. However, it is well known that the heat transfer capacity of a boiling system will be substantially reduced when the heat flux on the boiling surface exceeds the heat flux value corresponding to the departure from nucleate boiling. Such a critical heat flux (CHF) phenomenon and subsequent post-CHF scenario represent major limits for light water reactor (LWR) operation and safety. Therefore, modeling and prediction of post-CHF scenario, and the validation of these models are vital for the reactor safety analysis.

CTF [Salko et al. 2015] uses separate flow models for boiling heat transfer and two-phase flow, which consists of three fields, i.e., the liquid droplets, liquid film, and vapor. Supported by closure relations, CTF numerically solves the three sets of conservation equations of mass, momentum, and energy, one for each field, to obtain Quantities of Interest (QoI) of a certain scenario.

CTF decomposes a certain flow and heat transfer scenario into multiple flow regimes and heat transfer regimes. Criteria are set up to determine the transition between different regimes. For a given regime, multiple closure relations are incorporated into the conservation equations to make them numerically solvable. In CTF [Salko et al. 2015] the dispersed flow film boiling (DFFB) heat transfer regime is activated when the wall temperature is above both the critical heat flux temperature and the minimum film boiling temperature, and when the void fraction is higher than 0.95.

In the DFFB regime the heat transfer is a combination of three major mechanisms: convective heat transfer from the heated wall to the vapor phase, radiative heat transfer from the wall to vapor and liquid droplets and boiling/evaporative heat transfer when liquid droplets collide with the heated wall. The dynamics of liquid droplets plays a vital role in the DFFB heat transfer as it influences not only the radiative heat transfer, but also the boiling heat transfer. In the current practice of CTF, the radiative heat flux from the wall to the liquid droplets is modeled as:

$$q''_{r,l} = F_{wl}\left(T_w^4 - T_{sat}^4\right), \qquad \text{(Eq. 10.1)}$$

where $F_{wl}$ is the gray body factor that is determined by the interfacial area, wall emissivity and other properties of the liquid droplets. The determination of $F_{wl}$ relies on empirical correlations, which generally lack a comprehensive validation.

The boiling heat transfer flux in DFFB is calculated as the maximum of the CHF $q''_{CHF}$ in CTF and the droplet de-entrainment heat flux term $q''_{de}$. The latter is calculated as:

$$q''_{de} = h_{fg} C_{de} G_g, \quad \text{(Eq. 10.2)}$$

which is simply the product of the latent heat $h_{fg}$, a de-entrainment coefficient $C_{de}$, and total droplet mass flux $G_g$. The coefficient $C_{de}$ also relies on empirical correlations.

Since the modeling of DFFB in CTF still heavily relies on empirical correlations and the correlations are not well validated in the current practices; it is vital to design validation experiments that specifically aim to demonstrate application of the data-driven validation methodology with the ultimate goal of improving the modeling of DFFB in CTF.

Based on the modeling approach of DFFB in CTF, validation experiments are designed to provide high-fidelity data with well-quantified uncertainties that cover the major physical parameters that are considered sensitive to the QoIs in DFFB predicted by CTF. Such designs are summarized in the following chapters.

## 10.3. Scope of Work

The validation experiments were performed in a phased approach. Phase I experiments were designed to operate newly constructed experimental facility and obtain experimental data under room-temperature without heat transfers involved. The experimental facility for Phase I experiment is to use air-water to investigate the hydrodynamics of the water droplets in the DFFB flow regime. This phase of experiment is adiabatic in nature to verify the instrumentation for droplet measurements. There are four major systems of components, which are the test section, liquid supply system, air supply system and instrumentation. In the test section the primary data measurement and collection are made with proper instruments. The first three systems are connected with each other through tubing to form a hydraulic loop in the facility. Since no heat transfer is considered, the operating temperature and pressure are ambient conditions in the lab. A schematic of the facility is shown in Figure 10.49.

A platform was made available to accommodate all necessary optical instruments and synchronization and data acquirement system called ParticleMaster provided by LaVision. The platform is shown in Figure 10.50, and the configuration is shown in Figure 10.51. The platform consists of a rail system where all equipment is placed, including an LED light source, a high-speed camera with a microscope attached, a calibration plate along with a dummy plate, and the test section where the measurement is taken. The rail system allows the camera and light source to move in both x and y direction (parallel and perpendicular to the camera), which significantly enables physical adjustment of the camera and the light source for measurement. On one of the y-direction rail there is a dummy plate which is a piece of acrylic material with the same optical properties and thickness as the test section wall. Additionally, the calibration plate is placed between the light source and the dummy plate. During the calibration process, the calibration plate is placed at the location where the desired focal plane is in the test section flow channel, and the camera is then adjusted focused on the calibration plate. The presence of the dummy plate is to ensure the accurate location of the focal plane.

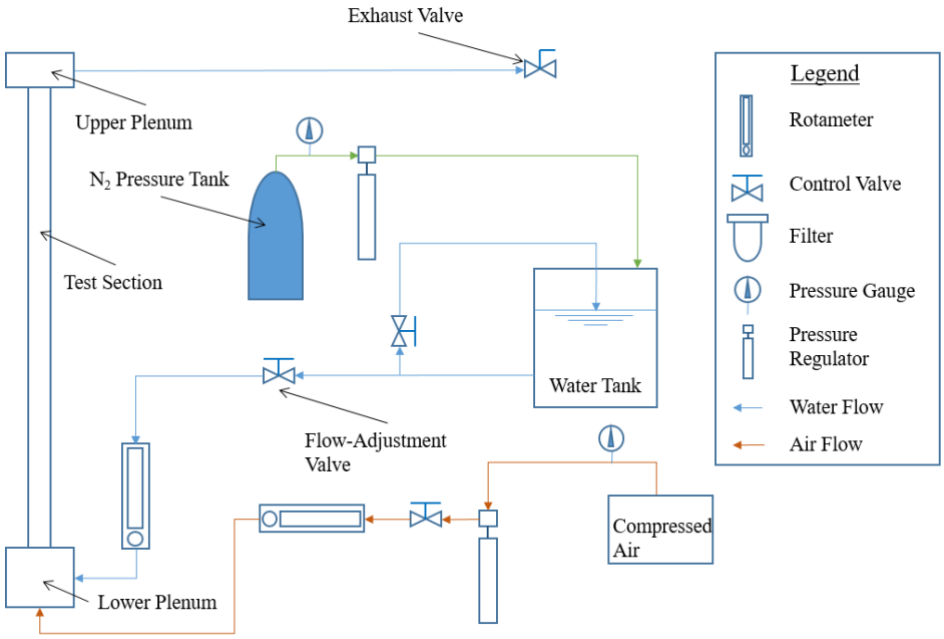


Figure 10.49. Schematic of the Phase-I experimental facility


Figure 10.50. Images of the optical instruments and the platform

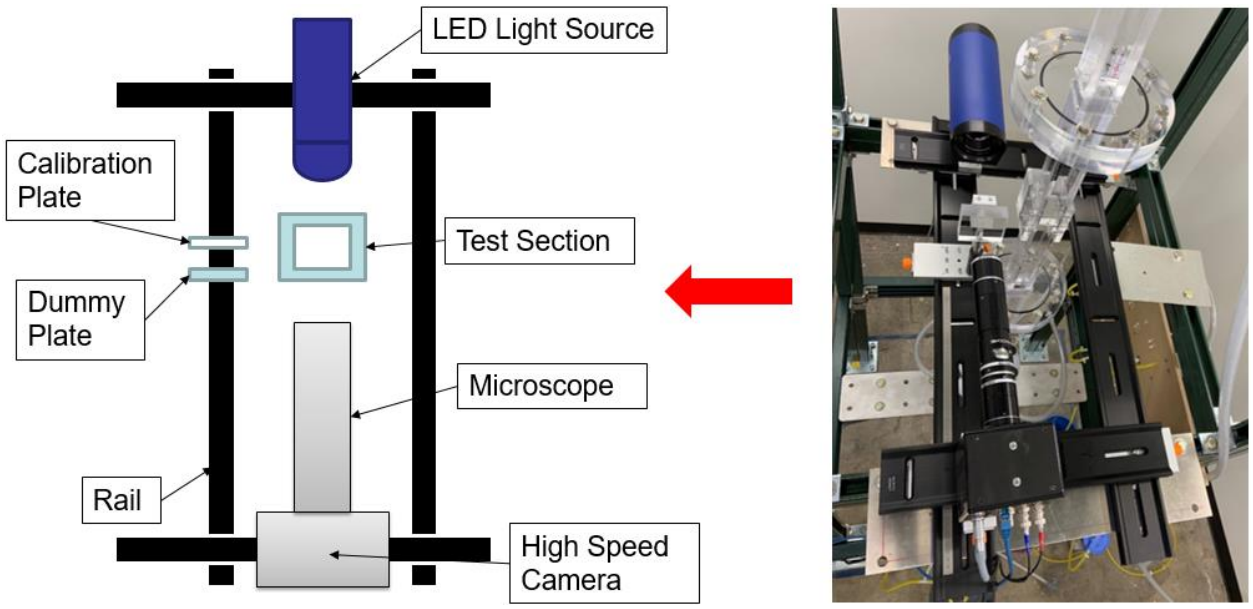


Figure 10.51. The configuration of the platform

## 10.4. Key Findings

### 10.4.1. Experimental Data

The objective of Phase I experiments was to obtain experimental data for air-water operating conditions. Figure 10.52 illustrates where the measurement was taken. The entire test section is divided into multiple areas, which are 4×4 mm square as majority, 4×2 mm in the periphery and 2×2 mm at corners. Within the red square are the measurement included in the dataset, as illustrated in Figure 10.52. Some measurement out of the red box is also included in the dataset.

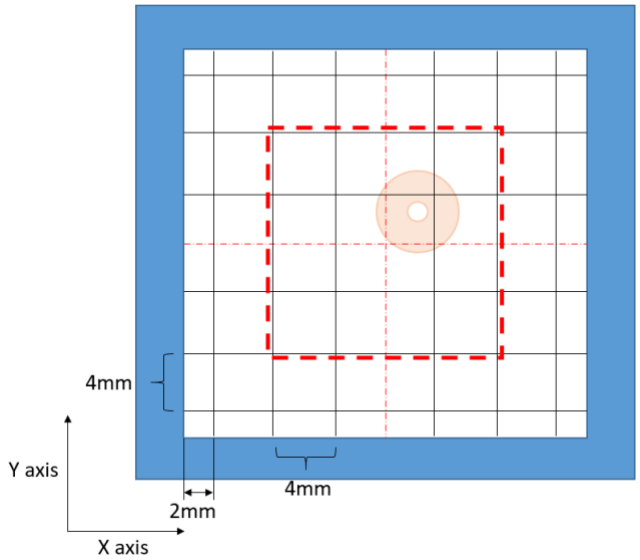


Figure 10.52. The dataset measurement in the test section (red dashed square)

There are several operating conditions in the measurement. Under each operating conditions there are three focal planes in Y axis (y = -4 mm, y = 0 mm and y = 4 mm). At each focal planes, there are 4 FOVs (the center of each FOV is x = -6 mm, x = -2 mm, x = 2 mm and x = 6 mm). In each FOV, there are three measurement sequence, each representing 4 seconds of the flow. Therefore, there are 108 measurements in all. The test matrix is shown in Table 10.15. All measurements are only for the polydisperse droplets. The nozzle that generates the droplets are slightly off aligned with the very center of the test section, as shown in Figure 10.52. The potential negative effect of such situation is unknown and needs further investigation.

Table 10.15. Operating conditions of the measurement (square duct D = 28 mm).

| Item | SYMBOL | UNIT | #1 | #2 | #3 |
|---|---|---|---|---|---|
| Droplet Diameter | $d$ | mm | 0.75 | 0.75 | 0.75 |
| Droplet Velocity | $u_d$ | m/s | 5 | 1 | 10 |
| Feedwater Flow Rate | $Q_b$ | mL/min | 120 | 120 | 145 |
| Air Reynolds Number | $\mathrm{Re}_c$ | n/a | 17,785 | 25,610 | 17,785 |
| Air Flow Rate | $V_{air}$ | L/min | 240 | 290 | 240 |
| Inlet Pressure | $p$ | psig | 11.5 | 18.0 | 11.5 |

Images taken in a typical measurement are no less than 4000, and each image is processed through the software with specified data processing parameters. Particles can be detected and recognized by shadow areas. Velocity information is automatically calculated through double frames in each image. However, since the dispersed flow is confined in a small square channel (28×28 mm) and the light has to go through two channel walls (front and rear wall), the droplets attached on the wall may have a negative effect on the image. Those unwanted droplets may project a vast grey area on the image as they are out of focus and present very blurry with no specific perimeter, which makes them look like part of the background. The drops-on-the-wall effect was not eliminated during the measurement, but the problem can be potentially solved by implementing heating close to the wall to quickly evaporate the drops or applying special wall that prevent drops retention.

Figure 10.53 show two typical example images with detected moving drops, background, interference and other complication. The left one shows two moving particles with diameter of 603.6 and 418.0 μm. They are very close to the exact focal plane as the shadow areas have sharp rim. Additionally, the interference from the drops on the wall is very noticeable as it presents several vast grey areas. One out-of-focus particle moving across the middle interference area is detected and recognized by the software, and the diameter is provided (430.6 μm), which becomes a false detection. Therefore, the presence of interference area (grey area) may inadvertently generate false detection and thus alter the detection accuracy. The right image shows another complicated situation: an out-of-focus drop moving across the camera projects irregular shadow area that presents three falsely detected particles. The reason of the irregularity of the shadow area is unclear. It is possible that the background which presents a grey area may interfere with the drop's shadow area. In general, particles that are slightly out of focus must satisfy the set criteria in order to be detected. One of the criteria is the minimum slope (which is discussed in the next section). As is shown, a particle that is out of focus is detected with diameter of 347.5 μm.

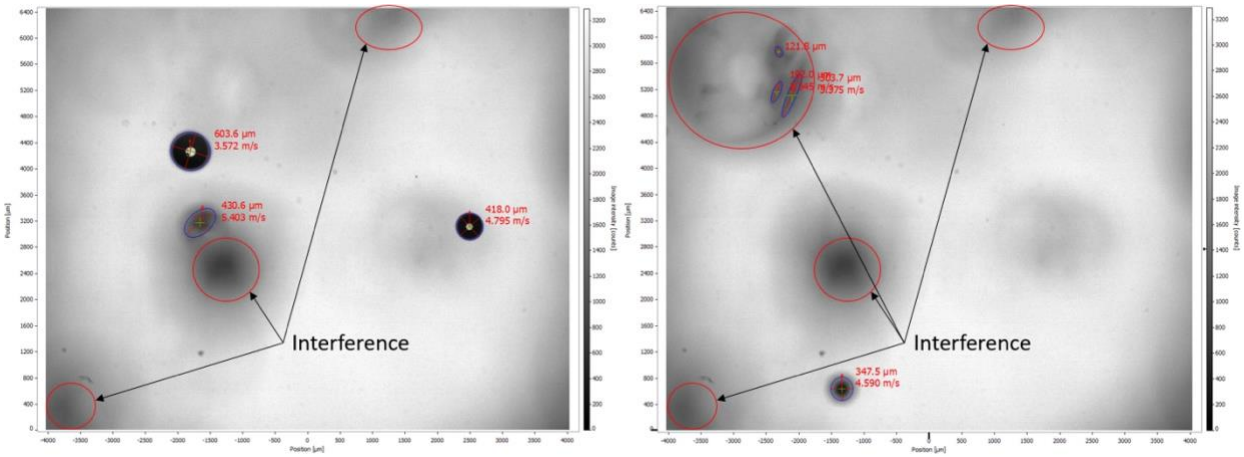


Figure 10.53. Example images that are taken in the same flow condition and at the same location but different timing.

In addition to particle images, the output data includes a complete list of particles detected with information such as diameter, perimeter, centricity, velocity, and statistical weight, etc., a histogram, a table of cumulative statistics and scatter plots as wanted (Figure 10.6). The histogram is usually about the diameter (or particle size) distribution, where the bin width is adjustable. Scatter plots are created for different use, but here it shows the particle detection locations. It is noticeable that the largest interference area is deficient in detected particles, which confirms its strong interference. Information provided in the cumulative statistics is consistent with the one calculated by the adopted data reduction method.

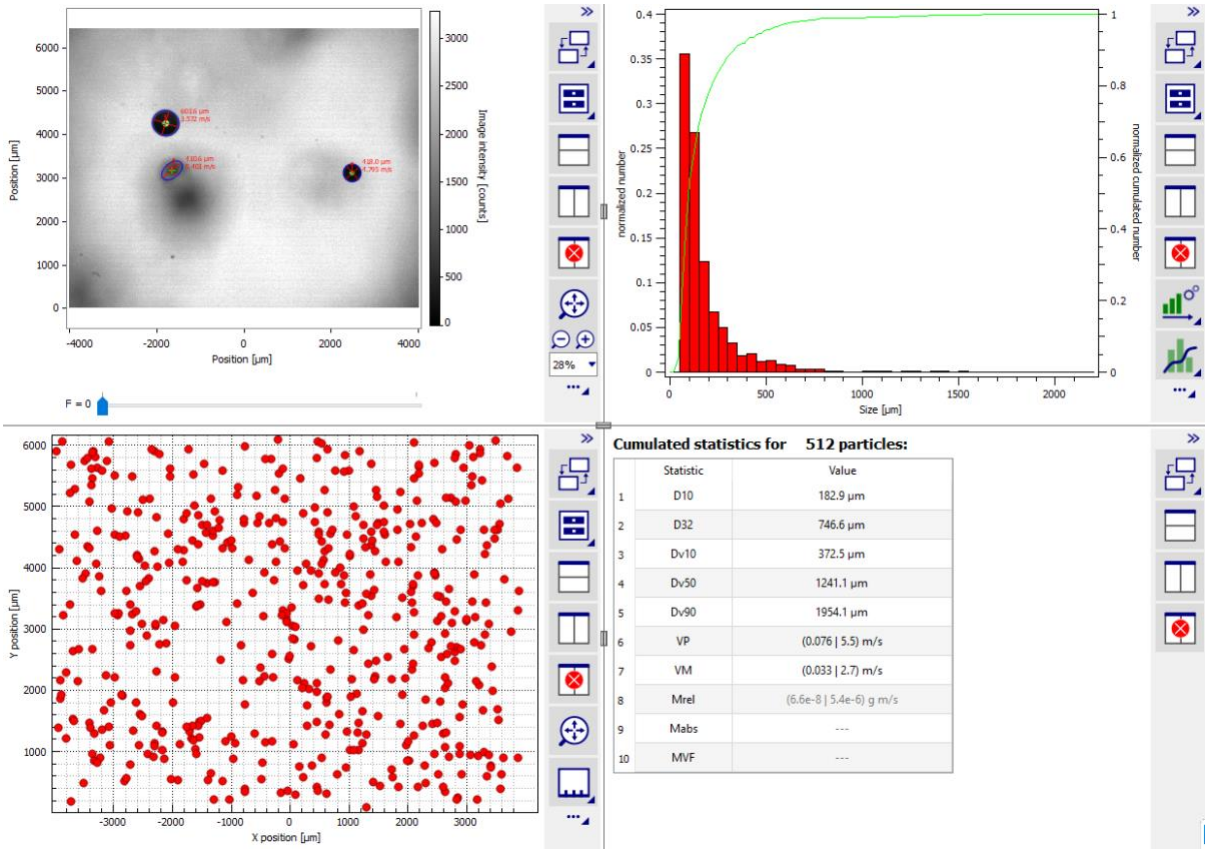


Figure 10.54. Example data including an image from the measurement, a histogram of diameter distribution, a scatter plot of particle detection location and cumulative statistics.

### 10.4.2. Uncertainty of Measurement

Measurement uncertainty is defined as the aggregate of all factors that affect the measurement of particles on the image deviating from the true dimensional scale. Since there are multiple procedures involved in the data collection that inevitably cause the uncertainty of in the measurement, the effect and sensitivity need to be further investigated. Some of the identified uncertainty associated with the measurement inaccuracy of particles' diameter include the algorithmic bias of particle detection in the image processing, the non-uniform distribution of light source on the image, the interference of both neighboring droplets and out-of-focus droplets' shadows to the measured particle image, the imperfect synchronization of the camera and light source, etc. Preliminary study on the calibration plate and its image indicates that the dots' diameters are consistent with a normal distribution, which means an individual particle measurement uncertainty (or estimated standard error) can be determined by its standard deviation of measurement, i.e., the particle diameter.

### 10.4.3. Uncertainty of Distribution Fitting

When we mention the uncertainty of droplets distribution, it can refer to the statistical quantities such as the mean and variance of one sample. Eventually, the uncertainty of droplets measurement is defined as the uncertainty of droplets diameter distribution. Therefore, it is important to determine the distribution function. There are two distributions considered in the data processing and analysis: normal distribution and log-normal distribution [Johnson et al. 1994], which is shown as follows:

$$f\left(x\right)=\frac{1}{\sigma\sqrt{2\pi}}e^{-\frac{1}{2}\left(\frac{x-\mu}{\sigma}\right)^2} \qquad \text{(Eq. 10.3)}$$

and

$$f\left(x\right)=\frac{1}{x}\cdot\frac{1}{\sigma\sqrt{2\pi}}\exp\left(-\frac{\left(\ln x-\mu\right)^2}{2\sigma^2}\right). \qquad \text{(Eq. 10.4)}$$

The probability density function (pdf) of the distribution is identified as a log-normal distribution based on literature review and collected data's observation. The recommended bin width selection method can be described as below:

$$\text{Bin Width}=2\frac{IQR\left(x\right)}{\sqrt[3]{n}}, \qquad \text{(Eq. 10.5)}$$

where *IQR(x)* is the interquartile range of the data and *n* is the number of observations in the sample. The statistical distribution fitting is used, which is to model the probability distribution of a single variable. The maximum likelihood method is commonly used for most statistical distribution fitting. Figure 10.55 shows the distribution comparison in a linear scale. It is shown that the distribution is consistent with different operating conditions and different location of measurement for the statistical model method. The uncertainties are listed in Table 10.16

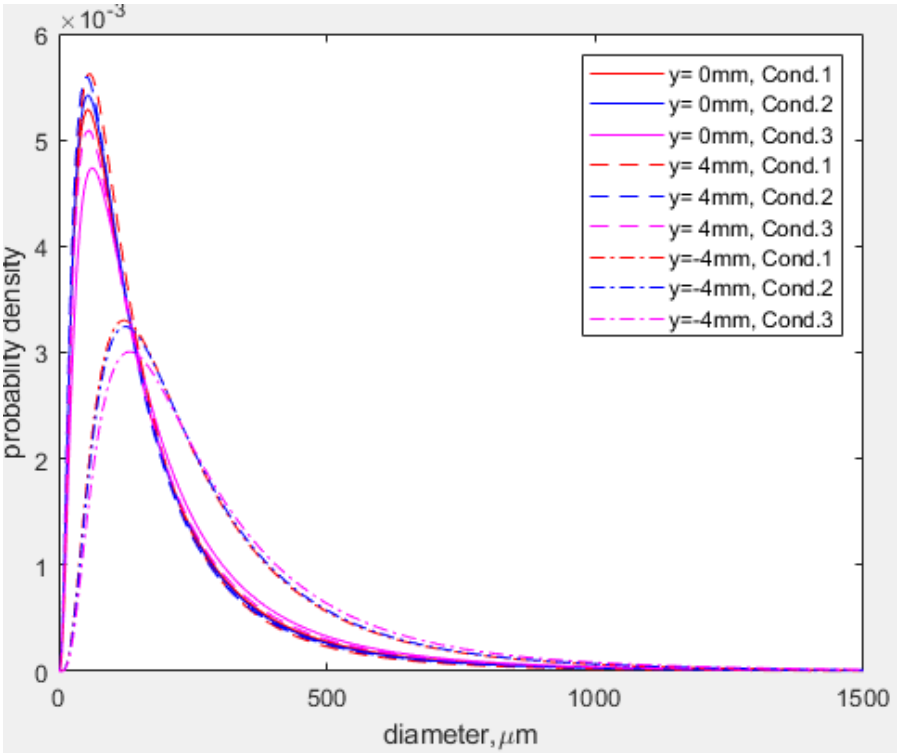


Figure 10.55. The droplet diameter distribution of 9 selected cases.

Table 10.16. The uncertainty analysis of 9 selected cases.

| CASE NO. | PARAMETER μ | PARAMETER N | MEAN | VARIANCE | RELATIVE ERROR | SAMPLE SIZE |
|---|---|---|---|---|---|---|
| 1 | 4.83 | 0.91 | 1.90E+02 | 4.721E+04 | 4.98% | 525 |
| 2 | 4.81 | 0.90 | 1.84E+02 | 4.231E+04 | 3.83% | 852 |
| 3 | 4.94 | 0.90 | 2.10E+02 | 5.535E+04 | 4.15% | 725 |
| 4 | 4.78 | 0.86 | 1.73E+02 | 3.223E+04 | 5.10% | 416 |
| 5 | 4.78 | 0.91 | 1.79E+02 | 4.103E+04 | 4.10% | 759 |
| 6 | 4.87 | 0.92 | 1.99E+02 | 5.325E+04 | 4.23% | 751 |
| 7 | 5.36 | 0.75 | 2.83E+02 | 6.047E+04 | 2.06% | 1780 |
| 8 | 5.38 | 0.75 | 2.88E+02 | 6.232E+04 | 1.51% | 3291 |
| 9 | 5.45 | 0.75 | 3.11E+02 | 7.398E+04 | 1.99% | 1942 |

A natural question will be how to quantify the uncertainty of the distribution fitting parameters such as parameter $\mu$ and $v$. A statistical method called bootstrap, based on resampling and the central limit theorem, is proven to be effective in determining the confidence interval of the parameter's estimate [DiCiccio et al. 1996]. This is because the bootstrap method creates a distribution of parameter estimates that follows a normal distribution. Due to the affordable computational requirement of the bootstrap method, it is hence used to calculate the confidence intervals for the uncertainty analysis.

There are generally two required parameters in bootstrap: the size of the resample from the available dataset and the repeated times of the distribution model fitting. Figure 10.56 shows a case study of the effect

of resampling size and number of resampling on the parameter estimation. The original dataset has 1,942 data points. It indicates that the increase of resampling size significantly reduces the estimated standard deviation of the parameter estimation distribution, yet the benefit for a better parameter estimate diminishes as the mean value of the estimate converges to a certain value. Similarly, a sufficiently large number of resamples result in a significantly narrow spread of the parameter estimate, but there exists a balance between accuracy and computational cost. Therefore, a sample size equal to 50% of the original dataset size and a number of resampling 1,000 is used for the uncertainty analysis.

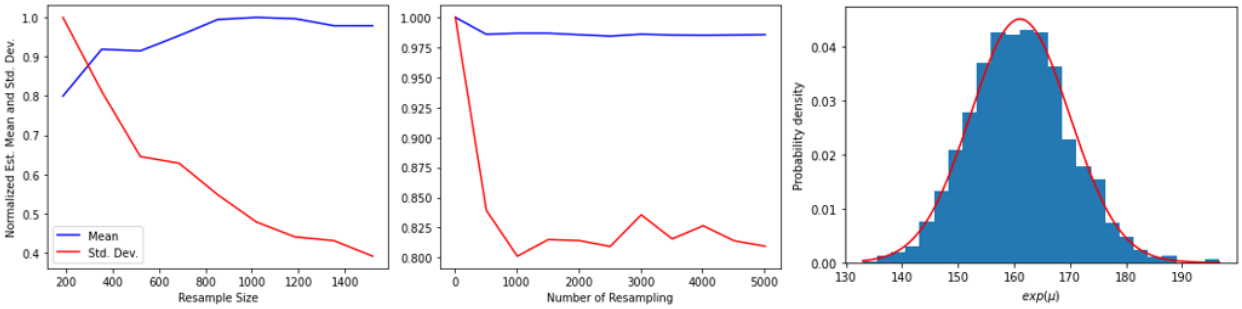


Figure 10.56. (Left) The effect of resample size and (middle) number of resamplings; (right) The estimated parameter exp(μ) follows a normal distribution.

There are three distribution parameters to estimate, which can be referred to as: the location, which dictates the translation on the variable axis; the scale factor, which is related to the scaling of PDF; and the shape factor, which dictates the overall shape. As it is introduced beforehand that the PDF of a lognormal distribution, we can have a more general formula according to (Eq. 10.4):

$$f(D) = \frac{1}{(D - D_{loc})s\sqrt{2\pi}} e^{-\left(\frac{\left(\ln(D-D_{loc})-\mu\right)^2}{2s^2}\right)}$$

$$= \frac{\frac{1}{\exp(\mu)}}{s} \frac{1}{\frac{D - D_{loc}}{\exp(\mu)}\sqrt{2\pi}} \exp\left(-\frac{\ln^2\left(\frac{D - D_{loc}}{\exp(\mu)}\right)}{2s^2}\right), \quad \text{(Eq. 10.6)}$$

with a transformation of $x = \frac{D - D_{loc}}{\exp(\mu)}$ and $f(D) = \frac{1}{\exp(\mu)} f(x)$, we can then obtain:

$$f(x) = \frac{1}{\sigma} \frac{1}{x\sqrt{2\pi}} e^{-\left(\frac{\ln^2 x}{2\sigma^2}\right)}. \quad \text{(Eq. 10.7)}$$

This indicates that *exp(μ)* is the scale factor; $D_{loc}$ is the location; and $\sigma$ is the shape factor. With the bootstrap method, we can obtain these three parameter distributions, which follow a normal distribution. Figure 10.57 shows box plots of the three parameters in nine groups of data. The location and scale factor are in μm, whereas the shape factor is in $\mu m^{-1}$. The box represents the interquartile range, and the middle line shows the sample mean. Additionally, dots represent the outliners. Box plots not only can show the overall distribution, but also illustrate the confidence interval range. Case (Group) 1 to Case (Group) 6 dataset's location parameters, for instance, has narrow spread, whereas their shape factors have relatively large uncertainties.

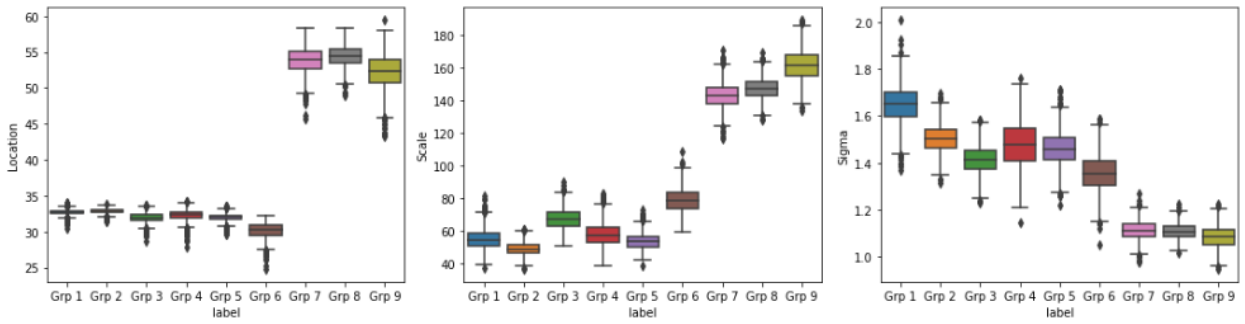


Figure 10.57. Distributions of parameter estimates: (left) location, (middle) scale and (right) shape factor.

The distribution model with the estimated parameters needs to be compared with the histogram that visualizes the distribution. Figure 10.58 shows such comparison, which is considered a good match. A more commonly used method to determine the goodness-of-fit is through the Kolmogorov-Smirnov test.

The Kolmogorov-Smirnov test can be served as a goodness-of-fit test [Massey 1951]. This is because that it is very likely that a distribution model does not perfectly match a real-world dataset. As can be seen in Figure 10.58, the q-q plot suggests that the distribution is heavy-tailed, asymptotic to a certain value, which makes it extremely right-skewed. This is consistent with the Kolmogorov-Smirnov test results, which suggests rejecting the null hypothesis. However, if we only look at the range with theoretical quantiles smaller than 2500, which covers most size range of particle diameters, we find that the overall goodness of fitting is satisfactory, also substantiated by the additional hypothesis test on that subset of data. The heavy tail can be explained by the fact that actual particle diameter has a physical upper bound. Literature [Ishii and Hibiki 2011] suggests a critical Weber number being around 12 dictates the upper limit of a liquid droplet in a continuous-phase flow. In fact, large droplets tend to disintegrate and become unstable. This is consistent with the observation from the available data. On the other hand, the lognormal distribution is a sheer mathematical expression of an idealized distribution. Therefore, the fitted distribution model can still be used to describe particle population smaller than around 1300 μm. This analysis can be generalized to other datasets, which is not shown here due to the length of this paper.

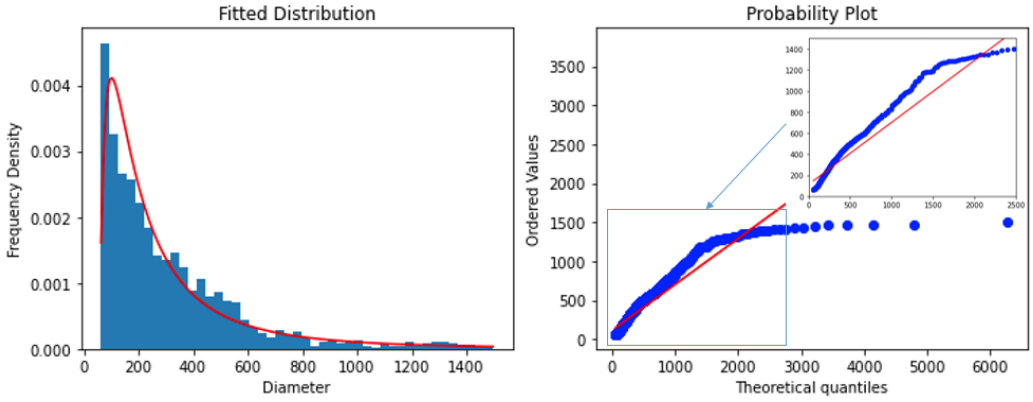


Figure 10.58. Distributions of parameter estimates: (left) location, (middle) scale and (right) shape factor.

### 10.4.4. Uncertainty of Characteristic Diameter

SMD (Sauter Mean Diameter) is selected to be calculated as the characteristic diameter of a DFFB flow. There are two available approaches to determine SMD: the calculation based on the dataset, according to the following equation [Kowalczuk et al. 2016]:

$$\mathrm{SMD} = \frac{\sum_{i=1}^{\infty} n_i D_i^3}{\sum_{i=1}^{\infty} n_i D_i^2}, \qquad \text{(Eq. 10.8)}$$

where $n_i$ is the number of drops in $i$ th diameter size class, $D_i$ is the diameter. and the one based on the obtained distribution models. The former approach suffers the potential lack of sample size of the population, thus the calculated SMD may not represent the true value; however, the latter one trades with the accuracy because of the heavy right-skewness towards large diameter, which is the nature of an idealized statistical model. A 'cutoff' value is imposed on the fitted distribution for the distribution-based SMD calculation to counter the heavy tail effect. The calculated SMD in both methods are presented in Table 10.17.

Table 10.17. Calculated SMD and nominal flow conditions

| Items | Case 1 | Case 2 | Case 3 | Case 4 | Case 5 | Case 6 | Case 7 | Case 8 | Case 9 |
|---|---|---|---|---|---|---|---|---|---|
| SMD/μm (dataset) | 439.3 | 469.7 | 473.3 | 380.8 | 473.7 | 629.2 | 548.0 | 538.4 | 575.7 |
| SMD/μm (distribution model) | 480.3 | 335.8 | 398.9 | 377.8 | 341.1 | 423.5 | 523.9 | 535.8 | 562.9 |
| Air flow rate/SLPM | 317 | 317 | 317 | 430 | 430 | 430 | 317 | 317 | 317 |
| Water flow rate/mLPM | 120 | 120 | 120 | 120 | 120 | 120 | 145 | 145 | 145 |

## **10.5.** Path Forward

The next step would be the Phase II/III experiment, which would involve modification of the facility used in Phase I. The purpose would be to use heating components to study steam-water droplet heat transfer mechanisms in DFFB regime. Phase-II and III experiments share most of the facility so the description of the facility is essentially the same. The facility shares some of the systems and components used in the Phase-I facility. However, due to the nature of heating elements, the majority of piping and tubing will be made of stainless steel. Thermal insulation will also be applied. The Phase-II facility consists of five major systems of components, four of which are similar to the Phase-I facility, i.e., the test section, liquid supply system, steam supply system and instrumentation. The last one is the electric heating system. Similarly, the primary data measurement and collection will be made in the test section with proper instruments. The first three systems are connected in an open hydraulic loop. There is no pump used in the facility, so the liquid and steam supply systems are pressurized to provide required hydraulic driving head. Saturated steam is generated in a boiler in the steam supply system. Additional heating elements are installed to heat up the steam to appropriate superheated state. The operating pressure ranges from the atmospheric pressure to 200 psi (14 bar). A schematic of the test facility is shown in Figure 10.59.

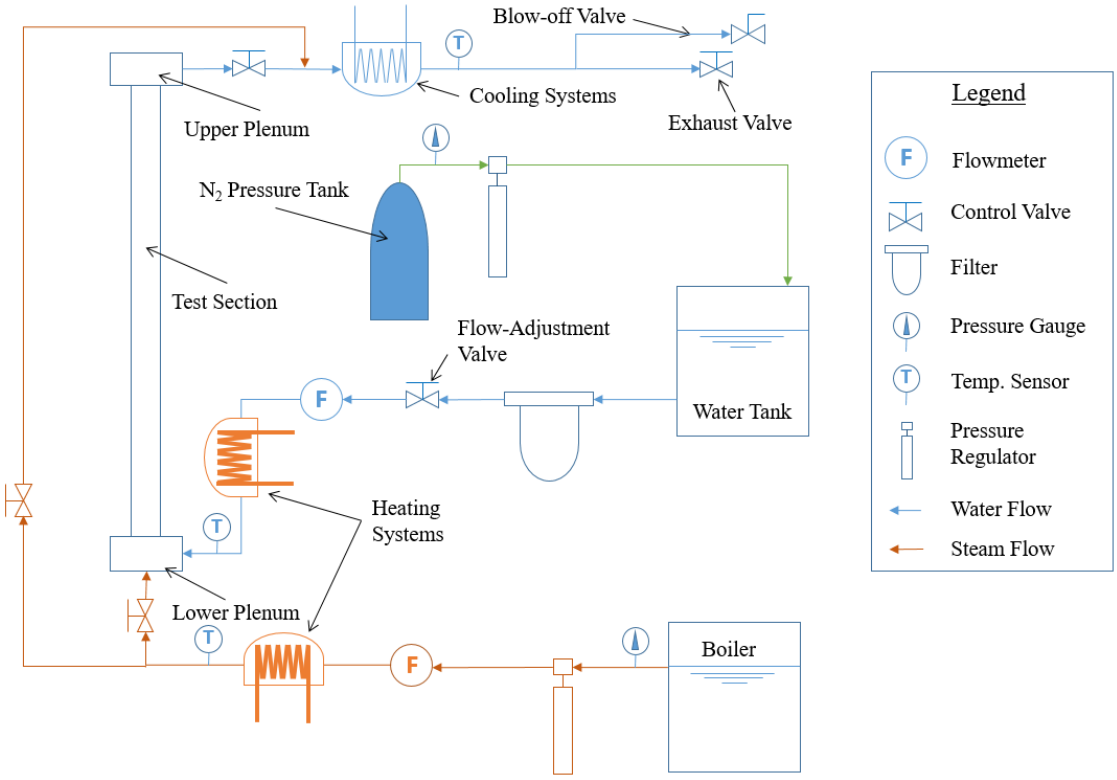


Figure 10.59. Schematic of Phase II/III experimental facility

## 10.6. Concluding Remarks

This report presents a major effort to provide procedures and approach for liquid droplets diameter and uncertainty analysis at a synthetic DFFB scenario. Key findings from the experimental data were summarized. Phase I facility with an optical instrument system was developed to facilitate the imaging which contains numerous droplet particle information. Data processing was completed using LaVision ParticleMaster package to obtain polydispersed droplets diameter and velocity statistics. Additionally, the particle diameter distribution modelling, i.e., the widely used lognormal distribution, was presented with discussion on the uncertainty quantification technique. The estimated parameters' confidence interval in the distribution model fitting process is properly quantified based on bootstrap resampling and central limit theorem. In the end, SMD calculation results based on two approaches were provided. It is believed that the characteristic parameters needed for a validation process include the fitted distribution of the population of polydispersed particles, uncertainty of the distribution as well as confidence interval of the distribution parameters, and calculated SMD based on the distribution. Also, along with the experimental data and its processing and analysis, significant experimental experience was accumulated for the future Phase II and III experiment, which would involve heat transfer testing.

### 10.6.1. Uncertainty quantification for multiphase flow simulations supported by high-resolution experiments

As a part of this work, the team (Liu et al., 2018, 2018, 2019, 2021) developed a machine learning-based Bayesian approach to inversely quantify and reduce the uncertainties of multiphase computational fluid dynamics (MCFD) simulations for bubbly flows. The proposed approach is supported by high-resolution two-phase flow measurements, including those by double-sensor conductivity probes, high-speed imaging, and particle image velocimetry. Local distributions of key physical quantities of interest (QoIs), including the void fraction and phasic velocities, are obtained to support the Bayesian inference. In

the process, the epistemic uncertainties of the closure relations are inversely quantified while the aleatory uncertainties from stochastic fluctuations of the system are evaluated based on experimental uncertainty analysis. The combined uncertainties are then propagated through the MCFD solver to obtain uncertainties of the QoIs, based on which probability-boxes are constructed for validation. The proposed approach relies on three machine learning methods: feedforward neural networks and principal component analysis for surrogate modeling, and Gaussian processes for model form uncertainty modeling. The whole process is implemented within the framework of an open-source deep learning library PyTorch with graphics processing unit (GPU) acceleration, thus ensuring the efficiency of the computation. The results demonstrate that with the support of high-resolution data, the uncertainties of MCFD simulations can be significantly reduced.

## 10.7. References


T. J. DiCiccio, and B. Efron, "Bootstrap Confidence Intervals," *Statistical Science*, **11,** no. 3, pp. 189-228 (1996)

M. Ishii and T. Hibiki, *Thermo-Fluid Dynamics of Two-Phase Flow*, NY, USA (2011).

N. L. Johnson, et al., "14: Lognormal Distributions", *Continuous univariate distributions*. **Vol. 1**, Wiley Series in Probability and Mathematical Statistics: Applied Probability and Statistics (2nd ed.), New York: John Wiley & Sons (1994).

P.B. Kowalczuk and J. Drzymala, "Physical Meaning of the Sauter Mean Diameter of Spherical Particulate Matter," *Particulate Science and Technology*, **Vol. 34**:6, pp. 645-647 (2016).

F. J. Massey, "The Kolmogorov-Smirnov Test for Goodness of Fit." *Journal of the American Statistical Association*, **Vol. 46**, No. 253, pp. 68–78 (1951).

R.K. Salko and M. Avramova, "COBRA-TF Subchannel Thermal-Hydraulics Code (CTF) Theory Manual," *CASL-U-2015-0054-000*, Pennsylvania State University, University Park, PA (2015).

Liu, Y., Shi, S., Qian, Y., Sun, X., and Dinh, N. Inverse Uncertainty Quantification of Turbulence Modeling in Multiphase-CFD Solver Using High-Resolution Data from Particle Image Velocimetry. In Proceedings of the Advances in Thermal Hydraulics (ATH-2018). Orlando, FL, USA, November, 2018.

Y. Liu, N. Dinh, Y. Sato, and B. Niceno, "Validation and Uncertainty Quantification of DNB Closures in MCFD Solver Using Inverse Bayesian Inference Method", Paper 198. Proceedings of ANS Conference on Best Estimate Plus Uncertainty (BEPU-2018), Lucca, Italy, May 2018

Yang Liu, Xiaodong Sun, and Nam T. Dinh, "Validation and Uncertainty Quantification of multiphase-CFD solvers: A Data-Driven Bayesian Framework Supported by High-Resolution Experiments", J. *Nuclear Engineering and Design*, 2019, Vol.354, 110200, pp.1-19.

Yang Liu, Dewei Wang, Xiaodong Sun, Yang Liu, Nam Dinh, and Rui Hu, "Uncertainty quantification for Multiphase-CFD simulations of bubbly flows: a machine learning-based Bayesian approach supported by high-resolution experiments", *Reliability Engineering and System Safety*, 2021 (in press).

# 11. High-fidelity Interface Capturing Simulations of the post-LOCA Dispersed Flow Film Boiling Regime for a Data-driven Modeling Framework

## 11.1. Introduction

The objective of developing a data-driven methodology, the focus of the current IRP project, implicitly necessitates the generation of a high fidelity, high resolution, and validated data archive, both from experiments and simulations. Recently, Chang et al [1] documented an extensive list of possible frameworks for a data-driven modeling approach. Further, to provide examples, several recent developments have demonstrated the applicability of machine learning approaches to turbulence modeling [2-4], boiling heat transfer prediction [5], mesh optimization [6] and coarse grid CFD error prediction [7]. All machine learning applications for model development underscore the demand for high volume of data for improving the predictive accuracy of these models.

The rapid advent of technology in the high-performance computing (HPC) arena, resulting in a substantial increase of large-scale computation capabilities, has enabled high resolution studies of complex flow phenomena which hitherto remained elusive, or prohibitively expensive, to be scrutinized by experiments. Direct numerical simulations (DNS) enable resolution of all relevant scales of turbulence without resorting to any closure models, thus providing high fidelity computations of the phenomena under investigation. Recently, DNS coupled with interface capturing method have been used to simulate multiple two-phase flow regimes in pressurized water reactor (PWR) sub-channels [8,9]. The dispersed flow film boiling (DFFB) regime, which exists under post loss-of-coolant accident (LOCA) conditions, is of extreme significance to safety margin characterization of PWRs [10]. Thus, data-driven closure modeling for system thermal hydraulic (STH) codes and turbulence modeling pertinent to DFFB flow conditions were a priori identified as the target applications for the demonstration of the RISMC [11] (risk informed safety margin characterization) framework under the IRP.

The DFFB regime is inherently transient, characterized by both mechanical and thermal non-equilibrium [12,13]. Phenomenologically speaking, it is best conceptualized by a mist type flow, with polydisperse droplets, corresponding to high void fractions (> 0.8). Heat transfer in the DFFB regime is a convoluted interplay of several different mechanisms. There is not an apparent single dominant heat transfer path, which, understandably, renders extreme complexity to the task of modeling/accounting for these phenomena in STH codes. As noted by Hochreiter et al [14], these mechanisms include, convection to superheated vapor from rod surface, surface radiation from rods to vapor and droplets, interfacial heat transfer between droplets and superheated vapor, direct contact heat transfer between the wall and entrained liquid (quenching), convective enhancement of the vapor by the entrained droplets and impact of spacer-grids to heat transfer enhancement due to flow acceleration and droplet break-up. In a recent publication Bajorek et al [15] presented their observations from the rod bundle heat transfer (RBHT) facility [16] experiments, summarizing key results from almost a decade of experimental tests of the post-LOCA regime. They emphasized the predominant effect of spacer-grids on the thermal hydraulics of the DFFB regime. All of the tests conducted at the RBHT facility, irrespective of high or low flooding rates, recorded a sharp increase in the heat transfer coefficient in the immediate downstream vicinity of the spacer-grid structures, contributing a significant proportion to the overall heat transfer of the core. Convective heat transfer enhancement was recorded for the initial single-phase experiments by Hochreiter et al [17], based on which Miller et al [18] and Riley et al [19] developed empirical correlations to account for the phenomenon in the system thermal hydraulic code COBRA-TF (or CTF) [20]. For the DFFB regime, several additional factors provide a positive feedback to heat transfer near the spacers, all owing to the droplet interaction with spacer-grid structures. Note that based on the flooding rate conditions, the phenomenology at the spacer-grids is quite different, resulting in different heat transfer mechanisms [21]. For high flooding rates, a film of coolant encapsulates the spacer grid structure due to de-entrainment from the bulk flow. For low flooding rates, on the other hand, the void fraction in the bulk is too high for a stable water film to develop on the

spacer surface. Sharp heat transfer augmentation is observed at the trailing edge of spacers, decaying exponentially with respect to the downstream distance [21-23]. The primary contribution comes due to the inertial impact of the droplets on the spacer-grid, resulting in breakup or deformation of the droplets and a drastic increase in the overall surface area. The heat transfer increase has been correlated with the observed decrease in the Sauter mean diameter (SMD) of the droplets. Ratio of the immediate upstream and downstream SMD, with respect to the spacer-grids, is an extremely important parameter used in modeling of the DFFB regime. A simplified mechanistic model was developed by Cheung et al. [24] to predict the downstream SMD of the droplets based on conservation of mass, kinetic and surface energies. A limited number of empirical correlations also exist in literature for SMD, subsequently used in modeling the interfacial source terms for closure relations in thermal hydraulic codes.

Other components, besides convective enhancement and decreasing SMD, through which the spacer-grids contribute, directly or indirectly, to the overall heat transfer in the DFFB regime, include direct radiation from the fuel rods to the spacer surface, thermal boundary layer separation and re-attachment and quenching due to impacting droplets. As a testament to their significance, not accounting for the spacer-grids in STH codes results in an over-prediction of the cladding temperature [25]. For modelling these phenomena or reducing the uncertainty of related models in STH codes, highly detailed insights into the droplet and fluid dynamics is imperative.

Thus, the overarching objective of the work documented herein is conducting *high-fidelity, single phase and interface capturing, representative simulations of the post-LOCA DFFB regime*. More specifically, large scale simulations are designed to resolve the droplet and fluid dynamics in the vicinity of spacer-grids. Large scale simulations are performed, realized by PHASTA [26], a strong scaling finite element method based numerical solver for the Navier-Stokes equations, on the Mira supercomputer at Argonne National Laboratory (ANL) [27]. Several ad hoc functionalities are implemented in PHASTA to make the simulations viable. Further, through the implementation of advanced MPI (message passing interface) routines, including MPI sub-communicators and MPI parallel I/O, high fidelity data is collected from the simulations enabling unprecedented insight into the flow physics of a PWR subchannel, including the effect of mixing vanes on downstream turbulence and anisotropy, the axial evolution of downstream SMD and the droplet feedback to turbulence. The data is archived and intended to be used for the development of data-driven turbulence and STH models, serving the broader goals of the IRP [28].

### 11.2. Scope of Work

Large scale simulations running on massively parallel supercomputers, which constitute the major objective of current research, pose several problems for their successful execution and subsequent, or in-situ, post-processing and data analysis. Major challenges with the simulations performed herein with PHASTA were, understandably, of a logistical nature, which required efficient data management code, either integrated as subroutines within PHASTA using advanced MPI libraries or developed as separate programs capable of handling large volumes of data.

The technical objectives of the large-scale simulations can, thus, be outlined as,

- Implementing code functionalities in PHASTA to make DFFB simulations feasible. This includes suite of tools to assign fully turbulent inflow boundary conditions, droplet injection at the upstream spacer-grid location and scalable MPI I/O routines for high data throughput.
- Single-phase and two-phase simulations on large scale supercomputers for a range of operating DFFB conditions, including different flow Reynolds numbers and droplet collision Weber numbers.
- Data collection, post-processing and analysis from single and two-phase simulations.
    - Study of turbulent flow features including mean flow properties, Reynolds stresses and turbulent anisotropy to gain insight into the effect of spacer-grids and mixing vanes.

- Analysis of the axial evolution of droplet volume, interfacial area and Sauter mean diameter, for different Weber numbers, and comparison with existing correlation in the STH code COBRA-TF [20] and empirical correlation from prior DFFB experiments, conducted at the rod bundle heat transfer facility
- Data archival to support future developments on data-driven, machine learning based turbulence and STH modeling.

This section provides an overview of the setup details for the single and two-phase simulations, including the accompanying assumptions. The section also includes a brief discussion on the technical and logistical challenges and the functionalities implemented in PHASTA for their resolution, especially the code implementations relevant to high resolution data collection, essential for data driven modeling.

### 11.2.1. Simulation Setup Details and Assumptions

The geometry used for both single and two-phase simulations in this work comprises a PWR sub-channel with spacer-grids and mixing vanes, shown in Figure 11.60. Fully developed turbulent profile is prescribed at the axial cross-section upstream of the spacer-grid structure and natural outflow boundary at the opposite longitudinal end. The hydraulic diameter of the sub-channel is $D_h = 12.976\ mm$, while the total axial length is $3.08\ D_h$. Periodic boundary conditions are prescribed across the lateral faces precluding the modeling any cross-flow, as is the case in realistic PWR conditions. This is the primary assumption of the simulations including that the flow is incompressible. The level-set interface capturing method is used for modeling the two phases, which allows for a smooth transition of properties across the interface informed by a contour field (see Saini [29] for details on numerical method).

The mesh for single and two-phase simulations consists of 55.8 and 367.5 million tetrahedral elements, respectively. It is designed to ensure that all relevant scales of turbulence, based on a priori estimates [30,31] made using bulk Reynolds number, are resolved. For two-phase simulations, it is imperative for the resolution of droplets and their collision with spacer grid structures to employ a finer mesh with extended boundary layer region near the walls. The mesh resolution was ensured to follow prior established guidelines for two-phase simulations by Fang et al [32]. Comprehensive details on the mesh design for all simulations are presented in Saini [29].

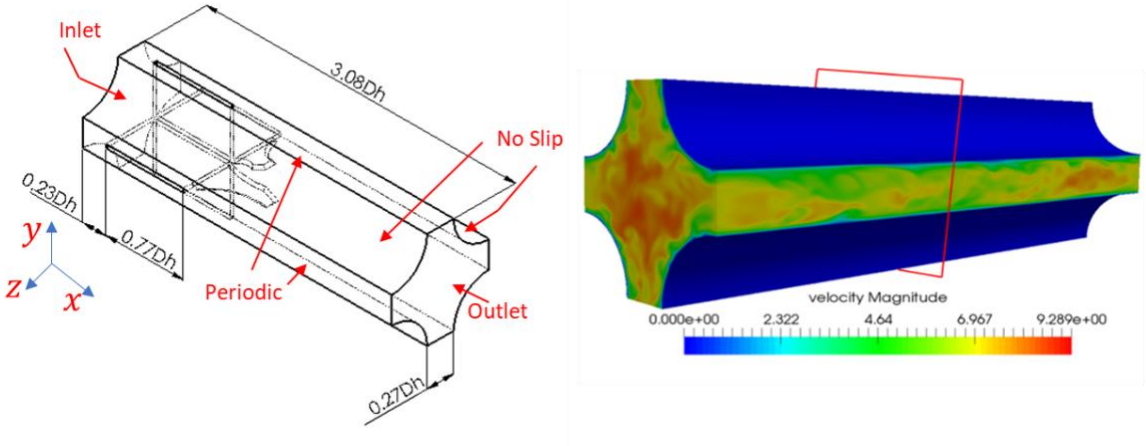


Figure 11.60: PWR sub-channel geometry with spacer-grid and mixing vanes (primary domain). Quasi-steady turbulent flow in periodic auxiliary domain (right).

Table 11.18: Properties for representative DFFB (two-phase) simulations.

| **Properties** | **Single phase** | **We55-Air** | **Properties @ 30 psi, steam superheat 100K** | | |
|---|---|---|---|---|---|
| | | | **We40 (Steam)** | **We55 (Steam)** | **We80 (Steam)** |
| Density ratio ($\rho_l/\rho_g$) | $\rho_g = 1.185\ kg/m^3$ | 1000 | 1029.59 | | |
| Viscosity ratio ($\mu_l/\mu_g$) | $\rho_g = 9.1 \times 10^{-6}\ Pa.s$ | 48 | 13.49 | | |
| Bulk Reynolds number, $Re_b = \rho_g u_{mean}^2 D_h/\mu_g$ | 11822 | | | | |
| Friction Reynolds number, $Re_\tau = u_\tau D_h \rho/3\mu_g$ | 242.539 | | | | |
| Collision Weber number, $We_c = \rho_l D u_d^2/\sigma$ | - | 55 | 40 | 55 | 80 |
| Aerodynamic Weber number, $We_a = \rho_l D u_{mean}^2/\sigma$ | - | 0.319 | 0.253 | 0.348 | 0.507 |
| Injected absolute droplet velocity, $u_d\ (m/s)$ | | 2.05 | 1.97 | | |
| Injected droplet diameter, $D\ (mm)$ | - | 1.0 | | | |
| Surface tension coefficient, $\sigma\ (N/m)$ | - | 0.091 | 0.118 | 0.086 | 0.059 |
| Gravity, $g\ (m/s^2)$ | -9.81 | | | | |

Two single-phase simulations are performed for $Re_b = \{5000, 11000\}$, which correspond to the near operating limits of the DFFB regime, as described by the experiments by Hochreiter et al [14]. For the two-phase simulations, all flow parameters and characteristic dimensionless numbers are listed in Table 11.18. One simulation was performed for air-water system properties at atmospheric conditions, which has higher viscosity ratio, while three other simulations were performed for steam-water system properties at system pressure of 30 psi and 100K superheat. The controlled parameters in all two-phase simulations are the bulk Reynolds number, $Re_b$, and the collision Weber number, $We_c$, of the injected droplets. To obtain a desired $We_c$, the surface tension coefficient is varied for different cases. The upstream injected droplets are assumed to be monodisperse and spherical, i.e., they all have a diameter, $D = 1mm$. Further, the initial velocity of the droplets, $u_d$, is assumed equal to the terminal velocity, estimated from the drag correlation by Morrison [33]. Finally, it is assumed that the droplets do not intersect at their inception point, maintained at a distance of $1.5D$ from each other and at a minimum distance of $0.75D$ from the sub-channel walls. These assumptions are informed by prior experimental observations of the flow dynamics in the DFFB regime [12,14,16,24,34,35]. Discussion on the rationale for selecting flow properties can be found in Saini [29].

### 11.2.2. Turbulent Inflow Boundary Conditions

The DNS scale turbulent flow CFD simulations in reactor sub-channels are often performed on relatively long domains computational domains with periodic boundary conditions across the axial ends of the domain [36] ($x/D_h \gg 1$). With a large enough domain, such that the largest scale eddies are reasonably resolved, periodic boundaries can emulate infinitely long sub-channels and generate a fully developed turbulent flow profile. For the ensuing DFFB simulations, however, we are concerned with droplet

interactions with the spacer-grids and mixing vane structures (Figure 11.60). The presence of these internal structures and axially evolving droplet dynamics compromises longitudinal periodicity of the domain, irrespective of the length used for the simulations.

To address the issue of specifying inlet boundary condition we use the, so called, boundary conditions transient (BCT) suite of tools, initially developed by Feng [37]. Straightforward conception of the application of BCT can be summarized as capturing the fully developed turbulent flow profile on the auxiliary flow domain, shown in Figure 11.60, and applying to the inlet cross-section of the primary domain. To achieve this, virtual "probes" are placed in the auxiliary domain, which correspond to the exact mesh node location of the primary mesh. Thus, a total of 29,389 probes were used to capture the instantaneous velocity field, which necessitated writing high volume of data output. This was enabled through the implementation of advanced MPI I/O routine in PHASTA, addressed in Section 11.2.3. For further details on BCT implementation refer Saini [29].

### 11.2.3. MPI Sub-communicators and MPI Parallel I/O

File I/O remains the most expensive operations for large-scale computations. For this reason, the simulation restart files are, often, sparingly written to the disk [38]. This imposes constraints on the post-processing analysis and the meaningful information that can be extracted from the simulations. In order to capture the turbulent velocity profile without loss of spatial resolution, as discussed in the previous section, all the computational nodes at the inlet cross-section of the primary mesh are used as velocity capturing probes on the auxiliary mesh, resulting in very large I/O buffers to be written to the disk at each simulation time step, which severely affects code performance.

Advanced MPI libraries were, therefore, implemented in PHASTA to greatly enhance the speed of write operations. The implementation involves a combination of MPI Sub-communicators and MPI parallel I/O. Details of the I/O algorithm are included in Saini [29]. Table 11.19 provides details on the PHASTA speed enhancement obtained from the MPI routines on the Cetus supercomputer at ANL, with a simulation running on 256 nodes and mesh split into 16,384 partitions. Comparison of number of simulation time steps with different number of probes, for collecting data, are made against single phase simulation without any data output. It is evident that without MPI enabled write operations, the penalty imposed on PHASTA by a single processor output made the simulation infeasible. This functionality not only made it possible to impose turbulent inflow boundary condition, but also enabled high resolution data collection, which is indispensable for data-driven modeling.

Table 11.19: Number of time steps performed during 1 hour of wall-clock time on Cetus.

| | **Single Processor** | | **171 Processors** | | |
|---|---|---|---|---|---|
| **Number of probes** | **Time steps** | **Penalty factor** | **Time steps** | **Penalty factor** | **Speed up ratio** |
| 0 (No recording) | 2887 | | | | |
| 5000 | 1267 | 2.28 | 2027 | 1.42 | 1.6 |
| 10000 | 75 | 38.5 | 1920 | 1.5 | 25.6 |
| 29839 | 9 | 320.78 | 1440 | 2.0 | 160.0 |

## 11.3. Key Findings

### 11.3.1. Single-phase Simulations

Single-phase steam experiments performed at the RBHT facility have demonstrated the effect of mixing vanes on enhancing the downstream turbulent kinetic energy [17], which serves as a strong component in augmenting heat transfer coefficient. Based on these experiments, Miller et al [18] and Riley

et al [19] developed empirical correlations to account for the phenomenon in CTF. Motivated by experimental findings, DNS simulations were conducted for $Re_b = \{5000, 11000\}$ (or $Re_\tau = \{110, 230\}$) and a large volume of data, from probes shown in Figure 11.61, was collected to gain further insight into the turbulent flow features in the primary domain.

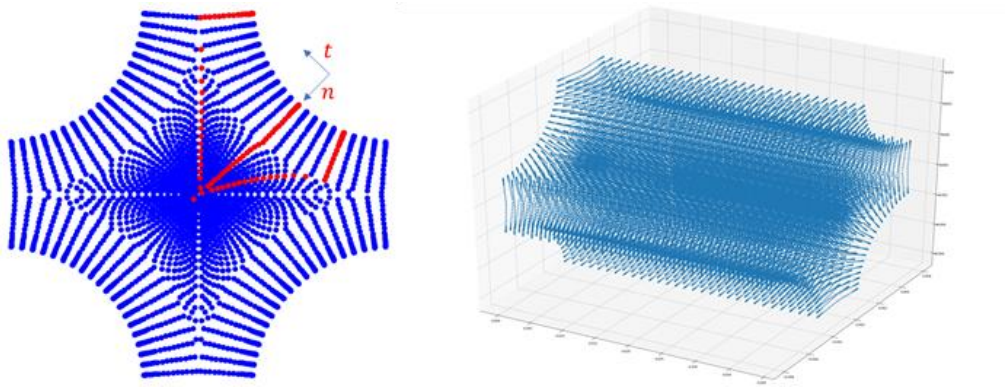


Figure 11.61. Probe configuration for data collection on a plane (left). All planes, along axial length, shown on right, totaling 84,908 probes.

### 11.3.2. Comparison with existing DNS Data

For comparison with existing DNS data, we focus on the results obtained for the plane at the inlet of the primary domain. Most widely used benchmark DNS data in literature is provided by Lee et al [39] for a typical flow channel. To enable a direct comparison with this data, the coordinate system is rotated, for each probe location, as shown in Figure 11.61, from $y - z$ to $t - n$, (rod) wall tangential-normal direction, with the normal pointing into the sub-channel.

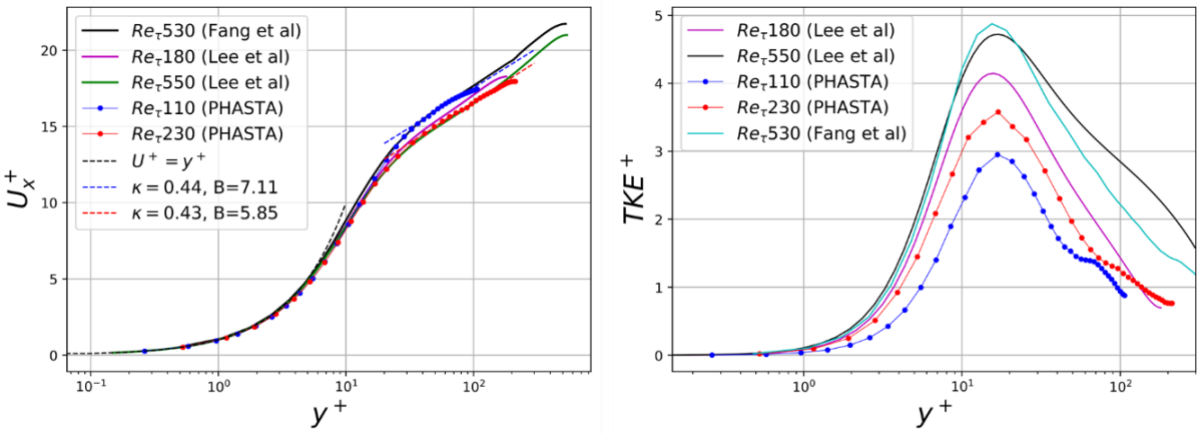


Figure 11.62. Comparison of normalized mean streamwise and TKE profile with DNS data for a sub-channel by Fang et al [40] and channel data by Lee et al [41].

Figure 11.62 shows the comparison of normalized mean streamwise velocity ($U^+ = U/u_\tau$) and turbulence kinetic energy ($TKE^+ = \overline{u_i' u_i'}/2u_\tau^2$ ) with that of flow between parallel plates [39] and sub-channel [40], albeit for different $Re_\tau$ values. Excellent agreement is obtained near the wall ($y^+ < 5$) for both cases with existing DNS data, ensuring that the mesh resolution and selected probe resolution captures the essential viscous sub-layer profile. The sub-channel results show the same trend of a decrease in the $U^+$ value with increasing Reynolds number as that of channel data in the log-layer region ($30 < y^+ < 100$). For the linear log law of the wall, $\kappa = 0.44$ and $0.43$ was obtained for $Re_\tau$=110 and 230, respectively, which are close to the widely accepted parameter, as given by Pope [42]. More relevant to the present study,

Fang et al [40] provided $\kappa = 0.43$ and 0.42, while $B = 6.7$, for their simulations in a PWR sub-channel with similar dimensions, for $Re_b = 29{,}079$ ($Re_\tau = 530$) and 80,774 ($Re_\tau = 1300$), respectively. The normalized principal Reynolds stresses in the streamwise and tangential directions are shown in Figure 11.63, compared with the results of Lee et al [39]. Although a direct comparison is not feasible due to difference in geometry and $Re_\tau$ values, the TKE and Reynolds stress profiles reveal important trend similarities, especially in the near wall region with channel simulations. Similar to a simple channel, most of the energy for the sub-channel geometry is contained in the streamwise fluctuations. Further, the TKE and $R_{xx}$ values peak at approximately the same wall distance, ($10 < y^+ < 15$), and then decline through the log-layer region. The log-layer trend for the tangential component $R_{tt}$ is also very similar to the channel data, with a peak obtained at $y^+ \sim 40$ for both geometries. However, the $R_{tt}$ profile plateaus towards the outer layers for the sub-channel more rapidly as compared to the channel data.

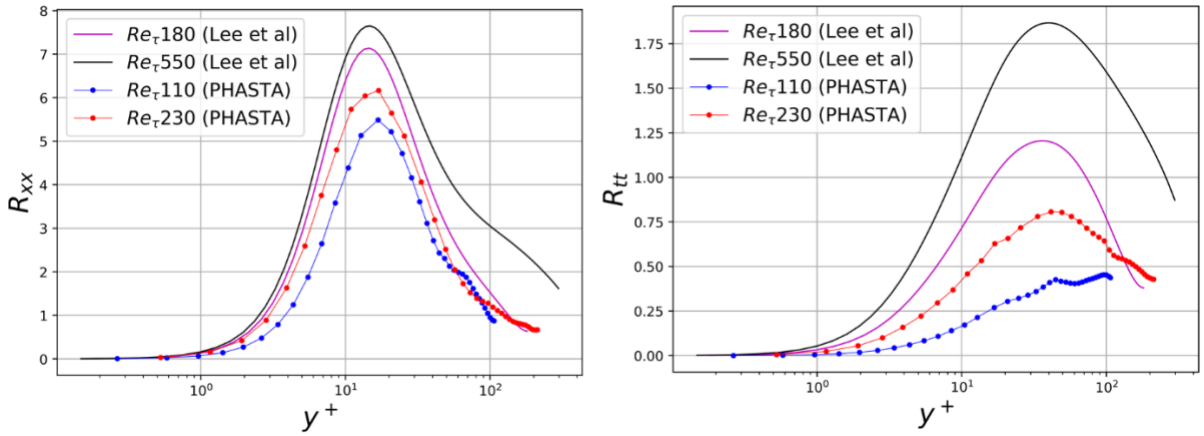


Figure 11.63. Comparison of normalized streamwise and tangential Reynolds stress profile with DNS data channel data by Lee et al [41].

### 11.3.3. Effect of Mixing Vanes on Downstream Turbulence

From the perspective of modeling the effects of spacer grids and mixing vanes on the convective heat transfer enhancement, it is imperative to understand their effect on the downstream dynamics of the flow. Figure 11.64 shows the normalized mean streamwise and tangential velocity profiles at two upstream (including the inlet) and six successive downstream locations. Note that the trailing edge of the mixing vane is located at the dimensionless axial distance of $x/D_h = 1.4$. Evidently, the mixing vanes transfer a significant amount of axial momentum of the flow to tangential components. The change in the streamwise velocity profile is not significant in the near wall region ($y^+ < 30$), however, it is significantly reduced in the immediate wake of the mixing vanes. The axial momentum is recovered to some extent as we move further downstream from the trailing edge. There is a distinct transition in the lateral velocity profile at a half distance, $y^+ \approx 100$, from the wall. The tangential velocity witnesses a very sharp increase in the near wall region ($y^+ < 20$), followed by a decline in the transition layer region. At further distance downstream, the tangential velocity in the near wall regions approaches zero, however, it is sustained in the bulk, in the opposite direction.

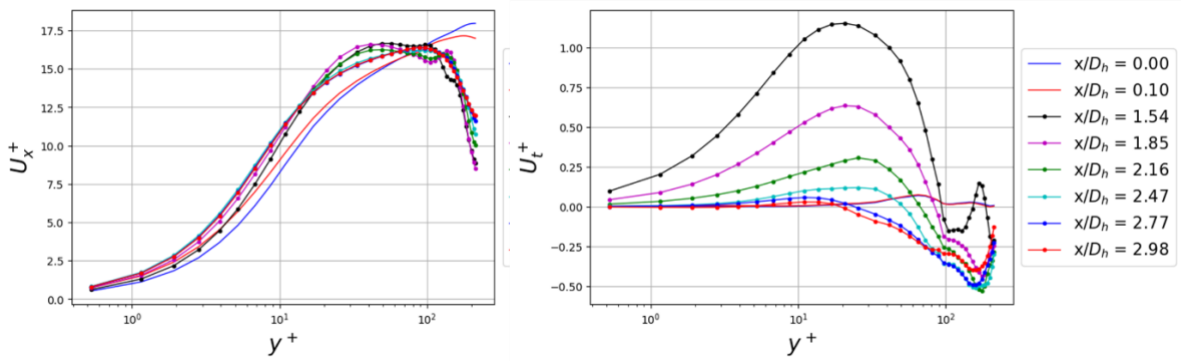


Figure 11.64. Comparison of upstream and downstream, relative to spacer-grid, normalized mean streamwise and tangential velocity profiles.

Observing the normalized principal Reynolds stress profiles, shown in Figure 11.65, it is evident that the mixing vanes impart a significant increase in energy to all components at the downstream location. The gradients of $R_{xx}$ and $R_{tt}$ are increased in the near wall regions ($y^+ < 10$), as compared to the upstream profile, and decrease progressively downstream. Further from the wall ($30 < y^+ < 100$) the trend for downstream profiles of $R_{xx}$ is similar to the upstream profile, however, further towards the center of the sub-channel another component is added due to the presence of mixing vanes. An especially sharp increase can be seen in the immediate wake of the mixing vanes. While the tangential component is insignificant in the upstream region, it shows an almost five magnitude order increase in the region $y^+ \sim 10$.

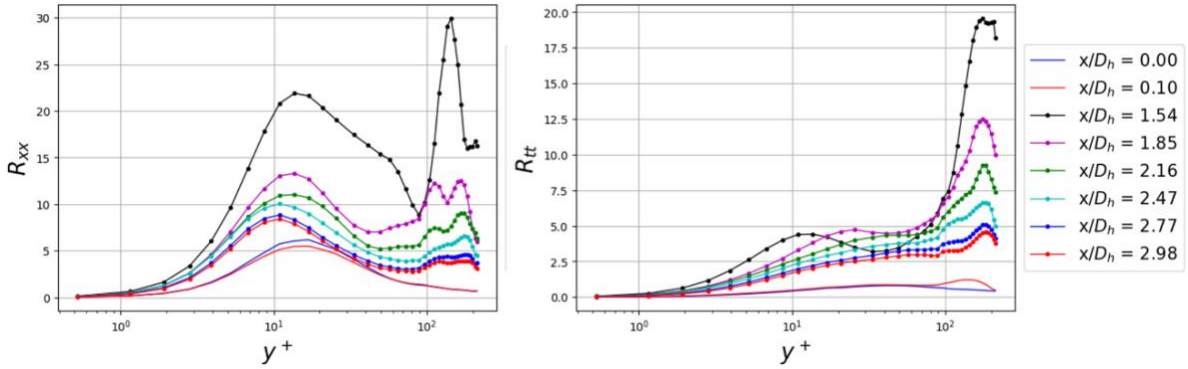


Figure 11.65. Comparison of upstream and downstream, relative to spacer-grid, normalized streamwise and tangential Reynolds stress profiles.

A relatively dense distribution of probe planes, as shown in Figure 11.61, allows the study of axial evolution of turbulence features. This data is pertinent to modeling in system thermal hydraulic codes, like CTF, since they involve cross-sectionally averaged governing equations. Figure 11.66 shows the axial evolution of principal Reynolds stresses and TKE for the $Re_\tau = 230$ case. A sharp increase in the turbulent energy is evident at the leading edge of the spacer and along the mixing vane profile, while the TKE decreases monotonously in downstream region.

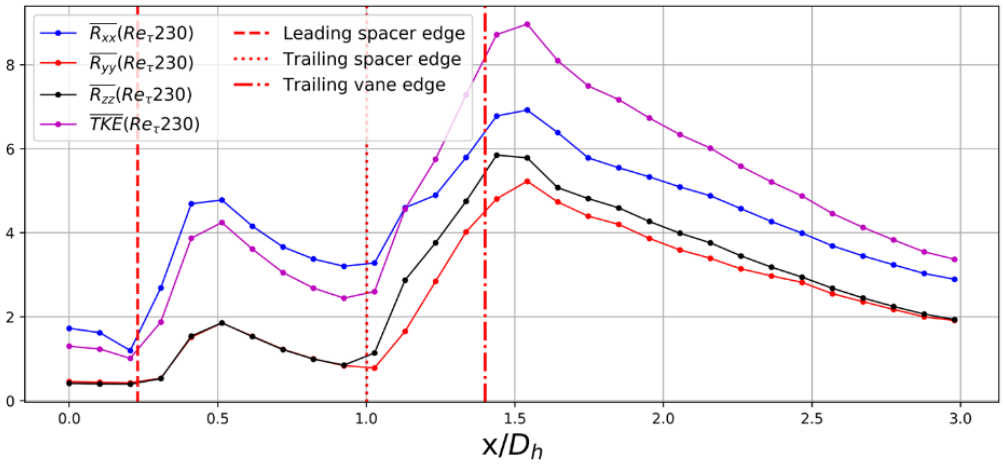


Figure 11.66. Axial evolution of plane averaged, normalized principal Reynolds stresses and TKE for $Re_\tau = 230$ case.

Further details and comprehensive discussion on the mixing vane effect on downstream turbulence, including the wall normal component of velocity and Reynolds stresses, the secondary stresses and anisotropy can be found in Saini [29].

### 11.3.4. Two-phase Simulations

Among the critical observations and results presented by Bajorek et al [15] for experiments conducted at the RBHT facility, the effect of heat transfer enhancement due to droplet collision with spacer-grid and mixing vane structures was particularly underscored. Droplet collision and subsequent breakup and/or deformation results in a very sharp increase in the interfacial area, which provides a positive feedback to several heat transfer paths. The reported increase in heat transfer coefficient has been empirically correlated to the Sauter mean diameter, which in turn was found to have a strong dependence on the upstream collision Weber number.

The steam-water system cases, as listed in Table 11.18, were run for a total simulation time of $t = \{14.75, 13.65, 13.35\} ms$ for We40, We55 and We80 cases, respectively. The droplet volume fraction for the cases at these time stamps were $\{3.14, 3.12, 2.91\}\%$, respectively. Instantaneous velocity contours for the steam-water system case with $We_c = 40$ at $t = 14.75\ ms$ and $We_c = 80$ at $t = 13.35\ ms$, are shown in Figure 11.67. For the We40 case the observed diameter of the droplets at the downstream location is evidently larger than the We80 case. For the former case, the droplets tend to coalesce into larger blobs while for the We80 case smaller droplet diameters, but a larger number of individual droplets can be seen in the domain, which is indicative of lower SMD value. Further, for the We40 case the droplets show a greater tendency to develop a liquid film over the leading edge of the spacer-grid structure, owing to a higher surface tension coefficient.

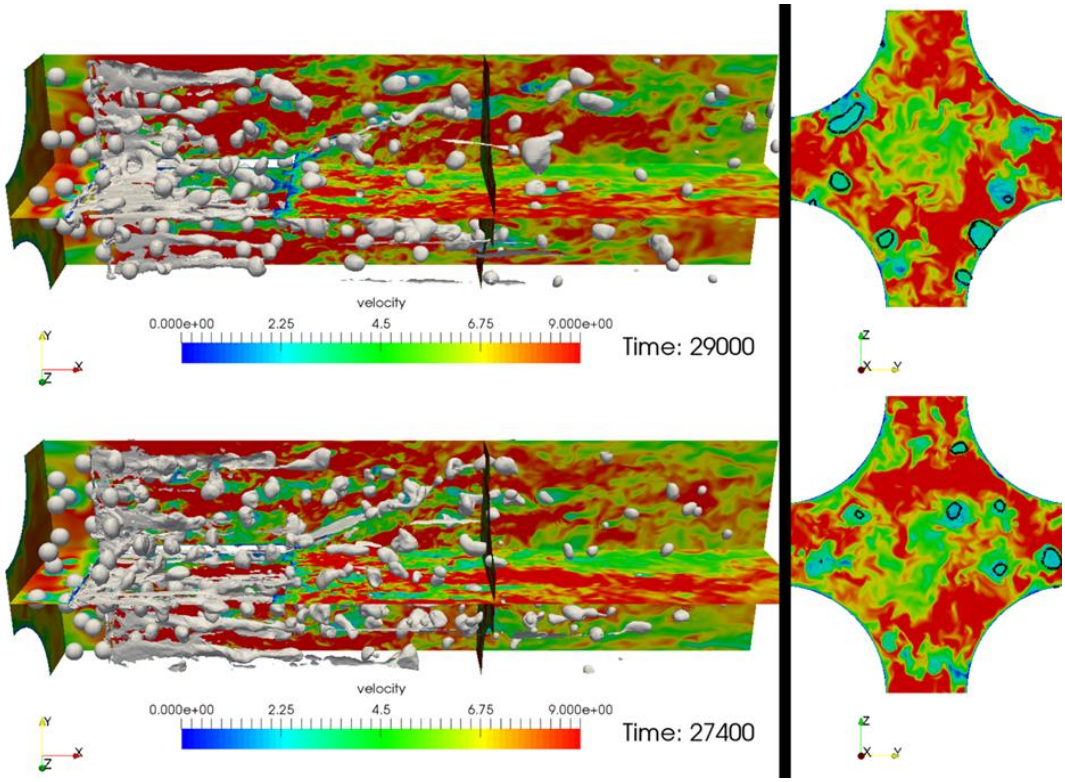


Figure 11.67. Axial evolution of plane averaged, normalized principal Reynolds stresses and TKE for $Re_\tau = 230$ case.

### 11.3.5. Axial Evolution of Droplet Dynamics

To quantify the axial evolution of droplet dynamics from the two-phase simulations, the domain is partitioned into 20 equi-spaced axial regions. The total droplet volume and interfacial area are captured at each simulation time step for each partition, which then allows for the calculation of SMD and studying its axial profile.

Figure 11.68 shows the time and cross-sectionally averaged profile of droplet volume and interfacial area in axial partitions. A sharp increase is evident at the leading edge of spacer-grid owing to droplet accretion due to collision, while a monotonous decrease is seen downstream of spacer-grid structure. This is a result of the higher acceleration experienced by the daughter or deformed droplets due to increased drag force relative to the gravitational force. The SMD profile is shown in Figure 11.69 and compared with the empirical correlation suggested by Cheung et al [24] based on RBHT data. Figure 11.70 shows the instantaneous SMD and time averaged profile for the We80 case, also compared with the existing CTF correlation [43]. The results show good agreement of time averaged SMD with these correlations at the downstream locations, Partition 14-19.

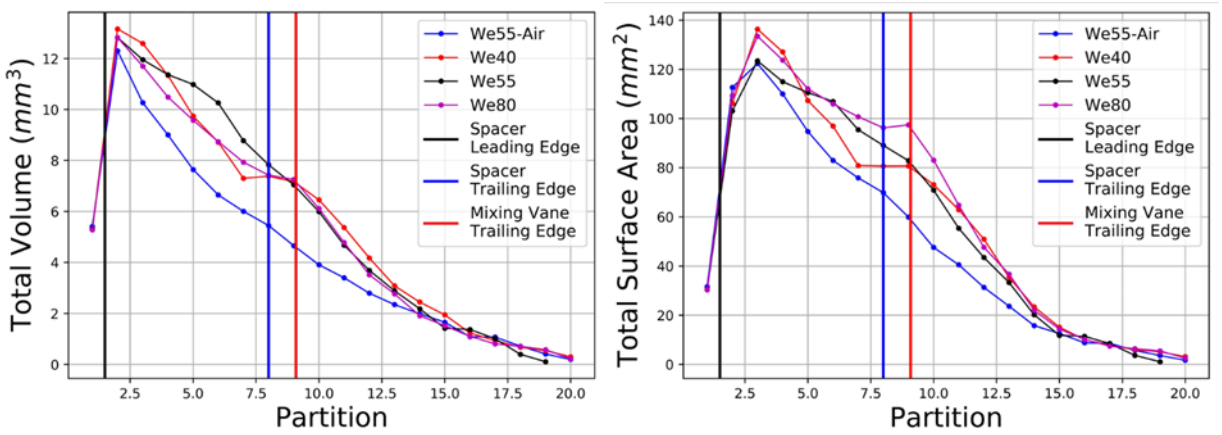


Figure 11.68 Axial profile of time averaged droplet volume (left) and interfacial area in axial partitions for all two-phase cases.

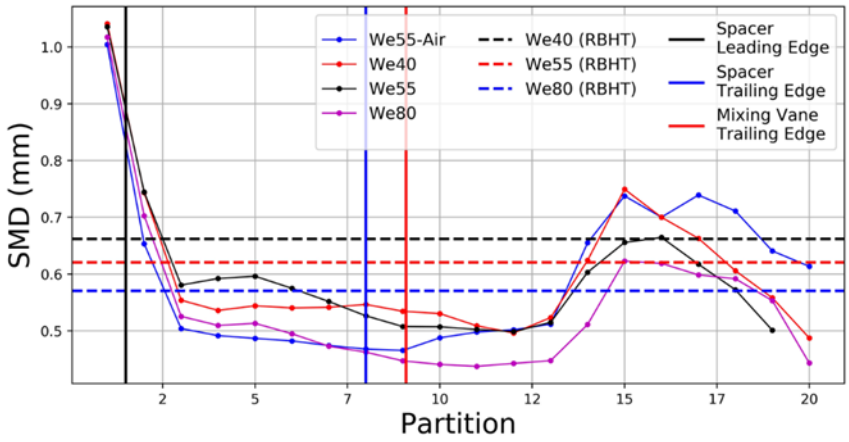


Figure 11.69. Axial profile of time averaged SMD in axial partitions for all two-phase cases. The values obtained with the RBHT correlation by Cheung et al [24] are also annotated.

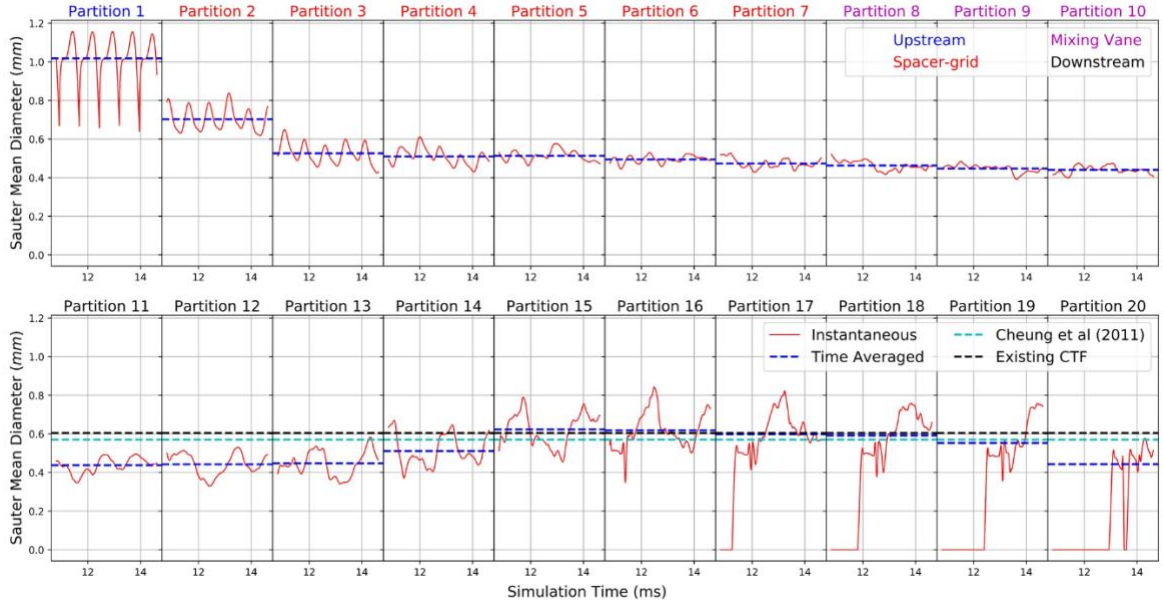


Figure 11.70. Instantaneous and time averaged SMD for the We80 case. Comparison with existing CTF and empirical correlation is shown for the downstream partitions.

### 11.3.6. Effect of Droplets on Downstream Turbulence

The presence of droplets in the computational domain decreases the effective hydraulic diameter for the steam/vapor flow. Thus, for the same flow rate maintained at the inlet cross-section, the droplets throttle the bulk flow, which is expected to increase the overall turbulent kinetic energy. From Figure 11.71 it is evident that the presence of droplets increases the streamwise velocity magnitude in the near wall region. The effect is more pronounced for the immediate downstream location $\frac{x}{D_h} = 1.54$ and the further downstream location past the vanes, with the near wall $U_x^+$ profile at $\frac{x}{D_h} = 2.77$ being almost identical. For the tangential component, however, the presence of droplets attenuates the momentum imparted due to mixing vanes, as compared to single phase case, in the wall region at $\frac{x}{D_h} = 1.54$. Away from the wall the droplets do not seem to have a significant effect on the mean components besides some re-organization of momentum.

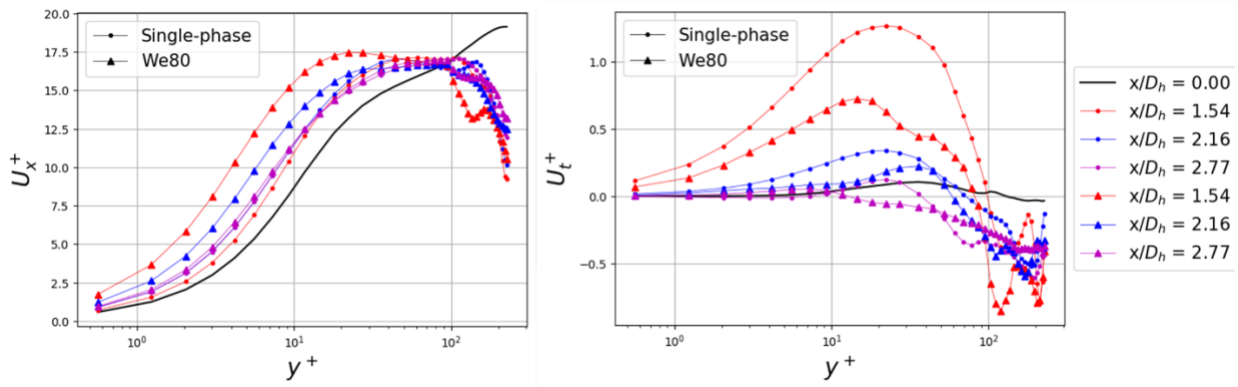


Figure 11.71. Comparison of normalized streamwise and tangential velocity for the single-phase and We80 case.

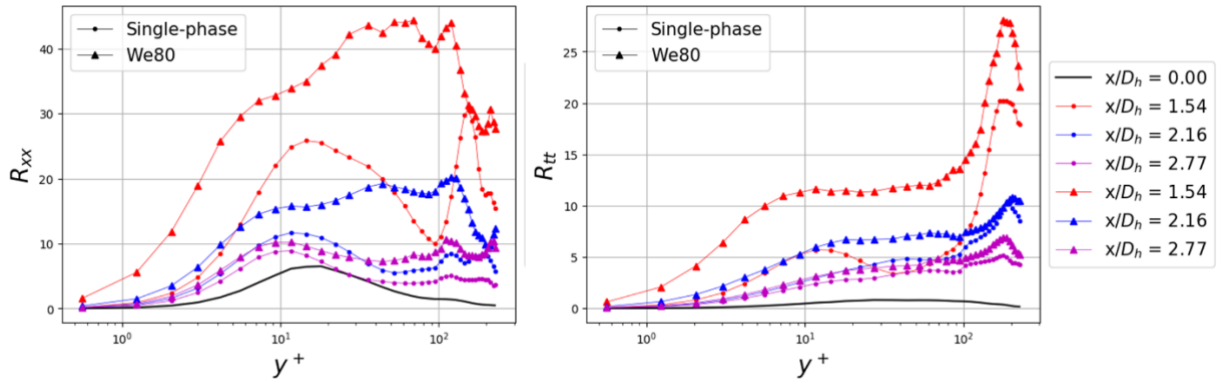


Figure 11.72. Comparison of normalized streamwise and tangential Reynolds stress for the single phase We80 case.

The presence of droplets imparts a significant positive feedback, across the $y^+$ distance, to the streamwise and tangential Reynolds stress components, especially at the immediate downstream location. The feedback is attenuated as we move further downstream, nevertheless an increase in the streamwise and tangential components is registered even at the $x/D_h = 2.77$ location. The massive feedback at the immediate downstream location can be owed to the mixing vane profile, which forces both the droplets and the bulk flow towards the peripheral regions. The results highlight the importance of considering droplet feedback to turbulence flow features and the need for modeling it in the DFFB regime.

## 11.4. Path Forward

The objectives achieved in this project clearly demonstrated the value of high-resolution simulations when the design and execution is implemented in collaboration with model developers and experimentalists.

In the future, the data generated and the capabilities developed will be applied to relevant problems in nuclear engineering thermal-hydraulics, including reactor operation and safety modeling problems. Of particular interest is the application of novel machine-learning based methods for model development and for gaining insight into flow physics.

The extensive data set provided (see data management, Section **Error! Reference source not found.**) will allow future data mining efforts for advanced model development, as well as investigating new algorithms for this data. The process, in turn, may identify additional fields and parameters which could be extracted from high resolution simulations in the future.

To summarize, given the potential future funding, the following objectives can be addressed in future projects:

- Apply and enhance interface tracking approach for a wide variety of two-phase flow problems in nuclear reactor relevant geometries.
- Utilize DNS for many advanced reactor designs.
- Enhance data collection algorithms to be suitable for a variety of modern ML-based methods.
- Develop scalable training databases for ML algorithms to continuously improve the models as more high resolution numerical and experimental data becomes available.
- Adding heat transfer / phase change effects (recently implemented in PHASTA) will greatly enhance the range of problems which can be studied using this approach.

## 11.5. Conclusions

The key conclusions from this project contribution are:

- The research herein highlights the capability of PHASTA, coupled with level-set method, to simulate the post-LOCA DFFB regime. Simulations with unprecedented resolution and fidelity were performed to illuminate droplet dynamics in this critical PWR regime.
- Advanced high-resolution data collection tools are implemented in PHASTA which enable detailed study of turbulence from DNS scale simulations, optimized for large scale supercomputers.
- The high spatial and temporal resolution of data collected from the single-phase and two-simulations is archived and would, potentially, serve as a data mine for the development of machine learning based turbulence and STH models.
- The results from single-phase simulations highlight the effect of spacer-grids and mixing vanes on convective enhancement. Further, invariant analysis of the data reveals that the mixing vanes modify the state of turbulence in the downstream region.
- The results from two-phase simulations emphasize the importance of considering droplet feedback to turbulence, in addition to the enhancement provided by spacer-grids and mixing vanes. The SMD results at the downstream locations match well with experimental data, establishing confidence in PHASTA and the incorporated level-set method in simulating the DFFB regime.
- All tools are in place for a more extensive parametric study of the DFFB regime, with a range of bulk Reynolds number and collision Weber numbers. Single droplet collision studies are recommended for characterizing uncertainties associated with collision events.
- The most limiting assumption of the current simulations, in contrast to the real DFFB conditions, is the lack of heat transfer modeling. Consideration of heat transfer mechanisms requires more

extensive development efforts in PHASTA, including methods for phase change, conjugate heat transfer and modeling of radiative heat transfer.

## 11.6. References


1. C. CHANG and N.T. DINH, "Classification of machine learning frameworks for data-driven thermal fluid models". *International Journal of Thermal Sciences* 135, 559-579 (2019).
2. J. WU, H. XIAO, E. PATERSON, "Data-driven augmentation of turbulence models with physics-informed machine learning". *arXiv preprint arXiv:1801.02762* (2018).
3. J. Wang, J. Wu, J. Ling, G. Iaccarino, H. Xiao, "A Comprehensive Physics-Informed Machine Learning Framework for Predictive Turbulence Modeling". *Preprint submitted to Elsevier* (2017).
4. J. LING, A. KURZAWSKI, J. TEMPLETON, "Reynolds averaged turbulence modelling using deep neural networks with embedded invariance". *J. Fluid Mech.* 807, 155-166 (2016).
5. Y. LIU, N. DINH, Y. SATO, B. NICENO, "Data-driven modeling for boiling heat transfer: using deep neural networks and high-fidelity simulation results". *Appl. Therm. Eng.* 144, 305-320 (2018).
6. H. BAO, N.T. DINH, J.W. LANE, R.W. YOUNGBLOOD, "A data-driven framework for error estimation and mesh-model optimization in system-level thermal-hydraulic simulation". *Nucl. Eng. Des.* 349, 27-45 (2019).
7. B.N. HANNA, N.T. DINH, R.W. YOUNGBLOOD, I.A. BOLOTNOV, "Coarse-Grid Computational Fluid Dynamic (CG-CFD) Error Prediction using Machine Learning". *arXiv preprint arXiv:1710.09105* (2017).
8. J. FANG, J.J. CAMBARERI, M. LI, N. SAINI, I.A. BOLOTNOV, "Interface-Resolved Simulations of Reactor Flows". *Nucl Technol* 206, 133-149 (2020).
9. N. SAINI and I.A. BOLOTNOV, "Interface capturing simulations of droplet interaction with spacer grids under DFFB conditions". *Nucl. Eng. Des.* 364, 110685 (2020).
10. L. HOCHREITER, F. CHEUNG, T. LIN, A. BARATTA, C. FREPOLI, *Dispersed Flow Heat Transfer Under Reflood Conditions in a 49-Rod Bundle: Test Plan and Design—Results from Tasks 1-10* (2000).
11. C. SMITH, D. SCHWIEDER, C. PHELAN, A. BUI, P. BAYLESS, *Light Water Reactor Sustainability Program Risk Informed Safety Margin Characterization (RISMC) Advanced Test Reactor Demonstration Case Study* (2012).
12. K. ARDRON and P. HALL, "Droplet hydrodynamics and heat transfer in the dispersed flow regime in bottom flooding". *CEGB, RD/B/5007N81, Berkeley* (1981).
13. LEE, N., 1982. PWR FLECHT SEASET Unblocked Bundle, Forced and Gravity Reflood Task Data Evaluation and Analysis Report. The Commission.
14. L. HOCHREITER, F. CHEUNG, T. LIN, C. FREPOLI, A. SRIDHARAN, D. TODD, et al., "Rod bundle heat transfer test facility test plan and design". *NUREG CR-6975.US Nuclear Regulatory Commission* (2010).
15. S.M. BAJOREK and F. CHEUNG, "Rod Bundle Heat Transfer Thermal-Hydraulic Program". *Nucl Technol* 205, 307-327 (2019).
16. L. HOCHREITER, F. CHEUNG, T. LIN, C. FREPOLI, A. SRIDHARAN, D. TODD, et al., "Rod bundle heat transfer test facility test plan and design". *NUREG CR-6975.US Nuclear Regulatory Commission* (2010).
17. HOCHREITER, L., 2014. Rod Bundle Heat Transfer Facility: Steady-State Steam Cooling Experiments. United States Nuclear Regulatory Commission, Office of Nuclear Regulatory ….
18. D. MILLER, F. CHEUNG, S. BAJOREK, "On the development of a grid-enhanced single-phase convective heat transfer correlation". *Nucl. Eng. Des.* 264, 56-60 (2013).
19. M.P. RILEY, "Spacer grid induced heat transfer enhancement in a rod bundle under reflood conditions". (2014).
20. M. AVRAMOVA and R.K. SALKO, *CTF Theory Manual* (2016).

21. M. RILEY, L. MOHANTA, F. CHEUNG, S. BAJOREK, K. TIEN, C. HOXIE, "Experimental studies of spacer grid thermal hydraulics in the dispersed flow film boiling regime". *Nucl Technol* 190, 336-344 (2015).
22. D. MILLER, F. CHEUNG, S. BAJOREK, "Investigation of grid-enhanced two-phase convective heat transfer in the dispersed flow film boiling regime". *Nucl. Eng. Des.* 265, 35-44 (2013).
23. S. YAO, L. HOCHREITER, W. LEECH, "Heat-transfer augmentation in rod bundles near grid spacers". *Journal of Heat Transfer* 104, 76-81 (1982).
24. F. CHEUNG and S. BAJOREK, "Dynamics of droplet breakup through a grid spacer in a rod bundle". *Nucl. Eng. Des.* 241, 236-244 (2011).
25. M. ANDREANI and G. YADIGAROGLU, "Difficulties in modeling dispersed-flow film boiling". *Wärme-und Stoffübertragung* 27, 37-49 (1992).
26. C.H. WHITING and K.E. JANSEN, "A stabilized finite element method for the incompressible Navier-Stokes equations using a hierarchical basis". *Int. J. Numer. Methods Fluids* 35, 93-116 (2001).
27. S. COGHLAN, K. KUMARAN, R.M. LOY, P. MESSINA, V. MOROZOV, J.C. OSBORN, et al., "Argonne applications for the IBM blue gene/Q, Mira". *IBM Journal of Research and Development* 57, 12: 1-12: 11 (2013).
28. T. Dinh N., "DOE-NEUP 16-10918". **2016** (2016).
29. N. SAINI and I.A. BOLOTNOV, "Interface capturing simulations of droplet interaction with spacer grids under DFFB conditions". *Nucl. Eng. Des.* 364, 110685 (2020).
30. J. KIM, P. MOIN, R. MOSER, "Turbulence statistics in fully developed channel flow at low Reynolds number". *J. Fluid Mech.* 177, 133-166 (1987).
31. R.D. MOSER, J. KIM, N.N. MANSOUR, "Direct numerical simulation of turbulent channel flow up to Re= 590". *Phys. Fluids* 11, 943-945 (1999).
32. J. FANG, M. RASQUIN, I.A. BOLOTNOV, "Interface tracking simulations of bubbly flows in PWR relevant geometries". *Nucl. Eng. Des.* 312, 205-213 (2017).
33. F.A. MORRISON, "Data correlation for drag coefficient for sphere". *Department of Chemical Engineering, Michigan Technological University, Houghton, MI* 49931 (2013).
34. Y. JIN, D.J. MILLER, S. QIAO, A. RAU, S. KIM, F. CHEUNG, et al., "Uncertainty analysis on droplet size measurement in dispersed flow film boiling regime during reflood using image processing technique". *Nucl. Eng. Des.* 326, 202-219 (2018).
35. M. ANDREANI and G. YADIGAROGLU, "Prediction methods for dispersed flow film boiling". *Int. J. Multiphase Flow* 20, 1-51 (1994).
36. J. FANG and I.A. BOLOTNOV, "Bubble tracking analysis of PWR two-phase flow simulations based on the level set method". *Nucl. Eng. Des.* 323, 68-77 (2017).
37. J. FENG, "Evaluation of Interfacial Forces and Bubble-Induced Turbulence Using Direct Numerical Simulation.". (2017).
38. K.T. CARLBERG, A. JAMESON, M.J. KOCHENDERFER, J. MORTON, L. PENG, F.D. WITHERDEN, "Recovering missing CFD data for high-order discretizations using deep neural networks and dynamics learning". *Journal of Computational Physics* (2019).
39. M. LEE and R.D. MOSER, "Direct numerical simulation of turbulent channel flow up to Re_tau 5200". *J. Fluid Mech.* 774, 395-415 (2015).
40. J. FANG, M. RASQUIN, I.A. BOLOTNOV, "Interface tracking simulations of bubbly flows in PWR relevant geometries". *Nucl. Eng. Des.* 312, 205-213 (2017).
41. M. LEE and R.D. MOSER, "Direct numerical simulation of turbulent channel flow up to $\mathit {Re} _ {{\it\tau}}\approx 5200$". *J. Fluid Mech.* 774, 395-415 (2015).
42. S.B. POPE, "Turbulent Flows". *Cambridge University Press* (2001).
43. M.N. AVRAMOVA and R.K. SALKO, *CTF theory manual* (2016).

# 12.Data-Driven Modeling and Validation Methods & Tools

This Chapter highlights key developments (by the project team and collaborators) in data-driven methods for thermal-fluid modeling, error evaluation, validation, uncertainty quantification, and scaling (scale bridging), including both STH and CFD.

## 12.1. Data-driven modeling (Hi2Lo)

Chih-Wei Chang and Nam Dinh, "Classification of Machine Learning Frameworks for Data-Driven Thermal Fluid Models", *International Journal of Thermal Science*, 135, pp.559-579, 2019.

> Thermal fluid processes are inherently multi-physics and multi-scale, involving mass-momentum-energy transport phenomena at multiple scales. Thermal fluid simulation (TFS) is based on solving conservative equations, for which – except for "first-principles" direct numerical simulation – closure relations (CRs) are required to provide microscopic interactions or so-called sub-grid-scale physics. In practice, TFS is realized through reduced-order modeling, and its CRs as low-fidelity models can be informed by observations and data from relevant and adequately evaluated experiments and high-fidelity simulations. This paper is focused on data-driven TFS models, specifically on their development using machine learning (ML). Five ML frameworks are introduced including physics-separated ML (PSML or Type I ML), physics-evaluated ML (PEML or Type II ML), physics-integrate ML (PIML or Type III ML), physics-recovered (PRML or Type IV ML), and physics-discovered ML (PDML or Type V ML). The frameworks vary in their performance for different applications depending on the level of knowledge of governing physics, source, type, amount and quality of available data for training. Notably, outlined for the first time in this paper, Type III models present stringent requirements on modeling, substantial computing resources for training, and high potential in extracting value from "big data" in thermal fluid research.
>
> The current paper demonstrates and investigates ML frameworks in three examples. First, we utilize the heat diffusion equation with a nonlinear conductivity model formulated by convolutional neural networks (CNNs) and feedforward neural networks (FNNs) to illustrate the applications of Type I, Type II, Type III, and Type V ML. The results indicate a preference for Type II ML under deficient data support. Type III ML can effectively utilize field data, potentially generating more robust predictions than Type I and Type II ML. CNN-based closures exhibit more predictability than FNN-based closures, but CNN-based closures require more training data to obtain accurate predictions. Second, we illustrate how to employ Type I ML and Type II ML frameworks for data-driven turbulence modeling using reference works. Third, we demonstrate Type I ML by building a deep FNN-based slip closure for two-phase flow modeling. The results show that deep FNN-based closures exhibit a bounded error in the prediction domain.

Yang Liu, Nam Dinh, Yohei Sato and Bojan Niceno, "Data-driven modeling for boiling heat transfer: using deep neural networks and high-fidelity simulation results", *Applied Thermal Engineering*, 144, pp.305-320, 2018

Chih-Wei Chang, Jun Fang and Nam Dinh; "Reynolds-Averaged Turbulence Modeling Using Deep Learning with Local Flow Features – an Empirical Approach", *Nuclear Science and Engineering*, Vol.00, pp.1-15, 2020 (online January 2020).

Yangmo Zhu, Nam T. Dinh, Nadish Saini, Igor A. Bolotnov, "An adaptive knowledge-based data-driven approach for turbulence modeling using ensemble learning technique under complex flow configuration: 3D PWR sub-channel with DNS data", Submitted for review, 2020

This work describes a new approach to increase the accuracy of Reynolds- averaged Navier–Stokes (RANS) in modeling turbulence flow leveraging the machine learning technique. Traditionally, different turbulence models for Reynolds stress are developed for different flow patterns based on human knowledge. Each turbulence model has a certain application domain and prediction uncertainty. In recent years, with the rapid improvements of machine learning techniques, researchers start to develop an approach to compensate for the prediction discrepancy of traditional turbulence models with statistical models and data. However, the approach has deficiencies in several aspects. For example, the amount of human knowledge introduced to the statistical model couldn't be controlled, which makes the statistical model learn from a very naive stage and limits its application. In this work, a new approach is developed to address those deficiencies. The new approach uses the "ensemble learning" technique to control the amount of human knowledge introduced into the statistical model. Therefore, the new approach could be adaptive to the multiple application domains. According to the results of case studies, the new approach shows higher accuracy than both traditional turbulence models and the previous machine learning approach. Furthermore, the new approach shows better performance in predicting the error caused by applying coarse mesh (insufficient mesh resolution) to the computational fluid dynamics (CFD) simulation, which indicates the potential of the approach to save the computational expense of RANS to the coarse-mesh level.

### 12.2. Data-driven error evaluation

Botros Hanna, Nam Dinh, Robert Youngblood, and Igor Bolotnov, "Coarse-Grid Computational Fluid Dynamic Errors Prediction by Machine Learning", *Progress in Nuclear Energy*, Vol.118 (2020) 103140 (online September 2019)

Computational Fluid Dynamics (CFD) is one of the modeling approaches essential to identifying the parameters that affect Containment Thermal Hydraulics (CTH) phenomena. While the CFD approach can capture the multidimensional behavior of CTH phenomena, its computational cost is high when modeling complex accident scenarios. To mitigate this expense, we propose reliance on coarse-grid CFD (CG-CFD). Coarsening the computational grid increases the grid-induced error thus requiring a novel approach that will produce a surrogate model predicting the distribution of the CG-CFD local error and correcting the fluid-flow variables. Given sufficiently fine-mesh simulations, a surrogate model can be trained to predict the CG-CFD local errors as a function of the coarse-grid local flow features. The surrogate model is constructed using Machine Learning (ML) regression algorithms. Two of the widely used ML regression algorithms were tested: Artificial Neural Network (ANN) and Random Forest (RF). The proposed CG-CFD method is illustrated with a three-dimensional turbulent flow inside a lid-driven cavity. We studied a set of scenarios to investigate the capability of the surrogate model to interpolate and extrapolate outside the training data range. The proposed method has proven capable of correcting the coarse-grid results and obtaining reasonable predictions for new cases (of different Reynolds number, different grid sizes, or larger geometries). Based on the investigated cases, we found this novel method maximizes the benefit of the available data and shows potential for a good predictive capability.

Han Bao, Nam T. Dinh, Jeffrey W. Lane, and Robert W. Youngblood, "A data-driven framework for error estimation and mesh-model optimization in system-level thermal-hydraulic simulation", *Nuclear Engineering and Design*, Volume 349, 1 August 2019, Pages 27-45

Over the past decades, several computer codes have been developed for simulation and analysis of thermal-hydraulics and system response in nuclear reactors under operating, abnormal transient, and accident conditions. However, simulation errors and uncertainties still inevitably exist even while these codes have been extensively assessed and used. In this work, a data-driven framework (Optimal Mesh/Model Information System, OMIS) is formulated and demonstrated to estimate simulation error

and suggest optimal selection of computational mesh size (i.e., nodalization) and constitutive correlations (e.g., wall functions and turbulence models) for low-fidelity, coarse-mesh thermal-hydraulic simulation, in order to achieve accuracy comparable to that of high-fidelity simulation. Using results from high-fidelity simulations and experimental data with many fast-running low-fidelity simulations, an error database is built and used to train a machine learning model that can determine the relationship between local simulation error and local physical features. This machine learning model is then used to generate insight and help correct low-fidelity simulations for similar physical conditions. The OMIS framework is designed as a modularized six-step procedure and accomplished with state-of-the-art methods and algorithms. A mixed-convection case study was performed to illustrate the entire framework.

### 12.3. Data-driven validation and uncertainty quantification

Yang Liu and Nam Dinh, "Validation and Uncertainty Quantification for Wall Boiling Closure Relations in Multiphase CFD Solver", *Nuclear Science and Engineering*. pp.1-19, 2018 (online Sep 2018)

Yang Liu, Nam Dinh, Ralph Smith, and Xiaodong Sun, "Uncertainty Quantification of Two-Phase Flow and Boiling Heat Transfer Simulation Through a Data-Driven Bayesian Modular Approach", *International Journal of Heat and Mass Transfer*, Volume 138, August 2019, Pages 1096-1116

Yang Liu, Xiaodong Sun, and Nam T. Dinh, "Validation and Uncertainty Quantification of multiphase-CFD solvers: A Data-Driven Bayesian Framework Supported by High-Resolution Experiments", J. *Nuclear Engineering and Design*, 2019, Vol.354, 110200, pp.1-19.

Yang Liu, Dewei Wang, Xiaodong Sun, Yang Liu, Nam Dinh, and Rui Hu, "Uncertainty quantification for Multiphase-CFD simulations of bubbly flows: a machine learning-based Bayesian approach supported by high-resolution experiments", *Reliability Engineering and System Safety*, 2021 (in press).

In this paper, we developed a machine learning-based Bayesian approach to inversely quantify and reduce the uncertainties of multiphase computational fluid dynamics (MCFD) simulations for bubbly flows. The proposed approach is supported by high-resolution two-phase flow measurements, including those by double-sensor conductivity probes, high-speed imaging, and particle image velocimetry. Local distributions of key physical quantities of interest (QoIs), including the void fraction and phasic velocities, are obtained to support the Bayesian inference. In the process, the epistemic uncertainties of the closure relations are inversely quantified while the aleatory uncertainties from stochastic fluctuations of the system are evaluated based on experimental uncertainty analysis. The combined uncertainties are then propagated through the MCFD solver to obtain uncertainties of the QoIs, based on which probability-boxes are constructed for validation. The proposed approach relies on three machine learning methods: feedforward neural networks and principal component analysis for surrogate modeling, and Gaussian processes for model form uncertainty modeling. The whole process is implemented within the framework of an open-source deep learning library PyTorch with graphics processing unit (GPU) acceleration, thus ensuring the efficiency of the computation. The results demonstrate that with the support of high-resolution data, the uncertainties of MCFD simulations can be significantly reduced.

### 12.4. Data-driven scale bridging

Han Bao, Nam Dinh, Linyu Lin, Robert Youngblood, Jeffrey Lane, Hongbin Zhang, "Using Deep Learning to Explore Local Physical Similarity for Global-scale Bridging in Thermal-hydraulic Simulation", *Annals of Nuclear Energy* journal Volume 147, November 2020, 107684

Current system thermal-hydraulic codes have limited credibility in simulating real plant conditions, especially when the geometry and boundary conditions are extrapolated beyond the range of test facilities. Because mesh size is one of the model parameters for these coarse-mesh codes with simplified boundary-layer treatments, the mesh-induced error and model error are tightly connected, which makes it difficult to evaluate mesh effect or model scalability independently, as in classical scaling analysis. This paper proposes a data-driven approach, Feature-Similarity Measurement (FSM), to establish a technical basis to overcome these difficulties by exploring local patterns using machine learning. The underlying local patterns in multiscale data are represented by a set of physical features that embody the information from a physical system of interest, empirical correlations, and the effect of mesh size. After performing a limited number of high-fidelity numerical simulations and a sufficient amount of fast-running coarse-mesh simulations, an error database is built, and deep learning is applied to construct and explore the relationship between the local physical features and simulation errors. As a result, a data-driven model can be developed to provide an accurate estimate on the simulation error even when global-scale gaps exist. Case studies based on mixed convection have been designed for demonstrating the capability of data-driven models in bridging global-scale gaps.

## 12.5. Concluding Remarks

At the time of the IRP proposal submission (2015-2016), data-driven methods in thermal fluid applications were in infancy. The investigations conducted in this project were exploratory; the developments were cutting-edge, building on advances in artificial neural networks (ANN), particularly “deep learning”. During the last three years, we witness a wave of interests in machine learning applications in thermal-fluid process modeling, validation, and uncertainty quantification. There is a critical mass of interests, talents, and technical capabilities to explore and exploit the potential of this new approach. However, it also becomes evident that data, both quantity and quality, present a bottleneck in data-driven methods’ success in new and complex applications.

# 13. Data Management Infrastructure to Support Validation Activities

## 13.1. Introduction

High-fidelity simulations (including CFD and DNS) and advanced experiments produce an unprecedented amount of data. However, the conventional framework was developed in the era when data storage and transfer were a weaker link. As a solution, empirical correlations were developed through experts' insight of the physics model. While methods of the formula and equation-centric era still remain important, they face increasing challenges from rapid data explosion. Their incapability in capturing and handling massive data, data irregularities, and complicated data interrelationships have resulted in considerable amount of data archives, experimental and computational, becoming corrupted, misinterpreted, and partially or completely lost over time.

To find solutions and address this problem, a complexity reduction approach is considered that would allow analysts to use high-fidelity models without having to develop empirical formulas. While the high-fidelity models can describe the system behavior at the finest scale, the range of model applicability often introduces numerous constrains, significantly reducing the effective dimensionality of the resulting datasets. This implies that the datasets are highly correlated with their true dimensionality much smaller than their nominal dimensionality. It has been shown by Bang, et. al. that reduced order modeling techniques can be used to identify so-called active degrees of freedom that can be used to reconstruct the big datasets from other datasets of much smaller dimensions, with the reconstruction errors being upper-bounded by preset tolerances over the wide range of conditions expected for model application (Bang, et al., 2012). This tactic not only affords a computationally efficient approach to processing and storing datasets, but also allows for much smaller number of metrics that can be used as a basis for the validation of large volume datasets associated with the high-fidelity models.

In the conventional equation-centric paradigm, four steps are involved in the workflow, i.e., (i) data analysis, (ii) model/correlation development, (iii) validation against data and quantification of uncertainty, and (iv) relevant data. In the new data-centric paradigm employed in the data-driven methodology, the workflow skips the two middle steps and goes directly from (i) data analysis to (iv) relevant data. Significant biases associated with (ii) and (iii) are thus eliminated. As more relevant data become available, the simulation becomes increasingly accurate. There is no data wasted in this framework. Validated simulations per se also become "data". Simulation control becomes knowledge management. Furthermore, it generates an incentive for community collaboration, with the common goal of reducing uncertainty through data sharing, experimental and computational alike. It follows that this new paradigm requires analytical capability to manage the data and complicated data interrelationships to ensure correct interpretation, extraction, and use of the data.

To achieve the data-driven goals, an advanced data management system is required to systematically collect, process, and manage data, and support all the relevant data operations on massive machine-readable data records. The system must meet the following requirements:

1. For infrastructure, tools, and protocols it should provide:
    - A web-accessible, searchable, quality-assessed, and user-friendly Database Management System.
    - A secure and access-controlled knowledgebase in compliance with partners-agreed technology control plan protocols.
    - A sustained platform enabling data (experimental, industrial, computational) collection, qualification, and preservation for a broad range of users, including non-developers and posterity.

- An efficient system with high traceability, accountability, and advanced data manipulation functionalities.
- Application Programming Interfaces (APIs) customized for intended simulation codes and Verification and Uncertainty Quantification (VUQ) analytical tools for data analytics, data mining, and data assimilation.

2. VUQ-enabling functionalities must be provided to ensure viable, effective workflows and protocols for collecting, assessing, processing, and managing validation data.

3. A Data File Warehouse is needed to support the following functions:
   - Data identification for preservation.
   - Data collection (primary sources of data in various types of electronic files such as spreadsheets, videos, photos, etc.).
   - Data tracking (data provenance and pedigree).
   - Data qualification (data quality assessment).

4. A Relational Digital Database is required to offer high traceability, accountability, and advanced data manipulation functionalities.

5. The system must provide functionalities that support predictive models (specified bounds for predictions):
   - Systematic and iterative evaluations.
   - Data characterization, i.e., assess, categorize, and rank the scalability, relevancy, and uncertainty of data for use in total data integration.
   - Data reconfiguration, i.e., converse/homogenize data of different types to formats compatible with VUQ methods, including converting raw data in analog media into digital data formats, reprocessing legacy data, and reformatting data as needed.
   - Interoperability, i.e., directly exchange data between the Relational Digital Database and the VUQ or simulation software in an automated fashion, with searching, sorting, and filtering capabilities.

6. The system must provide features that facilitate verification and validation activities:
   - Amenable to processing (with statistical and optimization methods and tools)
   - Specialized strict input, flexible, unlimited output/extraction
   - Creating dataset guided by questions Graphic User Interfaces (GUIs)
   - Knowledge accumulation (accumulative experience of using datasets)

7. The system must support integration of new and legacy experimental data for use in VUQ and M&S.

8. Compatible with engineering practice (current, and provision for future), e.g., VUQ methodologies including NRC regulatory guide.

Development of such a system requires considerable resources and time, which is obviously beyond the scope of the present project. A pragmatic approach would be to piggyback on an existing system and leverage its sustained resources and administrative support.

During the proposal preparation of the present project, the Department of Energy (DOE) was initiating the Nuclear Energy Knowledge and Validation Center (NEKVAC) in response to the strong support and recommendations from stakeholders at an Atlanta workshop organized in 2015 by DOE and the Idaho National Laboratory (INL) to brainstorm for developing such capabilities and particularly for advancing

the theory and practice of simulation code validation in the service of the nuclear industry. The NEKVAC was organized to operate through a Directorate composed of the Steering Committee, the Methods and Guidelines Committee, and a Knowledge Management Committee, with stakeholder members from government, academia, and industry organizations (Gougar, 2015). In addition to the three committees, the workshop also recommended establishing a knowledgebase and simulation code validation system using the Nuclear Energy Knowledgebase for Advanced Modeling and Simulation (NE-KAMS) Demo and the Radiation Safety Information Computational Center (RSICC) resources at the Oak Ridge National Laboratory (ORNL) to provide a tangible framework to support NEKVAC development and operation. It followed that as NEKVA took off, NE-KAMS would provide an ideal infrastructure to host the data for the present project, ensuring their compatibility with validation and uncertainty quantification, and most importantly, serving as a Validation Data Management System (VDMS) to implement the new data-centric paradigm. The homepage for NE-KAMS login is presented in Figure 13.1.

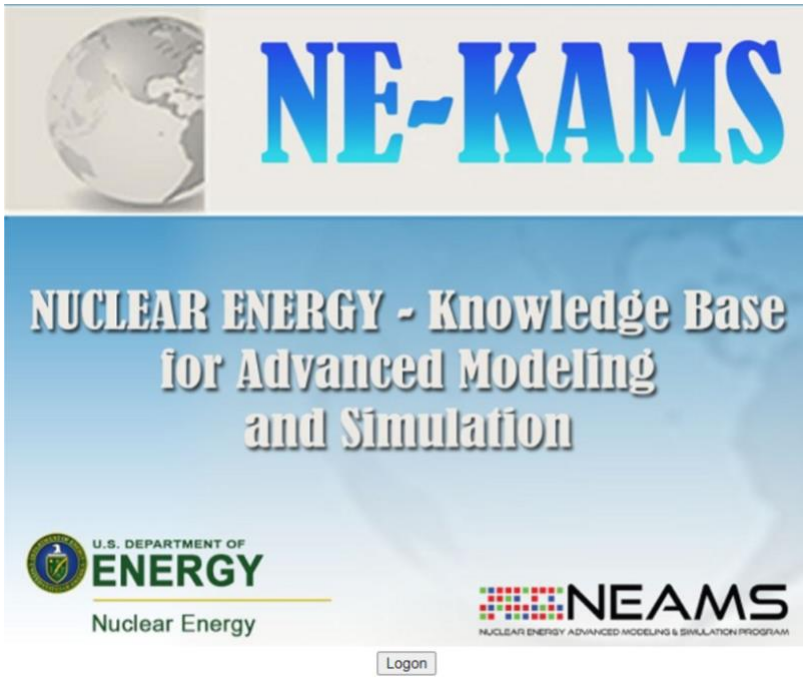


Figure 13.1. Homepage of NE-KAMS for authorized user login at http://nekams.ornl.gov/

The NE-KAMS Demo was sponsored by the DOE Nuclear Energy Advanced Modeling and Simulation (NEAMS) Program specifically to support verification and validation of advanced modeling and simulation [Lee, et. al., 2012; Ren, 2012; Lee, et. al., 2013]. Its development at the time was focused on a Data File Warehouse section to store and manage fluid dynamics and thermal hydraulics data files as foundation for further development of a Digital Database section to manage machine-readable digital data records. Standards and requirements for fluid dynamic code verification and validation data were also developed and archived in the NE-KAMS Data File Warehouse (Mousseau, et. al., 2011). To strive for time and cost efficiency, the NE-KAMS Demo was created in DOE's Gen IV Database Infrastructure that supports the Gen IV Materials Handbook project to manage nuclear materials data contributions from Canada, China, European Union, France, Japan, Korea, South Africa, Switzerland, and United States for international collaboration in development of the Generation IV Nuclear Energy Systems [Ren, 2008; Ren, 2013]. Over a decade of evolution, the infrastructure successfully fostered development of several other database and knowledgebase systems to support various programs, which included the Nuclear System Materials Handbook Database for all existing domestic reactor systems, the ASME Materials Properties Database for codes and standards of the American Society of Mechanical Engineers (ASME) (Ren, et. al., 2011a), and the Nuclear Concrete Materials Database for the Light Water Reactor Sustainability Program

(Ren, et. al., 2010; Ren, et. al., 2011b). To support the NEKVAC, a sophisticated implementation plan was developed for expansion and operation of NE-KAMS Demo (Ren, et. al., 2015). The plan considered prospective NE-KAMS users from government, academia, and industry organizations, offering an excellent opportunity for leverage by the present project.

## 13.2. Scope of Work

The Oak Ridge National Laboratory would provide the NE-KAMS System to support the present project in data collection and management, verification and validation of simulation results, as well as other related activities. Documents generated from the project, including publications, presentations, and important project files considered worth preserving, would also be uploaded to NE-KAMS and maintained in a well-organized fashion for posterity retrieval. Based on the collected simulation and experimental results, reliable predictions or development of new experiments would be suggested by NE-KAMS through its data mining functionality. Authorized participants of the present project would be provided with different access privileges needed for conducting their tasks. The developed was expected to create a NE-KAMS-based archive of validation data for scenarios considered in two Risk-Informed Safety Margin Characterization (RISMC) applications, i.e., flooding hazard simulation and analysis; and reactor system thermal-hydraulic analysis. Because these applications would involve new data types and unique information management functionalities and tools, requirements from RISMC methods and toolkit would necessitate modification and adaptation of the NE-KAMS System. Further, the development was also expected to provide advice and support in formulating requirements of RISMC-VDMS as a knowledge management system that is scalable and improvable, with growth potential through RISMC applications.

In the blueprint for development and implementation of RISMC-VDMS, the RISMC-VDMS was designed to initially consist of a validation data file warehouse, relational digital databases and associated interfaces and utilities, to provide support for a range of activities, namely (a) collection, documentation, and preservation of validation data into one data repository; (b) analysis, qualification and characterization of data; (c) processing, formatting, and archiving data for rapid and coherent access and use in VUQ activities and advanced M&S development via the construction of relational databases. Structural design of the system is presented in Figure 13.2.

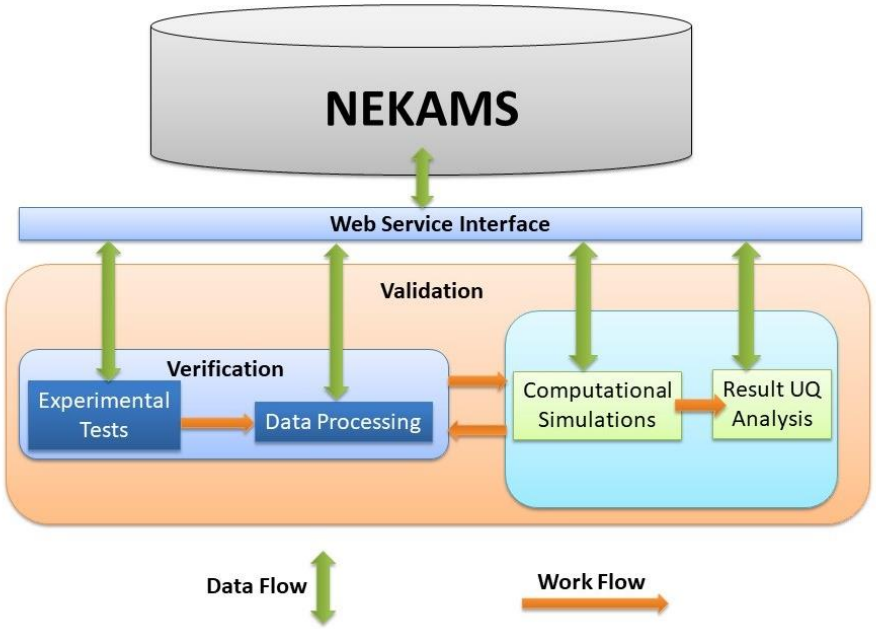


Figure 13.2. Structural design of the RISMC-VDMS of integrated data management, processing, and analysis workflow with NE-KAMS

Obviously, the desired development and implementation of RISMC-VDMS would require considerable effort in NE-KAMS structural and functional expansions. Since NE-KAMS was developed under the sponsorship of DOE for the specific purpose of supporting nuclear data collection and knowledge management, with the preparation of NEKVAC intensely underway, it was reasonably assumed that its further development under NEKVAC would provide adequate resources to support the needed expansion that could be leveraged by the present project.

### 13.3. Key Findings

To support the present and other DOE projects, the NE-KAMS Demo was upgraded to NE-KAMS Version 1.0 consisting of the following compartments with evolutionary expansions whenever resources became available under a piecewise development strategy.

- Operation Instructions
- Reports
- Experiment Unit Files
- Material Property Files
- Fluid Property Files
- Test Data Files
- Information Permit
- Quality Assessment
- Quality Assurance
- External Resources
- Presentations
- References
- Terminology Definitions

Each compartment is composed of a specific database schema that matches the data structure of the specific information domain. For example, Compartment Experiment Unit Files includes the following headings each containing a unique group of attributes:

- General Information
- Facility Information
- Structure and Geometry
- Surface Roughness
- Invasive Instrument
- Non-Invasive Instrument
- Data Acquisition System
- Test Control System
- Related Records
- Record Management Information
- Further Information

The access control system of NE-KAMS has been configured with two types of access privileges for the present project, i.e. READ users who can review and download data, and EDIT users who can review, download, upload, and edit data. Some project team members that needed NE-KAMS have been identified and granted access. NE-KAMS compartments that are applicable to the present project have also been configured with areas for "NCSU Released" and "NCSU Preparing," respectively. The "NCSU Released" areas are dedicated to data generated from this project that are qualified for public access. All NE-KAMS users can access such data. The "NCSU Preparing" areas are dedicated to data still under preparation. Only

the project EDIT users can access such data before the data are ready for release and moved to the "NCSU Released" areas.

Using the "NCSU Released" and "NCSU Preparing" structure in the Test Data Files Compartment, some test data file files were prepared, uploaded, and released. As shown in Figure 13.3, expandable folders named "NCSU/Thermal Hydraulics Test Data Files/Released" and "NCSU/Thermal Hydraulics Test Data Files/Preparing," respectively, are found in the compartment directory of the left pane. The first test data record is displayed in the right pan with test parameters and downloadable test result data files, as shown in Figure 13.3 (a). The records are hyperlinked at the bottom, as presented in Figure 13.3 (b), to their related records in other compartments so that users can browse conveniently through the information chain to understanding the data interrelationships and correctly interpret and use the data.

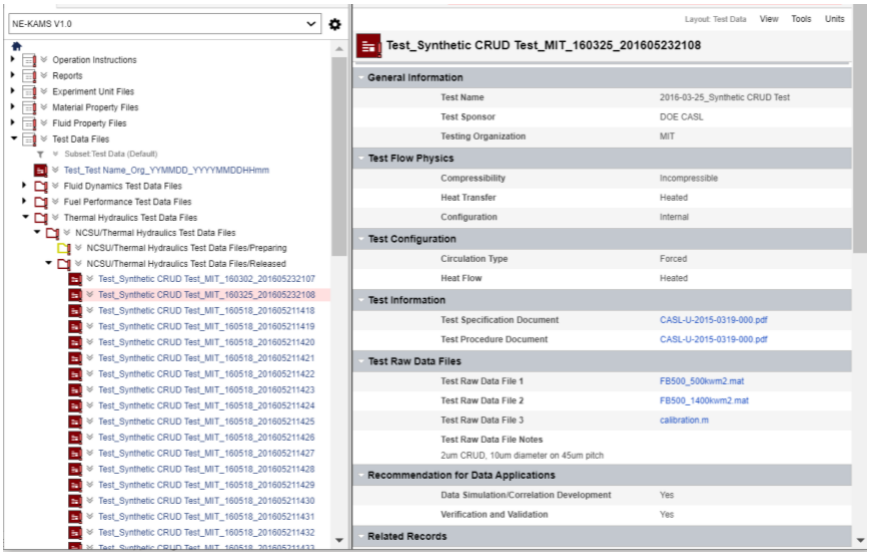


(a)

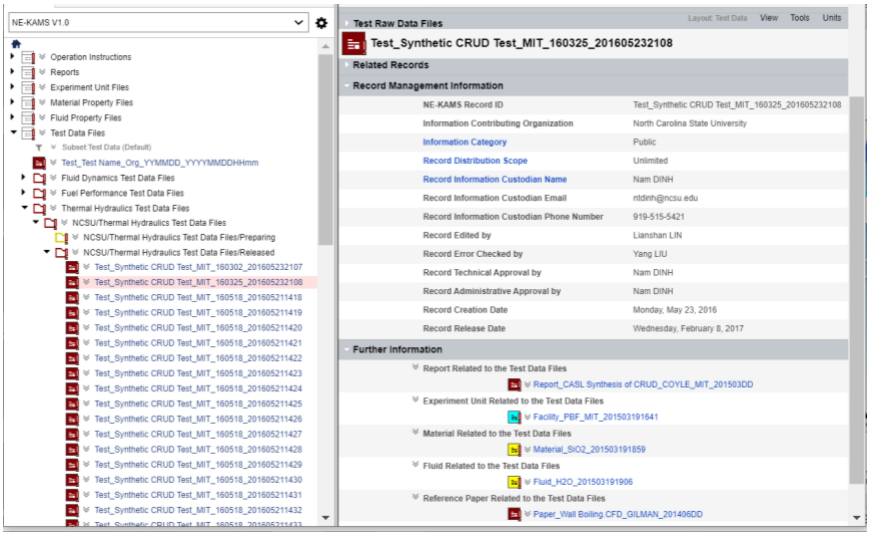


(b)

Figure 13.3. Data released and preparing areas for the present IRP in the Test Data File Compartment

Because a lot of important information of the project is summarized and reported in the periodic review meetings, a compartment for preservation of the meeting presentations was also developed for this project, as shown in Figure 13.4. These presentations provide auxiliary information for monitoring the project

progress, and more importantly, for understanding of the rationales of the validation data generation to ensure correct interpretation and use of the data, particularly for posterity who most likely will not have the full background knowledge that the present project participants have.

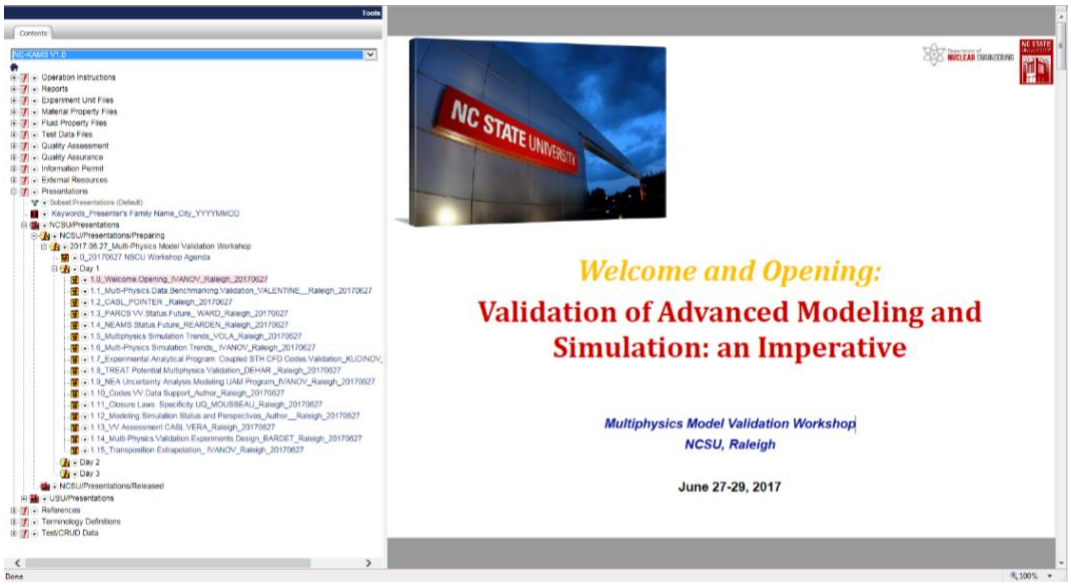


Figure 13.4. The Presentation Compartment and a record for the welcome and opening presentation for the Multiphysics Model Validation Workshop hosted by this IRP at NCSU in June 2017.

As the first step to provide APIs customized for the intended simulation codes and VUQ analytical tools for data analytics, data mining, and data assimilation, a data exchange web service interface was developed and successfully tested, in which the web service interface enabled a project participant at NCSU to access NE-KAMS data at ORNL from his computer at NCSU, and retrieved the data to remotely upload the data into a server at NCSU.

As previously discussed, the NE-KAMS structural and functional expansions required for development and implementation of RISMC-VDMS for the present project would largely rely on the NE-KAMS development under NEKVAC for adequate resources. With the initiation of NEKVAC intensely underway at the time, it was reasonably assumed that the required support would become available. Unfortunately, the situation did not pan out the desired way. NEKVAC was put on hold and eventually dissolved, despite the strong needs and the serious lack of effective information and knowledge management for advance modeling and simulation.

The dissolution of the NEKVAC had a significant negative impact on the present project. The ongoing development of schema for experiment data and simulation data was forced into a halt, and the work on V&V database infrastructure was also slowed down. Eventually it became clear that the desired structural and functional expansions of NE-KAMS could not be fully implemented during the period of this present project.

To prevent information loss and prepare for future opportunities, documents generated from the present project such as R&D reports, dissertations, and technical publications were preserved in NE-KAMS. For test data of large volumes, index records were created in NE-KAMS with descriptions of the data, background information, data structures, and hyperlinks to the data depositories so that posterity can correctly understand the information generated from the present project and easily locate the data when needed.

## 13.4. Path Forward

In order to ensure successful further development of the data-driven methodology, a major issue that must be addressed is the current lack of efficient knowledge management systems customized with a validation data structure. One of the major characteristics that made NE-KAMS stand out from the crowd during the INL-led nationwide survey of existing database systems for developing such a system was its customizable management of data and data interrelationships based on the data structure of interest [Lee, et. al., 2012]. The importance of customizable management of data and data interrelationships can be illustrated using Figure 13.5, where each circle represents a model, which may comprise multiple sub-models; and each line indicates a relation between the two models. The sub-models and sub-interrelationships multiply inside each circle. Data from the models and sub-models reflect the complex structure. Obviously, to fully develop the data-driven methodology, the complicated data interrelationships must be accurately maintained so that the information can be correctly interpreted, understood, and used with confidence.

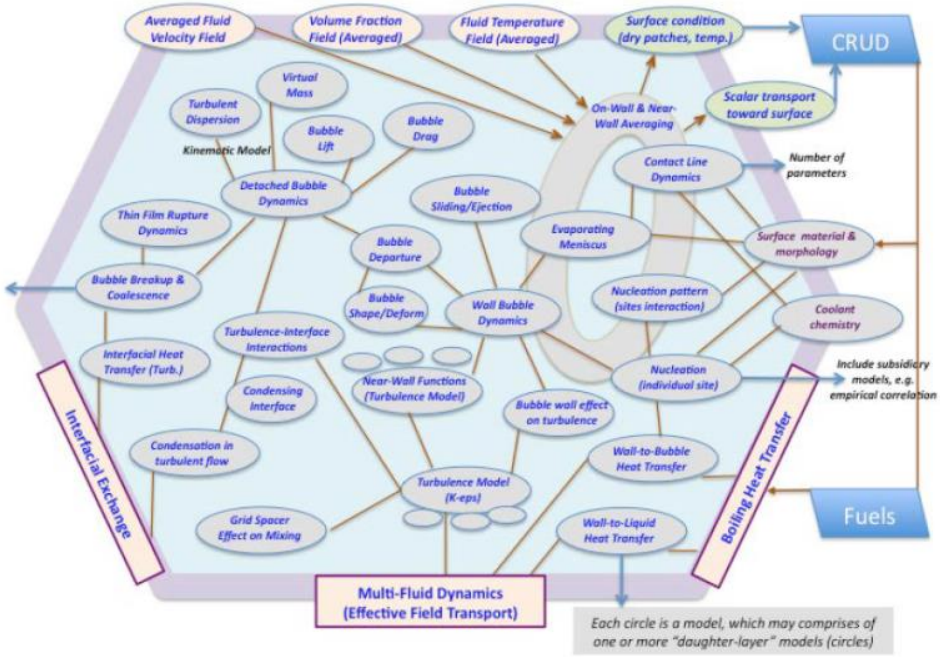


Figure 13.5 A schematic of multi-fluid dynamics modeling and simulation that demonstrates complexity of interrelationships among data generated.

Another major issue that must be addressed for successful development in the data-driven methodology is the sparse of validation data. This issue mainly has two folds: 1) the lack of qualified data, and 2) the lack of awareness about existing data. As more projects are conducted, more and more data will be generated to gradually improve the lack of qualified data situation. However, without a go-to focal point that registers and manages the characteristics and locations of all the generated data on a national or international scale, many datasets generated at high cost and stored in various places can quickly fade into oblivion.

In preparation for NEKVAC, a detailed implementation plan was developed by ORNL to delineate path forward in modernizing knowledge management for advanced simulation and modeling [Ren, et. al., 2015]. Today, the major principles and strategies discussed in the plan still provide valid guidance for path forward to support the data-driven methodology and other simulation and validation activities.

## 13.5. References

[Bang, et al., 2012] Youngsuk Bang, Jason M. Hite, and Hany S. Abdel-Khalik, "Hybrid Reduced Order Modeling Applied to Nonlinear Models," Int. J. for Numerical Methods in Eng., 91, 9, 929-949, August 2012.

[Gougar, 2015] "Introduction to NEKVAC," distribution to The Nuclear Energy Knowledge and Validation Center Directorate, May 2015.

[Lee, et. al., 2012] "NE-KAMS Demonstration Final Technical Report," INL/MIS-12-27348, DOE Office of Nuclear Energy, September 2012, Lee, Hyung; Mousseau, Kimberlyn C.; Johnson, Richard W.; and Ren, Weiju.

[Lee, et. al., 2013] "Nuclear Energy Knowledge Base for Advanced Modeling and Simulation FY 2013 Development Status Report," ORNL/TM-2013/411, Nuclear Energy Advanced Modeling and Simulation Program, U. S. Department of Energy, September 30, 2013, Lee, Hyung B. and Ren, Weiju.

[Mousseau, et. al., 2011] "Code Verification and Validation Data Standards and Requirements: Fluid Dynamics Version 1.0", Nuclear Energy Advanced Modeling and Simulation Program, Department of Energy, Nuclear Energy Office, September 2011, Mousseau, Kimberlyn C.; Johnson, Richard W.; Lee, Hyung; Oberkampf, William L.; Smith, Bart; Fort, James; Rider, William J.; and Weirs, V. Gregory.

[Ren, 2008] "Development of Digital Materials Database for Design and Construction of New Power Plants", Proceedings of 2008 International Congress on Advances in Nuclear Power Plants (ICAPP'08), American Nuclear Society Annual Meeting, Paper 8019, June 8-12, 2008, Anaheim CA, USA, Ren, Weiju.

[Ren, 2012] "Nuclear Energy Knowledge Base for Advanced Modeling and Simulation – Functionalities and Operation (Beta)," ORNL/TM-2012/ 464_Beta, Nuclear Energy Advanced Modeling and Simulation Program, Department of Energy, Nuclear Energy Office, September 30, 2012, Weiju Ren.

[Ren, 2013] "Gen IV Materials Handbook Functionalities and Operation (4A)", ORNL/TM-2013/406, U. S. Department of Energy Generation IV Nuclear Energy Systems Program, U. S. Department of Energy, September 15, 2013, Ren, Weiju.

[Ren, et. al., 2010] "Implementation Plan and Initial Development of Nuclear Concrete Materials Database for Light Water Reactor Sustainability Program", ORNL/TM-2010/177, U. S. Department of Energy Light Water Reactor Sustainability Program, U. S. Department of Energy, September 30, 2010, Ren, Weiju; Naus, Dan and Oland, Barry.

[Ren, et. al., 2011a] "ASME Materials Database Development Plan - A Database to Support American Society of Mechanical Engineers Codes and Standards", ORNL/TM-2011/160, American Society of Mechanical Engineers and the U.S. Department of Energy, June 30, 2011, Ren, Weiju and Ramirez, James.

[Ren, et. al., 2011b] "Nuclear Concrete Materials Database Phase I Development", ORNL/TM-2011/ 296, U. S. Department of Energy Light Water Reactor Sustainability Program, U. S. Department of Energy, September 30, 2011, Ren, Weiju; and Naus, Dan.

[Ren, et. al., 2015] "Nuclear Energy Knowledgebase and Simulation Code Validation System Development and Implementation Plan," ORNL/TM-2015/420, U. S. Department of Energy Nuclear Energy Knowledge and Validation Program, U. S. Department of Energy, August 30, 2015, Ren, Weiju and Valentine, Tim.

# 14.Project Data Management

## 14.1. High-Fidelity Simulation to Support System Thermal-Hydraulics Model Validation

### *Data Access*

The data repository from the single and two-phase simulations is archived on the *twophase* system at North Carolina State University's (NCSU) Nuclear Engineering department. To access the repository a user account needs to be created on the system. Contact Nadish Saini (nsaini3@ncsu.edu) or Igor Bolotnov (igor_bolotnov@ncsu.edu) for access to the machine and appropriate data archive.
To log into the machine from within the NCSU network, ssh using (replace 'user' with your username):

ssh -Y user@twophase.ne.ncsu.edu

If the user is outside the NCSU network, contact the above administrators for further instructions on getting access.

### *Repository Location*

The single-phase instantaneous data for probe locations shown in Figure 11.61 are located at:

/home/nsaini3/CASES/summer2019/singlephasethermal

The above directory includes four Reynolds number cases $\in Re_b = [5000, 20000]$. The binary files for instantaneous data for any given case are in:

/home/nsaini3/CASES/summer2019/singlephasethermal/Re11000/newvarts

Data for the two-phase cases have a similar directory structure. They are located at:

/home/nsaini3/CASES/summer2019/twoPhase

### *Data Format*

The instantaneous data is written from PHASTA in big endian binary format. Each single-phase contains data collected from 84,908 probes, with 28 variables written for each probe. The variable arrangement for a probe is as follows:

$$p, u, v, w, \Delta t, \frac{\partial u}{\partial x}, \frac{\partial v}{\partial x}, \frac{\partial w}{\partial x}, \frac{\partial u}{\partial y}, \frac{\partial v}{\partial y}, \frac{\partial w}{\partial y}, \frac{\partial u}{\partial z}, \frac{\partial v}{\partial z}, \frac{\partial w}{\partial z}, \frac{\partial T}{\partial x}, \frac{\partial T}{\partial y}, \frac{\partial T}{\partial z}, \frac{\partial p}{\partial x}, \frac{\partial p}{\partial y}, \frac{\partial p}{\partial z}, \frac{\partial^2 u}{\partial x^2}, \frac{\partial^2 v}{\partial y^2}, \frac{\partial^2 w}{\partial z^2}, x_p, y_p, z_p$$

Here $x_p, y_p, z_p$ are the probe coordinates, $p$ and $T$ are pressure and temperature, respectively, while the other variables are self-explanatory. Each instantaneous data file contains data written for 100 simulation time steps.

For the two-phase simulations, 9 variables were recorded arranged as,

$$p, u, v, w, \Delta t, x_p, y_p, z_p, \phi$$

where, $\phi$ is the local level-set field value at the probe location.

***Data Processing: Extracting Turbulent Statistics***

Python scripts for extracting turbulent statistics are located at the following Github repository: https://github.com/nandu90/dataDriven_IRP.

Owing to the large amount of instantaneous data and required memory requirements, the data is processed for each probe plane, as shown in Figure 11.61, separately. The necessary input file for running the Python script is $inputs.txt$. Details of the inputs are specified in the file. The most important inputs are described below:

```
inistep 5500    #Initial time step of binary file
laststep 9500   #Final time step of binary file
nprobes 84908   #Total number of probes
nsteps 100      #Total time-steps in each file
nplot 0         #Index of plane for which data is #to be extracted (0-29)
Rotate 0        #Rotates coordinate system to #tan-norm system with respect to #fuel rod walls
```

In the above example, the total number of time steps considered for averaging is 4000 (laststep-inistep). nplot parameter specifies the index of the plane, starting from the inlet of primary domain, Figure 11.60, for which the user chooses to extract the mean quantities. Rotate is a flag used to rotate the lateral coordinates to tan-norm system as described in Figure 11.61, necessary for comparing the statistical results with the existing DNS data, for instance the results shown in Figure 11.62. All output files are written in the *output/pln_*** directory. It contains CSV files for probe coordinates, mean velocities and Reynolds stresses.

## 14.2. Experimental Data to Support System Thermal-Hydraulics Model Validation

The processed data was properly stored for the future usage. Three ways of data storage were used: the virtual container in the DataFrame format supported by Pandas (for numerical values), which is a python package, cloud storage (for imagery information), and the one in compliance with the Nuclear Energy Knowledgebase for Advanced Modeling and Simulation (NE-KAMS). The list of large datasets is as follows:

Table 14.1. List of large datasets.

| Dataset | Description | Type | Size (Gb) | Storage Location |
|---|---|---|---|---|
| Y0OP1 | y = 0 mm, operating condition 1 | Images, Numeric | 2.1 | Pandas, Cloud |
| Y0OP2 | y = 0 mm, operating condition 2 | Images, Numeric | 2.5 | Pandas, Cloud |
| Y0OP3 | y = 0 mm, operating condition 3 | Images, Numeric | 3.1 | Pandas, Cloud |
| Y0OP4 | y = 0 mm, operating condition 4 | Images, Numeric | 2.9 | Pandas, Cloud |
| Y0OP5 | y = 0 mm, operating condition 5 | Images, Numeric | 3.6 | Pandas, Cloud |
| Y-4OP1 | y = -4 mm, operating condition 1 | Images, Numeric | 2.7 | Pandas, Cloud |
| Y-4OP2 | y = -4 mm, operating condition 2 | Images, Numeric | 2.3 | Pandas, Cloud |
| Y-4OP3 | y = -4 mm, operating condition 3 | Images, Numeric | 2.2 | Pandas, Cloud |
| Y-4OP4 | y = -4 mm, operating condition 4 | Images, Numeric | 3.5 | Pandas, Cloud |
| Y-4OP5 | y = -4 mm, operating condition 5 | Images, Numeric | 3.7 | Pandas, Cloud |
| Y4OP1 | y = 4 mm, operating condition 1 | Images, Numeric | 1.7 | Pandas, Cloud |
| Y4OP2 | y = 4 mm, operating condition 2 | Images, Numeric | 2.6 | Pandas, Cloud |
| Y4OP3 | y = 4 mm, operating condition 3 | Images, Numeric | 3.4 | Pandas, Cloud |
| Y4OP4 | y = 4 mm, operating condition 4 | Images, Numeric | 3.2 | Pandas, Cloud |

| | | | | |
|---|---|---|---|---|
| Y4OP5 | y = 4 mm, operating condition 5 | Images, Numeric | 2.7 | Pandas, Cloud |

## 14.3. Multi-Level Simulation to Support External Flooding Model Validation

### 14.3.1. Enhanced Spatial Resolution of Subdomain Meshes

Hundreds of terabytes of data are generated in ADCIRC full domain and subdomain simulations. These datasets include maximum elevation data, elevation time series, velocity time series, and boundary condition data. Considering the size of these datasets, they are archived and stored on servers at the United States Army Corps of Engineers, which have the capacity to store them.

Each case study considered is organized as follows:

**Directory Name:** StormName_Case StudyID/

**Subdirectories:**

**(1) RefinedFull_NoProject**

Input Files

a. ADCIRC mesh,
b. Meteorological data,
c. Nodal attributes file,
d. Full domain control file[1]

Output Files

e. Elevation time series
f. Velocity time series
g. Maximum Elevation data
h. Boundary conditions for all specified subdomains

**(2) RefinedFull_WithProject1**

Input Files

a. ADCIRC mesh,
b. Meteorological data,
c. Nodal attributes file,

Output Files

d. Elevation time series
e. Velocity time series
f. Maximum Elevation data

**(3) RefinedFull_WithProject2**

Input Files

a. ADCIRC mesh,
b. Meteorological data,
c. Nodal attributes file,

[1] Recorded in this file are boundary node numbers of subdomains mapped to full domain node numbers

Output Files

d. Elevation time series
e. Velocity time series
f. Maximum Elevation data

**(4) RefinedFull_WithProject3**

Input Files

a. ADCIRC mesh,
b. Meteorological data,
c. Nodal attributes file,

Output Files

d. Elevation time series
e. Velocity time series
f. Maximum Elevation data

**(5) Subdomains_WithProject:**

Input Files

a. Shape file (geometry using subdomain modeling scripts)
b. ADCIRC sub mesh,
c. Subdomain mapping files[2]
d. Meteorological data,
e. Nodal attributes file,
f. Subdomain boundary conditions file

Output Files

g. Elevation time series
h. Velocity time series
i. Maximum Elevation data

**ADCIRC-Neutrino coupling**. For this effort, the case studies considered are relatively simple and small. Thus, datasets are stored on desktop computers at USACE by Bukhari.

Each case study considered is organized as follows:

**Directory Name:** Case StudyID/

**Subdirectories:**

**(1) Full domain includes the following files:**

Input Files

a. ADCIRC mesh,
b. Meteorological data,
c. Nodal attributes file,
d. Full domain control file

Output Files

e. Elevation time series
f. Velocity time series

[2] Includes information of how subdomain nodes map to full domain nodes

g. Maximum Elevation data
h. Boundary conditions for all specified subdomains

**(2) SubdomainAroundNeutrinoDomain:**

Input Files
a. Shape file (geometry using subdomain modeling scripts)
b. ADCIRC sub mesh,
c. Subdomain mapping files
d. Meteorological data,
e. Nodal attributes file,
f. Subdomain boundary conditions file

Output Files
g. Elevation time series
h. Velocity time series
i. Maximum Elevation data

**(3) ADCIRCSubDataToNeutrinoData:**

Input Files
a. convertAdcirc2Neutrino.py
b. stations.dat
c. elevation time series
d. velocity time series

Output Files
e. SWData.csv

14.3.2. Verification and Validation

Datasets, models, and tools are maintained online in publicly accessible repositories, as described below.

**Alloy Case Studies on Scientific Computing**

Hurricane storm surge, sparse matrix computations, and other verification studies are maintained here:

https://people.engr.ncsu.edu/jwb/alloy/

**Sterling Visualizer for Alloy**

Sterling is Alloy extended to include visualizations generated using the alloy-js library. A local webserver is created when Alloy is initialized, and instance data is served automatically as solutions are found. The alloy-js library and supporting web pages are included to generate visualizations in the browser automatically.

The focus of this project is bringing better visualization techniques to Alloy, and so the name Sterling seemed particularly appropriate. After all, sterling silver is an alloy of silver that is generally used to make things that look nice.

Sterling website: https://sterling-js.github.io/

Github repository: https://github.com/alloy-js/sterling

**Components and Directory Structure**

We make use of the following tools:

- Gradle: Build tool responsible for gathering dependencies and generating the JAR file.
- Shadow: Gradle plugin used to create a fat JAR.
- Spark: Small webserver framework used to communicate with the browser.
- Alloy: Currently using Alloy 5.0.0.1

The project is laid out as follows (italicized items are not included in the repository but are generated by building the project):

- build/
    - libs/
        - Sterling-*.jar - The Sterling JAR file
- gradle/ - Gradle wrapper directory (more info)
- libs/ - Directory containing regular Alloy JAR files
- src/
    - main/
        - java/
            - gui/ - The main Alloy GUI (alloy4whole)
            - server/ - The Spark server code for communicating with the browser
            - sterling/ - Entry point and various Sterling specific classes
            - viz/ - The Alloy visualization window (alloy4viz)
        - resources/
            - public/ - Directory containing all web pages and Javascript to display visualizations
- build.gradle - The gradle build file that contains dependencies and build instructions
- gradlew - The gradle wrapper script (more info)
- gradlew.bat - The gradle wrapper script for Windows (more info)
- README.md - This file
- settings.gradle - The gradle settings file

## 14.4. SPH Simulation to Support External Flooding Model Validation

- A simulation with a particle size of 0.01 m (181,387 fluid particles total) takes about 16.7 hours for 30 cycles using an Intel Xeon central processing unit E5-2683 v3 @ 2.00 GHz with 28 core and 56 logical processors.
- Pressure data from the experiments was provided in 4 CSV format giving the time and pressure value for the four test cases. For validation 6 neutrino scene files were generated and used to reach optimal results. Results files from the simulations generated 6 pressure field result files.
- For the significant parameter work modified one main neutrino scene file into 35 varying scene files. The simulations resulted in 35 pressure field result files.